NASA Conference Publication 3088

Measurement and Characterization of the Acceleration Environment on Board the Space Station

Edited by
Charles R. Baugher
George C. Marshall Space Flight Center
Marshall Space Flight Center, Alabama

Proceedings of a conference implemented by
Teledyne Brown Engineering under contract with
NASA George C. Marshall Space Flight Center
and held at Lake Guntersville State Lodge
Guntersville, Alabama
August 11–14, 1986

NASA
National Aeronautics and
Space Administration
Office of Management
Scientific and Technical
Information Division
1990

FOREWORD

In the spring of 1986, members of NASA Headquarters and the George C. Marshall Space Flight Center came to the conclusion that a broad-based review and discussion of our knowledge concerning the anticipated acceleration environment on the Space Station would be desirable.

A contract was let to the Teledyne Brown Engineering Company (TBE) in Huntsville to organize and conduct a workshop with the theme "Measurement and Characterization of the Acceleration Environment On Board the Space Station." TBE mailed approximately 80 invitations to civilian and military government agencies, research organizations, and industries in the U.S., West Germany, France, and The Netherlands, with solicitation for contributed papers. A number of persons were personally invited to present papers.

The workshop took place at the Lake Guntersville State Lodge and Convention Center, 50 miles south of Huntsville, on August 11 to 14. Twenty-five papers were given, supplemented by many lively discussions. Among the 125 persons in attendance were astronauts Dr. Owen K. Garriott, Dr. Byron K. Lichtenberg, Dr. Ulf Merbold, and Dr. Lodewijk van den Berg.

Although the Workshop had originally been planned to address only questions related to the acceleration environment on the Space Station, presentations, and particularly discussions, covered a much larger scope. The fundamental question "how low must the acceleration level be, as a function of frequency, to assure that space-produced crystals, alloys, and other materials are substantially better than ground-produced materials?" came up again and again during the Workshop. A final answer to this question obviously does not yet exist. More experiments must be made that specifically address that problem.

Another sobering result of the Workshop was the recognition that the acceleration environment on all Shuttle flights -- inside and outside Spacelab -- was considerably worse than the environment required

for most of the materials experiments. It is anticipated that environmental conditions on the Space Station will not be substantially better than on the Shuttle. It will be necessary, therefore, to at least provide mechanical isolation mounts for the more sensitive experiments, or even to relegate them to unmanned, free-flying platforms with an absolute minimum of moving components.

A third problem that was given much attention during the Workshop was the measurement of the acceleration environment. Measuring very small levels of acceleration (on the order of 10^{-7} g) at very low frequencies (10^{-3} Hz) in the presence of accelerations up to 10^{-2} g at 1 to 100 Hz cannot be accomplished with any of the presently available accelerometers. Further efforts to develop accelerometer systems for such measurements will be needed.

Many attendees expressed the desire that a similar Workshop should be convened in the near future, perhaps in 1988.

For NASA/MSFC:	For Teledyne Brown Engineering:
Charles R. Baugher	Robert A. K. Mitchell
	Anthony Sharpe
	Edgar R. Pevey
	Daniel L. DeLong
	Ernst Stuhlinger

PARTICIPANTS WITH EXPERIENCE IN SPACE

Dr. Owen K. Garriott

Dr. Byron K. Lichtenberg

Dr. Ulf Merbold

Dr. Lodewijk van den Berg

TABLE OF CONTENTS

Paper No.	Title/Author	Page
1	Welcome - Edgar R. Pevey	1-1
2	Introduction (Outline of Workshop Program) - Anthony Sharpe	2-1
3	Overview of Space Station - Claude C. Priest	3-1
	Session 1. Effects of Accelerations on Materials Processing	
4	Desirable Limits of Accelerative Forces in a Space-Based Materials Processing Facility - Dr. Robert J. Naumann, NASA/MSFC	4-1
5	Implications of Acceleration Environments on Scaling Materials Processing in Space to Production - Ken Demel, NASA/Johnson Space Center	5-1
6	Acceleration Effects Observed in Optical Data Taken In Spacelab 3 FES - James Trolinger, SPECTRON Development Labs, Inc.; Ravindra Lal, Alabama A&M University; and Rudy Ruff, NASA/MSFC	6-1
7	Microgravity And Its Effects On Residual Motions In Fluids - J. Iwan D. Alexander and Charles A. Lundquist	7-1
	Session 2. Acceleration Measurements on Spacecraft	
8	The Microgravity Environment of the D1 Mission - H. Hamacher, U. Merbold, and R. Jilg	8-1
9	Low-g Measurements by NASA - Roger P. Chassay and Arthur Schwaniger, NASA/MSFC	9-1
10	Prediction and Reconstruction of On-Orbit Acceleration - Edward Bergmann, C. S. Draper Laboratory	10-1
11	Spacelab 3 Low-g Accelerometer Data from the Fluid Experiments System (FES) - Gary Arnett, BGB, Inc. ..	11-1
12	MSL-2 Accelerometer Data Results - Fred Henderson, Teledyne Brown Engineering	12-1
13	Mechanical Isolation for Gravity Gradiometers - David Sonnabend, Jet Propulsion Laboratory	13-1

TABLE OF CONTENTS (continued)

Paper No.	Title/Author	Page
	Session 3. Accelerometer Instrumentation	
14	The MESA Accelerometer for Space Application - William G. Lange and Robert W. Dietrich, Bell Aero-Space Textron	14-1
15	A New Accelerometer Recording System for Shuttle Use - Dr. Byron Lichtenberg, Payload Systems, Inc. .	15-1
16	New Accelerometers Under Development - Dr. Jerry Wald and Dr. M. Tehrani, Honeywell Systems and Research Center	16-1
17	Superconducting Six-Axis Accelerometer - Prof. H. J. Paik, University of Maryland	17-1
18	Presentation On A Space Acceleration Measurement System (SAMS) - Theodore L. Chase, NASA/LeRC	18-1
19	Acquisition and Analysis of Accelerometer Data - Keith R. Verges, Teledyne Geotech	19-1
20	Characterizing Performance of Ultra-Sensitive Accelerometers - Dr. Henry Sebesta, Applied Technology Associates, Inc.	20-1
	Session 4. Space Station Environment	
21	Free-Floating Experiments In Orbiter and Space Station - Owen K. Garriott, EFFORT, Inc.	21-1
22	Microgravity Acceleration Modeling For Orbital Systems - Dr. Walter Knabe, MBB-ERNO, Bremen	22-1
23	Low-g Payload Placement Constraints for Space Station - Anita S. Carpenter and Stanley N. Carroll, NASA/MSFC	23-1
24	Space Station Dynamics - Reg Berka, NASA/JSC	24-1
25	Space Station Structural Performance Experiment - Dick Gates, Boeing Aerospace Co.	25-1

TABLE OF CONTENTS (concluded)

Paper No.	Title/Author	Page
26	Effect of Science Laboratory Centrifuge On Space Station Environment - Nancy Searby, Lockheed	26-1
	Session 5. Panel: Desirable Acceleration Environment on Space Station	
27	Noise Power Spectral Density of The Sundstrand QA-2000 Accelerometer - Rex Peters and David Grindeland, Sundstrand Data Control, Inc.	27-1
	Session 6. Summary of Workshop	
28	The Perfectly Ideal Accelerometer (Summary of Workshop) - Dr. Ernst Stuhlinger, Teledyne Brown Engineering	28-1

1. WELCOME

Edgar R. Pevey*

Ladies and Gentlemen, on behalf of Teledyne Brown Engineering and the Microgravity and Materials Processing Facility (MMPF) Study team, welcome to Lake Guntersville State Lodge and, in particular, to the Workshop "Measurement and Characterization of the Acceleration Environment on board the Space Station". I am Ed Pevey, Study Manager of the MMPF Study. Prior to the start of the workshop, I wish to recognize some of our key players and those team members who are responsible for putting together this workshop.

First, from the Marshall Space Flight Center, I wish to recognize Mr. Charles Baugher, Contracting Officer's Representative (COR) for the MMPF Study. Charles is responsible for this microgravity workshop. Next, from TBE, the manager of our Advanced Programs Department, Mr. Tony Sharpe; my Workshop team: Dr. Ernst Stuhlinger, Mr. Dan Delong, and in back of the room, Ms. Becky Dew. These three are responsible for this workshop. They have been the workhorses.

At this time we are pleased to recognize and welcome former Astronaut/Mission Specialist, Dr. Owen Garriott, and three Payload Specialists, Dr. Lodewijk van den Berg, Dr. Byron Lichtenberg, and Dr. Ulf Merbold from West Germany. Dr. Merbold was the non-NASA member and first non-American in space aboard the Space Shuttle. We are pleased to recognize and welcome two participants from West Germany, Dr. Hans Hamacher, DFVLR, and Dr. Walter Knabe, from MBB/ERNO. Next, I wish to recognize our session chairmen: Session 1 - Dr. Trip Mookherji of TBE, Session 2 - Mr. James Fountain of the CSM Group, MSFC, Session 3 - Mr. Dan DeLong of TBE, Session 4 -Mr. Pete Priest of NASA/MSFC Space Station Program Office, Session 5 - Panel Moderators Dr. Bob Naumann and Charles Baugher, and Session 6 - Dr. Ernst Stuhlinger of TBE. Again, to all of you, both participants and attendees, a very warm Alabama welcome.

*Manager, Microgravity Materials Processing Facility Project, TBE

Our first speaker is Mr. Tony Sharpe, who will provide the outline of the workshop program. Mr. Sharpe has over 25 years of aerospace experience as manager and project manager of various systems engineering and space station definiton studies. Prior to coming to TBE, he was with the SPAR Aerospace Ltd. in Canada where he was manager of the Shuttle Remote Manipulator System Division. With Teledyne Brown Engineering, he is Manager, Advanced Programs Department, Space Programs Division. He received his Bachelor of Science Degree from the University of Leeds, England. Please welcome Mr. Tony Sharpe.

2. INTRODUCTION

Outline of Workshop Program

Anthony Sharpe*

When we need to make decisions concerning a subject matter about which we are grossly ignorant, we have two options. We can press on regardless, with a determination to "learn on the way" -- or, we can convene a workshop and try to eliminate at least some of our ignorance.

Both the Marshall Space Flight Center and its contractor, Teledyne Brown Engineering, find themselves in such a situation. We have to make decisions regarding acceleration measurements on board the Space Station, and we don't yet have enough knowledge to do so. Rather than forging ahead in the hope that knowledge will be picked up on the way, we have chosen the second option, and organized a workshop with the theme: "Measurement and Characterization of the Acceleration Environment On Board the Space Station."

We would like to extend a very warm welcome to all of you who have accepted our invitation to attend this workshop. Our aim, of course, is to "pick your brains"; but we also hope that these three days at the Guntersville Lodge will prove useful and rewarding to you in your own work.

In our opening presentation, we will familiarize you with the present Space Station concept, particularly its functions and structure.

The four main sessions of the workshop, today and tomorrow, will cover areas of critical importance to the materials processing scientist in the planning, preparation, and conduct of experiments in space.

The first session will address the effects that residual accelerations will have on materials processing under near-weightless conditions. Much theoretical, and some experimental, work has been done in

*Manager, Advanced Programs Department, TBE

this area during the past 15 years; but more work must be done before we can define with confidence the desirable acceleration limits for specific experiments.

In our second session, we will examine the acceleration environment experienced on previous spacecraft, ranging from rockets to the Space Shuttle -- and, in particular, Spacelab. Numerous measurements of this environment have been made, and they have provided a fairly clear picture of the residual accelerations that occurred during those flights. It is hoped that this session will provide a mechanism for consolidating this information and bringing the picture into clearer focus.

In our third session, we will review the acceleration measurement instruments presently available, or under development. Although a great number of accelerometer types have been developed and built during recent years, there may be a need for new developments that will cover the specific requirements of accelerometers for materials processing work.

Our fourth session will focus on the acceleration environment we expect on the Space Station.

With its large and relatively light structural members, its numerous running machines (such as fans, pumps, and compressors), its docking and undocking spacecraft, its moving astronauts, its air drag, and its gravity gradient, the Space Station will by no means offer a zero-g environment. Estimates of the residual accelerations expected on the operating Space Station will be presented.

Following these four sessions, there will be a Panel discussion, in which the subjects brought out during the sessions will be presented and debated by the session chairpersons (in this case chairmen) and some other workshop participants. We hope for strong audience participation in this Panel discussion.

On Thursday, there will be a summary of the entire Workshop, with an outline of the major findings, conclusions, recommendations, and remaining concerns that surfaced during the presentations and discussions of the previous two days. Again, we hope for lively discussions on the part of the attendees and participants of the Workshop.

A dinner is planned for Tuesday evening. We will have the great pleasure of an after-dinner speech by a real payload specialist/astronaut, Dr. Lodewijk van den Berg. Another payload specialist/astronaut, Dr. Byron Lichtenberg, will participate in the Workshop as a session speaker. Also participating in the Workshop as a session speaker, and as a Panel member, will be another real-life astronaut, Dr. Owen Garriott -- one of the "old timers" in space! We deeply appreciate the presence and participation of a fourth astronaut scientist, Dr. Ulf Merbold from West Germany, who flew on Spacelab 1.

It is our sincere wish that the outcome of this Workshop will, in terms of value, be greater than the sum of its parts, providing a much-enriched knowledge base from which we can all work.

I would like to extend my own very best wishes to all of you for an enjoyable and profitable time in this beautiful lodge.

It is now my pleasure to introduce our first speaker, Mr. Claude C. (better known as Pete) Priest.

Mr. Priest holds a Master of Science degree in mechanical engineering. He began his professional career with the Union Carbide Nuclear Company in Oak Ridge, Tennessee.

In 1962, he joined the Marshall Space Flight Center as a launch vehicle and flight systems engineer.

During the past four years, Mr. Priest has been a member of the Space Station Projects Office at the Marshall Center. He was detailed to NASA Headquarters in 1985 as Technical Assistant to the Associate Administrator for the Space Station.

Mr. Priest is Deputy Manager for the Laboratory Module in the Space Station Projects Office at the Marshall Space Flight Center in Huntsville.

He will give us an overview of the Space Station Program.

N91-12402

3. OVERVIEW OF SPACE STATION

Claude C. Priest*

This overview is primarily aimed at those workshop participants who may not be fully familiar with the Space Station program. I do not plan to discuss some issues that have appeared in the media lately relating to things like potential program organization changes, potential work package changes, center role responsibility changes, and impacts that may result to the program from the Shuttle redesign activities after the Shuttle Challenger accident. The major topics I would like to cover today will be the overall program guidelines that we laid out when we put the program together, a little about the international involvement, what our baseline configuration is today, and our plans as we proceed into the development phase this next fiscal year.

Over the last few decades, NASA has conducted numerous studies on space stations. There were even some serious attempts at initiating development. We have, in fact, flown the nation's first space station, which was Skylab. The current Space Station program officially began with the President's 1984 State of the Union address, in which he directed NASA to develop a permanently manned Space Station within a decade. This commitment has been reaffirmed in two succeeding addresses, in 1985 and again this past year, which I think is a rare occurrence for most NASA programs.

Earlier studies focused on a space station design that was singular in its function, such as a laboratory in space or an operations base. Out of the current planning came the desire that the Space Station (Figure 1) be a multipurpose facility, capable of the following functions: It should provide a laboratory in which we can conduct research and technology development in a pressurized environment, primarily in materials processing and similar sciences. It should also be a permanent observation post for both Earth and celestial observations. We are looking at it also as a servicing facility that would have the capability to extend satellite lifetimes as well as upgrade existing

*Deputy Manager, Laboratory Module Office, Space Station Projects Office, Marshall Space Flight Center

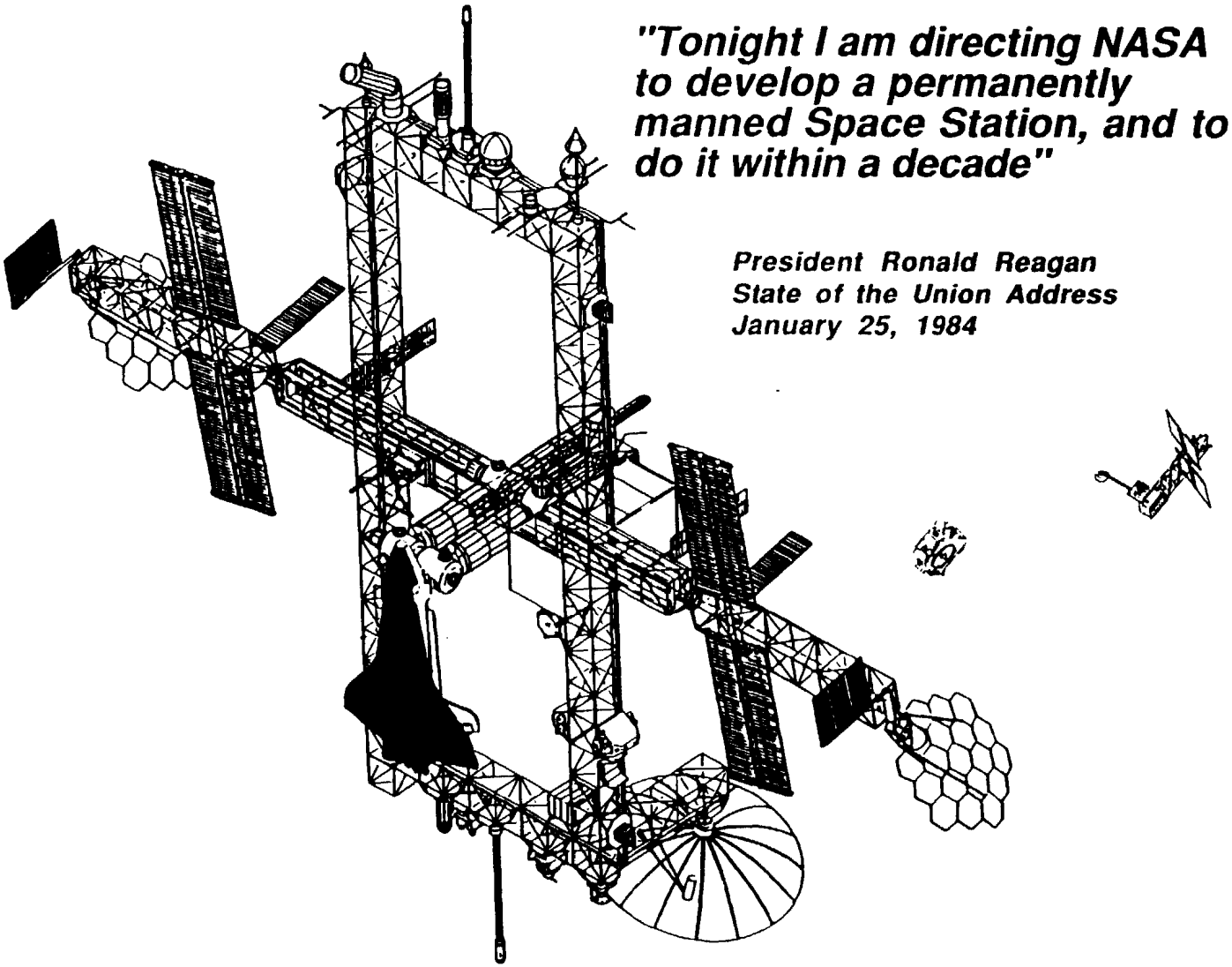

"Tonight I am directing NASA to develop a permanently manned Space Station, and to do it within a decade"

President Ronald Reagan
State of the Union Address
January 25, 1984

FIGURE 1.

space systems. This service and repair function has been designated a number one priority by NASA's Office of Space Science and Applications. We are also looking at it as a transportation node for delivering payloads to other near-Earth orbits, to geostationary orbits, or to interplanetary trajectories. It would also allow payloads too heavy to be launched on the Space Shuttle to be brought up separately, assembled at the Space Station, fueled, checked out, and launched to their destination. This would increase the payload size for future space missions.

The development of these capabilities, plus some others, as shown in Figure 2, made it difficult to avoid the conclusion that the Space Station should be evolutionary in its development, because we couldn't provide all of these functions at the outset. This evolutionary growth became an underlying theme in the Space Station planning. Early in the program there was a set of planning guidelines that were adopted for this definition process; it is interesting to note that during the past three years these guidelines have essentially remained unchanged. The guidelines, shown in Figure 3, are management-related and engineering-related. With respect to the engineering-related guidelines, we plan the Space Station to be continuously habitable to meet the President's direction of a permanent manned space station. It also will be dependent on the shuttle for launch and assembly, as well as for crew rotation. It will be consistent with the desires of the user community.

The Space Station will consist of both manned and unmanned elements; in fact, there will be a manned base as well as unmanned platforms. The program has been heavily focused on the Space Station users and their requirements to ensure that the facility to be developed will be customer- or user-friendly. The management-related guidelines show a three-year definition program; we are currently in the third year. We had planned to spend between 5 and 10% of the expected total cost of the Space Station, estimated at $8 billion in fiscal year 1984 dollars, for the definition phase so that it would put us in a sound position as we go into the development phase. This program has NASA-wide participation: all of the NASA space centers are involved. During Phase B, the

SPACE STATION

- a laboratory in space
- a permanent observatory
- a servicing facility
- a transportation node
- an assembly facility
- a manufacturing facility
- a storage depot
- a staging base

A space station is a multi-purpose facility

FIGURE 2.

SPACE STATION PLANNING
BASELINE GUIDELINES

MANAGEMENT RELATED

- Three year detailed definition
- NASA-wide participation
- Manage SE&I in-house
- Development funding in FY 1987
- IOC: "within a decade"
- Cost of initial capability: $8.0B
- Extensive user involvement
  - — Science and applications
  - — Technology
  - — Commercial
- International participation

ENGINEERING RELATED

- Continuously habitable
- Shuttle dependent
- Manned and unmanned elements
- Evolutionary
- Maintainable/restorable
- Operationally semi-autonomous
- Customer friendly
- Technology transparent
- Man-tended approach
- Automation and robotics focus

FIGURE 3.

system engineering and integration is being accomplished in-house. Consistent with the directive to complete the Space Station in a decade, we plan to have development funding beginning in the next fiscal year.

International participation has also been a fundamental requirement of the program, as directed by the President. When the President gave the direction to develop a permanently manned station, he also invited our friends and allies to participate (Figure 4). A year ago last spring, NASA signed bilateral MOUs (Memoranda of Understanding) with Canada, the European Space Agency, and Japan, and, in parallel with us, they are in the preliminary design phase. Canada is focusing on the Mobile Servicing Center (MSC), which provides support to attached payloads, as well as to the initial assembly of the Space Station. The European Space Agency is focusing primarily on a pressurized laboratory module as well as unmanned platforms. Japan is focusing on a Japanese experiment module that consists of a pressurized laboratory, with a pallet-like structure attached to the laboratory. So, the Space Station is going to be an international endeavor.

The result of these planning guidelines is a Space Station complex as depicted in Figure 5. The Station will be in a low-inclination orbit at 28.5°, in phase with unmanned co-orbiting platforms and supported by a maneuvering vehicle. The complex may also include an Earth observation platform in a polar orbit, supported by the Shuttle and also by a maneuvering vehicle. A manned base, a polar platform and co-orbiting platforms, are planned to be part of the IOC Space Station. The maneuvering vehicle, also called OMV, is being developed in a separate NASA program.

The major program phases are shown in Figure 6. Phase B, initiated a year ago last April, consists of two parts: a definition and a preliminary design. The definition part was concluded this past March with a systems requirements review. This led to a baseline configuration (Figure 7) in May of this year. Phase B is scheduled to be completed in January 1987. The design and development phase, C/D, should

SPACE STATION PROGRAM
INTERNATIONAL COOPERATION

- When directing NASA to develop a permanently manned Space Station, President Reagan invited friends and allies of the United Sates to participate in the Space Station endeavor
- International cooperation has been a hallmark of many NASA programs
- In the spring of 1985, NASA signed bilateral Memoranda of Understanding (MOU) with Canada, European Space Agency, and Japan that provide a framework for cooperation on Space Station during Phase B (Definition and Preliminary Design)
- International elements are part of the Space Station baseline configuration. Under study in Phase B preliminary design:

Canada — Mobile Servicing Center (MSC)
European Space Agency — Pressurized laboratory module, polar platform, resource module
Japan — Japanese Experiment Module (JEM)

- Negotiations on Space Station cooperation during Phase C/D and Operations begin in June, 1986

SPACE STATION IS AN INTERNATIONAL ENDEAVOR

FIGURE 4.

INITIAL SPACE STATION COMPLEX

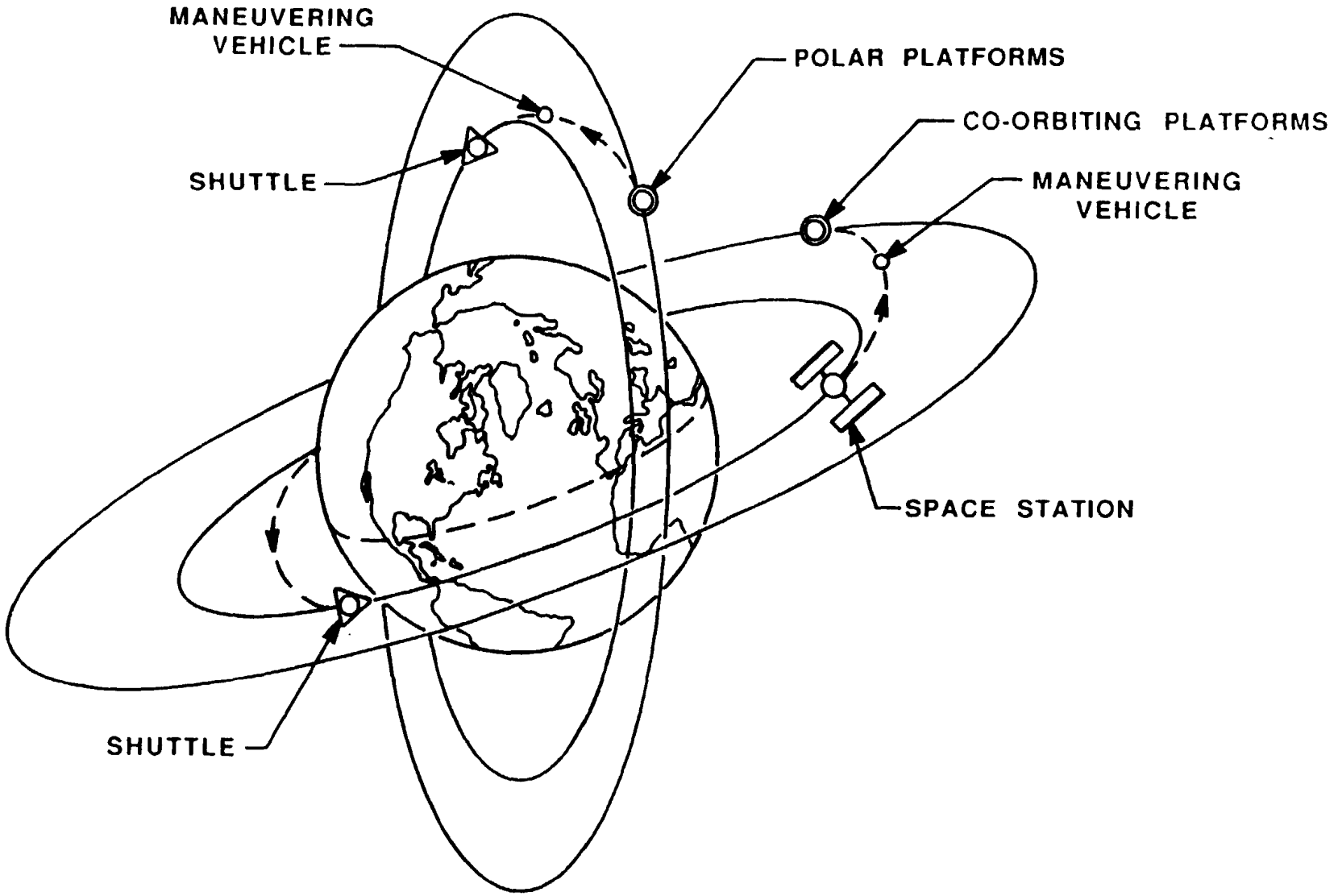

FIGURE 5.

SPACE STATION
PROGRAM PLANNING OVERVIEW

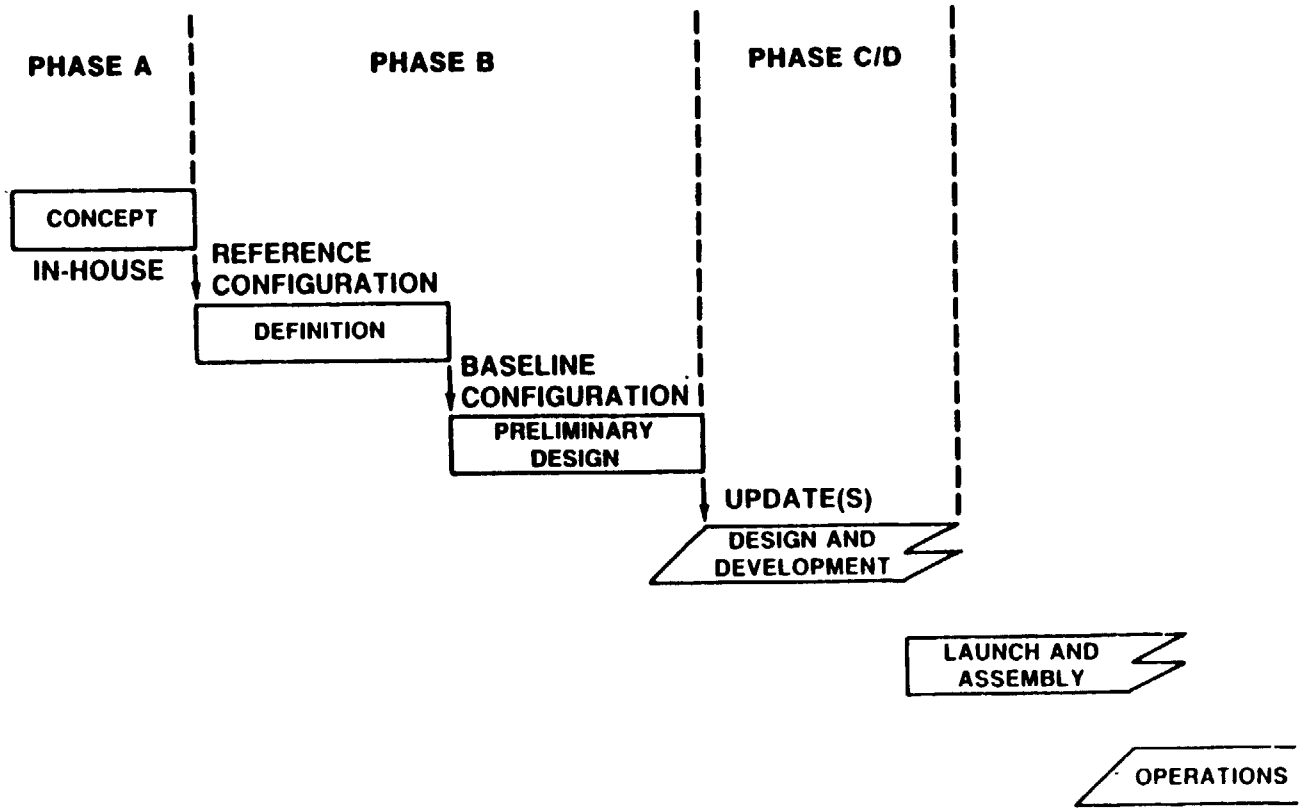

FIGURE 6.

DUAL KEEL SPACE STATION
BASELINE CONFIGURATION

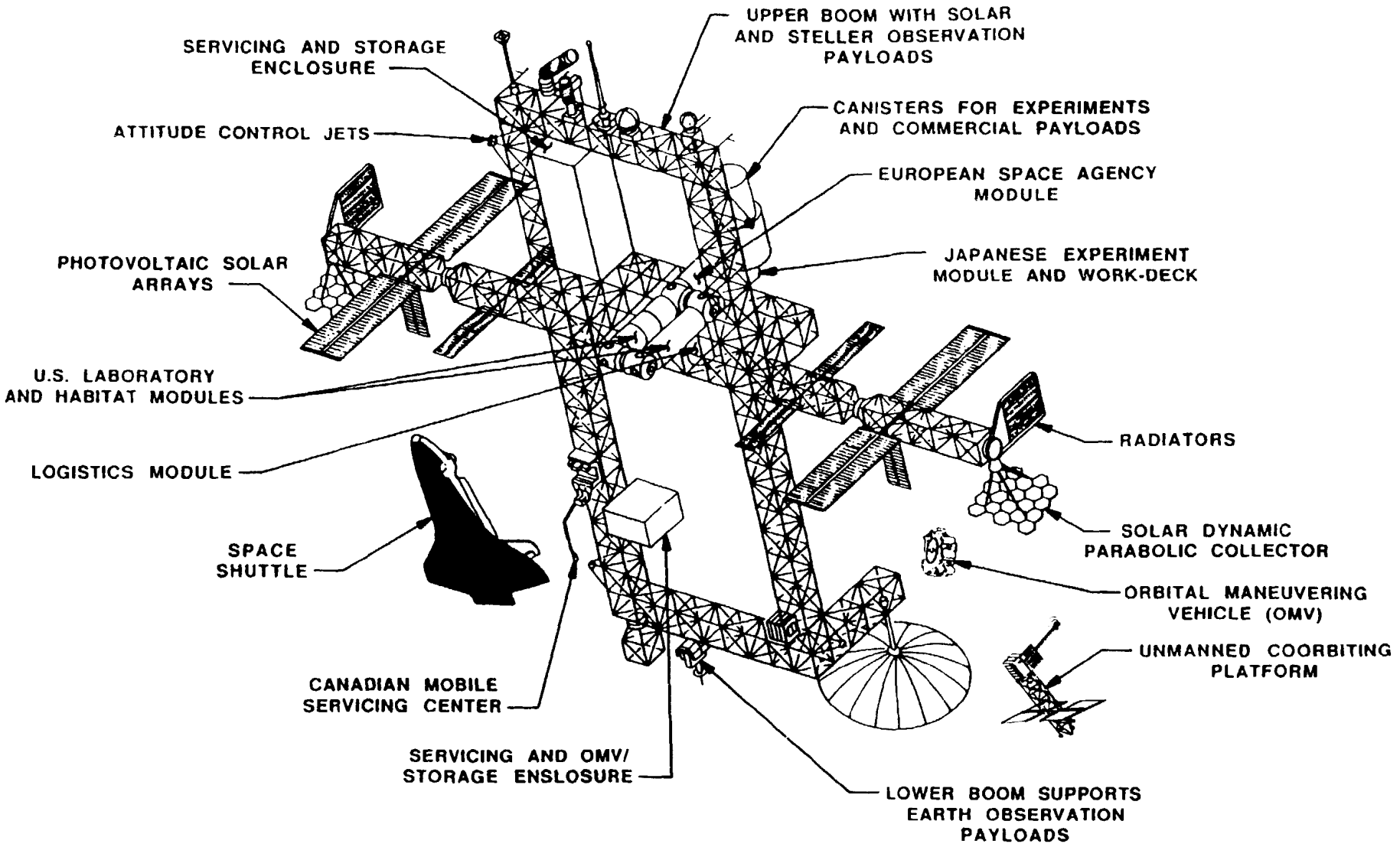

FIGURE 7.

be under contract by the middle of next year. This will lead, if we are successful, to a first-element launch in 1993, leading to the permanently manned capability about a year later, consistent with the President's directive.

There are four work packages in four NASA centers involved in the Phase B definition: Marshall Space Flight Center, Johnson Space Center, Goddard Space Flight Center, and Lewis Research Center. Most of the work on the manned base part of the Space Station is being done by Work Packages 1 and 2 and their contractors. Work Package 3 is primarily focused on the unmanned platforms and on the servicing and attached payload functions of the manned base. Work Package 4 is defining the power system for both the manned base and the platforms.

The baseline configuration that resulted from the definition phase, now under preliminary design, is shown in Figure 8. This configuration is called a dual-keel Space Station because of the two parallel vertical keels. The keels are about 360 ft long; the transverse boom, which runs from left to right on the figure, is about 500 ft long. The bases of these trusses are 5-m cubes. The Space Station will fly in an Earth-fixed attitude with the keels pointed toward the Earth. At the top of the keels are attached payloads, including instruments for stellar and solar observations.

The lower boom, attached to the two keels at the bottom, will support attached payloads observing the Earth. The transverse booms support the power systems at the ends, the thermal radiators, and the pressurized modules. The power system as planned today is a hybrid system of solar photovoltaic and solar dynamic design. The solar photovoltaic system will be put up initially to help support the base during assembly. When both of these power systems are in place, the total average power output will be 75 kW, with 50 kW being allocated to users and 25 kW for housekeeping or system support. There are servicing bays located between the keels, for servicing satellites and the OMV.

SPACE STATION

- ASSURE FREE WORLD LEADERSHIP IN SPACE DURING THE 1990's
- STIMULATE ADVANCED TECHNOLOGY
- PROMOTE INTERNATIONAL COOPERATION
- ENHANCE CAPABILITIES FOR SPACE SCIENCE AND APPLICATIONS
- DEVELOP FURTHER THE COMMERCIAL POTENTIAL OF SPACE
- CONTRIBUTE TO PRIDE AND PRESTIGE
- STIMULATE INTEREST IN SCIENCE AND ENGINEERING EDUCATION

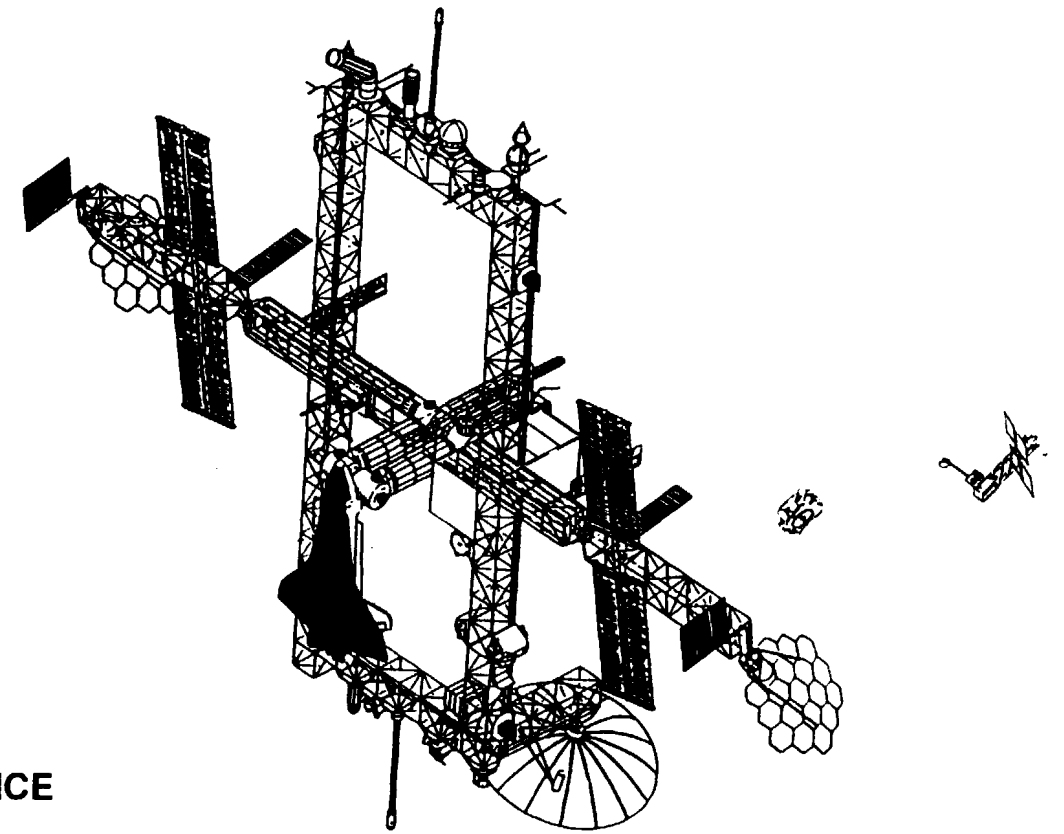

FIGURE 8.

The module assembly (Figure 9) consists of four major pressurized modules, two provided by the U.S., a habitation module and a lab, and one each provided by the European Space Agency and Japan. The length of the U.S. modules is on the order of 44 ft; the pressure level is the same as on Earth (14.7 psi). The environmental control system will be a closed-loop system with nitrogen resupply. The microgravity level that we want to achieve in the laboratory modules is on the order of 10E-5 g near the centerline of the U.S. Laboratory module. The Station will be assembled initially at an altitude of 220 n.mi. Later, it will be boosted up to its operating altitude of at least 250 n.mi. There are four major modules, all interconnected. Additionally, not shown in the figure, there is a logistics module and two airlocks. All the presurrized modules will incorporate a horizontal arrangement of floor, ceiling, and walls, much like Spacelab. A cross-section of a typical module is shown in Figure 10.

Four symmetrical longitudinal standoffs are used for utility runs down the module interior and also to support the racks that are mounted in the four quadrants of the modules. A utility interface will be provided between each two double racks that will provide power, data lines, and thermal ducts. Standard racks will be provided that can be replaced on orbit, either tilt-out or slide-out types. They will be interchangeable, with standard racks in all four modules. Both double and single racks will be provided; double rack width will be 42 inches, and two single racks will be capable of replacing one double rack. We are trying to maintain a minimum aisle space and a ceiling space of about 84 inches.

The U.S. and International modules currently have different module diameters, which will make the standard rack development more challenging. The U.S. module has about 166 inches internal diameter while the Japanese module is about 158 inches and the European module 157 inches in diameter.

SPACE STATION MODULE PATTERN

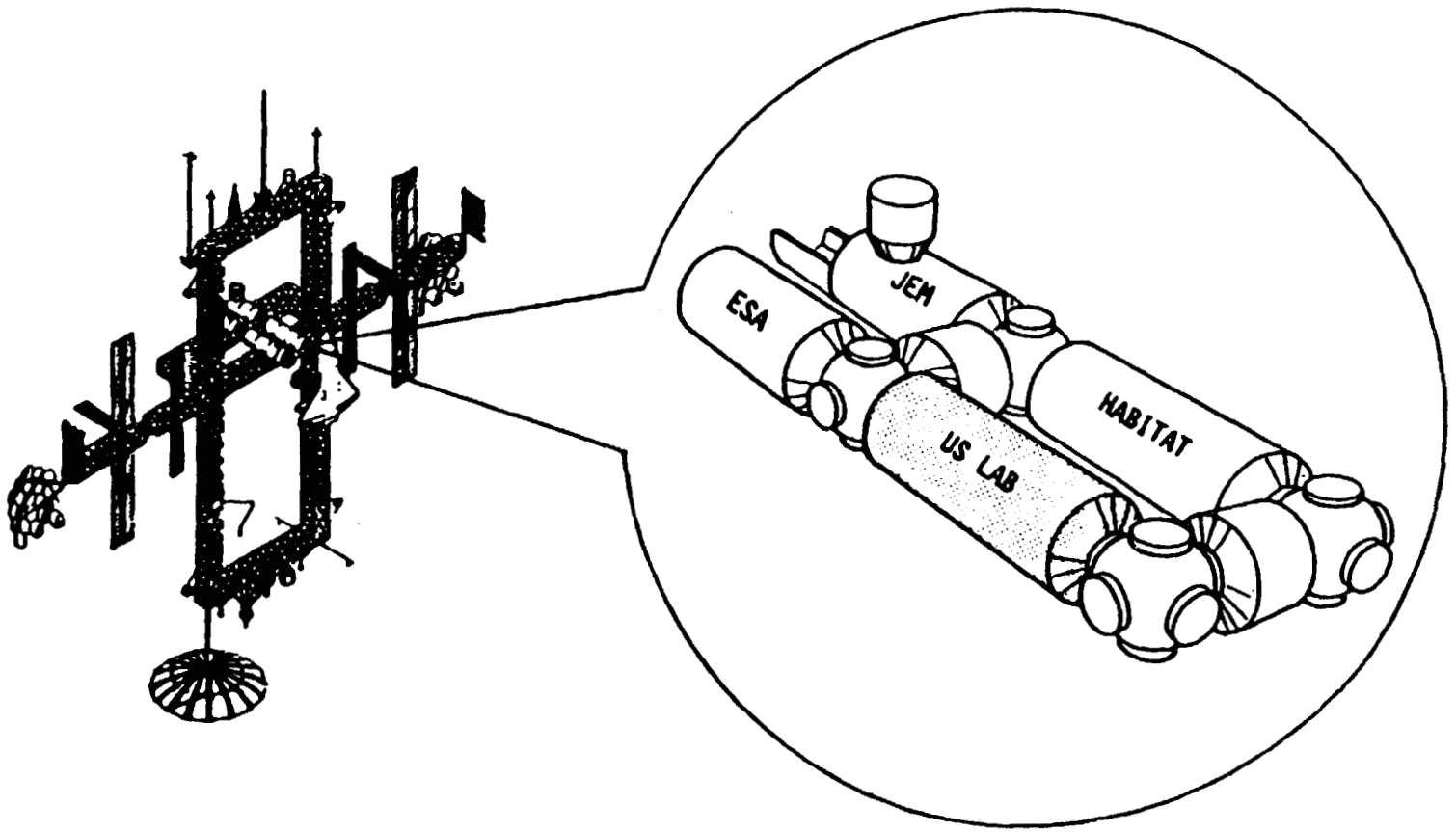

FIGURE 9.

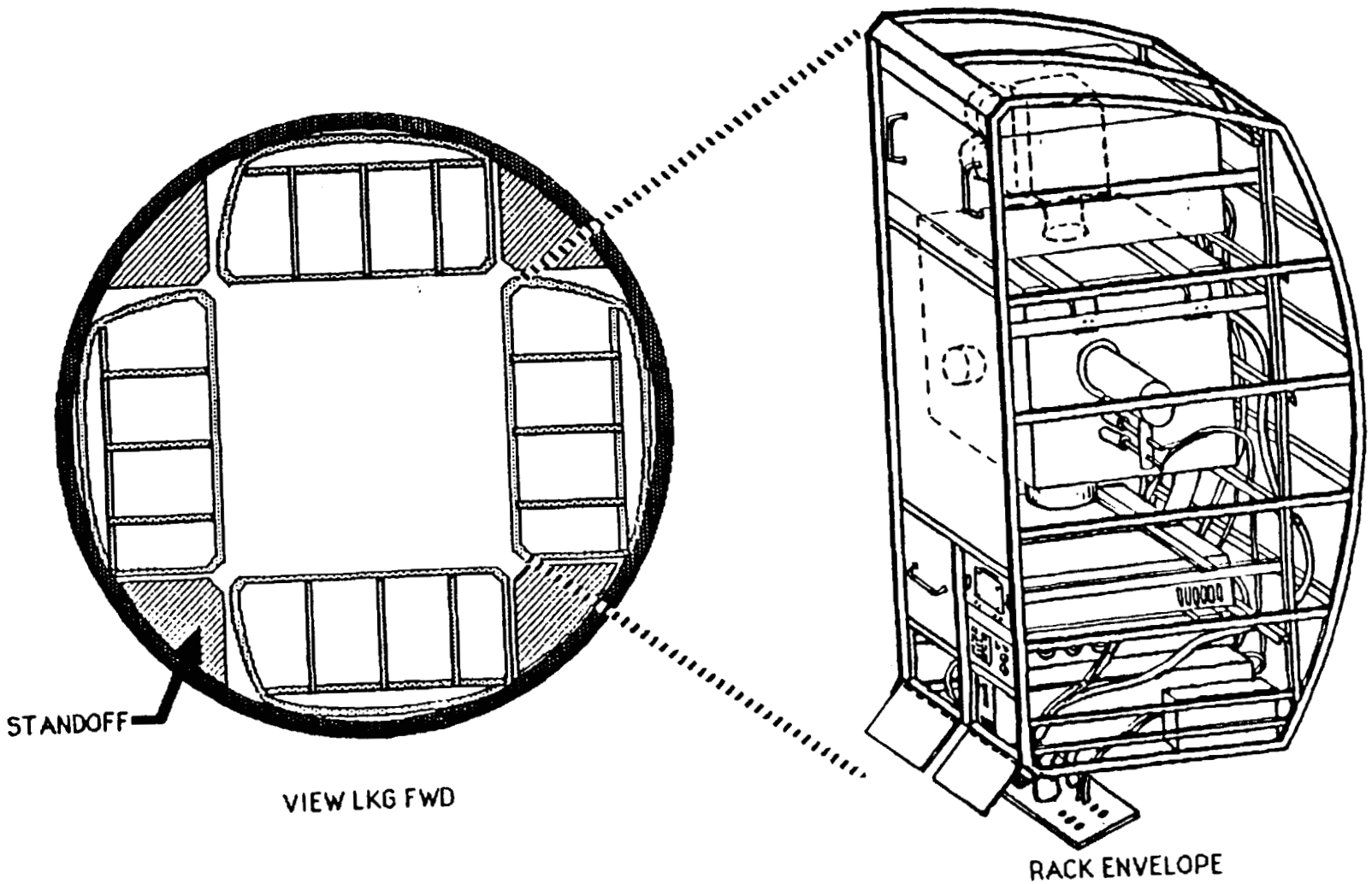

FIGURE 10.

The primary function that is going to be accommodated in the U.S. lab is materials reseach and development that would be most sensitive to acceleration environment.

There will also be control and monitoring space for user-provided pressurized modules that would be attached to the assembly. Such a module might be a production facility for commercial materials processing. The lab module will also be designed to accommodate life-sciences that would also require low acceleration levels. The life-sciences community has stated the need to have two centrifuges on board the space station. These will be variable-acceleration centrifuges to perform experiments on animals as well as humans. There will be a 1.8-meter-diameter centrifuge, to be available at the time of permanent man capability, which could be one year after the initial launch. There should also be a large centrifuge with 4-meter diameter about two years later. The 1.8-meter centrifuge can be rack mounted; it would have to be brought up in two double racks, and it would require some assembly on orbit. This centrifuge could be accommodated in either the U.S. lab or the European Space Agency Lab.

The 4-meter centrifuge will probably be carried up in a separate pressurized module and attached to the end of one of the laboratories. Such a module might be a derivative of a logistics module.

Figure 11 shows a typical floor plan of how the lab module might be laid out, with racks in the four quadrants, the ceiling, the floor, and the two walls. Floor and ceiling racks are primarily used for module subsystems as well as lab subsystems. The wall space is being reserved for user racks.

Figure 12 shows an artist's concept of one wall of the habitation module. Its primary function is for crew habitation. It will be designed to accommodate a crew of 8. The kinds of habitation facilities this module will include are shown on Figure 13 (galley, health maintenance, personal hygiene, crew quarters, ward room, workstations, and habitation storage). The hab module will also provide volume for the

U.S. LABORATORY
U.S. – PROVIDED MODULE

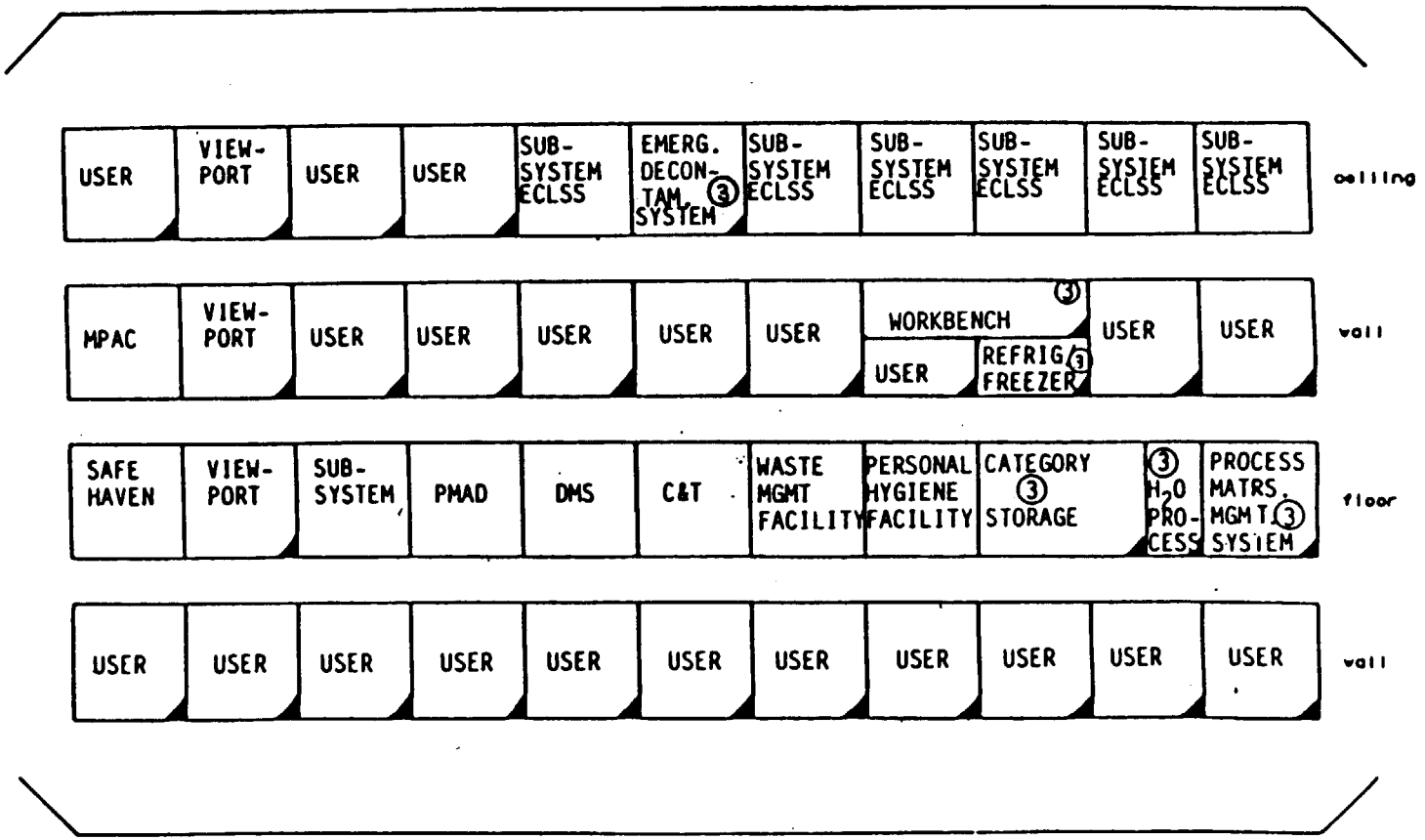

FIGURE 11.

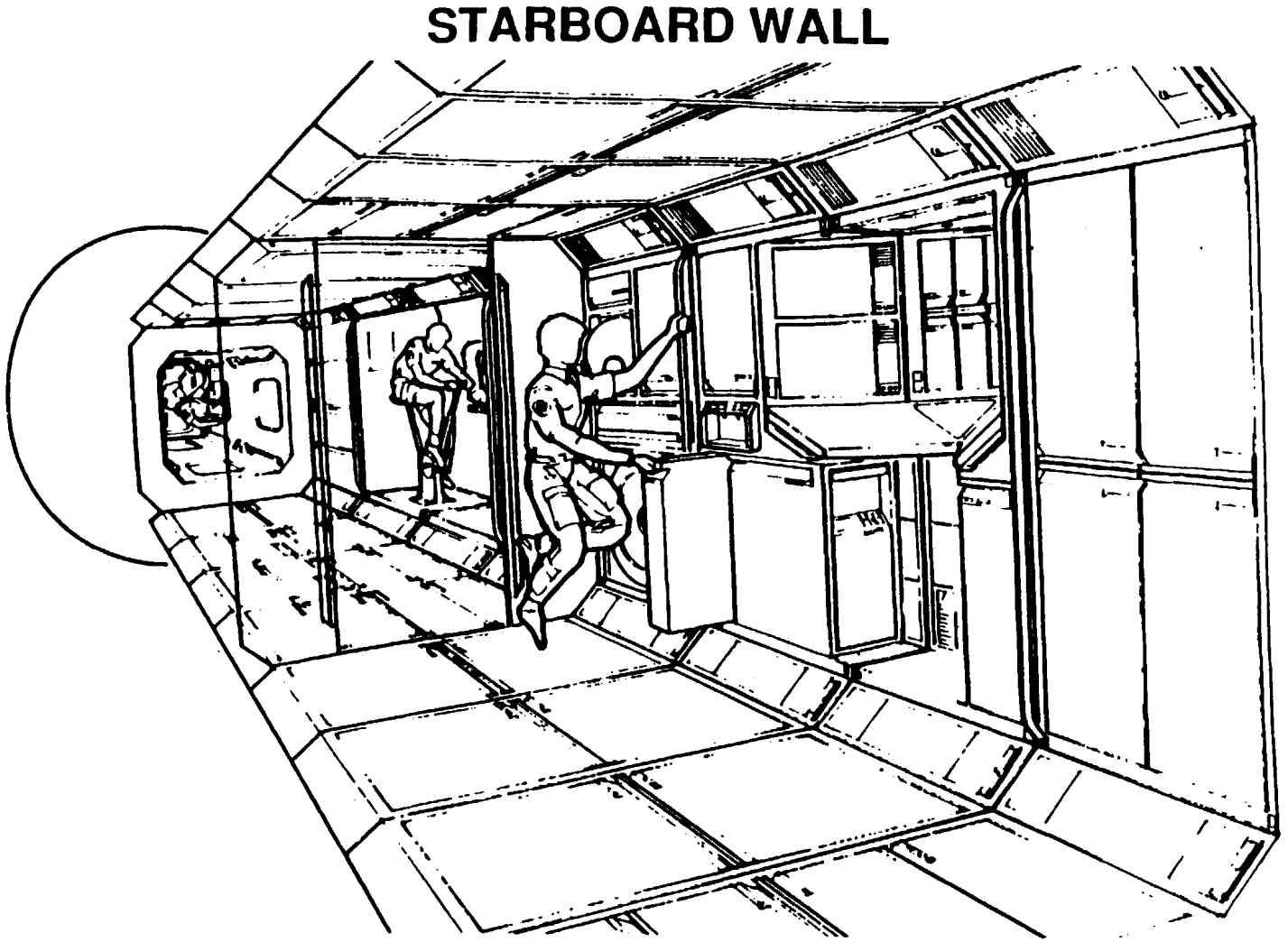

FIGURE 12.

HABITATION MODULE
U.S. – PROVIDED MODULE

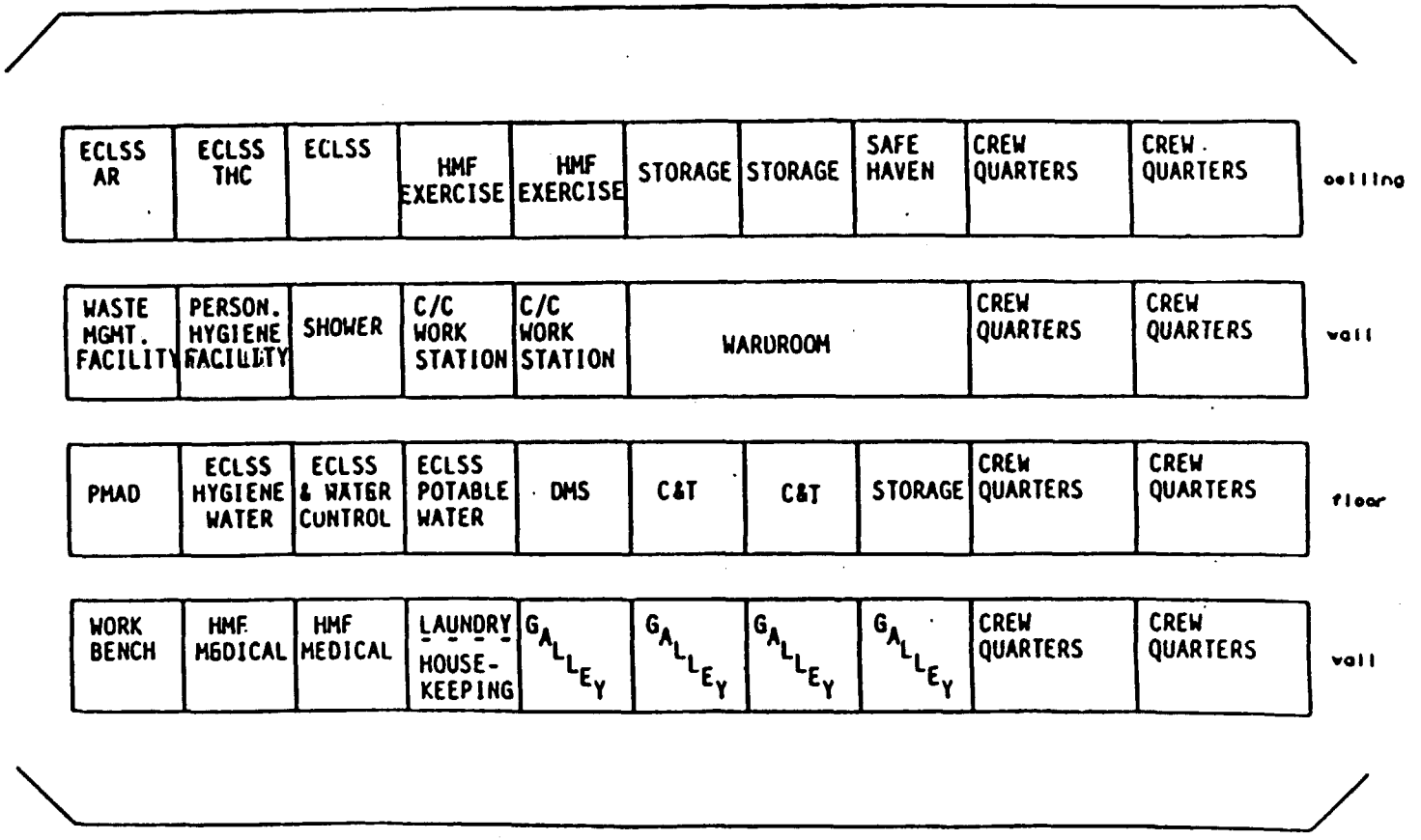

FIGURE 13.

equivalent of 44 double racks. The crew quarters, as shown here, are located at one end of the module complex for isolation. As in the lab module, the primary module subsystems are located in the ceiling and floor.

The Japanese experiment module (Figure 14) consists of a pressurized module, an experiment logistics module, exposed facilities, a local manipulator, and an equipment airlock so things can be moved in and out of the pressurized module. Activities planned in the Japanese experiment module include general science and technology R&D. The experiment logistics module is for the storage of experiment materials and equipment as well as fluids and gases. The experiment logistics module will also be used as a transportation device to get equipment up; currently, the experiment logistics module is planned to be changed out twice a year.

The exposed facility, a pallet-like structure, will serve for science observations and technology development, and also for some materials processing that may be too hazardous to be done in the pressurized modules. The airlock will be needed to transfer equipment between the pressurized module and the exposed facilities. Figure 15 shows a typical floor plan. The module has 24 racks; the Japanese module is shorter than the U.S. module. The wall space is again filled with user racks. The upper and lower boom-attached payload controls may also be located in this module as well as the control station for the Canadian Manipulator. Again, the floor and ceiling space is used for subsystems and storage. There may also be some overflow storage from the U.S. habitation module located in the Japanese module.

Figure 16 shows the European Columbus module; Figure 17 represents the floor plan arrangements for the Columbus laboratories. The European Space Agency is basing its design currently on a four-segment long spacelab module. The module would have a capability for 40 double racks; about one double rack less in length than the U.S. lab. Ten of the double racks in the module would carry overflow storage from the

SPACE STATION PROGRAM

REFERENCE CONFIGURATION
JAPANESE EXPERIMENT MODULE (JEM)

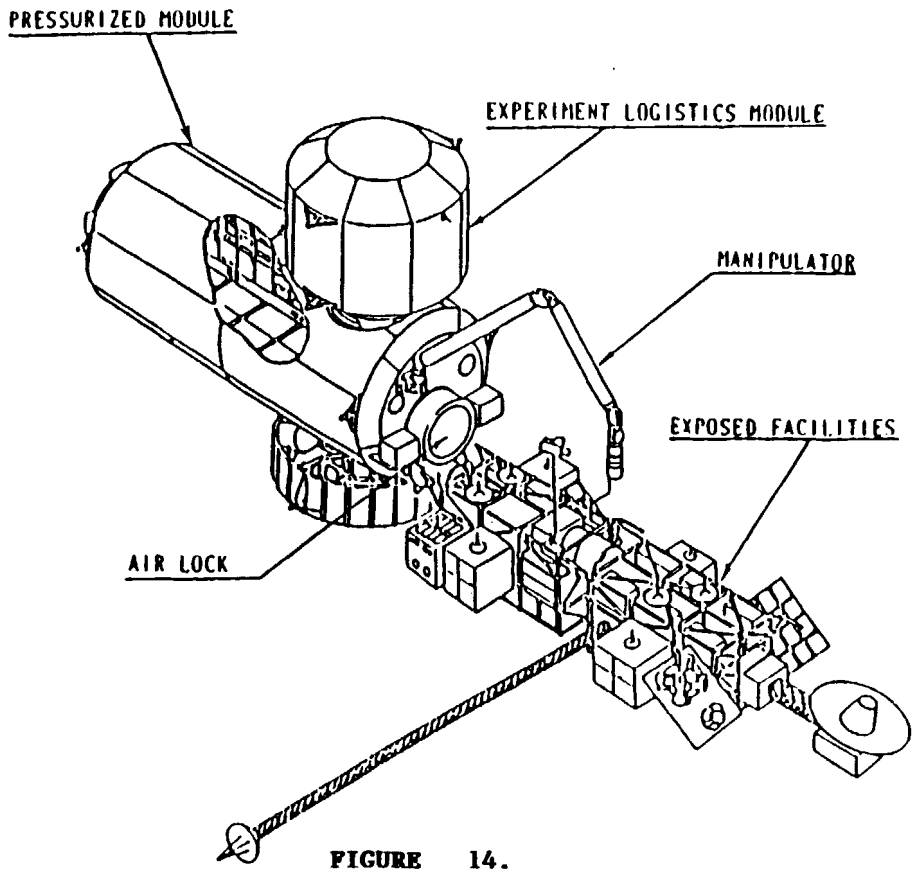

FIGURE 14.

JAPANESE EXPERIMENT MODULE (JEM)
JAPAN – PROVIDED MODULE

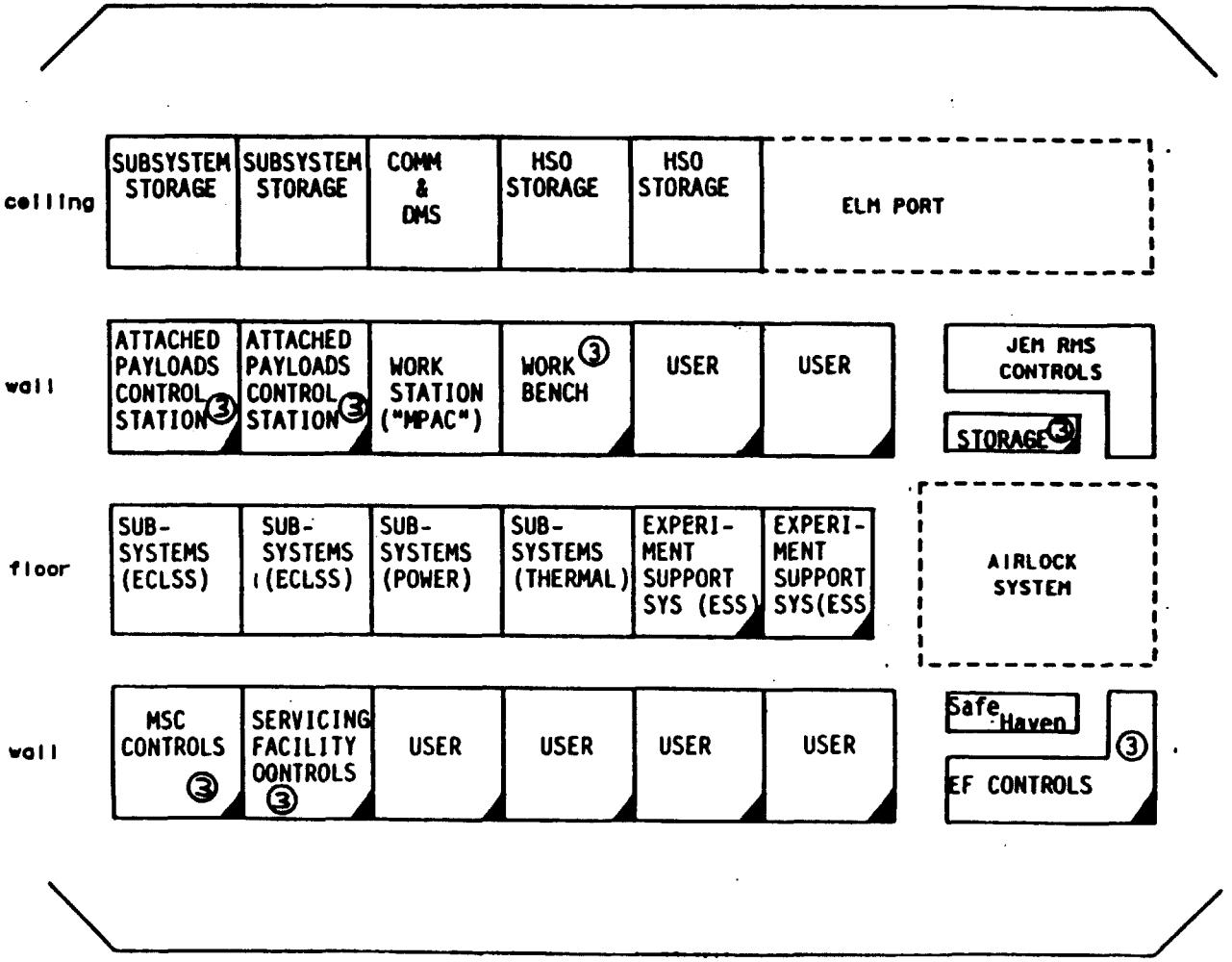

FIGURE 15.

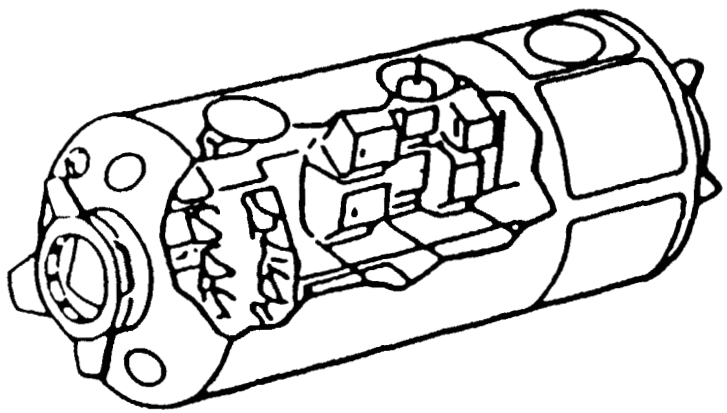

PRESSURIZED MODULE

ATTRIBUTES/REQUIREMENTS

- MULTIDISCIPLINE LABORATORY
  - LIFE SCIENCES
  - MATERIALS PROCESSING
  - GENERAL SCIENCE
- POWER REQUIRED 30 kW
  - HOUSEKEEPING (6 kW)
  - PAYLOADS (24 kW)
- CREW ACCOMMODATION 3
  - REQUIREMENT (5)

FIGURE 16.

COLUMBUS LABORATORY
ESA – PROVIDED MODULE

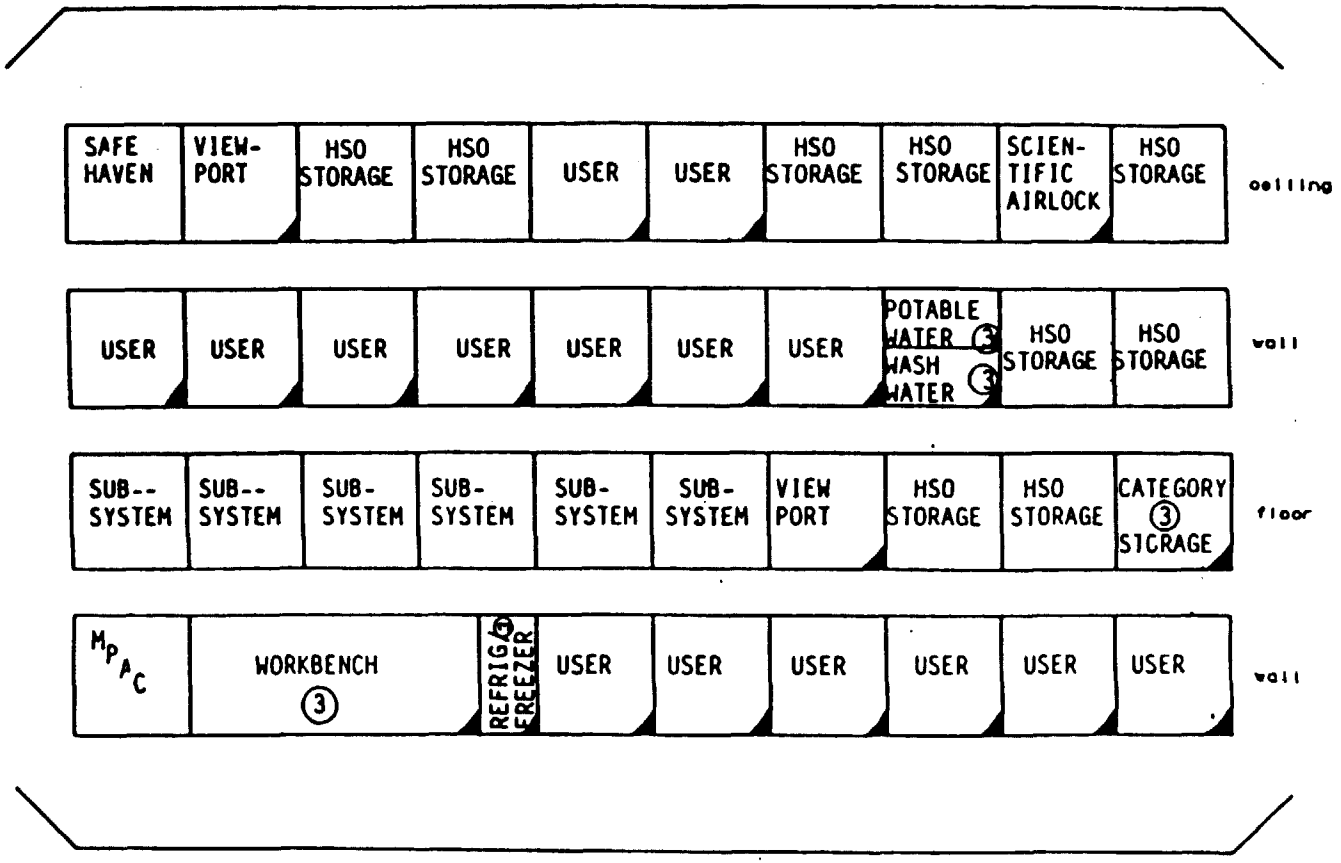

FIGURE 17.

U.S. Habitation Module. The Columbus module may support both life-sciences and materials processing, as well as general science. Again, the wall space is primarily used for user racks, and the floor and ceiling for subsystems and storage.

In addition to the U.S. Logistics pressurized module, there will be unpressurized elements such as fluid and gas containers and other materials that do not require pressurizing. It is currently planned to bring up a replacement logistics module about once every 90 days.

As a concluding remark, I would like to address the question: Why do we need a Space Station? I think a year ago we might have said that we needed a space station to maintain our leadership in space. I think today we would probably say that we need a space station to help us regain that leadership.

Question: What was the gravity level we want to maintain?

Priest: The current program requirement is that the acceleration level should not be higher than 10^{-5} g at the centerline of the U.S. Laboratory module.

Question: Will there be a safe haven?

Priest: The U.S. modules, both the hab and the lab module, are the only modules that have the total environmental control life-support systems. These modules will provide the basic safe haven capability. The race track configuration for the modules will allow crew escape to one of the two U.S. modules should there be a problem in a module that would necessitate that module being closed off.

4. DESIRABLE LIMITS OF ACCELERATIVE FORCES IN A SPACE-BASED MATERIALS PROCESSING FACILITY

Dr. Robert J. Naumann, NASA/MSFC

(The editors of this Proceedings Report compiled the following synopsis of Dr. Naumann's presentation, based on tape recordings taken during his talk).

There are three categories of accelerations to be encountered on orbiting spacecraft: (1) quasi-steady accelerations, caused by atmospheric drag or by gravity gradients, 10^{-6} to 10^{-7} g_o; (2) transient accelerations, caused by movements of the astronauts, mass translocations, landing and departure of other spacecraft, etc.; (3) Oscillary accelerations, caused by running machinery (fans, pumps, generators) (Figure 1).

Steady accelerations cause continuing displacements; transients cause time-limited displacements (Figure 2). The important aspect is "the area under the acceleration curve, measured over a certain time interval." (Note that this quantity is not equivalent to a velocity because of friction effects!)

Transient motions are probably less important than steady accelerations because they only produce constant displacements. If the accelerative forces were not equal and opposite, the displacement would increase with time. A steady acceleration will produce an increasing velocity of a particle, but eventually an equilibrium value will be reached where drag and acceleration forces are equal. From then on, the velocity will remain constant, and the displacement will increase linearly with time.

STEADY ACCELERATIONS:

ATMOSPHERIC DRAG: $2 \times 10^{-8}\ g_o$ - $2 \times 10^{-6}\ g_o$ (DEPENDING ON SOLAR CYCLE)

GRAVITY GRADIENT: $3.6 \times 10^{-7}\ g_o$ FOR EACH METER ABOVE OR BELOW C/M

TRANSIENT ACCELERATIONS:

REBOOST THRUSTERS:	0.0018 m/sec = $1.8 \times 10^{-4}\ g_o$ - sec (FEW MINUTES EVERY 90 DAYS)
ATTITUDE CONTROL THRUSTER:	$4.2 \times 10^{-4}\ g_o$ - sec (EVERY 2,100 sec FOR 5-deg DEAD-BAND) $2.0 \times 10^{-4}\ g_o$ - sec (EVERY 1,000 sec FOR 1-deg DEAD-BAND)
CREW MEMBER TRANSLATING AT 2.5 m/sec	$2 \times 10^{-4}\ g_o$ - sec (DURATION 1 TO 4 sec)
200-kg MASS TRANSLATING AT 1 m/sec	$1.7 \times 10^{-4}\ g_o$ - sec (DURATION 10 TO 100 sec)

OSCILLATORY ACCELERATIONS:

CREW MEMBER NODDING HEAD	$3 \times 10^{-5}\ g_o$ AT 1 Hz
ROTATING MACHINERY:	$3 \times 10^{-6}\ g_o$ AT 30 Hz (MORE SEVERE LOCALLY)
STRUCTURE FLEXING FROM CREW MOTION:	$2 \times 10^{-3}\ F_o\ g_o$ ($T_{IMPULSE} << 1/F_o$)

FIGURE 1. SUMMARY OF RESIDUAL ACCELERATIONS

FREE PARTICLE IN 10-cm-RADIUS CONTAINER, $X = \dot{X} = 0$ AT $t = 0$

ATMOSPHERIC DRAG, $g = 2 \times 10^{-7}\ g_o$; $t_{WALL} = 300$ sec

WORST-CASE G- GRADIENT, $g = 10^{-5}\ g_o$; $t_{WALL} = 45$ sec

TRANSIENT FROM THRUSTER, $gt = 2 \times 10^{-4}\ g_o$ - sec; $t_{WALL} = 50$ sec

TRANSIENT FROM CREW MOTION OF 10 m; $X_o = 0.6$ cm

TRANSIENT FROM 200-kg MASS OF 100 m; $X_o = 16.7$ cm, $t_{WALL} = 60$ sec

JITTER FROM HEAD MOVEMENT; $X_o = 8$ μm AT 1 Hz

JITTER FROM ROTATING MACHINERY; $X_o = 8$ nm AT 30 Hz

JITTER FROM STRUCTURE FLEXING; $X_o = 500\ \mu m/F_o$ AT F_o Hz

FIGURE 2. EFFECT OF RESIDUAL ACCELERATIONS ON FREE PARTICLE IN A BOX

In a transient mode of acceleration, the displacement will be constant if the accelerative force acts only in one direction. If the transient is oscillatory, the displacement goes back to zero after the transient. In all practical cases, a residual displacement should be expected because of non-linearity effects.

If a box with a free-floating particle were exposed to a drag force of 10^{-7} g_o, and if the initial distance between particle and box wall were 5 cm, the particle would hit the wall after about 300 sec. If the accelerative force were 10^{-5} g_o, the time would be 30 sec. With a thruster transient, it will hit the wall in 50 sec. A transient from crew motion will simply offset the particle by about 0.6 cm. Moving a 200 kg mass over a distance of 100 meters will bang the particle into the wall because its net displacement will be some 16 cm.

Nodding of an astronaut's head at 1 hertz produces an oscillating acceleration in the Space Station of about 10^{-5} g_o. Rotating machinery will cause particle displacements on the order of 8 nanometers. The natural frequency of Space Station structural flexing will be a few tenths of a hertz.

As an example, a protein crystal of 0.5-mm diameter, suspended in a 5-mm drop of water, would remain floating for 5 days if exposed to a steady acceleration of 3×10^{-7} g_o. A 1-cm crystal in a 10-cm vial under 10^{-5} g_o would take 2.5 hours before it hit the wall (Figure 3).

Transient effects, such as caused by astronauts nodding their heads, are mild. They may cause problems in float zone experiments, but they can be avoided by mechanical or magnetic vibration isolation.

"Steady accelerations can really kill you in a lot of processes."

The settling times of suspensions are controlled by the competing effect of Brownian motion and gravitational acceleration (Figure 4). Latex spheres of 0.2 micron diameter will remain suspended indefinitely even under 1 g_o (Figure 5). Blood cells require an acceleration level as low as 10^{-6} to 10^{-7} g_o to remain suspended. A mixture of molten lead

TYPE OF DISTURBANCE	CASE I	CASE II
AERODYNAMIC DRAG (2×10^{-7} g_o)	$\dot{X}$ = 0.048 cm/day t_{WALL} = 5.2 DAYS	$\dot{X}$ = 19 cm/day t_{WALL} = 6.3 hr
GRAVITY GRADIENT (WORST CASE) (1×10^{-5} g_o)	$\dot{X}$ = 2.4 cm/day t_{WALL} = 2.4 hr	$\dot{X}$ = 960 cm/day t_{WALL} = 7.5 min
THRUSTER FIRING (2×10^{-4} g_o - sec)	ΔX = 33 μm	ΔX = 1.3 cm
CREW TRANSLATION (10 min 4 sec)	ΔX = 33 μm → 0	ΔX = 1.3 cm → 0.71 cm
200-kg MASS TRANSLATION (100 min 100 sec)	ΔX = 28 μm → 0	ΔX = 1.1 cm → 0
JITTER FROM HEAD MOVEMENT	ΔX = ±80 nm	ΔX = ±7 μm
JITTER FROM MACHINERY	ΔX = ±0.8 nm	ΔX = ±0.8 nm
JITTER FROM STRUCTURE	ΔX = 50 μm, F_o < 10 Hz ΔX = 500/F_o μm, F_o > 10 Hz	ΔX = 2.1 cm, F_o < 0.02 Hz ΔX = 0.05/F_o cm, F > 0.02 Hz

CASE I: 0.5-mm-DIAMETER PROTEIN CRYSTAL IN 5-mm DROPLET, $\Delta\rho = 0.2\ \rho$, $\nu = 10^{-2}$ cm^2/sec

CASE II: 1-cm-DIAMETER CRYSTAL IN 10-cm-DIAMETER CONTAINER, $\Delta\rho = 0.2\ \rho$, $\nu = 10^{-2}$ cm^2/sec

FIGURE 3. EFFECTS OF RESIDUAL ACCELERATION ON PARTICLE IN VISCOUS MEDIUM

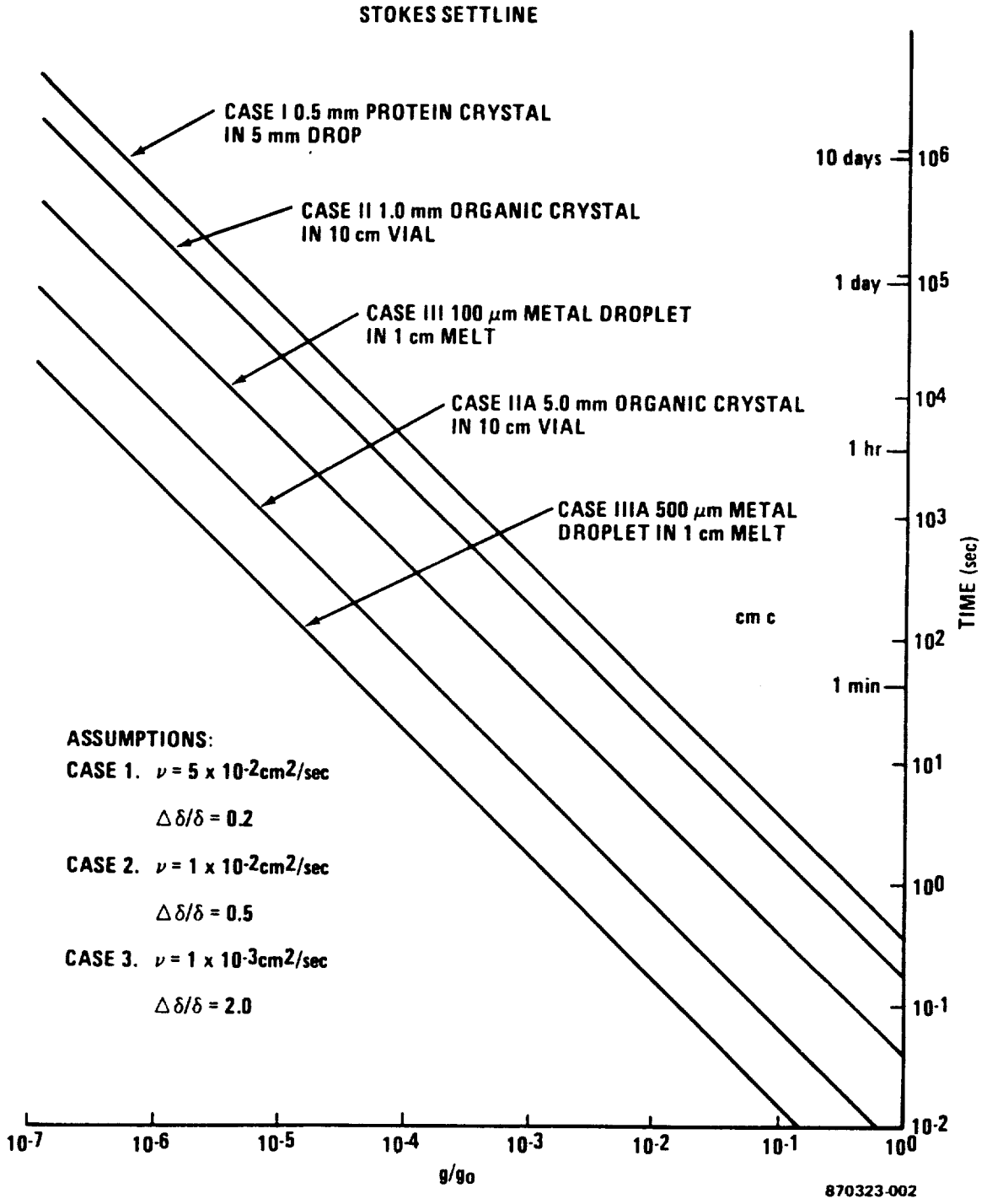

FIGURE 4. STOKES SETTLING

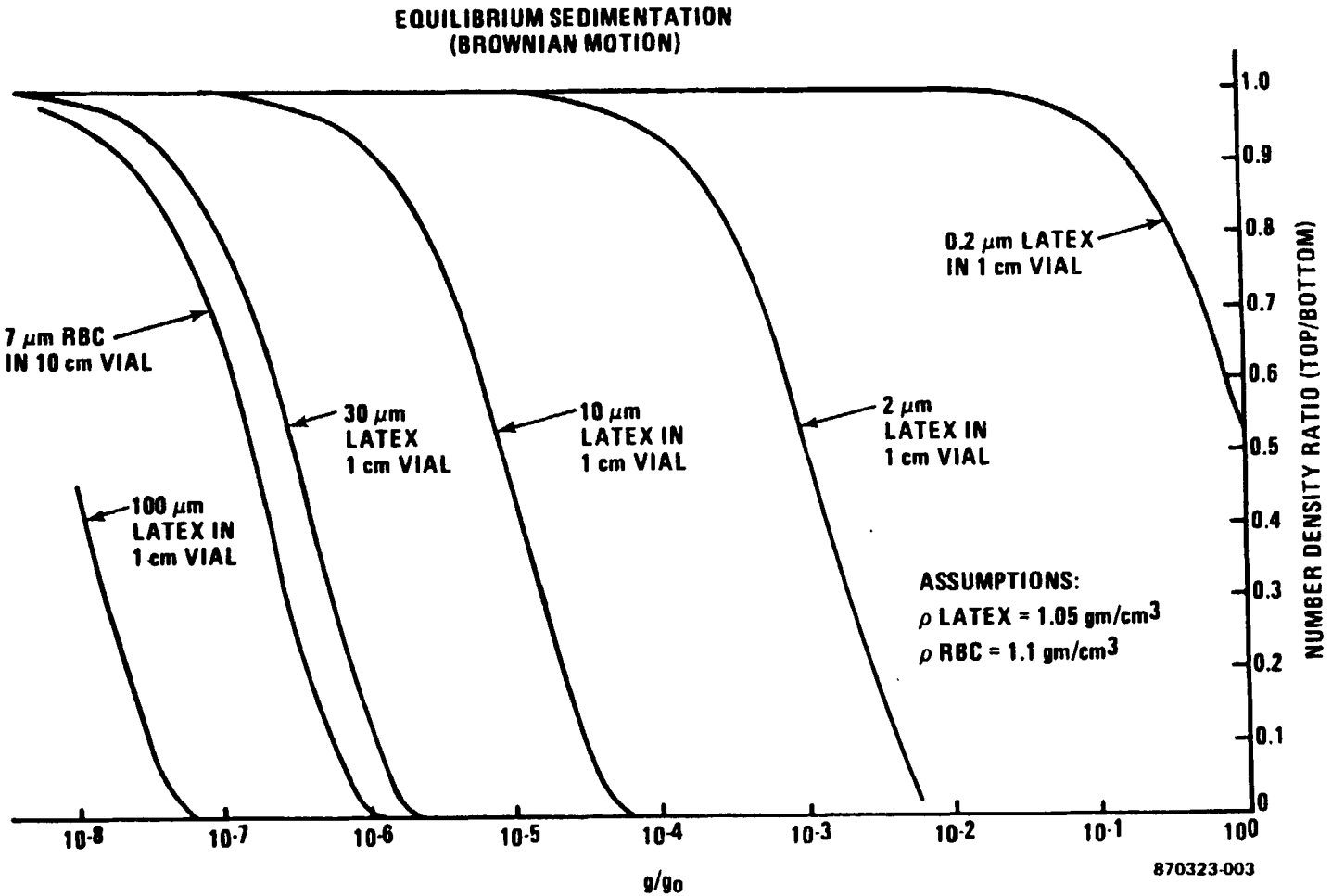

FIGURE 5. EQUILIBRIUM SEDIMENTATION (BROWNIAN MOTION)

and tin will remain homogeneous even at 10^{-6} g_o only when the mixture ratio tin:lead is smaller than 3.5 to 4% (Figure 6).

This latter case has been analyzed by Stan Coriell at the Bureau of Standards; it is an example of a situation in which the solution gradient is unstable, and the thermal gradient is stable ("double-diffusive convection").

If a crystal grows in a solution, the transport of material is influenced by diffusion and by convection. Under reduced gravity conditions, convection effects are reduced, diffusion effects are not. In the diagram of Figure 7, the line divides the regions where convection (above) or diffusion (below) is predominant.

The Peclet number measures the convective transport as compared to the diffusive transport. For the thermal case, it is defined as the characteristic velocity, v, times the characteristic length, ℓ, divided by the thermal diffusivity. At thermal Peclet numbers below ℓ, thermal fluctuations are suppressed. To suppress compositional fluctuations, solutal Peclet numbers must be kept below ℓ. Solutal Peclet numbers contain the chemical instead of the thermal diffusivity.

Substituting proper numbers in the Peclet expressions, the thermal Peclet number turns out as 10^2 g_o ℓ^3, and the solutal Peclet number as 10^6 g_o ℓ^3, for 1-cm samples. This means that accelerations must not be greater than 10^{-9} g_o if 10-cm samples without detrimental solutal convection effects are to be produced. Such a low level of gravitational acceleration cannot be attained on a space vehicle in low earth orbit. If the growth solution is a conductive medium, application of a magnetic field would greatly reduce diffusion - controlled convection. Experiments with magnetic fields have been carried out in ground-based labs.

Figure 8 was taken from a paper by Chang and Brown who analyzed the radial segregation in crystals grown by the Bridgman-Stockbarger

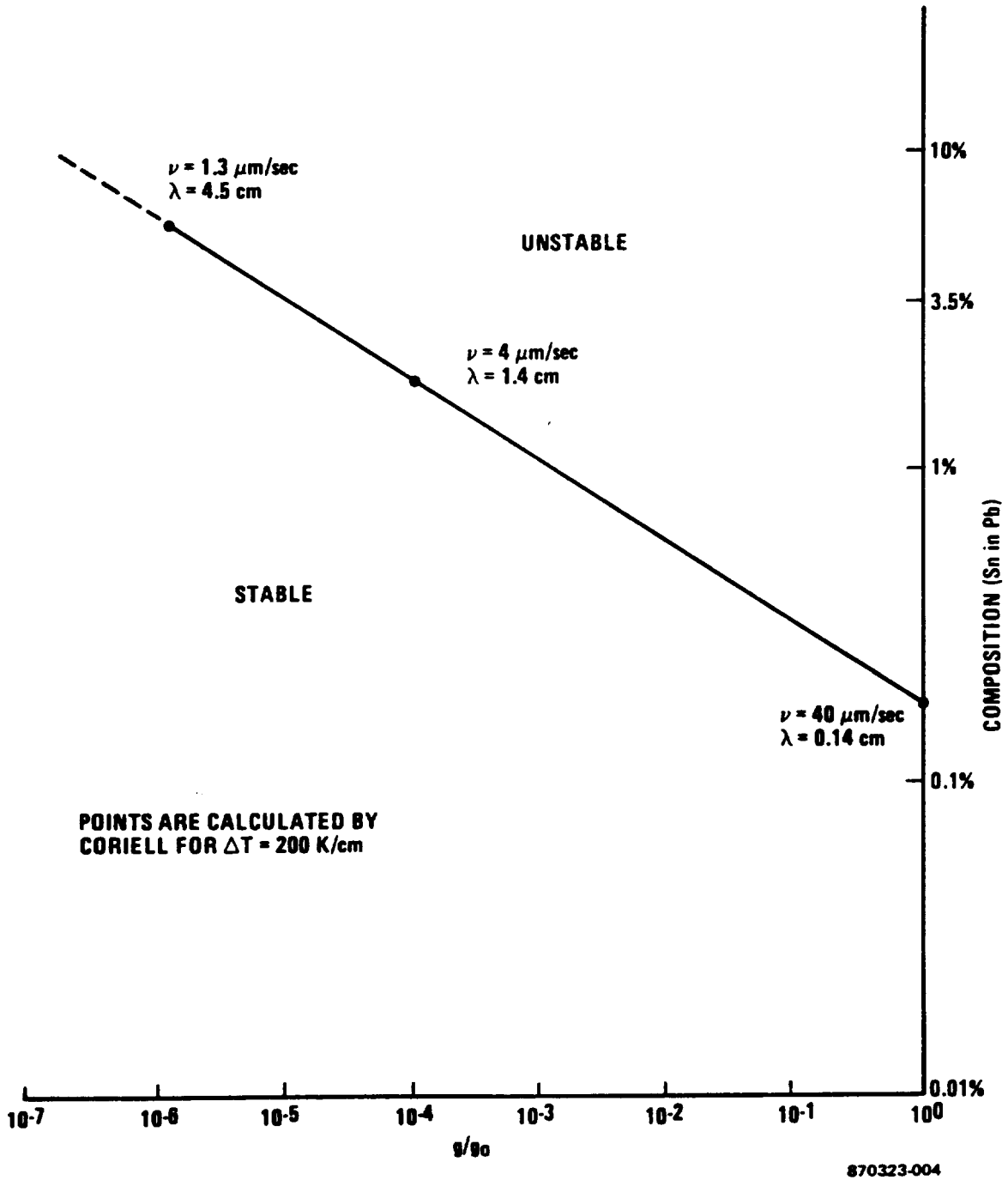

FIGURE 6. DOUBLE-DIFFUSIVE CONVECTION (Sn in Pb)

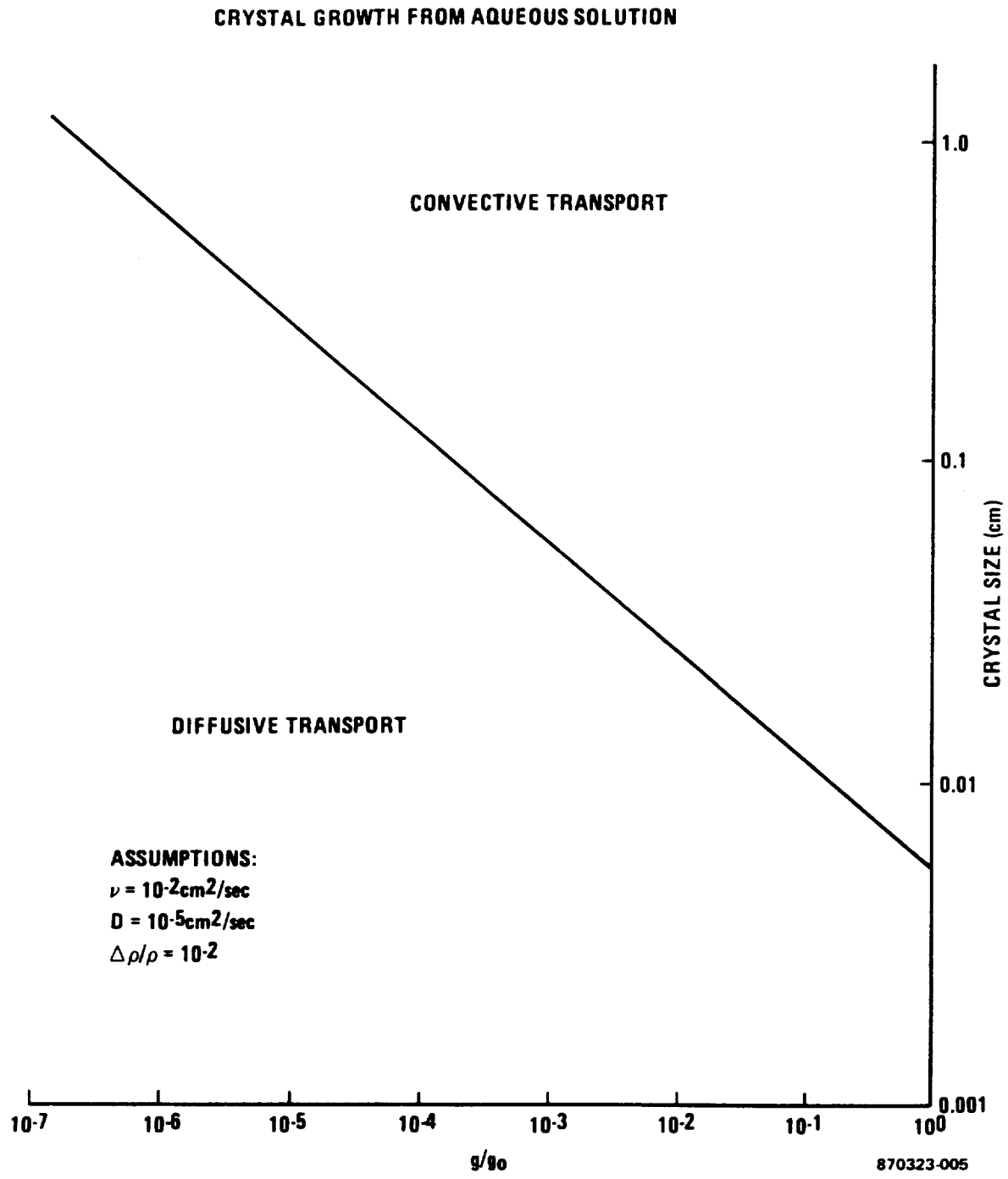

FIGURE 7. CRYSTAL GROWTH FROM AQUEOUS SOLUTION

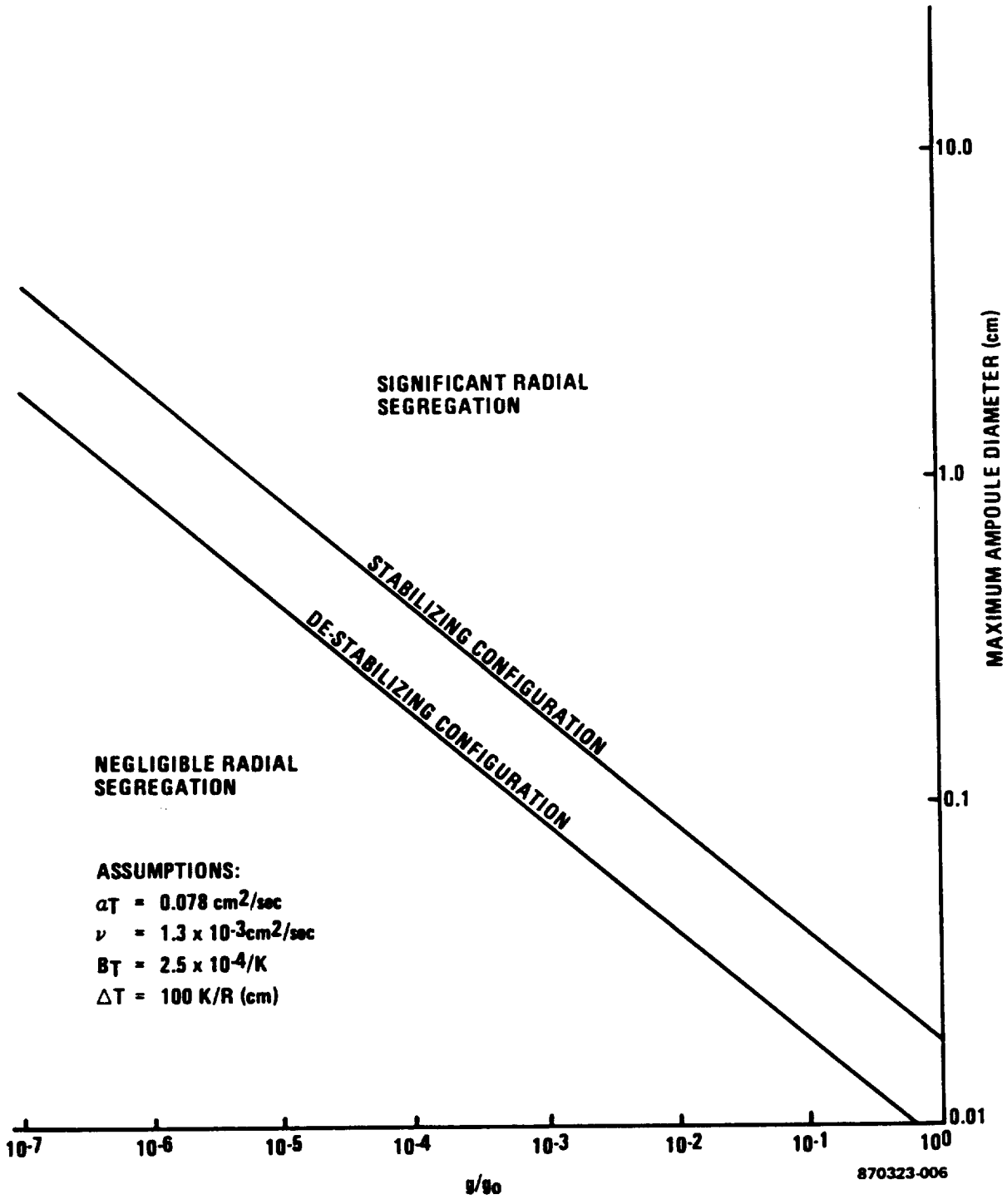

FIGURE 8. BRIDGMAN - STOCKBARGER GROWTH (FROM CHANG & BROWN)

method. Significant radial segregation occurs above the upper line and is absent below the lower line. For a one-centimeter sample, acceleration levels must not exceed 10^{-5} or 10^{-6} g_o if diffusion-controlled flow is to be maintained. To grow larger crystals, far lower levels will be needed. This might be achieved, in the case of conductive melts, by forcing a magnetic field on the system. Figure 9 shows the reduction of convective flow velocities as a function of magnetic field strength and electric conductivity of the melts. Crystals of less than 1 cm diameter can be grown under diffusion-controlled conditions without a magnetic field. To grow crystals up to about 10 cm requires only a fairly modest magnetic field, but strong fields will be needed for larger crystals.

Question (Reg Berka, JSC): Do all these curves refer to steady-state accelerations? How would transients and periodic accelerations affect these charts?

Naumann: If the transient is short as compared to the response time of the fluid, an average value of the acceleration should be taken. The response time of the fluid is on the order of the diffusive coefficient divided by the square of the length scale.

"We have reasons to believe that on Spacelab 3 steady state accelerations were on the order of 10^{-7} g_o, substantially better than Space Station specifications. We believe that a level of 10^{-5} g_o, specified as a requirement for the Space Station, is way too high. With the new configuration of the Space Station where the line of the center of mass will be located within the lab module, steady accelerations will be much better than 10^{-5} g_o." (Note that this statement refers only to steady state accelerations, but not to transient and oscillating accelerations.)

If steady state accelerations on the Space Station are not kept near 10^{-7} g_o, crystals that can be grown on the Space Station will be severely limited in size. "We think that would be a fatal error ...

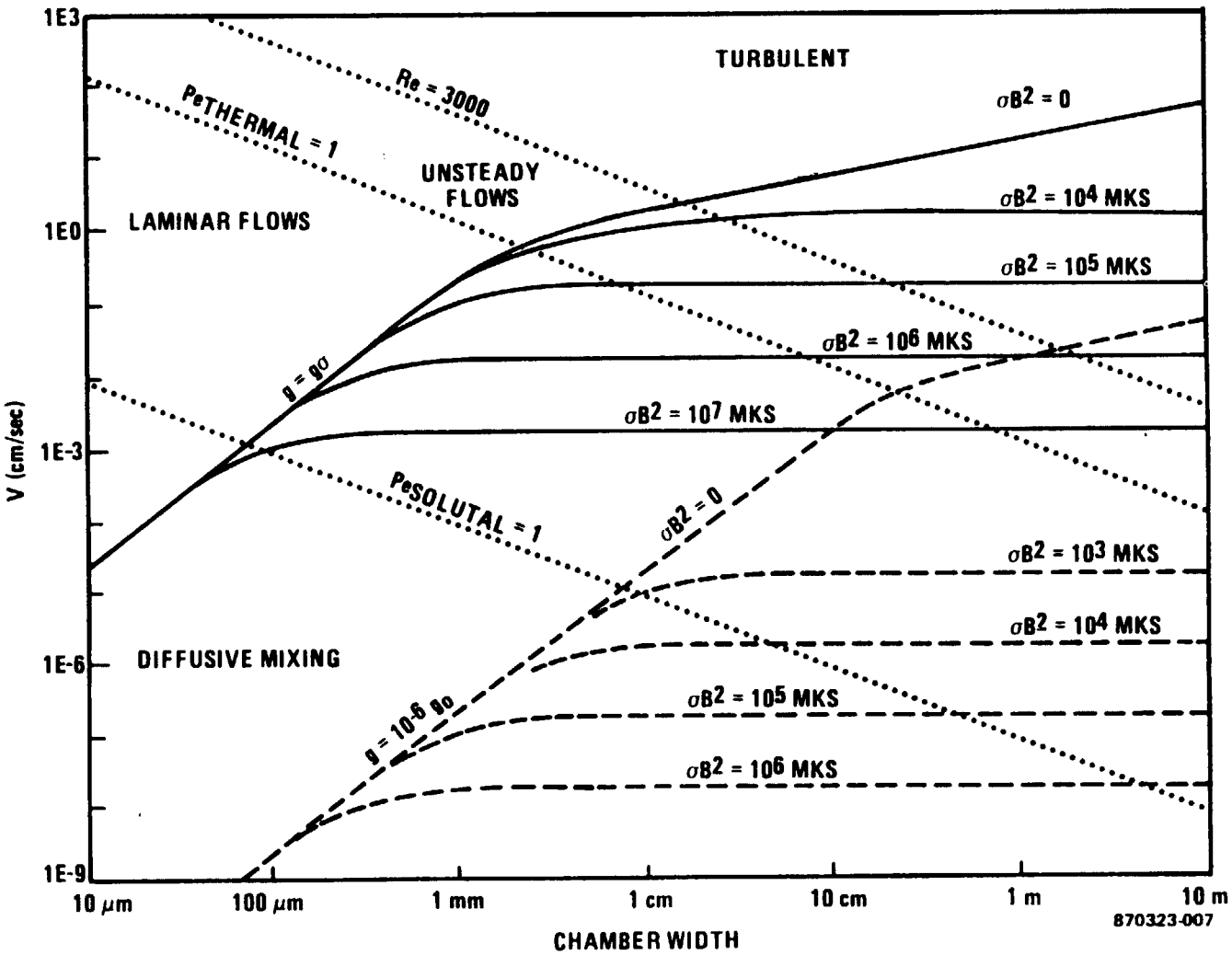

FIGURE 9. CONVECTIVE FLOW VELOCITY AS A FUNCTION OF MAGNETIC FIELD STRENGTH, ELECTRIC CONDUCTIVITY, AND CHAMBER SIZE, AT VARIOUS GRAVITATIONAL ACCELERATIONS

unless we can find industries that are willing to accept crystals of less than 1 cm in size, which I think is unlikely, you really don't have an industrial constituency ... As far as accelerometer development goes, those are the accelerations we really want to measure. I'm not sure that measuring peak accelerations is the right thing to do; I think the more useful thing to do would be to measure the acceleration x time product, over varying time intervals."

Question (Larry Collins, Alabama A&M University): What are the units for the magnetic field expression?

Naumann: The units are the product of sigma times B squared, in MKS units; sigma being the conductivity in siemens (mho-meters), and B is measured in tesla. The strongest fields would be 10^5 or 10^6 tesla.

Question: (Not understandable)

Naumann: There is a very nice paper by Bob Dreslin who was at NASA Headquarters, which gave the closed form solution of the flow of a fluid in a circular container when a thermal gradient is present. A brief overview of flow conditions when thermal gradients are present is shown in Figure 10.

Question: How can a measured profile of acceleration versus time be applied to the diagram that shows "acceptable" and "desirable" acceleration versus frequency?

Naumann: You first take the acceleration profile and decompose it into the three coordinate components. Then, you decompose each of these profiles into its Fourier components; this will give you an amplitude versus frequency plot. If this measured amplitude versus frequency plot is below the lines in the diagram, you are in good shape. (Note that this analysis is not without problems, as pointed out quite drastically by Ken Demel; see "Summary of Workshop," p. 28-3).

Question (Fred Henderson, Teledyne Brown): The experimenters of the French Mephisto experiment have requested an accelerometer sensitive

Must keep $Pe_{Thermal} = \frac{\hat{v}L}{\alpha}$ <<1 to suppress thermal fluctuations

Must keep $Pe_{Solutal} = \frac{\hat{v}L}{D}$ <<1 to suppress compositional fluctuations

To estimate $\hat{v}$ for steady acceleration, consider 2-D flow in:

a. channel

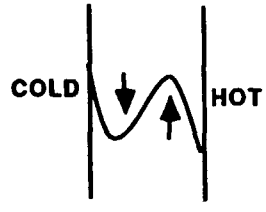

$$\hat{v} = \frac{\beta g \Delta T L^2}{72\sqrt{3}\,\nu}$$

b. circle

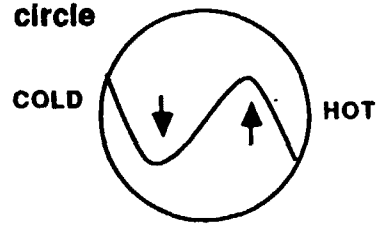

$$\hat{v} = \frac{\beta g \Delta T R^2}{48\sqrt{3}\,\nu}$$

c. cylinder

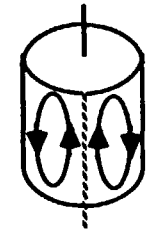

$$\hat{v} = \frac{\beta g \Delta T R^2}{48\,\nu}$$

For $\beta = 10^{-4}$, $g = 10^3 g_o$, $\Delta T = 10k$, $\nu = 10^{-3}$ cm^2/sec

$$\hat{v} \simeq \frac{10^{-4} \times 10^3 g_o \times 10}{10^2 \; 10^{-3}} L^2 = 10\, g_o L^2 \text{ (cm/sec)}$$

For $\alpha = 10^{-1}$ cm^2/sec, $D = 10^{-5}$ cm^2/sec

$$Pe_{Thermal} = 10^2 g_o L^3, \; Pe_{Solutal} = 10^6 g_o L^3$$

FIGURE 10. ESTIMATE OF REQUIRED G-LEVELS

SP87-093

to 10^{-4} g_o at 100 Hz, and they had a theoretical argument for this request. Are you familiar with their rationale?

Naumann: I really don't know why they specified that high a frequency. They said that's what they need, and we just accepted it. They may know something we don't know, or we may know something they don't.

Question (Byron Lichtenberg, Payload Systems Inc.): I would like to refer to your earlier statement about an astronaut nodding his head. Your assumption was for a 5 kilogram mass coupled to a rigid body giving a 20 micro-g acceleration. The assumption is that a person's head is a 5 kg mass driven by an electric motor and rigidly coupled to the floor. In reality however there is a considerable amount of fluid damping.

Naumann: Yes, that's what I assumed; a rigid body coupled to the floor. Then I realized later that if you hold something in your hand, and if you move it with a displacement of 10 centimeters at a frequency of 1 Hz, that will be equivalent to 0.1 g_o. Thus it is very difficult to move things around by hand and not to exceed large acceleration levels.

Ken Demel, JSC: But analysis will show that this is less of a problem than it would be if it were a steady state acceleration.

Question: Have magnetic suspensions and other isolating mechanisms been considered for use on the Space Station?

Naumann: There are a number of suspension systems available, both mechanical -- using airbags or springs with dashpots -- and magnetic, that isolate the region of the experiment from the main structure. They will isolate an experiment on a spacecraft from transient and oscillatory motions. But there are limits to how far you can go. The major limit will be the amount of free travel of the isolated platform relative to the rest of the spacecraft. Theoretically, you could keep the experiment totally suspended and fly the spacecraft around it if you were free to move the center of mass of the spacecraft, but that would be rather difficult to accomplish. You could

keep the accelerative forces transmitted to the experiment absolutely zero if you had a large enough free space around it ... In practice, you could probably isolate very well down to 10 Hz, maybe 1 Hz or even 0.1 Hz. However, lower frequencies you would not be able to isolate within a reasonable structure.

Question (Ed Bergmann, C. S. Draper Laboratory): Isolating the motion is not at all that impossible, as Owen Garriott will discuss later. I just wanted to mention that it has actually been done; there have been some simulations where the orbiter was flown around an experiment.

Naumann: Oh yes, but that assumes that the spacecraft is maneuverable; unfortunately, the Space Station is not.

Question: I don't understand why you are not concerned with jitter.

Naumann: The question is: would jitter effects produce microscopic motions at the interface that could cause problems? The answer is: yes, they probably could. I think we need to be concerned about it. I'm less concerned about it because I can do something about it if I need to; I can isolate.

The macroscopic effects, such as the influx of fluid of a different concentration to the interface of a growing crystal, can really mess up diffusion-limited growth. This is a first-order effect, and it is more worrisome than the second-order effects caused by jitter. The latter may consist of the displacement of an element of fluid by a few microns over the interface. We don't really know what consequences that may have. We have not studied that yet, and I would say that this is probably a second-order effect. I would be concerned about it only after the first-order problem has been solved.

Table 1 lists a number of conclusions regarding low-acceleration work on the Space Station.

TABLE 1. CONCLUSIONS

- Spacelab module contains the center of mass of the system. Measured steady accelerations are 3.8×10^{-7} g_o at the FES.
- A steady acceleration level of 10^{-5} g_o presently specified for Space Station is 26 times worse than we have now and will limit the usefulness of Space Station as a national microgravity facility.
- The most serious consequence will be the size of electronic-electro-optical materials and aligned in situ composite alloys that can be grown without significant gravity effects. This will greatly restrict commercial interest.
- Examples:
  - Uniform doping can only be achieved in Bridgman-grown crystals up to 0.8-cm diameter.
  - Alloy compositions will be limited to a few percent (3 wt % for Sn in Pb unless diameter << 2.5 cm).
  - Diffusion-controlled transport cannot be maintained for solution-grown crystals larger than a few millimeter diameter (3.3 mm for triglycine sulphate).
  - Rotation will be needed to maintain free suspensions, even for 0.5-mm protein crystals.
- Access to the vicinity of the flight path of the center of mass is needed to provide the same steady-state accelerations presently available on Spacelab.
- Tolerance to transient or periodic accelerations increases as ω^2. Additional attenuation can be obtained by shock mounting or by active isolation control.
- Additional development is needed to reduce effects of steady or very low frequency distrubances.
  - Possibly experiment rotation and/or magnetic damping.

5. IMPLICATIONS OF ACCELERATION ENVIRONMENTS ON SCALING MATERIALS PROCESSING IN SPACE TO PRODUCTION

Ken Demel, NASA/Johnson Space Center

I will cover some considerations regarding materials processing from a commercial perspective. There's a lot of science and research involved, but I think that the product potential in the commercial sector will ultimately pull the research and science programs along to benefit mankind in keeping with the NASA charter. The best mechanism we have for dispersing scientific results of these programs to mankind in general is through a process called commercialization. Like it or not, that's our best distribution system. I represent Space Station Level B and have been working with the commercial advocacy group. We are starting from a perspective that had been pronounced by President Reagan in his state of the union addresses, and we're also considering the amendment to the Space Act in Public Law 98-361 given on the bottom of Figure 1. The amendment says that while you're doing things for all mankind, for national security, and domestic welfare, encourage commerce also. This is essentially the charter that we've taken for developing a commercial perspective that includes materials processing in space. Figure 2 indicates a number of commercial utilization areas that have been developed. The communications industry is well advanced. There is activity in earth and ocean remote sensing as well. The bottom of the figure indicates the promising area that we're here to discuss, and the commercial requirements regarding materials processing that are driving the Space Station design. Several key areas include power, proprietary data, operational requirements (including logistics), and also the center of gravity (c.g.) location, and control of that location with respect to materials processing payloads. The previous speaker, Bob Naumann, talked about small samples, whereas I am going to go through a rationale that says why you have to be even more careful as you expand the scale and go to larger samples.

Executive and Legislative Pronouncements

"We will soon implement a number of executive initiatives, develop proposals to ease regulatory constraints, and with NASA'S help, promote private sector investment in space"

State of the Union Address, 1984

"In the zero gravity of space, we could manufacture in 30 days life saving medicines it would take 30 years to make on earth. We can make crystals of exceptional purity to produce super computers. Creating jobs, technologies and medical breakthroughs beyond anything we ever dreamed possible."

State of the Union Address, 1985

The Congress declares that the general welfare of the United States requires that the National Aeronautics and Space Administration seek and encourage, to the maximum extent possible, the fullest commercial use of space."

Public Law 98-361 (Ammendment to Space Act of 1958)

Figure 1.

COMMERCIAL UTILIZATION

- SPACE IS ALREADY COMMERCIALIZED: COMMUNICATIONS INDUSTRY
- ENCOURAGING PRIVATE SECTOR IN SPACE IS PART OF U. S. NATIONAL SPACE POLICY AND PART OF NASA's STATUTORY MANDATE
- SEVERAL NASA ACTIVITIES HAVE A COMMERCIAL DIMENSION:
  - -- EXPENDABLE LAUNCH VEHICLES
  - -- LANDSAT
  - -- SPACE STATION
  - -- UPPER STAGES
  - -- NASA/INDUSTRY RESEARCH
- A SPACE STATION COULD PROVIDE LABORATORY AND SERVICING CAPABILITIES TO PRIVATE SECTOR'S ENDEAVORS IN SPACE
- SPACE STATION PLANNING INCLUDES:
  - -- COMMERCIAL WORKING GROUP
  - -- CONTRACTOR OUTREACH TO NON-AEROSPACE INDUSTRIES
- ONE PARTICULARLY PROMISING AREA: MATERIALS PROCESSING
- COMMERCIAL REQUIREMENTS INFLUENCE SPACE STATION DESIGN:
  - -- POWER
  - -- PROPRIETARY DATA
  - -- OPERATIONAL REQUIREMENTS
  - -- CG LOCATION & CONTROL WITH RESPECT TO MPS PAYLOADS

Figure 2.

We are aware of the "Why Materials Processing in Space" (Figure 3). Generally it is to apply another method of controlling the outcome of an experiment with a material. Every time a new process parameter has been added to our repertoire in processing materials there has been a great advance in materials capability. Progress, technological and otherwise, marches on materials capability, so it is for the reasons given here that we think materials processing could have a dramatic payoff. Buoyancy, sedimentation, and hydrostatic pressure and their adverse effects are well documented in the literature.

Figure 4 gets to the heart of the issue from the commercial standpoint. To determine whether one wants to enter a commercial enterprise, one does market surveys and finds out what he has to make to give himself a niche in the market for a consumer base. That dictates the size of the product to support his application market as indicated in the upper left hand corner of Figure 4. That in turn drives his space station resources, dictates his demand for resources, and his production rate and logistics flow that has to be implemented to maintain a market so that he can stay in business. Both the size of the product and the production rate drive factory investment requirements, and all that (market demand and production management) determines whether there is a positive return on investment. And if that little block, Return on Investment (ROI), doesn't come out right, he's not a participant. He can't afford to be. He is doing it on his own money. It's going through this sort of a model that leads to the issues shown in Figure 5, "Product Mortality versus Cost".

In Figure 5, the commercial endeavor starts out with the same process that experimenters start with, that is, science and research. It goes through a number of development sequences, then through engineering, and finally into production. While the venture capital is going at risk, as shown on a log scale, the objective is ROI past the break-even point on the far right in an appropriate time. Getting through those detailed steps of going from the possible approaches on

WHY MATERIALS PROCESSING IN SPACE?

"MICROGRAVITY" ENVIRONMENT ADDS NEW DIMENSION TO PROCESSING AND PROCESS CONTROL
- A NEW UNIQUE PROCESS PARAMETER

- BUOYANCY-DRIVEN CONVECTION DISAPPEARS
  - DIFFUSION CONTROL IS DOMINANT
  - UNWANTED MIXING IS ELIMINATED
  - THERMAL AND COMPOSITION FLUCTUATIONS VANISH

- SEDIMENTATION CEASES
  - HETEROGENEOUS SUSPENSIONS ARE MAINTAINED
  - MATERIAL PHASE MIXTURES ARE LONG LIVED
  - PROCESS BATCHES CAN BE CONTAINERLESS

- HYDROSTATIC PRESSURE GOES TO ZERO
  - LIQUIDS ARE SHAPED BY SURFACE TENSION
  - FLOAT ZONE PROCESSING AT LOW SURFACE TENSION

BONUSES - ULTRA HIGH VACUUM, HIGH PUMPING SPEED, HIGH HEAT REJECTION

Figure 3.

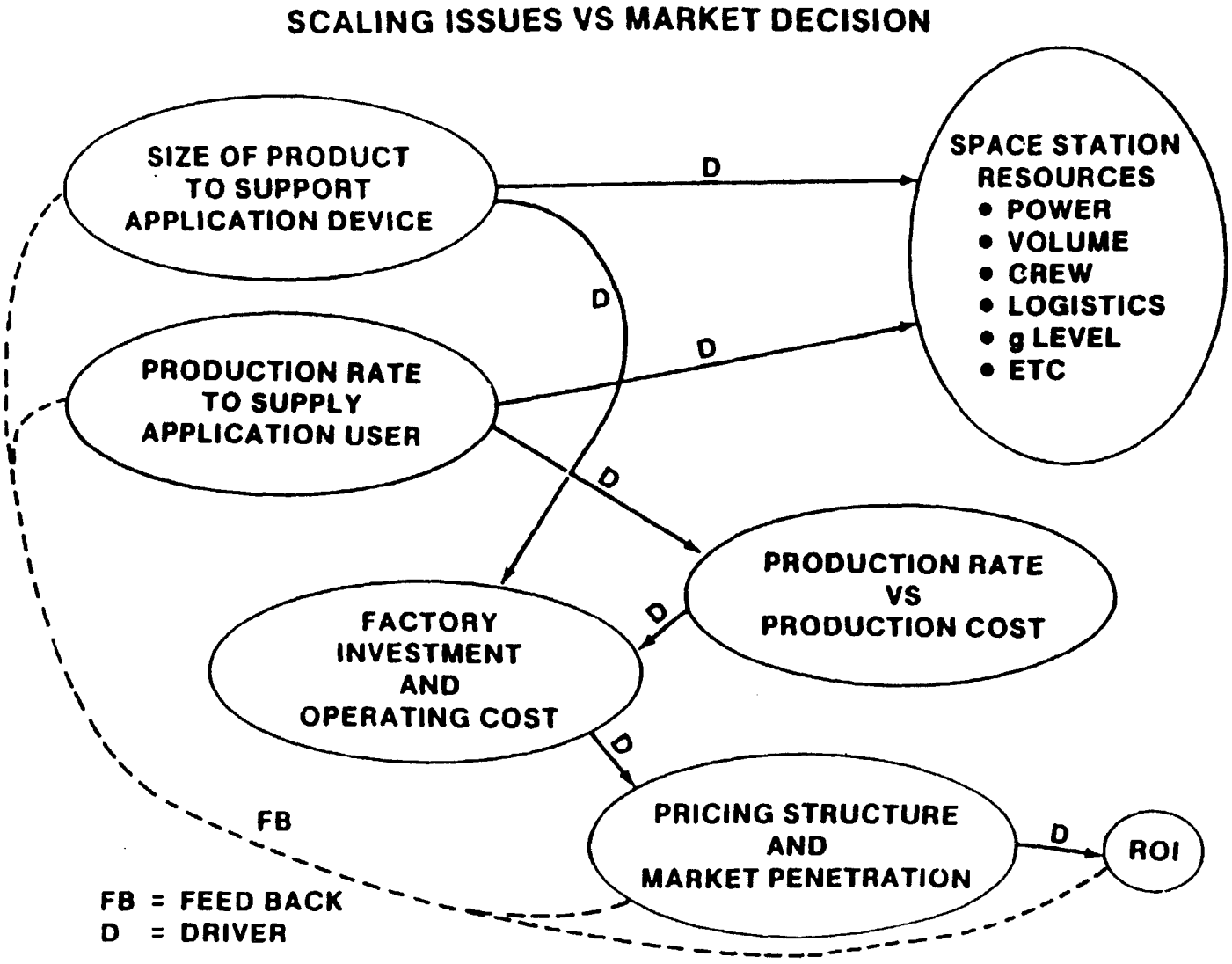
SCALING ISSUES VS MARKET DECISION
SIZE OF PRODUCT TO SUPPORT APPLICATION DEVICE
PRODUCTION RATE TO SUPPLY APPLICATION USER
SPACE STATION RESOURCES
• POWER
• VOLUME
• CREW
• LOGISTICS
• g LEVEL
• ETC
PRODUCTION RATE VS PRODUCTION COST
FACTORY INVESTMENT AND OPERATING COST
PRICING STRUCTURE AND MARKET PENETRATION
ROI
D
FB
FB = FEED BACK
D = DRIVER

Figure 4.

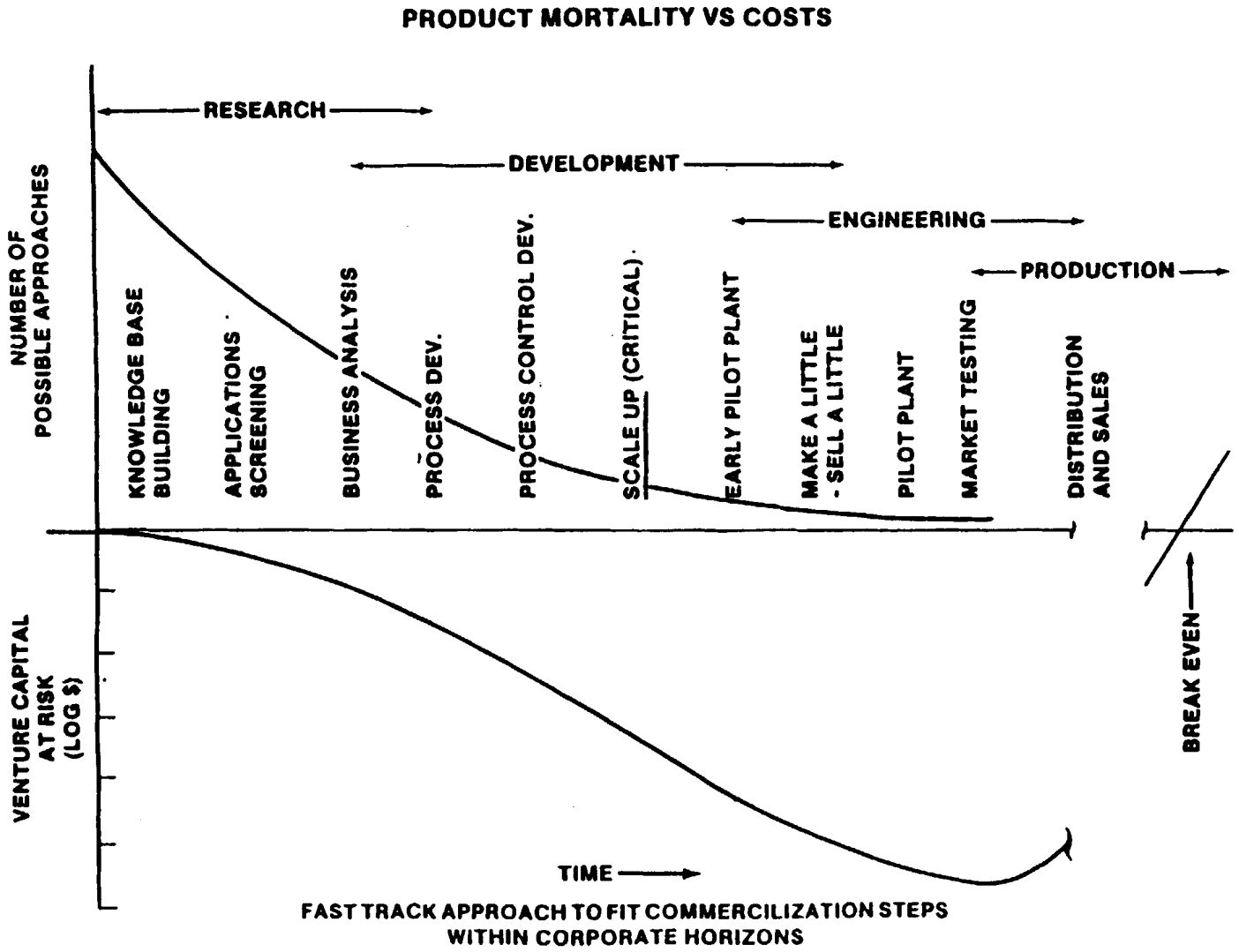
PRODUCT MORTALITY VS COSTS
RESEARCH
DEVELOPMENT
ENGINEERING
PRODUCTION
NUMBER OF POSSIBLE APPROACHES
KNOWLEDGE BASE BUILDING
APPLICATIONS SCREENING
BUSINESS ANALYSIS
PROCESS DEV.
PROCESS CONTROL DEV.
SCALE UP (CRITICAL)
EARLY PILOT PLANT
MAKE A LITTLE - SELL A LITTLE
PILOT PLANT
MARKET TESTING
DISTRIBUTION AND SALES
BREAK EVEN
VENTURE CAPITAL AT RISK (LOG $)
TIME
FAST TRACK APPROACH TO FIT COMMERCILIZATION STEPS WITHIN CORPORATE HORIZONS

Figure 5.

the left to a final product and output on the right, leads the commercial endeavor through a number of hurdles. Knowledge base building and a certain amount of application screening are shown on the left hand side. There's a lot of process development, control development, scale-up, pilot plant, and so on to go through. We are working toward developing the Space Station that will support this activity. Whether materials production will occur on the Space Station or not is yet to be determined. Throughout this entire process, that scale-up issue is a critical one and Bob Naumann alluded to that in his talk.

Figure 6 expands on the scaling process between research and production. It essentially involves calibration of research, or process results versus the process environment. The process environment here is a parametric definition of the thermal, the pressure, the electromagnetic environment, and so on. Those are all process control parameters, and we are adding the new one of the weightlessness in trying to determine how to exploit it so that it augments those other process parameters.

Figure 7, entitled "Scaling Issues," shows this a little more graphically. Indicated is a hypothetical application size which is a crystal of the order of 4 quarts, or about a gallon, in some configuration. If one starts out by doing a number of process experiments (P_i) at a given volume (shown here as a volume of about 7 or 8 cc on the horizontal axis) and does this experiment as a function of g, buoyancy driven convection and scaling from dimensional analysis would indicate that there would probably be process thresholds as shown by the diagonally drawn family of curves. Point P_1 shows what would be perhaps unacceptable results. The second trial is also unacceptable. Finally, one gets low enough g at point P_5 to get diffusion growth control in this particular process. Using the the Space Station Materials Lab, one would hope to map out an environment where you knew what the process threshold was, and then you still might be faced with a projection from what you could do on a Space Station laboratory to a point design required for production. That's critical because if you do a straight-

CRITICALLY ESSENTIAL STEP

- IN SCALING FROM RESEARCH TO PRODUCTION

CALIBRATE

PROCESS RESULTS

VERSUS

PROCESS ENVIRONMENT

- PROCESS ENVIRONMENT IS DEFINED PARAMETRICALLY BY PROCESS PARAMETERS
  - THERMAL
  - PRESSURE/VACUUM
  - ELECTRO MAGNETIC FIELDS
  - GEOMETRY
  - TIME
  - •
  - •
  - •
  - WEIGHTLESSNESS (THE NEW ONE)

Figure 6.

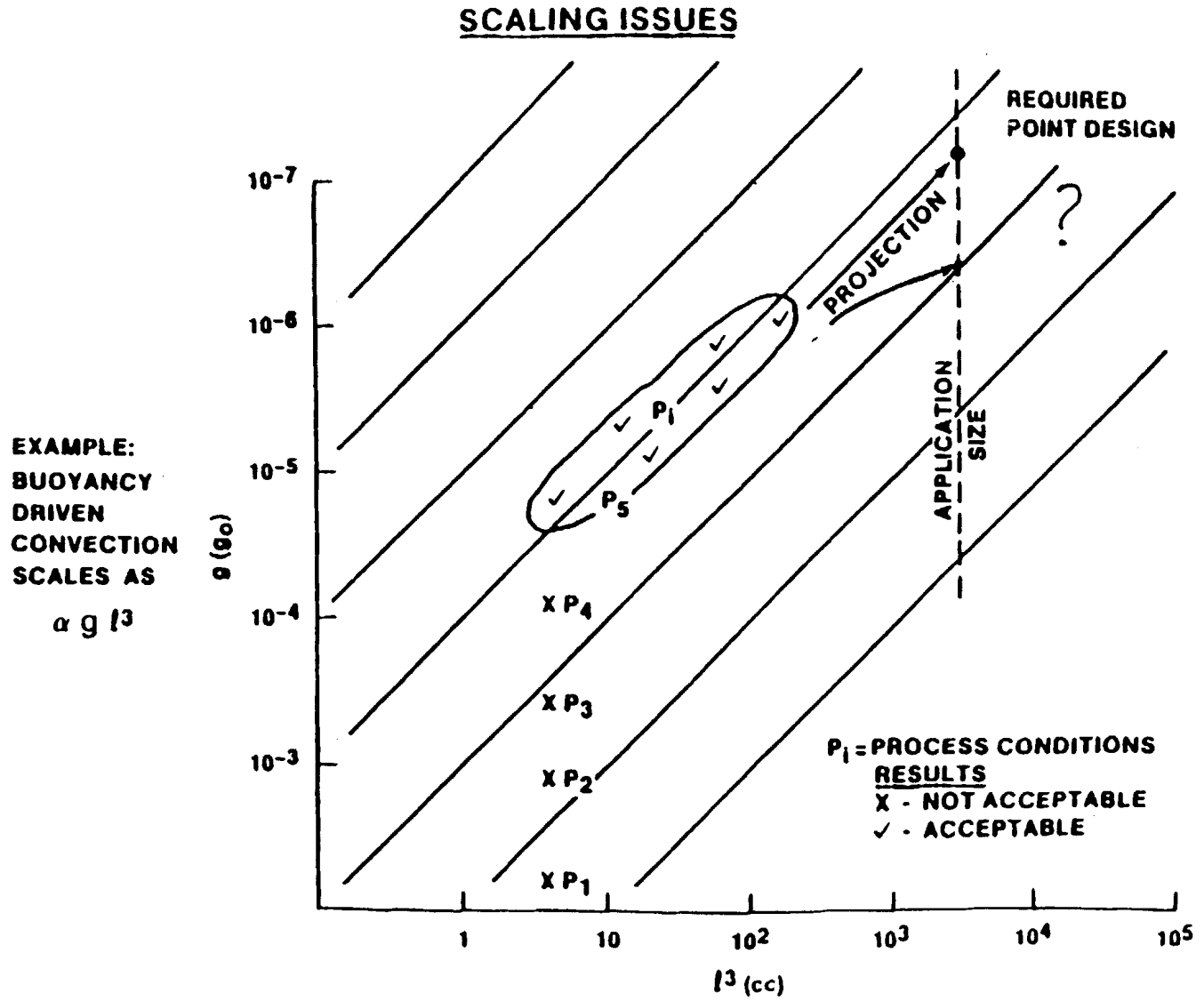
SCALING ISSUES
EXAMPLE:
BUOYANCY
DRIVEN
CONVECTION
SCALES AS
α g l3
g (go)
10-7
10-6
10-5
10-4
10-3
REQUIRED
POINT DESIGN
PROJECTION
?
APPLICATION
SIZE
P1
P5
X P4
X P3
X P2
X P1
Pi = PROCESS CONDITIONS
RESULTS
X - NOT ACCEPTABLE
✓ - ACCEPTABLE
1
10
10²
10³
10⁴
10⁵
l3 (cc)

Figure 7.

line projection (if that's really what it is) it drives you to much lower g levels. If there's some limiting mechanism occurring that makes the process threshold veer off horizontally, that is going to be a much less costly design to implement for production, and that becomes risk reduction to any commercial people who might be interested in this activity.

Figure 8 shows a number of process thresholds, and this does not have the scaling aspect in it, these are just different processes that we've developed with the help of Dr. Naumann and his associates. The acceleration environment in the orbit (0 to about 0.05 Hz, labeled on the horizontal axis on the bottom) includes the structural resonance regime and the vibration and noise regime. Each of those areas has its specific cause and countermeasures; and each has its specific detrimental effects on materials processing. The orbital effects, for example, drag or any frequency attributed to flying solar inertial and having the g vectors rotate, occur around 2×10^{-4} Hz. Things like the centrifuge operating at 22 rpm are at about 0.3 Hz. That's right in the middle of the structural resonance or close to the structural resonance of the Space Station as it's now understood. Those are issues that the materials people have to deal with when they do a detailed relation to some of the principles that Bob discussed earlier.

One item that we've come across quite a bit is that accelerometers on previous spacecraft have measured 10^{-3} g, and adequate experimental results were achieved. The data points at about 10 Hz are quite high, but because of the considerations that Bob gave earlier, they are of no consequence to these particular processes. One cannot take 10^{-3} at 10 Hz and move to the left on the chart to 0 Hz and get by with 10^{-3}. Our understanding of the fluid mechanics is getting to the point where we're quite sure that operating on that assumption would be devastating. Saying that 10^{-3} g is adequate at all frequencies since it is okay at 10 Hz is like saying that aerodynamic designs at subsonic regimes are acceptable for hypersonic flight.

EXAMPLE MICROGRAVITY REQUIREMENTS RELATED TO PROCESS

FREQUENCY VS ACCELERATION

G-LEVEL TOLERANCE FOR MONOCHROMATIC OSCILLATING DISTURBANCES POINTS AT A & B ARE SPACE LAB 3 ACCELERATION MEASUREMENTS

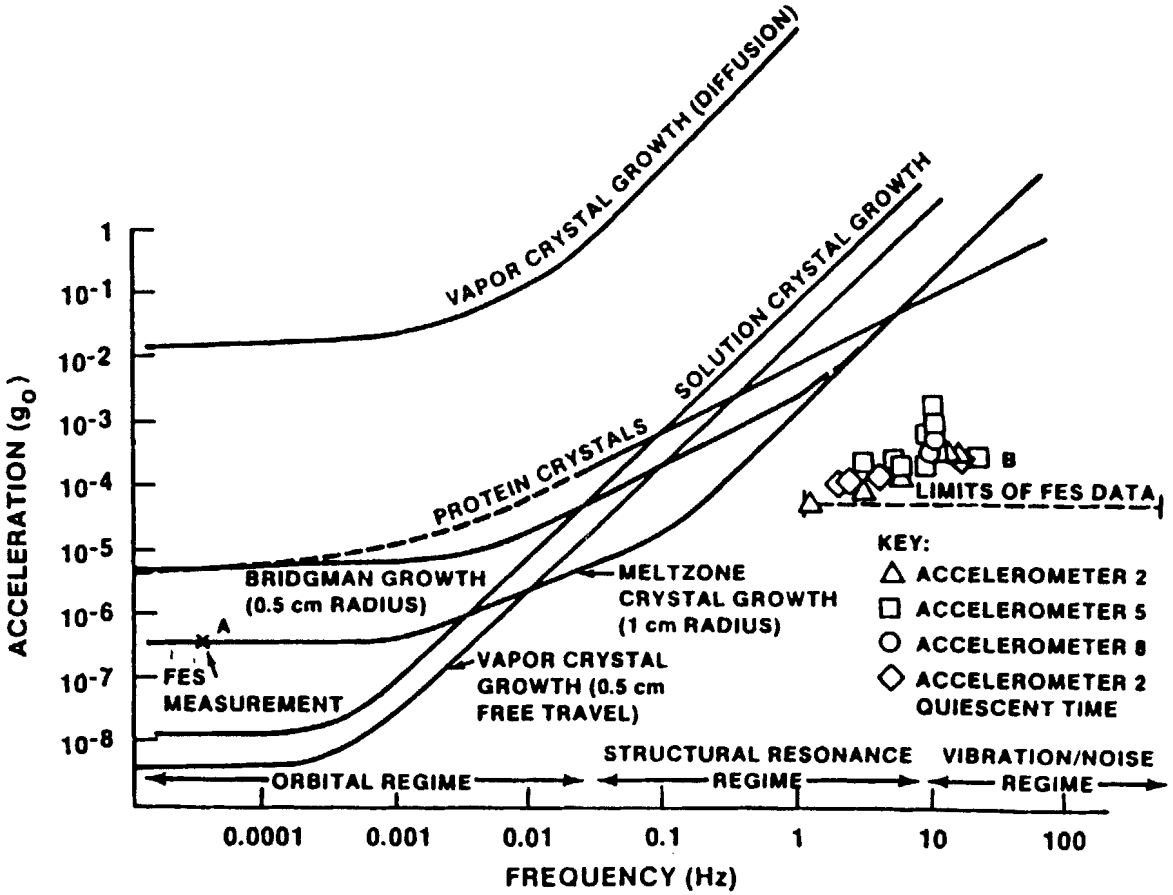

Figure 8.

Figure 9 shows another sequence of such threshold curves, g-level versus frequency, and here are indicated three options that we're studying at level B. The current Space Station requirements document officially says 10^{-5} g and that's the straight dashed line given in the figure as Option 1. As far as the wording is concerned, that acceleration level is a constant with frequency. We're looking at the option 2, which would start at 10^{-6} in the low frequency regime and then increase in the structural resonance area and the noise and vibration area to the right. These curves are a family that, for Bridgman crystal growth, correspond to the 1-, 2-, and 4-cm diameter curves for the stabilizing growth configuration with the hot part of the melt over the cold part. Another set of three curves are for the destabilizing condition, where the cold elements in the melt are over the hot elements. In that particular case, when the process is destabilized thermally, the g-level requirements go down by an order of magnitude. This would preclude a solar inertial rotation vector from being of use. Complicated schemes for rotating process payloads within the equipment that has to fit inside a universal double rack assembly that's less than a meter deep and has height and volume restrictions, power leads and other process lines are probably not feasible. I haven't seen any design that would accommodate that sort of an approach.

Tight calibration between process results and process environment will need to be done to keep the transition from research to production from being haphazard. Within that control is the calibration of the environment. There's a very detailed characterization of the g environment in all of the regimes that I mentioned, including the oscillatory area, the transient domain, and so on. What we get out of this in terms of process results will be useless in terms of projection to production if we do not know what is necessary to duplicate the process environment. So if you do have a good research result for a small sample and you don't know what environment you have to provide for a sample that's five times larger for an application market, you don't know what to do to go into production.

G-LEVEL TOLERANCE FOR MONOCHROMATIC OSCILLATING DISTURBANCES

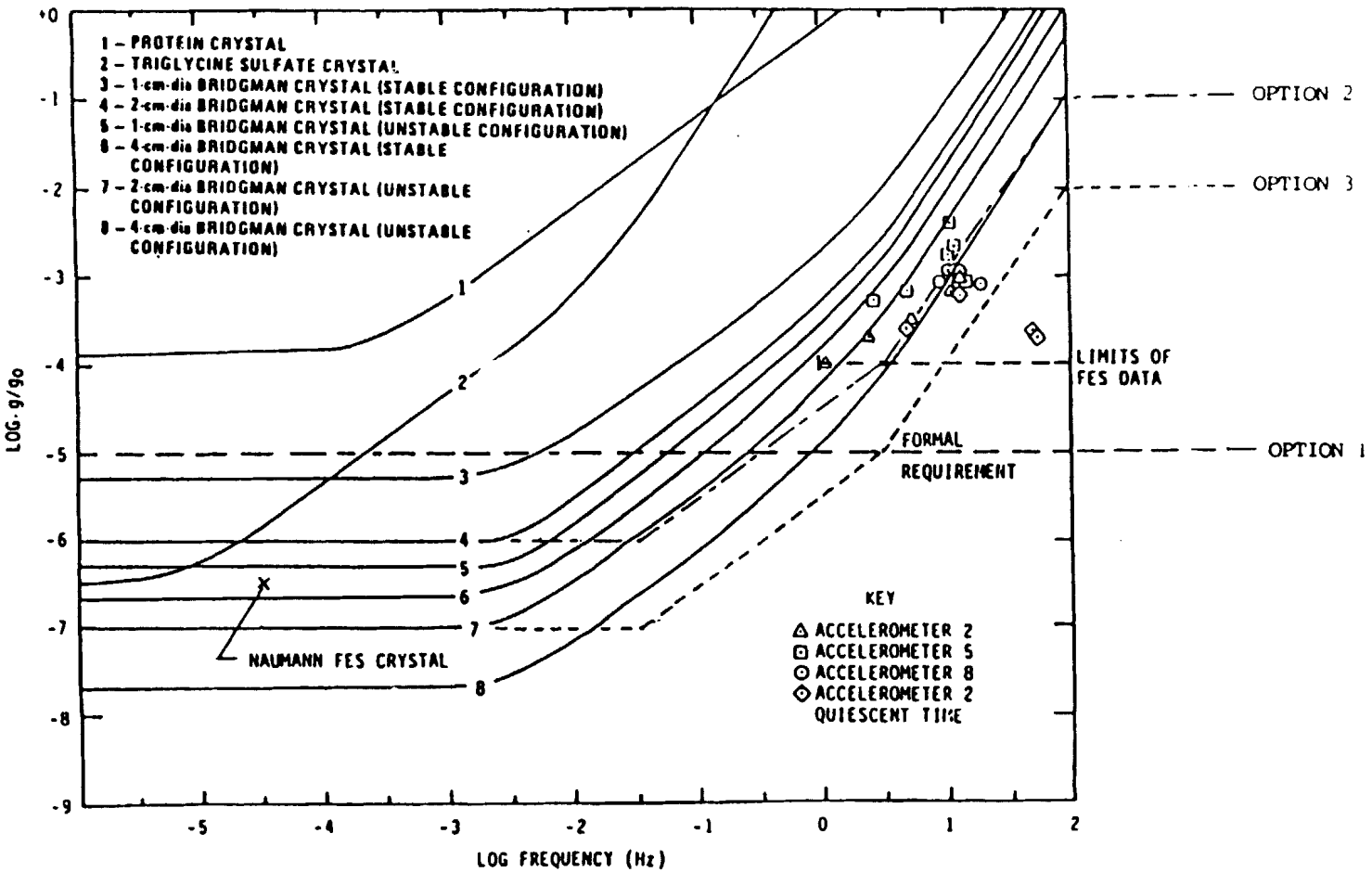

Figure 9.

I think we have learned how to deal with the thermal process parameters since the start of the bronze age. We've learned how to deal with the vacuum parameter since James Watt started using it. This new process parameter falls into that sort of a framework, but the sophistication of our methods now in fluid mechanics and so on is advanced enough so that we should be able to make great strides quickly, if we just do that tight calibration and the tight analytic modeling that are required. Figure 10 indicates a set of calibration data that we think the commercial community definitely needs. The Vander Slice Committee, which was a parallel to the current science task force on Space Station headed by Dr. Banks, made a big point that data bases are required to support commercial activity.

Characterization of the process, the environments, what you might expect to gain, are needed to map out the convective regimes that are shown in the S-1 area (Figure 10) versus the diffusive growth regimes in the S-2 area. This is a lot of detail based on dimensional analysis. We're trying to separate convective growth from diffusive control, which is the main issue. Diffusive control, as shown in Figure 11, maps detail nomograms for assessing how to scale up to a production device. This figure pertains to germanium-gallium; it has thermal gradients as one parameter. The H on the chart is the crystal diameter; R is the growth rate. Concentration gradients are shown across the horizontal axis on the bottom, and could be related to dollars in the market place at a given size. Large crystals are to the lower left-hand part of this diagram, where the g-levels keep going down. One g is shown at the top on the left-hand axis, 10^{-6} g_o at the bottom. This is the framework that we need to provide, or to develop data for, so that we can assess the risk of going to a production effort.

Figure 12 shows the environment that needs to be characterized. It's a lot more detailed than is given here, but this shows the relative magnitudes of drag-induced accelerations, the acceleration due to attitude wobble on the Space Station, the gravity-gradient accelera-

FLUID DYNAMICS PROVIDES SCALING RELATIONS FOR SEPARATING "CONVECTIVE DIFFUSIVE" FROM "DIFFUSIVE" REGIMES

S_1 CONVECTIVE

S_2 DIFFUSIVE THROUGHOUT

S_3 & S_4 DIFFUSIVE OVER LIMITED LAYER

DIMENSIONAL ANALYSIS METHODS USED IN EARTHBOUND PROCESS CONTROL IS EXTEMDED TO LOW G USING "SCHMIDT", "GRASHOF", AND "PECLET" NUMBERS

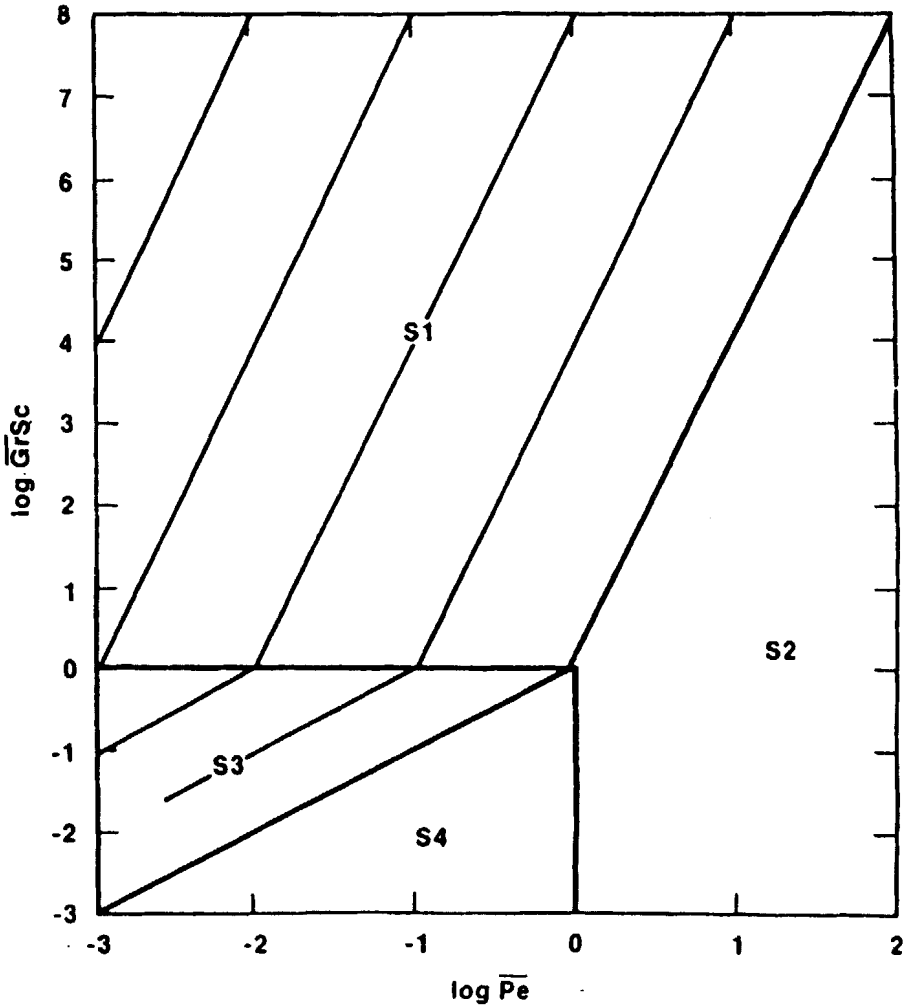

Figure 10.

G LEVEL VERSUS SIZE AND CONCENTRATION FOR THE GERMANIUM-GALLIUM SYSTEM FOR HOMOGENEOUS CRYSTALS

□ TEXUS

★ ASTP

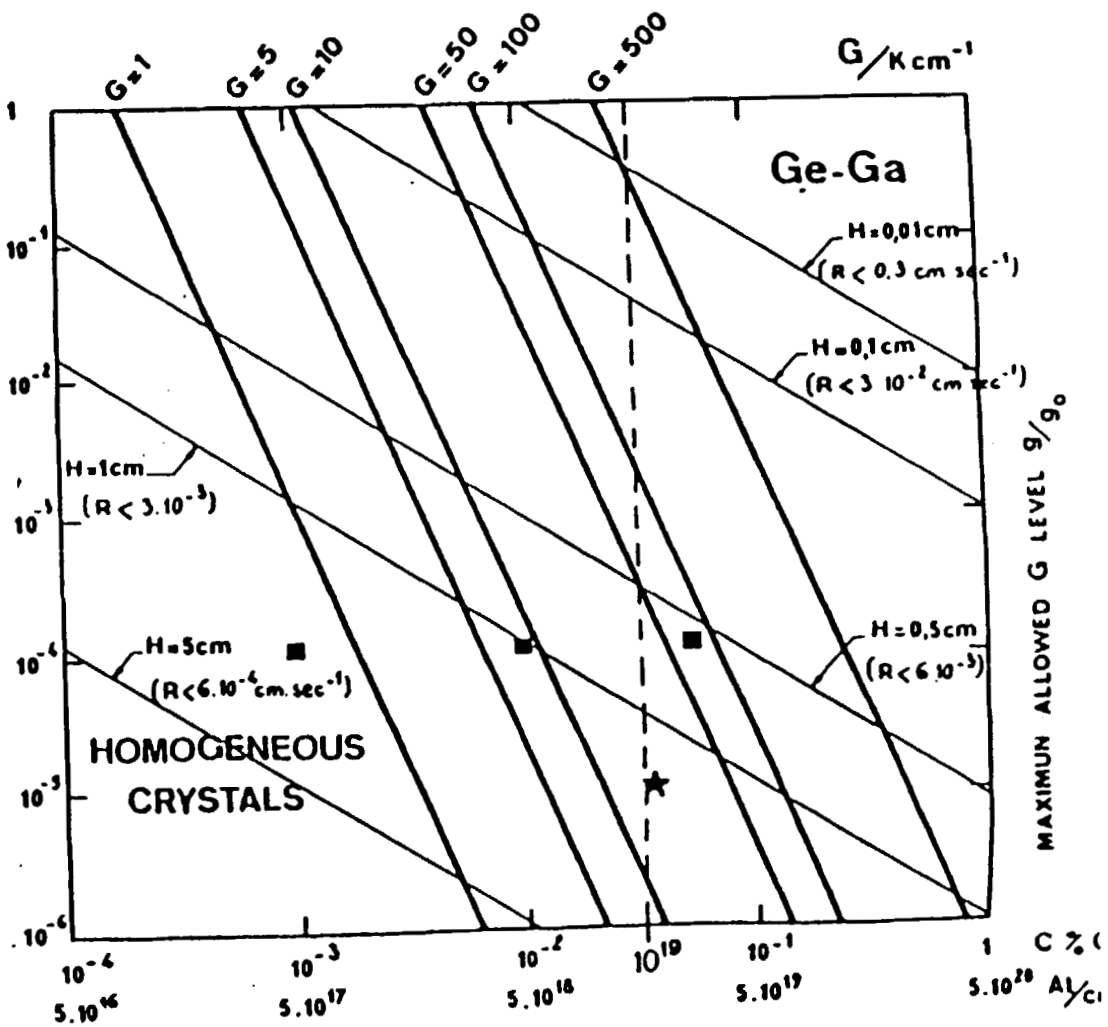

Figure 11.

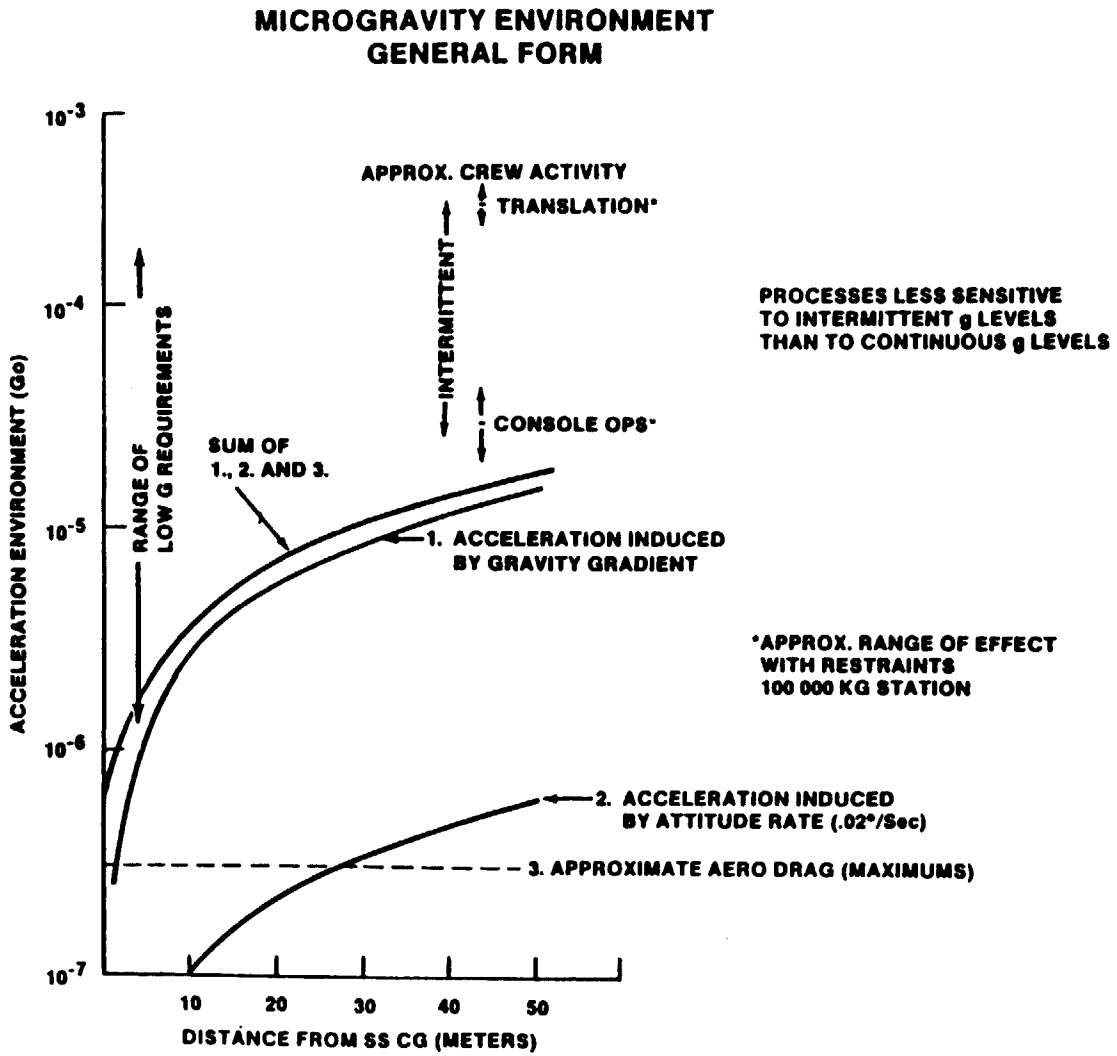
MICROGRAVITY ENVIRONMENT
GENERAL FORM
ACCELERATION ENVIRONMENT (Go)
10^{-3}
10^{-4}
10^{-5}
10^{-6}
10^{-7}
RANGE OF LOW G REQUIREMENTS
APPROX. CREW ACTIVITY
TRANSLATION*
INTERMITTENT
CONSOLE OPS*
SUM OF 1., 2. AND 3.
1. ACCELERATION INDUCED BY GRAVITY GRADIENT
2. ACCELERATION INDUCED BY ATTITUDE RATE (.02°/Sec)
3. APPROXIMATE AERO DRAG (MAXIMUMS)
PROCESSES LESS SENSITIVE TO INTERMITTENT g LEVELS THAN TO CONTINUOUS g LEVELS
*APPROX. RANGE OF EFFECT WITH RESTRAINTS 100 000 KG STATION
10
20
30
40
50
DISTANCE FROM SS CG (METERS)

Figure 12.

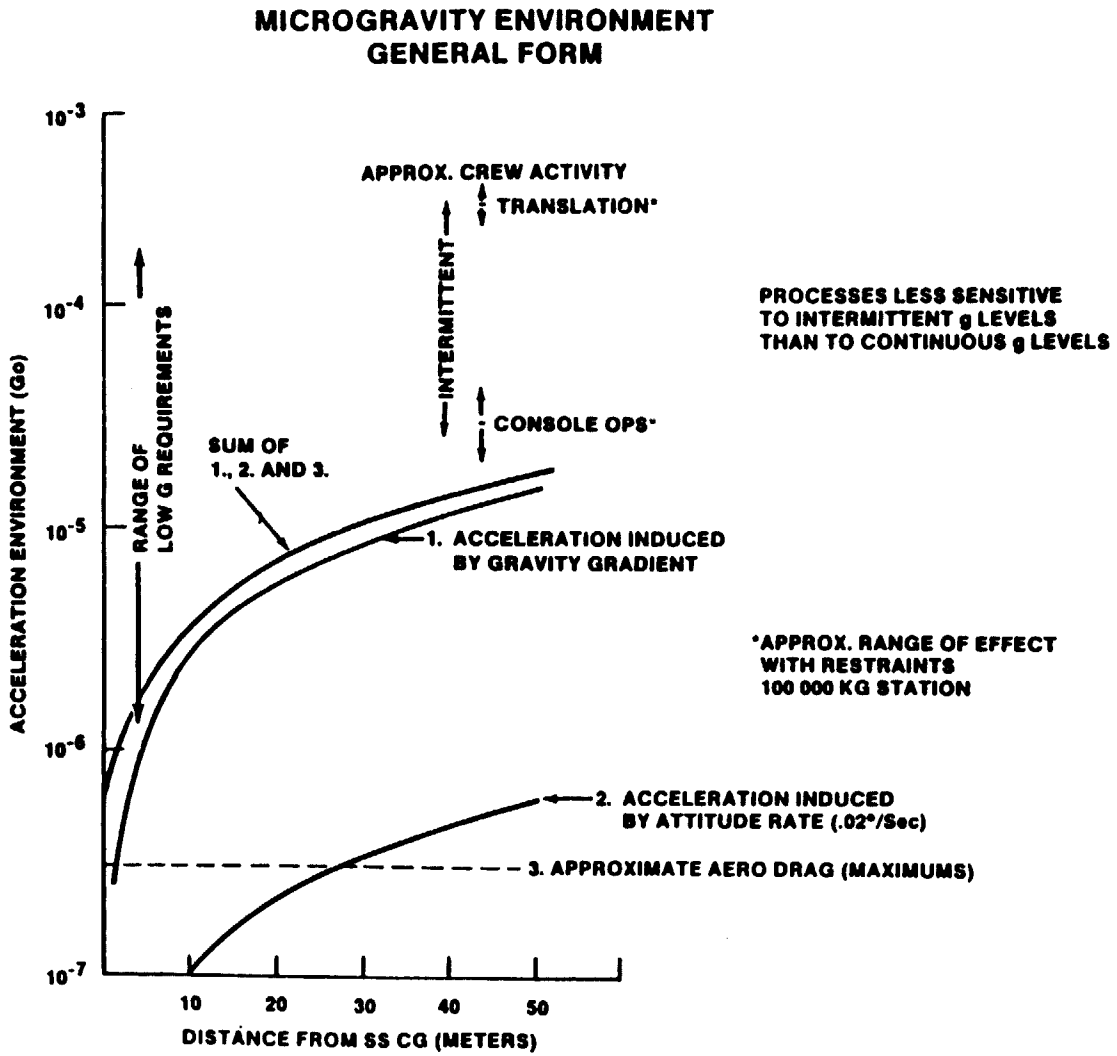
MICROGRAVITY ENVIRONMENT
GENERAL FORM
ACCELERATION ENVIRONMENT (Go)
10^{-3}
10^{-4}
10^{-5}
10^{-6}
10^{-7}
RANGE OF LOW G REQUIREMENTS
APPROX. CREW ACTIVITY
TRANSLATION*
INTERMITTENT
CONSOLE OPS*
SUM OF 1., 2. AND 3.
1. ACCELERATION INDUCED BY GRAVITY GRADIENT
2. ACCELERATION INDUCED BY ATTITUDE RATE (.02°/Sec)
3. APPROXIMATE AERO DRAG (MAXIMUMS)
PROCESSES LESS SENSITIVE TO INTERMITTENT g LEVELS THAN TO CONTINUOUS g LEVELS
*APPROX. RANGE OF EFFECT WITH RESTRAINTS 100 000 KG STATION
10
20
30
40
50
DISTANCE FROM SS CG (METERS)

Figure 12.

CHARACTERIZATION OF MICROGRAVITY ENVIRONMENT

- 3- DIMENSIONAL VECTOR FIELD
  - VS FREQUENCY
  - VS TIME
  - LINEAR COMPONENTS
  - ROTATIONAL COMPONENTS
- NEEDED SENSITIVITY LEVELS MIGHT COME FROM COMPUTATIONAL FLUID DYNAMICS
- DATA FORM SHOULD FIT EXPERIMENT DESIGN

Figure 13.

tions, the range of the intermittent activity on the Station and so on. All of the frequency scale is on one chart, so one should not read in here that the intermittent activity has the same effect as the g at the same level for, say, gravity gradient. One has to go back to the frequency curves on Figures 8 and 9 to get that component of the data. Figure 13 indicates the type of characterization that we need to do to the g field, and the instrumentation to do it with, with emphasis on 10^{-3} to 10^{-4} Hertz.

Figure 14 is a picture of the acceleration level that one can acheive in the current Space Station configuration in the local vertical-local horizontal mode. In the lower right-hand corner are the sizes of that elliptic torus around the Earth. At 10^{-6} g, that's 16 m by 5.3 m. At a nano-g that's 16 mm by 5.3 mm, so anybody that needs a nano-g has problems if he has something as large as a marble to work with. Figure 15 indicates the issue more clearly. Here again is that scaling chart from Figure 7, and in the upper right-hand area, there are some intersect lines on process thresholds. That's the approximate cap on what you can do in low-earth orbit because the sample starts getting bigger than the environment that's available. What this implies is that, as you go into assessing production, you may well run into that cap. For example, there is an asterisk along the horizontal axis on the left that is an approximate location of a curve for a Bridgman crystal growth of germanium-gallium. Obviously, that curve would intersect the application size above the limit where, from an acceleration standpoint, you could do it. That's a regime above which the magnetic methods that Dr. Naumann mentioned would be in order. The other mechanism would be to go to a much higher orbit. If you went to about a 4,000 n.mi. orbit, you'd be two Earth radii out from the center of the Earth and that cap would move off and cross through the "C" in Commercial. Going to a much higher orbit and incurring a much different, harsher environment does buy you something, but it's extremely expensive. The main point I'd like to leave with you here is that this gives a strategic framework from which to decide where to put the thrust for later

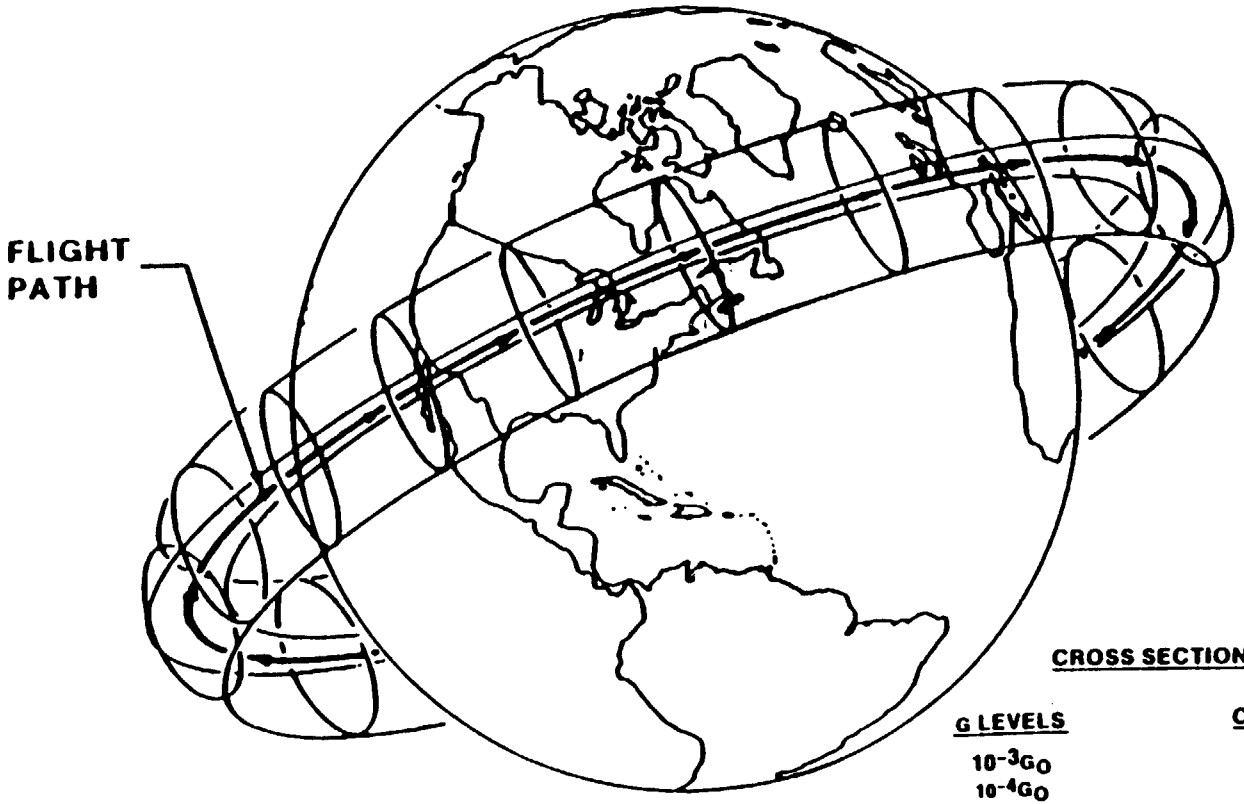

CROSS SECTION OF ISO G ENVELOPES

G LEVELS	MAJOR AXIS CROSS PLANE	MINOR AXIS RADIALLY
$10^{-3}G_O$	16000 M	5300 M
$10^{-4}G_O$	1600 M	530 M
$10^{-5}G_O$	160 M	53 M
$10^{-6}G_O$	16 M	5.3 M
$10^{-7}G_O$	1.6 M	.53 M
$10^{-8}G_O$	16 CM	5.3 CM
$10^{-9}G_O$	16 MM	5.3 MM

Figure 14.

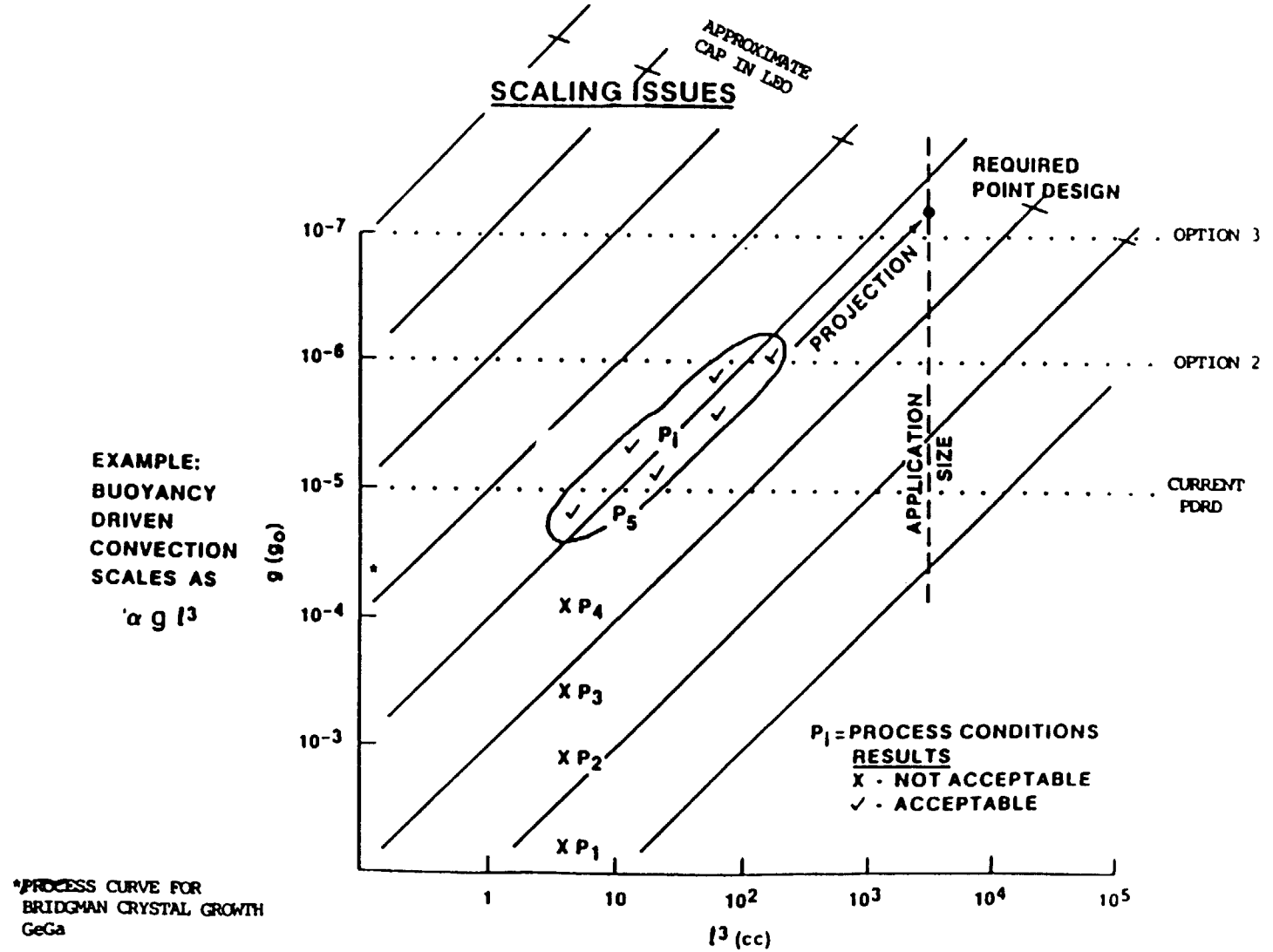
SCALING ISSUES
APPROXIMATE CAP IN LEO
REQUIRED POINT DESIGN
OPTION 3
OPTION 2
CURRENT PDRD
PROJECTION
APPLICATION SIZE
EXAMPLE:
BUOYANCY DRIVEN CONVECTION SCALES AS
α g l3
g (go)
10-7
10-6
10-5
10-4
10-3
P1
P5
X P4
X P3
X P2
X P1
P1 = PROCESS CONDITIONS
RESULTS
X - NOT ACCEPTABLE
✓ - ACCEPTABLE
1
10
10²
10³
10⁴
10⁵
l3 (cc)
*PROCESS CURVE FOR BRIDGMAN CRYSTAL GROWTH GeGa

Figure 15.

production. We need to be careful with our commercial constituency in materials processing and point out that there are certain things that we might not be able to bring to fruition in low-Earth orbit. It might take a higher orbit and a much more capable transportation system. It might be something that is available 100 years from now instead of 10 years from now.

Figure 16 is a view that you've seen previously but our basic configuration in which 10^{-5} g_o is easy to get. That is indicated on Figure 17. The large ellipse is the profile of 10^{-5} g_o at the dc level, not the oscillatory, the bump, the grind, the rattle and roll activity on the Station, but just the gravity gradient component. The small ellipse is the 10^{-6} contour. I don't think we can change the c.g. of this configuration to get the laboratory modules out of the 10^5 envelope. I think we need to consider a micro-g or 2 micro-g for the static g-level. This would require c.g. maintenance and control as we add payloads to the upper and lower booms, and may be a critical technology for the countries involved in the Space Station activity.

Figure 18 is a recap showing the LVLH configuration and its g environment shown on the left, and the solar inertial configuration on the right. The solar inertial has a high degree of vector direction change. Stable processing configurations would go to unstable processing configurations, whereas the environment on the left lets you stack modules longitudinally along the flight path. You can't do that on the right with the solar inertial. The small total volume that you can exploit in the solar inertial, unless your process happens to be ideally suited for reversal of the field, is just too great a penalty to pay.

Figure 19 shows another way of looking at the structure of the field that we need to start considering. As you move around in the fluid element in your process, up is not always the same direction. It moves around. If your process element represented that sphere, the forces on the surface of that sphere are shown with respect to the radial direction, which is up and the cross-plane direction, which is

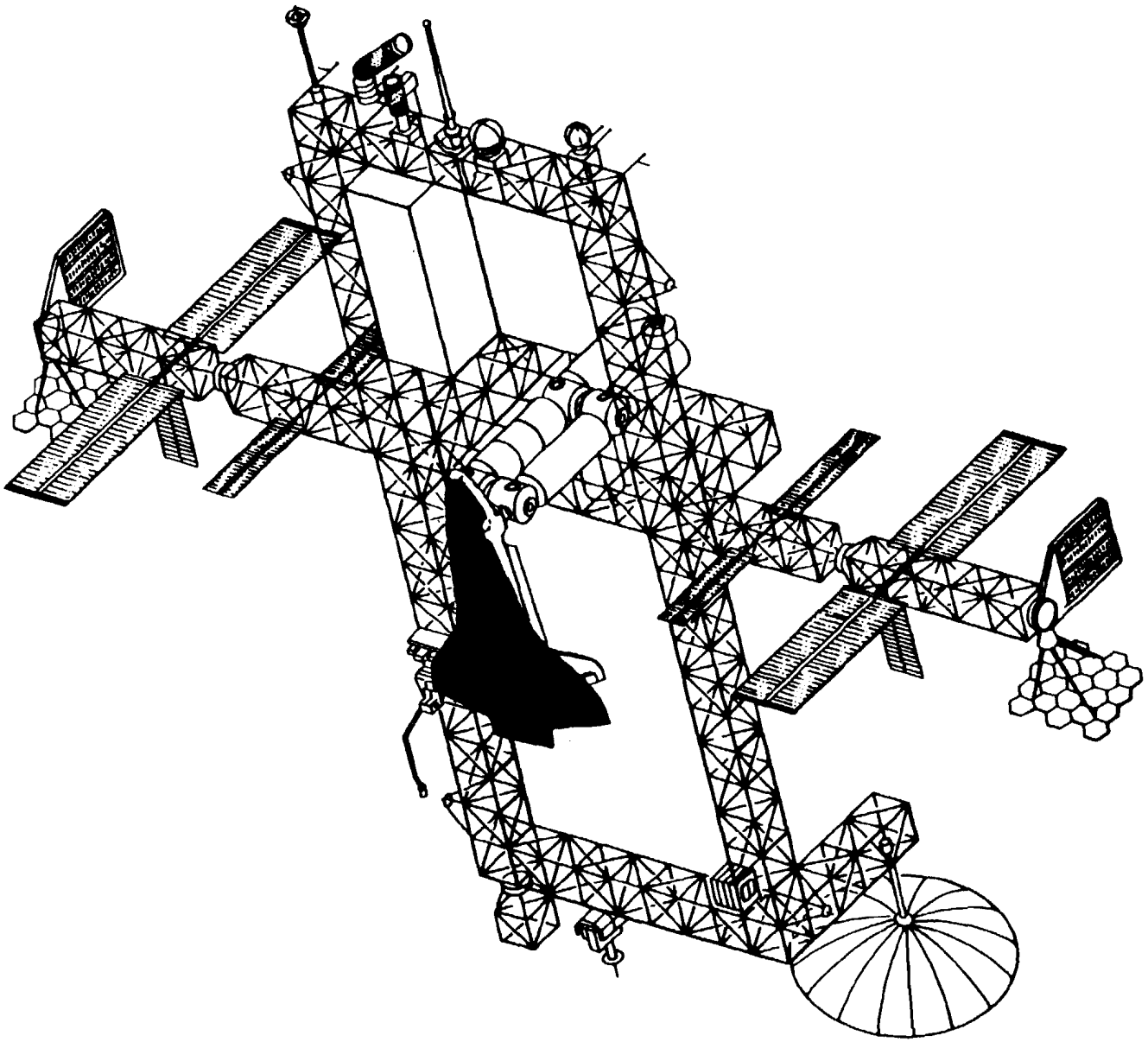

Figure 16.

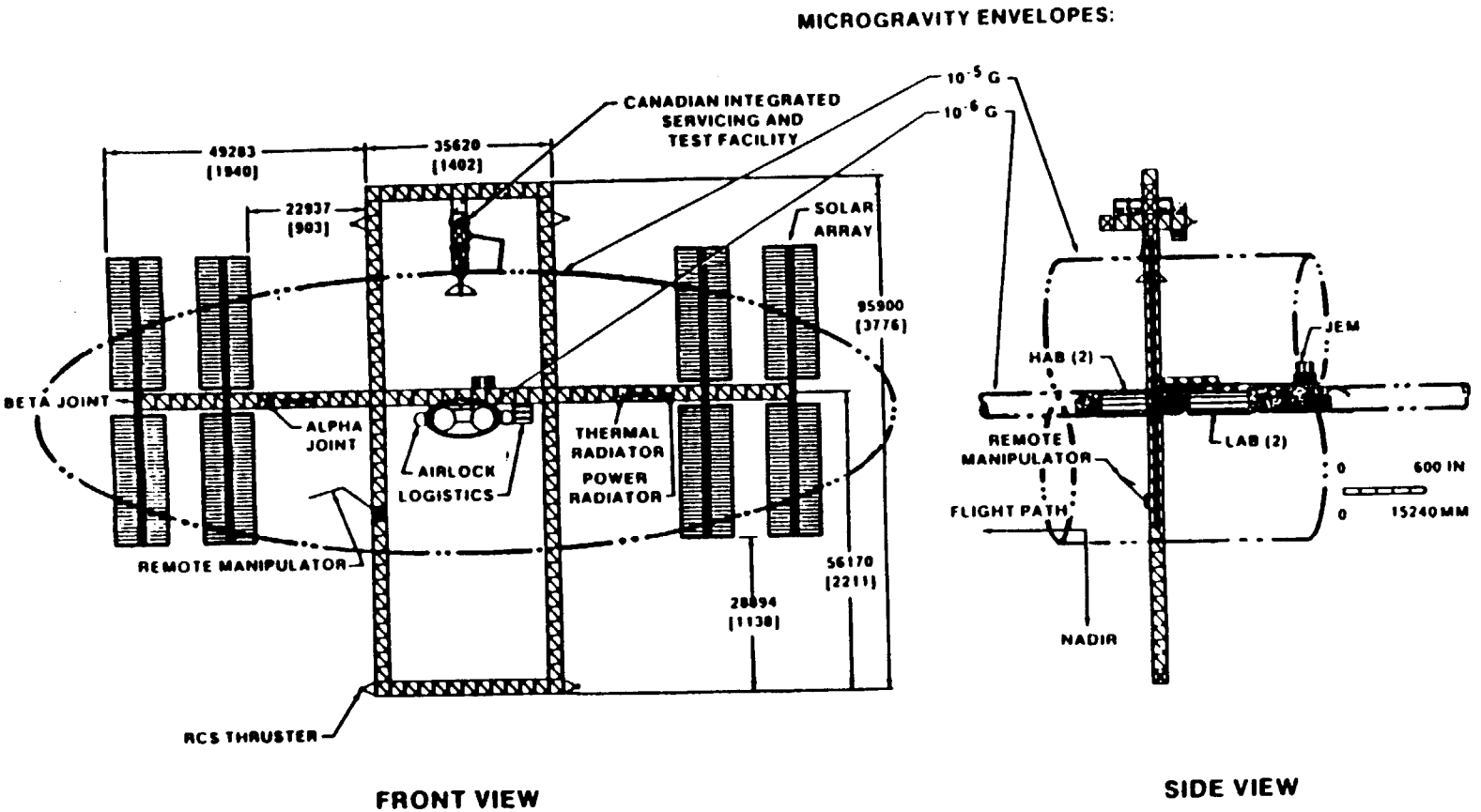

Figure 17.

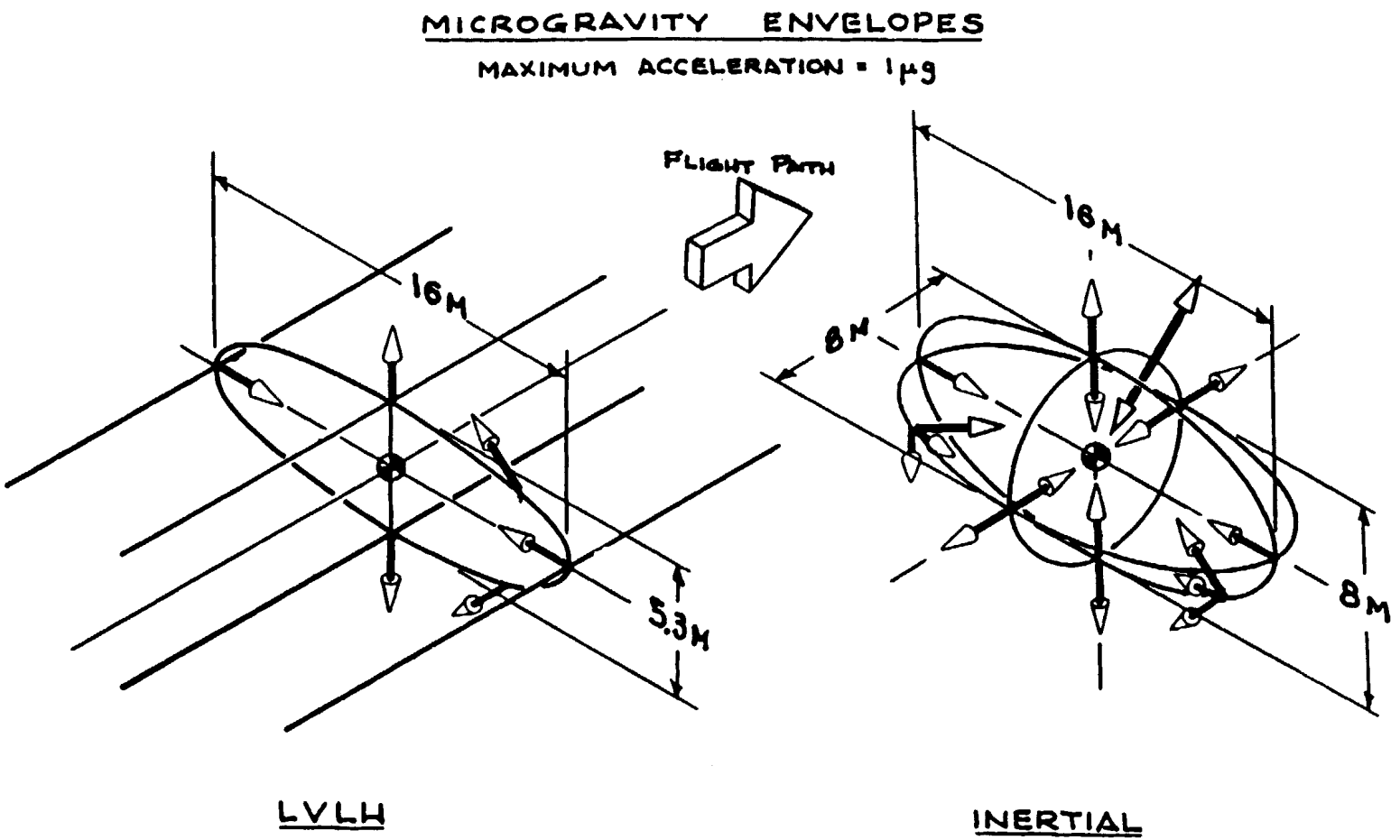
MICROGRAVITY ENVELOPES
MAXIMUM ACCELERATION = 1μg
FLIGHT PATH
16M
5.3M
LVLH
16M
8M
8M
INERTIAL

Figure 18.

STRUCTURE OF GRAVITY GRADIENT FIELD

FOR A CIRCULAR ORBIT, THE ACCELERATION DUE TO GRAVITY GRADIENT EFFECTS ON A POINT R METERS FROM THE FLIGHT PATH OF THE CG CENTER OF GRAVITY IS:

DISTANCE FROM CG (M)	ACCELERATION ($10^{-6}G_O$) RADIAL	CROSS PLANE
R	A_R	A_{CP}
1	0.375	0.125
2	0.75	0.25
4	1.50	0.50
8	3.00	1.00
16	6.00	2.00
32	12.00	4.00
64	24.00	8.00

- ORBIT ALTITUDE: 270nm, 500km
- Z AXIS RADIAL FROM EARTH
- Y AXIS CROSS PLANE
- X AXIS VELOCITY VECTOR (⊥ TO CHART)

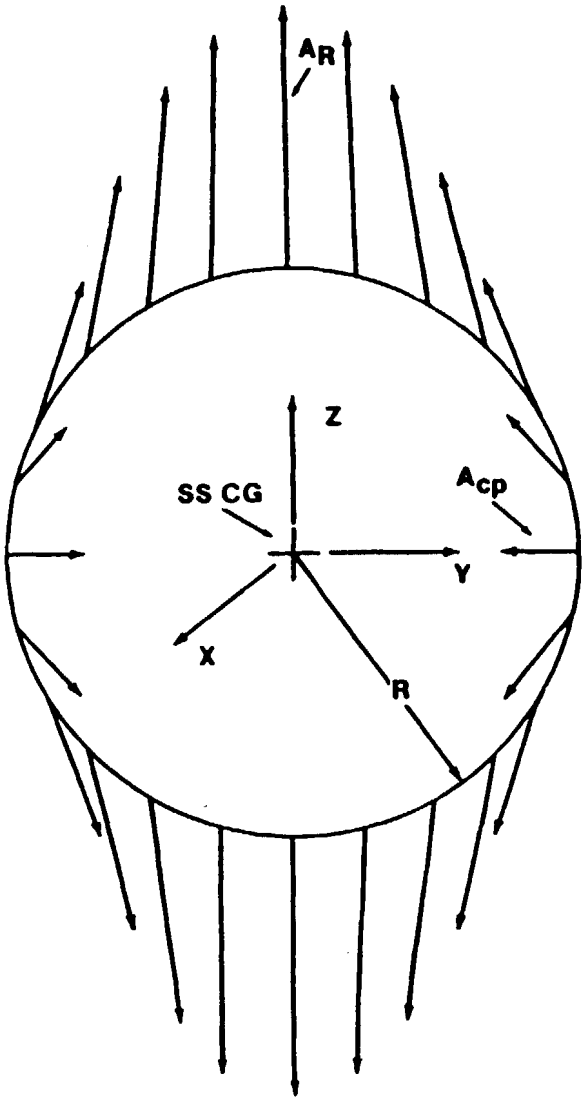

Figure 19.

horizontal on this chart. Figure 20 shows what's happening inside this spherical fluid element. The fields are changing throughout, and our fluid dynamics modeling shows the field to be generally constant and in a constant direction. These are time stationary fields, but they do change with position. There could very easily be some damping characteristics that one might be able to utilize in this regard, but what they are is a question for the expert in computational fluid dynamics.

Figure 21 indicates some of the drag aspects that we're faced with. Currently the program is taking the approach that it's going to design a station so that it could operate at an altitude that would incur an average drag of 0.3 micro-g. But within the orbit, we won't be flying a constant fixed drag acceleration because that requires moving up and down. The Space Station altitude has not yet been specifically picked, only the design range of the station has been set. Somebody will want to fly the Station to its extreme altitudes so it could still be a threat, so the altitude flight issue must still be addressed.

Figure 22 is a list of things to watch on the station from a user and an implementer's viewpoint in the materials processing area. TEA is torque equilibrium attitude. The station doesn't fly exactly with the boom structure vertical to the Earth's surface; there can be two or three degrees of wobble, depending on momentum conservation considerations in the attitude control system. There will be significant changes when the Shuttle docks. Generally it will be noisy enough and we'll be doing enough things in the laboratory where we would probably shut down operations while the Shuttle is docked. We don't envision the Shuttle to be there for long. The TEA limit of a few degrees is the most likely limit. As you get out farther and farther on the cantilever, flying along the flight path of the center of gravity, any torque equilibrium attitude can tip you up right out of your required g environment. The center of gravity will migrate with growth, as some of the payloads are several tens of thousands of pounds, and are going to get mounted to the upper or lower booms. The center of gravity would move tens of feet. There is a possibility for manifesting the payloads

GRAVITY GRADIENT STRUCTURE FOR EXTENDED VOLUMES

THE COMPOSITE STRUCTURE OF THE GRADIENT FIELD OVER EXTENDED VOLUMES IS INDICATED HERE. R_0, R_1, & R_2 ARE THE RADII OF THE OUTER, MIDDLE & INNER CIRCLES

DISTANCE FROM CG (M) R	ACCELERATION ($10^{-6}G_o$) RADIAL A_R	CROSS PLANE A_{CP}
1	0.375	0.125
2	0.75	0.25
4	1.50	0.50
8	3.00	1.00
16	6.00	2.00
32	12.00	4.00
64	24.00	8.00

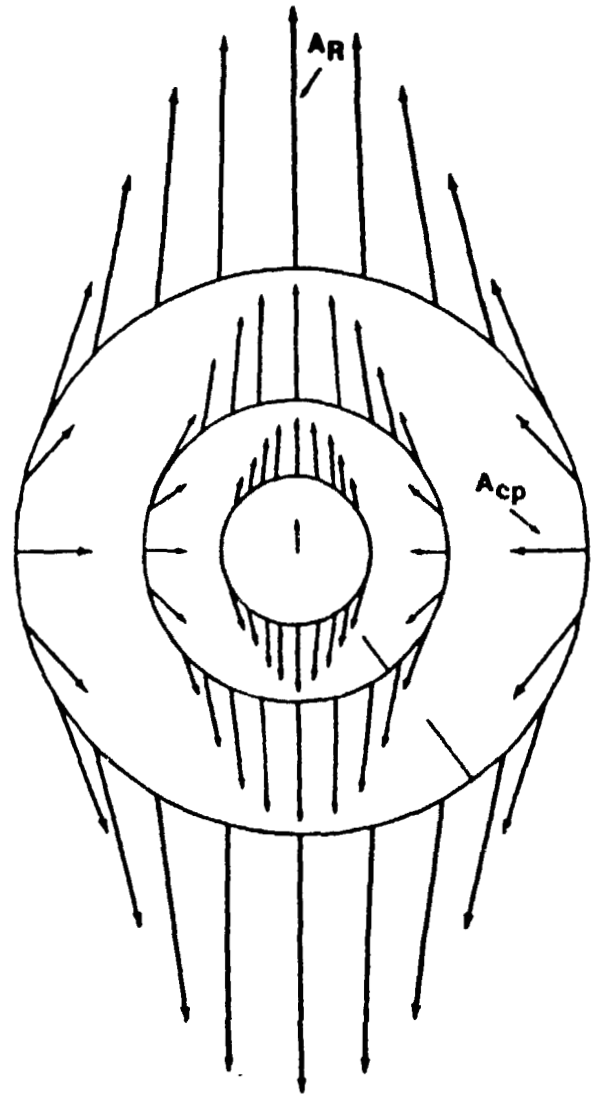

Figure 20.

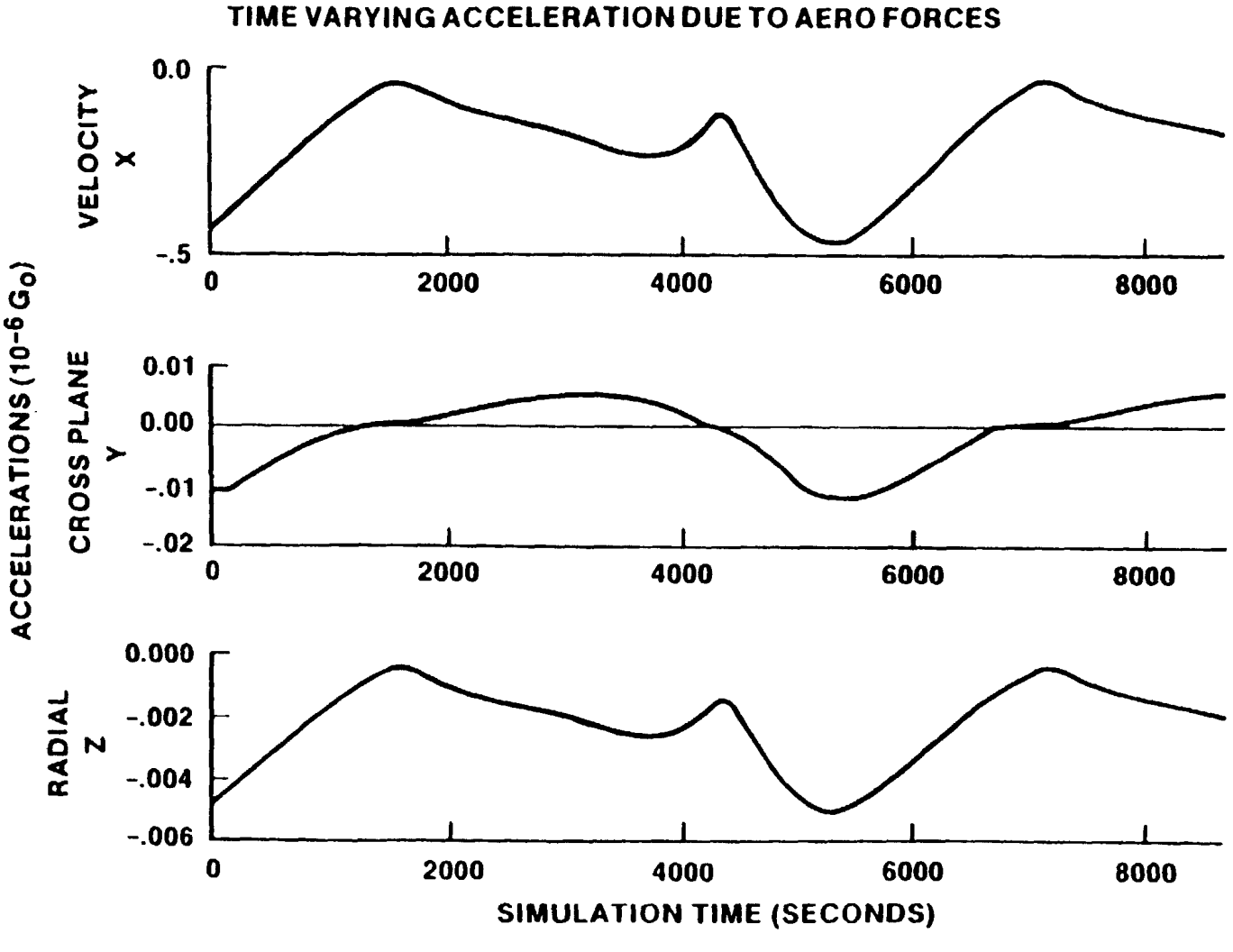
TIME VARYING ACCELERATION DUE TO AERO FORCES
ACCELERATIONS (10-6 Go)
VELOCITY X
0.0
-.5
CROSS PLANE Y
0.01
0.00
-.01
-.02
RADIAL Z
0.000
-.002
-.004
-.006
0
2000
4000
6000
8000
SIMULATION TIME (SECONDS)

Figure 21.

SPACE STATION THINGS TO WATCH

- TEA - FLIGHT ATTITUDE/MODE
- CG MIGRATION W GROWTH
- CG FLUTTER W OPS
- DRAG PROFILE
- STRUCTURAL RESONANCE
- VIBRATION & NOISE
  - ROTARY & RECIPROCAL EQUIPMENT
  - CREW - ANIMALS
- LOCATION OF

Figure 22.

THE KEY TO THE GORDIAN KNOT
OF EXPLOITING MICROGRAVITY
AND SCALE UP

FLUID DYNAMICS
AND
COMPUTATIONAL FLUID DYNAMICS
WITH
EXPERIMENTAL RESEARCH & DEVELOPMENT

Figure 23.

in such a way that that doesn't happen. There's still room for using ballast units of waste solid or liquid materials on the station to do this. This really hasn't been addressed yet, but people like you will have to bring the message for the need to stay at a micro-g or two micro-g.

Question: Is there is any effort in fluid dynamics?

Demel: The answer is yes. Code E, that's Dick Halpern's organization in NASA Headquarters, has a considerable effort in computational fluid dynamics. It's getting bigger. At level B in the Space Station, we're funding, or will be funding, some activity in that regard to tailor the answers of the work that we need to characterize the environment for the Space Station, what the implications are on Space Station design. Aerodynamics on the Shuttle were done by computational fluid dynamics and it was supported by wind tunnel testing. But a lot of the data base that is used in Shuttle operations comes from the computational part. I think that's a very valid model for us to use here in materials processing.

Alex Lehoczky, NASA/MSFC: Couldn't forces in the melt due to solute concentration gradients be a major factor as well?

Demel: Alex was making the point that all of this is based upon convection considerations and not solution considerations or concentration considerations, that's true. Getting the thermal aspects under control I think is essential to providing the access to the problems so you can address the solutal aspects.

Lehoczky: What I'm referring to is the driving force.

Demel: Yes.

Ulf Merbold, ESA/ESTEC: Have you looked at thrusters to exactly counteract the drag forces?

Demel: Yes. Bob made mention of the DISCOS experiment or the TRIAD experiment that was flown in the early 70's, I think around '74 or so. That was a drag-free satellite oriented toward assessing true

gravity orbits nonaffected by drag, photon pressure, electric fields, or whatever. But in that experiment they demonstrated a sensing and control capability to maintain down to 10^{-11} or 10^{-12} g in the very core of a test mass, not for a very large volume. It still has dimensions of a few microns at those levels. But the control technology has been with us, for a satellite, since the early 70's. Now applying that control technology to the station is another issue. We have been discussing the resistojets for drag make-up but in terms of having engines that would have a variable thrust to exactly counter drag as it varies in the orbit, we haven't really addressed that. The people who are concerned with reboost are concerned about the reliability of the engines and making sure the Space Station doesn't get into an attitude or altitude where it deorbits and that sort of thing. We have been reviewing that constant drag makeup to do a detailed counteraction of drag in the orbit as a growth capability on the station and really not made a big point of it at this point. That's something we can fix later; we're concentrating on those things that have to be fixed now in the basic configuration, but yes that is a way to take care of that drag component.

Fred Henderson, Teledyne Brown Engineering: That drag level -- there may be something about the geometry I didn't understand, but it would seem that atmospheric drag you could move the center from the very center of the geometry rather than fly a reaction type acceleration.

Demel: No, when you do your vector summation of all the effects, and take in account the attitude wobble on the spacecraft, the volume at a given g level is shifted in the velocity direction as you mentioned. But you're continually driving or going to a lower altitude. You're spiraling in continuously at tens to a 100 meters per orbit. When you insist that a process chamber spiral in with you, it's experiencing the same drag forces constantly that the station does.

N91-12405

6. ACCELERATION EFFECTS OBSERVED IN OPTICAL DATA TAKEN IN SPACELAB 3 FES

James Trolinger, SPECTRON Development Labs, Inc.
Ravindra Lal, Alabama A&M University
Rudy Ruff, NASA/Marshall Space Flight Center

ABSTRACT

Optical instrumentation in the Fluids Experiment System (FES) is briefly decribed. Samples of the data produced by the schlieren and holography systems during the Spacelab 3 flight are then presented with some of the holographic interferometry data being presented for the first time. Acceleration effects that can be observed in these data are discussed and the potential for using them as a basis for measurement is explored. This includes the tracking of deliberately introduced tracer particles and density gradients in the FES, the analysis of the existing concentration gradients, and a new fiber optic G-meter concept. Finally, some of the plans for acceleration measurement in the upcomng IML-1/FES are described.

I am going to describe some of the data from the Spacelab 3 flights that are relevant to this meeting. Dr. Lal of Alabama A&M University was the principal investigator and Rudy Ruff of NASA/Marshall Space Flight Center helped me put this presentation together. Figure 1 is a summary of the things I want to talk about, with particular attention given to some of the effects that are caused by residual acceleration. It also seems relevant to mention a particular additional acceleration instrument that we have been developing, and to mention some of the plans for the International Microgravity Laboratory (IML) experiments for measuring acceleration in the Fluids Experiment System.

SUMMARY

* FES OPTICAL INSTRUMENTATION
* SPACELAB 3 OPTICAL DATA
* OBSERVED EFFECTS OF ACCELERATION IN SPACELAB 3
* SOME IDEAS MAKING USE OF THE OBSERVED EFFECTS
* PLANS FOR IML-1/FES ACCELERATION MEASUREMENTS

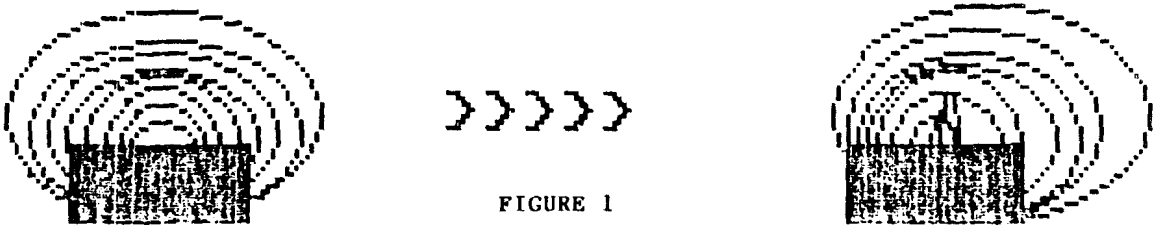

FIGURE 1

The optical instrumentation is summarized in Figure 2. It includes a Schlieren system, which observes the refractive index gradients while the crystal is growing in a diffusion-dominated field. The region around the crystal is depleted of solute which changes the refractive index. Therefore, instruments that measure refractive index will show this region around the crystal. You can also observe shadows or diffraction patterns of other things that may be in the flow field. I will show some examples of free-floating crystals that depict this. One nice thing about the Schlieren system is that it is a real-time system; you can observe by downlink on the closed-circuit TV while the experiment is operating.

The other system I'll discuss is the holographic system. It records holograms of the flow fields around the crystal from two different angles. In this system, there is a complete three-dimensional picture of any solids or materials that are moving around the crystal so that one has a quantitative measure of density, or refractive index, and ultimately the concentration of the solute surrounding the crystal.

For the Schlieren system, Figure 3, a helium-neon laser beam is expanded and collimated. The laser is located immediately above the crystal. A collimated beam of light travels across the crystal and is focused by a parabolic mirror before it crosses the knife edge and enters the vidicon camera.

Woven into this same optics are actually two holographic systems. The one shown in Figure 4 beams directly across the crystal, through the test cell,; onto the primary hologram film. Along the optical train, a beam is split off and that beam is mixed to provide a reference wave for the hologram. When this hologram is reconstructed, it is reilluminated with this reference wave and the full three-dimensional field and the restored wavefront are reconstructed from the hologram. Diagnostics can be applied to that reconstructed wavefront just as they could to the original wavefront.

C-2

FES OPTICAL INSTRUMENTATION

* SCHLIEREN SYSTEM OBSERVABLES
  - *REFRACTIVE INDEX GRADIENTS
  - *SOLID MATERIALS OF SUFFICIENT SIZE (DIFFRACTION PATTERN)
  - *OBSERVED ON CCTV IN REAL TIME

* HOLOCAMERA
  - *REFRACTIVE INDEX
  - *SOLID MATERIALS (3-D IMAGE)
  - *OBSERVED WITH HOLOGRAMS AT A LATER TIME

FIGURE 2

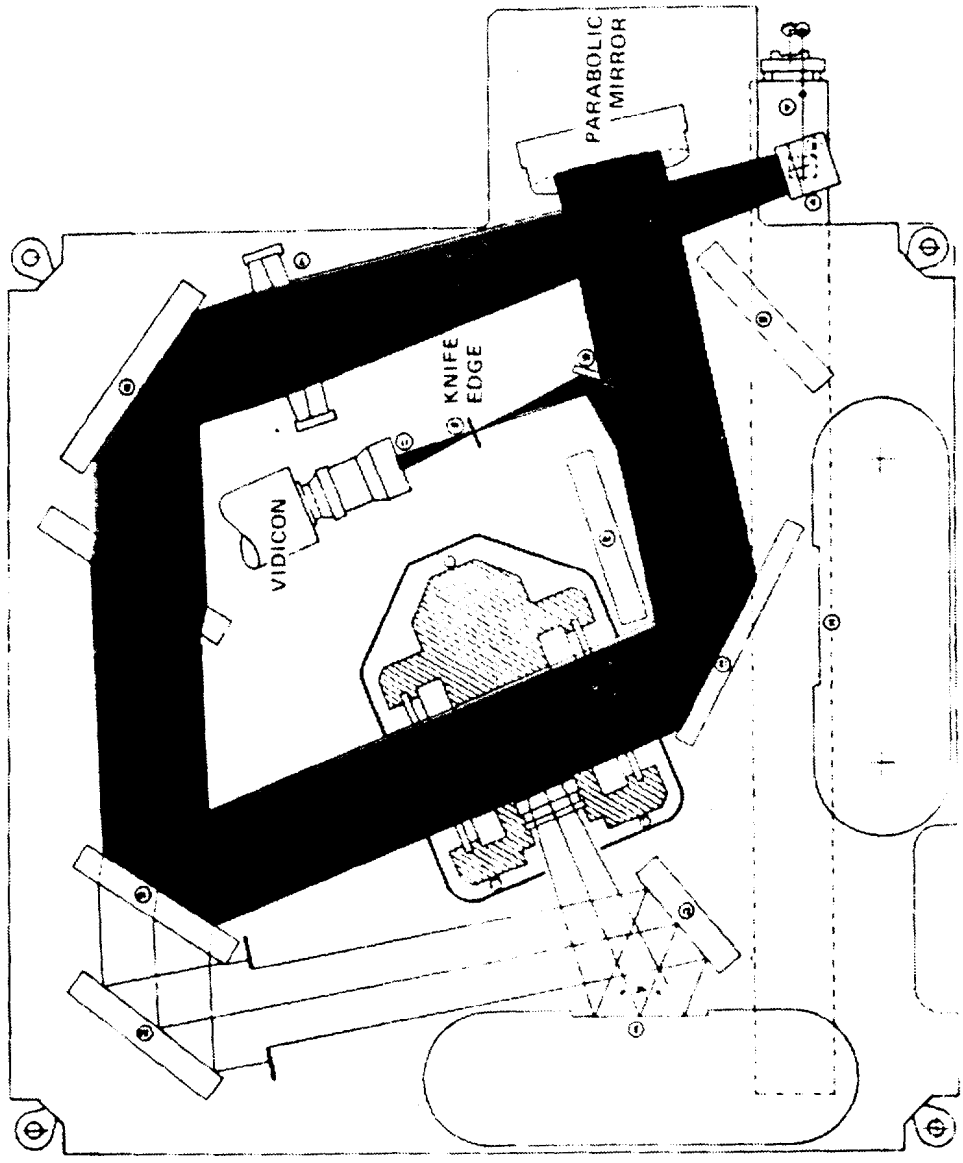

FIGURE 3.

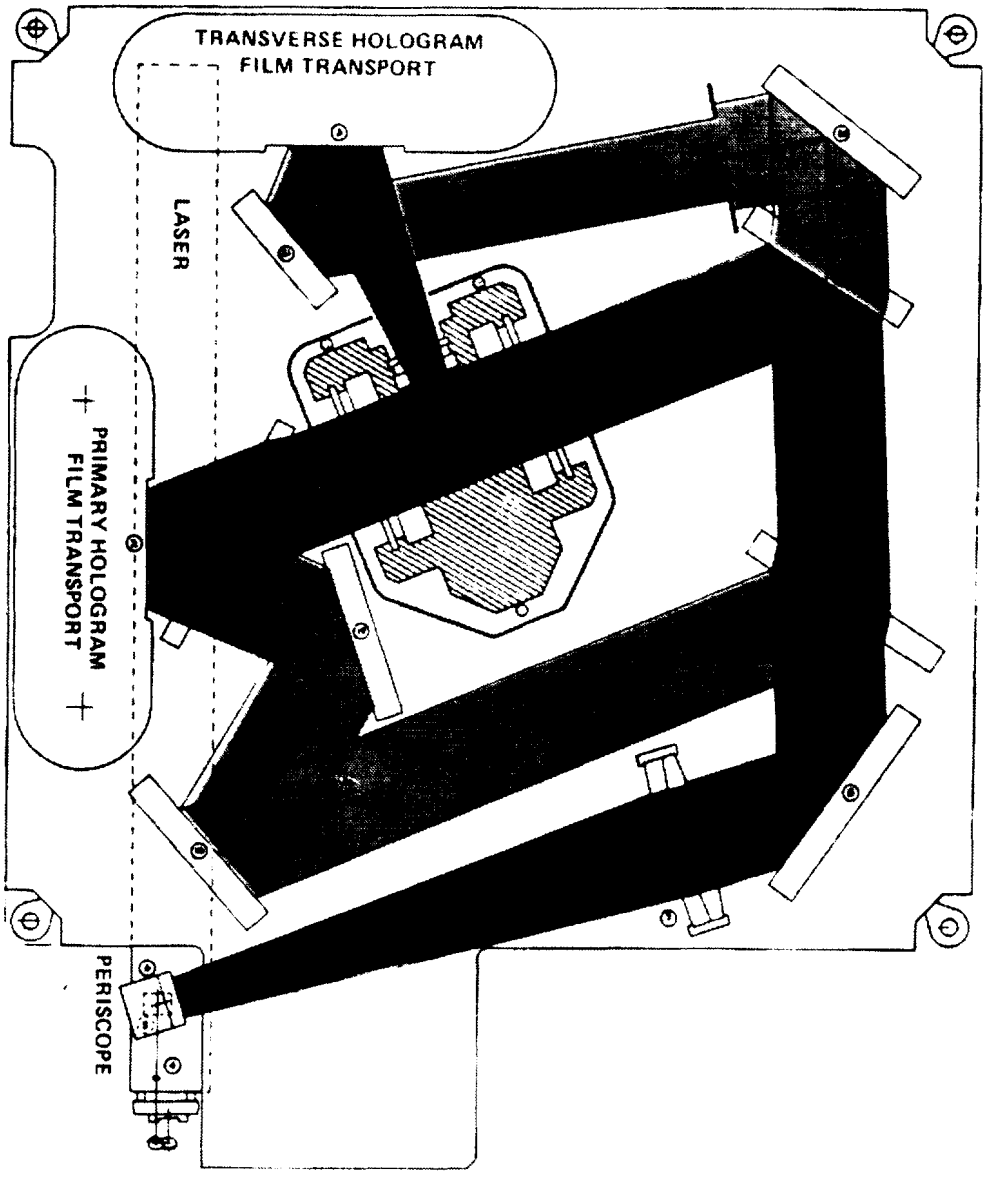
TRANSVERSE HOLOGRAM
FILM TRANSPORT
LASER
PRIMARY HOLOGRAM
FILM TRANSPORT
PERISCOPE

FIGURE 4.

These holograms are generated almost continuously during the experiment after the cap is removed from the crystal and growth has started. These holograms were generated every few seconds. The holographic data disadvantage is that it cannot be examined until the mission is over. This was the first time holograms have been made in space and we were not sure that the system would produce good holograms in space, because of a number of considerations that were not possible to test in the earth's environment.

Figure 5 summarizes the observations made with the holographic system. The system worked almost flawlessly for the entire flight, with hundreds of holograms and many hours of video tapes made. There are tremendous amounts of data which we are just beginning to analyze. A bonus that was not expected was the observation of free-floating crystals. These crystals could also be used for measurements. Refractive index changes and the effects of accelerations on these were observed. The concentration and, consequently, the refractive index around the crystal should be symmetrical and uniform for proper crystal growth. Acceleration was observed to push this back and forth and make the concentration nonsymmetrical. In some cases, impulses, dumps, or large motions (accelerations) were indicated by the crystals making large movements in short periods of time.

The crystal is shown in Figure 6, and the rays of light pass through the zone of concentration gradients. As the concentration increases, as during crystal dissolution, the rays will be bent toward the increasing refractive index. As the crystal grows, the region immediately surrounding it is depleted, and the refractive index decreases, so that the light ray coming through that zone gets blocked. The closed-circuit television camera shows a picture of the crystal and the surrounding zone of different concentration.

The lower portion of Figure 6 shows the effects of acceleration on the differing concentration region. During null acceleration, you see a more or less symmetrical dark region. The figure on the right shows the rays that have been bent and moved out of the field. A free-

OBSERVATIONS

* SUSPENDED CRYSTAL MOTION (FLOATERS)
* REFRACTIVE INDEX FIELD CHANGES
* UNSYMMETRICAL REFRACTIVE INDEX FIELD
* CONVECTIVE MOTION PERSISTING FOR HOURS
* IMPULSES EASILY OBSERVED
* MICROGRAVITY AND SMALL VARIATIONS MORE DIFFICULT

FIGURE 5

SPACELAB 3 OPTICAL DATA- SCHLIEREN

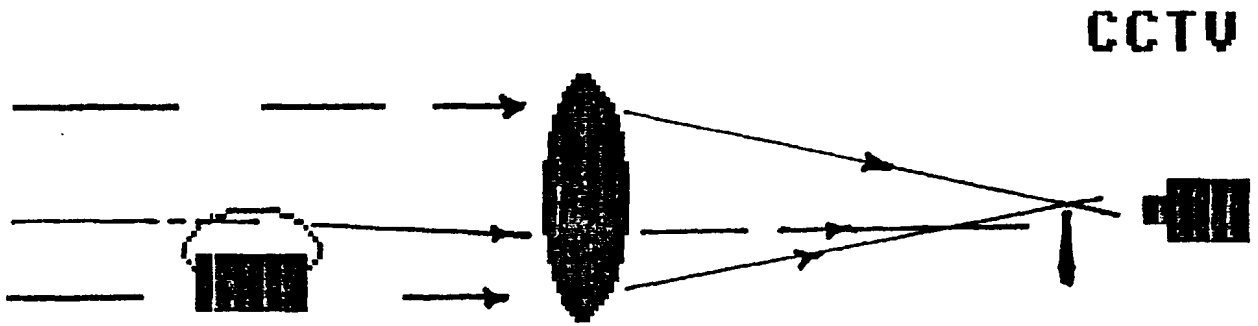

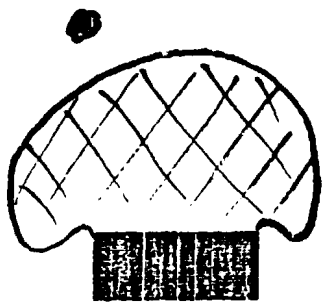

NO ACCELERATION

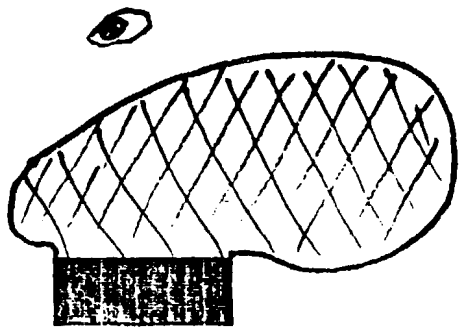

ACCELERATION

FIGURE 6

floating particle would be similar. It would be a small spherical blob that is surrounded by a dark region because a free-floating crystal is also growing. Under acceleration one may observe quite drastic movement of the plume off to one side, and the free-floating crystal would move with the appearance of a comet. It would drag the region of lower refractive index at a different velocity.

Figure 7 shows an actual picture from the closed-circuit TV screen. You are looking through the cell and can see the crystal and the plume. This was early in the experiment, when the acceleration was low and significant acceleration effects are not observed. Later, it becomes extremely difficult to analyze the data quantitatively. One must make some assumptions about symmetry. Once the field moves to the side, it becomes impossible to know what the symmetry is, the data cannot be analyzed in a quantitative sense.

A similar effect for the holographic interferometry is shown in Figure 8. There were several types of holographic recordings done. The passage of the light beam is again delayed over the crystal and the wavefront is phase-shifted as it passes through the region of different refractive indices. This information is stored on the hologram. The standard interferometry technique is to reconstruct just the starting wave, and mix it with an interferometer reference wave, which gives an inteferogram. For the null-acceleration case, the interferogram has field lines that look symmetrical, and the free-floating crystal is surrounded by a circular set of fringes. At the onset of acceleration, these fringes push off to the side. This can be viewed as a buoyant force pushing the bubble in the opposite direction of the acceleration.

Figures 9 and 10, were made by Bill Witherow of NASA and I think Bob Naumann used a similar set to calculate the g forces taking place as the particle moved. These are double exposure holographic interferograms, and there are a number of things to see in these figures. You can see a free-floating crystal that is sitting on the corner of the TGS crystal, which is no longer a cylinder. It has taken a different shape now. Five hours later the crystal has moved, and two hours after that it has moved even more. Ultimately, it moved out of the field of view.

FIGURE 7.

SPACELAB 3 OPTICAL DATA- HOLOGRAPHY

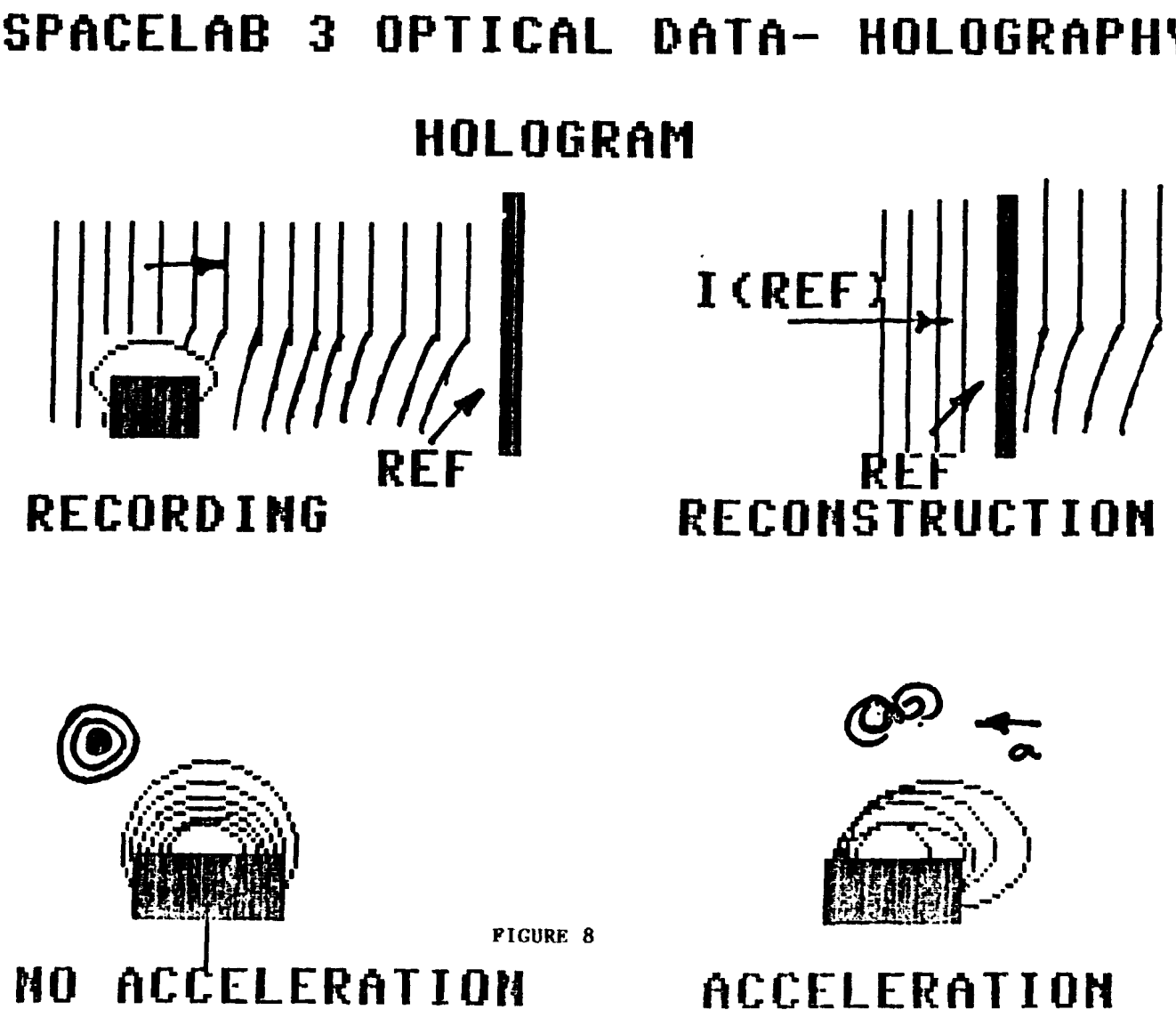

FIGURE 8

MET 79:44:26

MET 84:44:30

MET 86:57:53

MET 87:13:02

MET 89:43:34

DOUBLE EXPOSURE HOLOGRAMS
(FES CELL 203)
SL3

FIGURE 9.

DOUBLE EXPOSURE HOLOGRAMS
(FES CELL 203)
SL3

FIGURE 10.

The crystal is moving extremely small amounts during the time between two exposures. You cannot really see motion of the crystal itself, but you can see the region around it because the change in the concentration produced a set of fringes. There was virtually no change in the crystal itself between these two times, or in the concentration around the crystal, so you see no fringes on some of the figures. In other cases, there is a small change but definitely a concentration gradient change between the two exposures.

I have summarized the consequences of what was seen in Figure 11. The FES experiment is not particularly interested in acceleration, but in convective flow, whether the process is diffusion-controlled or not. There is obviously convective flow that is being measured by several things. This flow will lead to a non-uniform concentration, but the question is: how much? That is yet to be analyzed and modeled, and is presently being done. This potentially would lead to a non-uniform growth. A side effect is that it makes the experiment and analytical calculations difficult, but we have developed an alternate solution.

We have looked at some ideas for measuring acceleration in Figure 12, more specifically, convective flow in the FES. It was a bit of serendipity that the free-floating crystal could be used to measure acceleration. We are considering deliberate seeding of the FES and that will probably be done in the IML-1 experiment. There is a potential problem if you put particles into the flow, in that one of those particles will certainly wind up where it is not wanted. So it would be nice if one could put a dissipative seeding that would not reach the crystal. We considered the possibility of stretching a wire with exposed centers across the fluid, so one could actually add a temperature change, or density gradient, into the flow. One could then add tracer refractive index gradients anywhere in the fluid that could be traced with the Schlieren and the holography systems. Dr. Lal and his team are considering modeling the plume by adding acceleration as a parameter. He and Dr. Wilcox have created a general model for the crystal growth. It can predict what the density gradients or the concentration gradients will be, but it could include acceleration for ultimate use as a measurement tool.

CONSEQUENCES

* CONVECTIVE FLOW OVER CRYSTAL
* NON UNIFORM CONCENTRATION
* NON UNIFORM GROWTH
* ERROR IN ABEL INVERSION OF DATA

FIGURE 11

ACCELERATION MEASUREMENT ON SPACE PLATFORMS

SPECTRON
A TITAN Company

IDEAS FOR ACCELERATION MEASUREMENT

* ADD TRACER PARTICLES-MONITOR MOTION
* ADD TRACER REFRACTIVE INDEX CENTERS
* MODEL EXISTING PLUME RE ACCELERATION
* FIBER OPTIC G SENSOR

FIGURE 12

Bubble mechanics is a subject that has not been treated much in zero g. Think, in the general sense, of a bubble which is a density of one value, within a density of another value, as shown in Figure 13. I have separated this into three effects; acceleration, diffusion, and density. If there is no acceleration, then is there is a diffusion of one density into the other. In this case, there is a diffusion layer that looks like the second picture. So, this bubble essentially grows. In the G-field, the bubble does two things. The center of gravity will move, but the bubble will not hold its shape because of viscous forces and drag. It will be distorted. The bubble in the acceleration field will change shape due to a combination of these effects as shown at the bottom of the figure. Those two effects must be separated in order to use this as a measure. That is a reason to want very small bubbles in the flow field -- their center of gravity would be easier to locate. The distortion effects of the bubble would not play a big role.

We have developed a number of fiber optic sensors (Figure 14) to measure electric fields, magnetic fields, gravitational fields, and flow fields. Basically, the device injects a wave front into the fiber. One of the paths is a fixed leg of the Mach Zehnder interferometer and the other has the sensing element on it. In the case of measuring gravity, there is a mass on that element. Analysis of the phase differs between the two legs, leads to measurable function of acceleration. In the case of a flow field, the drag across the fiber stretches one leg of the Mach Zehnder interferometer. Appendix A shows the simple derived relationship. The longer the fiber, the more sensitive the accelerometer is, and the larger the mass the more sensitive it is. We have not yet demonstrated this for gravitational fields, but we have demonstrated it for electric and magnetic fields. Putting numbers into this equation for some practical geometries, fiber types, and measurement of phase, shows that nano-g sensitivity is achievable.

Figure 15 is a summary of some of IML-1 plans that make use of things that we have learned from Spacelab 3. The IML will seed the flow field, probably with polystyrene spheres, and track the motion to measure acceleration or to measure convective flow. Because of the problem

DENSITY GRADIENT IN A G FIELD

-BUBBLE MECHANICS-

ZERO-G DIFFUSION-DISTORTION-CG MOTION

COMBINATION OF ABOVE

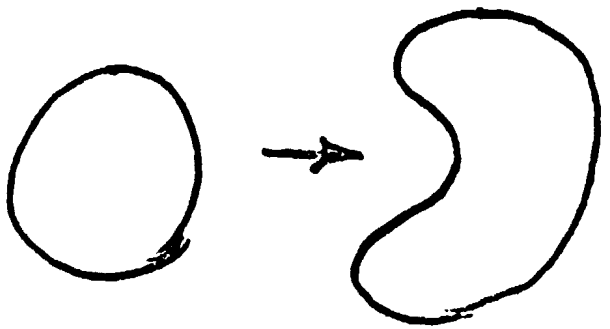

FIGURE 13

FIBER OPTIC G-SENSOR

* OPTICAL FIBER STRETCHED ACROSS FLUID
* FIBER LENGTH OR POSITION CHANGED BY ACCELERATION
* FIBER SENSOR IS ONE BRANCH OF A MICHELSON INTERFEROMETER
* ATTAINABLE SENSITIVITY 10^{-9} G

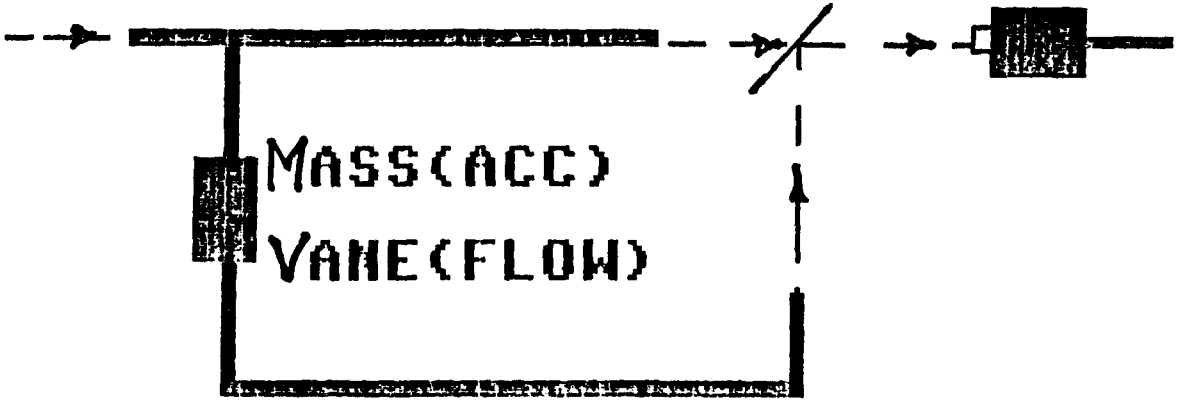

FIGURE 14

ACCELERATION MEASUREMENT ON SPACE PLATFORMS

SPECTRON
A TITAN Company

IML-1 PLANS

* SEED FES WITH POLYSTYRENE SPHERES
* TRACK SPHERE MOTION
* THREE VIEWING ANGLES
* MEASURE CONVECTIVE FLOW

HOE

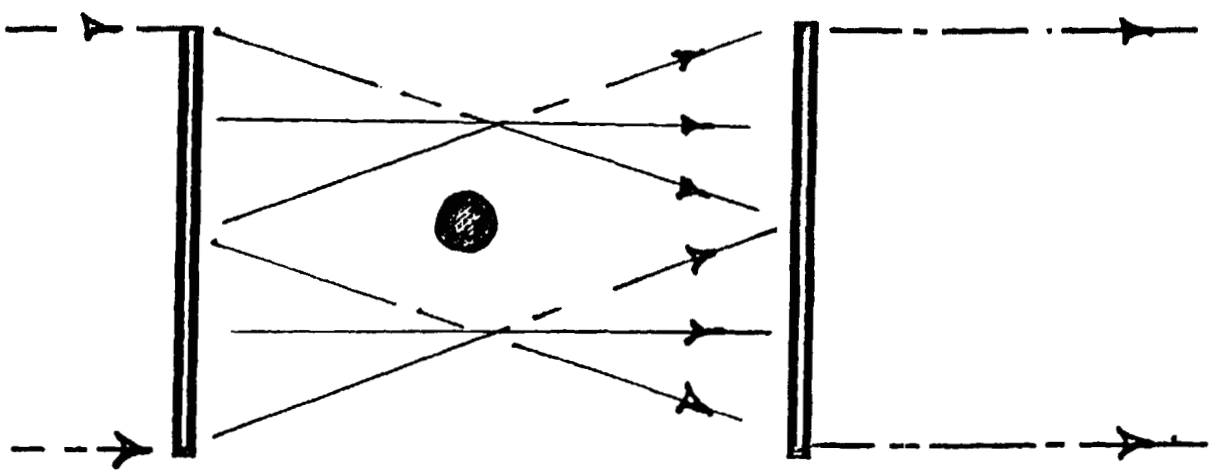

FIGURE 15

that is now known as non axi-symmetry in the growth field, there are plans to look across the crystal at a number of angles so that this can be compensated. We have tomography equations that are reasonably accurate for views across the crystal at $\pm$15 degrees, providing a full three-dimensional density distribution.

We will use a holographic element on one side of the crystal to split the beam into three beams across the crystal and another one on the opposite side to recombine the beams. This will also help to track particles in three dimensions, and it will give a higher resolution.

Ken Demel, NASA/Johnson Space Center: Do you have any quantitative correlations between displacements and accelerations?

Trolinger: As far as I know the only calculations that yield hard numbers on gravity are those by Bob Naumann. We haven't actually modeled the flow field or any of the density gradients to try to do this yet.

John Williams, the Center for Space and Defense Technology: Early in the FES program we talked in terms of a performance parameter on being able to detect the change in index of refraction of 10^{-5} or so. Do you have a feel for where we stand now as far as detection sensitivity?

Trolinger: I think we met all of those specifications. Among others, I was surprised at how well the system really worked. The holography system and holographic interferometry system was extremely rewarding in how well the data is coming out. There are some problems here and there, but basically I think most of the specifications of the original design were met.

Lodewijk van den Berg, EG&G: I have a flippant answer to that but it's of course due to the extreme care taken by the people that were operating the equipment (Dr. van den Berg was the payload specialist for this experiment). In all these extraneous motions that you saw in the solution, is it possible to track those motions in the quality of the crystal that was obtained? In other words can you see the dif-

ferent regions in the crystal that are damaged by these motions or is the crystal just homogeneous throughout, in other words, this kind of much lower than 1-g motions, did it have an effect on the crystal?

Trolinger: I will call on Ravi Lal to answer since he has the crystal.

Lal: We cannot, at the present time, correlate the motions observed in the solution due to the disturbances with the defects in the grown crystal. However, we have found different amounts of growth at different locations of the seed. This is an anomaly and can only be attributed to time-periodic growth rate.

Question: Did you take the motion of the free-floating crystal around the fixed crystal to calculate the local gravity gradient?

Trolinger: The question was were we assuming the gravity gradient background to calculate the motion of the particle. Bob Naumann's answer is yes.

Bob Naumann, NASA/Marshall Space Flight Center: I'm not quite sure that the calculations agree properly. We still have work to do on that.

Byron Lichtenberg; Payload Systems, Inc: Could the free-floating crystals explain the distorted concentration?

Trolinger: The data shown for the free-floating crystal was from one cell. The third cell, from which the interferometry data was shown, actually did not have any free-floating crystals, so you really couldn't explain that with distortion. There would be some distortion, certainly, by the free-floating crystal. Also those free-floating crystals were only present during a small part of the mission. Ultimately a larger acceleration would scoot those things off to the side and they would be completely out of the field of view. Also there were some actual correlations, especially with the water dump near the end of the mission. That was postponed as long as possible. The plume was sitting there, and when that occurred, it just swooshed over. So accelerations were actually correlated with some of the gradients in concentration.

APPENDIX A

A SENSITIVE FIBER-OPTIC ACCELEROMETER

K. A. Arunkumar
Spectron Development Laboratories, Inc.
3303 Harbor Blvd., Suite G-3
Costa Mesa, California 92626
(714) 549-8477

Abstract

A sensitive fiber-optic accelerometer which can measure accelerations down to nano-g's has been proposed.

The Proposed Accelerometer

Fiber-optic interferometric accelerometer with μg sensitivity has been demonstrated by Tveten.[1] In this communication, we propose a simple method to improve its sensitivity by at least a couple orders of magnitude. The accelerometer in reference 1 employs axial stretching of one of the arms of an all fiber Mach-Zehnder and the measured phase difference $\delta\phi$ is related to the acceleration by

$$\text{Acceleration } a = \frac{\lambda r^2 Y}{2m2L}\,\delta\phi \qquad (1)$$

where r, 2L and Y are the radius, length, and Young's modulus of the fiber, respectively, and m is the mass undergoing acceleration.

Accelerations can also be measured when the moving mass bows one arm of the interferometer instead of stretching it axially (transverse accelerometer), see Figure 1.

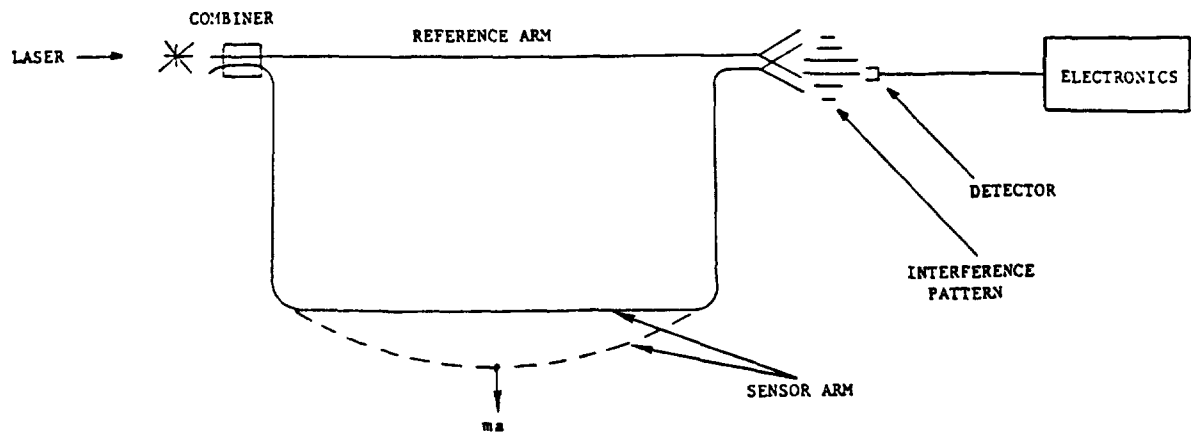

Fig. 1. Schematic of the Proposed Accelerometer

KAA-26/19

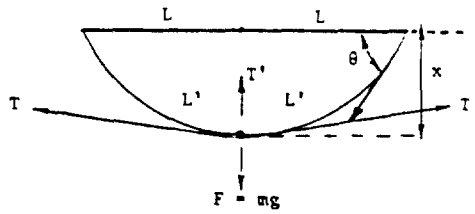

Figure 2. Fiber Bowing When Subjected to Acceleration

Analysis

For small displacement y, the phase difference

$$\delta\phi = \frac{4\pi}{\lambda}\left[\sqrt{x^2 + L^2} - L\right] \text{ and } x = \left(\frac{L\lambda}{2\pi}\right)^{1/2} \delta\phi^{1/2}$$

Under equilibrium conditions, $F = T' = 2T \sin\theta$ where T is the tension in the fiber. Using the definition for Young's modulus, $\delta\phi$ can also be expressed as

$$\delta\phi = \frac{2\pi}{\lambda}\frac{2L}{Y}\frac{T}{\pi r^2}$$

Combining the above relations, we have for the phase difference

$$\delta\phi = \frac{2\pi}{\lambda}\frac{2L}{Y}\frac{F}{2x}\frac{\sqrt{x^2 + L^2}}{\pi r^2} \quad \text{and for}$$

acceleration

$$a = \left(\frac{\lambda}{2\pi L}\right)^{3/2} \cdot \frac{Y}{m} \cdot \pi r^2 \cdot (\delta\phi)^{3/2} \tag{2}$$

where it is assumed that $L = L'$ for $y \ll L$.

Discussion

A 10 kg mass undergoing 9.8×10^{-6} m/sec^2 (μg) acceleration can cause a $\delta\phi \sim 1.4 \times 10^3$ rad when a fiber of active length 1m and $r = 2\mu$ is stretched longitudinally (axial accelerometer). Under the same condition, transverse stretching (bowing) results in a phase shift of 1.36×10^4, an order of magnitude greater than the former. This property of the latter will be helpful while measuring ng (nano-g) accelerations.

Under ng acceleration, the axial accelerometer will produce a phase shift of 1.414 rad whereas the transverse accelerometer will induce a $\delta\phi$ of 135.6 radians. The phase change detection technique for the latter can be much simpler than that to be used for the former. Moreover, acceleration measurement using the fiber bowing technique can greatly simplify the experimental setup.

Reference

A. B. Tveten, A. Dandridge, C. M. Davis, and T. G. Giallorenzi, Electron. Lett., Vol. 16, pp. 854-855, 1980.

7. MICROGRAVITY AND ITS EFFECTS ON RESIDUAL MOTIONS IN FLUIDS

J. Iwan D. Alexander* and Charles A. Lundquist**

ABSTRACT

The primary reason for conducting many materials science experiments in space is to minimize or eliminate undesirable effects that might result owing to convective motions in fluids that are driven by buoyancy effects. Of particular concern are the low frequency accelerations caused by the Earth's gravity gradient field, spacecraft attitude motions, and atmospheric drag. In order to gain a limited understanding of the effects of these accelerations we have calculated the Stokes' motion of a spherical particle in a fluid for various types of spacecraft attitudes. In addition, we have assessed the effect of slowly rotating the experimental system relative to the spacecraft in order to reduce the rate at which the particles accumulate against the container wall.

NOMENCLATURE

q_{K*} - position of the spacecraft mass center with respect to the geocentric inertial frame.

x_{K*} - position of the particle with respect to the origin of the geocentric inertial frame.

x_K - position of the particle with respect to the origin of the spacecraft frame.

x_k - position of the particle with respect to the origin of the experimental frame.

R_{kK} - rotation of the spacecraft frame into the experimental frame.

A_{KK*} - rotation of the geocentric frame into the inertial frame.

G_{kK} - Gravity gradient tensor expressed in terms of the experimental frame.

*USRA Visiting Scientist, NASA/MSFC
**Director of Research, University of Alabama in Huntsville

$q = G_c M_e$, where G_c is the gravitational constant, and M_e is the mass of the earth.

ω_b - angular speed of the spacecraft.

$\alpha = 4.5\ \mu/\rho_s \omega_b R^2$, is the dimensionless Stokes coefficient.

$\delta = (\rho_s - \rho_f)/\rho$ is the buoyancy coefficient.

$\bar{\rho} = \rho_s - (\rho_f/2\rho_s)$.

R - radius of the particle (assumed to be small compared to the size of the experimental system).

μ - fluid viscosity.

ρ_s - particle mass density.

ρ_f - fluid mass density (assumed to be constant)

1. INTRODUCTION

The accelerations experienced within experimental systems aboard orbiting spacecraft occur over a broad range of frequencies. Of particular concern to materials scientists are the low frequency accelerations since it is known that these can give rise to sustained fluid motion[1,2,3]. Sources of residual accelerations include the effects of the Earth's gravity gradient tides, spacecraft motions, and atmospheric drag, to the higher frequency "g-jitter" caused by machinery vibration, cooling systems, spacecraft vibrations, and ephemeral disturbances such as crew motions and thruster firings.

In order to improve our understanding of the effects of some of the low frequency accelerations (for certain types of spacecraft attitude there will be steady accelerations) we examine the Stokes motion of a spherical particle subject to the effects of the earth's gravity gradient field, atmospheric drag, and spacecraft attitude motions. In addition, we also investigate the possibility that the residence time of a particle in a given region of the fluid may be increased by a continuous rotation of the experimental system relative to the spacecraft. It is assumed that the fluid is "spun up".

For an experiment aboard a spacecraft in gravity gradient stabilized attitude it is found that rotations of the experiment at rates corresponding to twice, and one-half the orbital rate can substantially reduce the extent of the particle motion relative to the experimental frame of reference. The most effective rotation appears to be about an axis perpendicular to the orbital plane, at twice the orbital rate, and in the opposite sense to the direction of motion of the spacecraft.

2. FORMULATION

2.1 Frames of Reference and Coordinate Systems

We shall refer to three frames of reference in this work (see Figure 1). The first is an inertial geocentric frame, the second is a moving frame which is rigidly attached to the spacecraft and may rotate with respect to the inertial frame. The third frame is the experimental frame which is free to rotate with respect to the spacecraft. Each frame of reference will be characterized by a cartesian coordinate system such that the position of a particle at time t will be denoted by either $\tilde{x}_k$, $\tilde{x}_k$, or $\tilde{x}_{K*}$, k, K, K* = 1,2,3, where a miniscule subscript refers to the spacecraft frame and an asterisk superscript on a majescule subscript refers to the geocentric inertial frame.

It is convenient to formulate this problem in terms of nondimensional variables[3]. Distance is scaled using a_o, the initial value of the osculating semi-major axis* of the spacecraft orbit, and to scale time using $(\gamma/a_o^3)^{1/2}$ which physically corresponds to the angular speed, ω_o, of the spacecraft in a circular orbit of radius a_o. An additional length scale "d", a characteristic distance within the spacecraft, is also used which is used to scale distance within the spacecraft. The dimensionless variables and parameters are:

$$x_{K*} = \tilde{x}_{K*}/a_o, \quad q_{K*} = \tilde{q}_{K*}/a_o, \quad t = \tilde{t}(\gamma/a_o^3)^{1/2}$$

$$\epsilon\, x_k = A_{kK*}(x_{K*} - q_{K*}), \quad \epsilon = d/a_o \ll 1. \tag{1}$$

*Since the spacecraft is subject to an atmospheric drag force the spacecraft gradually spirals in toward the earth. As a result the orbital elements cannot be defined in the usual sense. The instantaneous values of these elements are referred to as the osculating elements.

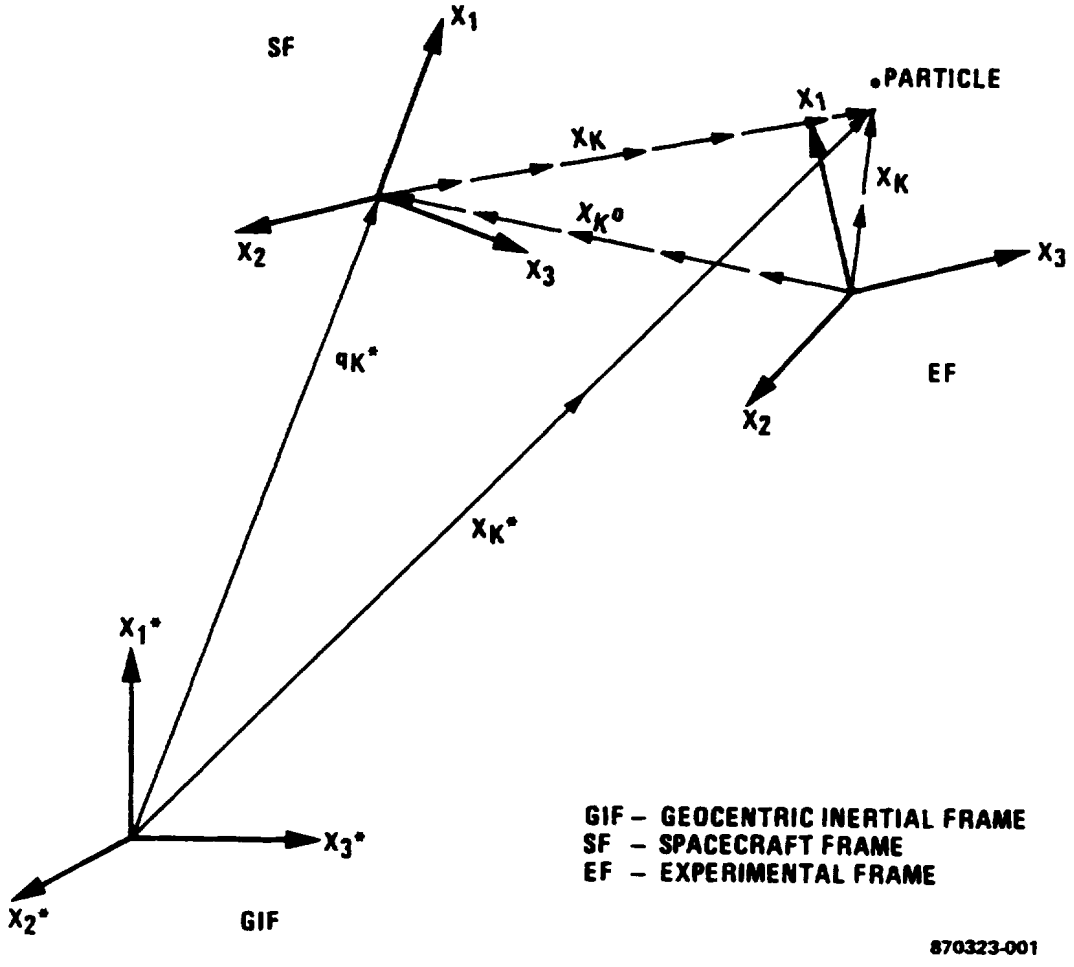

FIGURE 1. FRAMES OF REFERENCE

2.2 The Gravity Gradient

The body force acting on a particle at $k_{K*}(t)$ is taken to be

$$F_{K*}(x_{K*}) = - (1/r^3)x_{K*}, \quad K^*, = 1,2,3, \tag{2}$$

where

$$r^2 = x_{M*}x_{M*}. \tag{3}$$

Similarly, the body force acting at the mass center of the spacecraft is assumed to be

$$F^o_{K*} = - (1/r_o^3)q_{K*}, \quad K^*, = 1,2,3, \tag{4}$$

where q_{K*} is the position of the mass center of the spacecraft in the geocentric inertial frame.

$$r_o^2 = q_{M*}q_{M*}. \tag{5}$$

If $x_{K*} - q_{K*}$ is small, we can expand (2) in a Taylor series about $x_{K*} = q_{K*}$ and obtain

$$F_{K*} = F^o_{K*} + \epsilon\, G_{K*M*}A_{mM*}x_{m*} + O(\epsilon^2), \quad K^*, = 1,2,3, \tag{6}$$

where

$$G_{K*M*} = DF_{K*}(q_{M*}), \quad K^*, \; M^* = 1,2,3, \tag{7}$$

is the gravity gradient tensor. It can be shown that[3,5]

$$G_{K*M*} = - (1/r_o^3)I_{K*M*} + (3/r_o^3)e_{K*}e_{M*}\ , \tag{8}$$

where $e_{K*}(t)$ is a unit vector parallel to q_{K*}, and I_{K*M*} is the identity tensor.

In the experimental frame of reference the gravity gradient force can be expressed as:

$$G_{km}(x_m - x^o_m) = R_{kK}A_{kK*}G_{K*M*}\,(x_{M*} - q_{M*}), \tag{9}$$

where $R_{kK}A_{kK*}$ is the rotation of the geocentric inertial frame into the experimental frame about an axis passing through the origin of the experimental frame.

2.3 Equations of Motion for a Spherical Particle Subject to a Stokes Drag

The accelerations, relative to the experimental frame experienced by the particle, are given by[3,7]

$$\frac{d^2x_k}{dt^2} = \delta F(b)_k + \alpha \frac{dx_k}{dt} \tag{10}$$

where δ is the buoyancy coefficient that includes the effects of added mass, α is the dimensionless Stokes' coefficient, and $F^{(b)}{}_k$ is the effective buoyancy force given by

$$F^{(b)}{}_k = \left(\frac{dQ_{km}}{dt} + Q_{kp}Q_{mp}\right) x_m + 2Q_{km}\frac{dx_m}{dt} + R_{kK}\ 2W_{KM}R_{KM}\frac{dx_m}{dt} + \left(W_{KP}W_{MP} + \frac{dW_{KM}}{dt}\right) R_{mM}\,(x_m - x^o{}_m) + G_{km}\,(x_m - x^o{}_m) = f^{(d)}{}_k, \tag{11}$$

where Q_{km} and W_{KM} are skew tensors that represent the rates of rotation of the experimental frame with respect to the spacecraft frame and the rate of rotation of the spacecraft frame to the geocentric inertial frame. It is implicit in the above equations that we have neglected the "history integral" which appears in the Basset-Boussinesque-Oseen equations[7].

The above equations together with the initial conditions:

$$\frac{dx_k}{dt} = 0,\ x_k = X^o{}_k \tag{12}$$

were solved numerically for various values of the parameters δ and α, and for different rotations of the experimental system relative to the spacecraft, with the orbital parameters given in the appendix.

3. RESULTS

Selected results of our calculations are presented in Figures 2 and 3. For the cases in which the experiment was rotated relative to the spacecraft the axis of rotation passed through the origin of the

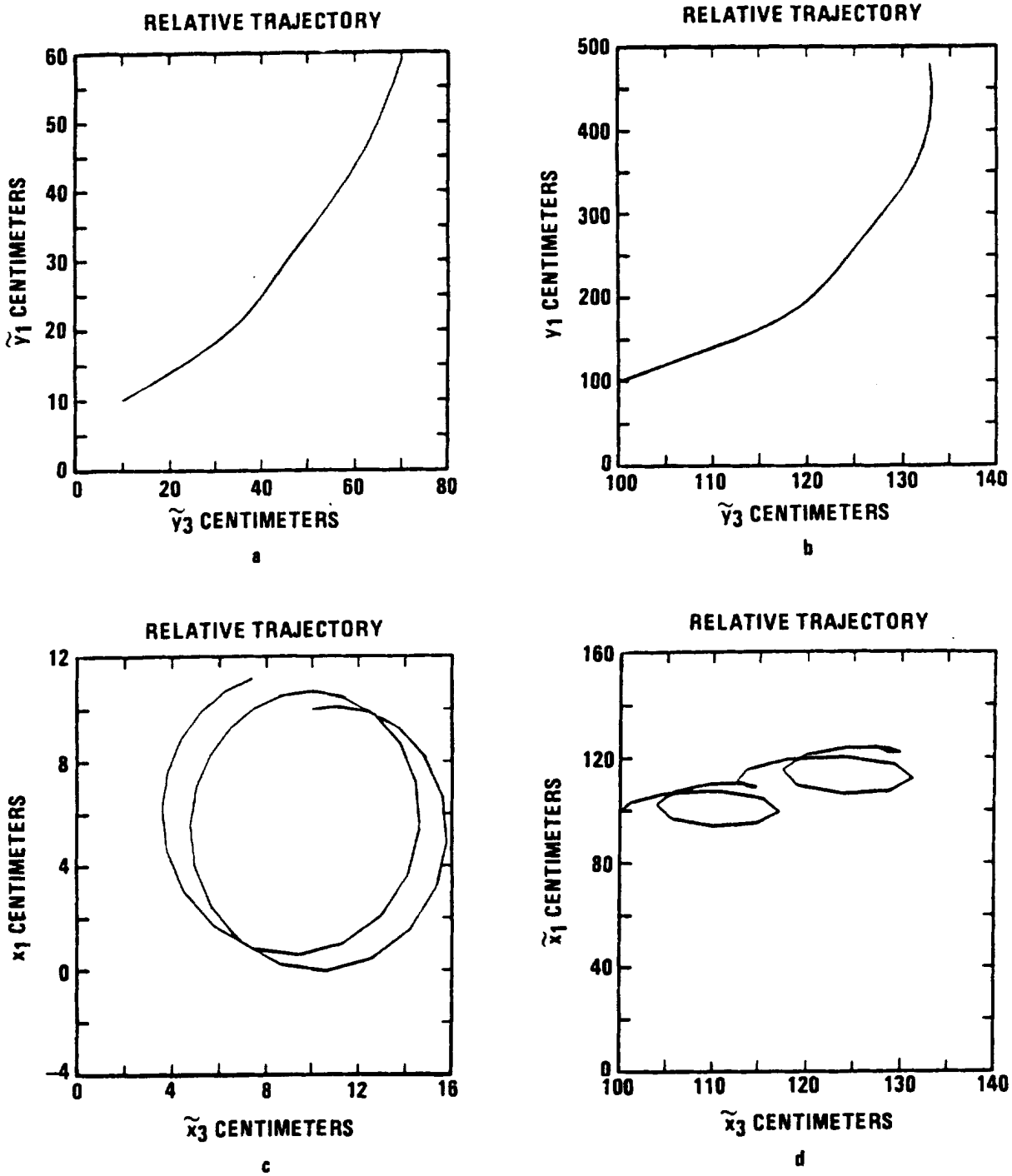

FIGURE 2. PARTICLE TRAJECTORIES; a, b - RADIAL FRAME
c, d - INERTIAL FRAME

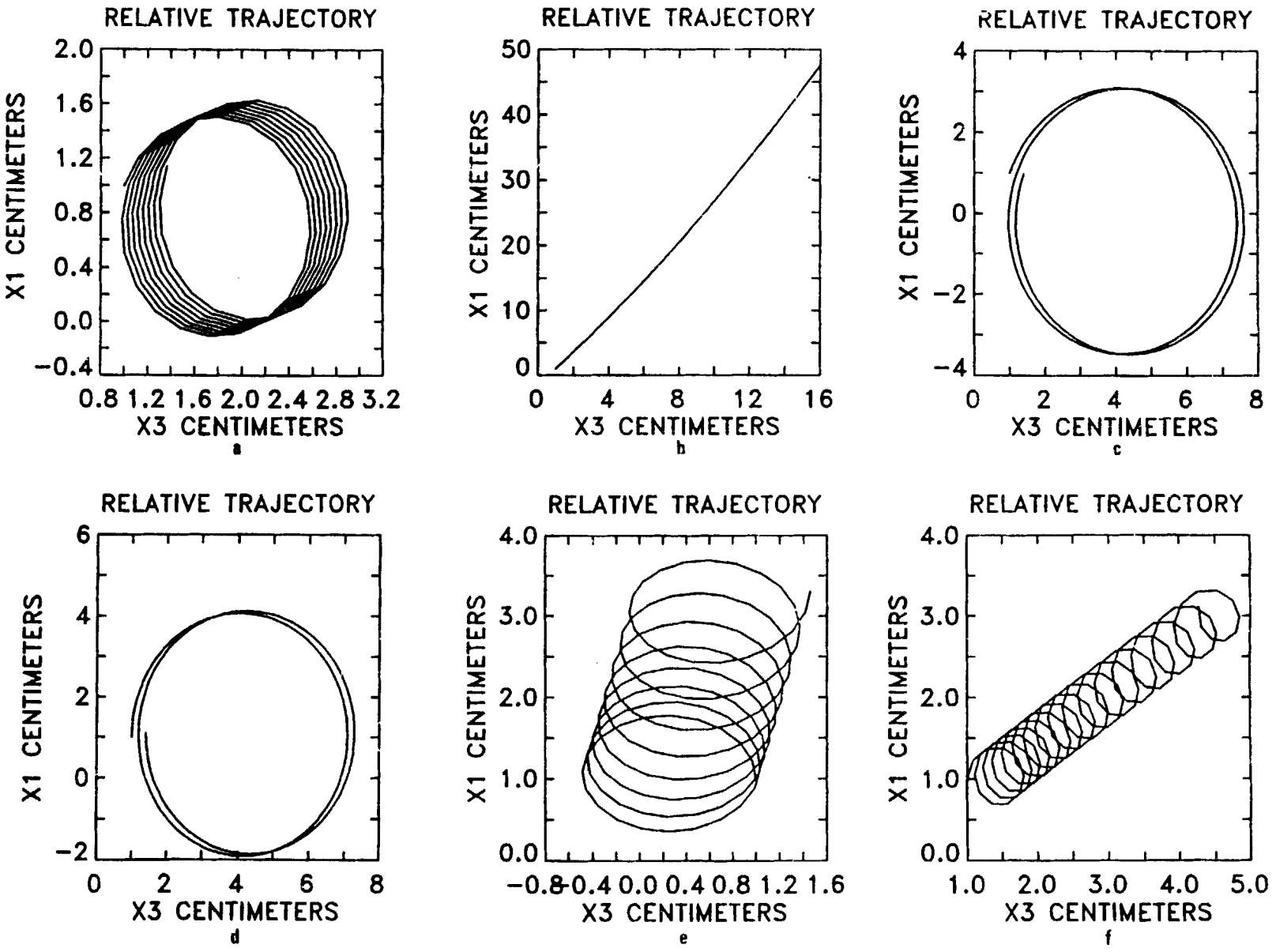

FIGURE 3. PARTICLE TRAJECTORIES: EXPERIMENTAL FRAME

experimental frame of reference and was oriented perpendicular to the orbital plane. Each trajectory is shown as seen by an observer in the experimental frame of reference.

Figure 2 depicts particle trajectories for particles subject to Stokes drag. The dimensionless Stokes coefficient is 20 and the buoyancy coefficient is 0.82 (physically this would correspond to a steel ball of radius 0.25 cm in water). The spacecraft is subject to atmospheric drag. The origin of the experimental frame of reference is taken to coincide with the mass center of the spacecraft. The initial velocity is zero. For Figures 2a and 2b the spacecraft is in a gravity gradient stabilized attitude and hence the spacecraft frame rotates with respect to the geocentric inertial frame. For Figures 2c and 2d the spacecraft frame does not rotate with respect to the geocentric inertial frame (as would occur in the case of the solar inertial attitude).

a) $x_k(0) = (10,0,10)$cm,
b) $x_k(0) = (100,0,100)$cm,
c) $x_k(0) = (100,0,100)$cm
d) $x_k(0) = (10,0,10)$cm

Figure 3 shows trajectories of particles relative to the experimental frame of reference. The origin of the experimental frame of reference is taken to be at $x_k = (1,0,1)$m from the spacecraft mass center. The dimensionless Stokes coefficient is 100, the buoyancy coefficient is 0.5. The initial velocity was zero. The initial position of the particle in the experimental frame is (1,0,1) cm. The motion was calculated for four orbits of the spacecraft about the earth (approximately six hours).

a) Relative rate of rotation: $-2.0\ \omega_0$
b) Relative rate of rotation: 0.0
c) Relative rate of rotation: $-0.5\ \omega_0$ (no atmospheric drag)
d) Relative rate of rotation: $-0.5\ \omega_0$
e) Relative rate of rotation: $2.0\ \omega_0$
f) Relative rate of rotation: $-4.0\ \omega_0$

4. CONCLUSIONS

The residual accelerations associated with the gravity gradient, centrifugal accelerations, Euler accelerations*, and atmospheric drag forces can cause sustained motions in fluids. For a spherical particle immersed in a viscous fluid the residence time of that particle in a given region of the fluid can be increased substantially by an appropriate rotation of the experimental frame relative to the spacecraft frame. The most effective choices of rotation were twice and half the angular speed of the spacecraft. The best was at twice the orbital rate in the opposite sense to the direction of motion of the spacecraft.

5. REFERENCES

1. Langbein, D. "Allowable G-levels for Microgravity Payloads," to be published, European Space Agency Journal, 1986.

2. Kamotani, Y. Prasad, A., and Ostrach, S., AIAA Journal, 19, 511-516, 1981.

3. Alexander J.I.D., and Lundquist, C. A., "Residual Motions Caused by Microgravitational Accelerations," MSFC Space Science Lab. preprint ser. no. 86-132, to be published in Journal of the Astronautical Sciences., 1986.

4. Bauer, H. F., ZFW, 10, 22-33, 1986.

5. Forward, R.L., Phys. Rev. D, 26, 735-744, 1982.

6. Lundquist, C. A., AIAA Guidance and Control Conference Proceedings, August 15-17, paper no. 83-2261, 665, 1983.

7. Monti, R., Techno-systems Rep. no TS-7-84, Technosystems Developments, Napoli Italy.

8. Basset, A. B., "A treatise on Hydrodynamics," 2, p. 291, Dover, 1961.

9. Sterne, T. E., "An Introduction to Celestial Mechanics," p. 206, Interscience, N.Y., 1960.

10. Mullins, Aerodynamic Design Databook, Vol. 1, Orbiter Vehicle, SD-732-sh-0060-1k, Rockwell Int., Nov. 1977.

*Apparent accelerations in a rotating frame resulting from a non-constant rate of rotation.

APPENDIX

The spacecraft orbits were calculated using the following parameters:

$$a_o = 6688 \text{ km}, \quad C_D A/2m = 1.02(10)^{-2},$$

where C_D is the drag coefficient, A is the effective cross section area, and m is the mass of the spacecraft. We determined the values of C_D and A appropriate for the space shuttle for the orbits under consideration using data from Mullins[10]. The initial osculating eccentricity was taken to be $(10)^{-6}$. The atmospheric density is a function of altitude. We used a model atmosphere discussed by Sterne[9] and used by Alexander and Lundquist[2].

37th International Astronautical Congress. Innsbruck, Austria.
Oct 4-11, 1986. Paper IAF-86-268.

8. THE MICROGRAVITY ENVIRONMENT OF THE D1 MISSION

H. HAMACHER[1], U. MERBOLD[2], R. JILG [1]
[1] Deutsche Forschungs- und Versuchsanstalt für
Luft- und Raumfahrt e.V. (DFVLR), Köln, FRG
[2] European Space Agency (ESA), Paris, France

Abstract

Some characteristic features and results of D1 μg-measurements are discussed as performed in the Material Science Double Rack and MEDEA. Starting with a brief review of main potential disturbances, the payload aspects of interest to the analysis and the accelerometer measuring systems are described. The μg-data are analysed with respect to selected mission events such as thruster firings for attitude control, operations of Spacelab experiment facilities, vestibular experiments and crew activities. The origins are divided into orbit, vehicle,and experiment induced perturbations. It has been found that the μg-environment is dictated mainly by payload-induced perturbations. To reduce the μg-level, the design of some experiment facilities has to be improved by minimizing the number of moving parts, decoupling of disturbing units from experiment facilities, by taking damping measures, etc. In addition, strongly disturbing experiments and very sensitive investigations should be performed in separate mission phases.

1. Introduction

The Spacelab Mission D1 was primarily dedicated to carry out experiments which made use of the low level of gravitation aboard an orbiting spacecraft. Although reduced by several orders of magnitude compared to 1g on ground, the residual microgravity (μg-)level still affects physical processes in very individual ways [1]. Hence, the knowledge of the actual μg-environment during the processing time is an important basis for the final scientific analysis of the results. In contrast to the steady-state gravitational field on earth, the μg-vector field aboard a spacecraft is characterized (i) by a steady-state dc component and (ii) by a fluctuating ac contribution called g-jitter, being inherently local and statistical in nature with peak values usually far above the level of the dc component.

To measure the microgravity history achieved during D1, various payload elements were equipped with accelerometer packages. Figure 1 shows on the starboard and the portside of the payload locations and measurement axis of the accelerometers installed [2]. The knowledge of the actual μg-environment is also an important basis to examine and improve the design and operational concept of the payload.

In this paper characteristic features and results of μg-measurements are presented as performed in the Material Science Double Rack (MSDR) and in MEDEA. Starting with a brief review of main potential disturbances, the payload aspects of interest to the analysis and the accelerometer measuring systems will be described. This is followed by the discussion of μg-data with respect to their potential causes.

2. Causes of Main Disturbances

It is one of the unique possibilities of space flight that a freely orbiting spacecraft offers a virtually zero-gravity state to its interior objects without time limitations by trajectory kinematics. For the spacecraft center of mass (CM), the gravitational force is balanced by the centrifugal force. Zero gravity, however, is an ideal state that cannot be accomplished completely in a real spacecraft due to a number of deviations from the model of a freely drifting mass point. The residual μg vector field may be described by

$$\vec{a} = \Sigma\ (\vec{a}_s + \vec{a}_{tr})$$

where $\vec{a}_s$ and $\vec{a}_{tr}$ are a quasi steady and a transient vector, respectively. $\vec{a}_s$ has a frequency typical of the order of the orbital frequency. $\vec{a}_{tr}$ is characterized by a wide spectral range of frequencies large in comparison with that of $\vec{a}_s$.

2.1 Quasi Steady Accelerations

2.1.1 Atmospheric Drag

Due to e x t e r n a l forces, mainly the residual atmospheric drag, the orbiter is not in a freely drifting state, giving rise to a quasi s t e a d y acceleration a_d of the CM, acting opposite to the orbital velocity vector [3]. The level of a_d versus altitude as predicted for various orbiter flight modes is depicted in Fig. 2. For the D1 nominal flight altitude of 324 km, a maximum of $a_d \cong 1 \cdot 10^{-6} g_o$ (g_o = 9.81 ms^{-2} the gravitational acceleration on ground) is expected for the flight mode with the largest projected cross-sectional area [4]. As a result of the atmospheric density variations along one orbit there is always a pulsation of twice the orbital frequency [5].

2.1.2 Gravity Gradient Effects

For objects located off CM gravity and centrifugal forces are no longer balanced completely, giving rise to a "tidal acceleration" a_t which is proportional to the displacement r from CM (Fig. 3). In case of 324 km altitude and Gravity Gradient Mode yields [3]

$$a_t = 1.36 \cdot 10^{-7}\ g_o\ [m^{-1}] \begin{pmatrix} 0 & 0 & 0 \\ 0 & -1 & 0 \\ 0 & 0 & 3 \end{pmatrix} \begin{pmatrix} x \\ y \\ z \end{pmatrix}$$

Figure 4 shows the location of the MSDR and MEDEA with respect to the total CM. Based on a typical displacement of $r \leq 2{,}5$ m it may be stated that a_t is always below $10^{-6}\ g_o$.

2.1.3 Orbiter Rotation

Orbiter rotation for attitude changes were performed by rotation rates $\omega_r \leq 0.2$ deg/sec, resulting in a centrifugal acceleration at r = 2.5 m of

$$a_c = r\omega_r^2 \leq 3.1 \cdot 10^{-6} g_o.$$

This steady acceleration $\vec{a}_c$ is always superimposed by the tidal vector $\vec{a}_t$ which rotates relative to $\vec{a}_c$ by $2 \cdot \vec{\omega}_r$. The magnitude of the quasi steady vectors are depicted in the g/g_o vs frequency plot Fig. 5. It follows that the magnitude of $\vec{a}_c$ may exceed both the drag and the tidal acceleration. The only existing measurement value of the quasi steady component results from an analysis of the path of a freely floating particle. It was recorded by the Fluid Experiment System FES during SL-3 [5]. This value conforms fairly well with the predictions of drag and tidal acceleration.

2.2 Transient Accelerations

A variety of transient external and internal forces give causes to transient accelerations, resulting in exitations of the spacecraft flexibility modes. The induced g-j i t t e r are characterized by a wide frequency spectrum. Transient e x t e r n a l forces may result from operational activities, such as thruster firings for attitude control and extra vehicular activities. These forces in general exert also a torque to the vehicle, resulting in a transient rotational acceleration phase and followed by a quasi steady acceleration period due to a constant rotation around CM.

The mass allocation inside a spacecraft is changing due to the motion of mechanical parts, crew activities, etc., giving rise to i n t e r n a l forces. These forces do not involve a momentum change to the spacecraft CM system. Impulses caused by internal forces are always compensated by equal and opposite impulses with a time delay. Even though the induced g-jitter may reach high peak values, the resulting displacement of particles with respect to the CM is small because of its compensated and random nature.

3. Acceleration Monitoring Systems

The analysis presented in this paper is based on data of the MSDR package and the three-axis sensor of MEDEA (Fig. 1). The technical data are listed in Table 1 [5]. The detection range covered by these systems are indicated in Fig. 5. It may be seen that none of the systems is suited to detect the steady state component.

Table 1: Technical Data of the D1 Accelerometer Systems [2]

	MSDR	MEDEA[1)]
Measurement axis	u, v, w	x, y, z
Detection mode	peak detection	equally spaced time axis
Sampling rate, Hz	1	107
Range, mg	10^{-2} - 10	10^{-1} - 100
Resolution, mg	10^{-3}	$5 \cdot 10^{-2}$
Band width, Hz	0 - 100	0 - 10

1) High Precision Thermostat (HPT) package

The MSDR accelerometer was operated in a peak detection mode to reduce the total amount of data. Peak values within intervals of Δt = 1 sec were detected from an analogue random response in positive and negative direction of the coordinate considered (Fig. 6). The resulting step functions a are the envelopes of the analogue signal. Figure 7 shows a typical reading of the MSDR system. The lowest value detectable by peak detection is determined (i) by periodic vibrations having frequencies higher than the sampling rate, (ii) by steady accelerations and (iii) by a zero point offset. As a result, the data recorded by peak detection do not allow for zero point corrections, calculation of the resultant acceleration vector, and any frequency analysis.

The MEDEA package was operated in a high rate sampling mode, suited to perform frequency analysis up to about 5 Hz.

4. Data Analysis

In the following, examples of different classes of disturbances will be discussed with respect to their causes as identified by correlation with the mission timelines and onboard video recordings. The examples are subdivided into vehicle and experiment induced perturbations, the latter also including those originating from crew activities.

4.1 Orbiter Induced Disturbances

The first series of measurements are orbiter-induced perturbations caused by firing the different thruster systems. Figure 8 shows a MSDR reading taken during the firing of the Vernier Thruster System (VRCS), being part of the Reaction Control System (RCS). The Vernier Thrusters serve to initiate and to stop orbiter rotation for attitude changes. The spikes induced are of the order of 1 mg. The number of attitude maneuvers necessary during a mission depends on the kind of experiments aboard Spacelab. In a microgravity oriented mission the orbiter is flown preferably in the gravity gradient stabilized attitude with a minimum of thruster firings needed. As given in the as-flown timeline of D1 [6], 29 % of the SL-activated time have been flown in the Gravity Gradient Mode within five time phases lasting between 7 1/2 and 12 hours each. The comparison with SL-1 with 4 % in Gravity Gradient Mode reflects the µg-dedicated character of D1 and the multidisciplinary nature of SL-1.

The second group of thrusters incorporated in the RCS are the Primary Thrusters (PRCS) utilized for velocity changes, docking maneuvers, etc. Firings of the PRCS are rather rare events during a mission. Figure 9 shows the test firing prior to the descent as recorded by the MEDEA system. This series of firings shows highest spikes in z-direction (60 mg) and a decay time of the structural vibration as long as about 11 sec.

4.2 Disturbances by Experiment Operations

The second group of perturbations analysed in this paper are those caused by the payload itself. Starting with vestibular experiments, MSDR perturbations and crew activities will be discussed.

4.2.1 Vestibular Experiments

Vestibular experiments frequently have strong effects on the µg level [7]. Severe disturbances have been detected during the "Hop and Drop" experiments. One of the science astronauts was jumping along the positive z-coordinate while "hopping" and was pulled down to the Spacelab floor by elastic cords. Figure 10 is the time history of a "hop" series as recorded in MEDEA. The dominating response is in the z-axis which was the jump direction. An effective tool for discussing the signals are the corresponding power spectral density (PSD) functions describing the power distribution over the time history of fig. 10. The peak at 1.7 Hz in the z-plane represents the "hop" frequency. The dominating peak at 5 Hz, appearing in all coordinates, indicates the eigenfrequency of the Spacelab module in its suspension.

The second part of this experiment was the "drop" exercise. It was started from a holding of the science astronaut on the upper part of a SL-rack. After the release he was pulled down to the floor by the cords. The time history of a series is depicted in Fig. 12, showing decay times of the order of 6 sec. In the corresponding PSD functions (Fig. 12) a second dominating spike appears between 7 and 8 Hz, which is the eigenfrequency of the rack row in the suspension, excited by the hold of the astronaut.

A second example is the Vestibular Sled Facility consisting of a motor-driven seat and a 4 m runway which is fixed in the Spacelab aisle. Numerous profiles of acceleration to the test person have been carried out, as for example sinusoidal or trapeziform. A record taken in MEDEA during trapeziform acceleration of 200 mg maximum is shown in Fig. 14. The ramp in the x-axis of 0.28 mg average corresponds well to the calculated value for the rigid case. It is interesting to note that the structural vibrations in z-axis exceed temporary x-axis level.

4.2.2 MSDR-Induced Disturbances

Operations of experiment facilities and auxiliary equipment installed in the MSDR naturally have a strong impact on the μg-level detected by the MSDR package. The Fluid Physics Module FPM has been selected as an example to demonstrate the consequences of both the design concept and the operation of a facility on the μg-environment. The FPM induced g-jitter during the operation of rotating and vibrating parts, handling of samples, film changes, etc. For the latter acitivities, the FPM had to be extracted from the rack on telescopic slides. Figure 15 shows a sequence of FPM-induced perturbations. In the first phase, the facility was extracted causing spikes up to full scale. This was followed by a handling period and an operation phase in the oscillation mode generating a relatively uniform pattern. The record taken during the same time phase by the MEDEA system is shown in Fig. 16. Many FPM-induced spikes of the MSDR plot can be correlated with the MEDEA readings. Few of them are indicated by the arrows in Figures 15 and 16.

4.2.3 Crew Activities

From a detailed analysis of the D1 flight video tapes numerous spikes have been identified as a result of crew activities. Two examples are shown in Fig. 17. The spikes exceeding full scale of a_u were generated by closing a container door located in the Spacelab ceiling. The second group of peaks resulted from a Science Astronaut holding to and working at the extracted FPM.

4.2.4 Quiet Phases

The examples discussed are primarily strong disturbing events which are by no means representative for the entire mission. A quiet period, standing for many others of the mission, is shown in Fig. 18 in terms of the magnitude of the resulting vector calculated from MEDEA data.

5. Summary and Discussion

The results of the analysis have been summarized in the g vs f-plot of Fig. 19. Also indicated is the microgravity level recommended for the US Space Station (SS) [3]. In the quasi-steady regime the Spacelab data of the non-rotating case are below the SS requirements [FES, SL-3].
The high frequency regime regime is determined by perturbations generated during the operation of the payload itself with the exception of the PRCS firings which were rather rare events during D1. It may be seen from Fig. 19 that the μg quality can be improved by shifting the vestibular experiments to separate mission phases outside the processing time of sensitive experiments. To further reduce the μg-level, various precautions are possible and necessary. The design concept of some experiment facilities, e.g. the FPM, has to be changed drastically by minimizing the number of moving parts during operation and handling, decoupling of disturbing units (motors, fans) from experiment facilities, by taking damping measures, etc. Moreover, the Science Astronauts should be trained in causing as little accelerations as possible. Another fact, the need for dedicated missions, has been discussed frequently in the past. The D1 Mission was a step in this direction.

In addition to the design and operational precautions, the μg measuring technique aboard Spacelab has to be improved. The peak detection method allows the analysis of transient contributions to the g-jitter and a correlation to their origins. Steady state contributions, however, are hard to identify. This method also suffers from the disadvantage that a possible zero point offset of the system cannot be observed and eliminated from the μg-data, and any frequency analysis is not possible.

Acknowledgement

The authors are indebted to Dr. N. Trappen of DFVLR for his valuable support in processing the μg-flight data.

References

[1] R.J. Naumann, "Susceptibility of Materials Processing Experiments to Low-Level Accelerations", NASA Conf. Publ. 2199 (1981), pp. 63-68

[2] - "Microgravity Environment Acceleration Monitoring Systems of D1-Payload Elements", MBB/ERNO, D1-IN-TN-139-ER (1983).

[3] H. Hamacher, "Simulation of Weightlessness", in "Materials Sciences in Space", edited by B. Feuerbacher, H. Hamacher, R.J. Naumann, Springer (1986), pp 31-51

[4] - "Spacelab Payload Accommodation Handbook", NASA, SPL/2104, Main Vol., Issue 2, Revision 0 (1985)

[5] - "Low Acceleration Characterization of Space Station Environment", Teledyne Brown Engineering, Huntsville (AL), Sp 85-2928, Final Report, Revision B (1985).

[6] - "D1 Timeline As Flown", DFVLR, D1-OP-TN-012-RF (1986).

[7] H. Hamacher, U. Merbold, "The Microgravity Environment of the Materials Science Double Rack During Spacelab-1", Proc. of the AIAA Shuttle Environment and Operations II Conference, Houston, TEX., 13-15 Nov.1985, pp. 228-238.

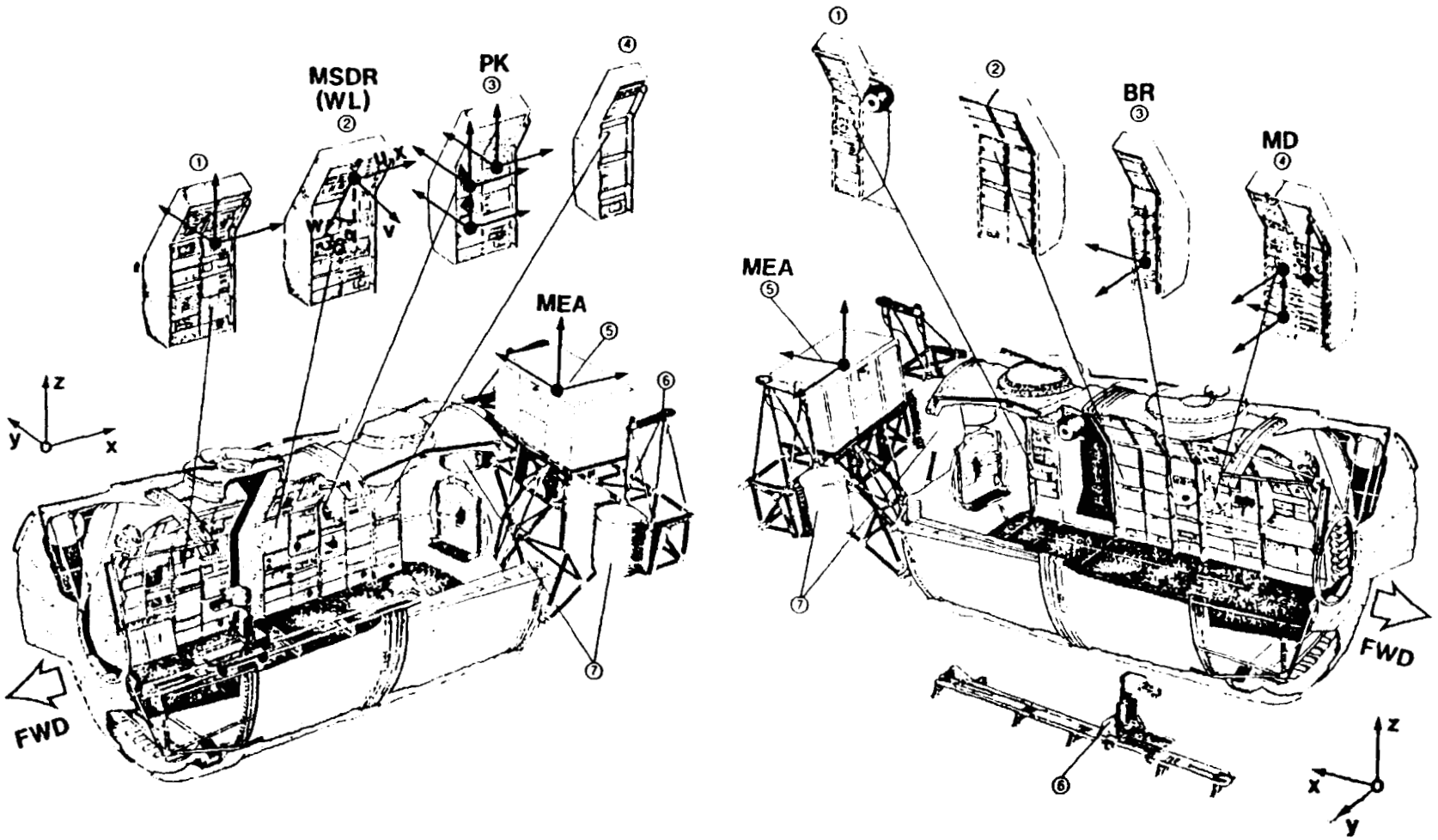

Fig.1. Locations and measurement axis of the accelerometer packages of the D1 payload [2].

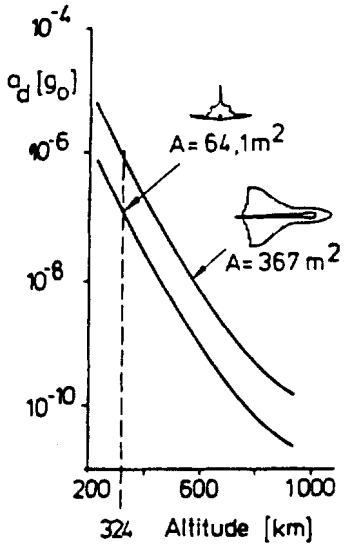

Fig.2.
Calculated effects of atmospheric drag on the Orbiter, m=90718 kg [4].

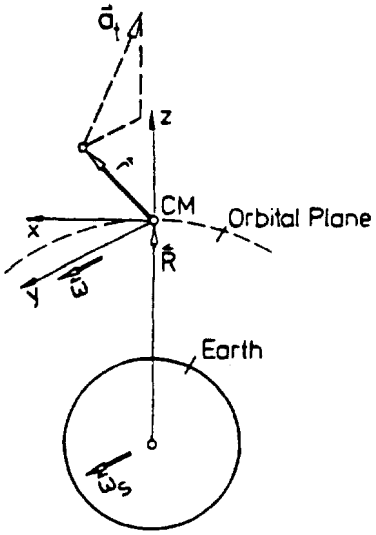

Fig.3.
Definition of the tidal acceleration $\vec{a}_t$.

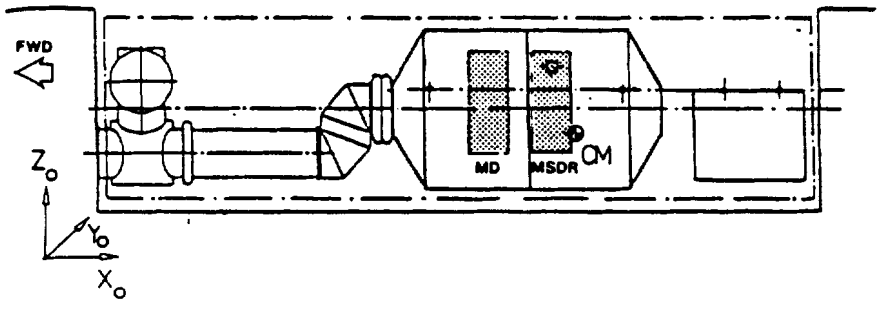

Fig.4. Location of MSDR and MEDEA (MD) relative to the total center of mass (CM).

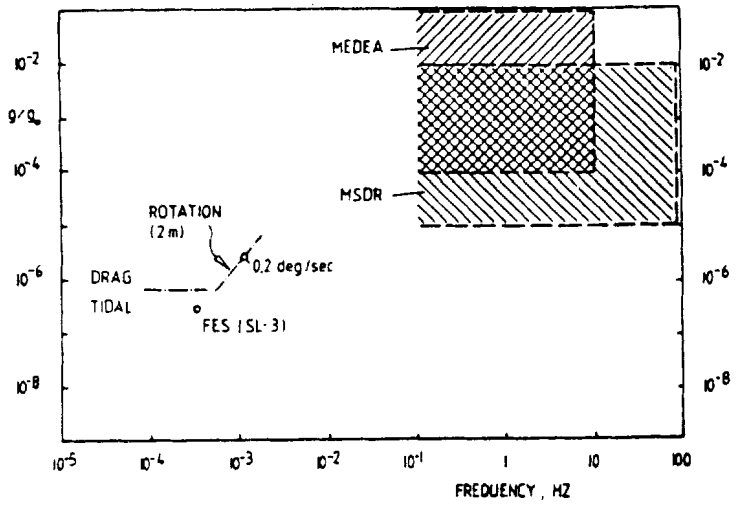

Fig.5.
Measurement range of the MSDR and MEDEA systems.
Quasi-steady components of the Orbiter.

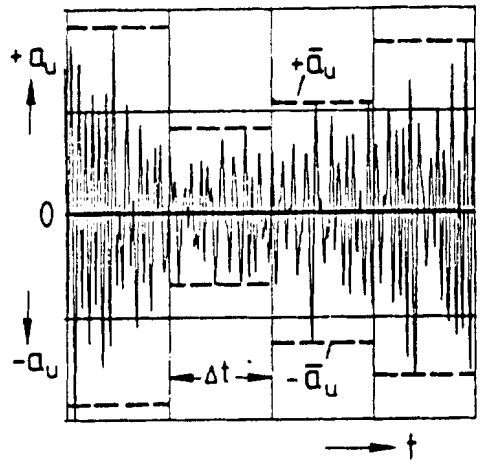

Fig.6.
Illustrating the principle of the peak detection method. The maximum amplitudes within Δt are detected from an analog signal for each direction.

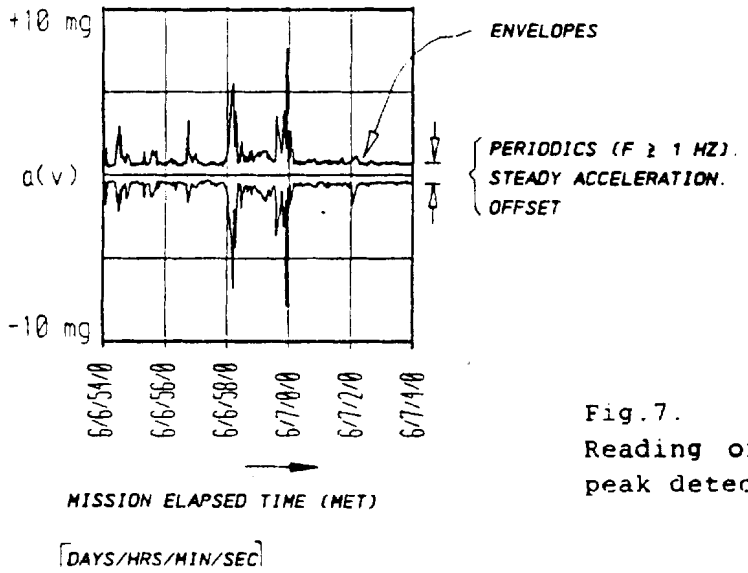

Fig.7.
Reading of the MSDR system in peak detection mode.

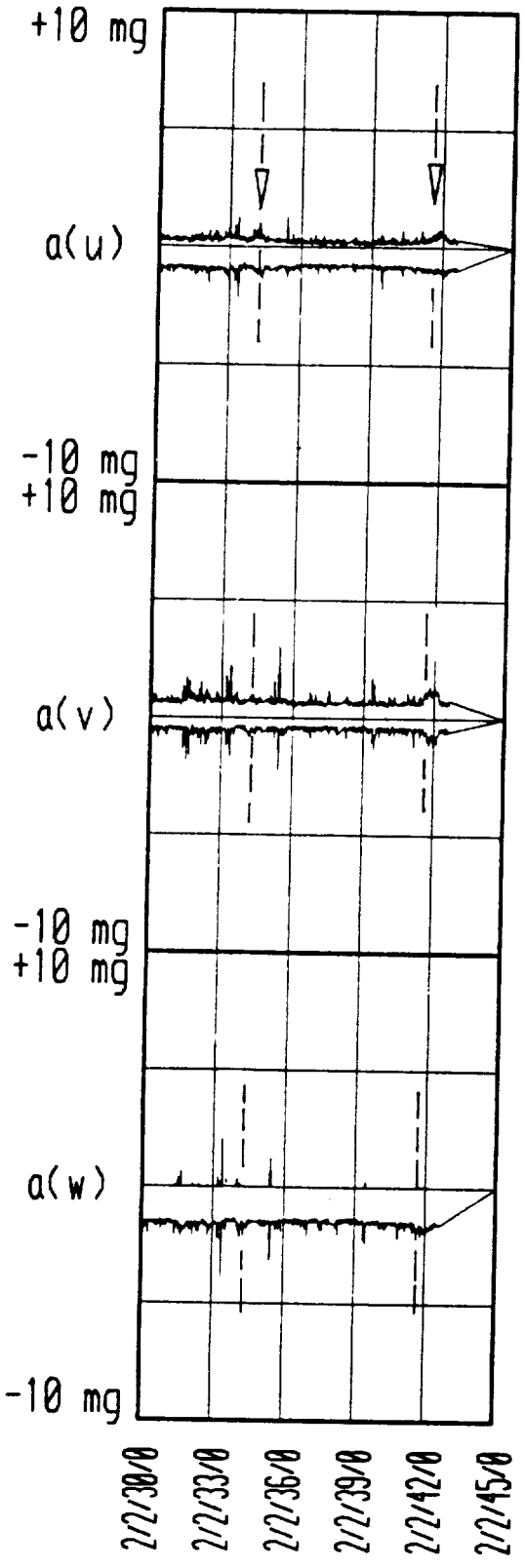

Fig.8.
Two RCS Vernier Thruster firings indicated by arrows (MSDR).

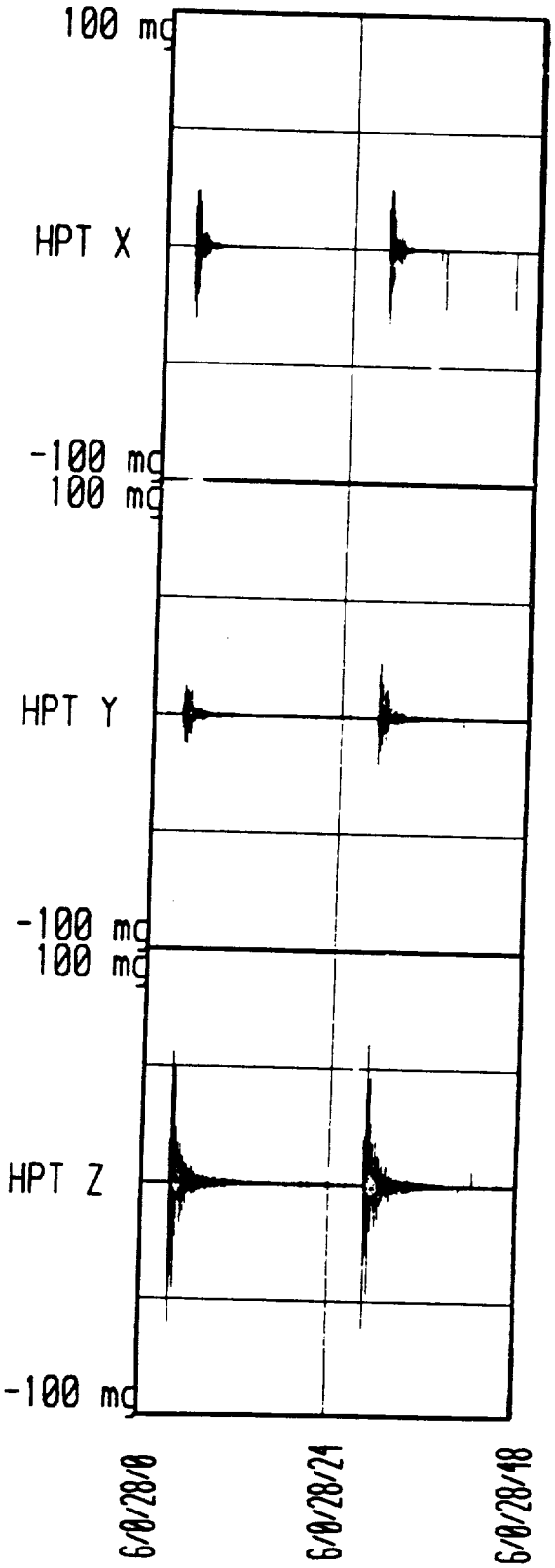

Fig.9.
Two RCS Primary Thruster firings (MEDEA).

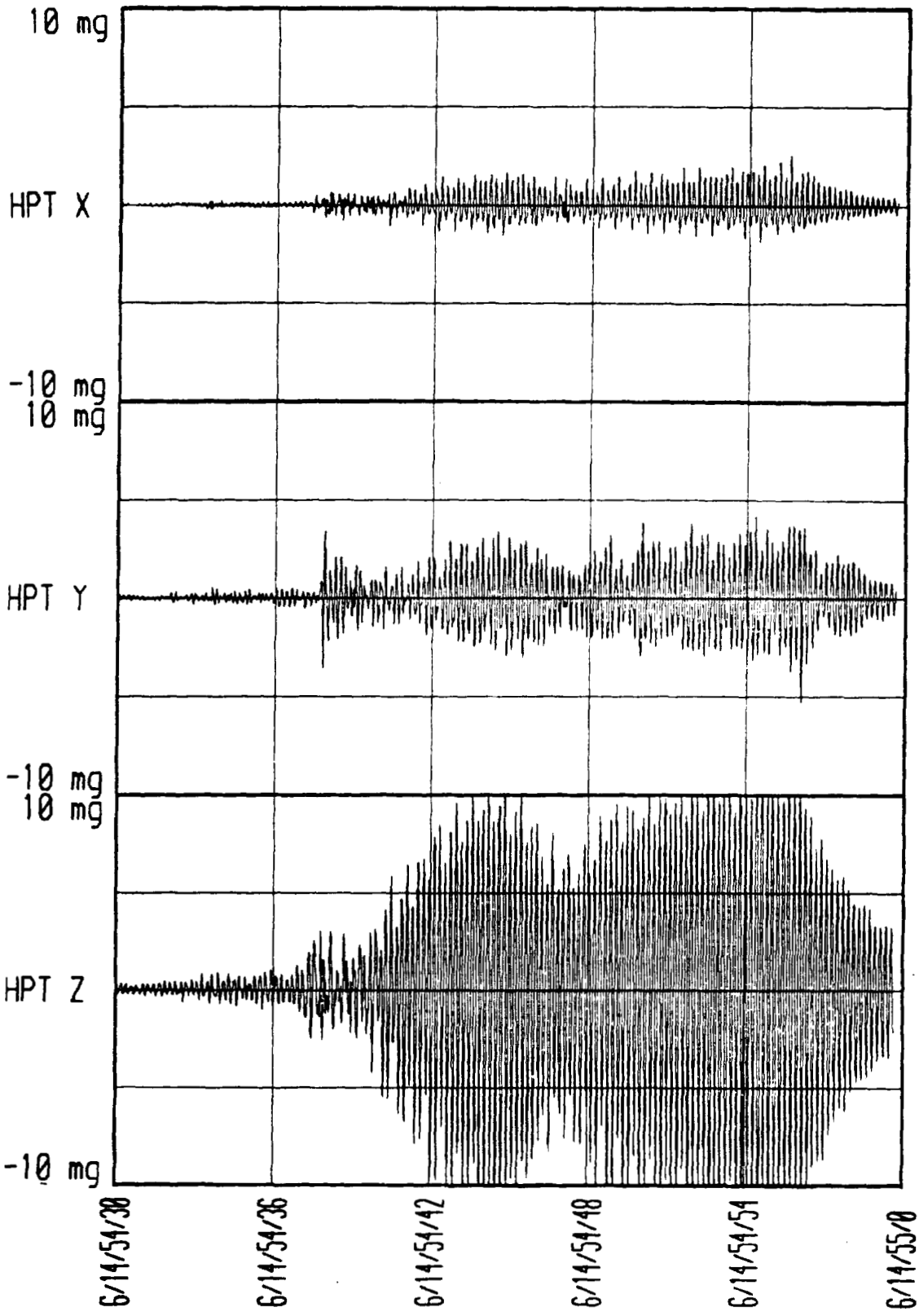

Fig.10. Time history of the "Hop and Drop" experiment, "Hop" phase (MEDEA).

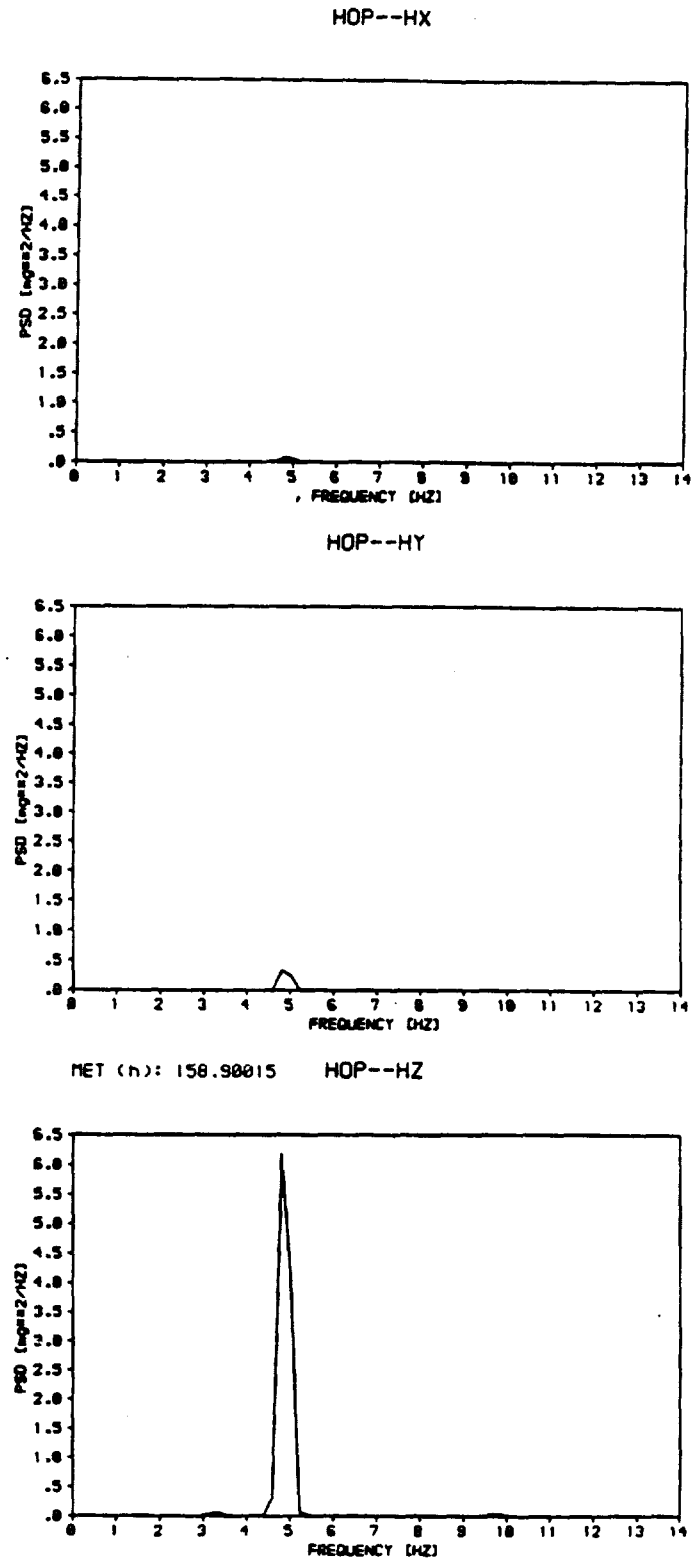

Fig.11. Power spectral density function of "Hop" phase (Fig. 10.).

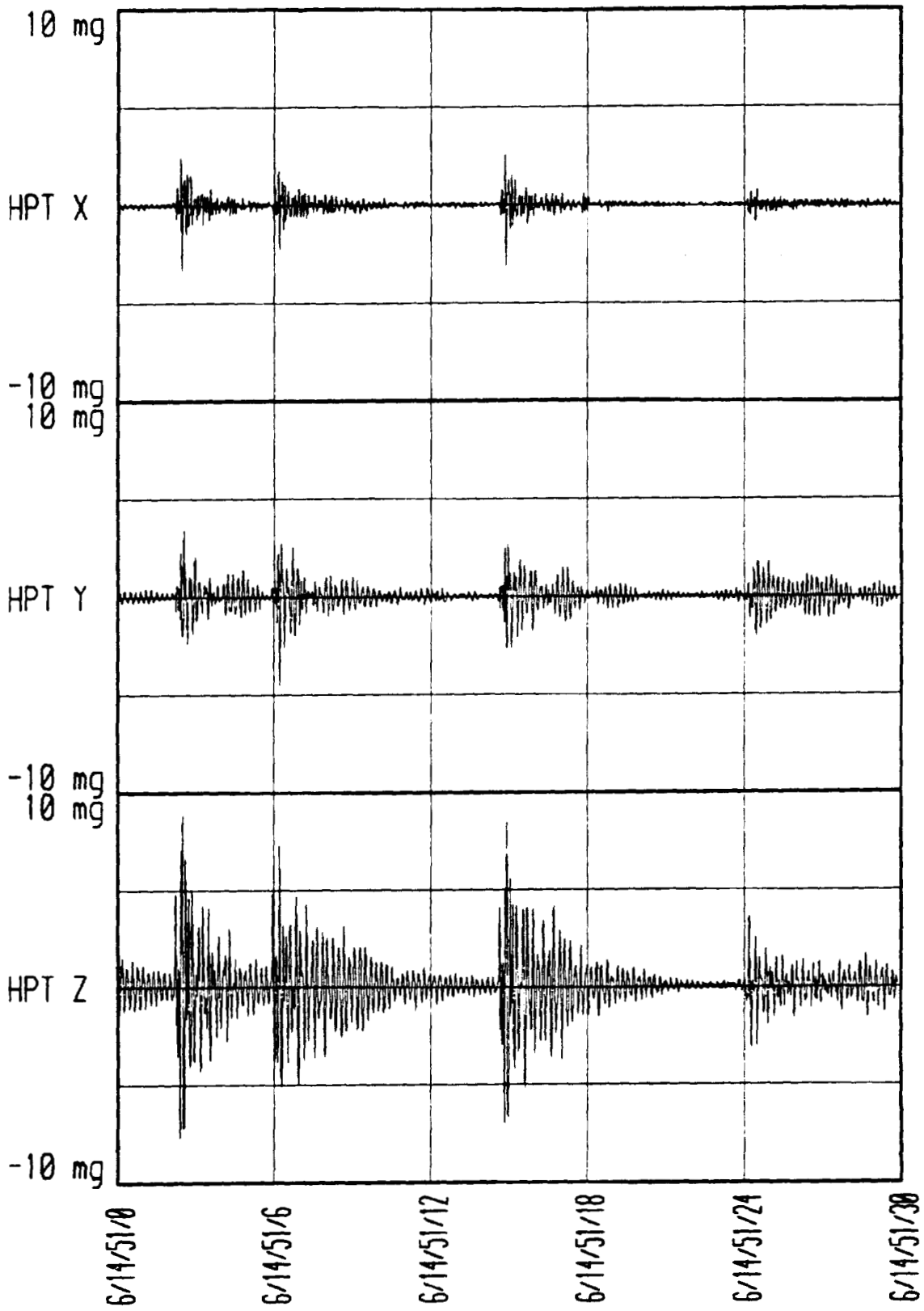

Fig.12. Time history of the "Hop and Drop" experiment, "Drop" phase (MEDEA)

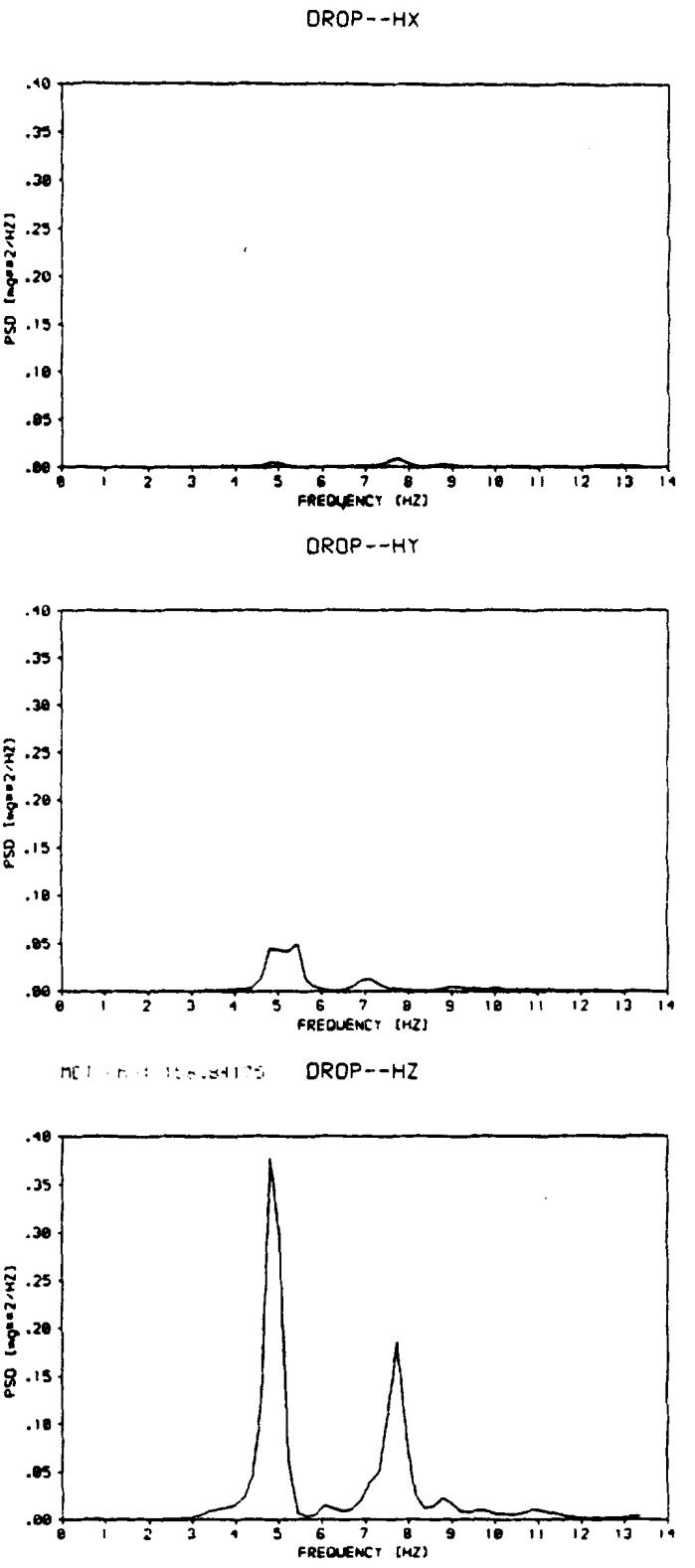

Fig.13. Power spectral density function of "Drop" phase (Fig.12).

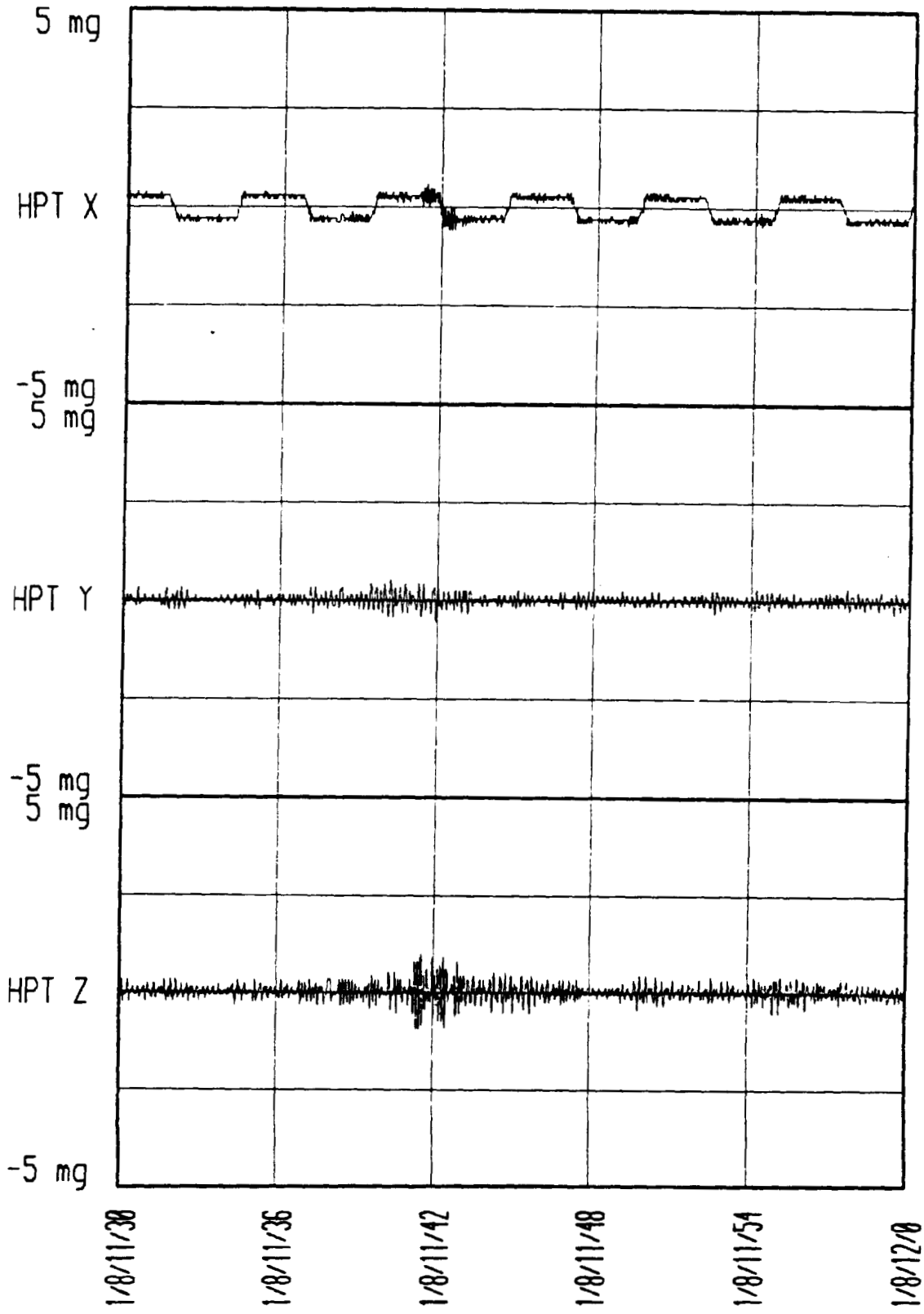

Fig.14. Time history of a Sled run in the trapeziform operation mode.

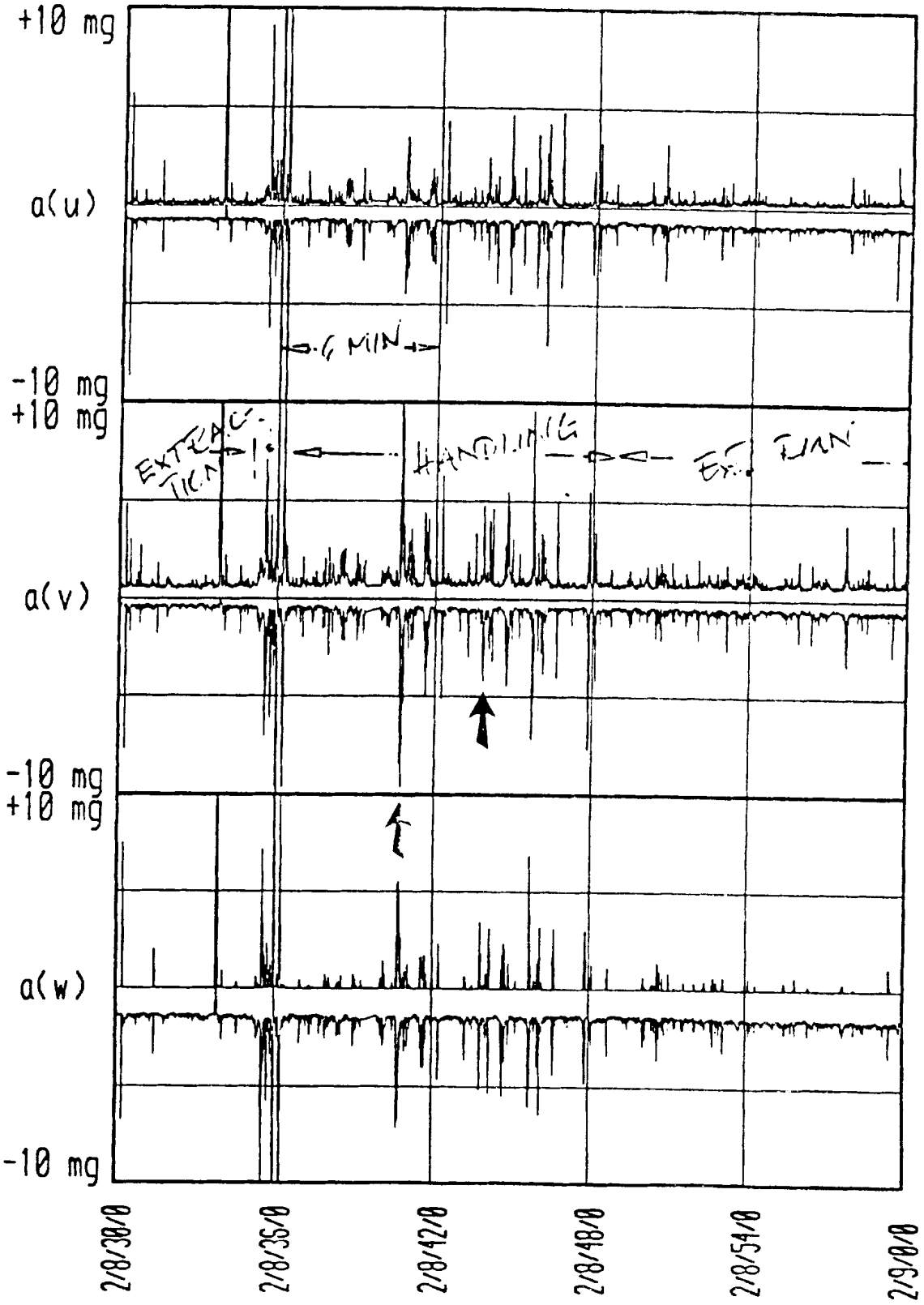

Fig.15. FPM activities (MSDR).

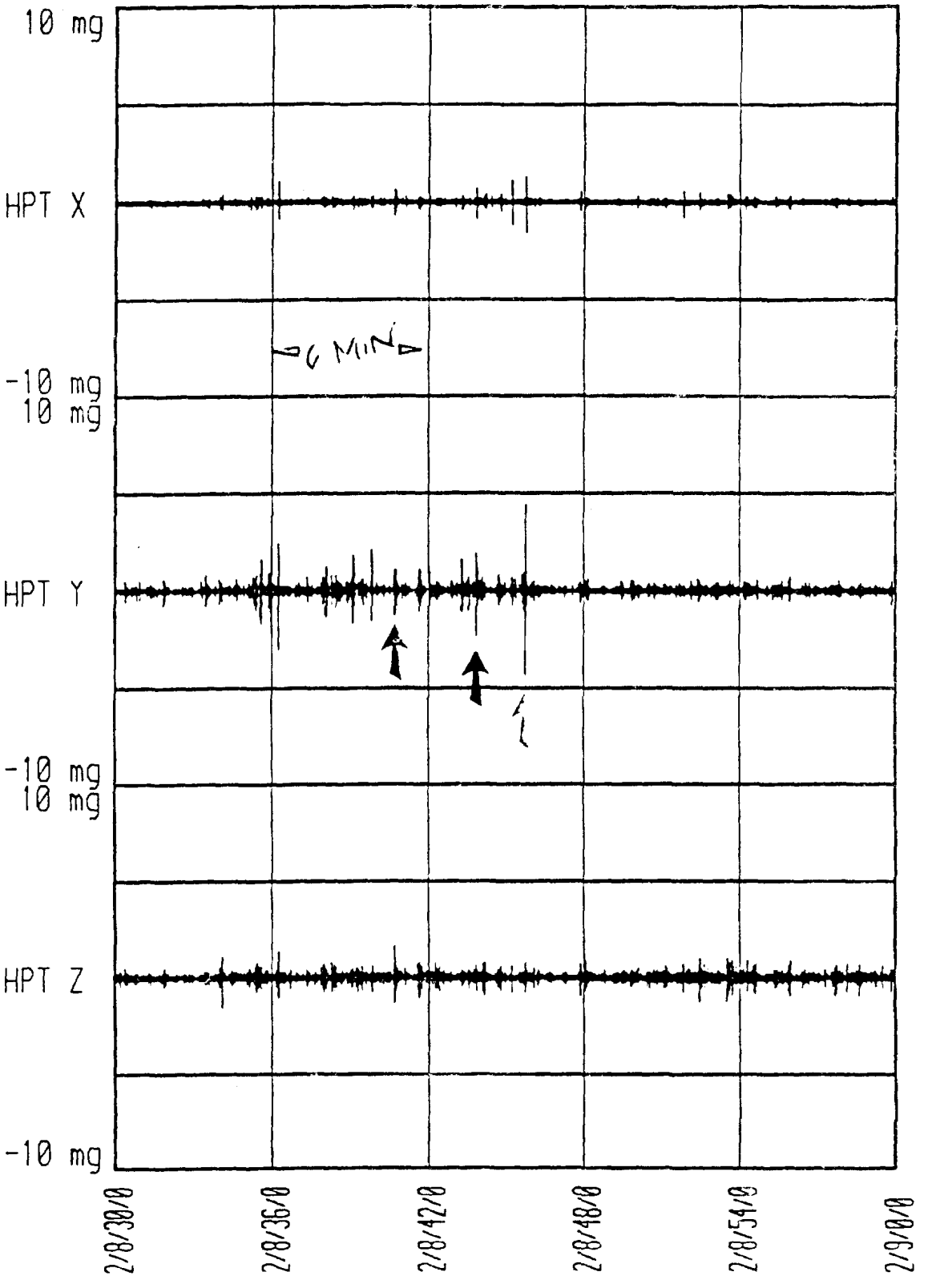

Fig.16. FPM activities of Fig.15 as detected in MEDEA.

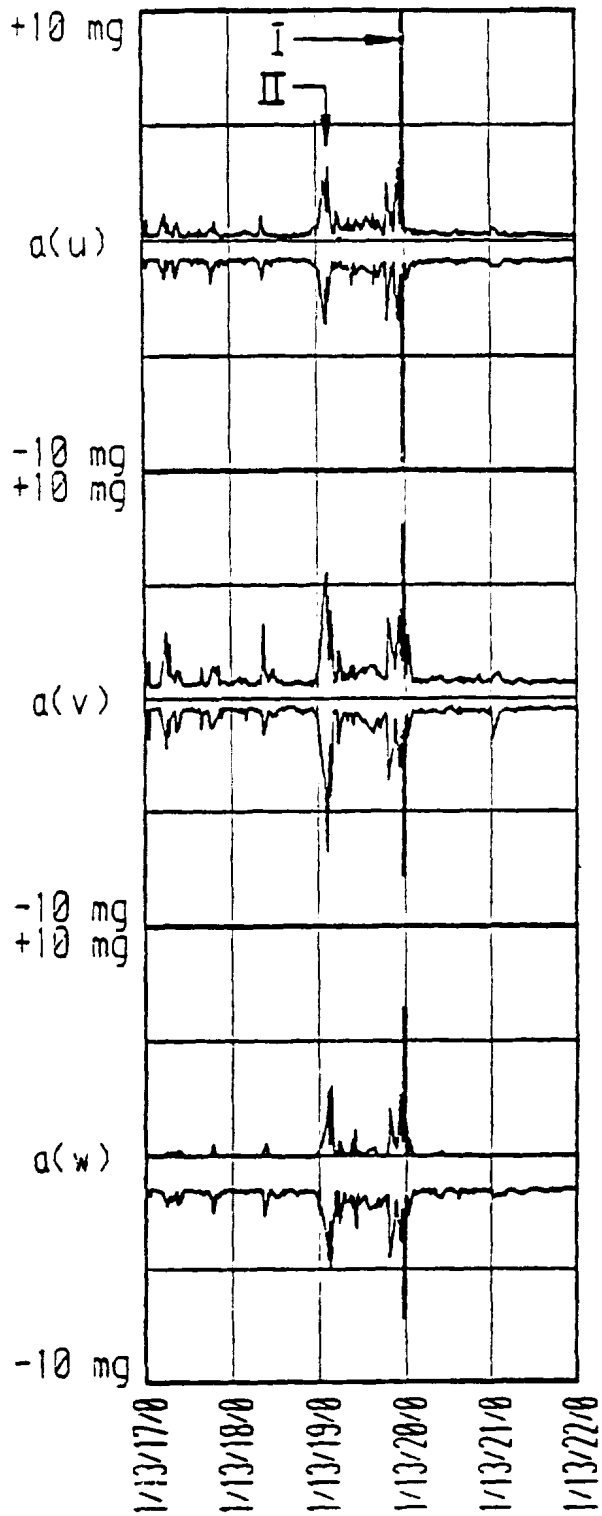

Fig.17. Examples of disturbances due to crew activities.
I Close of a container door
II Hold on the extracted FPM

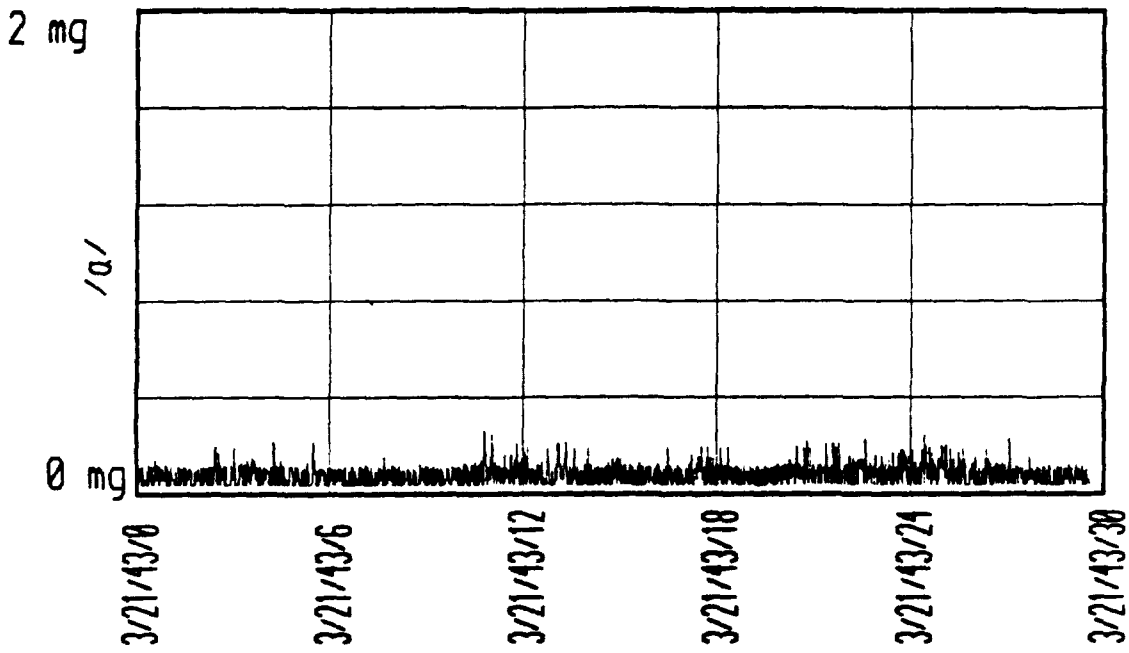

Fig.18. Example of a quiet phase. Magnitude of the resulting vector (MEDEA).

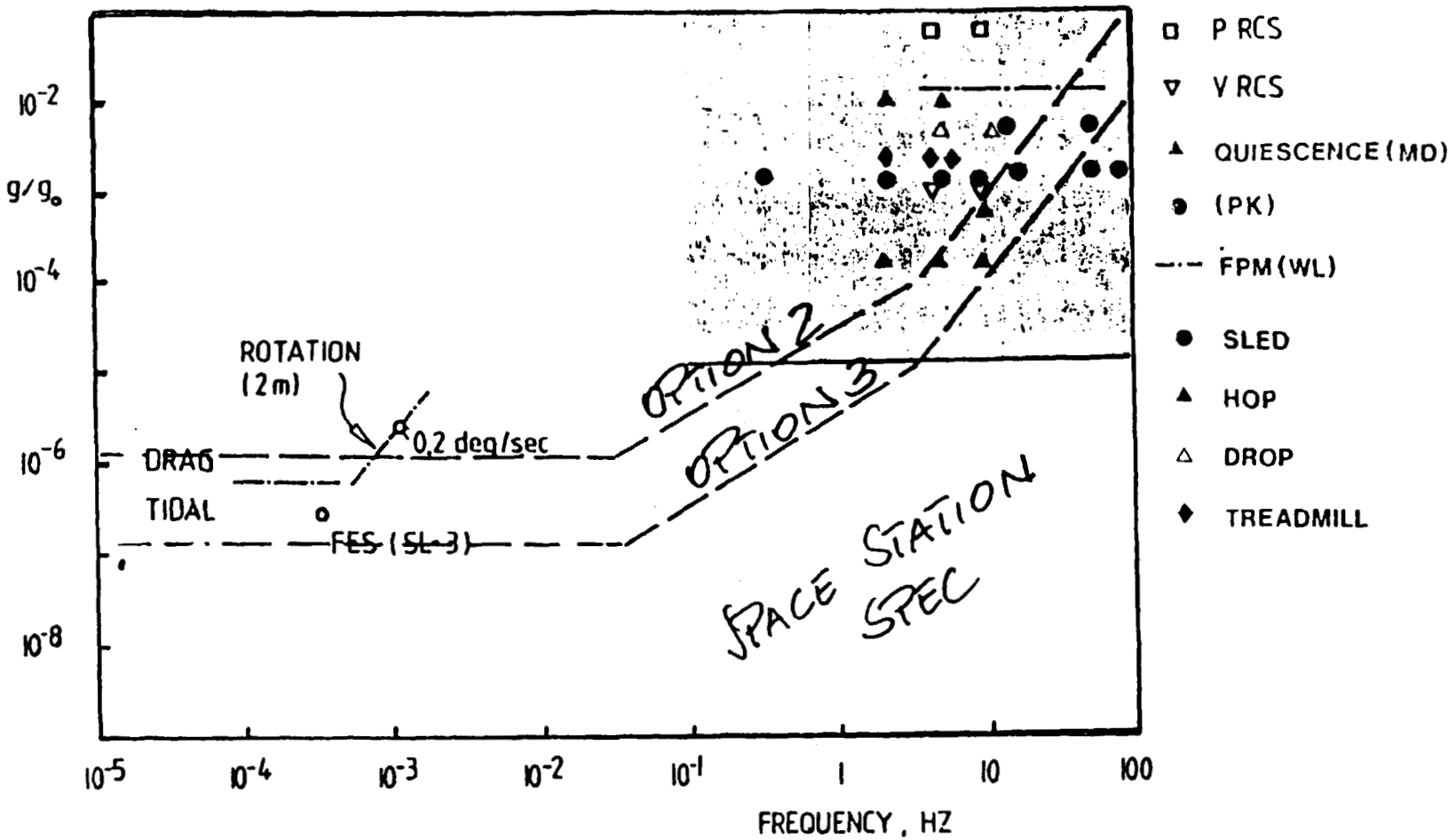

Fig.19. Summary of the measurement results.

N91-12408

9. LOW-G MEASUREMENTS BY NASA

Roger P. Chassay*, NASA/MSFC
Co-Author: Arthur Schwaniger, NASA/MSFC

ABSTRACT

NASA has utilized low-g accelerometers on a variety of flights for over ten years. These flights have included aircraft parabolas, suborbital trajectories, and orbital missions. This large quantity of data has undergone only limited in-depth analyses. Highlights of this low g data are presented along with brief discussion of the instruments used and the circumstances of the data collection.

INTRODUCTION

Some aspects of low-g environment during flight of a spacecraft have been of interest since the beginnings of manned spaceflight. Virtually all engineers and scientists involved in spaceflight during the sixties and early seventies assumed that acceleration was reduced to zero once earth orbit had been achieved. Hence the term "zero-g," which is still heard occasionally today, although we are much more enlightened now and know that "zero-g" is only theoretical.

Studies of the effects of astronaut crew motion on spacecraft stabilization and control systems were conducted in the early 1960's. A flight experiment to assess the characteristics of astronaut crew motion disturbances was conducted on the second manned Skylab mission in August 1973. Although the Skylab was not instrumented with low-g accelerometers, forces exerted by the astronauts were determined and acceleration levels were inferred (Reference 1). The flights of materials processing experiments on aircraft in parabolic maneuvers and on suborbital rockets brought low-g accelerometer instrumentation into use to provide experiment investigators a record of the acceleration environment; this, in turn, provided a means of correlating experiments results with residual accelerations.

*Acknowledgments: Key inputs were provided by Gary Arnett (BGB, Inc.), Fred Henderson (TBE), Rudolph Ruff (MSFC), John Scott (NTI), and Malcolm Tagg (MDAC)

The following topics provide typical examples of data that have been collected and analyzed over a period exceeding 12 years. Acceleration information from flights of KC-135 aircraft, Spacelab, and the Materials Science Laboratory are included, along with other low-g acceleration data. Some discussion of the challenges associated with the data collection and analysis is also given.

CHALLENGES

Handling of low-g data is definitely not straightforward. One of the challenges (Figure 1) in obtaining useful low-g data is that the signal is extremely small when measuring, say, one-millionth of normal Earth gravity or 10^{-6} g. Even at 100 times greater levels (10^{-4} g), we are still measuring a very small signal, i.e., 1/10,000th of g. These tiny signals can easily be masked by ordinary electronic noise and the data user may be misled into believing he has accelerometer data when he may actually have nothing but a useless record of electronic noise. Therefore, it is very important to have quieting circuits built into the electronics and to assure that the signal-to-noise ratio is greater than 1.0 for the end application.

Another challenge in handling low-g data is that the accelerations can be self-induced. At times, the microgravity scientist or engineer overlooks the subtle, but influential accelerations induced by fans, pumps, etc., internal to the experiment aparatus, while at the same time levying stringent acceleration limits on equipment provided by others. Obviously, the key here is to stress objectivity in flight equipment selections, regardless of the source of the equipment, so that minimal accelerations occur at the low-g critical sites.

Another area that requires attention in assessing low-g data is the shifts in accelerometer calibration that occur with these sensitive instruments; these shifts require corrections to the amplitude offset bias, which occurs in the low-g data.

- **CHALLENGES**
  - ACCELERATIONS CAN BE FALSE, e.g. ELECTRONIC NOISE
  - CALIBRATION OF SENSORS CAN SHIFT
  - ACCELERATIONS CAN BE SELF-INDUCED
  - ACCELERATIONS CAN BE INDUCED BY UNKNOWN FORCES NEVER IDENTIFIED
  - AXES IDENTIFICATION CAN BE AMBIGUOUS
  - ENORMOUS AMOUNT OF DATA MAKES ANALYSIS A VERY LARGE TASK, (e.g., ONE HALF MILLION DATA POINTS DURING A TYPICAL MISSION FOR EACH SAMPLE/SEC).

FIGURE 1

Attention must also be paid to the variety of different axes systems that are in use by different sectors of the aerospace and scientific community. Occasionally, axes assignments are casually made for convenience of a single organization. More frequently, axes assignments are made formally, based upon either technical logic or tradition. Overall, several different axes assignments are typically used, e.g., for payload layout, for flight operations, for experiment-unique considerations, etc. The informed user or processor of low-g acceleration data should benefit from the learning adventure of the authors that X-axis data from someone else are not necessarily X-axis data in the axes system you are using.

Another challenge is the enormity of the data, i.e., for each sample per second on one axis we obtain one-half a million data points on a typical shuttle mission. A common, workable method for handling this large amount of low-g data is yet to be devised.

The single greatest challenge in working with low-g data is the difficulty in correlating mission events (which are known to cause accelerations) with the notable features of the low-g data in a cause-and-effect relationship. In the vast majority of cases, we observe an apparent lack of correlation, even though a cause-and-effect phenomenon is known or probable. In the preponderance of cases, we routinely observe unusual accelerations, then search for causes, and then cannot positively or even remotely identify the cause or causes. For example, a mysterious 17 Hz acceleration seems to occur on most Shuttle missions for which we have data, but no one has yet come close to positively identifying the cause for this acceleration. In other cases, we know an acceleration-inducing event occurred, but this event is not reflected in the data, for reasons not readily obvious; after some effort some of these reasons become known, but others remain a mystery.

In grappling with these difficulties, we have pursued the data analyses up to now only to a very limited extent, primarily since many of the low-g data users have not as yet determined the specific use to

which the data will be put. They know fundamentally that if the residual accelerations, however low, can possibly have significant or even profound effects on the low-g experimental results, then these residual accelerations should be characterized via low-g measurements during the experiment. However, the specific application of the low-g data for an investigator, such as a metallurgist or crystallographer, may require that the investigator be capable of readily assimilating low-g data, converting it to meaningful effects on fluid dynamics, converting that in turn to concentration gradients, and that to effects at the solid-liquid interface. This series of events certainly is not at all straightforward and beyond the time or resources available to many of the low-g investigators or frequently beyond their experience base. Therefore, until the need for fully analyzed low-g data becomes more prevalant, only limited resources will be invested in this complex activity.

VARIETY IN THE FORMS OF DATA PRESENTATION

Low-g data have been presented in a wide variety (Figure 2) of narrative, graphic, and tabular forms. Various degrees of detail and processing were included. Analyses such as filtering, inverse filtering, RMS accelerations, power spectral density, and shock spectra were used with no standardized approach. In the case of Spacelab, a summary table of ranges of acceleration levels and frequency content was given.

LOW-G ACCELERATION MEASUREMENTS IN A GROUND LABORATORY

We have stated that experiments conducted in low gravity can be adversely affected by accelerations which are "self-inflicted," i.e., accelerations caused by equipment within the experiment apparatus such as pumps, fans, acoustic levitators, camera mechanisms, coolant flow, and vent ports. For two of the MSFC suborbital SPAR low-g payloads, special tests were performed prior to flight to measure these self-induced accelerations. These payloads included furnaces and levitators which contained components suspected of generating undesired acceler-

- VARIETY IN THE FORMS OF DATA PRESENTATION:
  - NARRATIVE
  - TIME HISTORIES
  - POWER SPECTRAL DENSITIES
  - RMS
  - SHOCK SPECTRA
  - FILTERED
  - INVERSE FILTERED

FIGURE 2

ations. Figure 3 shows a sample of one of the higher level power spectral density plots acquired from low-g acceleration readings during one of these simulated flight functional testings of the experiment payload; the payload was suspended on an overhead crane to avoid the damping of accelerations that would occur if the payload rested on a solid support, such as a laboratory floor (Reference 2).

LOW-G ACCELERATION MEASUREMENTS DURING PARABOLIC AIRCRAFT FLIGHT

Short periods of low-g can be obtained during parabolic flight in aircraft. NASA has frequently utilized a KC-135 aircraft, among others, to conduct low-g experiments. Many parabolas are executed during a typical flight, resulting in alternating periods of low-g and high-g as well as some one-g periods when level flight is needed to reset or repair experiments between runs. Figure 4 provides a sample of acceleration versus time as four parabolas are flown.

Digitized data from a Sunstrand Model 303T15 accelerometer, tabulated in Table 1, provide a more quantitative history for a similar KC-135 flight. Accelerations from 1 to 10 milli-g are recorded in the separate axes during a period of low acceleration levels, which lasted up to 20 seconds.

LOW-G-ACCELERATION MEASUREMENTS DURING SUBORBITAL FLIGHT

A Low-Gravity Accelerometer System (LGAS) was flown as a piggyback item on a suborbital mission, October 4, 1974, to demonstrate the feasibility of measuring low-g accelerations during free fall of a rocket payload; the LGAS had been developed at MSFC using Singer-Kearfott C70 -2412 sensors. Figure 5 indicates the successful demonstrated flight results, which provided a time history of low-g accelerations in each of three orthogonal axes (Reference 3). Figure 6 provides similar data for one axis during the SPAR X suborbital flight on June 17, 1983. SPAR operated much as an unmanned "FREE FLYER" and, thus, provided one of the very best low-g environments of any carrier to date. Measurements on SPAR payloads I-IV are reported in Reference 4.

ED5474

SELF-INDUCED ACCELERATIONS IN SPAR PAYLOAD GROUND TEST

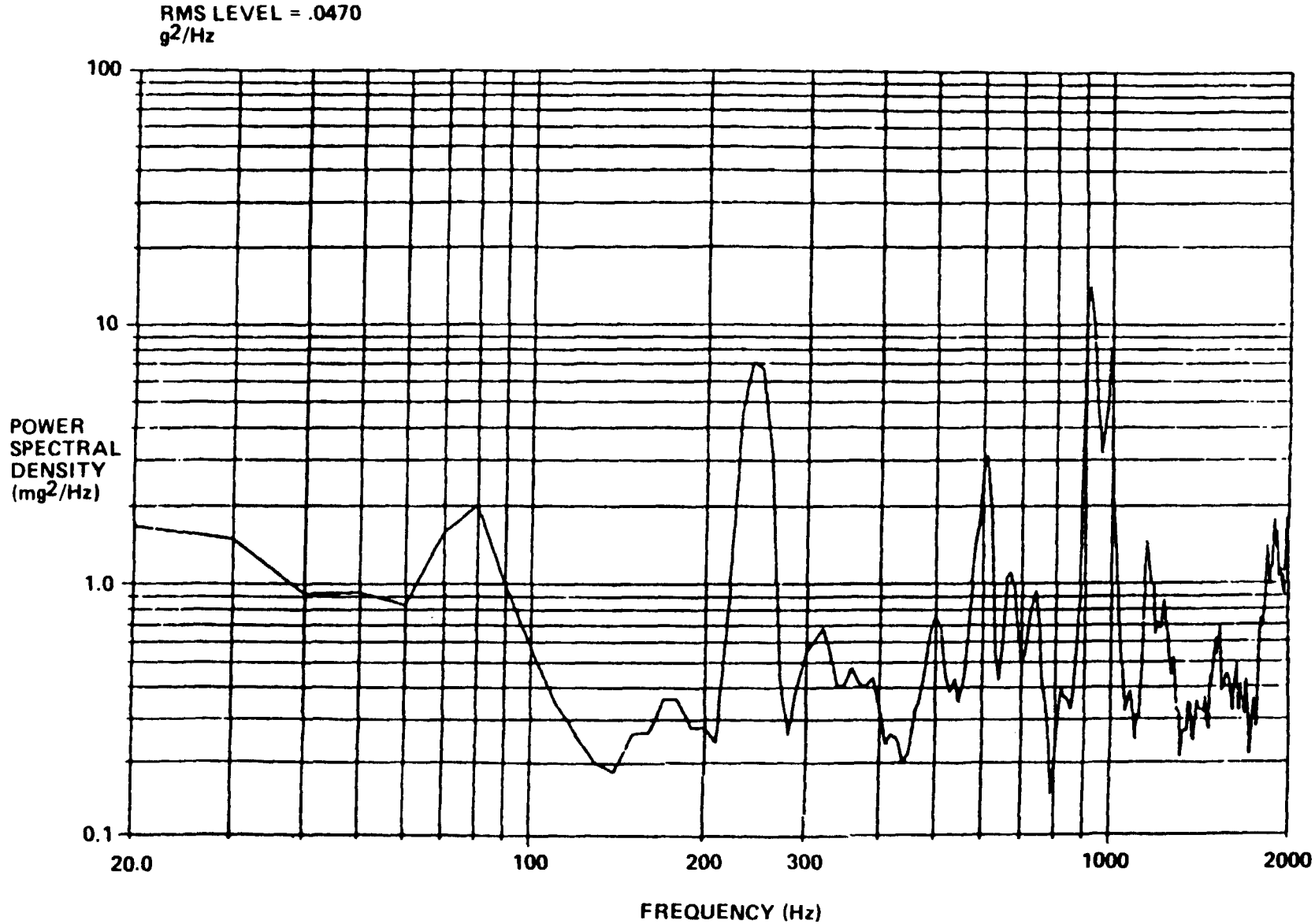

FIGURE 3

RAW DATA FROM KC–135 FLIGHT

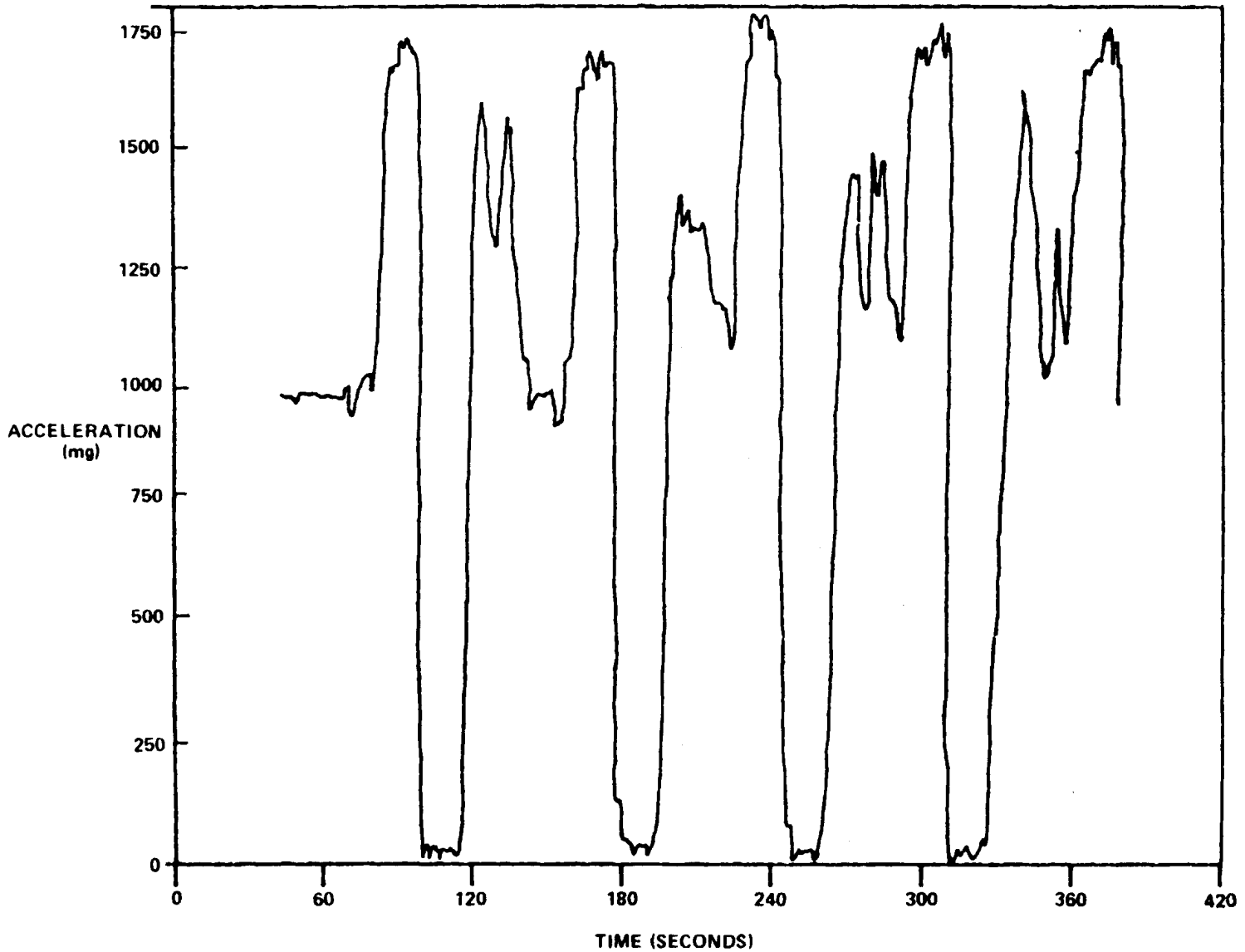

FIGURE 4

TABLE 1

RAW DIGITIZED DATA FROM KC–135 FLIGHT

TIME	X AXIS (mg)	Y AXIS (mg)	Z AXIS (mg)
20 SEC	+ 122	+1,742	+ 58
21 SEC	+ 129	+1,748	+ 39
22 SEC	+ 132	+1,715	+ 18
23 SEC	+ 134	+1,646	+ 28
24 SEC	+ 135	+1,564	+ 43
25 SEC	+ 75	+1,028	+ 33
26 SEC	+ 21	+ 449	+ 10
27 SEC	– 2	+ 269	+ 2
28 SEC	– 11	+ 160	+ 11
29 SEC	– 11	+ 73	+ 18
30 SEC	– 10	+ 51	+ 16
31 SEC	– 9	+ 28	+ 5
32 SEC	– 10	– 2	– 1
33 SEC	– 8	– 2	– 3
34 SEC	– 8	+ 5	+ 2
35 SEC	– 7	+ 5	+ 8
36 SEC	– 7	+ 4	+ 10
37 SEC	– 7	+ 7	+ 6
38 SEC	– 8	+ 10	0
39 SEC	– 8	– 6	– 2
40 SEC	– 9	– 9	0
41 SEC	– 10	– 8	+ 4
42 SEC	– 10	– 4	+ 8
43 SEC	– 12	+ 10	+ 5
44 SEC	– 13	+ 9	0
45 SEC	– 16	– 10	– 2
46 SEC	– 14	– 6	0
47 SEC	– 19	+ 35	+ 8
48 SEC	– 17	+ 71	+ 6
49 SEC	– 22	+ 209	+ 4
50 SEC	– 22	+ 416	+ 4

ED5460

SUBORBITAL ACCELERATIONS DURING DEMONSTRATION FLIGHT

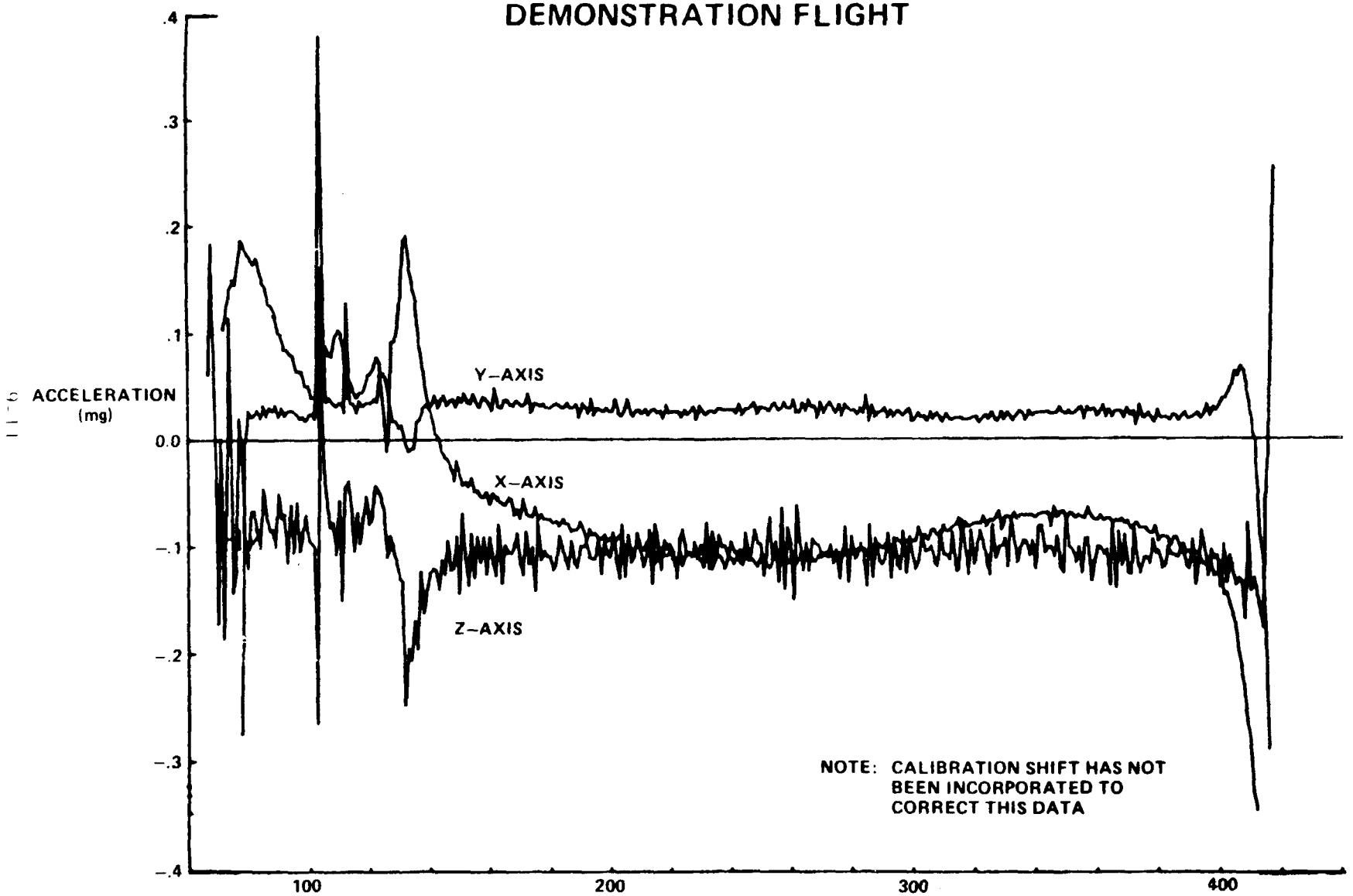

FIGURE 5

SUBORBITAL ACCELERATION DURING SPAR X "FREE FLYER" MISSION

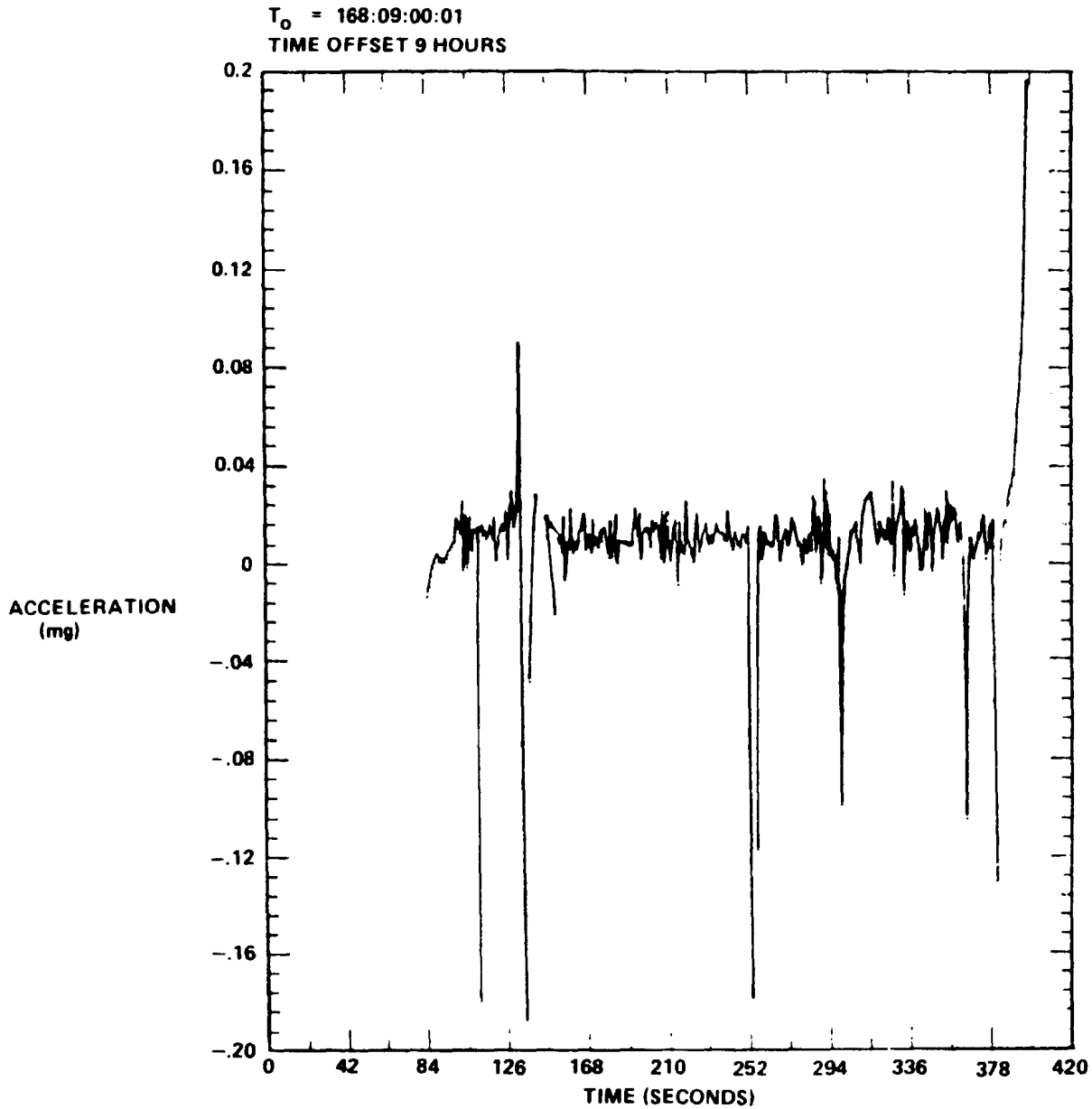

FIGURE 6

LOW-G ACCELERATION MEASUREMENTS IN THE STS ORBITER MIDDECK

Small low-g experiments are conducted in the Orbiter Middeck area on many Shuttle Transportation System (STS) missions. To provide some indication of the low-g environment, a Micro-g Acceleration Measurement System (M-GAMS) was initially utilized during the STS-3 mission in March 1982. The M-GAMS includes a two-axis capability provided by SA-100 sensors from Columbia Research Laboratories. Figure 7 provides a narrative characterization of the acceleration readings obtained during the Electrophoresis Equipment Verification Test on that STS mission (Reference 5). Figure 8 contains similar information plotted as a function of time (Reference 6). Note that much of the actual low-g data are marked by background electronic noise. The noise has a magnitude of 1 bit or 10^{-4} V/g and occurs in both the positive and negative directions. Therefore, we only know that the g-levels were below the false signals caused by the electronic noise.

LOW-G MEASUREMENTS IN THE MATERIALS EXPERIMENT ASSEMBLY OF STS-7

The Materials Experiment Assembly (MEA) is a carrier for microgravity experiments in the STS Orbiter Bay. The MEA contains a Low-g Accelerometer System (LGAS), which is very similar to the one described above for use during suborbital SPAR flights. Figure 9 displays a low-g time history during MEA experiments when an STS thruster firing is known to have occurred. The data obtained from the LGAS are in the form of an integrated average of the accelerations during each one-second interval in each axis. Notice that the acceleration caused by the thruster firing is masked by the one-second averaging and the induced acceleration cannot be observed in these data (Reference 7). However, recent investigations have determined that the very low frequency vibrations and dc accelerations are more detrimental to low-g experiments, in general, and therefore an event such as a rapid thruster firing may not be of as much interest as previously thought.

ED5473

ACCELERATIONS OBSERVED ON STS–3 IN THE ORBITER MIDDECK

- TYPICALLY THE ACCELERATION READINGS WERE LESS THAN 2.5 MILLI-G IN ONE AXIS AND LESS THAN 1.25 MILLI-G IN AN ORTHOGONAL AXIS. (THE THIRD AXIS WAS NOT MEASURED).

- MAXIMUM ACCELERATION READINGS OCCURRED DURING A PERIOD OF LESS THAN TWO HOURS.
  - 137 ACCELERATION EVENTS
  - EACH EVENT WAS $\geq$38 MILLI-G
  - DAMPING OF EACH EVENT WITHIN 3-4 SECONDS
  - FREQUENCY CHARACTERISTICS: 10 TO 25 HZ

FIGURE 7

ED5455

SAMPLE ACCELERATION DATA FROM STS-11 MIDDECK (ACES EXPERIMENT)

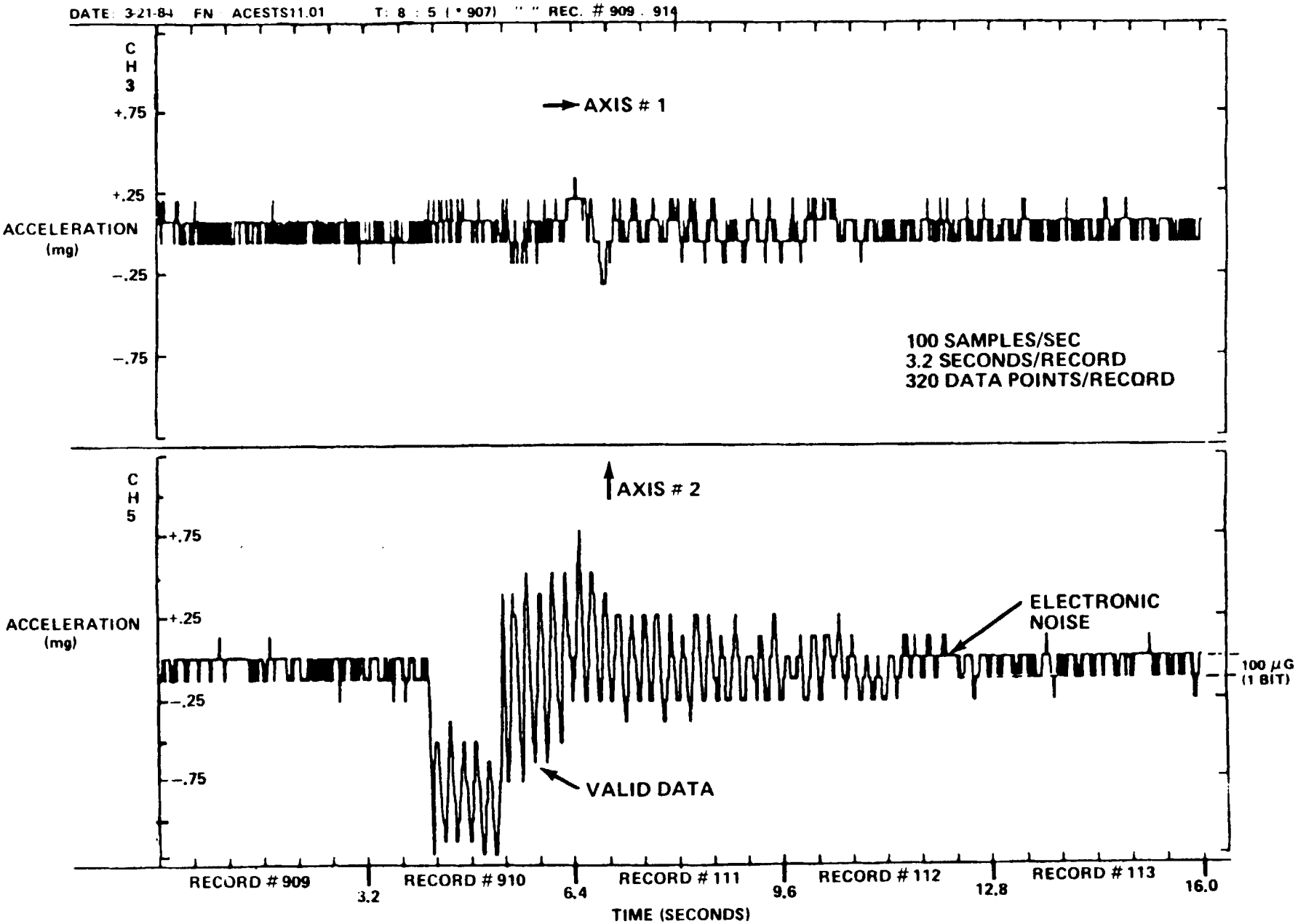

FIGURE 8

ED5449

RAW DATA FROM STS-7 MEA EXPERIMENTS (AVERAGE ACCELERATION AT 1 SEC INTERVALS)

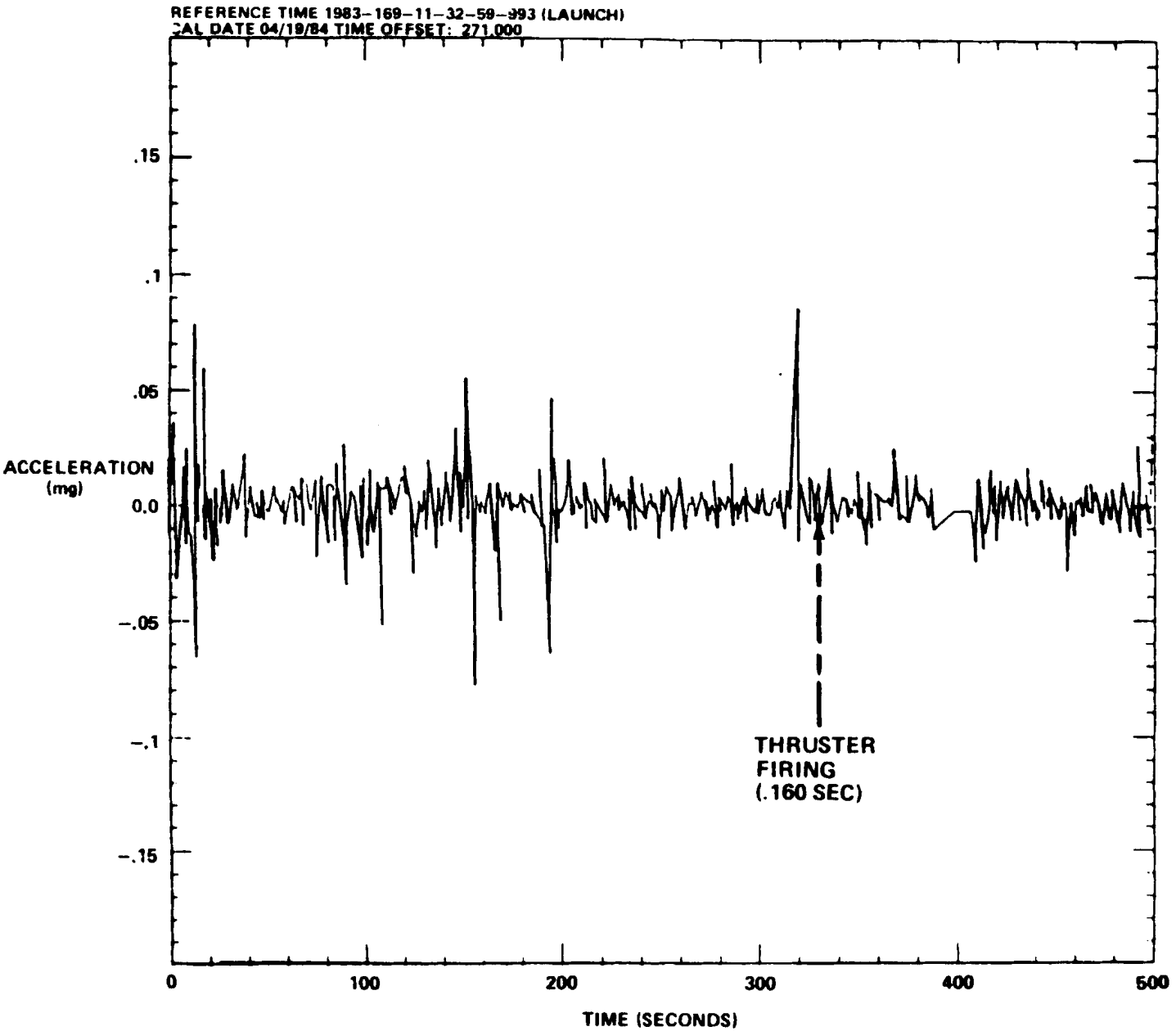

FIGURE 9

LOW-G ACCELERATION MEASUREMENTS ON SPACELAB 1

The flight of Spacelab 1 occurred in November-December 1983 and was instrumented with 14 Systron-Donner linear accelerometers. Each accelerometer had a sensitivity of 10 micro-g and a bandwidth of 30 Hz. Data were recorded at the rate of 80 samples per second. One example of data taken during a time when the crew activity was constrained to a cough test is shown in Figure 10 (Reference 8). The acceleration peaks were less than one milli-g and, in fact, the time history shown is very comparable to "quiet time" periods.

Figure 11 shows the shock spectra for the acceleration history shown in the previous figure. The shock spectra are derived by using the acceleration time history as a forcing function to drive a massless spring (with natural frequency Omega and damping, which gives an amplification factor of 20). The frequency is varied from 0 to 100 Hz and the peak acceleration response of the spring at each frequency determines the shock spectrum amplitude. The maximum value at 10 Hz shown on this figure is 5.6 milli-g.

Table 2 recaps the acceleration levels and the frequencies at which they occur on both the Spacelab module and pallet. During the quiet time, the acceleration ranged from 0.25 to 0.65 milli-g in the module and from 0.13 to 0.45 milli-g on the pallet. Frequencies ranged from 8 to 40 Hz.

During the "cough test", accelerations ranged from 0.2 milli-g on the pallet to 2.8 milli-g in the Z direction in the module. Frequencies ranged from 8 to 11 Hz. For the crew's "push off" test, the accelerations occurred in the X-direction for a Y-direction pushoff at 0.1 milli-g and the largest acceleration also occurred (with a Y-direction pushoff) in the Z-direction at 2.4 milli-g.

Lower level (111 Newtons) vernier thruster firings of the Orbital Rate Control System produced 0.3 to 1.0 milli-g while higher level (3870 Newtons) primary thrusters produced up to 20 milli-g. A Spacelab disturbance attributed to sudden release of tunnel trunnion frictional

CREW- INDUCED ACCELERATION ON SPACELAB 1 (VIA "COUGH TEST")

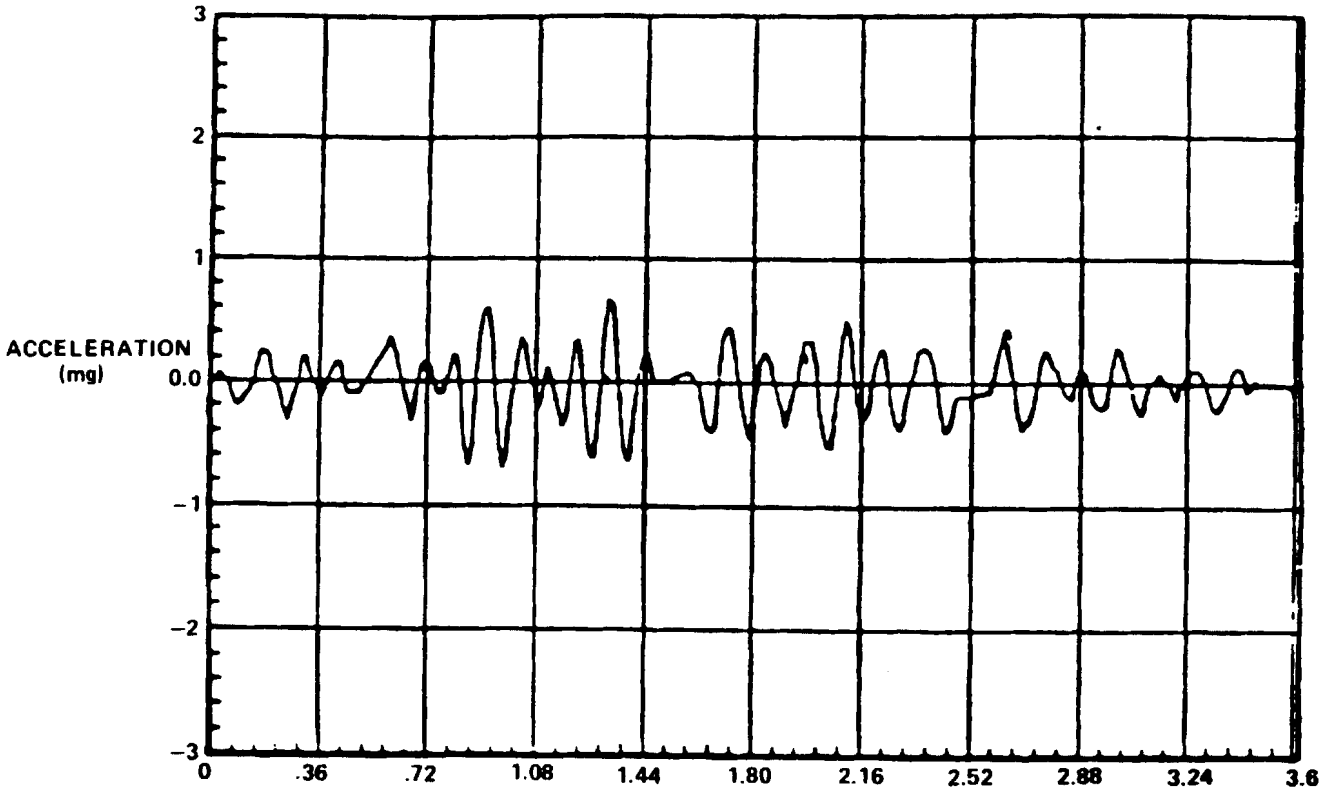

FIGURE 10

SHOCK SPECTRA FROM SPACELAB 1 CREW- INDUCED ACCELERATION (VIA "COUGH TEST")

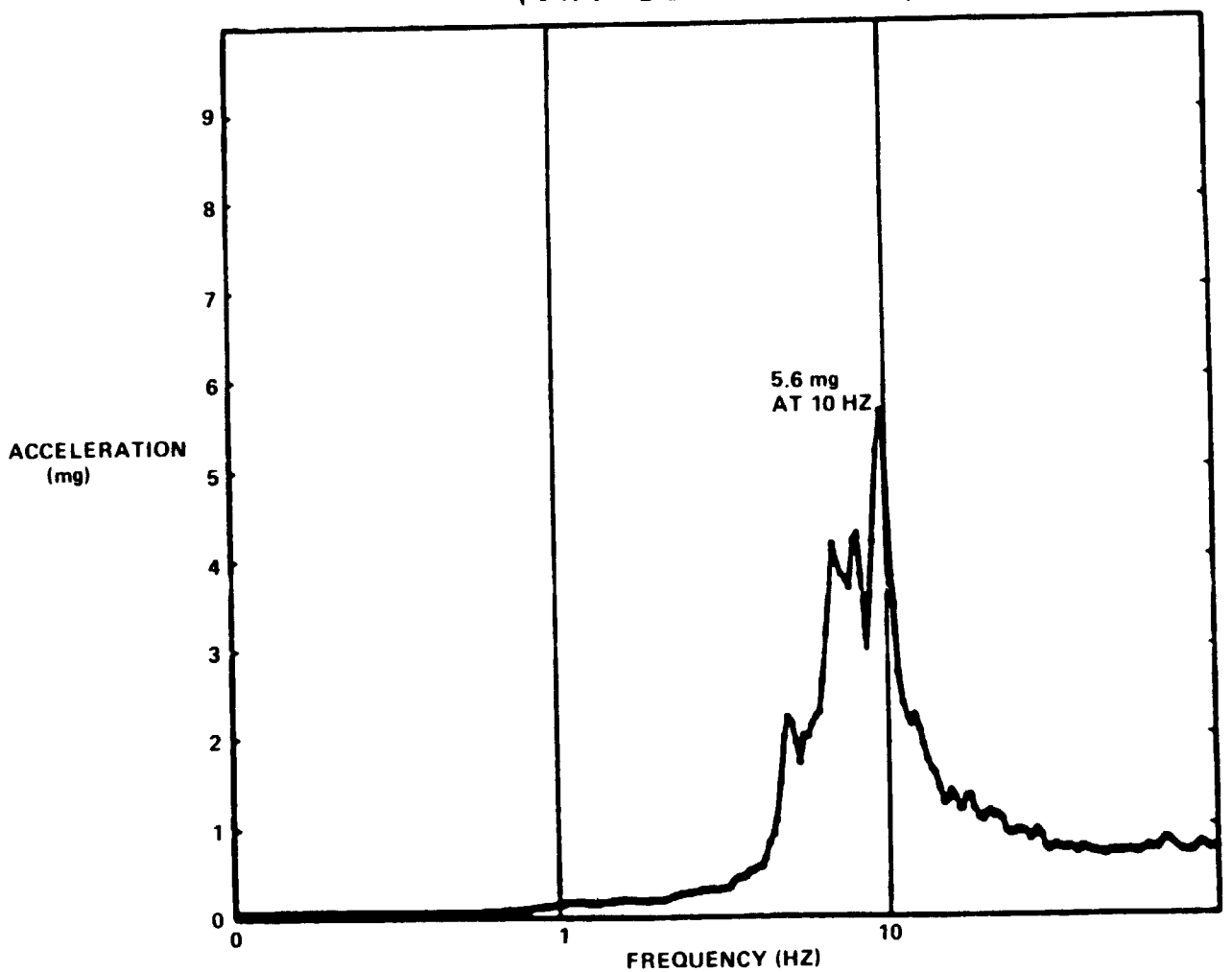

FIGURE 11

TABLE 2

PEAK ACCELERATIONS FROM SPACELAB 1

	MODULE			PALLET		
	X–DIRECTION	Y–DIRECTION	Z–DIRECTION	X–DIRECTION	Y–DIRECTION	Z–DIRECTION
"QUIET TIME" 11.18–11.23 HRS AMPLITUDE (mg) FREQUENCY (Hz)	0.35 – 0.4 20 –35	0.25 22 – 40	0.5 – 0.65 17 – 40	0.13 – 0.25 22	0.2 – 0.45 22	0.13–0.25 8 – 16
COUGH TEST 11.314 – 11.315 HRS AMPLITUDE (mg) FREQUENCY (Hz)	1.0 10	1.0 11	2.8 9	0.2 10	0.3 8	0.7 10
X–PUSH–OFF 11.340 – 11.355 HRS AMPLITUDE (mg) FREQUENCY (Hz)	2.8 12	3.0 21	2.5 9	0.6 12	1.0 6	1.2 8
Y–PUSH–OFF 11.375 – 11.385 HRS. AMPLITUDE (mg) FREQUENCY (Hz)	0.1 16	1.0 21	2.4 8	0.3 18	0.5 15	0.5 8
Z PUSH–OFF 11.404–11.406 HRS. AMPLITUDE (mg) FREQUENCY (Hz)	1.1 12	1.0 20	1.7 16	0.7 15	1.1 17	1.0 9
VERNIER THRUSTER FIRING 202050–202110 SEC. (111 NEWTONS) AMPLITUDE (mg) FREQUENCY (Hz)	0.3 – 0.5 17	0.3 – 0.6 25	0.5 – 1.0 18	NOT AVAILABLE	NOT AVAILABLE	NOT AVAILABLE
PRIMARY THRUSTER FIRING 188.870–188.930 HRS. (3,870 NEWTONS) AMPLITUDE (mg) FREQUENCY (Hz)	25 – 29 9	20 – 29 9	2.5 – 2.9 9	10 – 15 8	10–15 16	20 – 29 16
TUNNEL TRUNNION DISTURBANCE 188.431 – 188.435 HRS. AMPLITUDE (mg) FREQUENCY (Hz)	12 13	6.0 20	9.0 15	2.5 12	2.4 25	3.0 12

forces produced 2.4 to 12.0 milli-g. Note that the accelerations experienced out on the pallet were significantly attenuated as compared to those inside the Spacelab Module, which were very close to the acceleration source.

LOW-G ACCELERATION MEASUREMENTS ON SAFE

On the OAST-1 Solar Array Flight Experiment (SAFE), the base of the solar array was instrumented with Sunstrand model QA1101 accelerometers measuring parallel to the axes of the STS Orbiter.

Figure 12 shows a time history of the low-g data taken at the base of the SAFE, taken in the X-direction over a 100-sec period. A "steady state" amplitude bias of about 0.35 milli-g is apparent in these data, but the cause is not identified in available records. It is probably a calibration shift, which would have been removed in more refined versions of the data. In an attempt to reproduce some of the SAFE data, we learned that all the processed data had been deleted from the computer tape library and only the original analog data tapes remain. Thus, to reproduce data for this flight would require a complete repeat of the entire post-flight data processing operation, at considerable additional cost. This highlights the fact that data are not stored indefinitely in all forms, primarily due to data storage capacity limitations (Reference 9).

LOW-G ACCELERATION MEASUREMENTS ON SPACELAB 3

The flight of Spacelab 3 on STS-51B in April-May 1985 carried the Fluids Experiment System (FES). The experiment was mounted on a 135-kg optical bench that was, in turn, mounted on the double rack inside the manned Spacelab module. A package of Bell Miniature Electrostatic Accelerometers (MESA) was mounted on the optical bench. For experiment purposes, measuring axes of the X and Z accelerometers were rotated 65.7 degrees clockwise (facing the FES rack) from the X- and Z-operational axes of the Orbiter. The resolution of the accelerometers

RAW DATA FROM SOLAR ARRAY FLIGHT EXPERIMENT

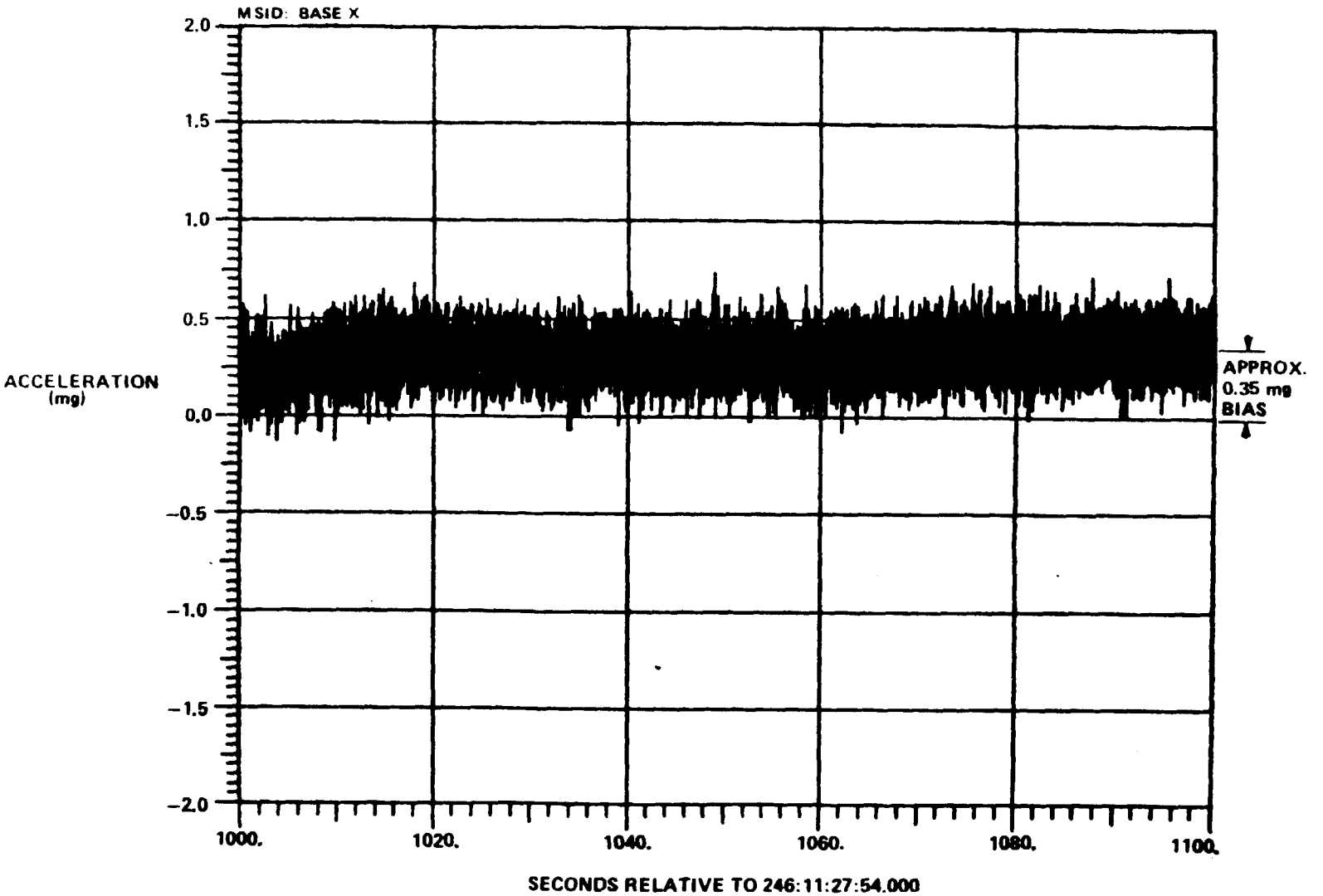

FIGURE 12

is 1 micro-g and the bandwidth is 50 Hz. Data were recorded at 300 samples per second. We have included several samples of low-g data from this experiment as it, perhaps, has been the subject of more analyses at MSFC than any other. Table 3 shows the form of data as received in real time at the MSFC Huntsville Operations Support Center. Average and peak-g levels are given for each axis in units of micro-g for 1-sec and 60-sec time intervals. The notes at the bottom of Table 3 are recorded by the person monitoring the data.

RAW DATA AND POWER SPECIAL DENSITY FROM SPACELAB 3

Figures 13 and 14 deal with a 14-sec time slide of data taken during the Spacelab 3 mission when the FES was not active, but the accelerometers were functioning. An unidentified disturbance occurs at about 5 sec into the interval and damps out in about 3 sec. A power spectral density for the entire time period shows dominant frequencies of 5.8 Hz, 17.2 Hz, 34 Hz, and 138 Hz. A band-pass filter was applied to these data and the results are discussed next.

FILTER DATA AND POWER SPECTRAL DENSITY (PSD) PLOTS FROM SPACELAB 3

The frequency spectrum was filtered to display the 0 to 7.5 Hz acceleration time history shown in Figure 15. The effect of the same unidentified disturbance is clearly visible in this figure. In Figure 16, the PSD plot shows that this filtered sample is also entirely made up of the 5.8 Hz oscillation.

ACCELERATION "CALIBRATION" DURING SPACELAB 3

During Spacelab 3 we were concerned with the higher-than-expected low-g readings. To aid in identifying the source(s) of the accelerations, we requested that all flight crewmen leave the Spacelab module and remain as motionless as practical in the Orbiter. We then had one crewman re-enter Spacelab and perform routine experiment tasks, so we could attempt to correlate his actions with low-g readings.

ED5470

TABLE 3

REALTIME ACCELERATION DATA FROM SPACELAB 3 (FES EXPERIMENT)

NOTE: DATA DISPLAYED ARE NOT TRUE AVERAGE OR PEAK VALUES SINCE ONLY EVERY 30TH DATA POINT IS USED IN CALCULATIONS. ALSO NEGATIVE PEAK VALUES WERE NOT CALCULATED CORRECTLY.

PB HRMGMT 123:06:21:46
MET 4:13:25:19
GMT 124:05:27:37

	G–LEVEL (E–6G'S)	
	1 – SEC PERIOD	60 – SEC PERIOD
X AVERAGE	– 2179	– 801
Y AVERAGE	– 1212	– 1226
Z AVERAGE	– 1913	– 1517
X PEAK	1100	91000
Y PEAK	60	12700
Z PEAK	– 680	11500

NOTES:

TAPE 22:44 → 4/13 25:19 LODEWIJK VAN DEN BERG AT OCP & THAGGARD IS AT MID–MODULE

4/13:27:03	L.V. CLOSED LH OB DOOR (& THEN REOPENS IT TO ALLOW RH DOOR TO CLOSE)
4/13:27:05	L.V. CLOSED RH OB DOOR
4/13:27:06	L.V. CLOSED LH OB DOOR

ED5451

RAW DATA FROM SPACELAB 3

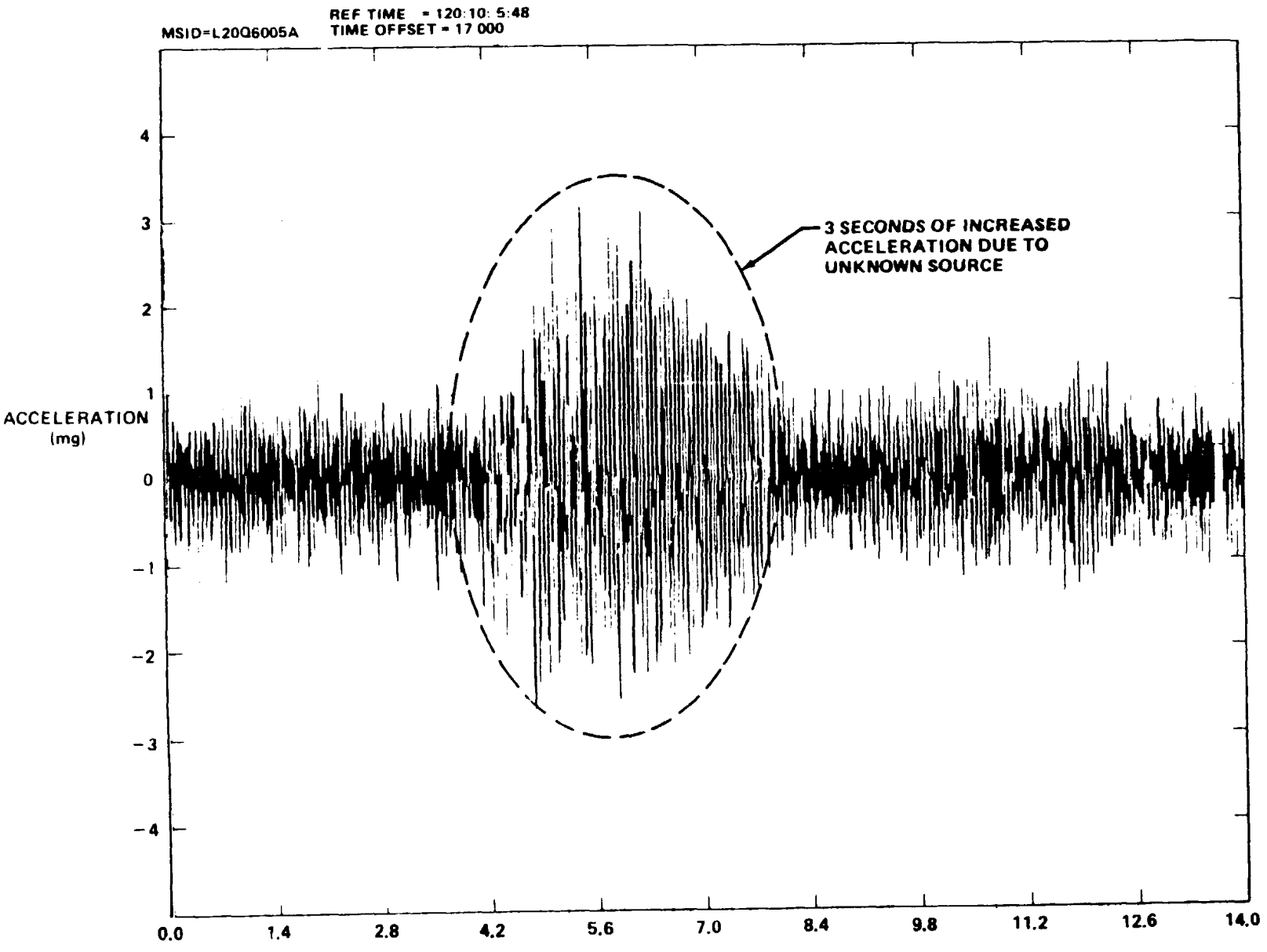

FIGURE 13

POWER SPECTRAL DENSITY FROM SPACELAB 3 (RAW DATA)

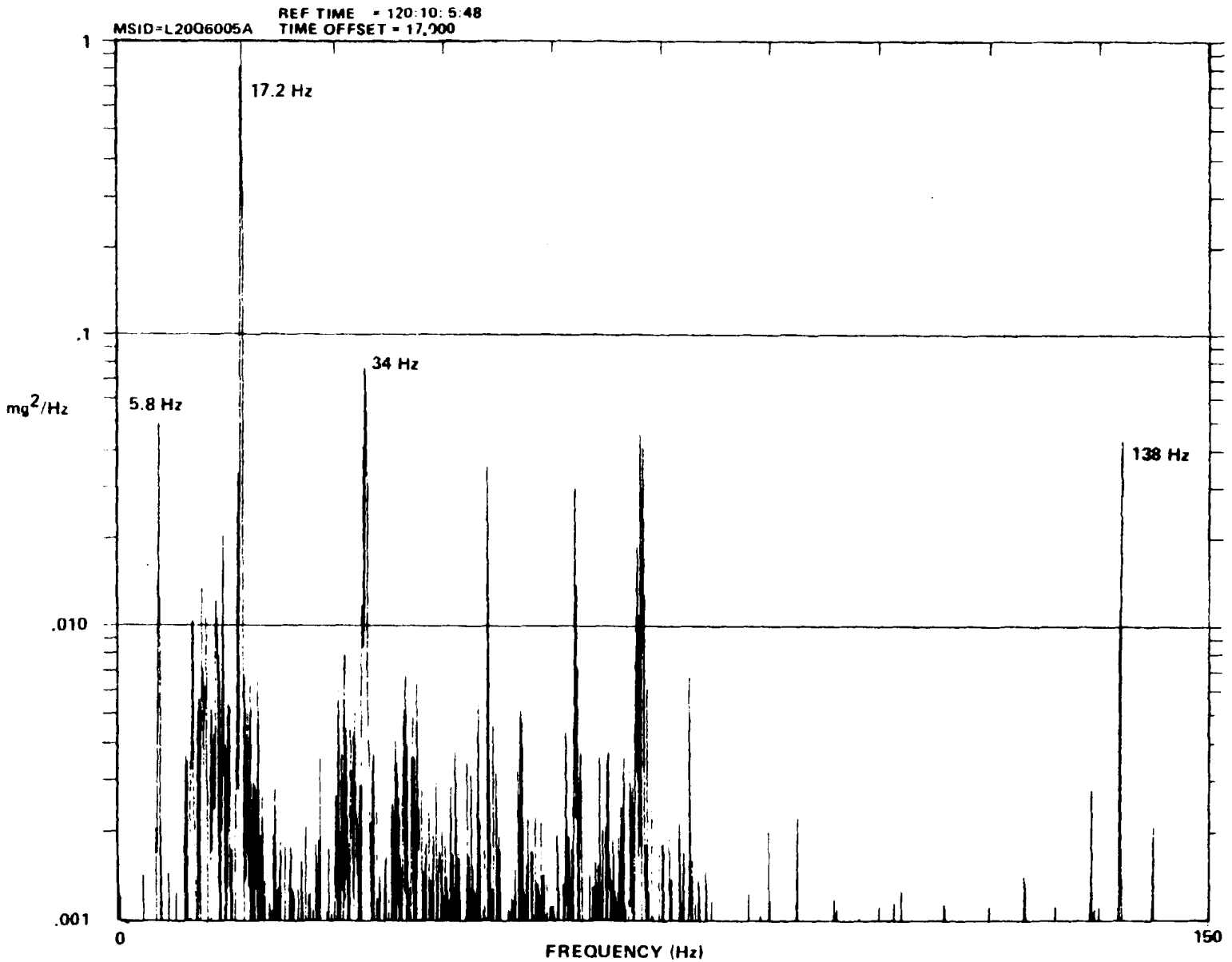

FIGURE 14

ED5453

FILTERED DATA FROM SPACELAB 3
(0 TO 7.5 HZ BANDPASS)

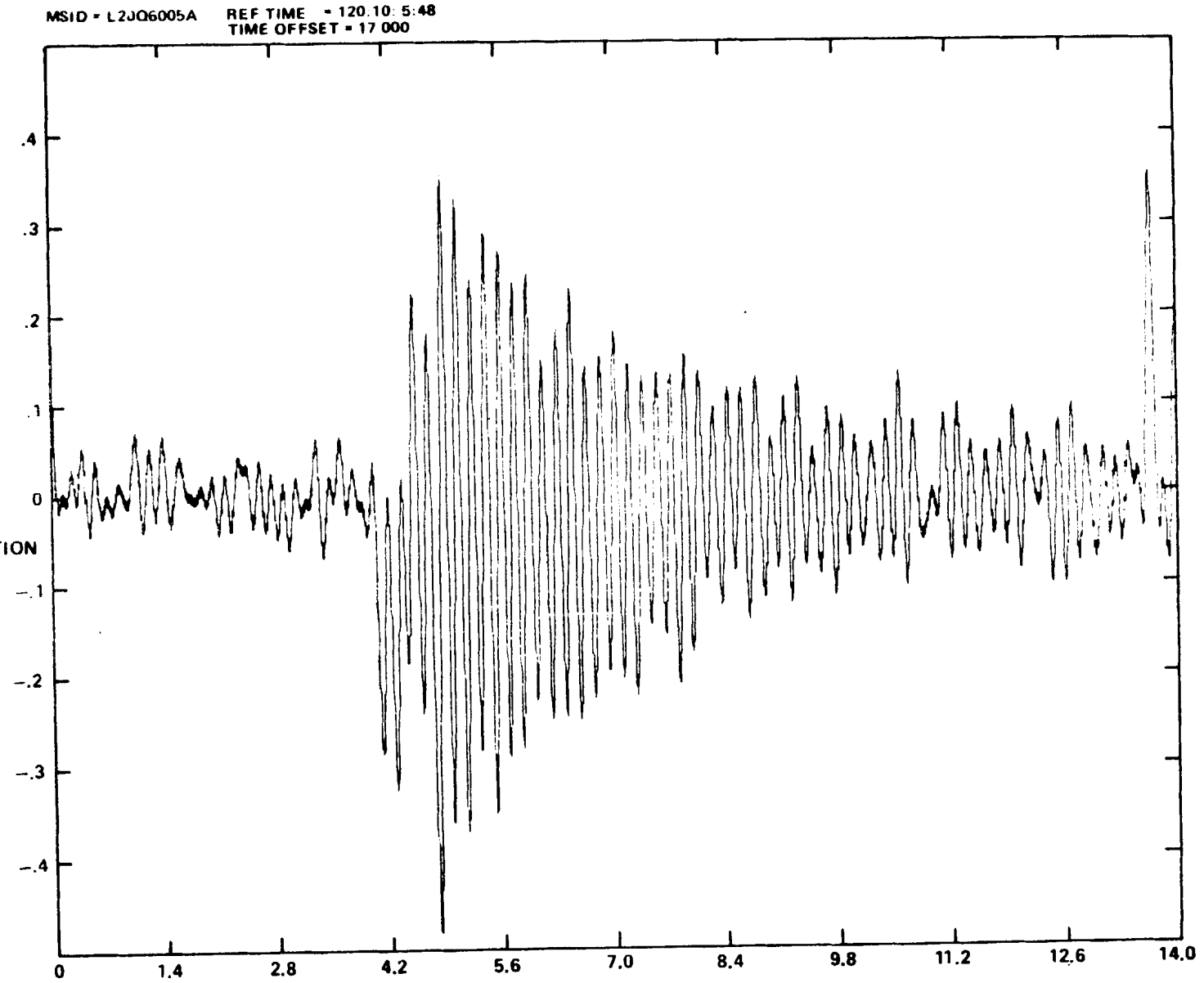

FIGURE 15

POWER SPECTRAL DENSITY FROM SPACELAB 3
(FILTERED DATA: 0 TO 7.5 HZ BANDPASS)

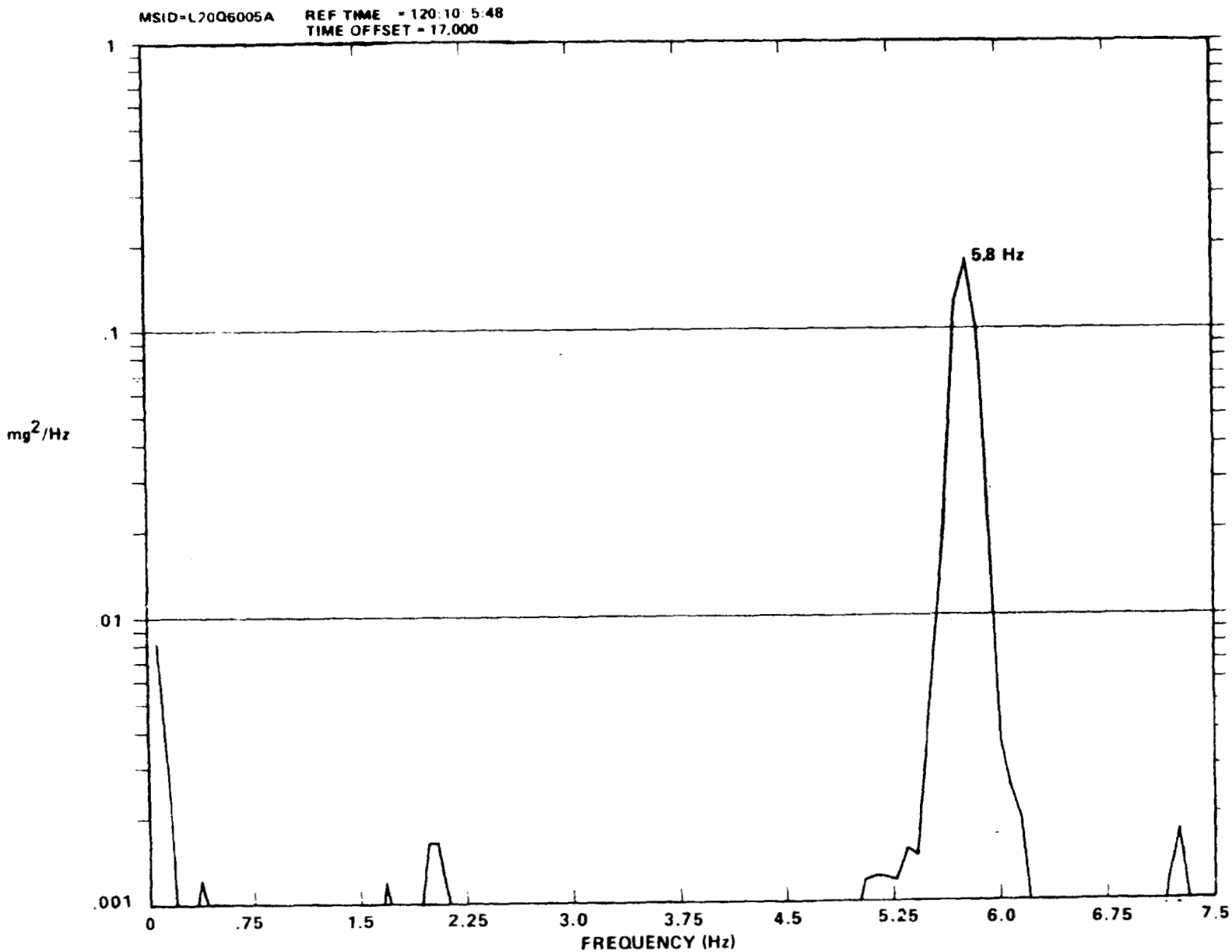

FIGURE 16

Figure 17 gives a record of specific activity of the one crewman. A video tape record of these actions was made in real time during the mission. After the mission, the tape was viewed and the tabulation of activity and timing were made. This record was used to correlate events with spikes in the accelerometer data for the same time period.

ACCELERATION PEAKS WITH LATCH OPENINGS

Figure 18 shows the distinct peaks in "self-inflicted" acceleration, which occurred as the latches on the FES Optical Bench doors were opened. The background acceleration is fairly steady, with peaks slightly greater than 1 milli-g. The peaks at latch openings range from about 4 to 8 milli-g.

ACCELERATION CHANGE WITH CHANGE IN DOOR POSITION

Figure 19 shows a much longer time period (1,600 sec). For the first 750 sec, the Optical Bench doors were in the closed position. For the next 300 sec, the doors were in the open position and then, for the remaining interval, the doors were again in the closed position. The acceleration level shows a marked decrease in amplitude while the doors were open. The exact cause of this phenomenon has not been determined, but the effect of configuration alteration is clear.

LOW-G ACCELERATION MEASUREMENTS ON SPACELAB 2

Spacelab 2 was flown on STS-51F in July-August 1985. Similar to Spacelab 1, it was instrumented with Systron-Donner linear accelerometers and data were accumulated over periods of varied activity. Two examples of the Spacelab 2 data are included here.

CREW-INDUCED ACCELERATION ON SPACELAB 2

Figure 20 shows the acceleration history resulting from crew pushoff from one wall of the module. Only small disturbances appear in the particular axis shown. Wider ranges of acceleration occur when all

ACCELERATION CALIBRATION DURING SPACELAB 3 (FES EXPERIMENT)

REMOVE CREWMEN FROM SL–3 THEN:

TAPE INDICATOR READING		
0:30:21	START VCG ROTATION	
0:35:13	HOLOGRAM TAKEN	
0:36:49	PUSH OFF FROM FES	
0:37:02	UNLATCH FES DOORS	
0:37:10	OPEN FES DOORS	~ 5 MINUTES
0:37:56	ENTER FES	
0:38:20	RE–ENTER BENCH	
0:42:27	CLOSE FES DOORS	
0:42:50	PUSH OFF FROM FES	
0:43:25	PUSH OFF FROM FES	
0:44:40	OPEN PREHEAT DOOR	
0:45:11	CLOSE PREHEAT DOOR	
0:49:40	RE–ENTERING CREW MEMBER	

START	MET	05:13:31:48	TAPE	0:17:33
END	MET	05:14:06:14	TAPE	0:51:55

FIGURE 17

ACCELERATION PEAKS WITH LATCH OPENINGS
SPACELAB 3

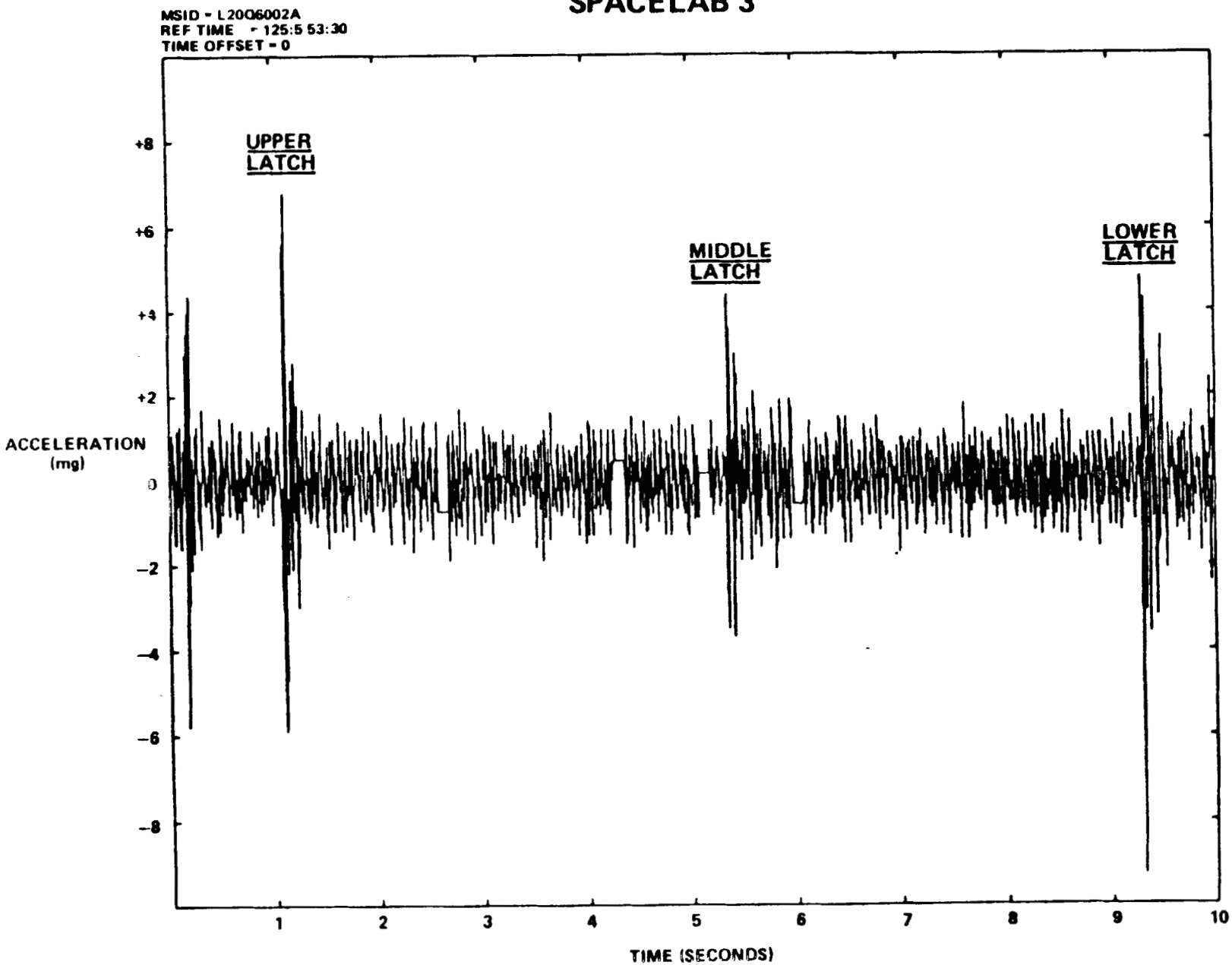

FIGURE 18

ACCELERATION CHANGE WITH CONFIGURATION MODIFICATION

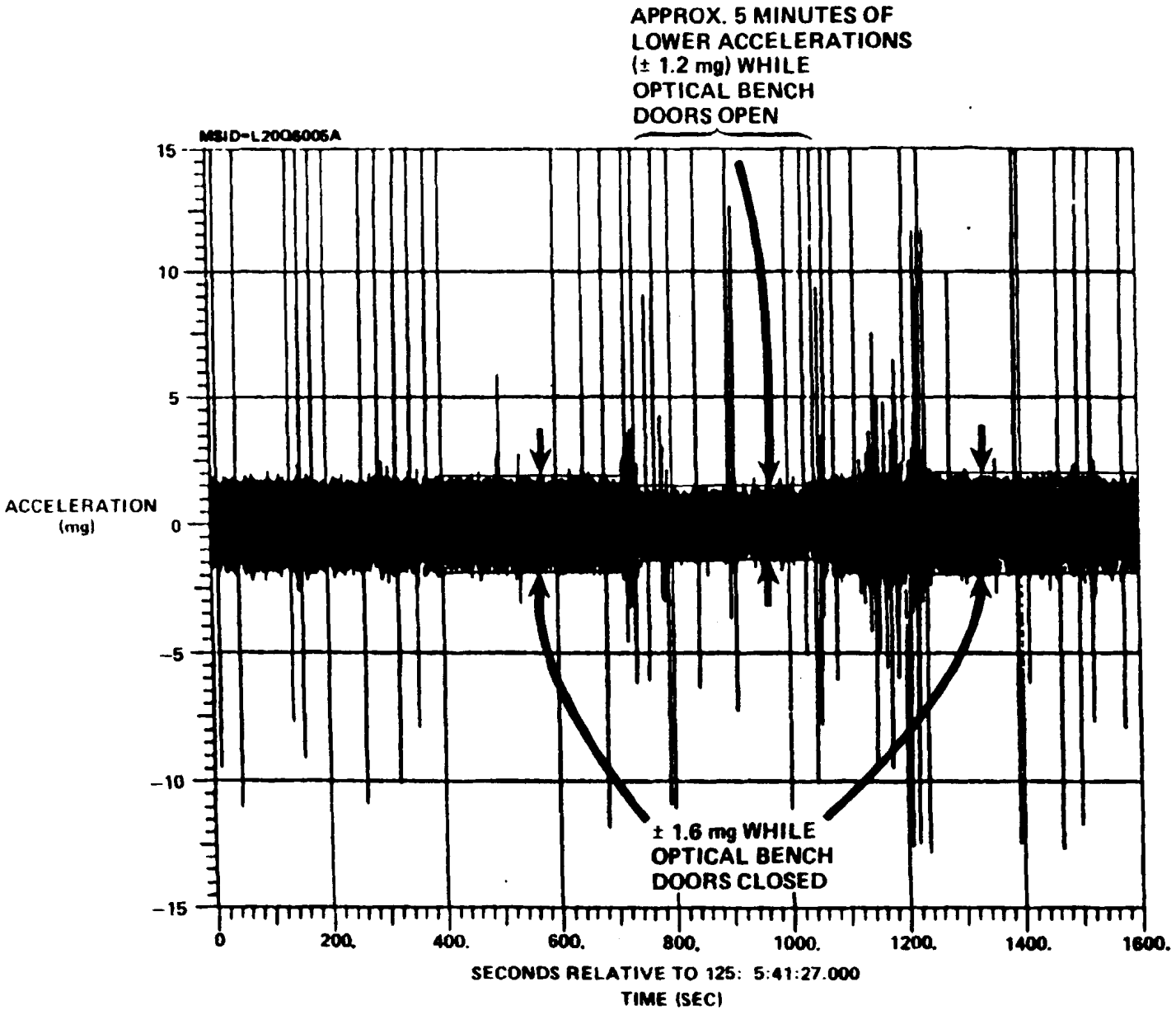

FIGURE 19

CREW INDUCED ACCELERATION ON SPACELAB 2 (VIA PUSHOFF FROM WALL)

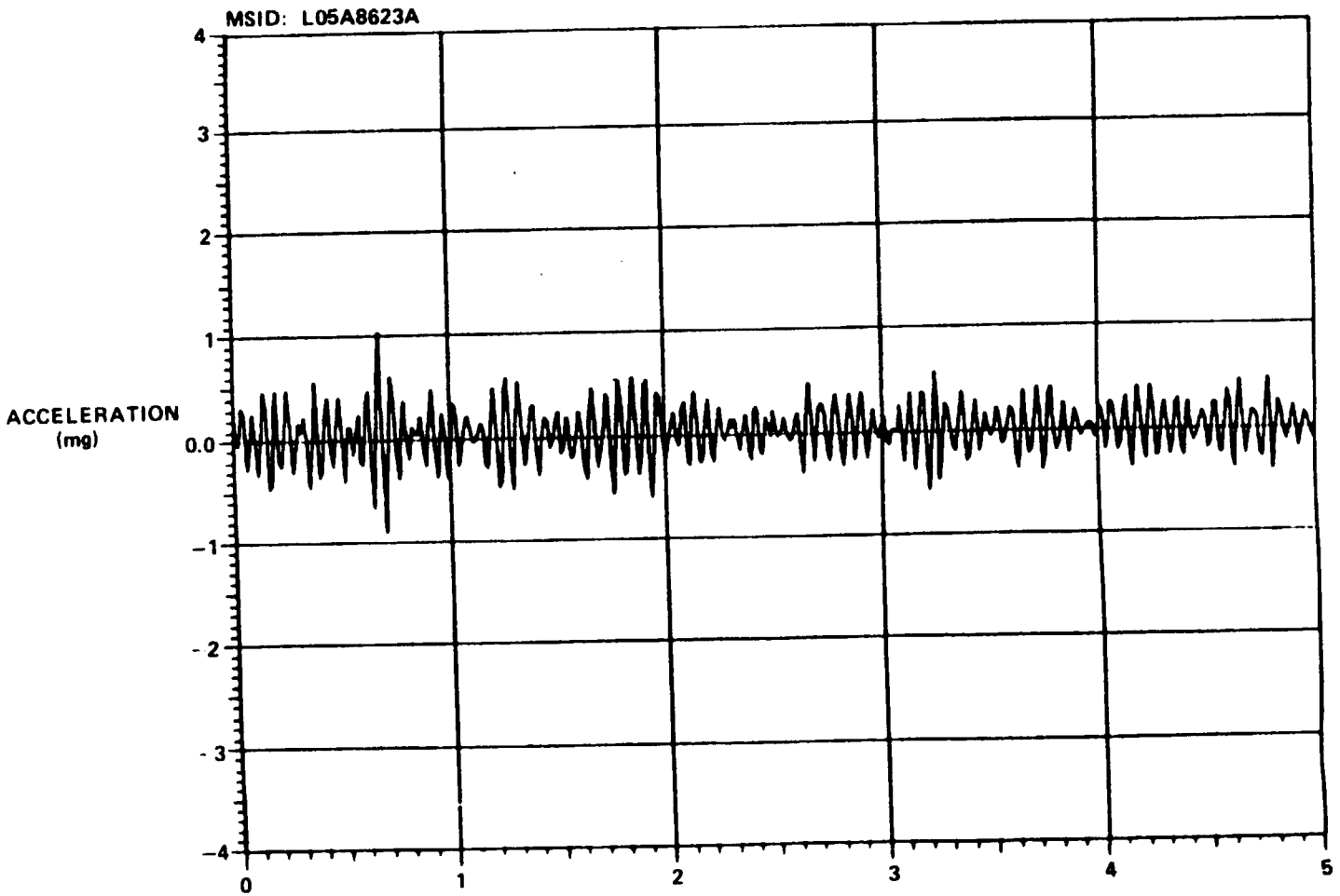

FIGURE 20

axes are considered, as was indicated previously for Spacelab 1. Shock spectra were generated for the Spacelab 2 data. The shock spectra from the pushoff data just shown are presented in Figure 21. The peak response is 6.5 milli-g at 17.4 Hz.

ORBITAL MANEUVERING SYSTEM BURN DURING SPACELAB 2

An example of the relatively large accelerations due to firing of the Orbital Maneuvering System (OMS) thrusters is shown in Figure 22. The initial shock of the thruster produces peaks of 30 milli-g. After about 3.5 sec, a near-steady level of -12 to -14 milli-g is reached. Figure 23 shows the shock spectra for this OMS burn with a peak of 235 milli-g at 5.58 Hz (Reference 10). The measuring direction for this example is the Z axis of the orbiter, which is perpendicular to the wing plane. Accelerations along the long axis of the orbiter due to the OMS thruster are on the order of 50 milli-g.

LOW-G ACCELERATION MEASUREMENTS ON MATERIALS SCIENCE LABORATORY

The Materials Science Laboratory 2 (MSL 2) was carried aboard STS-61C in January 1986. It was instrumented with two Bell Aerospace Model #6471-300001 accelerometers with a range of +/- 0.512 milli-g, an accuracy of +/- 5%, and frequency response of 0.01 to 20 Hz. The data were collected at a rate of 125 samples per second.

This accelerometer data system was obtained from the cancelled Advanced Gimbal System (AGS) project and the range was not wide enough to accommodate peak data during periods of vigorous activity. However, useful data were collected. Some examples follow.

ACCELERATION INDUCED BY TREADMILL USAGE BY FLIGHT CREWMAN ON MSL 2

Figure 24 shows a 5-sec time history of the acceleration environment during treadmill usage by a flight crewman on MSL 2. (Figure 25 is a photo that shows a flight crewman using a treadmill on another STS

SHOCK SPECTRA FROM SPACELAB 2
CREW- INDUCED ACCELERATION
(VIA PUSHOFF FROM WALL)

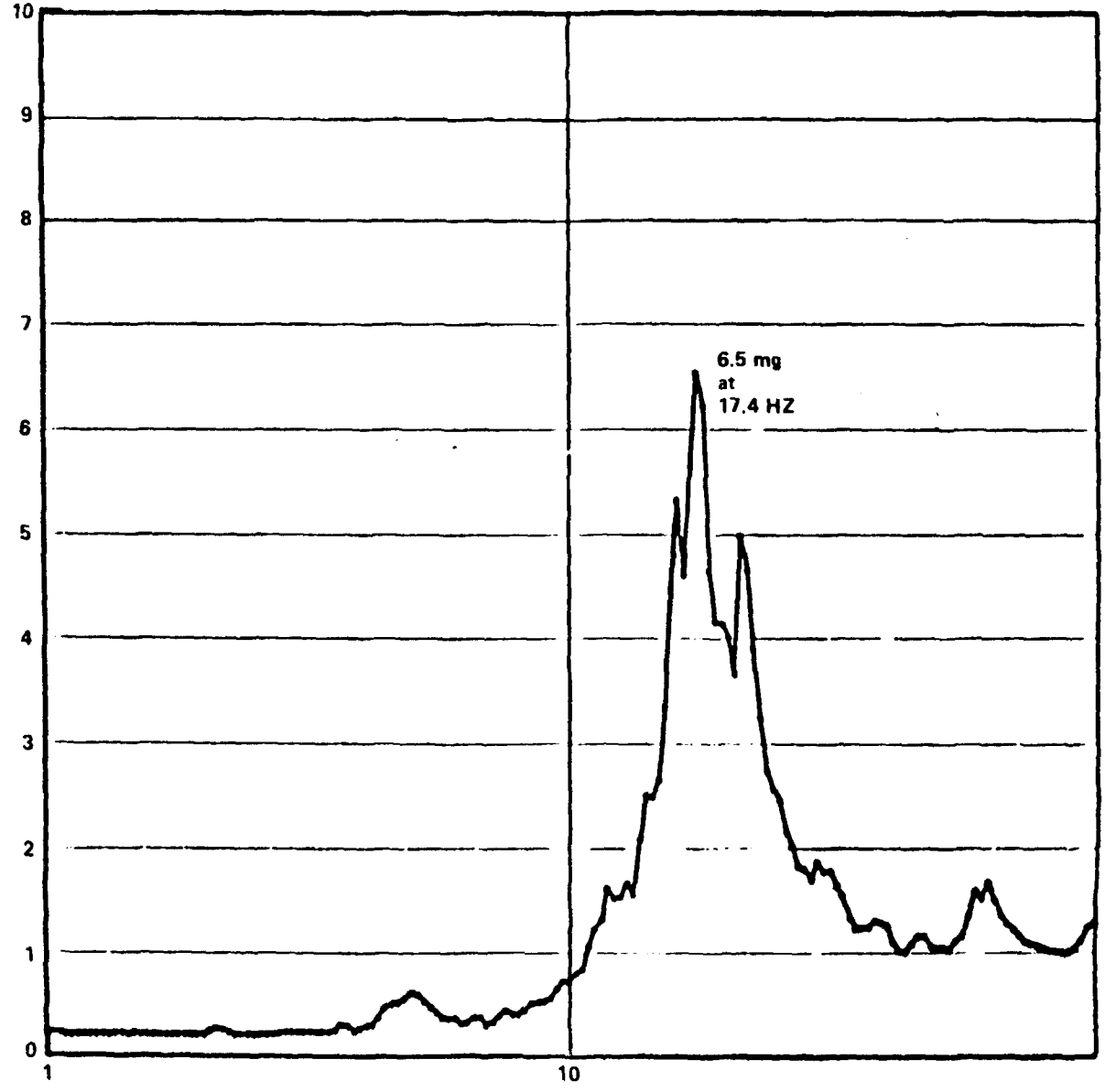

FIGURE 21

RAW DATA FROM SPACELAB 2 OMS BURN

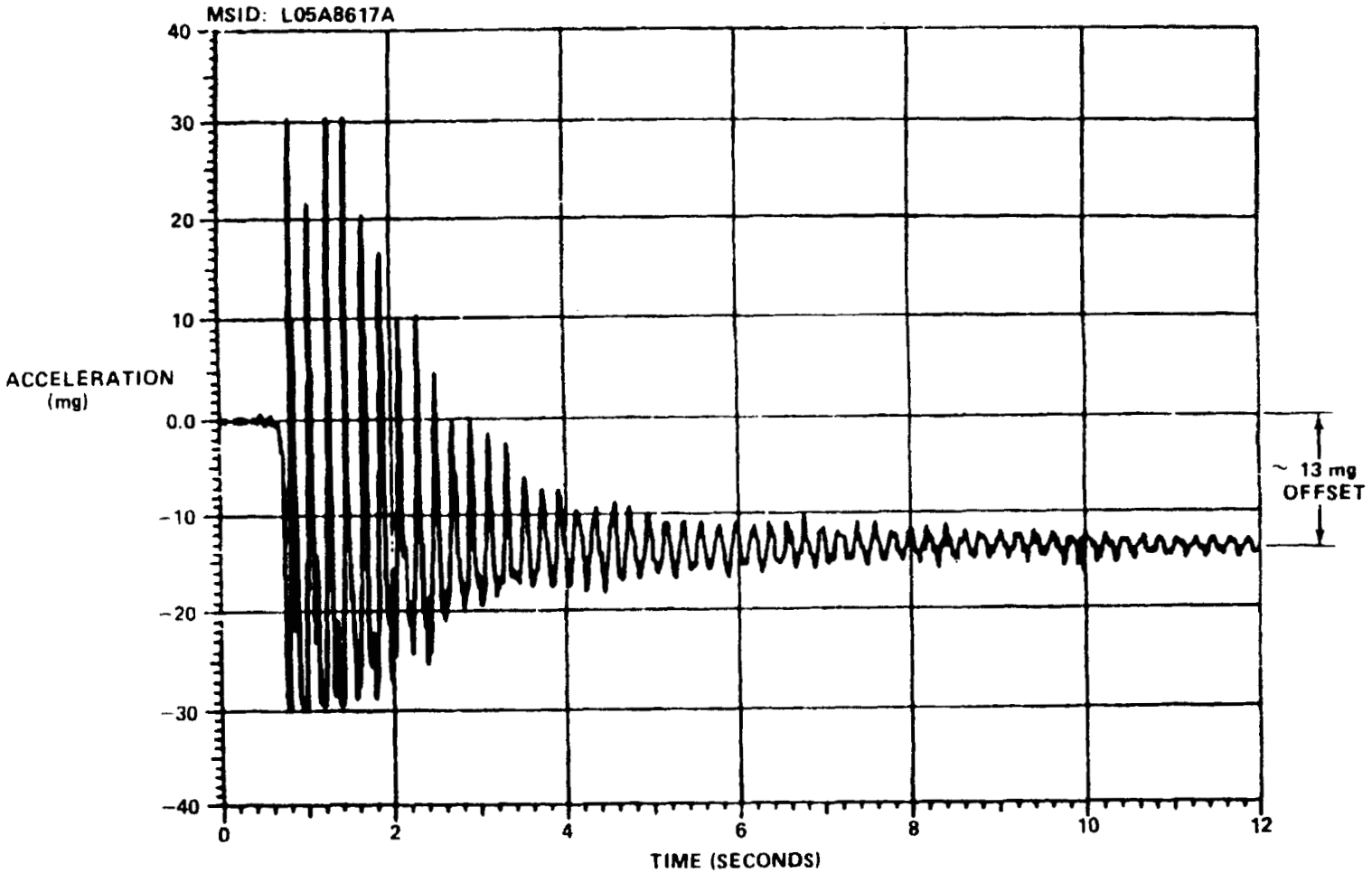

SECONDS RELATIVE TO 1985:216:16:59:26: 0

FIGURE 22

SHOCK SPECTRA FROM SPACELAB 2 OMS BURN

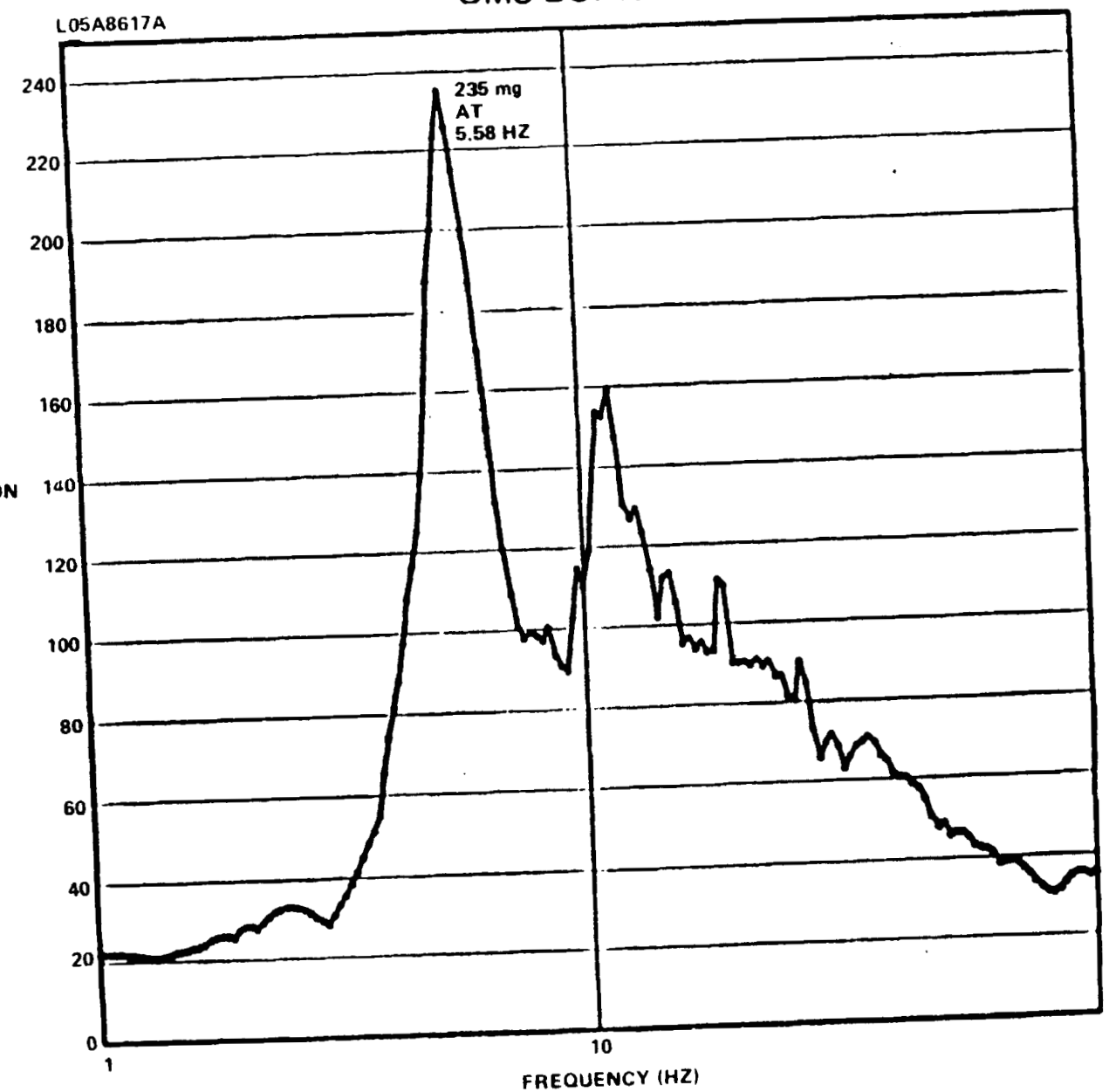

FIGURE 23

ACCELERATION INDUCED BY TREADMILL ON MSL-2
(IN–FLIGHT FILTERED DATA)

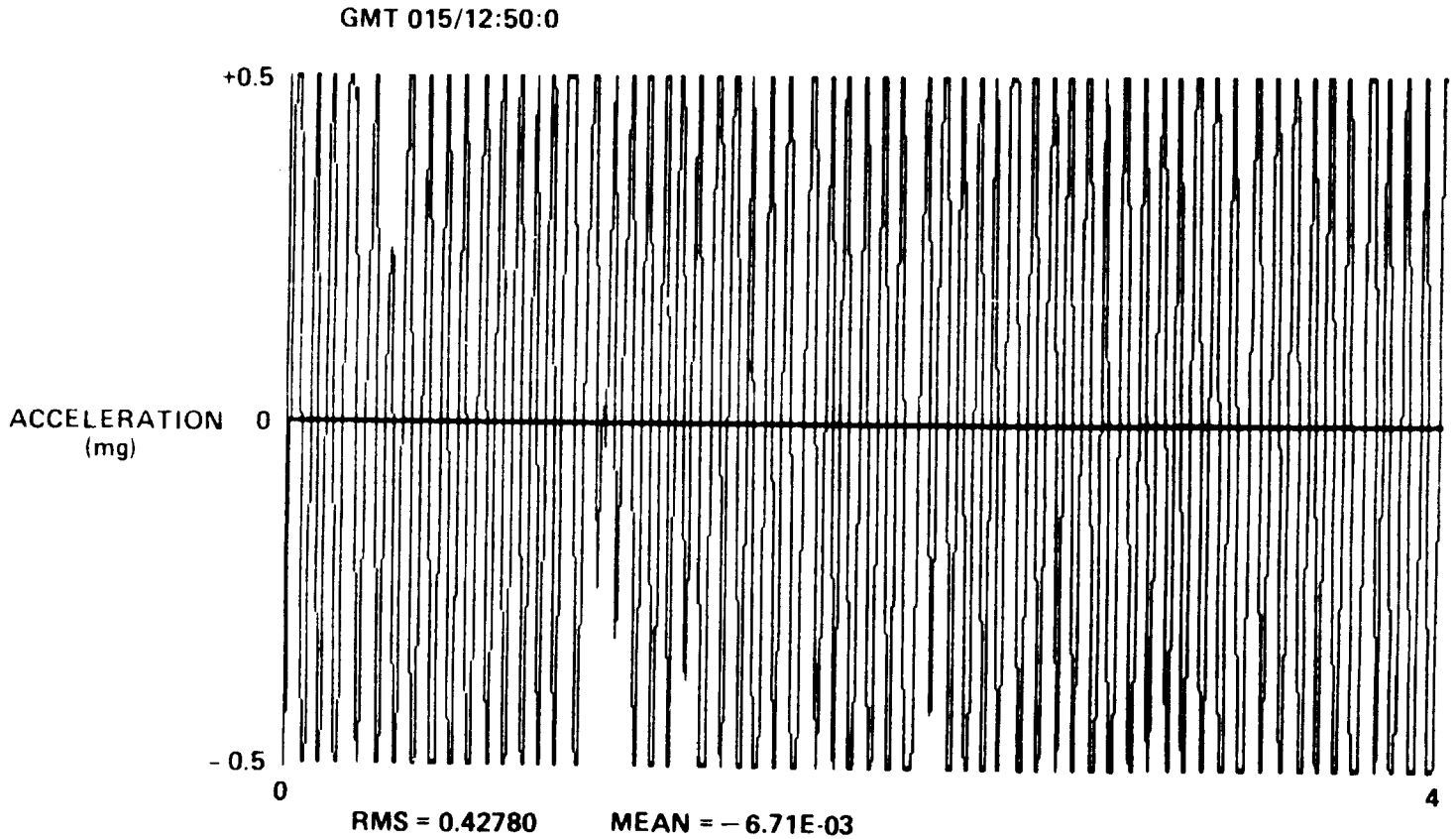

FIGURE 24

FIGURE 25. MSL-2 TREADMILL USAGE

flight). During the vigorous MSL 2 treadmill activity, the data peaks were frequently clipped by the limited range of the system. The rolloff of the frequency response of the accelerometer is such, however, that the higher frequency data are not clipped. Thus, by using "inverse filtering," the data can be reamplified and the output expressed in the correct wider range than that originally recorded. The sample shown in Figure 24 was prior inverse filtering. Figure 26 shows the same data after being adjusted by this inverse filter procedure. Several peaks of more than 1 milli-g appear here (Reference 11).

LOW-G ACCELERATION MEASUREMENTS FROM THE HIGH RESOLUTION ACCELERATION PACKAGE (HIRAP)

The HIRAP is a separate associated major subassembly of the Aerodynamic Coefficient Identification Package (ACIP). It is mounted on the Orbiter ACIP mounting shelf. The ACIP contains linear and angular accelerometers used to collect aerodynamic and flight dynamic data during shuttle ascent, orbit, and re-entry flight for spacecraft design and operational considerations. The angular accelerometers are in a Systron-Donner model 5612 triaxial assembly using model 4595 single axis angular accelerometers. The linear instrument is a Bendix GSD triaxial linear accelerometer. The HIRAP uses three orthogonally mounted, gas damped, Bell Aerospace Model X1 linear accelerometers. The HIRAP instruments are better than those in the ACIP for characterizing the low-g environment. They have 1 micro-g resolution and a range of +/- 8.0 milli-g and an accuracy of better than 0.125%. The frequency response is limited, however, by low-pass filters to 2 Hz and 20 Hz. Inverse filtering can be used as previously mentioned to adjust the output (Reference 12). One example of HIRAP data from this reference is shown in Figure 27. It shows a relatively long period of 2,000 sec consisting initially of a quiet period, then a period of primary (3870 Newtons) thruster firings, and finally a period of vernier (111 Newtons) thruster firings of the Orbital Rate Control Systems. The relative magnitudes of acceleration in the different periods is readily apparent.

ACCELERATION INDUCED BY TREADMILL ON MSL-2
(POST–FLIGHT INVERSE FILTERED DATA)

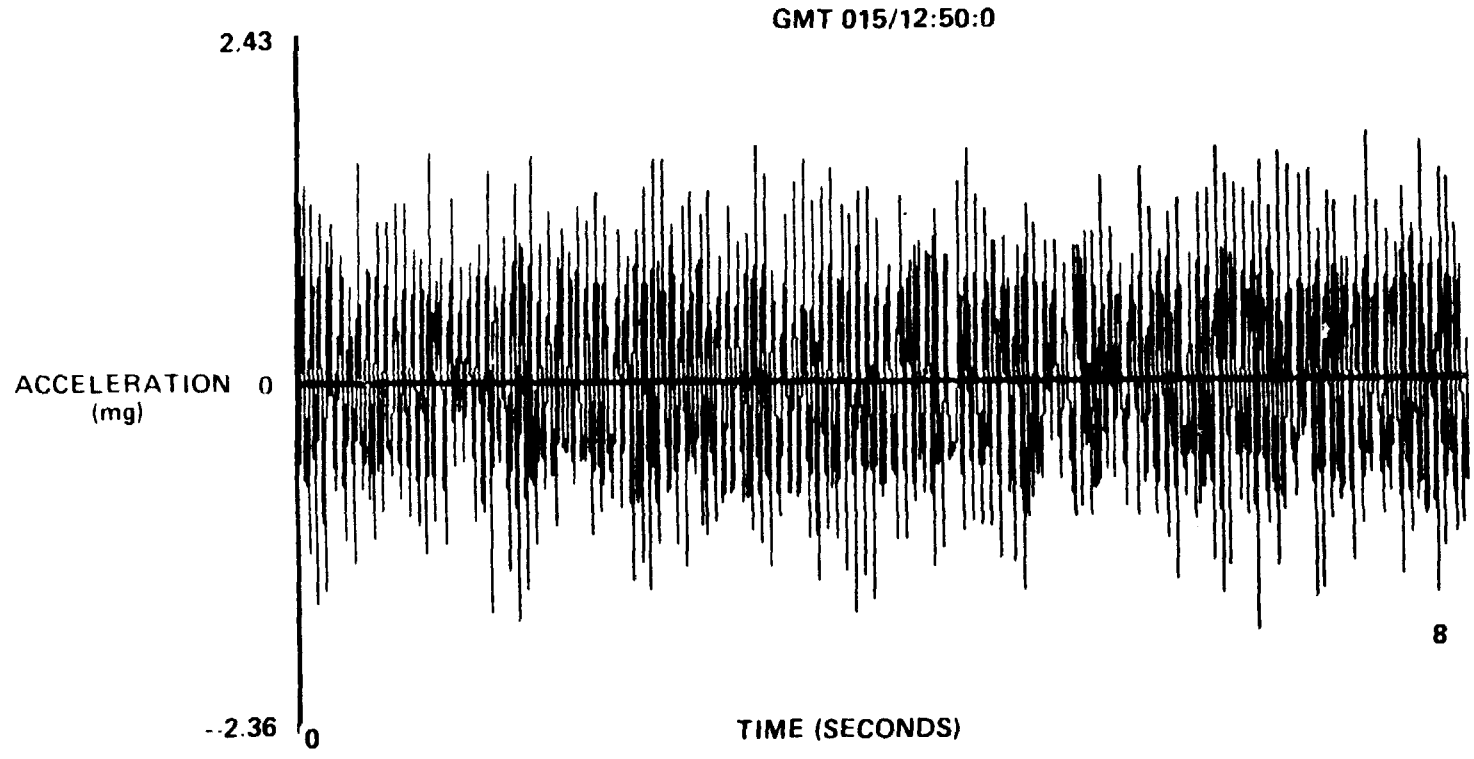

RMS = 0.67535 MEAN = 2.89E-03

FIGURE 26

ACCELERATION CHANGE WITH REACTION CONTROL SYSTEM (RCS) FIRINGS (FROM HIRAP)

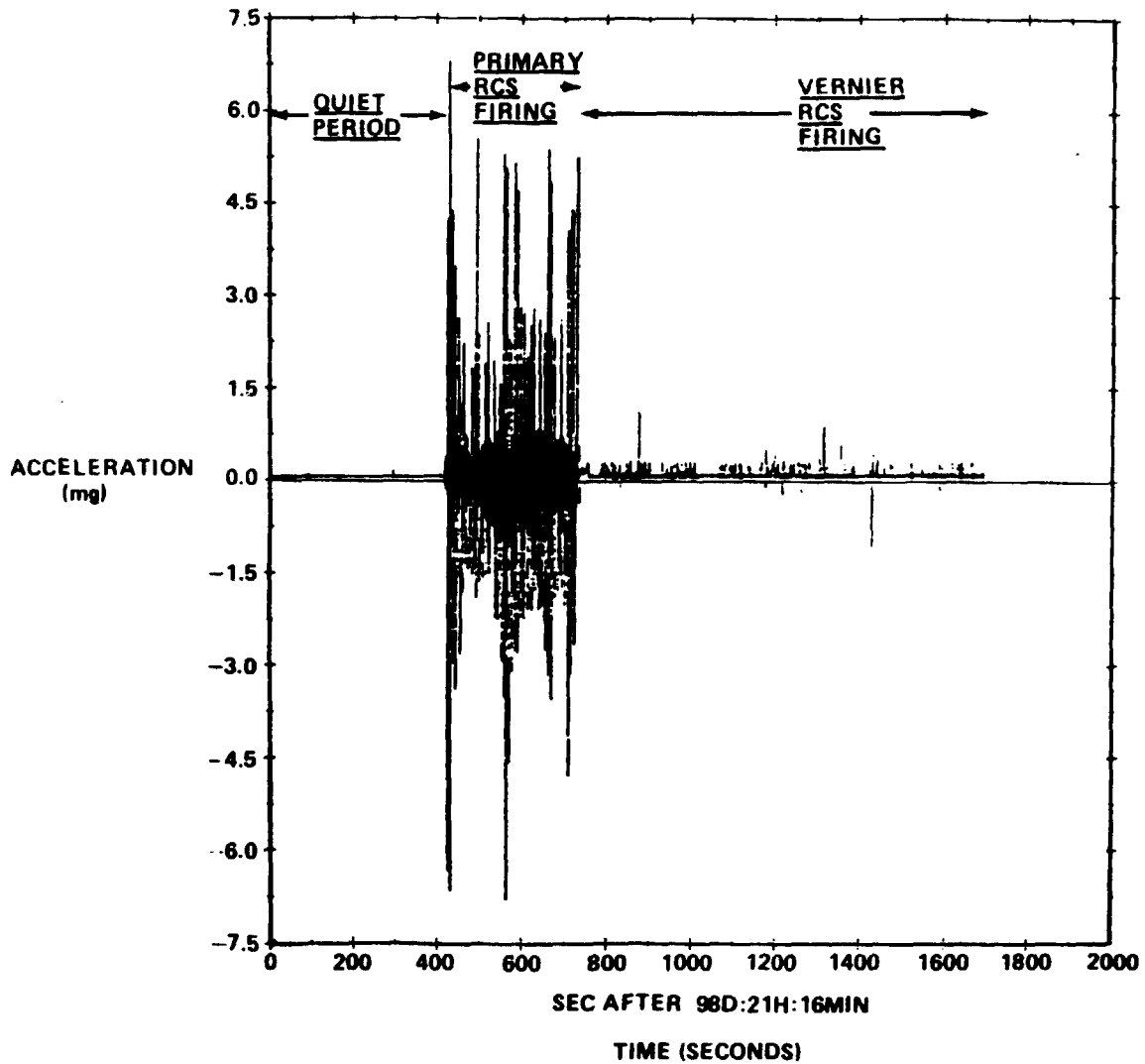

FIGURE 27

To date, the emphasis on analysis of HIRAP data has been on their use in deriving the aerodynamic forces exerted on the Orbiter in the early stages of reentry, but it appears that the HIRAP can contribute to the analysis of the on-orbit low-g environment as well. Reference 13 gives a list of ACIP and HIRAP data available and also some examples of the data available from some missions.

CONCLUSIONS

Perhaps the most significant message from this summary (Figure 28) of 12 years of low-g data is highlighted by our choice of units in which to present the bulk of the material, i.e., milli-g rather than micro-g. We had initially hoped for 10^{-6}g maximum, but decided to request a more achievable 10^{-5}g on STS missions. Instead, we were promised 10^{-4}g maximum, but actually were provided 10^{-3}g of jitter. So we "lost" three orders of magnitude. (The extent to which this can be improved on Space Station is yet to be shown.) So on low-g carriers thus far, we typically have been using a "milli-g" environment; micro-g will be a future goal.

One other significant problem is that detailed records of mission events (particulary crew activity, but also mechanical events and activity) are difficult to obtain and very difficult to correlate with acceleration data.

A problem that surfaced during preparation of this paper is that all the processed forms of data cannot be stored indefinitely. Thus, prompt analysis and reduction of data to encompass the significant information and storage of that information is essential.

RECOMMENDATIONS

More systematic data acquisition and reduction techniques are needed for low-g data; previous efforts have been highly individualized and relatively ineffective.

● CONCLUSIONS AND RECOMMENDATIONS

- LOW–G PEAKS OF STS SEEMS TO BE QUITE OFTEN ON THE ORDER OF MILLI–G'S RATHER THAN MICRO–G'S
- DETAILED MISSION EVENT HISTORIES ARE DIFFICULT TO OBTAIN AND ALSO VERY DIFFICULT TO CORRELATE WITH ACCELERATION TIME HISTORY DATA
- LOW–G DATA IS PERISHABLE (DUE TO STORAGE CAPACITY LIMITATIONS) AND SHOULD BE RETRIEVED AND REDUCED SHORTLY AFTER EACH MISSION
- MOST OF LOW–G DATA ACQUIRED TO DATE HAS UNDERGONE ONLY MINIMAL ANALYSES DUE TO LACK OF A PROVEN, ECONOMICAL APPROACH AND DUE TO LACK OF INVESTIGATOR USABILITY
  - MORE SYSTEMATIC LOW–G DATA ACQUISITION AND REDUCTION TECHNIQUES ARE NEEDED.
  - LOW–G DATA USERS NEED TO STRATEGIZE THEIR SPECIFIC USE OF LOW–G DATA

FIGURE 28

The body of well-qualified scientists that need low-g is composed mostly of metallurgists, crystallographers, or physicists who are expert in their fields of speciality, but who may not be adept at: (1) taking low-g data and converting that to the effects on fluid dynamics; (2) converting that, in turn, to effects on concentration gradients; and, (3) transforming that into an understanding of the effects on crystal microstructure. Therefore, low-g users need to strategize their specific use of low-g data very early in their experiment planning, so that the low-g data can be smoothly integrated into the in-flight and post-flight experiment analyses--not overlooked, as prevalent today.

The volume of low-g data is massive and the extent of analysis of the data is still limited. However, interest in the results is growing and NASA has created an STS Orbiter Environment Panel to gather information on all aspects of the on-orbit environment into a central data base; the Orbiter Motion Subpanel (which was originally chaired by one of the authors and is currently chaired by the other) is charged with gathering the low-g data for the above panel. Continued effort will be applied by the Orbiter Motion Subpanel to characterizing and understanding the low-g environment on the STS Orbiter and taking measures to improve the environment for the many investigators who need a more quiescent acceleration environment for acceptable experiment results. Obviously, these same types of measures should be diligently incorporated into the Space Station planning, design, and operation. It is of utmost importance that acceleration levels on Space Station be held to a minimum and that characterizing and understanding those residual accelerations be a standard real-time Space Station task.

REFERENCES

1. A summary of the Skylab Crew/Vehicle Disturbances Experiment T-013, Bruce A. Conway and T. C. Hendricks, NASA, Langley Research Center, NASA TND-8128, March 1976.

2. SPAR IX Self-Induced Vibration, William W. Cleaver, George C. Marshall Space Flight Center, ED23-80-118, December 1980.

3. Accelerations Experienced During Low-G Flight of Black Brant VC (NAS 21.015) on October 4, 1974, Ralph Kissel, NASA, TMX-64903.

4. Measurement of Acceleration Forces Experienced by Space Processing Applications, S. Toth and M. Frayman, Goddard Space Flight Center, Contract No. NAS5-23438, Mod. 23, ORI INC, Technical Report 1308, March 1978.

5. Memorandum for Record. Preliminary Results of Low Level G Force Monitoring During Conduct of Electrophoresis Equipment Verification Testing on STS-3, Cletis R. Boohrer, Lyndon B. Johnson Space Center, SE3/5-82/88, May 18, 1982.

6. Micro-g Acceleration Measurement System (MGAMS) Data From STS-11, Johnson Space Center Memorandum SE3/3-84-22 (undated).

7. Materials Experiment Assembly (MEA) Acceleration Summary, STS-7, Earle G. Harris, Marshall Space Flight Center, JA62-004, July 1984.

8. Effects of Spacelab Deformations and Disturbances on Optical System Alignment and Pointing, McDonnell Douglas Corp., MDTSCO Huntsville Operations, TM SEAD-85038A, May 1985.

9. Unpublished material on Solar Array Flight Experiment furnished by Gene Young, Marshall Space Flight Center, TA81.

10. Unpublished material on Spacelab 2 furnished by Malcolm Tagg, MDTSCO Huntsville Operations.

11. Materials Science Laboratory 2 (MSL-2), Acceleration Study, Fred Henderson, Teledyne Brown Engineering, August 1986.

12. SDI Space Shuttle Based Experiments for Acquisition, Tracking, and Pointing, JPL Contract No. 957337, The Charles Stark Draper Laboratory, Inc., CSDL-R-1868, April 15, 1986.

13. Microgravity Disturbances on the STS During Orbital Operations, Leonard S. Nicholson, Johnson Space Center, TM2-86-18, June 1986.

Ken Demel, Johnson Space Center: Are most of that data that you were talking about in the 5- to 20-Hz frame? What is our sensitivity below 5 or certainly below 1 Hz, and how does all of this experience compare to what we think we're seeing in the reduced sensitivity of liquids in the higher frequency readings?

Roger Chassay: It's hard to tell. The question is, Do we see in the bulk of these data that most of the data are in the order of 5 to 20 Hz and did we see any other in a range where it might have more impact on experiments such as the various modes and frequencies? It seems to me that we have not made a systematic study of that, but just taking a look at some of the samples that we have been shown here today there are many samples that we've shown that happen to fall into the 5- to 20-Hz region or above.

Ravinda Lal, Alabama A&M University: I saw on one of the viewgraphs you showed that the data in the module and the pallet were quite different and some exceeded one tenth of data in module. Do we believe that the structure problem of the Shuttle to Spacelab we are not communicating the disturbances into the cabin? Is that going to be a big problem in the space station?

Chassay: The question is the data where we compared the accelerations out on the pallet with the accelerations inside the module, there is a rather drastic reduction in the accelerations out on the pallet as compared to those inside the module. I think the answer to that is that the accelerations, especially the cough test and the push-off-the-wall, were occurring inside the module, I believe, and so therefore one would expect the accelerations closer to the source would be a higher level, because there is some attenuation over most mechanical joints and so out in the pallet area with the additional mechanical joints there would be an additional attenuation.

Ed Bergmann, C.S. Draper Laboratory: I'm interested in one of your charts where you showed a large peak at 17.4 Hz. I've done quite a bit of work with the ASIP and HIRAP and it turns out that those instruments have fluid pumps that give a signal of 17.4 Hz in the

output from those instruments. Was this taken with a different instrument or with ASIP/HIRAP?

Chassay: _____ shows up in the HIRAP data that was shown in Figure 26, it turns out that 17 Hertz shows up in some of the data. You'll see it later in one of the other talks, and in the other data it does not show up and that is rather mysterious. I think that is a good topic for the panel discussion tomorrow night. We felt that 17 Hertz might be a hard fact of some data processing we were doing but we were unable to find any major 17 Hertz input that would be coincident with all the places that we were seeing it and also be absent at the time we were not seeing the 17 Hertz.

Bergmann: All that I am saying is that in talking to the manufacturer of the ASIP instrument they indicated that there's a fluid pump in the suspension of the instrument that oscillates the ASIP at 17 Hertz.

Chassay: That's valuable input, some how it looks as though that 17 Hertz topic does need additional discussion, perhaps during the panel discussion.

10. PREDICTION AND RECONSTRUCTION OF ON-ORBIT ACCELERATION

Edward Bergmann, C. S. Draper Laboratory

ABSTRACT

As the number of acceleration sensitive experiments to be carried on each Shuttle or Space Station mission increases, the requirement for either low-g environment or for accelerometry at each experiment location also increases. Preflight planning of such experiments in the past has not always included detailed analyses of the acceleration environment at the experiment location that had a serious impact on the experiment. Careful modeling of the mission activities and their effect on the experiment in many cases would have been beneficial to these experiments. In some cases, the experiment was not compromised, but insufficient instrumentation was available onboard to directly measure accelerations at the experiment location. This paper describes the type of preflight modeling available to assist in experiment design and mission integration and the use of that tool postflight to enhance flight data when sensors are not ideally suited to experiment analysis. Examples of recent shuttle flight experiments are presented.

My presentation is going to appear different from those of my predecessors; they presented data actually measured on orbit with accelerometers. The specific subject I want to discuss is what to do in a situation where there is no appropriate instrumentation to support analysis of the experiments. The way that I got into this particular quandary was that during mission 61-B I met the principal investigator of the 3M experiment, who was very interested in precise, low g environment. When I started talking to the experimenter, it became apparent to

me that there was no single source of g-levels at various locations on the Shuttle. As a result, we are expending a significant effort trying to reconstruct the accelerations that the Shuttle induced on the DMOS experiment during that mission. We are trying to see how we can either interpret what happened to the experiment as a result of these accelerations that were induced by the Orbiter or redesign the experiment and refly it to avoid these by taking advantage of operational considerations.

I don't think I need to go through the numbers except that I want to indicate to you that most of the effects that would influence an experiment in the milli-g or micro-g range have either been studied mathematically or calibrated by in-flight measurements and verified against simulations on the ground. What that leads to is that we have a fairly good ability to predict and model the kinds of effects that the various environmental disturbances would have on the vehicle, probably down to the micro-g range. I can't say that we have a good model of some of the effects of things like solar radiation pressure and cabin leakage but they are at or below this range. We also have a very good way of modeling the control disturbances that are induced on the experiment.

The DMOS experimenters were not aware of the fact that Mission 61-B included the flight test of a new control system, which would maneuver the vehicle considerably more than most of the other Shuttle flights had been maneuvered. So there was a great deal of jet activity on that mission and, as a result there were very large jet thrust-induced disturbances on the experiment. The disturbance-level numbers were generated specifically in support of the DMOS experiment, which was in a middeck locker.

In trying to piece together what happened on that mission we first went back to the kinds of data that are normally available from a Shuttle mission. There are two primary sources of information on what occurred during a mission in terms of the dynamic environment. First is

the normal Shuttle telemetry of a large number of flight control, guidance, and navigation parameters to reconstruct the Shuttle state, trajectories, and the control activities. In addition, on the orbiter Columbia there is also the Aerodynamic Coefficient Identification Package/High Resolution Accelerometer Package (ACIP/HIRAP). This is a set of linear accelerometers, angular rate gyros, and angular accelerometers that were originally installed in support of entry aerodynamic studies. The ACIP has been available since STS-3 and the HIRAP has been available since STS-6. We have borrowed them for on-orbit measurements to calibrate RCS jets and to verify disturbance levels, as shown in Figure 1. Unfortunately, 61-B was flown on Atlantis, which does not have an ACIP/HIRAP. Direct accelerometer data were therefore not available from the instruments in support of the experiment.

One of the types of information that we did have available was in the telemetry; it is the state feedback through the flight control system and the navigation system. For flight control and navigation the orbiter relies on an inertial measurement unit, which is simply a four-axis set of gyros for measuring attitude, capable of about 20 arc seconds quantitization. There is also a set of accelerometers mounted on the stable member of the IMU that have a resolution on the order of 1 cm/sec^2.

Normally for on-orbit operation there are no other onboard state data available. There are ground tracking data available but the resolution of that data is somewhat less than needed for analysis of an experiment.

In the on-orbit flight control system there is no rate gyro in the loop. The angular rate information that is supplied by the flight control system on the orbiter is actually inferred from the attitude measurements and from the control supplied by the autopilot of the vehicle and is basically generated by a two-part filter. That filter is very similar to a Kalman filter, based on the difference of the estimated vehicle attitude and IMU. It generates an estimate of the vehicle angular rates and the undesired acceleration.

One interesting problem in using these data to analyze what happens at a particular location in the orbiter is that the navigation system is navigating the Orbiter center of gravity and the DMOS experiment was located in the orbiter middeck, which is 45 feet forward of the center of gravity. The result is that the acceleration at that location consists of the jet accelerations, centripetal, and Coriolis terms, which actually become quite significant when the Orbiter is maneuvering in attitude. There are also significant accelerations due to the gravity gradient, aerodynamic, and vibration. Most of these have been observed in the past and have been modeled mathematically. These models have been compared to measurements, so it is not unreasonable to build a simulation of these effects to infer what is going on at the middeck location of the orbiter from jet firing activity and flight control activity.

We have used the HIRAP to observe vehicle response to individual jet firings and also to validate the frequencies and some of the modal amplitudes of the structural model of the Orbiter. Figure 1 shows processed HIRAP linear accelerometer data. This is a time history of the response to a series of vernier jet firings and you can see a very strong jump in the acceleration when the vernier jets are fired. These are all very short firings and the oscillation is indeed the Orbiter structure. We have removed most of the known electrical and instrument noise and in doing the analysis of these data, we found frequencies that correspond very closely to the predicted structural frequency of the orbiter. This gave us a fair amount of confidence in the structural models of the orbiter that were generated by the standard finite element techniques. We also have flight data that can be used to model the structural response of the orbiter, at a given station, to individual jet firings.

The HIRAP is mounted very close to the orbiter center of gravity, close to the keel of the orbiter, about 10 feet below and 10 feet behind the center of gravity of the orbiter. So it is a very good measurement of what the Orbiter center of gravity is doing.

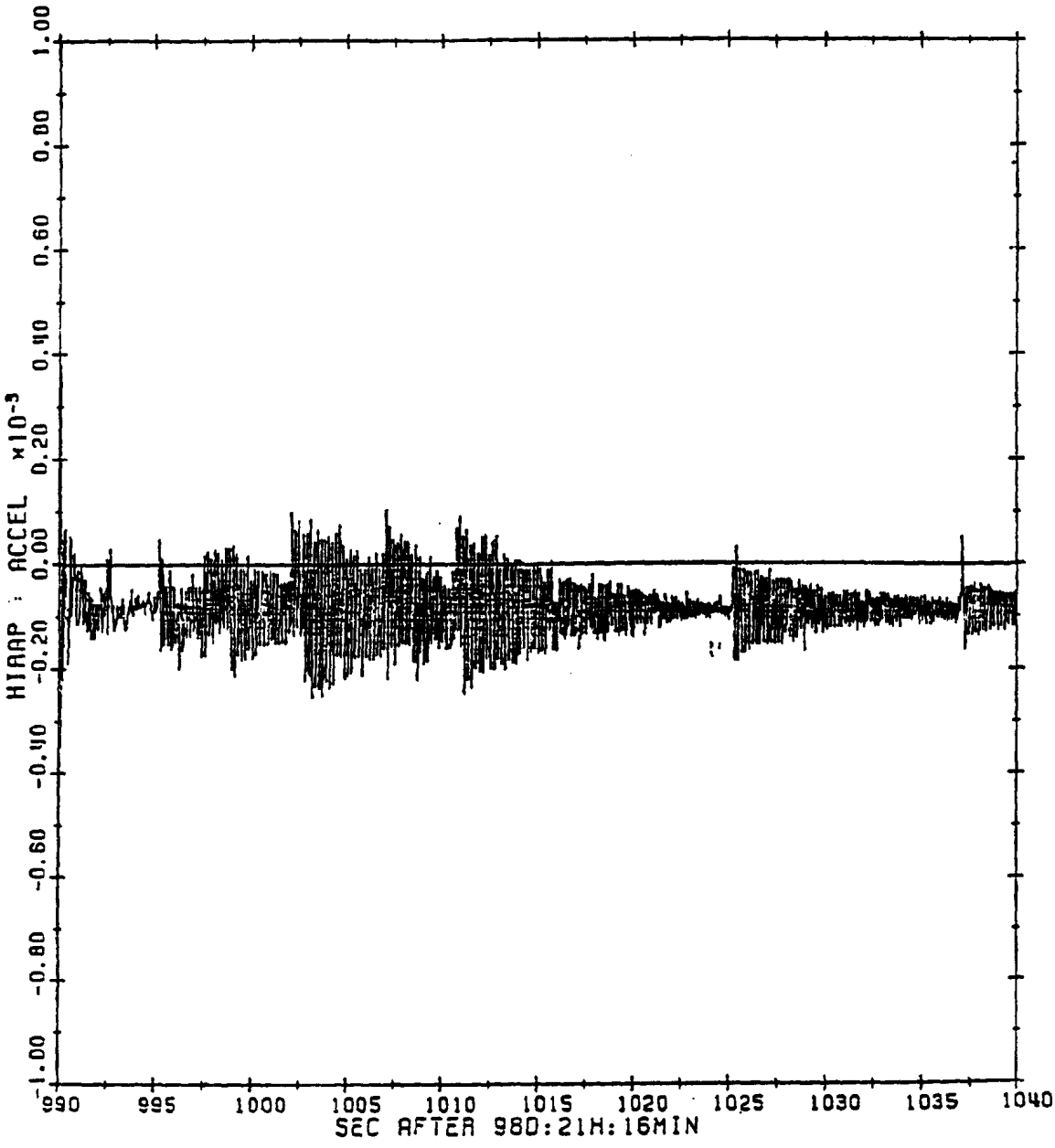

FIGURE 1. HIRAP (X) LINEAR ACCELEROMETER; TIME HISTORY, VRCS REGION, COMPENSATION (20 Hz BANDWIDTH) (G)

Data are generally telemetered at 1 Hz. The flight control system on the orbiter, however, operates at 12½ Hz. There is a sampling problem that can occur, if we were to plot the flight data represented by the circled points shown on Figure 2. There is a great temptation to simply connect the points and say this is what happened. You can miss significant events, in this case a pair of jet firings, that get you back to the same state, but produce some motion of the vehicle in between these points. So using 1 Hertz telemetry data and then doing things like sampling at high rate can actually be misleading. You can miss some disturbances acting on the vehicle. Fortunately, the jet firing activity is sent down at 12 Hz, and that means that we see all the jet firings that are being applied to the vehicle. So, we do know every time that a jet is fired on the orbiter and that's a highly reliable system. In fact, there are two separate indications each time a jet is fired. We can look at the data at 1 Hz then notice a jet firing in between these points. We then have to do some work to find out what happened to that measurement, as a result of those jet firings. That leads us into the kind of analysis that we are doing for DMOS.

The simulation we developed is a tool that will also be available for the space station. For analysis of flight control design on shuttle, we built a model of the shuttle flight control system which is now used in doing analysis in flight experiments. Going back to our math models of the environmental disturbances, reactions of the vehicle, jet torques, and so forth, we can build a model of the rigid motion of the orbiter that we use to predict performance. We have actually used this to design some of the in-flight control experiments.

We have compared that with the results of flight data after similar activities were performed and found that it is a highly accurate measure of what the vehicle would do in response to certain control inputs. In addition, we have a model of the flight control and guidance system and this model is directly traceable to the flight code and can be made to interact with the environment in exactly the same way that

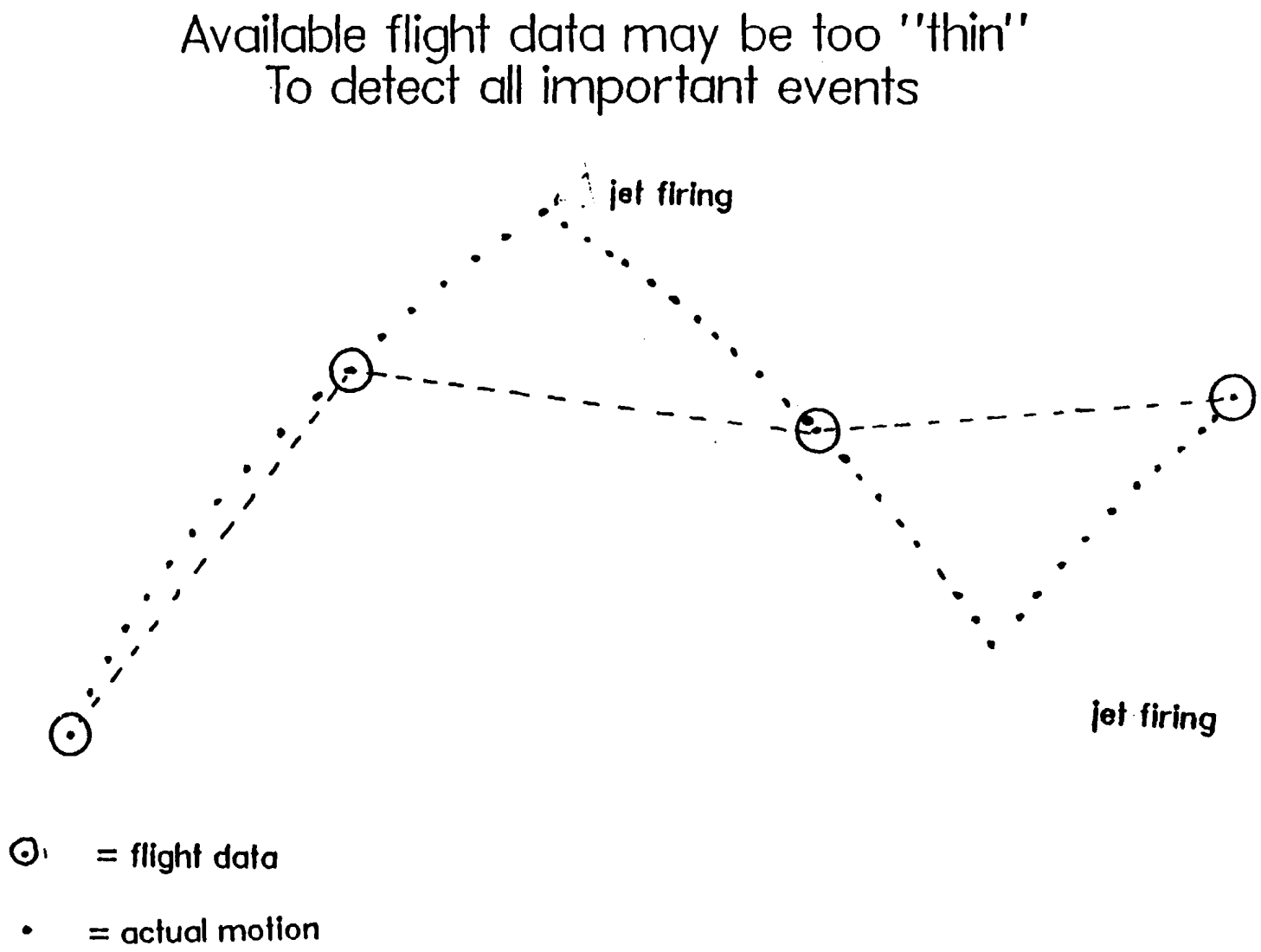

FIGURE 2. AVAILABLE FLIGHT DATA MAY BE TOO "THIN" TO DETECT ALL IMPORTANT EVENTS

the orbiter flight control system interacts with the orbiter. Jet firings act on the orbiter and the IMU data are fed back to the flight control system, which processes that data and acts upon it.

For the 61-B mission there were actually two ways we could reconstruct what happened. Using a tape from NASA of all the jet firings that occurred during a portion of the mission, we can turn off our avionics model and simply drive our environment model with the jet firing activity. We integrate the equations of motion to generate a history of the vehicle state. We can then apply the corrections that correspond to the difference in the motion of the vehicle at the cg, or in any particular location on the vehicle, accounting for the gravity gradient terms, the transverse and centripetal terms, the input flex terms, and then produce some representation of what motion occurred at that location.

In other situations, and fortunately 61-B was not one of them, where the telemetry drops out, we can get into this very dilemma of good data up to a point and have a gap because the telemetry was lost for an interval. However, we can take the last data point and use that as an initial condition in our simulation, and since our simulation mimics the flight control and dynamics of the vehicle, we can fill in the gap. We use the next data point as a check, that we have indeed arrived at a correct statement when the data are picked up again. So we have two positions and basically we are solving differential equations between those positions, so we can also use this to fill in intervals where data are not available.

One of the reasons that one can't simply take the accelerometer data from ACIP, HIRAP, and the navigation data at the center of gravity is that the orbiter does rotate. In fact, the normal mode of operation for the orbiter is to rotate at orbital rates to keep the payload bay pointing at the earth (about 0.06 degrees per second). There are also quite a number of attitude maneuvers that are performed as a part of the normal orbiter operations to align the IMU or to satisfy certain experimental requirements. Any time such a rotation happens, the orbiter

naturally rotates about the center of gravity and an experiment in the middeck will be accelerated. If there is a particle suspended in a volume that particle would eventually collide with the side of the vessel.

This rotation could be from a control input for an attitude maneuver, or it could be the gravity gradient trying to position the Orbiter a certain way. The only message here is: the orbiter is going to rotate about the cg, and because the middeck is on a lever arm it will swing like the mast of a boat, and you had better take that into account. The navigation data is really telling you where the center of gravity is going, not where you're going, that's the motivation for the corrections that we apply to the results of this simulation. There are further corrections that you would have to apply to navigation data or any ACIP data to determine what happened in the middeck.

One of the things we did for the DMOS experimenter on Mission 61-B was to demonstrate some of the typical maneuvers that he would have seen during the mission. Figure 3 is a simulation of one of the vernier yaw maneuvers on the mission. You can see the vernier jets firing to accelerate the vehicle at about two tenths of a degree per second. The angular rates in the other axes are moving up and down due to the way the autopilot decouples the vernier jets. It will generally fire one or two jets continuously and cycle other jets to cancel the off-axis acceleration. After the rate is achieved, it will coast throughout the maneuver. Occasionally you'll see a firing in the middle of the maneuver and then jets fire to take out the angular rate. Most of the maneuvers are performed going from a local vertical track so you are starting at 0.06 degree per second and going to a vertical track. This maneuver had a great deal of jet coupling in it, and looking at what happened to the orbital center of gravity during that maneuver, you can see the acceleration level cycling as the jets cycle off and on. There is a constant level at the beginning of the maneuver. During the closing phases of the maneuver there is a near-zero level of acceleration because the angular rate is so small and you can see jet cycling again as the maneuver stops. Figure 4 shows what happens at the center of gravity.

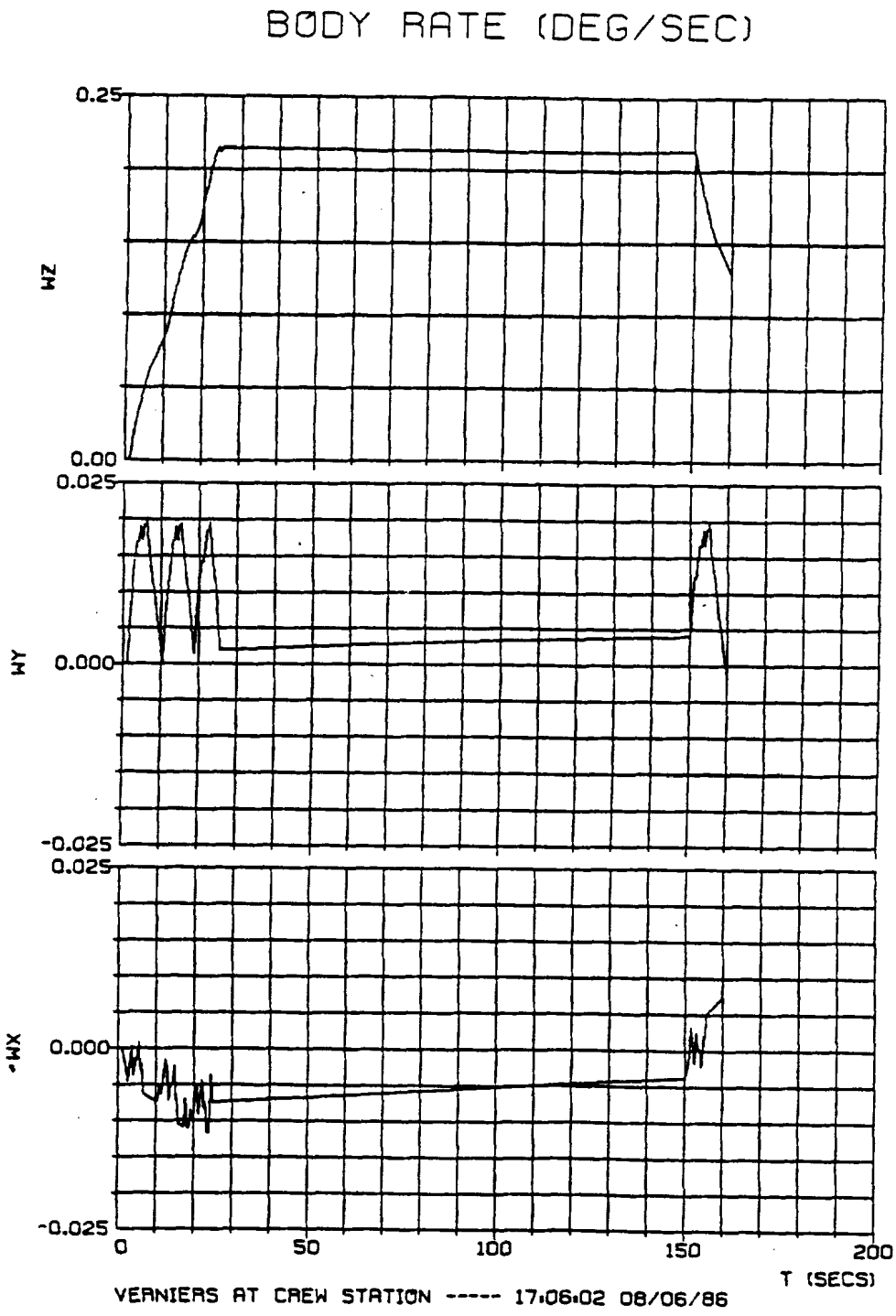
BØDY RATE (DEG/SEC)
0.25
0.00
ZM
0.025
0.000
-0.025
MY
0.025
0.000
-0.025
-MX
0
50
100
150
200
T (SECS)
VERNIERS AT CREW STATION ----- 17:06:02 08/06/86

FIGURE 3.

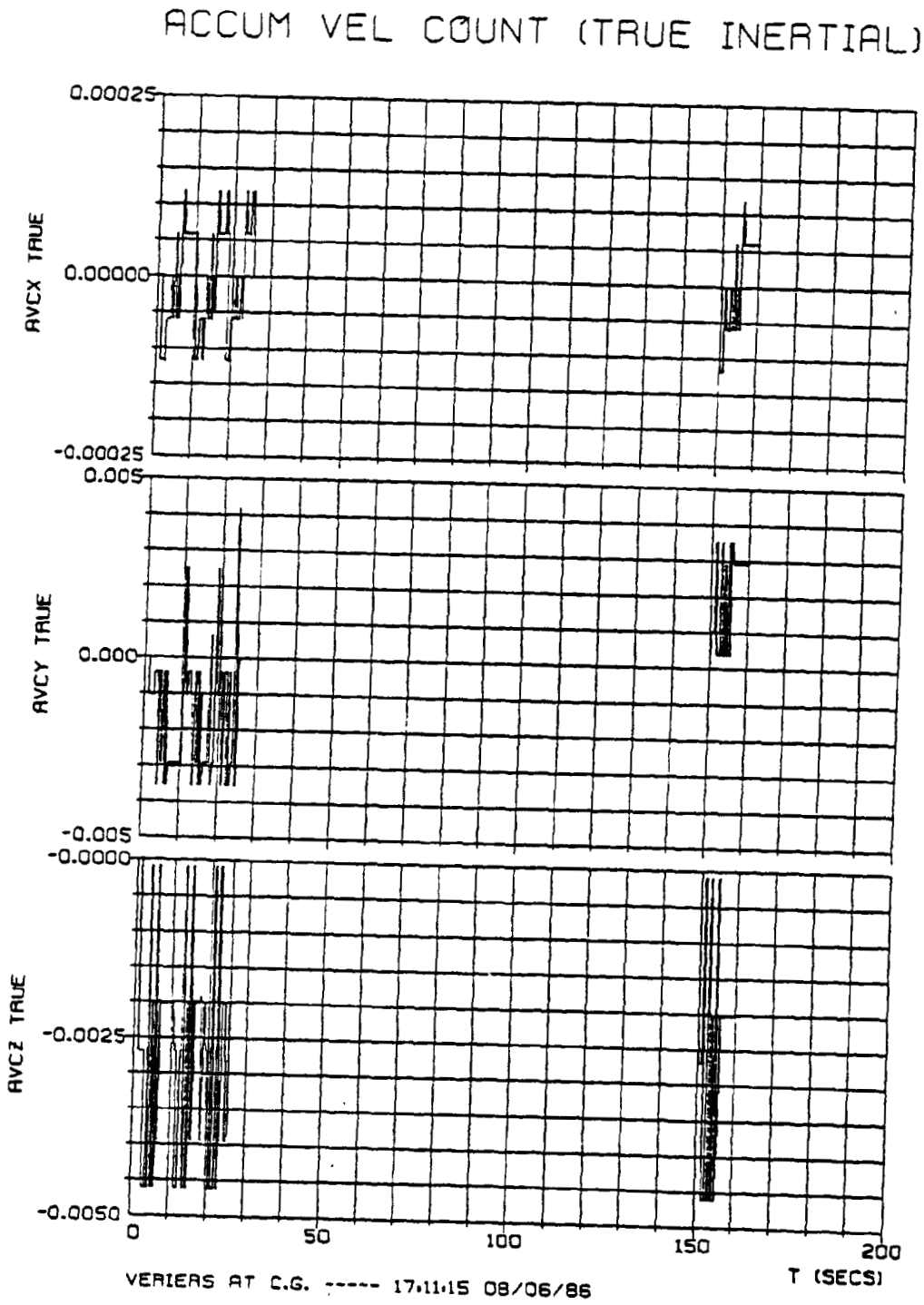
ACCUM VEL COUNT (TRUE INERTIAL)
0.00025
0.00000
-0.00025
AVCX TRUE
0.005
0.000
-0.005
AVCY TRUE
-0.0000
-0.0025
-0.0050
AVCZ TRUE
0
50
100
150
200
T (SECS)
VERIERS AT C.G. ----- 17:11:15 08/06/86

FIGURE 4.

When we consider that our experiment is not at the center of gravity we get a plot that looks very similar (Figure 5), you can see the jets cycling. You can see that this plot looks very similar except the scales differ by an order of magnitude approximately, and that ratio comes out to be about a 50-foot lever arm. Had the experimenter been supplied with ACIP/HIRAP data, or had he been supplied with navigation data to tell him what happened during his experiment, he would have gotten a very misleading impression of the acceleration that his experiment saw as a result of this maneuver.

The second thing that occurred on that mission showed us that the orbiter doesn't always rotate about the center of gravity, depending on what the control system is trying to accomplish. At one point in the mission we deployed a small radar reflector from the forward end of the payload bay. After the commander maneuvered the orbiter back about 35 feet from the payload, he practiced moving around relative to the reflector, to assess the ability to control the vehicle position using a different auto pilot than the one we have now. The commander had to rely primarily on visual cues to determine what motion occurred.

The control system was configured to control the center of gravity of the vehicle and we actually ran into a couple of interesting things that could have misled the commander during that experiment. When we asked him to perform this task the commander put the vehicle in a mode which held the attitude automatically so he didn't have to worry about the vehicle orientation. He used translation hand controller to change the velocity of the vehicle incrementally. Each deflection of the controller changes the vehicle velocity by approximately 0.1 ft/sec. At one point during this activity, he attempted to move the vehicle to the side in the Y direction. He told us the vehicle didn't move and we weren't sure why because the telemetry said the jet fired, the vehicle responded, and the center of gravity moved. The motion at his location, however, was an order of magnitude smaller than the spike at the center of gravity.

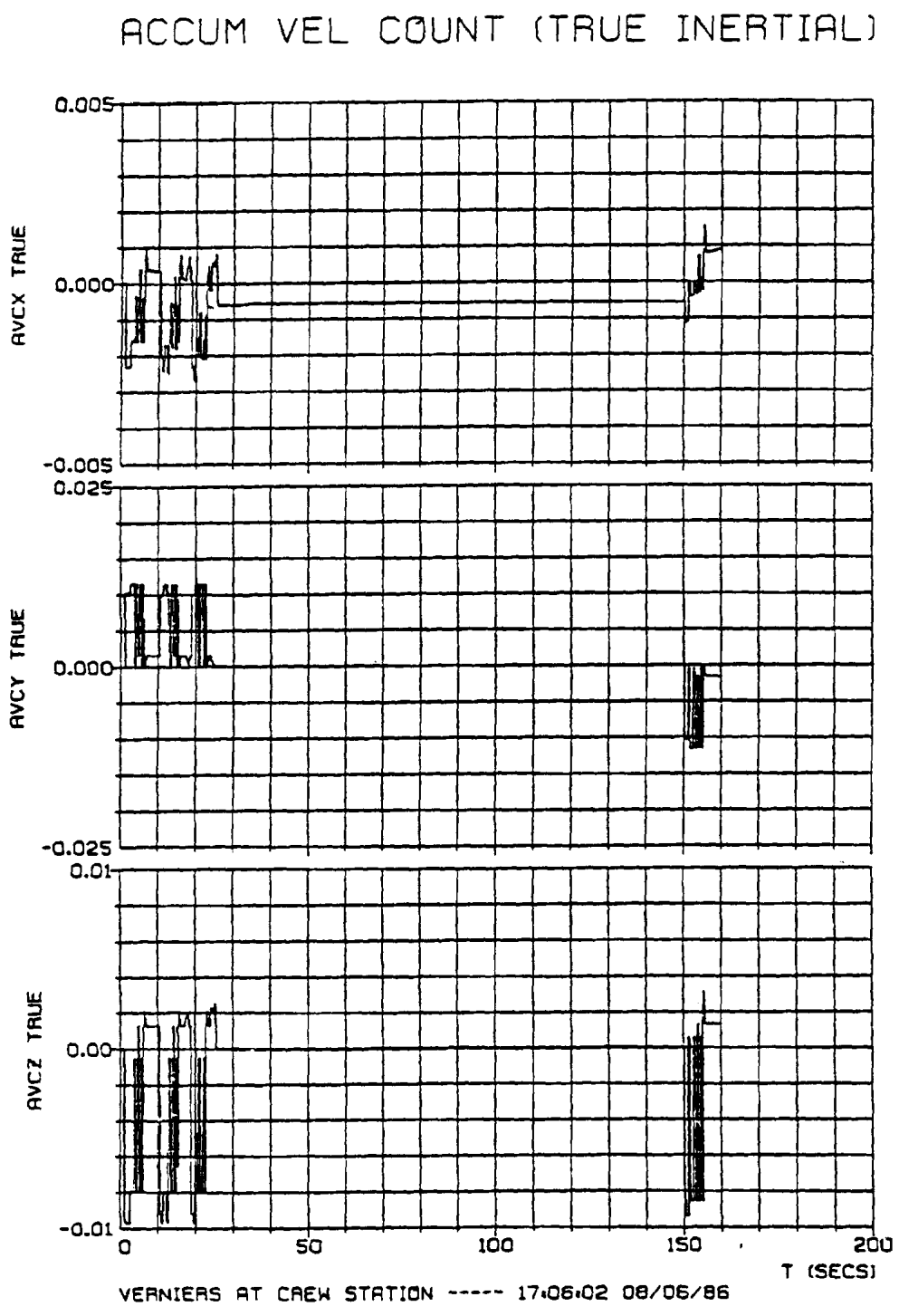
ACCUM VEL COUNT (TRUE INERTIAL)
AVCX TRUE
0.005
0.000
-0.005
AVCY TRUE
0.025
0.000
-0.025
AVCZ TRUE
0.01
0.00
-0.01
0
50
100
150
200
T (SECS)
VERNIERS AT CREW STATION ----- 17:06:02 08/06/86

FIGURE 5.

The vehicle had actually controlled attitude and translation at the same time. The control system was trying to find the optimal way to take out the attitude errors and to simultaneously satisfy the translation of the cg that the commander wanted. So instead of doing what the commander thought it was going to do, it actually rotated around him; the center of rotation was instantaneously moved to where the commander was. To satisfy the angular rate requirement and the translation requirement at the same time it fired one jet that resulted in an instantaneous center of rotation that was not the center of gravity because the CG was translating. Therefore, it is possible to make the vehicle rotate about any point you want.

It is important to try to plan to have accelerometers near your experiment and not rely upon the system. In the past you didn't always have them where you wanted them, and there are going to be times when they fail. What we are finding now is we can accurately fill in some of those gaps by reconstructing the vehicle motion based on the information that we have. In addition, we also want to warn you that when you're planning an experiment that requires micro g's, talk to the people planning the mission. Find out what they're doing and look very carefully at the kind of motion you're going to get. Perhaps if you do these kinds of simulations you can save yourselves a lot of trouble.

Ray Yoel, Boeing: This simulation work that you've done. It can be used to predict accelerations in future flights?

Ed Bergmann: The question was if this acceleration work could be done to predict accelerations on future flights?

In fact, one of the things that we have done with the simulation is to use it to support the development of crew procedures for certain experiments and one of the products is the center of gravity acceleration of the vehicle. In general, the procedures for a mision are laid out long in advance of the mission, and since the vehicle most of the time is operated in automatic mode, and we have a model of

that mode, we can give you a pretty good prediction of what's going to happen. It's a little tougher when it's controlled manually because people fly the thing differently.

The same is true of the space station, except it's a little premature right now because the design is not firmly pinned down but in principle one can do the same thing for a space station.

Rudy Ruff, Marshall Space Flight Center: You mentioned knowing the structural frequencies of the orbiter. Do they correlate with what we heard this morning from Dr. Hamacher?

Bergmann: The structural frequencies that we found in looking at the flight data correspond well with the lowest structural frequencies that were predicted by the prime contractor of the orbiter. I think that most of the data that people have seen do confirm the correctness of the frequencies of the orbiter structural models. One has to be careful in using that data however, because those frequencies change dramatically when the payload bay doors open and close and they change dramatically based on the payload configurations. In addition, one thing I'd like to mention is there are a number of flexible payloads that are attached to the orbiter. One of our efforts, at Johnson Space Center, is to investigate how the addition of those flexible payloads interacts with the control system so that you can actually, depending on what your payload is, and if it's flexible, see other modes superimposed on the orbiter structural modes. It can be quite significant, enough to interact with the control system.

Bob Naumann, Marshall Space Flight Center: I may have misinterpreted what you said. You said that the orbiter is actually just flying and maintaining its local vertical or whatever, you put a centrifugal force in there due to the fact you've got a moment arm away from the center of mass. Is that what you mean to say?

Bergmann: The question was when the orbiter is tracking the local vertical there's centrifugal force because this point is away from the center of mass?

Naumann: This is what I'd like to point out because you are always in that mode where you are actually earth oriented. The centrifugal forces exactly balance the gravitational forces and you don't have any additional acceleration from that.

Bergmann: I guess you don't. That's true at the center of gravity of the vehicle.

Question: No, it's true anywhere along the flight path of the center of gravity.

Bergmann: As long as you are at the same altitude as the center of mass of the vehicle.

Ken Demel, Johnson Space Center: Have you looked at any of the Space Station rates on attitude maneuvering? When you do a desaturation of the gyros and that sort of thing, what I have seen is that you're talking about 0.02 degrees per second or less and $r\omega^2$ is less of a problem than gravity gradient.

Bergmann: The question has to do with the Space Station maneuvering rates during desaturation and so forth, and the answer is that the rates people typically think of are well below a tenth of a degree per second and you're right. In those cases those terms can be relatively small. But when you're talking microgravity or something like that, those are marginal on that scale. The other thing is it is physically possible to rotate the space station at a higher rate which could occur in some kind of accident or contingency, or where you have got to do something quickly, but I don't want to preclude that kind of capability because of my ability to model what the vehicle is doing.

N91-12410

11. SPACELAB-3 LOW-g ACCELEROMETER DATA FROM THE FLUID EXPERIMENTS SYSTEM (FES)

Gary Arnett, BGB, Inc.

ABSTRACT

The FES flown aboard SL-3 contained a "Miniature Electrostatic Accelerometer" (MESA). This accelerometer was purchased from Bell Aerospace, Textron and had three range (auto switching), bidirectional, three orthogonal axis capability. BGB, Inc. is in the process of examining the total mission data from this instrument. From these data, areas of interest are identified and related back to mission events. The basic format of the data for the total mission is RMS, with two (2) hours per plot.

My talk today is about a program where we are primarily looking into the accelerometer data that came from Dr. Lal's FES Experiment. We have titled the study very appropriately "The Spacelab 3 Low-g Accelerometer Data from the FES" as shown in Figure 1.

We looked at the data and know that many people, especially here, have a use for gravitational data from Spacelab 1, 2, and 3, whatever it might be, because it may help them reduce their own data. Another experiment that I know can use this kind of data is the Geophysical Fluid Flow Cell. We are just getting into this program, so I'm not going to give you any startling conclusions, but we are going to show you the track that we are taking. The first thing that we wanted to do was to provide a total mission format that the basic user could compare with his own experiment data. Our data might help him select areas of special interest in his own data. The first of our overall objectives is to take this whole mission data, find a format that is of

BGB, Inc.
4321 University Drive • Suite 300
Huntsville, Alabama 35816-3009 • Phone (205) 895-0341

PROGRAM
SL-3 LOW-G ACCELEROMETER DATA FROM THE FLUID EXPERIMENT SYSTEM (FES)

NAME
G. ARNETT

DATE
AUGUST 1986

CHART NO.

OBJECTIVES OF STUDY

- PROVIDE USEABLE FORMAT OF TOTAL MISSION DATA FROM FLUID EXPERIMENT SYSTEM (FES), LOW-G ACCELEROMETER.
- IDENTIFY AREAS OF INTEREST AND ATTEMPT TO CORRELATE WITH BASIC MISSION EVENTS.
- IDENTIFY SPECIFIC G DATA OF INTEREST TO FES RESULTS (I.E. G-DATA DURING TIME OF HOLOGRAM EXPOSURES).

Figure 1.

general use and make it available to the user. Then when you get into the data reduction, you want to correlate the data with basic mission events. One of the best jobs that I've seen done on that was in the earlier presentation by Dr. Hamacher. His talk was very informative, but we are taking the opposite approach, we are looking at the g-data and going back and identifying things that might cause it. Since we are working very closely with Dr. Lal on his FES results, we want to overlap some of the things that would be of interest to him, especially the holograms you saw in an earlier presentation.

The FES was located radially, slightly more than a meter off the center of gravity of the orbiter. The FES accelerometer orientation is shown in Figure 2. You must decide which set of coordinates you want to use. This set actually is in terms of the structure of the orbiter where the X axis is measured toward the tail or away from the cabin. If you think in terms of dynamic coordinates, you must turn those coordinates around and the plus X axis is toward the cabin. Figure 2 depicts that the accelerometer unfortunately could not be mounted with its X, Y, Z axes totally aligned with the Shuttle's X, Y, Z axes. We are off from the positive Y axis and the XZ plane is rotated in the structural coordinate system 112.5 degrees, or if you want to think in terms of the dynamic axis, it's off by the complement of that, or 67.5 degrees. The Y-axis is in plane and the XZ plane is rotated.

Some basic background information on the accelerometer that was used is shown in Figure 3. It was a miniature electrostatic accelerometer and had automatic switching with three ranges. The three ranges were 127 micro-g, 1.27 milli-g, and 12.7 milli-g. The really important information shown is the measurement rate of about 300 samples/second. I think Roger Chassay said that sample rate would produce 150 million pieces of data. That is factor of about 100 too many when you start looking at the data. There was a force rebalance loop (Figure 4) on the X and Y axis, and Z was very similar. You had an ac pickoff and the dc forcing function.

FLUIDS EXPERIMENT SYSTEM
ACCELEROMETER ORIENTATION

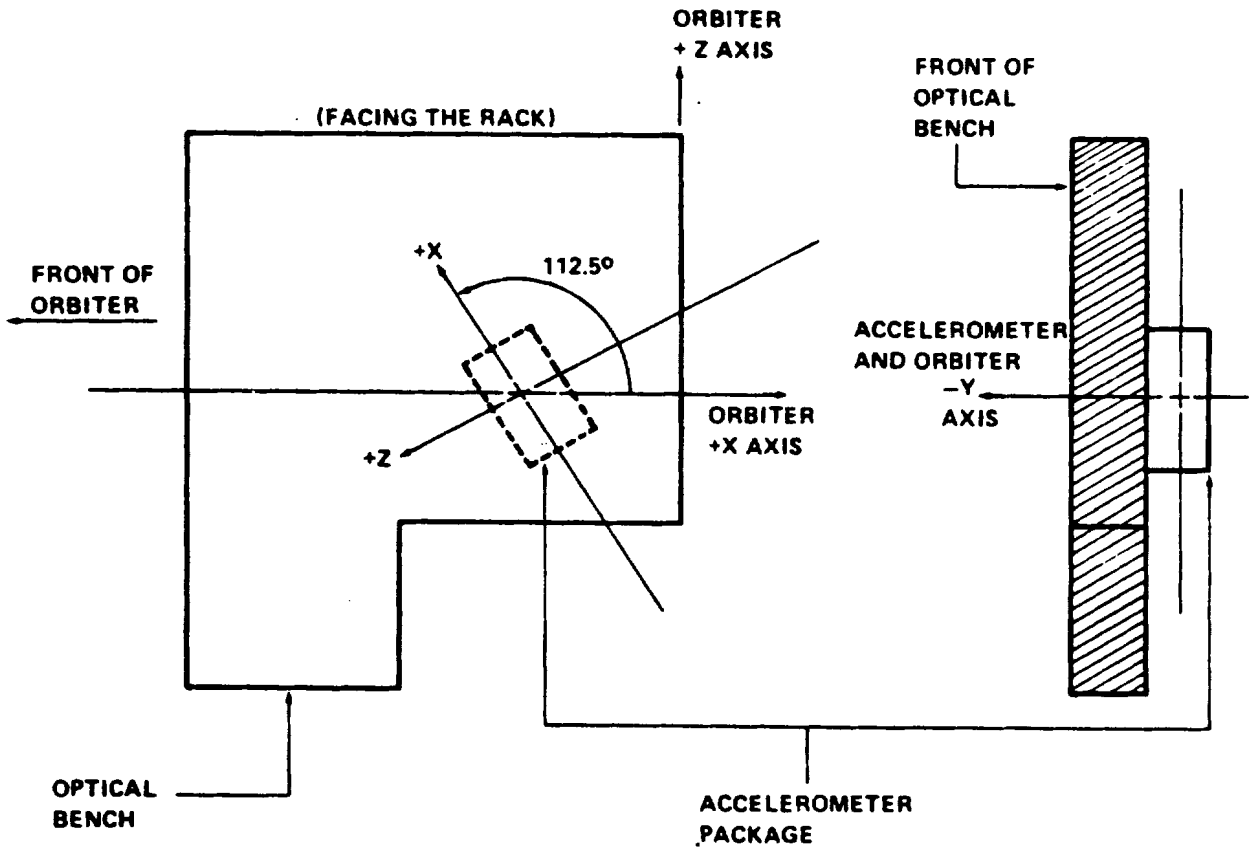

FES MEASUREMENT NUMBER	FES ACCEL. AXIS
L20Q6002A	X
L20Q6005A	Y
L20Q6008A	Z

Figure 2.

BGB, Inc.
4321 University Drive • Suite 300
Huntsville, Alabama 35816-3009 • Phone (205) 895-0341

PROGRAM: SL-3 LOW-G ACCELEROMETER DATA FROM THE FLUID EXPERIMENT SYSTEM (FES)

NAME: G. ARNETT

DATE: AUGUST 1986

CHART NO.:

TYPE: MINIATURE ELECTROSTATIC ACCELEROMETER (MESA)

MANUFACTURER: BELL AEROSPACE, TEXTRON

CAPABILITY:

- THREE RANGES (AUTOMATIC RANGING):
  - 1 MICRO-G RESOLUTION AT 127 MICRO-G FULL SCALE
  - 10 MICRO-G RESOLUTION AT 1.27 MILLI-G FULL SCALE
  - 100 MICRO-G RESOLUTION AT 12.7 MILLI-G FULL SCALE
- BI-DIRECTIONAL
- THREE INDEPENDENT ORTHOGONAL AXIS
- MEASUREMENT RATE: 300 SAMPLES/SEC

CONFIGURATION:

- CYLINDRICAL "PROOF MASS" ELECTROSTATICALLY SUSPENDED IN A CYLINDRICAL, HERMETICALLY-SEALED CASING

OPERATION:

- "PROOF MASS" POSITION IS SENSED CAPACITIVELY
- DC ELECTROSTATIC FORCE IS GENERATED TO RESTORE TO NULL POSITION
- DC VOLTAGE IS CONVERTED TO FREQUENCY PROPORTIONAL TO ACCELERATION
- FREQUENCY PULSES COUNTED FOR FIXED DURATION
- FINAL SUM OUTPUT AS DIGITAL VALUE PROPORTIONAL TO ACCELERATION ON "PROOF MASS"

Figure 3.

FORCE REBALANCE LOOP, X AND Y AXES (Y ONLY SHOWN)

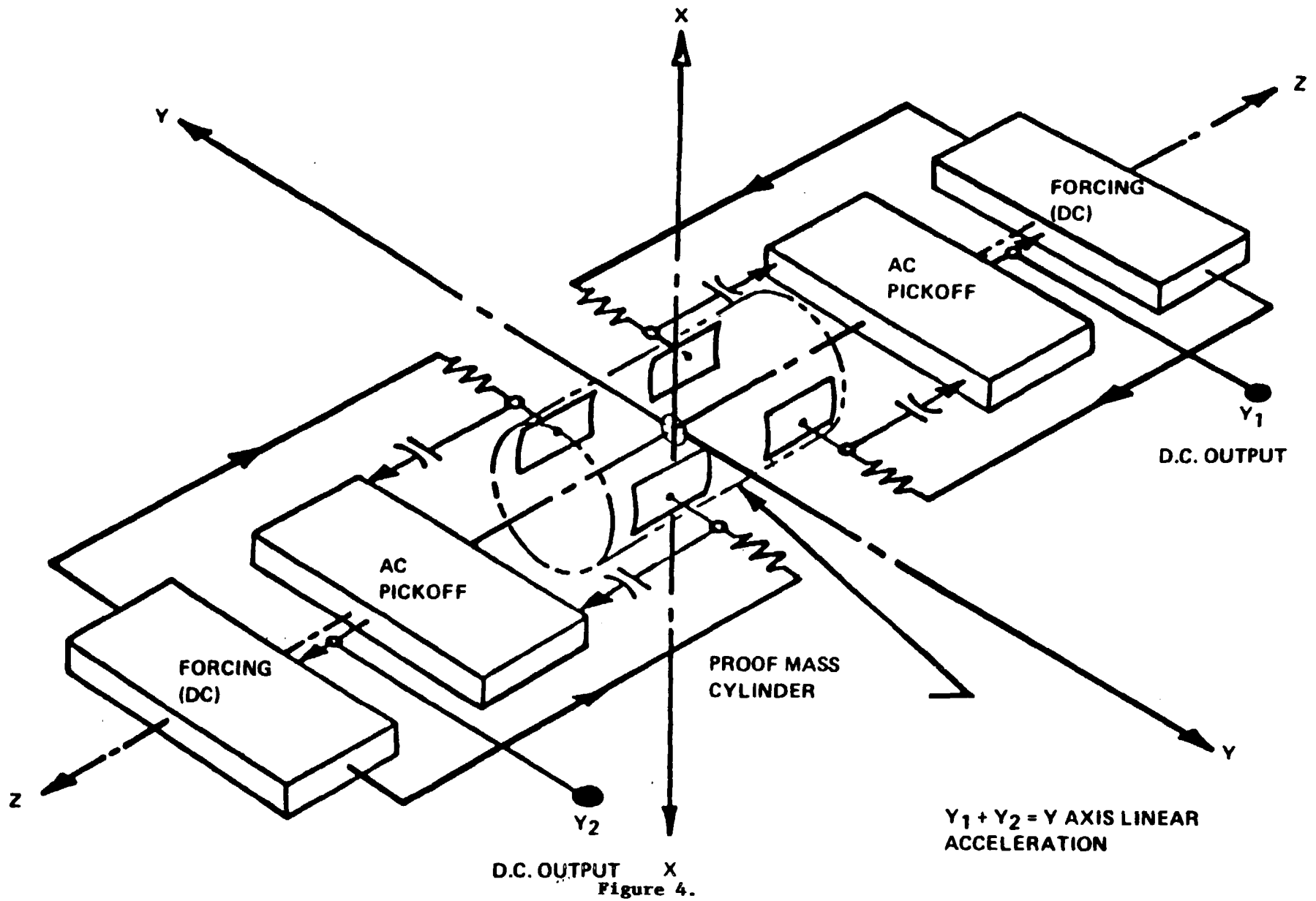

Figure 4.

JA-11,673-86

There are some terms (Figure 5) that I want to define before showing our data reduction results. We have tried to format the data to meet that first objective where people look at it and identify those areas of interest to themselves. We ended up integrating over a 10-second period of time. That meant that we were integrating about 3,000 points for each point that we plot. We define that time interval as delta HST. This is the format that the Computation Lab at Marshall gives us the data. We plotted our data as an RMS, or a standard deviation plot with a delta HST of 10 seconds. We defined a crest factor which is the peak value within that 10-second period divided by the RMS. All of these are designed to smooth the data because with 300 points per second, your data looks very rough and I will discuss that later. We define power spectral density as a plot of the power input versus the frequency.

One of the things that we have done so far is to look at the real effect of the RCS engines. In the upper right corner of Figure 6 we selected six typical engines that we would try to track to see their effects. We would look at the time they were moderately active and when very active. The F location, as seen in the upper left corner, is in the forward module, the 5 means that it was through that manifold number, and in the upper center is a definition of what A, F, L, R, U, and D mean in terms of thruster plume direction. The box in the right center shows the direction of thruster plume which causes a movement in the opposite direction. The dynamic body coordinates are shown in the lower right-hand box, and the structural coordinates are shown at the lower left, where poxitive X goes from the cabin back, if you are looking for a station location.

The typical raw data we started out with is shown in Figure 7 and, as you can see, we had to do something with the data. There was something in the hardware/software cycle that drove us over scale at a very regular period of time. I had a discourse on this from our software people from the Computation Lab, and their first recommendation was

BGB, Inc.
4321 University Drive • Suite 300
Huntsville, Alabama 35816-3009 • Phone (205) 895-0341

PROGRAM
SL-3 LOW-G ACCELEROMETER DATA FROM THE FLUID EXPERIMENT SYSTEM (FES)

NAME
G. ARNETT

DATE
AUGUST 1986

CHART NO.

DEFINITIONS

ΔHST = TIME INTERVAL OVER WHICH THE RAW DATA IS INTEGRATED

= 10 SECONDS ON TOTAL MISSION DATA

RMS = ROOT MEAN SQUARE OF DATA WITHIN THE ΔHST TIME PERIOD, OR STANDARD DEVIATION OVER THE 10 SECOND TIME PERIOD

$$\text{CREST FACTOR} = \frac{\text{PEAK VALUE WITHIN } \Delta\text{HST}}{\text{RMS}}$$

PSD = POWER SPECTRAL DENSITY - DISTRIBUTION OF POWER (ENERGY) INPUT VERSUS FREQUENCY

Figure 5.

F5L L5D R5R

F5R L5L R5D

DATA USED FROM THESE THRUSTERS

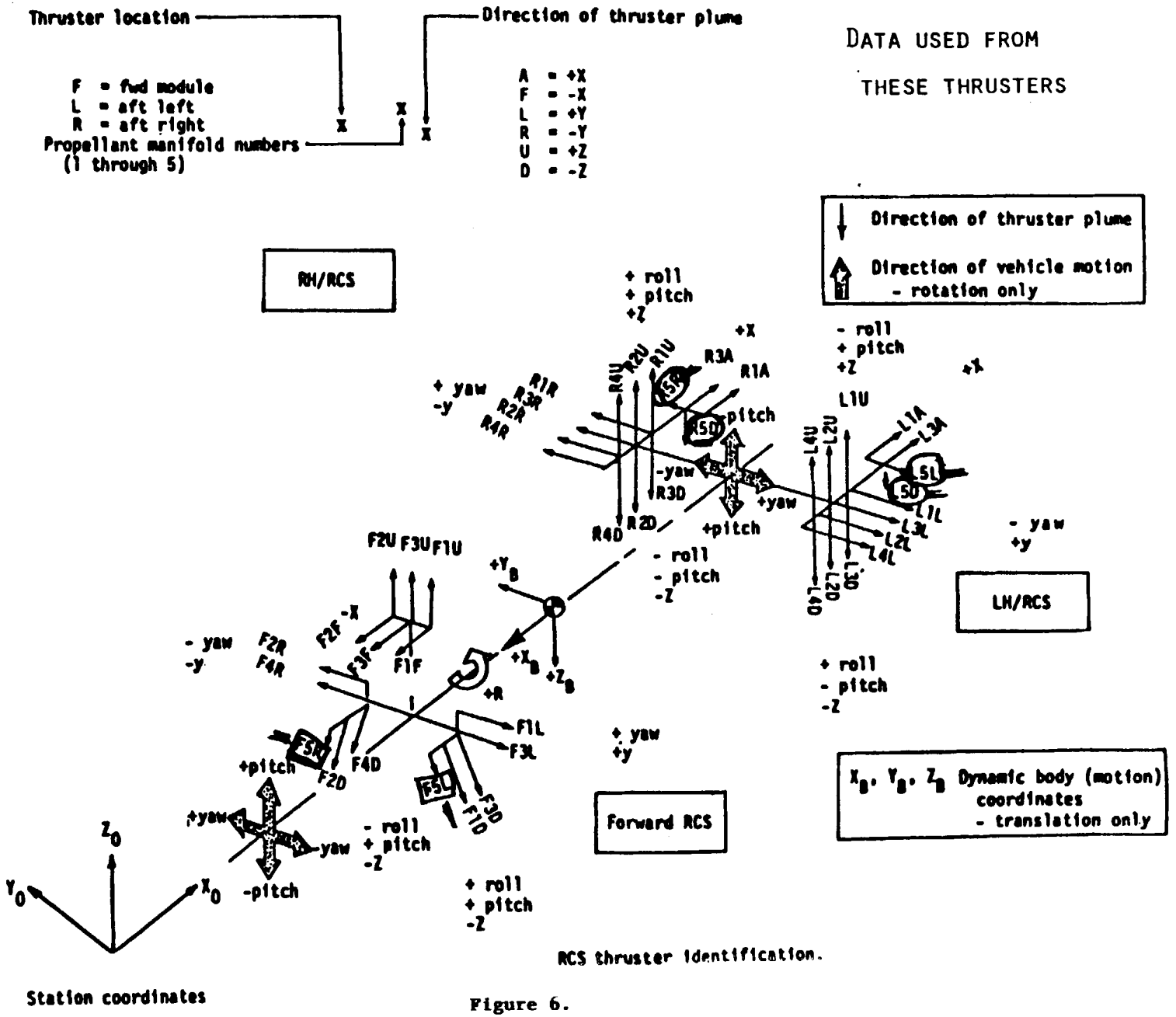

RCS thruster identification.

Figure 6.

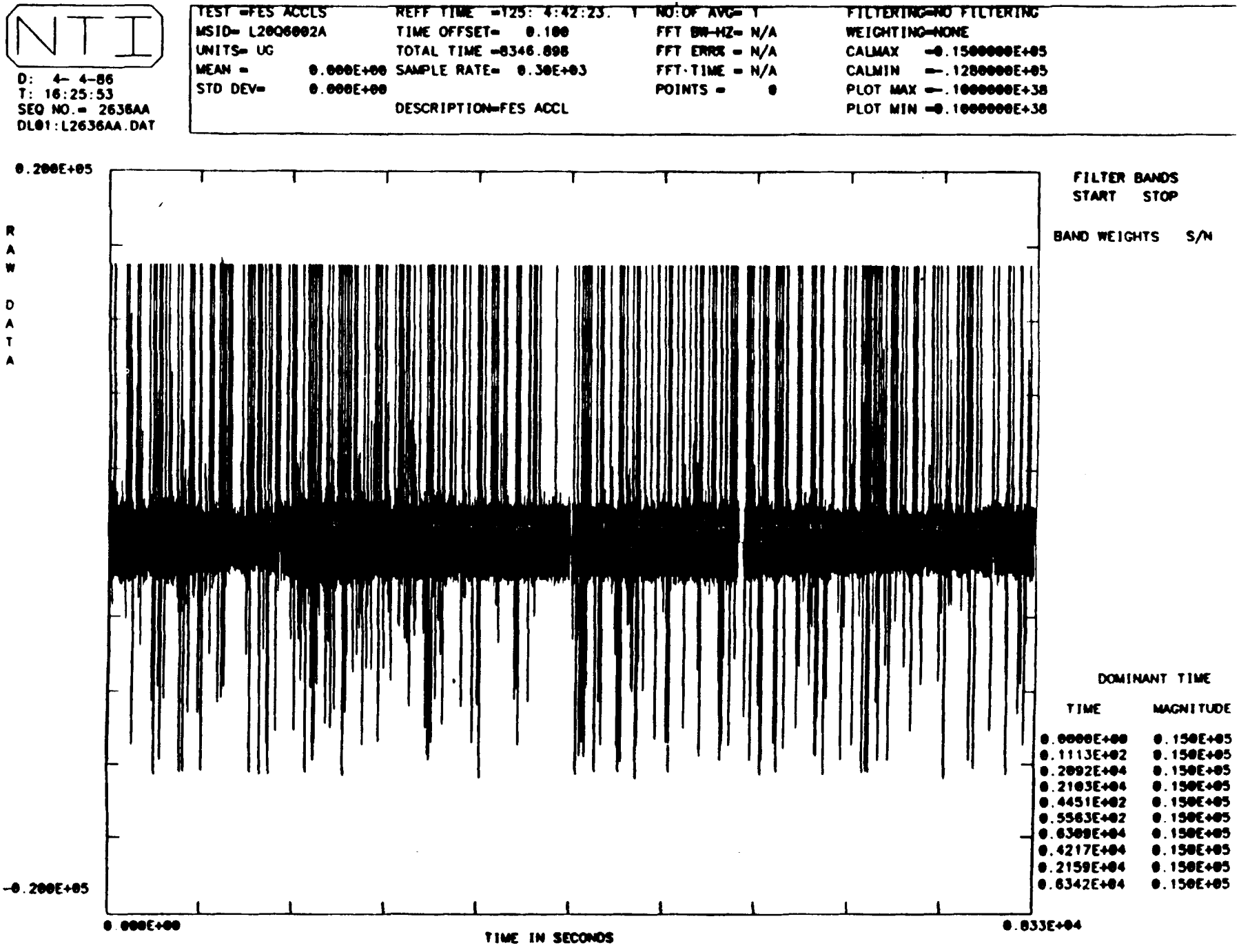
NTI
D: 4- 4-86
T: 16:25:53
SEQ NO.= 2636AA
DL01:L2636AA.DAT
TEST =FES ACCLS
MSID= L20Q6002A
UNITS= UG
MEAN = 0.000E+00
STD DEV= 0.000E+00
REFF TIME =Y25: 4:42:23. Y
TIME OFFSET= 0.100
TOTAL TIME =8346.898
SAMPLE RATE= 0.30E+03
DESCRIPTION=FES ACCL
NO OF AVG= Y
FFT BW-HZ= N/A
FFT ERR% = N/A
FFT TIME = N/A
POINTS = 0
FILTERING=NO FILTERING
WEIGHTING=NONE
CALMAX =0.1500000E+05
CALMIN =-.1200000E+05
PLOT MAX =-.1000000E+38
PLOT MIN =0.1000000E+38
0.200E+05
RAW DATA
-0.200E+05
0.000E+00
TIME IN SECONDS
0.833E+04
FILTER BANDS
START STOP
BAND WEIGHTS S/N
DOMINANT TIME
TIME MAGNITUDE
0.0000E+00 0.150E+05
0.1113E+02 0.150E+05
0.2092E+04 0.150E+05
0.2103E+04 0.150E+05
0.4451E+02 0.150E+05
0.5563E+02 0.150E+05
0.6309E+04 0.150E+05
0.4217E+04 0.150E+05
0.2159E+04 0.150E+05
0.6342E+04 0.150E+05

Figure 7.

to throw out every thing that is over scale -- something about a bit-flipping and then it would drive the reading over scale, and then come back and give an accurate reading. What we are really doing is peaking out and this is really not good data. Often, you could be throwing away a piece of data, but when you are trying to look at so much data, you may have to throw away a piece or two of good data in your data reduction.

QUESTION: Can you say that is data, or is it electronic noise?

ANSWER: It was described to me as not necessarily noise but a characteristic of the software in the reduction cycle. Some of it could be noise and some of it could be real data. What I'm trying to explain to you is what we settled on as a data reduction method and format.

A part of the RMS time history in the same timeframe is shown in Figure 8. This is just slightly over one hour of data, and we used a 5-second integration time. We did identify that the peak was a true peak.

In Figure 9, we were trying to plot two hours of time and make it meaningful, so you would have only about 70 rather than 1,000 pieces of paper to scan through the mission g-data. We used a 10-second integration time for this plot and found that the real data was retained. We settled on this two-hour format with a 10-second integration time for the basic mission data reduction.

I want to show a very significant event which was a roll maneuver which is depicted in Figures 10 through 12. This was after the FES experiment was over, but the optical bench was still on. They left the optical bench on so we could utilize the accelerometer to ensure that we could see an event such as a roll maneuver. If you have events spread over a relatively large period of time, you should see it in the RMS time history. Crest is peak value over RMS value, so if you have a peak value for quite a period of time, the RMS value is going to equal peak value, and you will not see a large long time period event. The crest value is intended to bring out more isolated events. So RMS shows you some of the long time period events, and crest value shows the isolated

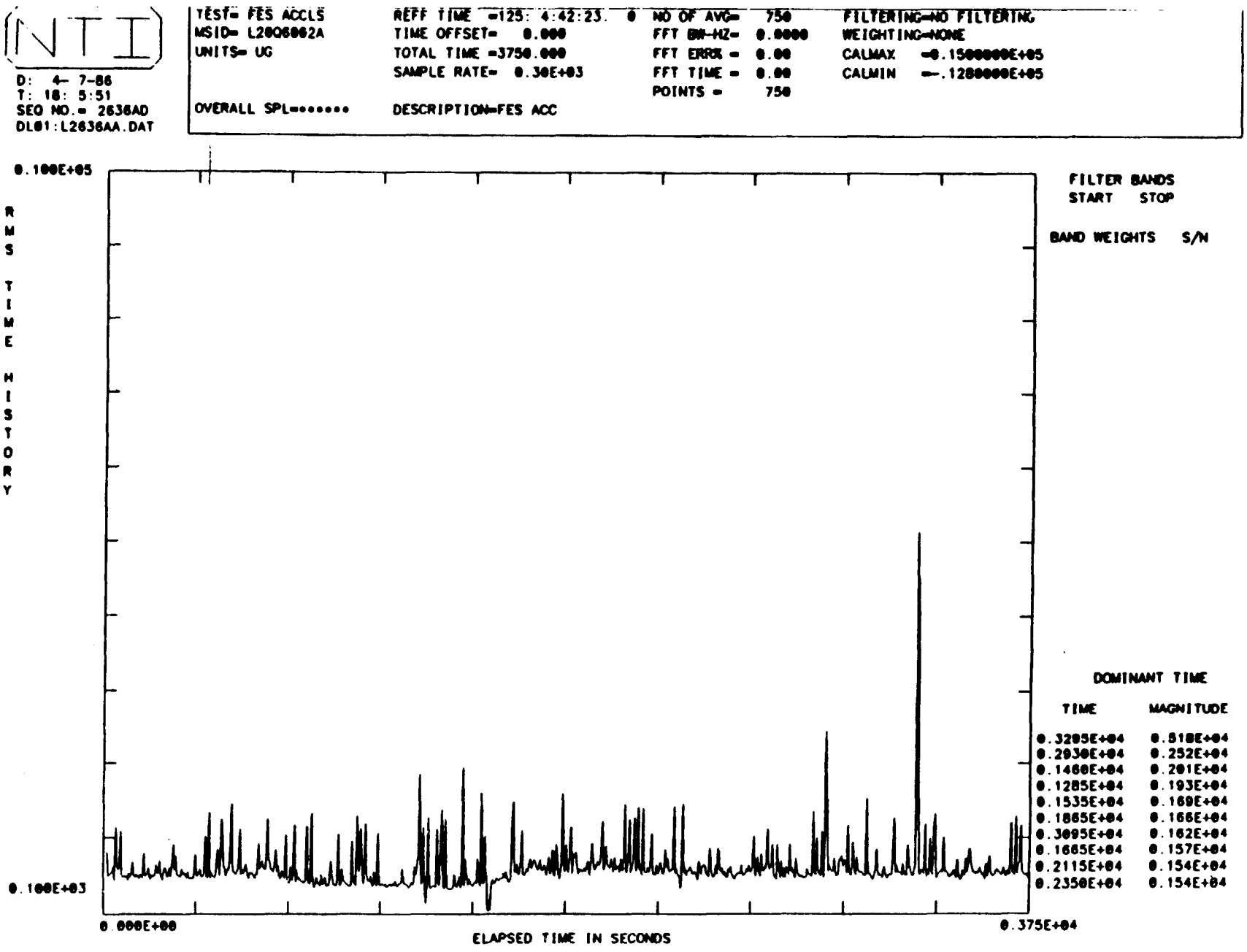
NTI
D: 4- 7-86
T: 18: 5:51
SEQ NO.= 2636AD
DL01:L2636AA.DAT
TEST= FES ACCLS
MSID= L20Q0002A
UNITS= UG
OVERALL SPL=******
REFF TIME =125: 4:42:23. 0
TIME OFFSET= 0.000
TOTAL TIME =3750.000
SAMPLE RATE= 0.30E+03
DESCRIPTION=FES ACC
NO OF AVG= 750
FFT BW-HZ= 0.0000
FFT ERR% = 0.00
FFT TIME = 0.00
POINTS = 750
FILTERING=NO FILTERING
WEIGHTING=NONE
CALMAX =0.1500000E+05
CALMIN =-.1200000E+05
0.100E+05
0.100E+03
RMS TIME HISTORY
FILTER BANDS
START STOP
BAND WEIGHTS S/N
DOMINANT TIME
TIME MAGNITUDE
0.3295E+04 0.518E+04
0.2930E+04 0.252E+04
0.1460E+04 0.201E+04
0.1285E+04 0.193E+04
0.1535E+04 0.169E+04
0.1865E+04 0.166E+04
0.3095E+04 0.162E+04
0.1665E+04 0.157E+04
0.2115E+04 0.154E+04
0.2350E+04 0.154E+04
0.000E+00
0.375E+04
ELAPSED TIME IN SECONDS

Figure 8.

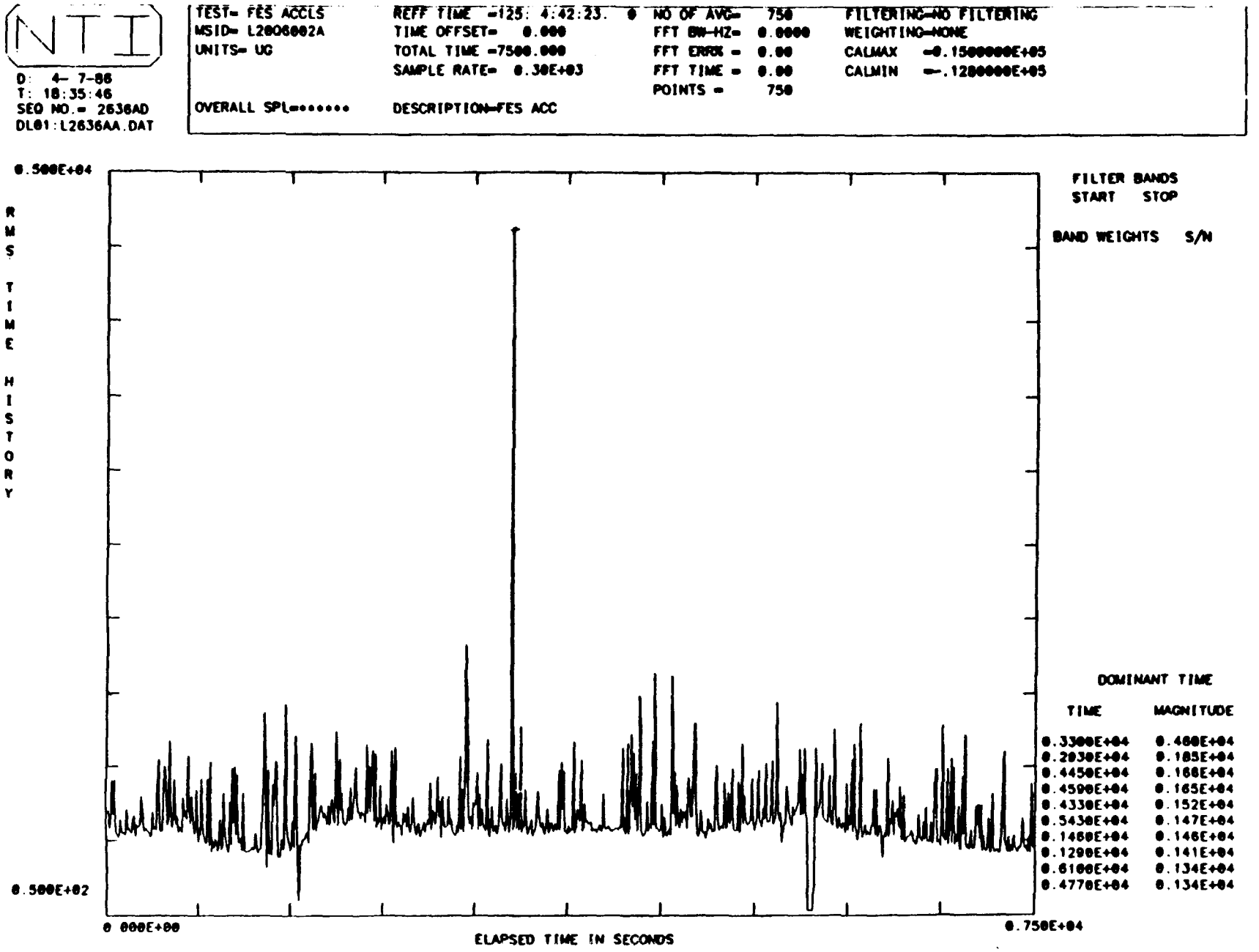
NTI
D: 4- 7-86
T: 18:35:46
SEQ NO.= 2636AD
DL01:L2636AA.DAT
TEST= FES ACCLS
MSID= L2806002A
UNITS= UG
OVERALL SPL=******
REFF TIME =125: 4:42:23. 0
TIME OFFSET= 0.000
TOTAL TIME =7500.000
SAMPLE RATE= 0.30E+03
DESCRIPTION=FES ACC
NO OF AVG= 750
FFT BW-HZ= 0.0000
FFT ERROR = 0.00
FFT TIME = 0.00
POINTS = 750
FILTERING=NO FILTERING
WEIGHTING=NONE
CALMAX =0.1500000E+05
CALMIN =-.1200000E+05
0.500E+04
RMS TIME HISTORY
0.500E+02
0.000E+00
0.750E+04
ELAPSED TIME IN SECONDS
FILTER BANDS
START STOP
BAND WEIGHTS S/N
DOMINANT TIME
TIME MAGNITUDE
0.3300E+04 0.460E+04
0.2030E+04 0.185E+04
0.4450E+04 0.160E+04
0.4590E+04 0.165E+04
0.4330E+04 0.152E+04
0.5430E+04 0.147E+04
0.1460E+04 0.146E+04
0.1290E+04 0.141E+04
0.6100E+04 0.134E+04
0.4770E+04 0.134E+04

Figure 9.

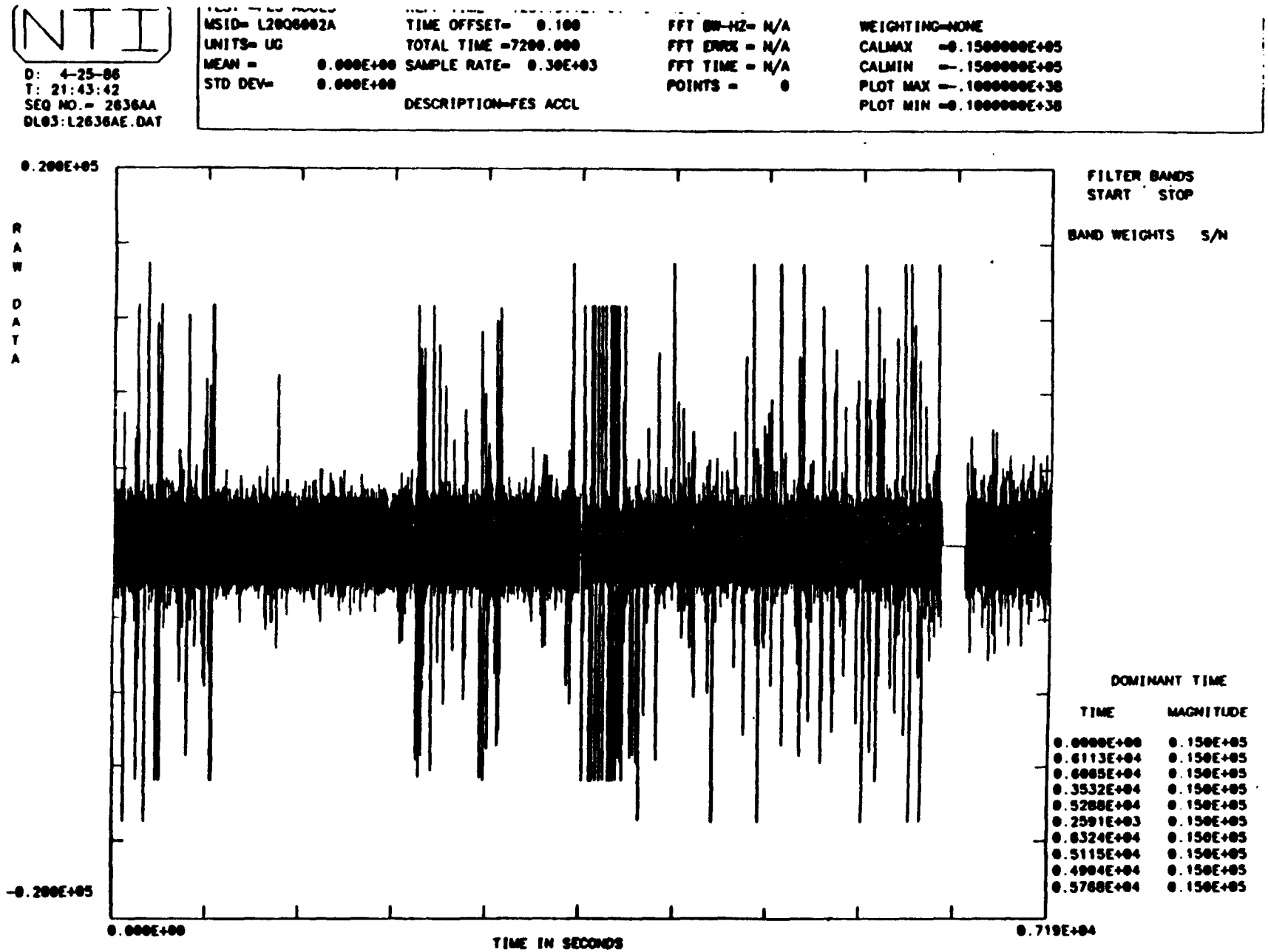
NTI
D: 4-25-86
T: 21:43:42
SEQ NO.= 2636AA
DL03:L2636AE.DAT
MSID= L20Q6002A
UNITS= UG
MEAN = 0.000E+00
STD DEV= 0.000E+00
TIME OFFSET= 0.100
TOTAL TIME =7200.000
SAMPLE RATE= 0.30E+03
DESCRIPTION=FES ACCL
FFT BW-HZ= N/A
FFT ERR% = N/A
FFT TIME = N/A
POINTS = 0
WEIGHTING=NONE
CALMAX =0.1500000E+05
CALMIN =-.1500000E+05
PLOT MAX =-.1000000E+38
PLOT MIN =0.1000000E+38
0.200E+05
RAW DATA
-0.200E+05
0.000E+00
TIME IN SECONDS
0.719E+04
FILTER BANDS
START STOP
BAND WEIGHTS S/N
DOMINANT TIME
TIME MAGNITUDE
0.0000E+00 0.150E+05
0.6113E+04 0.150E+05
0.6085E+04 0.150E+05
0.3532E+04 0.150E+05
0.5288E+04 0.150E+05
0.2591E+03 0.150E+05
0.6324E+04 0.150E+05
0.5115E+04 0.150E+05
0.4904E+04 0.150E+05
0.5768E+04 0.150E+05

Figure 10.

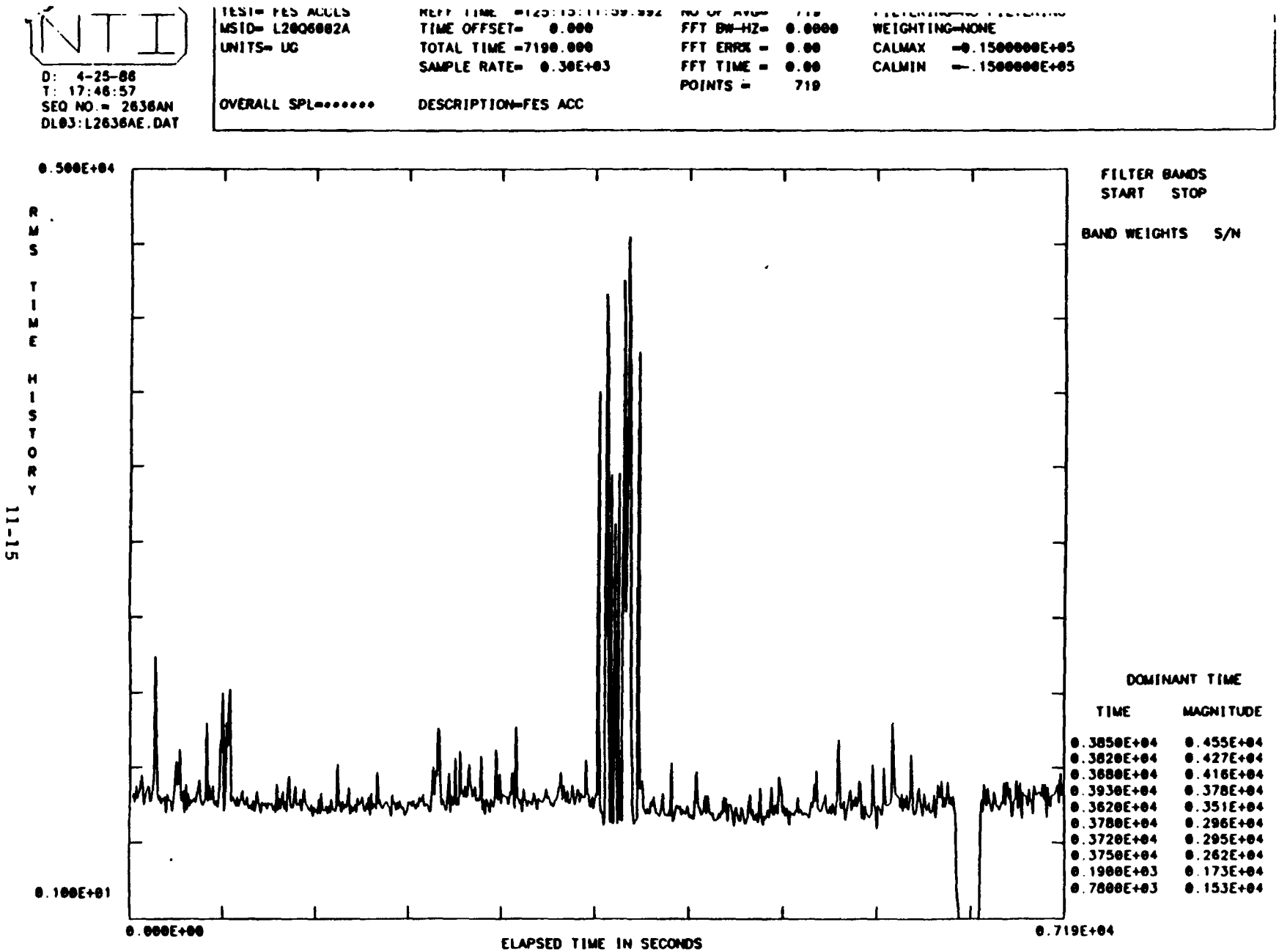
NTI
D: 4-25-86
T: 17:46:57
SEQ NO.= 2636AN
DL0J:L2636AE.DAT
TEST= FES ACCLS
MSID= L20Q6002A
UNITS= UG
OVERALL SPL=******
TIME OFFSET= 0.000
TOTAL TIME =7190.000
SAMPLE RATE= 0.30E+03
DESCRIPTION=FES ACC
FFT BW-HZ= 0.0000
FFT ERR% = 0.00
FFT TIME = 0.00
POINTS = 719
WEIGHTING=NONE
CALMAX =0.1500000E+05
CALMIN =-.1500000E+05
0.500E+04
RMS TIME HISTORY
0.100E+01
0.000E+00
ELAPSED TIME IN SECONDS
0.719E+04
FILTER BANDS
START STOP
BAND WEIGHTS S/N
DOMINANT TIME
TIME MAGNITUDE
0.3850E+04 0.455E+04
0.3820E+04 0.427E+04
0.3680E+04 0.416E+04
0.3930E+04 0.378E+04
0.3620E+04 0.351E+04
0.3780E+04 0.296E+04
0.3720E+04 0.295E+04
0.3750E+04 0.262E+04
0.1900E+03 0.173E+04
0.7800E+03 0.153E+04

Figure 11.

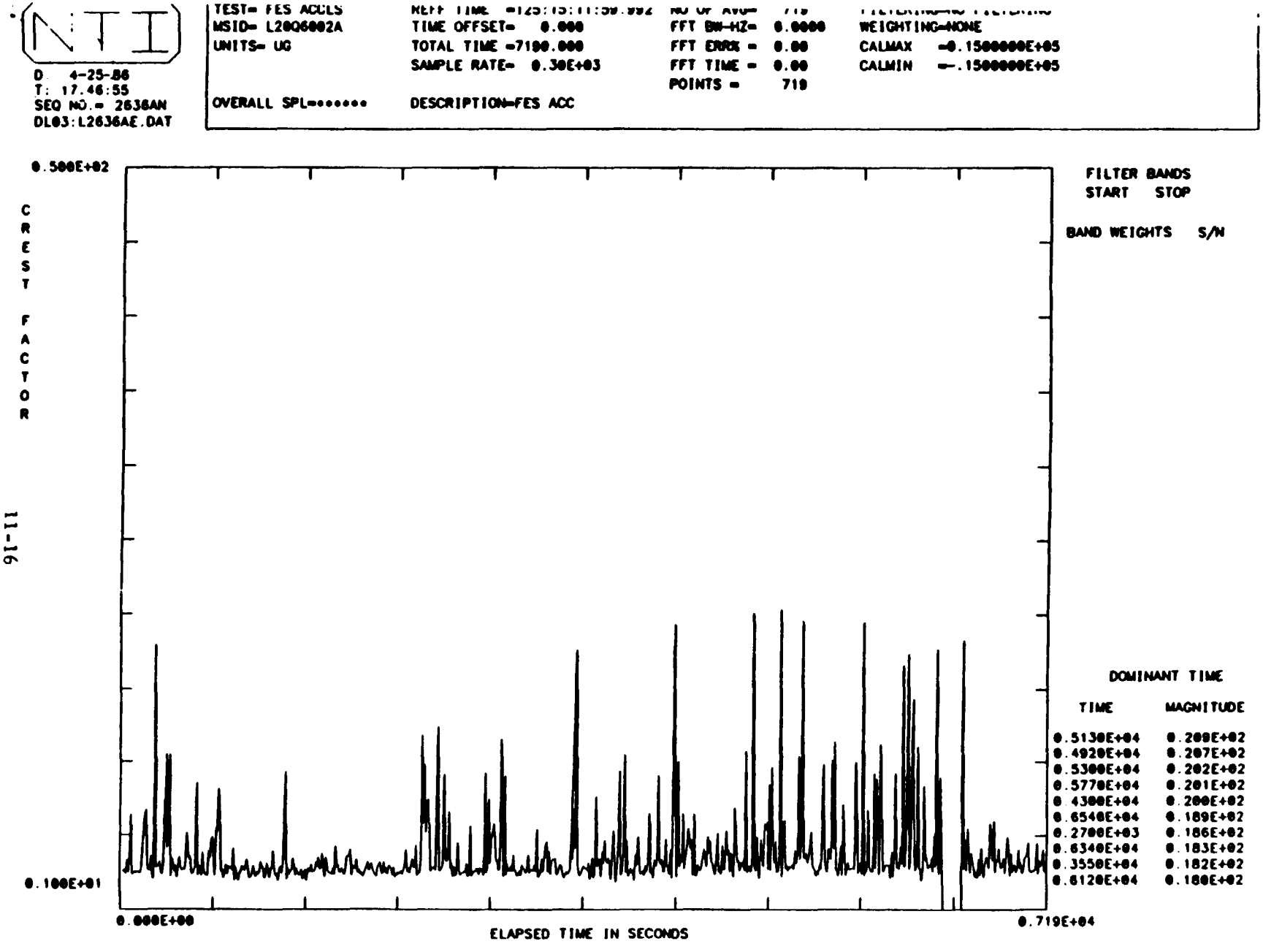
NTI
D 4-25-86
T: 17.46:55
SEQ NO.= 2636AN
DL03:L2636AE.DAT
TEST= FES ACCLS
MSID= L28Q6002A
UNITS= UG
TIME OFFSET= 0.000
TOTAL TIME =7190.000
SAMPLE RATE= 0.30E+03
FFT BW-HZ= 0.0000
FFT ERR% = 0.00
FFT TIME = 0.00
POINTS = 719
WEIGHTING=NONE
CALMAX =0.1500000E+05
CALMIN =-.1500000E+05
OVERALL SPL=******
DESCRIPTION=FES ACC
0.500E+02
CREST FACTOR
0.100E+01
0.000E+00
ELAPSED TIME IN SECONDS
0.719E+04
FILTER BANDS
START STOP
BAND WEIGHTS S/N
DOMINANT TIME
TIME MAGNITUDE
0.5130E+04 0.208E+02
0.4920E+04 0.207E+02
0.5300E+04 0.202E+02
0.5770E+04 0.201E+02
0.4300E+04 0.200E+02
0.6540E+04 0.189E+02
0.2700E+03 0.186E+02
0.6340E+04 0.183E+02
0.3550E+04 0.182E+02
0.6120E+04 0.180E+02

Figure 12.

events. You can see the roll maneuver very clearly in the RMS plot in Figure 11 and if you look at the same timeframe for the crest value in Figure 12 you really don't see anything, so the data reduction seems to be working.

The data shown in Figure 13 is the computer plot of the X, Y, and Z components of the acceleration RMS time history for the same timeframe. Figure 14 shows the crest factor for X, Y, and Z components for the same timeframe. So, this is the basic format for the presentation of our reduced data. In Figures 10 through 14 there is a total dropout of data that shown at about 6,400 seconds elapsed time. This is not considered significant but is mentioned to aid in understanding the data presentation.

To improve the usefulness of the data, we overlay the times when the reaction control system was either moderately active or very active as shown in Figure 15. Also included is a time overlay of the experiment operating modes. This is what we did for the FES experiment. Mode ten was when the cap was being removed from the crystal and mode eleven was when the crystal growing process was initiated. Until you overlay this RCS information for the whole mission the principal investigator does not have a complete story. I think when Dr. Lal saw this data he was quite interested to see that there was quite a bit of RCS activity at that particular time.

A plot of the crest value, Figure 16, for the same timeframe, doesn't show signifiant events because we were seeing broadband, long-term events. The format of the RCS data we will provide to users is shown in Figures 17 through 22. The thruster location is shown at the top center of each figure as F5L, F5R, etc., and represents locations as defined in Figure 6. There is a figure for each of six thruster locations, 2 forward, 2 aft right, and 2 aft left. The timeframe is the same for each figure; it starts at a GMT of 121:12 and is two hours long. Referring to the timeframe in Figure 16 this was the transition of the FES experiment from mode ten to mode eleven. There was signifi-

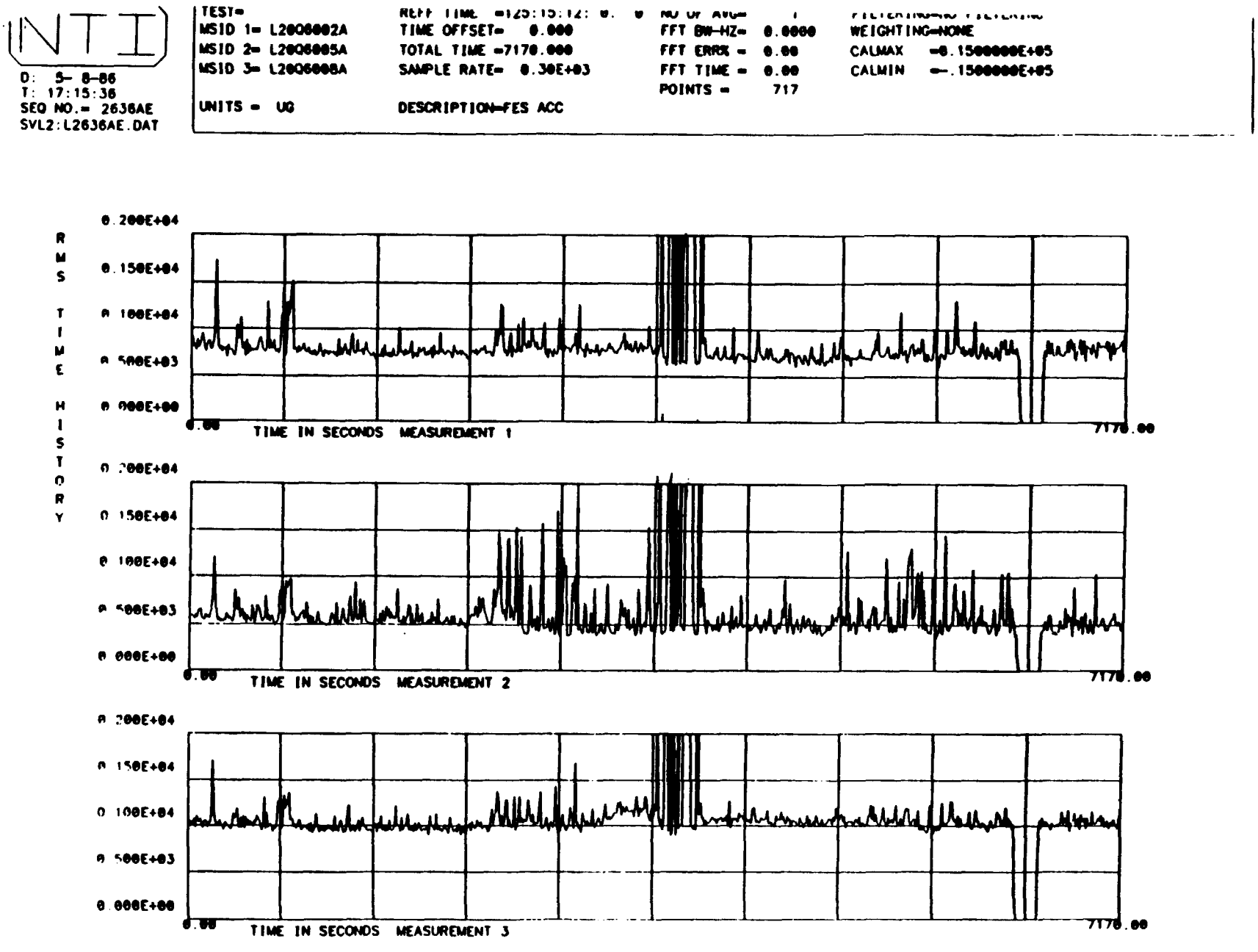

Figure 13.

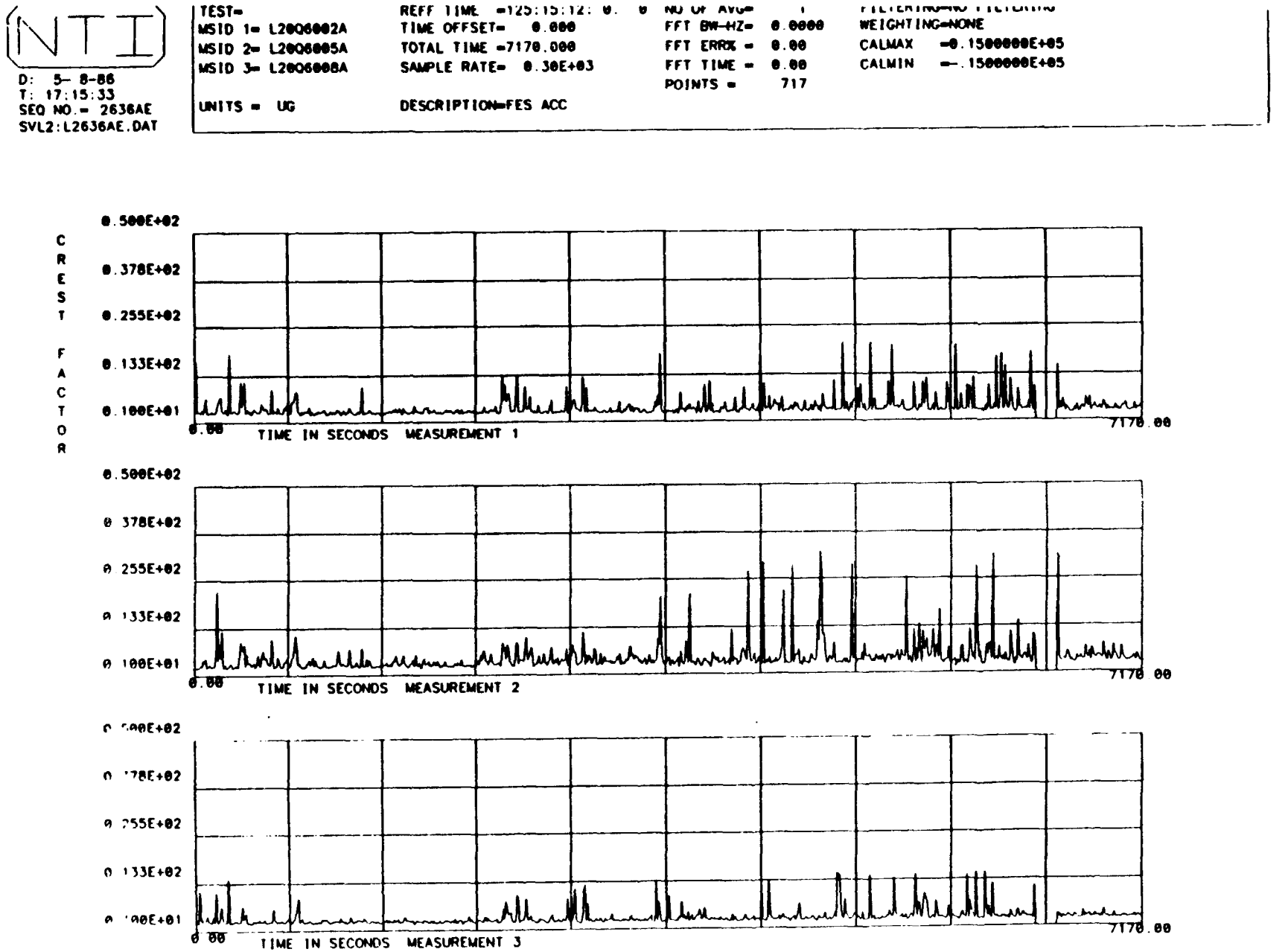

Figure 14.

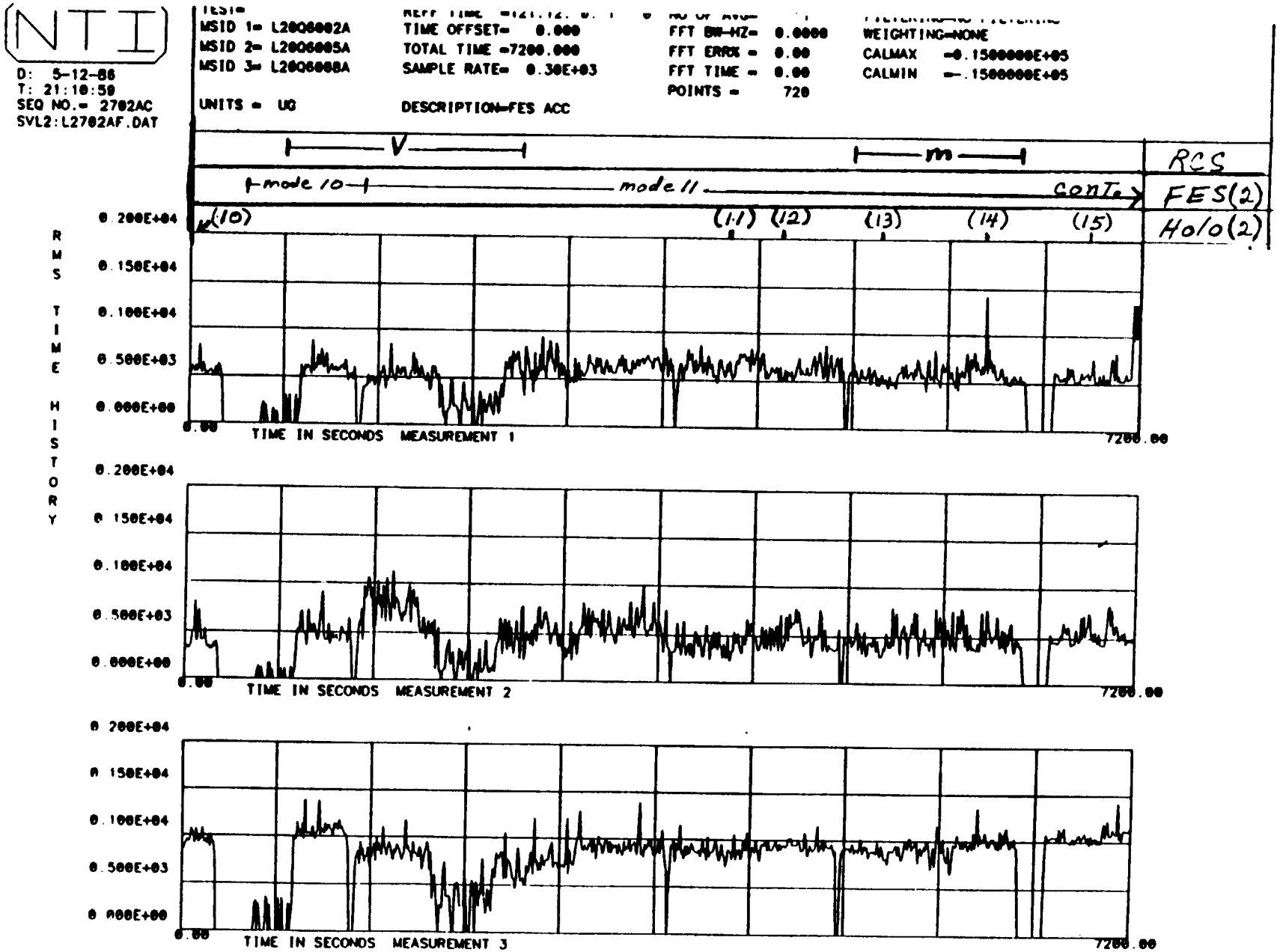
NTI
D: 5-12-86
T: 21:10:59
SEQ NO.= 2702AC
SVL2:L2702AF.DAT
MSID 1= L26Q6002A
MSID 2= L26Q6005A
MSID 3= L26Q6008A
UNITS = UG
TIME OFFSET= 0.000
TOTAL TIME =7200.000
SAMPLE RATE= 0.30E+03
DESCRIPTION=FES ACC
FFT BW-HZ= 0.0000
FFT ERR% = 0.00
FFT TIME = 0.00
POINTS = 720
WEIGHTING=NONE
CALMAX =0.1500000E+05
CALMIN =-.1500000E+05
V
m
mode 10
mode 11
cont.
RCS
FES(2)
Holo(2)
(10)
(11)
(12)
(13)
(14)
(15)
RMS TIME HISTORY
0.200E+04
0.150E+04
0.100E+04
0.500E+03
0.000E+00
TIME IN SECONDS MEASUREMENT 1
TIME IN SECONDS MEASUREMENT 2
TIME IN SECONDS MEASUREMENT 3
7200.00

Figure 15.

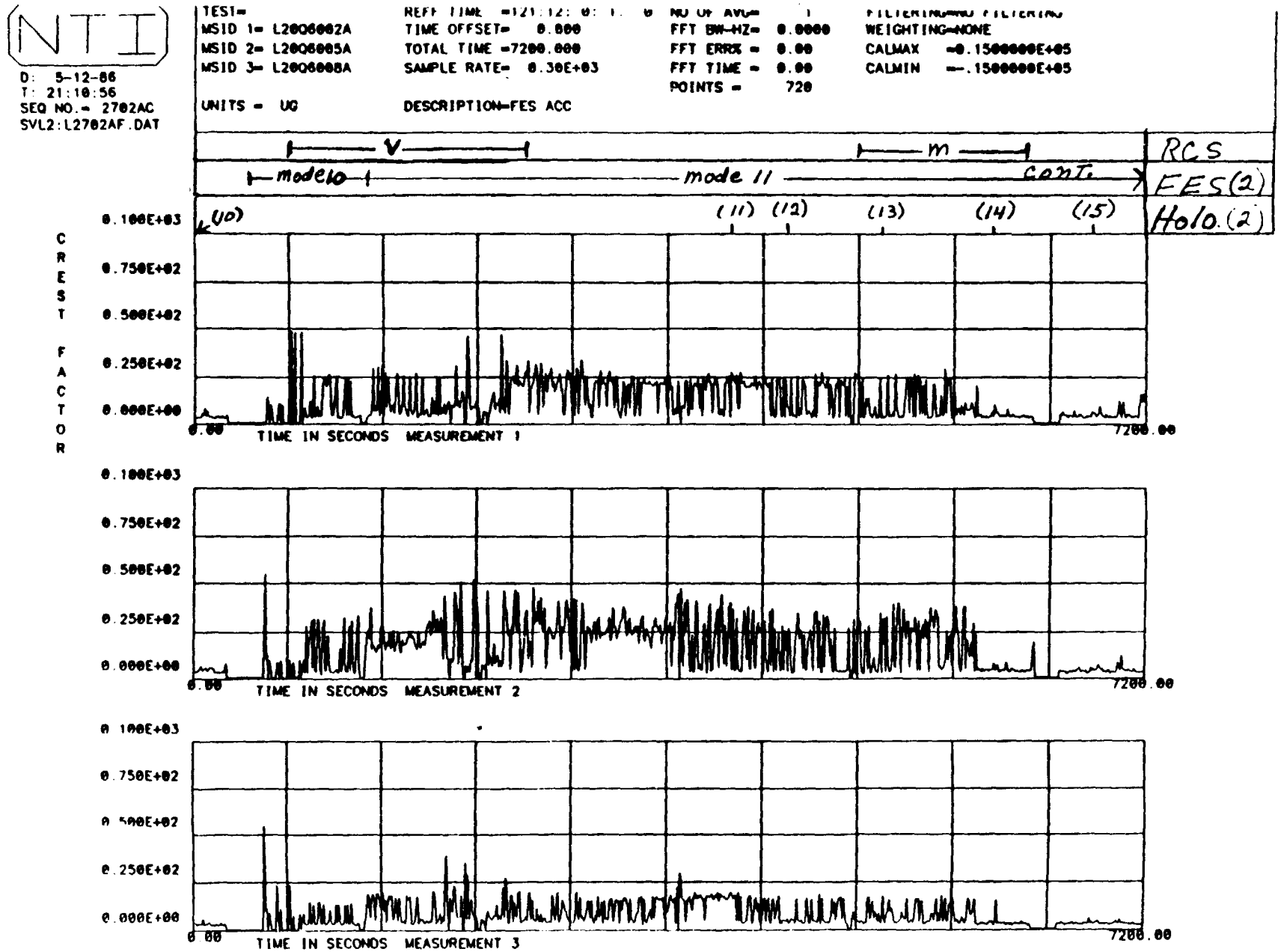
NTI
D: 5-12-86
T: 21:10:56
SEQ NO.= 2702AC
SVL2:L2702AF.DAT
TEST=
MSID 1= L2006002A
MSID 2= L2006005A
MSID 3= L2006008A
UNITS = UG
TIME OFFSET= 0.000
TOTAL TIME =7200.000
SAMPLE RATE= 0.30E+03
FFT BW-HZ= 0.0000
FFT ERR% = 0.00
FFT TIME = 0.00
POINTS = 720
WEIGHTING=NONE
CALMAX =0.1500000E+05
CALMIN =-.1500000E+05
DESCRIPTION=FES ACC
V
M
mode10
mode 11
cont.
RCS
FES(2)
Holo.(2)
(10)
(11)
(12)
(13)
(14)
(15)
CREST FACTOR
0.100E+03
0.750E+02
0.500E+02
0.250E+02
0.000E+00
0.00
TIME IN SECONDS MEASUREMENT 1
7200.00
TIME IN SECONDS MEASUREMENT 2
TIME IN SECONDS MEASUREMENT 3

Figure 16.

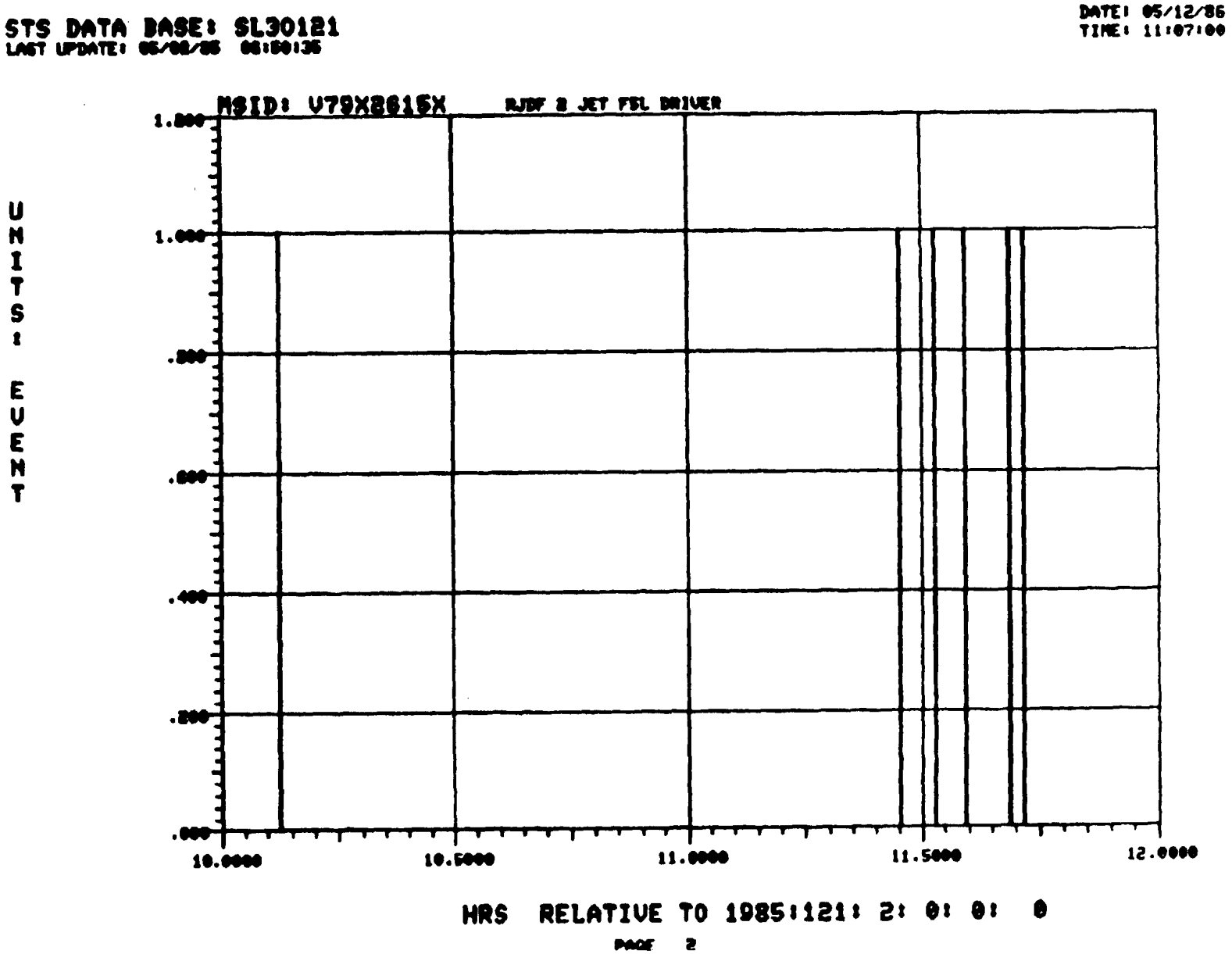
STS DATA BASE: SL30121
LAST UPDATE: 05/08/86 08:00:35
DATE: 05/12/86
TIME: 11:07:00
MSID: V79X8615X
RJBF 2 JET FEL DRIVER
UNITS: EVENT
1.000
.800
.600
.400
.200
.000
10.0000
10.5000
11.0000
11.5000
12.0000
HRS RELATIVE TO 1985:121: 2: 0: 0: 0
PAGE 2

Figure 17.

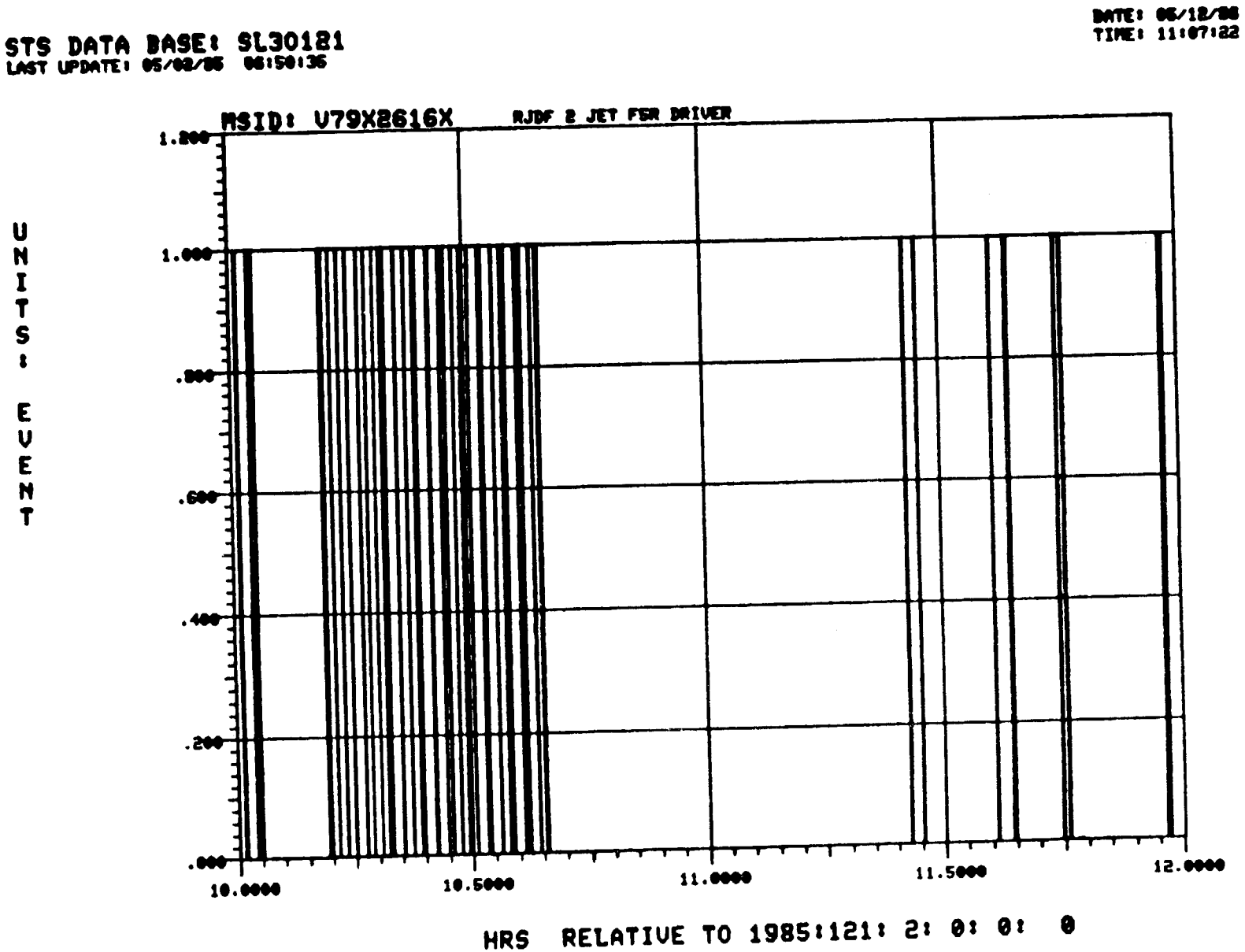
STS DATA BASE: SL30121
LAST UPDATE: 05/02/85 06:50:36
DATE: 05/12/85
TIME: 11:07:22
MSID: V79X2616X
RJDF 2 JET FSR DRIVER
UNITS: EVENT
1.200
1.000
.800
.600
.400
.200
.000
10.0000
10.5000
11.0000
11.5000
12.0000
HRS RELATIVE TO 1985:121: 2: 0: 0: 0
PAGE 3

Figure 18.

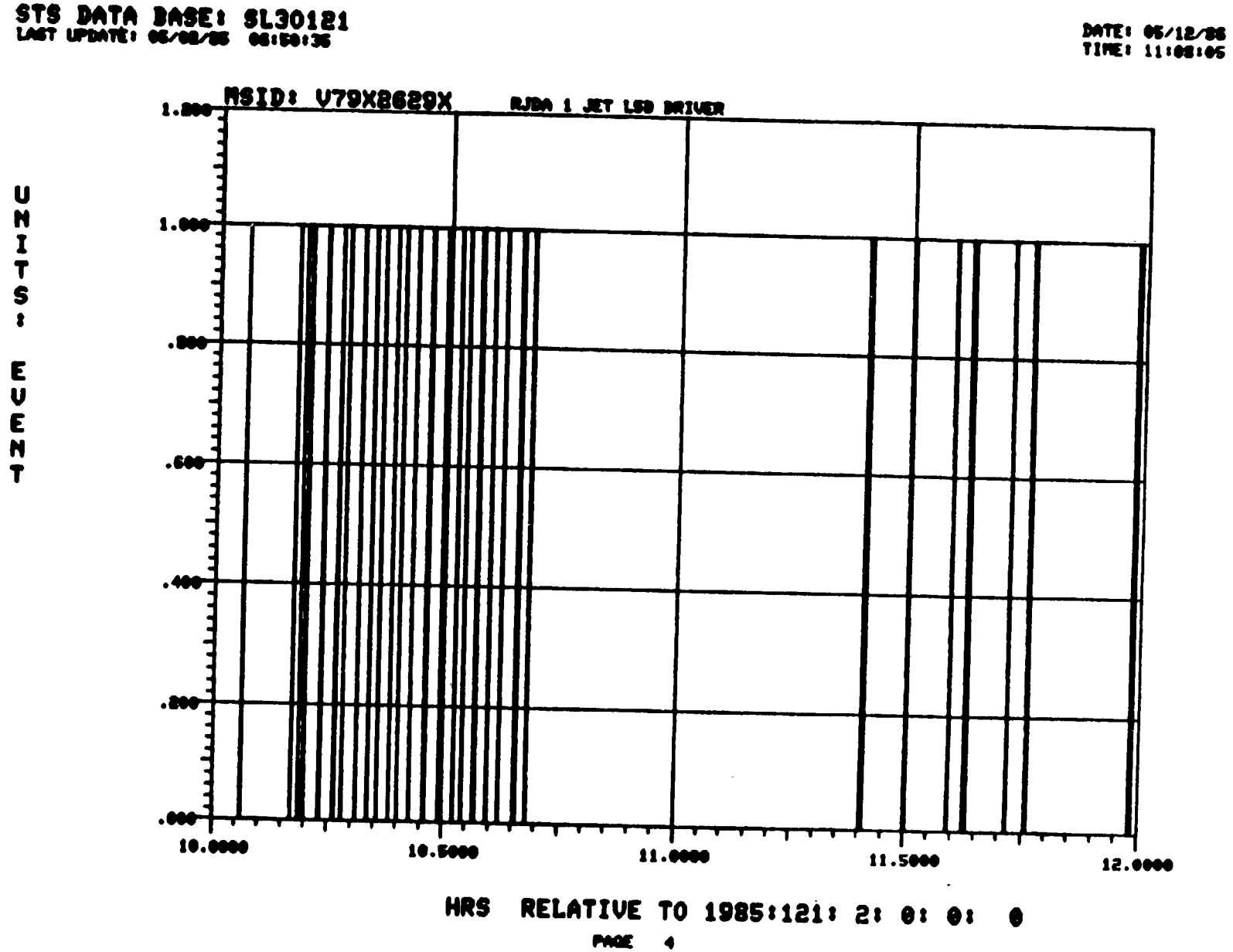
STS DATA BASE: SL30121
LAST UPDATE: 05/08/86 08:50:35
DATE: 05/12/86
TIME: 11:08:05
MSID: V79X8629X
RJBA 1 JET LSB DRIVER
UNITS - EVENT
1.000
.800
.600
.400
.200
.000
10.0000
10.5000
11.0000
11.5000
12.0000
HRS RELATIVE TO 1985:121: 2: 0: 0: 0
PAGE 4

Figure 19.

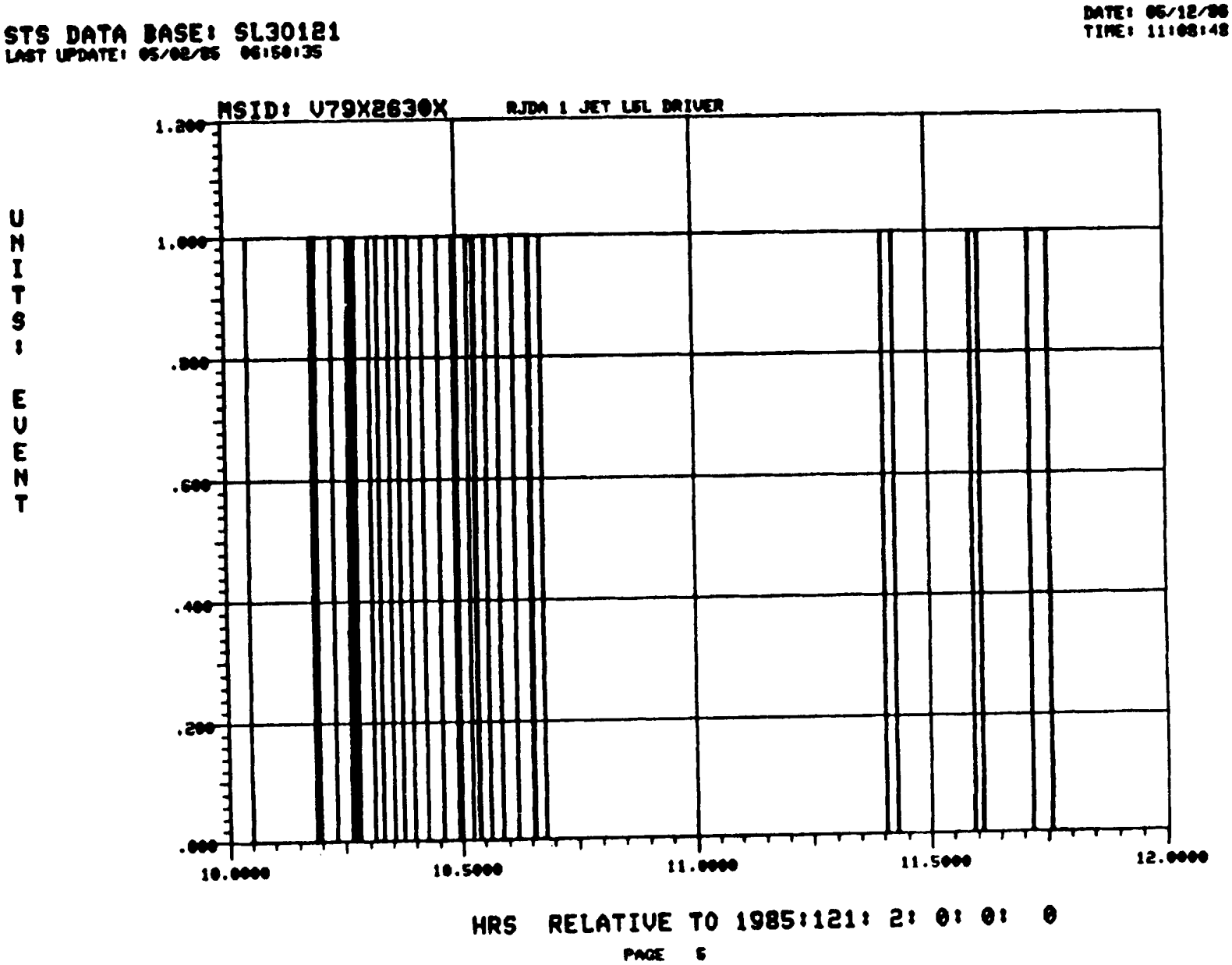
STS DATA BASE: SL30121
LAST UPDATE: 05/02/85 06:50:35
DATE: 05/12/85
TIME: 11:08:48
MSID: V79X2630X
RJDA 1 JET LGL DRIVER
UNITS: EVENT
1.200
1.000
.800
.600
.400
.200
.000
10.0000
10.5000
11.0000
11.5000
12.0000
HRS RELATIVE TO 1985:121: 2: 0: 0: 0
PAGE 5

Figure 20.

STS DATA BASE: SL30121
LAST UPDATE: 05/08/86 08:50:35

DATE: 05/12/86
TIME: 11:09:15

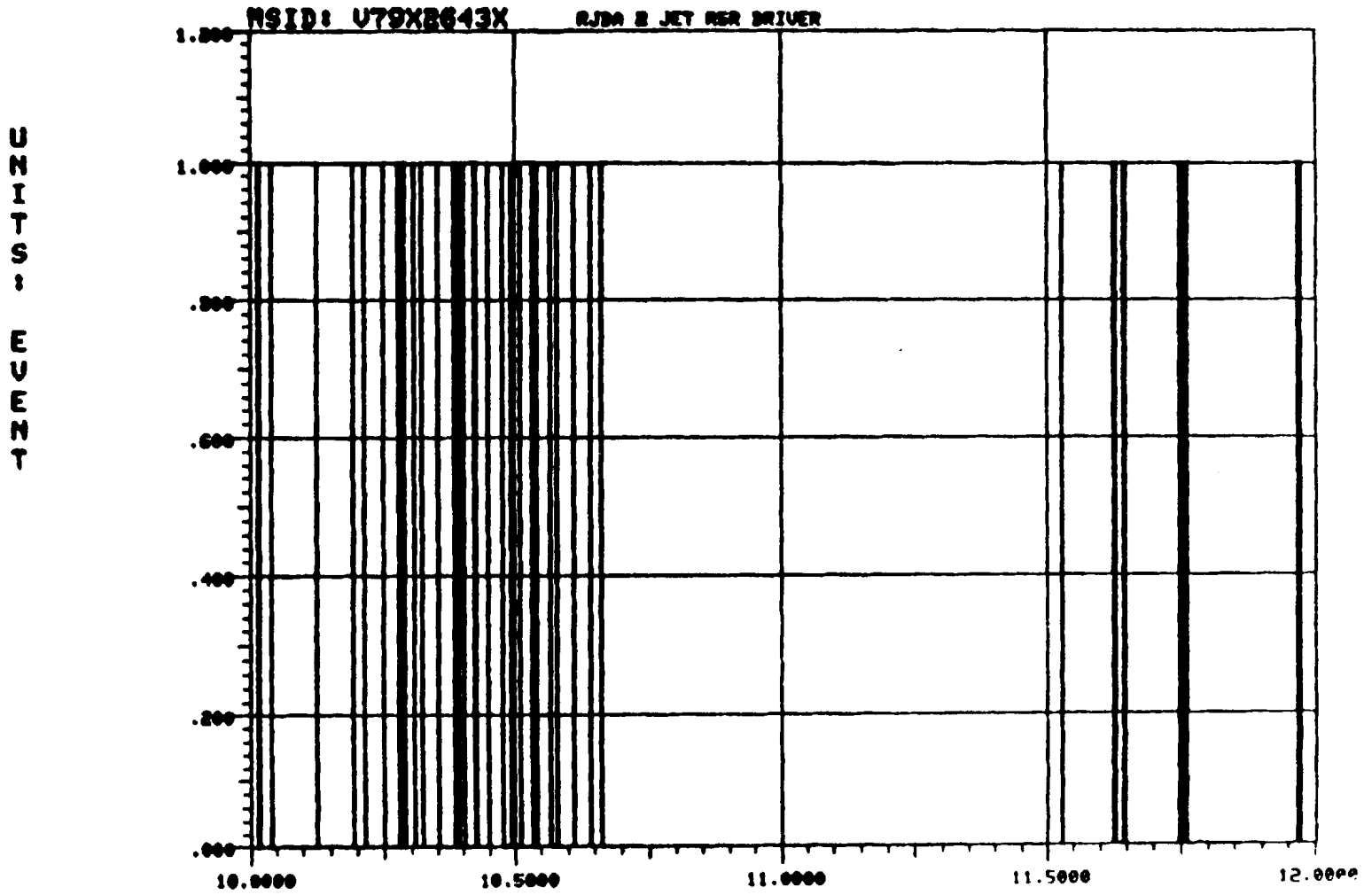

PAGE 6

Figure 21.

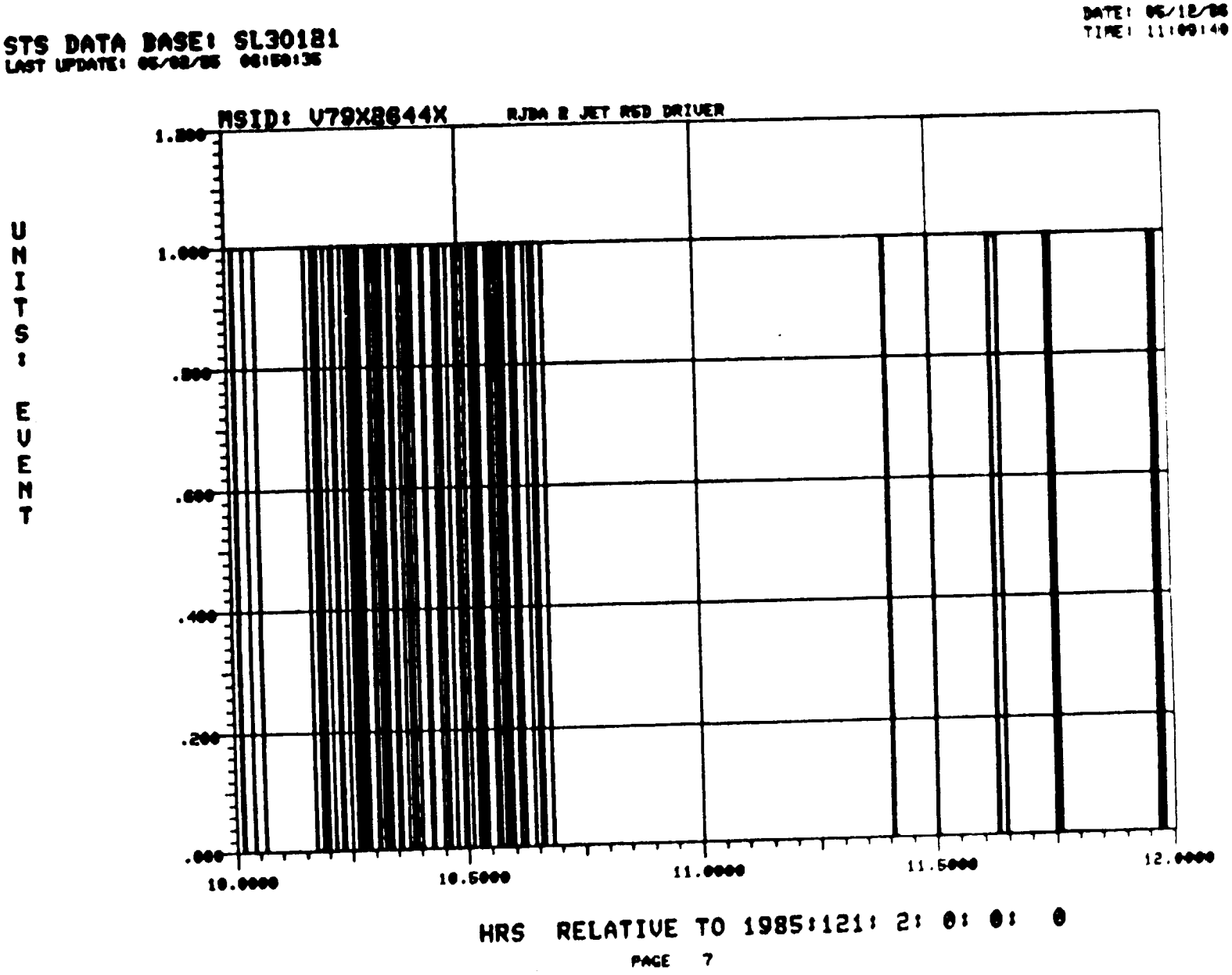
STS DATA BASE: SL30181
LAST UPDATE: 05/02/85 08:50:35
DATE: 05/12/85
TIME: 11:09:40
MSID: V79X8644X
RJDA 2 JET RCD DRIVER
UNITS: EVENT
1.200
1.000
.800
.600
.400
.200
.000
10.0000
10.5000
11.0000
11.5000
12.0000
HRS RELATIVE TO 1985:121: 2: 0: 0: 0
PAGE 7

Figure 22.

cant activity during that timeframe, and I think these six figures show the source. Of the six RCS firings we picked there was only one that was not very active during this time period. You can correlate these RCS firings with the periods identified as a very active RCS time and as a moderately active time in Figure 16. When you look at the g effects, it becomes really important, not only that these lines are fairly close together, but when you get a broad line it means that particular RCS engine is firing very rapidly. It only fires for about 80 milli seconds, I believe, but it is firing very rapidly to try to maintain its proper attitude.

Another area where we identified very pronounced activity is shown in Figures 23 and 24. I can not say that was definitely an RCS engine but it sure looks like it. If we look at the crest value, again the disturbance doesn't show up. The set of thruster firings are shown again for the six locations (Figures 25 through 30). If you look at the first firing it was relatively benign at the time of the pronounced disturbance in Figure 23. Looking at the other five examples (Figures 26 through 30) of the RCS engines, two in the front, two in the aft left, two in the aft right, we see fairly active firing during the period of interest. Other activities may have supplemented the disturbances in X, Y, and Z, but the RCS firings seem to fit the timeframe of interest. This was at a relatively critical stage in the FES crystal growth process. I have not yet superimposed any of the substeps within mode eleven, but that particular timeframe was a fairly critical period.

I think Hans Hamacher mentioned in his talk that not every time that the RCS's are firing is there a bad environment on the Shuttle or Space Station, or in this case, the Spacelab. Well here is another event that I thought had a relatively significant effect (Figure 31). Figure 32 is a good example of the crest factor and how it does not show you the broad events. There are some definite events shown in the crest factor after the RMS has levelled off and I do believe that these are definite events that are happening throughout the mission. It could be some of the treadmill events that have been identified earlier. Some of

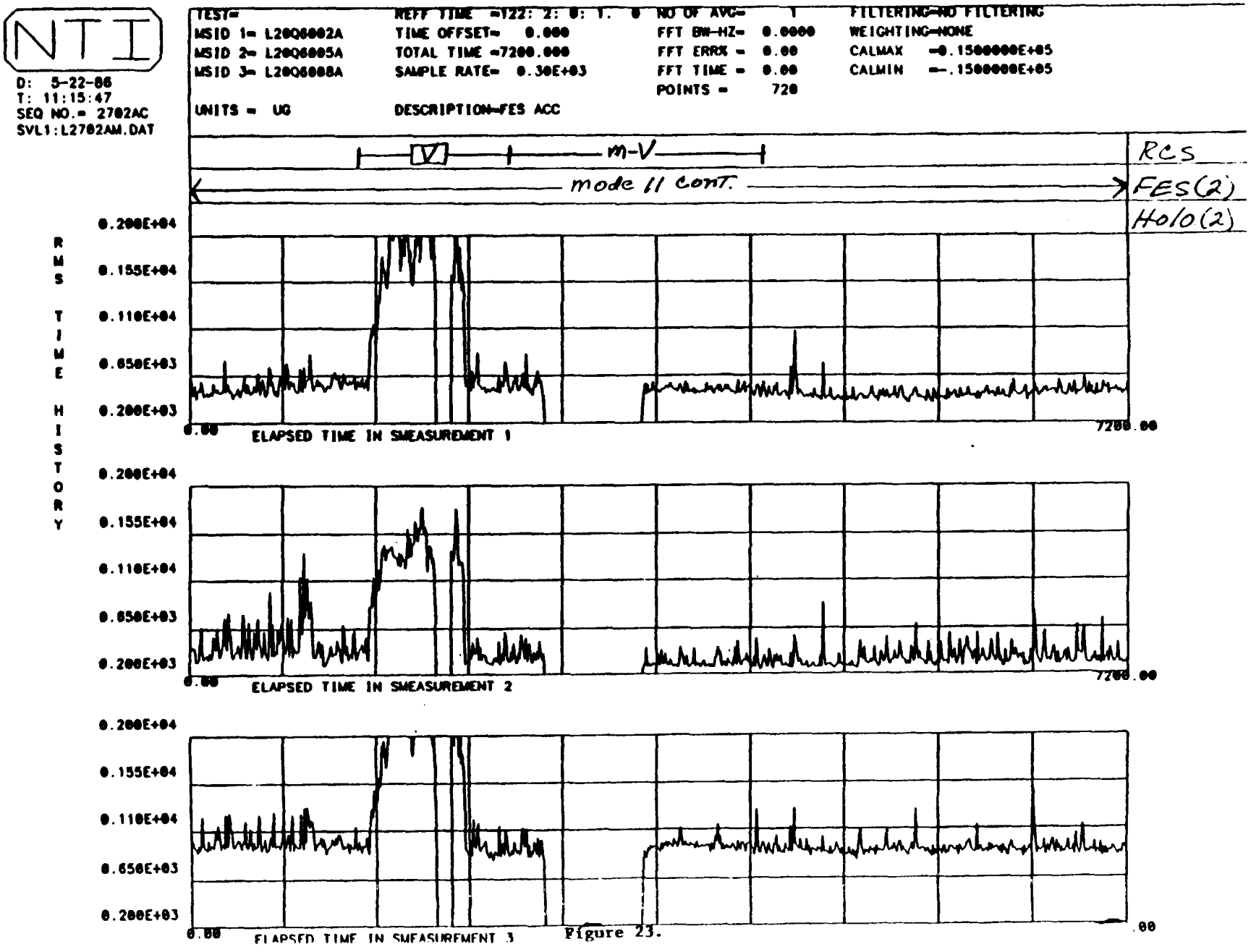
NTI
D: 5-22-86
T: 11:15:47
SEQ NO.= 2702AC
SVL1:L2702AM.DAT
TEST=
MSID 1= L20Q0002A
MSID 2= L20Q0005A
MSID 3= L20Q0008A
UNITS = UG
REFF TIME =Y22: 2: 0: 1. 0
TIME OFFSET= 0.000
TOTAL TIME =7200.000
SAMPLE RATE= 0.30E+03
DESCRIPTION=FES ACC
NO OF AVG= 1
FFT BW-HZ= 0.0000
FFT ERR% = 0.00
FFT TIME = 0.00
POINTS = 720
FILTERING=NO FILTERING
WEIGHTING=NONE
CALMAX =0.1500000E+05
CALMIN =-.1500000E+05
m-V
mode 11 cont.
RCS
FES(2)
Holo(2)
RMS TIME HISTORY
0.200E+04
0.155E+04
0.110E+04
0.650E+03
0.200E+03
0.00
7200.00
ELAPSED TIME IN SMEASUREMENT 1
ELAPSED TIME IN SMEASUREMENT 2
ELAPSED TIME IN SMEASUREMENT 3

Figure 23.

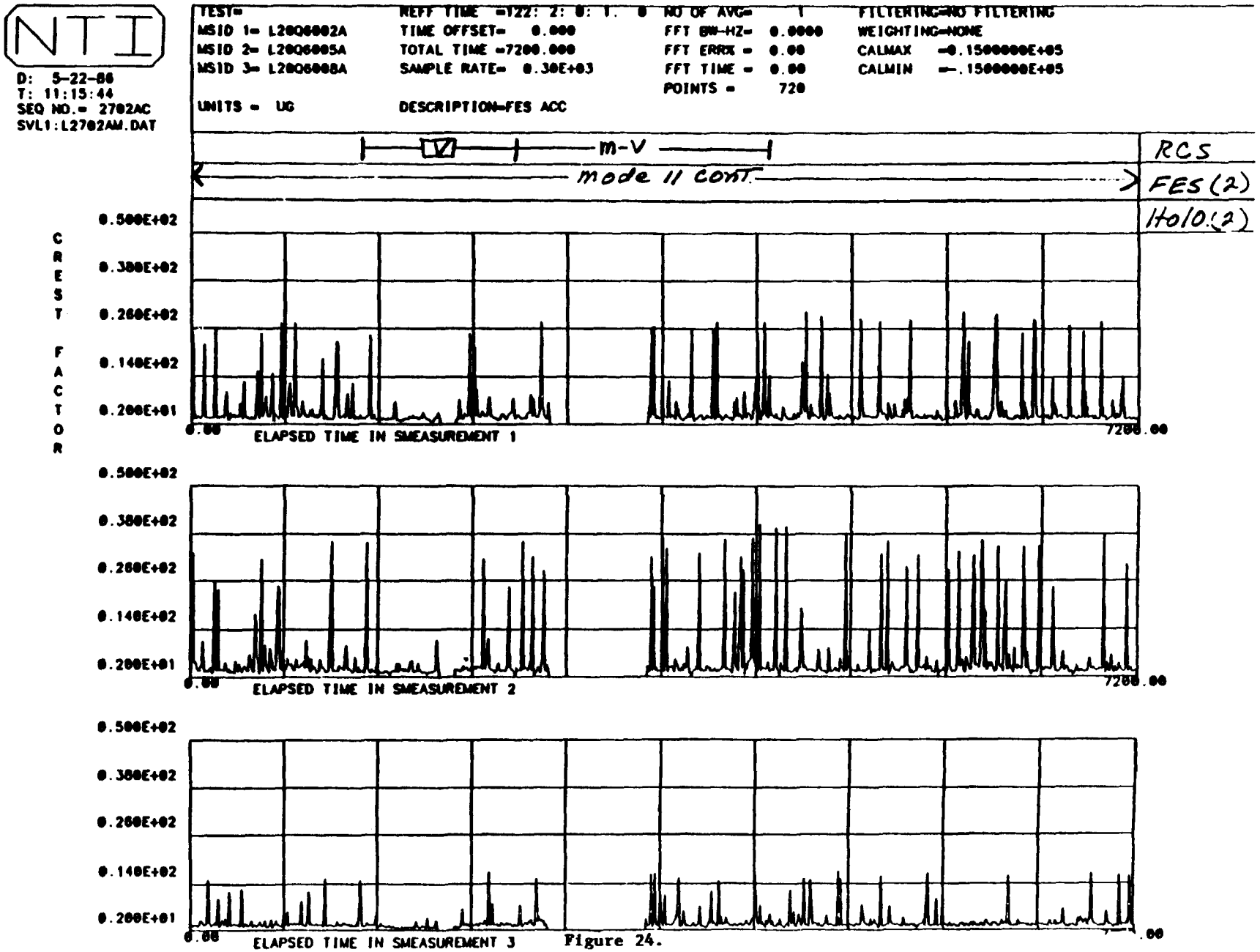

Figure 24.

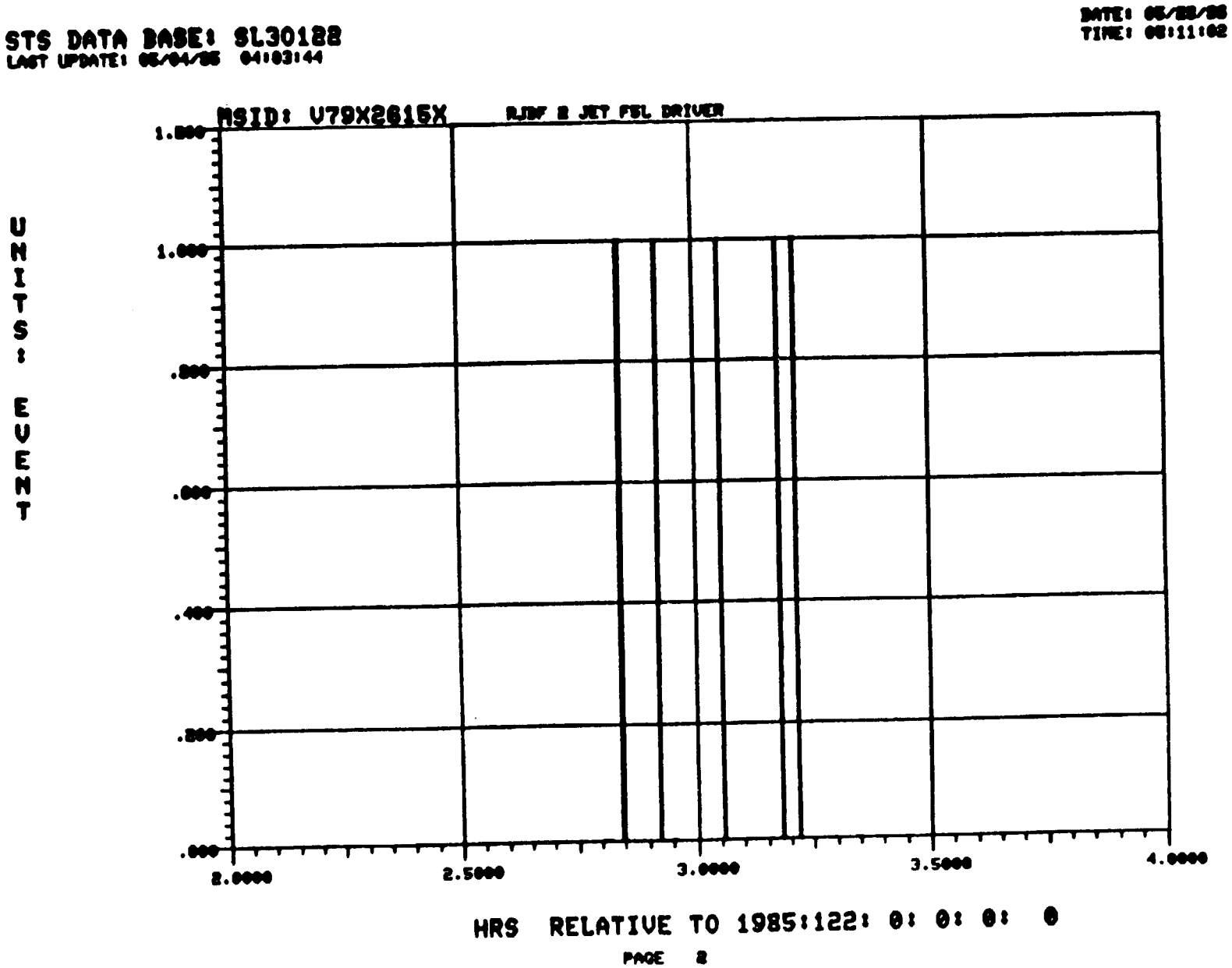
STS DATA BASE: SL30188
LAST UPDATE: 05/04/85 04:03:44
DATE: 05/08/85
TIME: 08:11:02
MSID: V79X2615X
RJBF 2 JET FEL DRIVER
UNITS: EVENT
1.000
.800
.600
.400
.200
.000
2.0000
2.5000
3.0000
3.5000
4.0000
HRS RELATIVE TO 1985:122: 0: 0: 0: 0
PAGE 2

Figure 25.

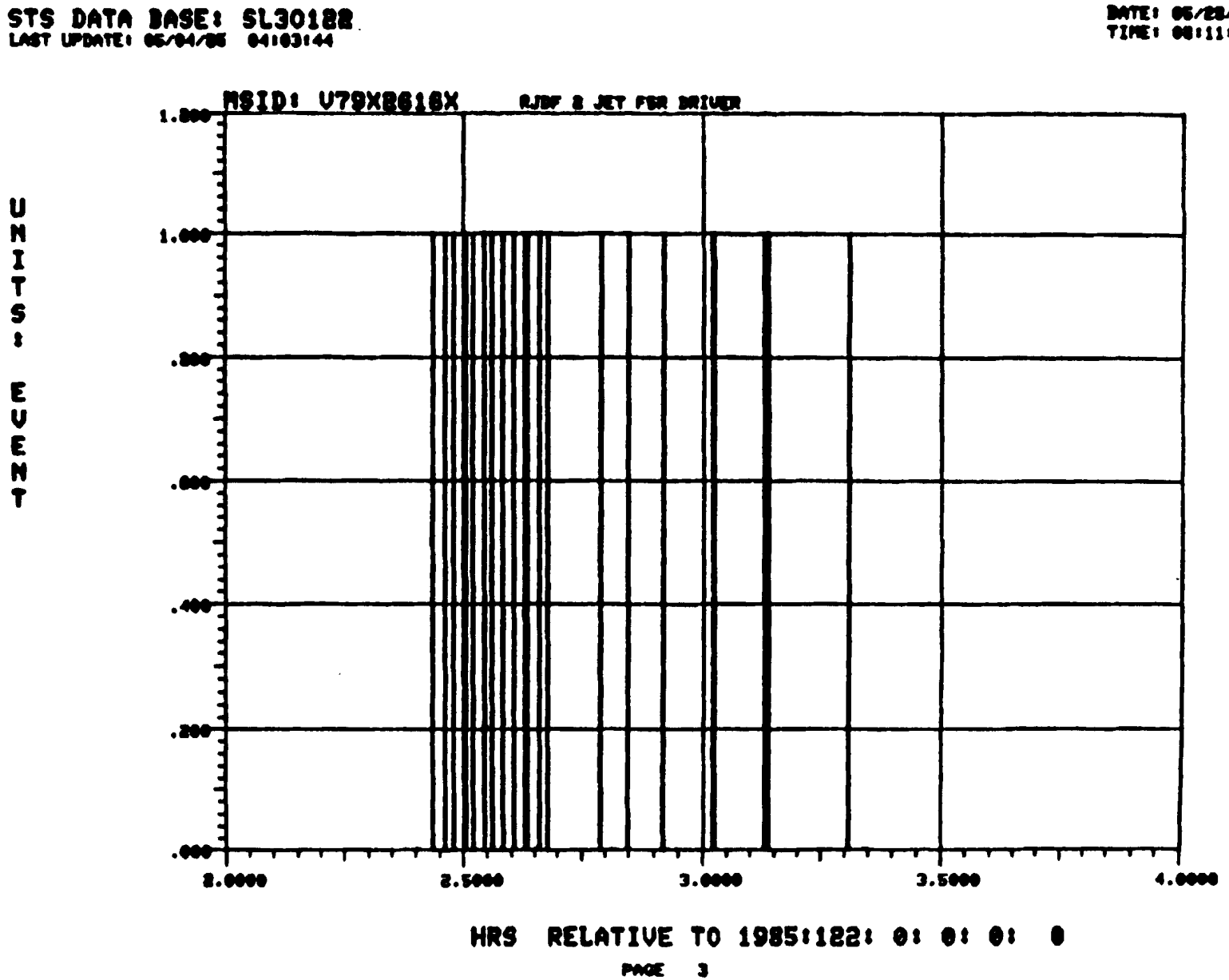
STS DATA BASE: SL30182
LAST UPDATE: 05/04/85 04:03:44
DATE: 05/23/85
TIME: 08:11:39
MSID: V79X2618X
RJDF 2 JET FOR DRIVER
UNITS = EVENT
1.200
1.000
.800
.600
.400
.200
.000
2.0000
2.5000
3.0000
3.5000
4.0000
HRS RELATIVE TO 1985:122: 0: 0: 0: 0
PAGE 3

Figure 26.

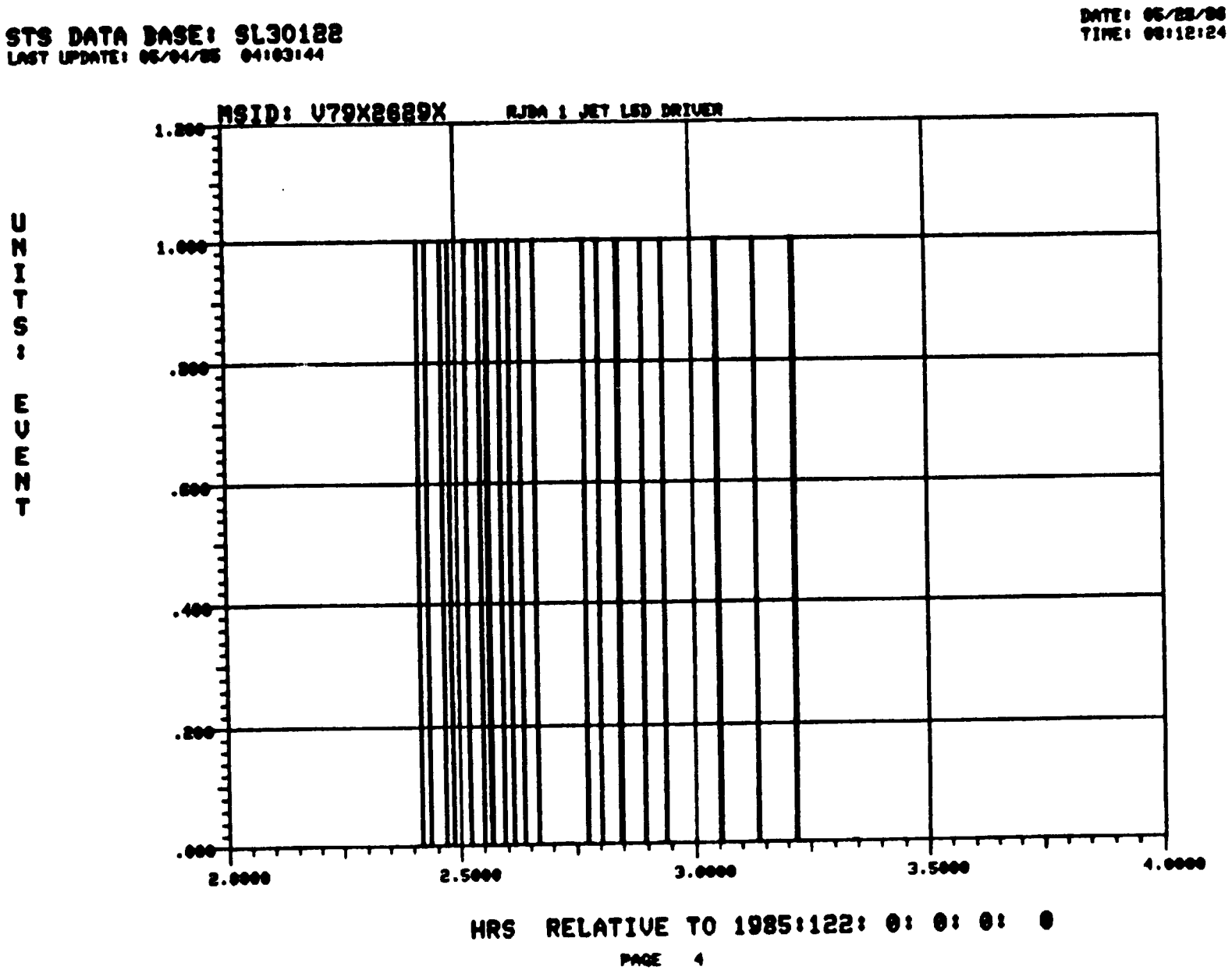
STS DATA BASE: SL30122
LAST UPDATE: 05/04/85 04:03:44
DATE: 05/22/85
TIME: 08:12:24
MSID: V79X2629X
RJDA 1 JET LSD DRIVER
UNITS: EVENT
1.200
1.000
.800
.600
.400
.200
.000
2.0000
2.5000
3.0000
3.5000
4.0000
HRS RELATIVE TO 1985:122: 0: 0: 0: 0
PAGE 4

Figure 27.

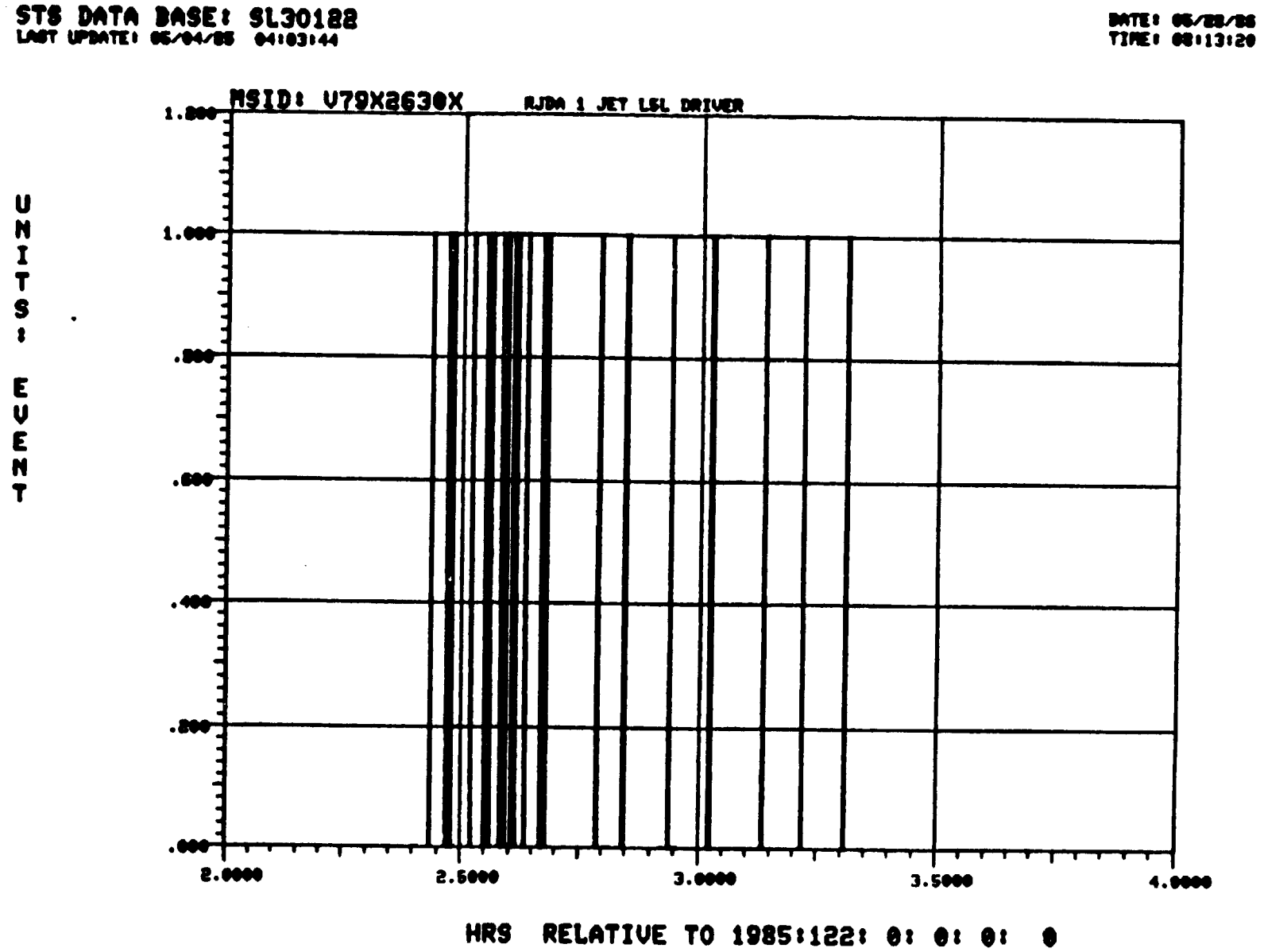

Figure 28.

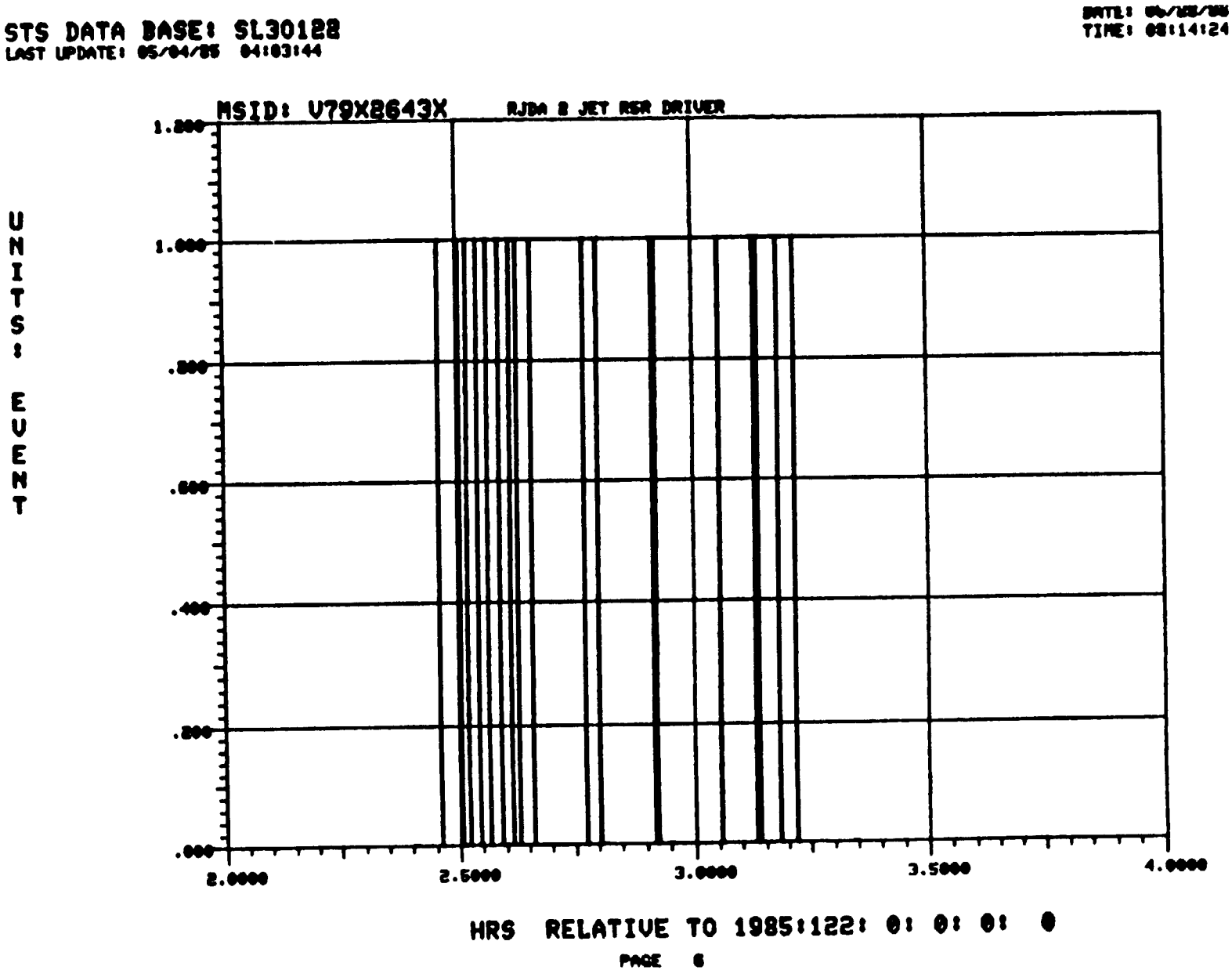

Figure 29.

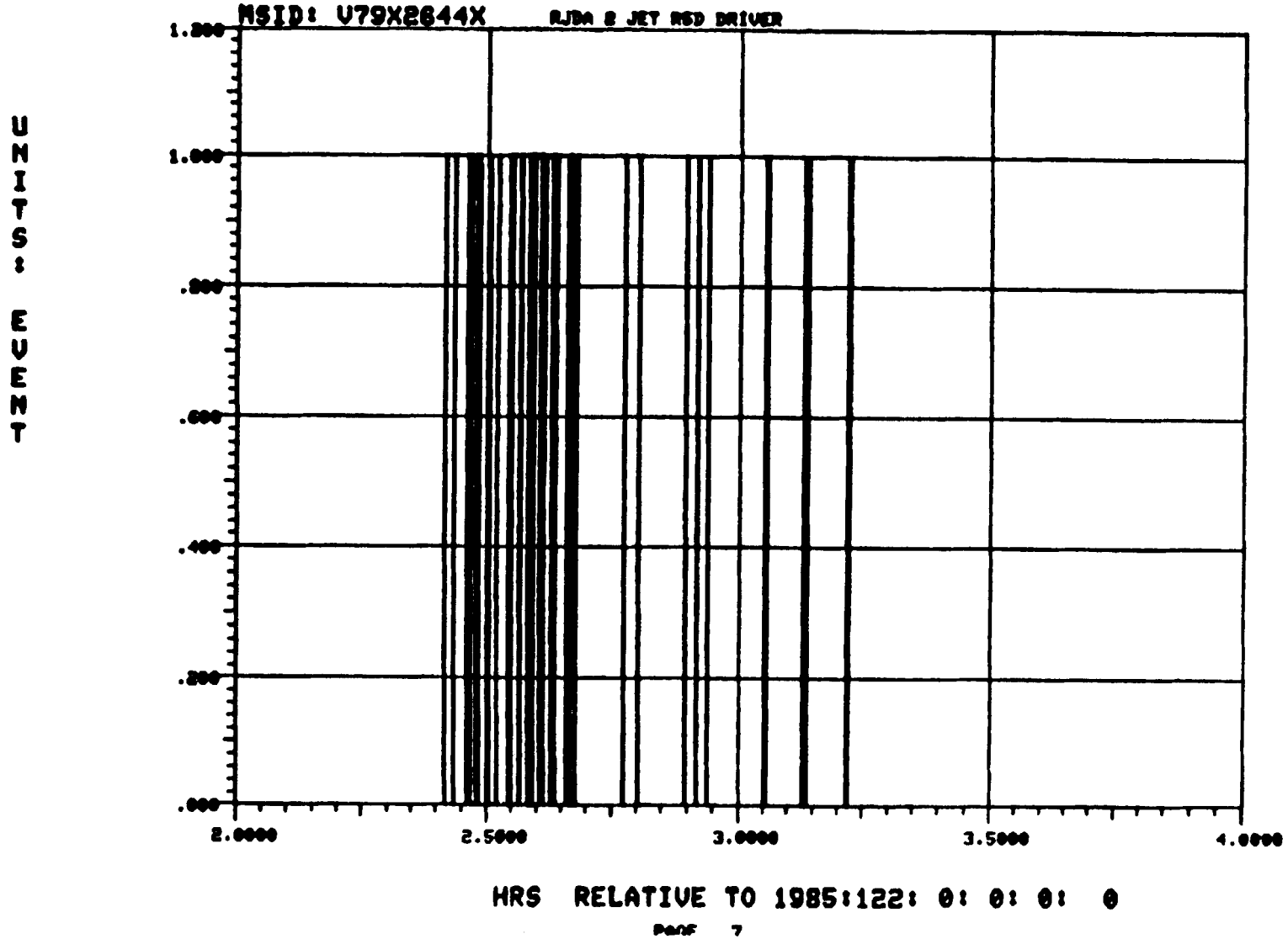
STS DATA BASE: SL30122
LAST UPDATE: 05/04/86 04:03:44
DATE: 05/28/86
TIME: 08:15:47
MSID: V79X2644X
RJDA 8 JET RCD DRIVER
UNITS: EVENT
1.200
1.000
.800
.600
.400
.200
.000
2.0000
2.5000
3.0000
3.5000
4.0000
HRS RELATIVE TO 1985:122: 0: 0: 0: 0
PAGE 7

Figure 30.

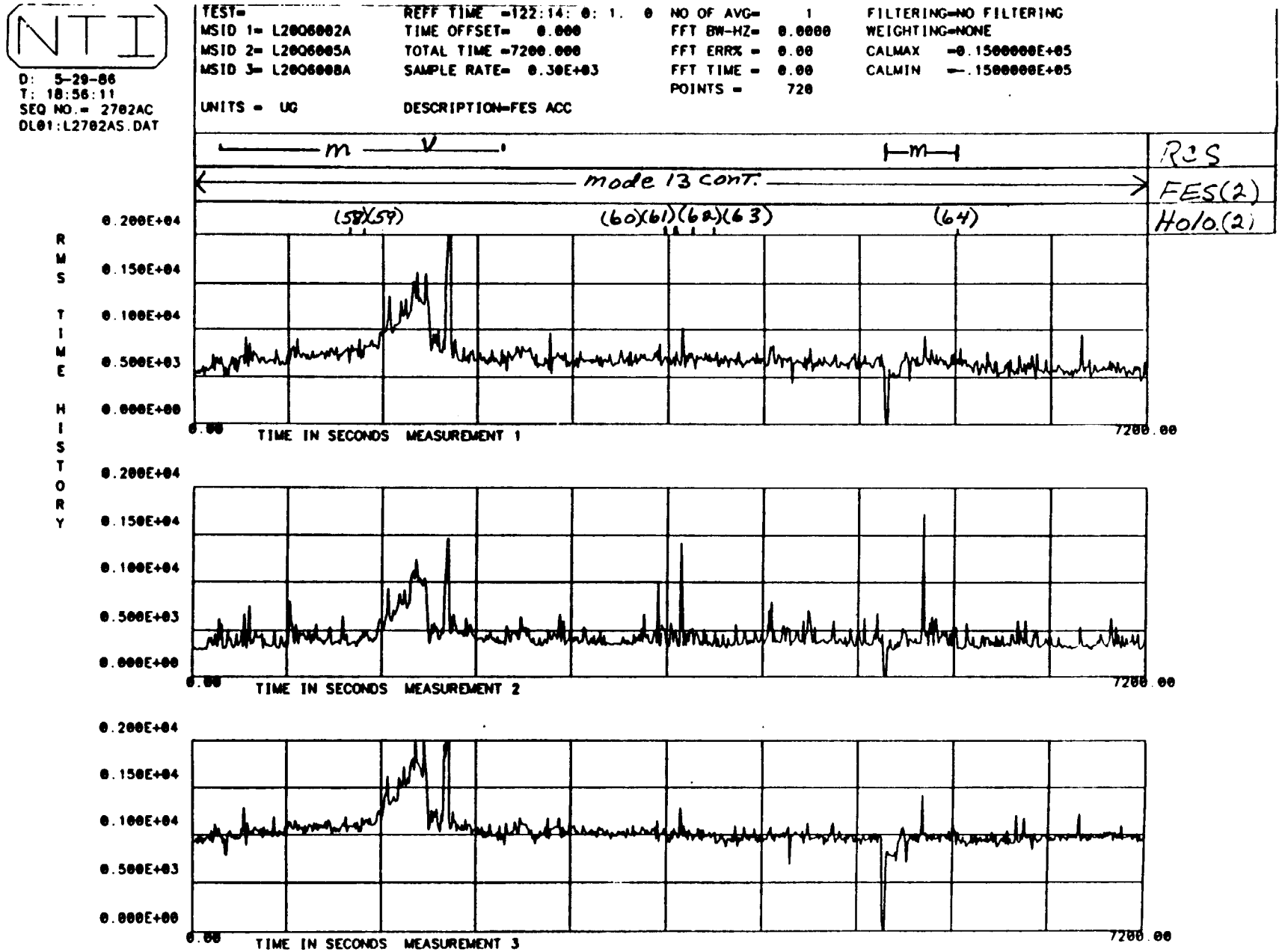
NTI
D: 5-29-86
T: 18:56:11
SEQ NO.= 2702AC
DL01:L2702AS.DAT
TEST=
MSID 1= L20O6002A
MSID 2= L20O6005A
MSID 3= L20O6008A
UNITS = UG
REFF TIME =122:14: 0: 1. 0
TIME OFFSET= 0.000
TOTAL TIME =7200.000
SAMPLE RATE= 0.30E+03
DESCRIPTION=FES ACC
NO OF AVG= 1
FFT BW-HZ= 0.0000
FFT ERR% = 0.00
FFT TIME = 0.00
POINTS = 720
FILTERING=NO FILTERING
WEIGHTING=NONE
CALMAX =0.1500000E+05
CALMIN =-.1500000E+05
m v
m
mode 13 cont.
R2S
FES(2)
Holo.(2)
(58)(59)
(60)(61)(62)(63)
(64)
RMS TIME HISTORY
0.200E+04
0.150E+04
0.100E+04
0.500E+03
0.000E+00
0.00
TIME IN SECONDS MEASUREMENT 1
7200.00
TIME IN SECONDS MEASUREMENT 2
TIME IN SECONDS MEASUREMENT 3

Figure 31.

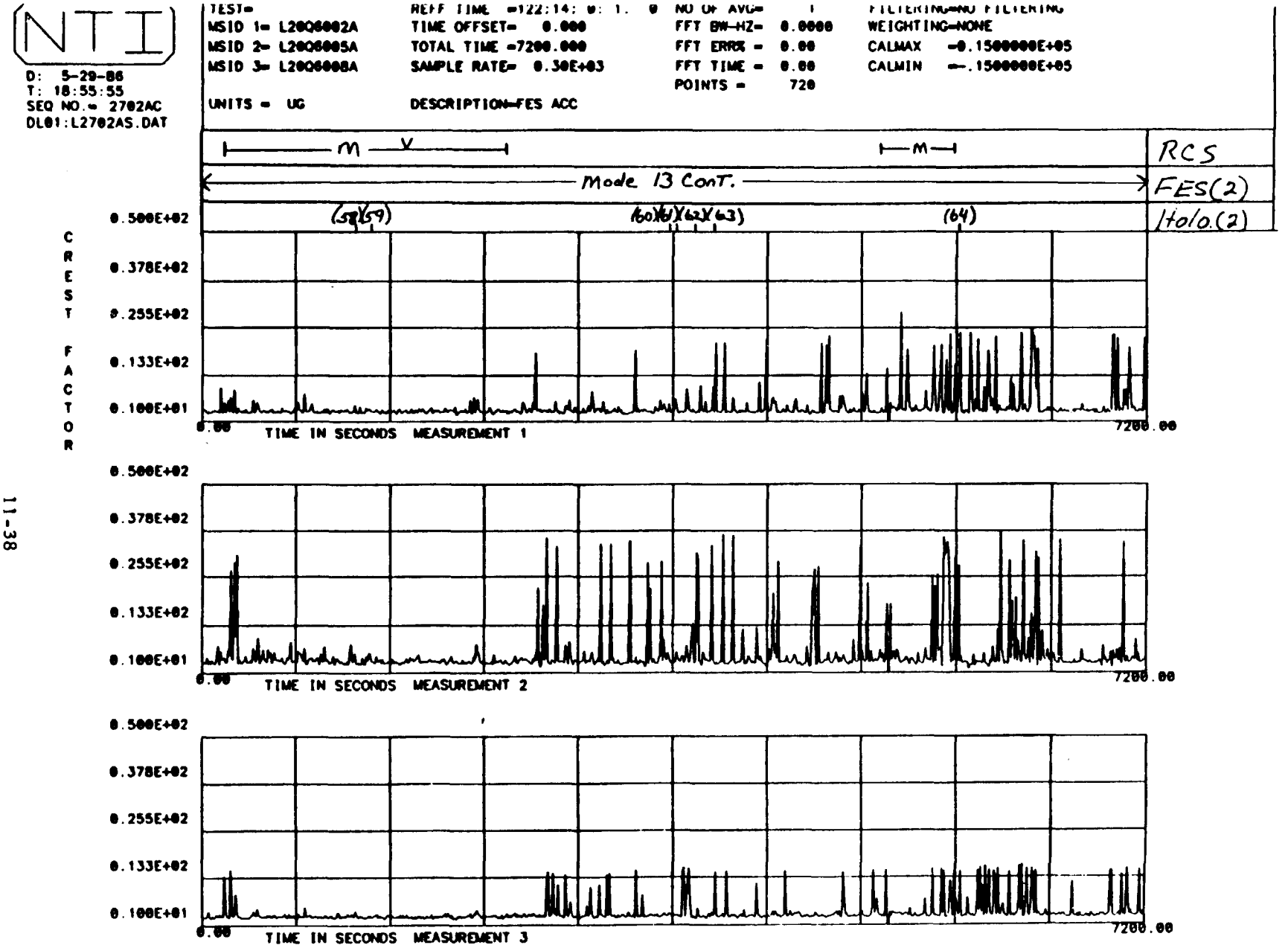

Figure 32.

our next steps will be to try to identify the most interesting areas, especially for the FES. You see in Figure 32 the crest is about two and a half. The crest factor is unitless. You are really looking at a relative effect, like there is some meaning between one peak and the size of another peak, but it has no meaning in absolute terms.

There was something going on in a 12-hour cycle. It may be just happenstance, but a disturbance we looked at was at exactly 122:2 and another was at 122:14 reference time. We looked ahead at the 123:2 time frame and there was another peak. At later mission times, the disturbance disappeared from the 12-hour cycle. So there were three cycles of twelve hours where something interesting was going on.

During some time periods the RCS thrusters were very active (Figures 33 and 34) and we had a pretty benign type of atmosphere, as far as g-level is concerned. It is like Hans Hamacher said, sometimes you are going to see some of these effects and sometimes you are not. I don't understand it, but we intend to look at this much closer than we have so far. Another interesting event is shown in Figure 35. This is raw data spread over a 10-second time period. So raw data can be very useful too. It doesn't look quite as bad as when we plotted it in a two-hour timeframe. I wanted to point out that this type of event is something that Rudy Ruff has been looking into more than we have. But this agrees with some other things that were said today and this type of event seems to be very prevalent. Figure 36 is a PSD plot, or spectrum level, and you can see that 17-Hz factor that has been discussed. The dominant frequency is shown at 17.1 Hz. Somebody was talking about 17.4 Hz being a fan of some kind, but we see the 17 Hz very predominantly throughout the whole mission. Figure 37 shows a timeframe about 40 seconds downstream where we saw another event that appears to be a real event. We did a power spectrum on it (Figure 38), and that peak had shifted by a factor of two, up to about 34 Hz, and the 17 Hz is not showing up at all. So there may have been something cutting in or out or it could be a node that we are seeing. We feel that the recurring 17 Hz disturbance is definitely worth looking into further.

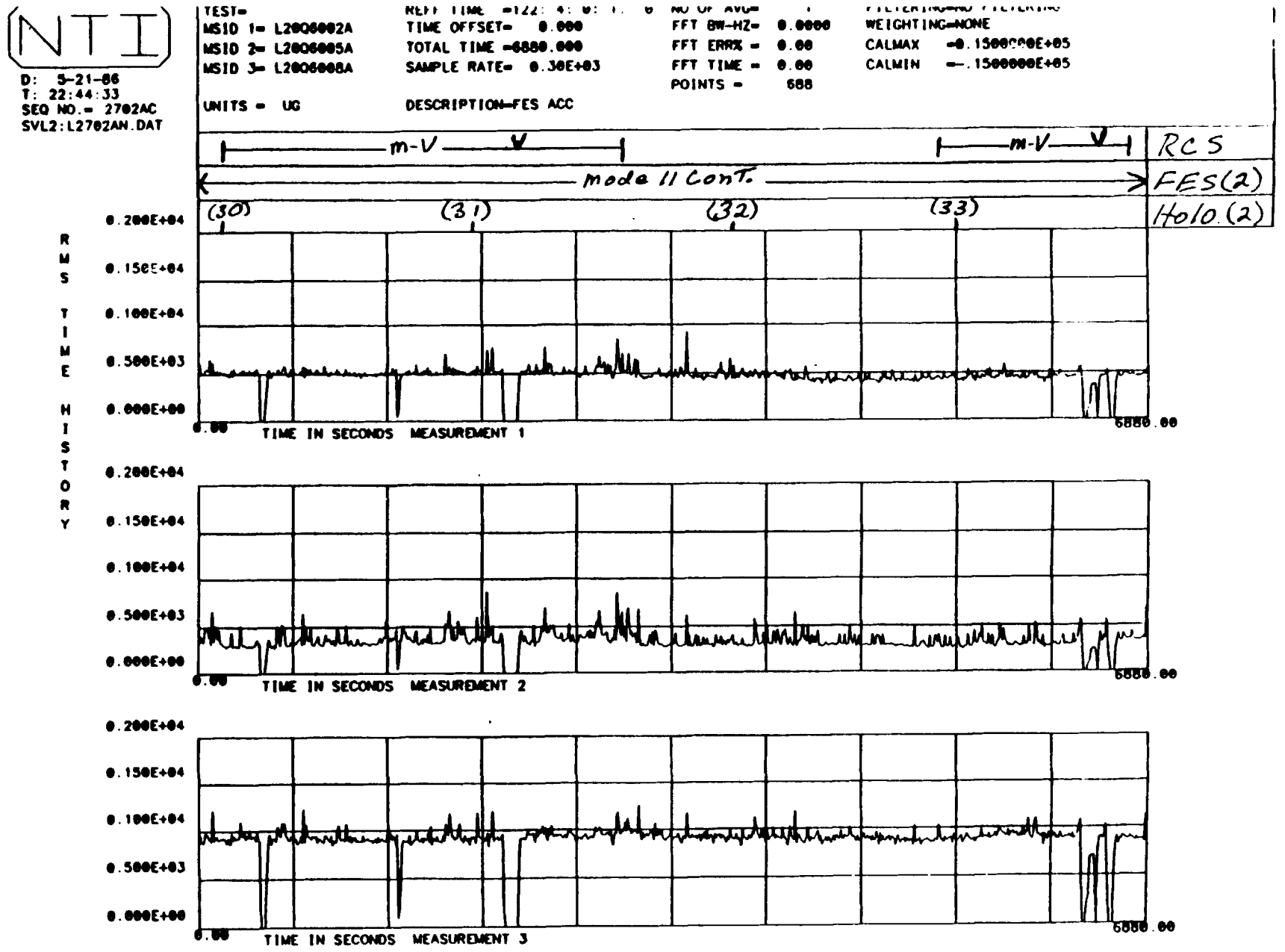
NTI
D: 5-21-86
T: 22:44:33
SEQ NO.= 2702AC
SVL2:L2702AN.DAT
TEST=
MSID 1= L2QQ6002A
MSID 2= L2QQ6005A
MSID 3= L2QQ6008A
UNITS = UG
TIME OFFSET= 0.000
TOTAL TIME =6880.000
SAMPLE RATE= 0.30E+03
DESCRIPTION=FES ACC
FFT BW-HZ= 0.0000
FFT ERR% = 0.00
FFT TIME = 0.00
POINTS = 688
WEIGHTING=NONE
CALMAX =0.1500000E+05
CALMIN =-.1500000E+05
m-V
m-V
RCS
mode 11 Cont.
FES(2)
Holo.(2)
(30)
(31)
(32)
(33)
RMS TIME HISTORY
0.200E+04
0.150E+04
0.100E+04
0.500E+03
0.000E+00
0.00
TIME IN SECONDS MEASUREMENT 1
6880.00
TIME IN SECONDS MEASUREMENT 2
TIME IN SECONDS MEASUREMENT 3

Figure 33.

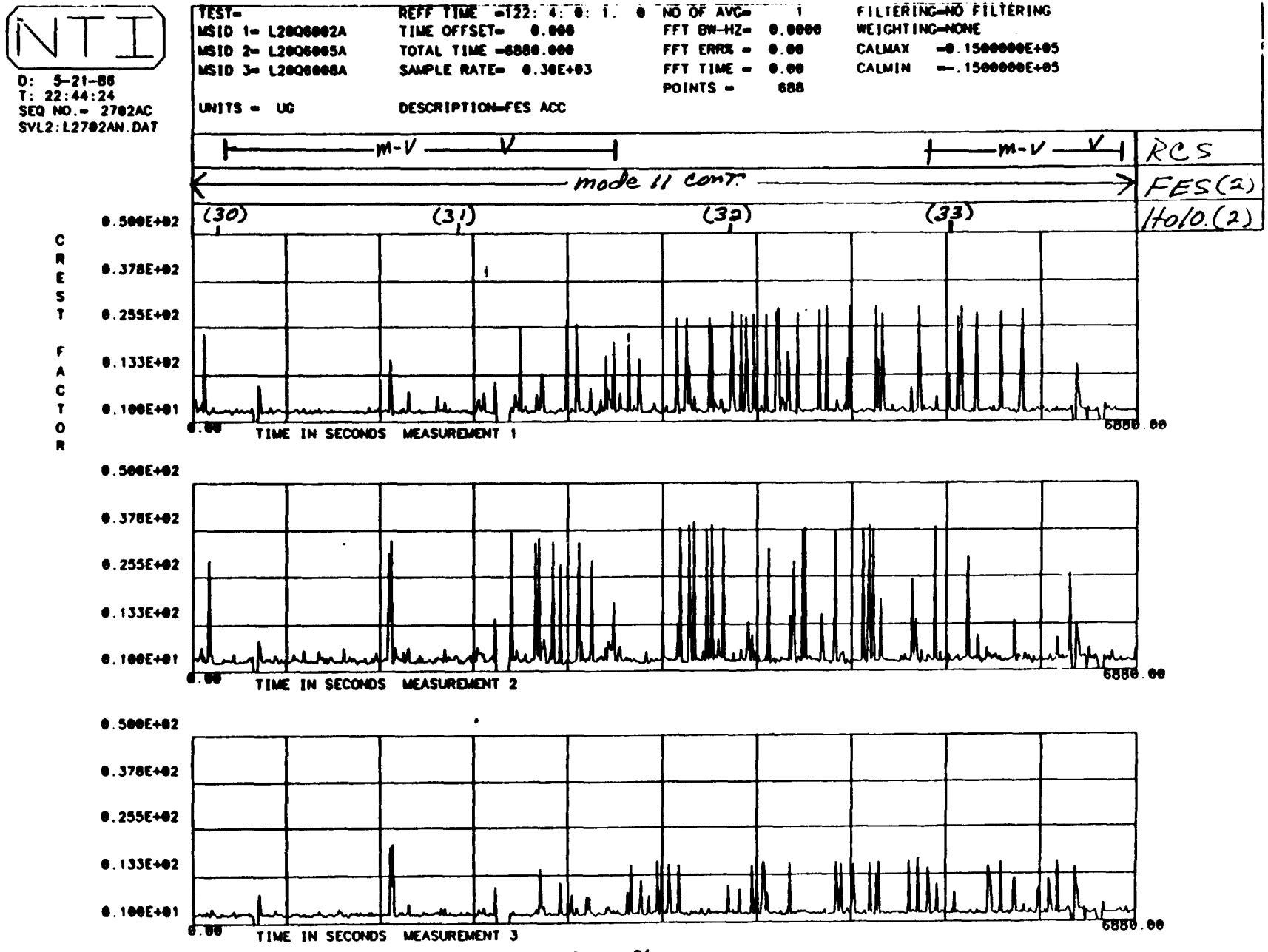
NTI
D: 5-21-86
T: 22:44:24
SEQ NO.= 2702AC
SVL2:L2702AN.DAT
TEST=
MSID 1= L20Q6002A
MSID 2= L20Q6005A
MSID 3= L20Q6008A
UNITS = UG
REFF TIME =122: 4: 0: 1. 0
TIME OFFSET= 0.000
TOTAL TIME =6880.000
SAMPLE RATE= 0.30E+03
DESCRIPTION=FES ACC
NO OF AVG= 1
FFT BW-HZ= 0.0000
FFT ERR% = 0.00
FFT TIME = 0.00
POINTS = 688
FILTERING=NO FILTERING
WEIGHTING=NONE
CALMAX =0.1500000E+05
CALMIN =-.1500000E+05
m-V
V
m-V
V
RCS
mode 11 cont.
FES(2)
Ho/O.(2)
(30)
(31)
(32)
(33)
CREST FACTOR
0.500E+02
0.378E+02
0.255E+02
0.133E+02
0.100E+01
0.00
TIME IN SECONDS MEASUREMENT 1
6880.00
TIME IN SECONDS MEASUREMENT 2
TIME IN SECONDS MEASUREMENT 3

Figure 34.

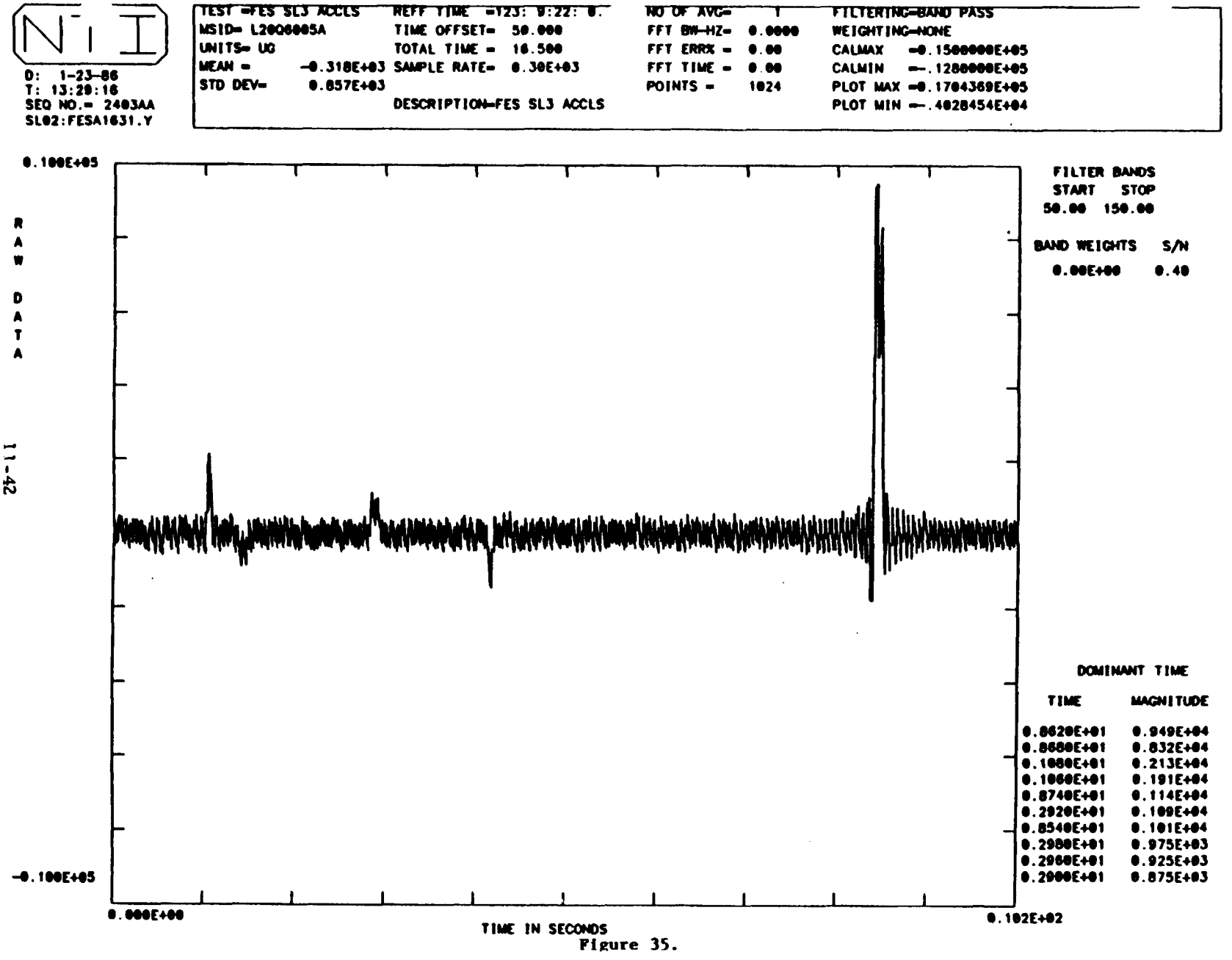
D: 1-23-86
T: 13:20:16
SEQ NO.= 2403AA
SL02:FESA1631.Y
TEST =FES SL3 ACCLS
MSID= L20Q6005A
UNITS= UG
MEAN = -0.318E+03
STD DEV= 0.857E+03
REFF TIME =123: 9:22: 0.
TIME OFFSET= 50.000
TOTAL TIME = 16.500
SAMPLE RATE= 0.30E+03
DESCRIPTION=FES SL3 ACCLS
NO OF AVG= 1
FFT BW-HZ= 0.0000
FFT ERRX = 0.00
FFT TIME = 0.00
POINTS = 1024
FILTERING=BAND PASS
WEIGHTING=NONE
CALMAX =0.1500000E+05
CALMIN =-.1200000E+05
PLOT MAX =0.1704369E+05
PLOT MIN =-.4028454E+04
0.100E+05
RAW DATA
-0.100E+05
0.000E+00
0.102E+02
TIME IN SECONDS
FILTER BANDS
START STOP
50.00 150.00
BAND WEIGHTS S/N
0.00E+00 0.40
DOMINANT TIME
TIME MAGNITUDE
0.8620E+01 0.949E+04
0.8680E+01 0.832E+04
0.1080E+01 0.213E+04
0.1060E+01 0.191E+04
0.8740E+01 0.114E+04
0.2920E+01 0.109E+04
0.8540E+01 0.101E+04
0.2980E+01 0.975E+03
0.2960E+01 0.925E+03
0.2900E+01 0.875E+03

Figure 35.

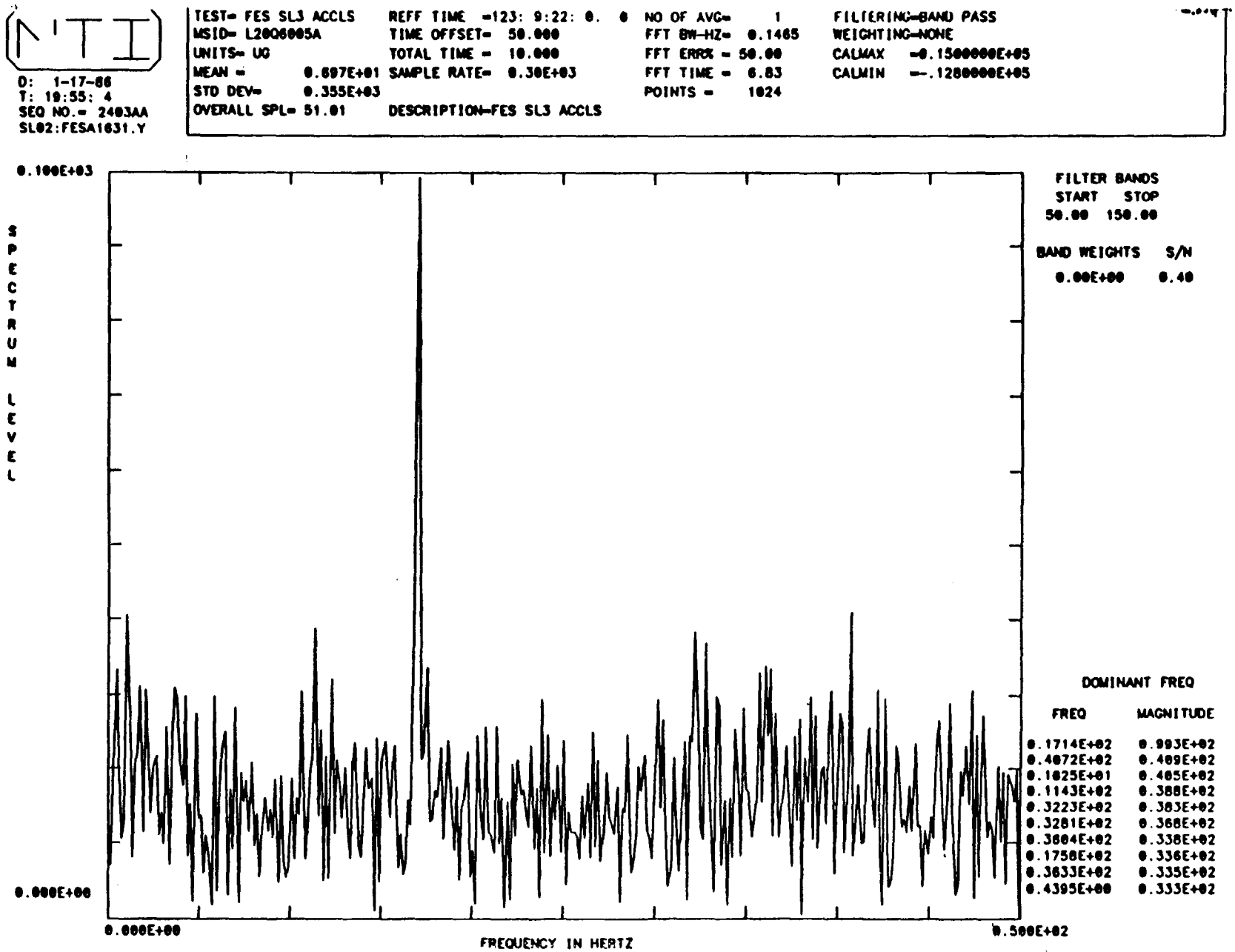
NTI
D: 1-17-86
T: 19:55: 4
SEQ NO.= 2403AA
SL02:FESA1631.Y
TEST= FES SL3 ACCLS
MSID= L2006005A
UNITS= UG
MEAN = 0.697E+01
STD DEV= 0.355E+03
OVERALL SPL= 51.01
REFF TIME =123: 9:22: 0. 0
TIME OFFSET= 50.000
TOTAL TIME = 10.000
SAMPLE RATE= 0.30E+03
DESCRIPTION=FES SL3 ACCLS
NO OF AVG= 1
FFT BW-HZ= 0.1465
FFT ERR% = 50.00
FFT TIME = 6.83
POINTS = 1024
FILTERING=BAND PASS
WEIGHTING=NONE
CALMAX =0.1500000E+05
CALMIN =-.1200000E+05
0.100E+03
SPECTRUM LEVEL
0.000E+00
0.000E+00
0.500E+02
FREQUENCY IN HERTZ
FILTER BANDS
START STOP
50.00 150.00
BAND WEIGHTS S/N
0.00E+00 0.40
DOMINANT FREQ
FREQ MAGNITUDE
0.1714E+02 0.993E+02
0.4072E+02 0.409E+02
0.1025E+01 0.405E+02
0.1143E+02 0.388E+02
0.3223E+02 0.383E+02
0.3281E+02 0.368E+02
0.3604E+02 0.338E+02
0.1750E+02 0.336E+02
0.3633E+02 0.335E+02
0.4395E+00 0.333E+02

Figure 36.

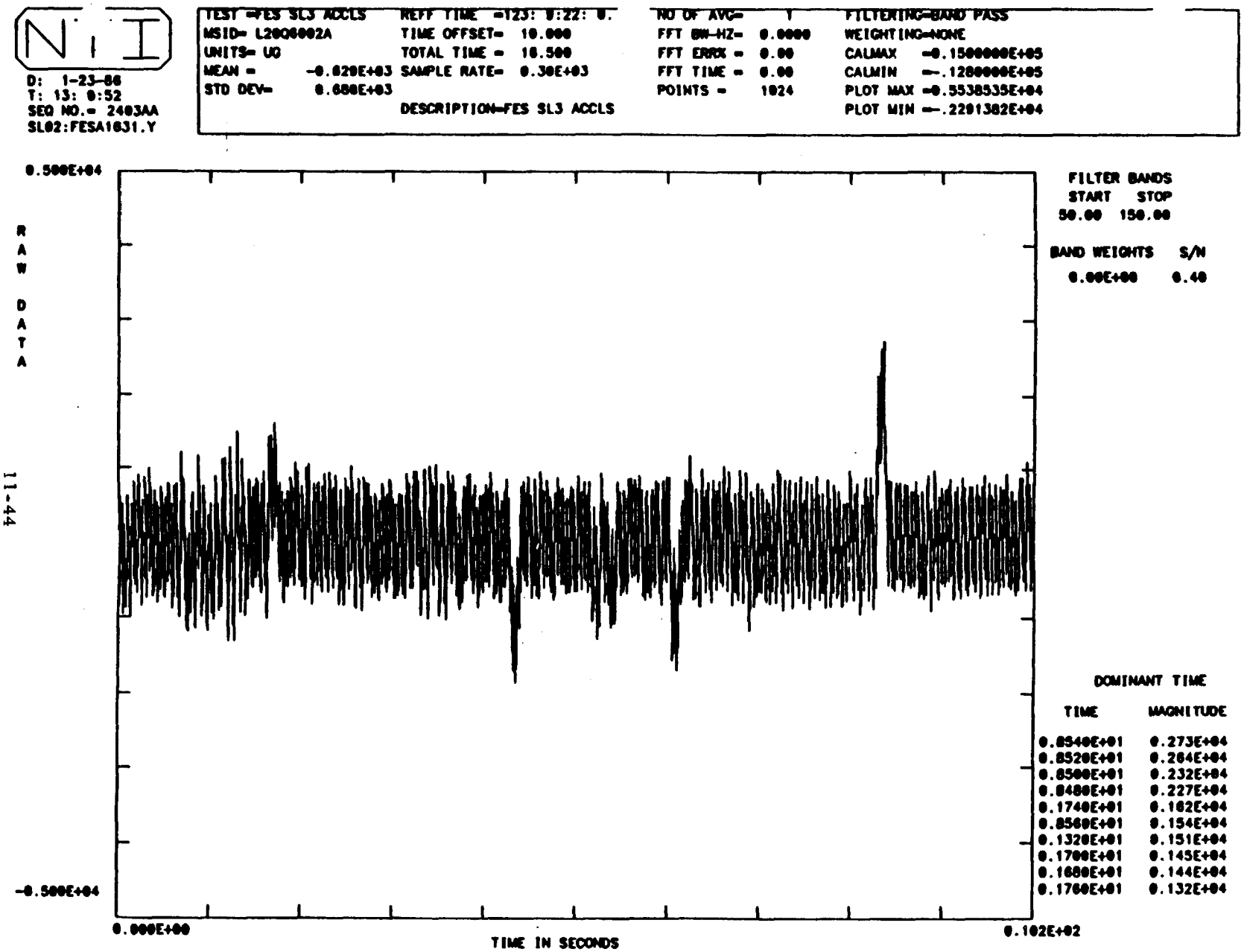

Figure 37.

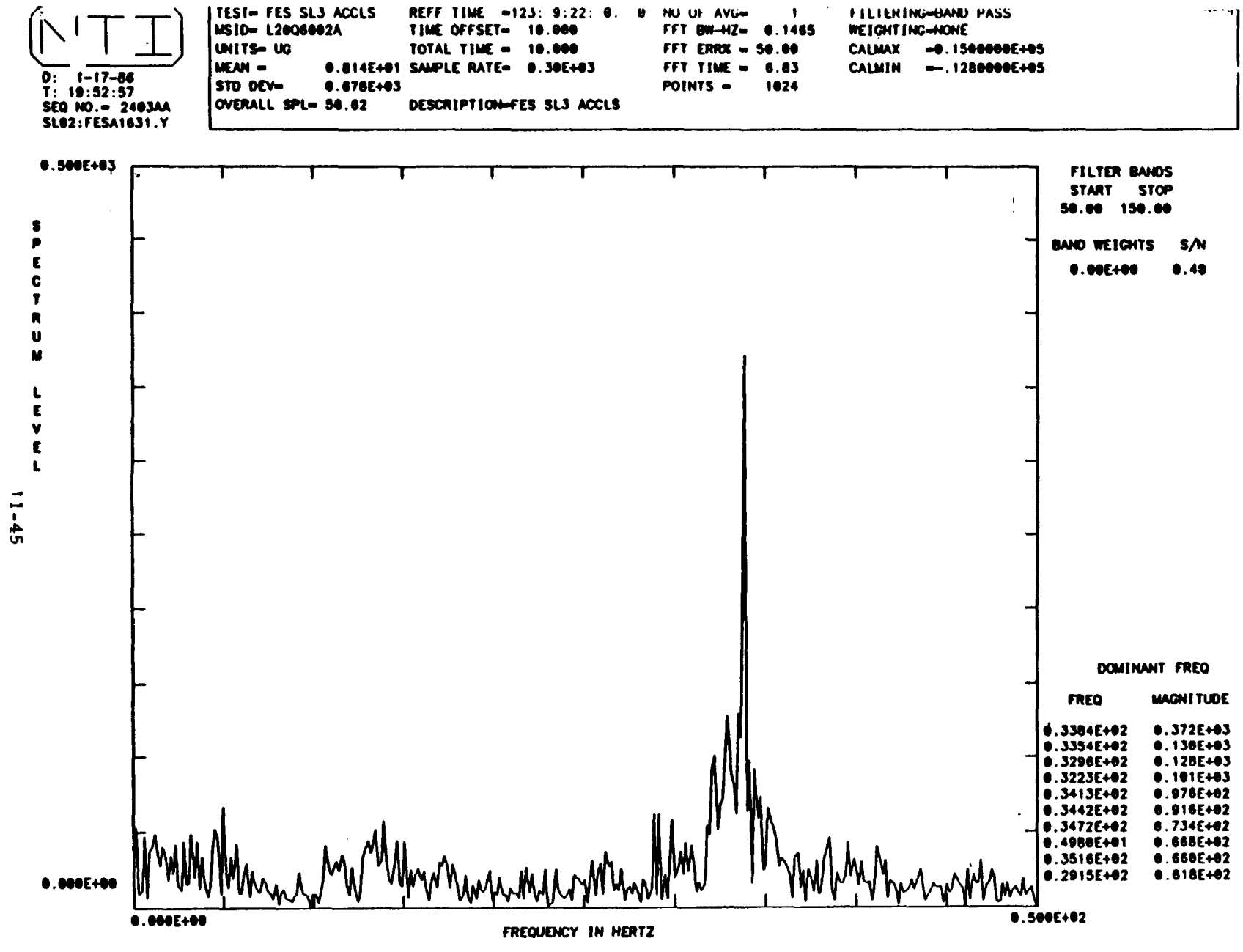
NTI
D: 1-17-86
T: 19:52:57
SEQ NO.= 2403AA
SL02:FESA1631.Y
TEST= FES SL3 ACCLS
MSID= L20Q0002A
UNITS= UG
MEAN = 0.814E+01
STD DEV= 0.678E+03
OVERALL SPL= 56.62
REFF TIME =123: 9:22: 0. 0
TIME OFFSET= 10.000
TOTAL TIME = 10.000
SAMPLE RATE= 0.30E+03
DESCRIPTION=FES SL3 ACCLS
NO OF AVG= 1
FFT BW-HZ= 0.1465
FFT ERROR = 50.00
FFT TIME = 6.83
POINTS = 1024
FILTERING=BAND PASS
WEIGHTING=NONE
CALMAX =0.1500000E+05
CALMIN =-.1280000E+05
0.500E+03
SPECTRUM LEVEL
0.000E+00
0.000E+00
0.500E+02
FREQUENCY IN HERTZ
FILTER BANDS
START STOP
50.00 150.00
BAND WEIGHTS S/N
0.00E+00 0.49
DOMINANT FREQ
FREQ MAGNITUDE
0.3384E+02 0.372E+03
0.3354E+02 0.130E+03
0.3296E+02 0.128E+03
0.3223E+02 0.101E+03
0.3413E+02 0.976E+02
0.3442E+02 0.916E+02
0.3472E+02 0.734E+02
0.4980E+01 0.668E+02
0.3516E+02 0.660E+02
0.2915E+02 0.618E+02

Figure 38.

One of the most interesting things to Dr. Lal is to review the holograms, select the interesting areas, expand those areas, and relate the data back to the asymmetry that they see in some of their holograms. We can not do that right now. The FES experiment people have started reducing their data from cell three first, because of some interesting things on that crystal. We have started from the beginning of the mission. So we will be able to do that later and we will be comparing some of our data to their data.

Question: In your time history plot, and also in the power spectral density, you seem to have background when you don't see the events. Are they seismic or is it electronics noise, and what is the level of that?

Arnett: Well the levels were all indicated on the RMS charts. We are seeing an awful lot of things that are coming up and giving a two-milli g disturbance, two to five, two to seven. In that basic range we are seeing a lot of disturbances.

Question: The background that you see is about 2 milli-g's?

Arnett: No, I thought that you were talking about events that we could really pull out.

Question: Not events, away from events, what is the background? Is it electronics noise?

Arnett: The background is down pretty low. I guess I really haven't tried to look at exactly what our background is. I guess what you are identifying as the background has been running around 10^{-3}.

Question: Eliminating these events, what would be the background noise level? If you can eliminate those events, what would be the background noise level?

Arnett: What is this g level here? It's running at somewhere around 1.5 times 10^{-4} up to the 10^{-3} range, just about exactly where the other people have been finding it to lie, and I think if you went back to one of the other viewgraphs you could see that a little bit better. I can show you after the talk if you would like.

12. MSL-2 ACCELEROMETER DATA RESULTS

Fred Henderson
Teledyne Brown Engineering

The Materials Science Laboratory-2 (MSL-2) mission flew the MSFC-developed Linear Triaxial Accelerometer (LTA) on the STS 61-C Shuttle mission launched January 21, 1986. Flight data have been analyzed to verify the quietness of the MSL carrier and to characterize the acceleration environment for future MSL users. The MSL was found to introduce no significant experiment acceleration; and the effects of crew treadmill exercise, Orbiter vernier engine firings, and other routine flight occurrences were established. The LTA was found to be well suited for measuring nominal to very quiet STS acceleration levels at frequencies below 50 Hz. Special processing was used to examine the low-frequency spectrum and to establish the effective rms amplitude associated with dominant frequencies.

The Materials Science Laboratory (MSL) was developed to provide a flexible cargo bay interface for experiments.

An objective of the MSL-2 Flight Accelerations Study was to evaluate Linear Triaxial Accelerometer (LTA) data obtained during the STS 61-C mission to determine the contribution, if any, of the MSL carrier to susceptible future experiments. Another primary objective was to quantify the acceleration environment for use by future MSL users (Figure 1).

The MSL-2 mission provided good data to satisfy these objectives, since LTA data were recorded continuously throughout most of

the six-day mission, and a wide variety of on-orbit circumstances were noted. Unlike Spacelab, there were periods when the entire crew slept, which enabled evaluation of a quiescent Shuttle. The effects of known crew-commanded disturbances were examined, and so was the behavior of the Shuttle during "quiet" periods of crew sleep.

- **VERIFY QUIETNESS OF MSL CARRIER SUBSYSTEMS**
- **QUANTIFY THE STS/MSL ACCELERATION ENVIRONMENT FOR MSL USERS**

FIGURE 1. OBJECTIVES

The STS 61-C cargo configuration, as depicted in Figure 2, consisted of one SATCOM satellite, which was deployed within hours of reaching orbit, several Get Away Special (GAS) canister experiments mounted on the GAS Bridge and on Hitchhiker-G1, and the MSL-2 payloads. The MSL was activated almost immediately upon start of on-orbit operations.

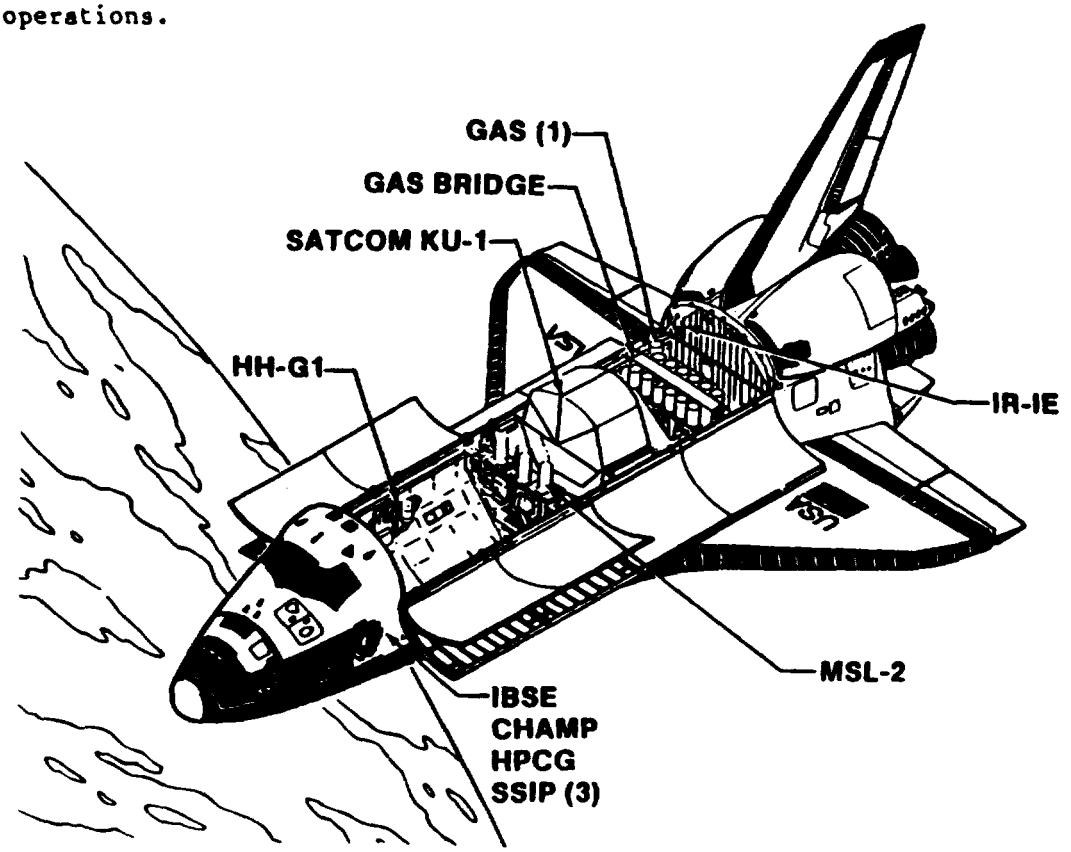

FIGURE 2. STS 61-C CARGO CONFIGURATION

The LTA is mounted on the aft side of the MSL carrier (Figure 3) with the signal junction box and instrumentation signal conditioners close to the OFT Freon pump. For this reason, the effect of pump operation was of some concern, although prior analysis had indicated that the 10,000-rpm rate of the pump would cause little carrier vibration.

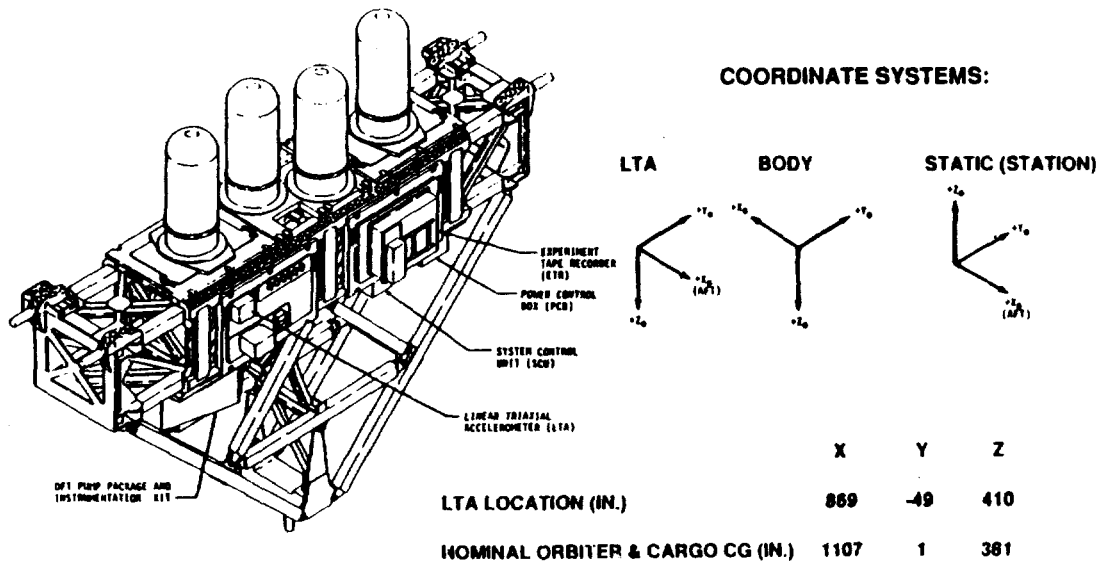

FIGURE 3. LTA ORIENTATION ON MSL

The location of the MSL is provided in static coordinates, as used to assign mechanical locations to the carrier. Orbiter body coordinates, LTA coordinates, and static coordinates all share the same respective axes but vary in declaration of the positive direction.

The LTA signal output range, resolution, accuracy, and frequency response are as specified in the accelerometer specification (Figure 4). The 125 sample/sec data acquisition rate for each channel was sufficient to determine frequencies well beyond the high filter corner frequency of 20 Hz.

• RANGE:	± 512 MICRO G
• RESOLUTION :	1 MICRO G
• ACCURACY:	± 5%
• FREQUENCY RESPONSE:	.01 TO 20 HZ
• SAMPLE RATE:	125 SPS

FIGURE 4. LTA CHARACTERISTICS

The lowpass filter of the LTA passes useful information well above the corner frequency of 20 Hz, as shown in the calculated plot (dashed line) and breadboard measured electrical response chart (solid line) of Figure 5. Discussions with the accelerometer vendor disclosed that the 20-Hz cutoff frequency was not the result of LTA mechanical limitations, but the addition of electronic anti-aliasing filters. The filter cutoff was based on an earlier intended application of the accelerometer, which required a slower sampling rate. Although attenuated, a significant portion of the input amplitude is passed through the electronic filter at frequencies less than the Nyquist frequency of 62 Hz.

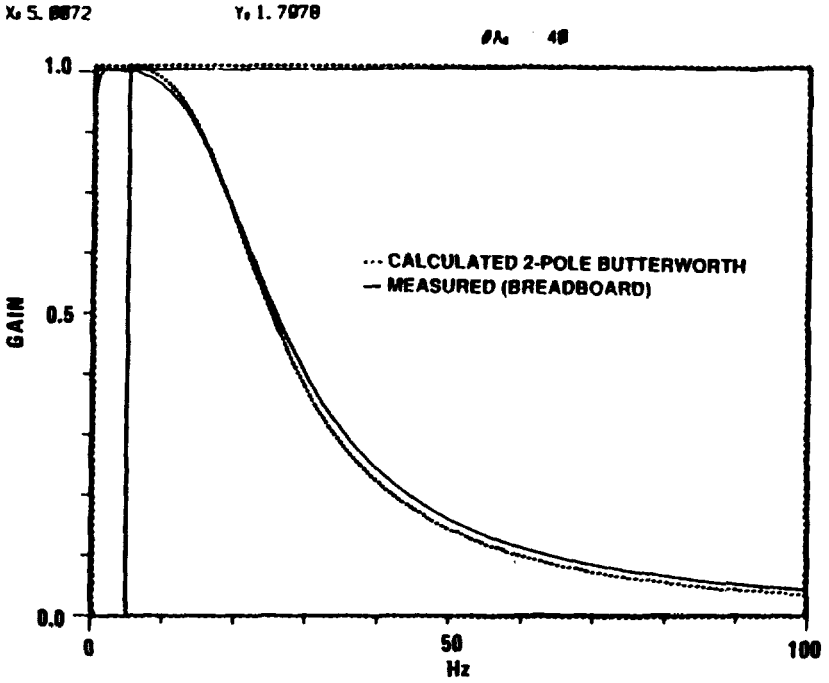

FIGURE 5. LTA LOWPASS FILTER RESPONSE

Including a mathematical model of the inverse lowpass filter function in the processing of LTA data enabled restoration of data as if the filter had not been present over the extended frequency range. This increased the susceptibility of the higher frequencies to random noise but enabled higher frequency spectral peaks to be observed. The effectiveness of the anti-aliasing filters on eliminating frequencies higher than 62 Hz was reduced, but no more so than the original anti-aliasing filter with respect to the original 20-Hz cutoff. The stages of the process used to effectively extend the frequency range is shown in the following discussion.

Data reduction techniques used to interpret LTA data began with the plotting of data from each axis on 2-hour plots (Figure 6). Although coarse, with the width of a line corresponding to over 2,000 data points, these plots were useful in showing periods of activity and quiet on a reasonably long time scale. Even so, 36 plots were required for each day of flight operation.

- TWO HOUR TIME HISTORIES
  - ESTABLISH PERIODS OF ACTIVITY
  - ESTIMATE DURATION OF QUIET PERIODS
- SHORT DURATION TIME HISTORIES (SECONDS)
  - SHOW STRUCTURE OF ACCELERATION HISTORY
  - CORRESPOND TO POWER SPECTRAL DENSITIES (PSD'S)
- POWER SPECTRAL DENSITIY
  - AS RECORDED IN FLIGHT
  - WITH AND WITHOUT FILTER COMPENSATION
  - LOW FREQUENCY EXPANSION USING POINT AVERAGING
  - RMS AMPLITUDE AVERAGE OVER SPAN OF PSD
    - TOTAL AMPLITUDE
    - CONTRIBUTION NEAR DOMINANT FREQUENCY
- DISPLACEMENT HISTORY

FIGURE 6. DATA REDUCTION TECHNIQUES

From these long-time-span charts and logs of mission activity, representative cases were chosen for further analysis. Representative plots spanning intervals from several seconds to minutes were examined to determine the nature of disturbances and to verify suitability for further treatment by application of Fast Fourier Transform (FFT) analysis.

For selected cases, power spectral densities (PSDs) were plotted, both from raw data and with filter compensation. Where low-frequency signals were present, plots of the low-frequency spectrum were expanded. An N point smoothing routine was added to permit measurement of very low frequencies approaching the 0.01-Hz low-frequency cutoff of the LTA while preserving the benefits of oversampling. Also, the ability to calculate in-band effective root mean square (rms) of PSD amplitudes around dominant frequencies was incorporated in the FFT program. In addition to in-band rms, rms calculations were also used to determine the total effective energy of data for all frequencies for comparison with the rms of time-history data. Agreement on total rms amplitude helped ensure validity of the process.

The PSD techniques, however, are limited in application to instances where conditions persisted over one to several seconds. While important in determining the nature of many disturbances, FFT analysis does not easily interpret irregular or occasional acceleration spikes that may also be damaging to low-g experiments. Consequently, a technique was developed to determine peak velocity and peak displacement resulting from LTA-sensed accelerations. Such calculations require that assumptions be made concerning a restoring system; otherwise, slight acceleration bias in the acceleration data will cause a gradual growth in derived velocity and quadratic growth in displacement. Insufficient data have been processed by this technique to publish results and and so are not included here. Examples of some acceleration spikes, however, are included to illustrate the nature of LTA data.

One technique employed in LTA data analysis was the determination of effective rms amplitude of prominent PSD peaks. The reason for this is the possibility of slight frequency variations in LTA data causing a spreading of the PSD maximum amplitude. In such a case, as shown in Figure 7, the peak PSD amplitude of a pure frequency (as shown on the left) may be several times higher than the peak amplitude of a signal of identical amplitude (shown on the right) that exhibits slight variation in frequency. Computing the rms of PSD amplitudes surrounding the peak compensates for the frequency variation and yields a number proportional to the amplitude of the input signal. In each case shown, if the peak amplitude of the sinusoidal input were 10 mg, the rms amplitude reported would be 7.07 mg.

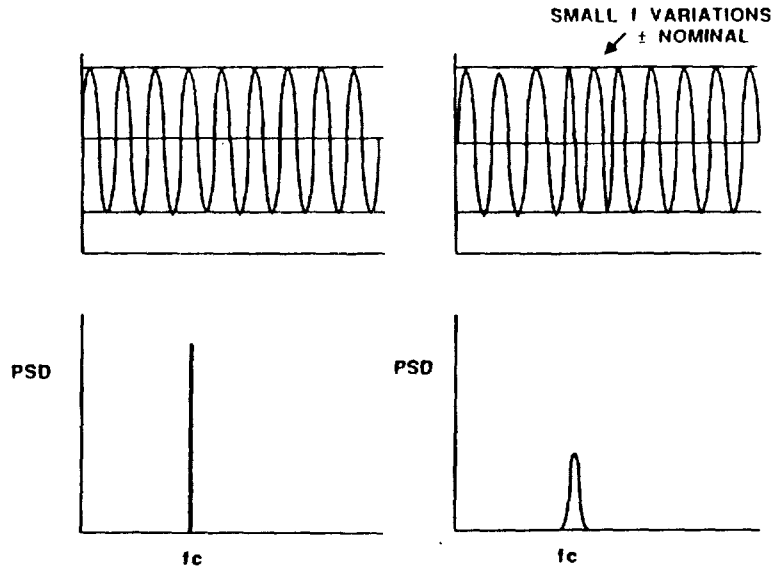

FIGURE 7. EXPLANATION OF IN-BAND RMS

Figure 8 shows the times when MSL equipment was active during the STS 61-C mission. Greenwich Mean Time (GMT), Mission Elapsed Time (MET), and MET hours are all shown on the scale across the top. The initial vertical line corresponds to launch on January 12, 1986, at 11

hours and 55 minutes. Other vertical lines are drawn at 24-hour intervals from the launch.

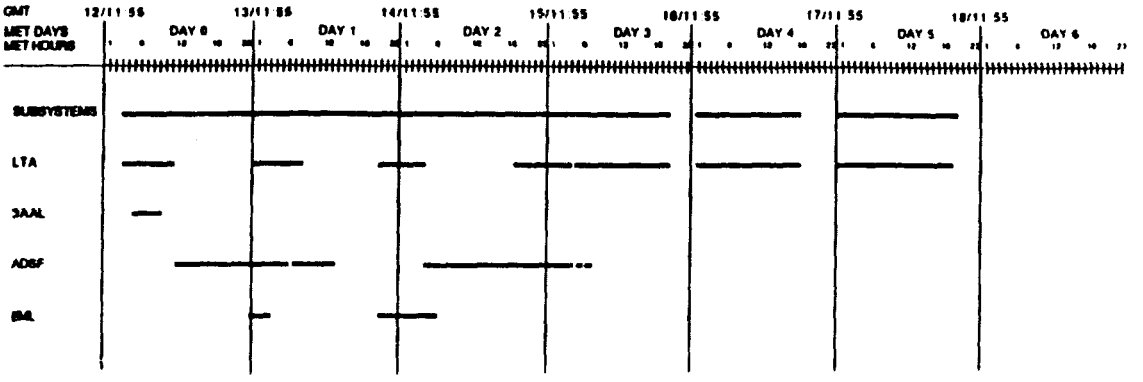

LTA – LINEAR TRIAXIAL ACCELEROMETER
ADSF – AUTOMATED DIRECTIONAL SOLIDIFICATION FACILITY
3AAL – THREE-AXIS ACOUSTIC LEVITATOR
EML – ELECTRO-MAGNETIC LEVITATOR

FIGURE 8. MISSION TIME PROFILE

As shown, the LTA acquired data for recording on the MSL Experiment Tape Recorder throughout most of the mission. MSL subsystems were activated soon after reaching orbit and remained on except for two periods later in the mission. These two periods of deactivation accompanied Shuttle landing preparations, which had to be deferred because of bad weather in the Shuttle landing area.

The notes in Figure 9 are shown to explain the representation of the acceleration data in the various time-history and PSD plots throughout this paper.

- REPRESENTATIVE AXIS CHOSEN FOR BREVITY
  - QUIETEST BACKGROUND PLOT USED TO SHOW NON-INFLUENCE
  - MOST ACTIVE AXIS USED TO SHOW SEVERITY
  - ALL AXES SHOWN IN MSL-2 FLIGHT REPORT, VOL. 2
- ACCELERATION AMPLITUDES ARE IN MILLI-G'S (MG'S)
- GMT DAYS 12-18 REFER TO CALENDER DAYS JAN. 12-18,1986
- MAXIMUM VALUES NOTED ON PLOTS ARE IN ORDINATE UNITS (NOT RMS)
- RMS VALUES NOTED ON PLOTS REFER TO TOTAL DATA SET
- AMPLITUDES GREATER THAN LTA SATURATION LEVELS ARE VALID FOR FILTER COMPENSATED (ADJUSTED) PSD'S

FIGURE 9. DATE NOTES

A short time-history plot of LTA Y-axis data is shown in Figure 10. Full-scale amplitude is ± 0.512 mg beginning on January 18 at 2:48:00 and continuing for slightly over 4 sec. Also reported is the RMS amplitude of data and the mean amplitude.

As with subsequent figures, a representative axis has been chosen for brevity. Here the axis with the lowest background noise was chosen to show absense of pump interference. In other instances, the axis with the greatest amplitude is used to show severity of disturbances.

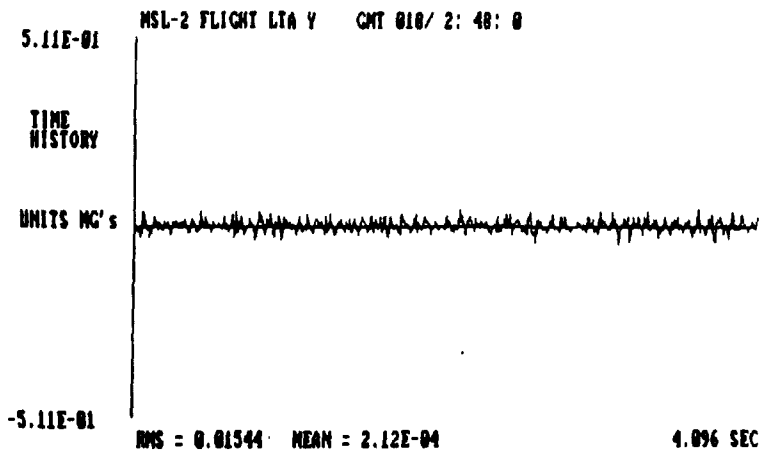

FIGURE 10. PUMP ON, 4-SEC TIME HISTORY

The PSD corresponding to the previous time-history (Figure 11) shows a moderate spectral peak around 13 Hz and a fairly random distribution elsewhere. Units are in milli-g's squared per hertz,and the maximum spectral intensity of 1.7×10^{-4} at 13.3 Hz is reported. The PSD-derived RMS amplitude of 0.01544 mg agrees with that derived from raw data samples on the previous chart. The FFT bandwidth of 0.2441 Hz is the width of each spectral band in the PSD.

The frequency domain data were treated by the inverse filter model and the PSD obtained as shown in Figure 12. As expected, the amplitude of-high frequency contributors was amplified.

To verify repeatability, a second 4-sec sample of data was analyzed in the same way as the first (Figure 13), immediately following the first sample.

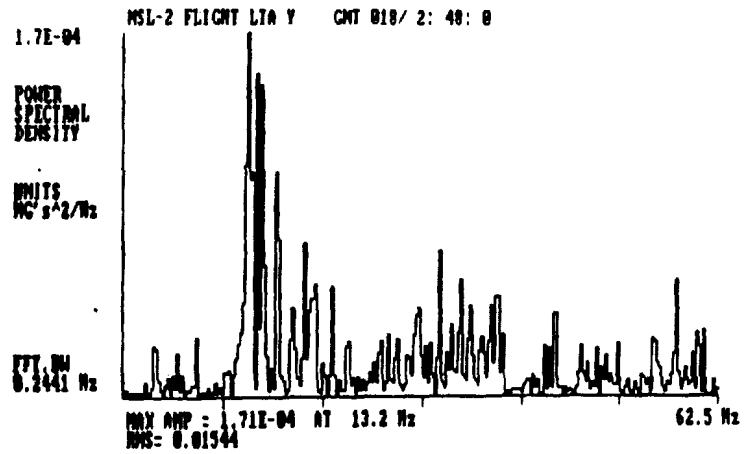

FIGURE 11. PUMP ON, 4-SEC PSD

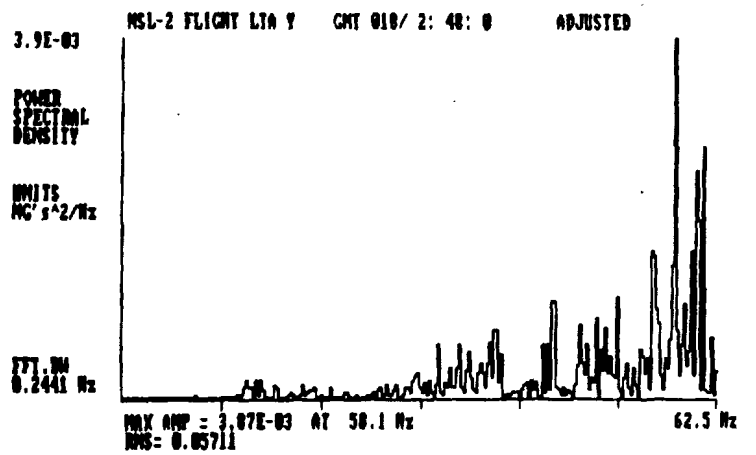

FIGURE 12. PUMP ON, 4-SEC PSD-ADJUSTED

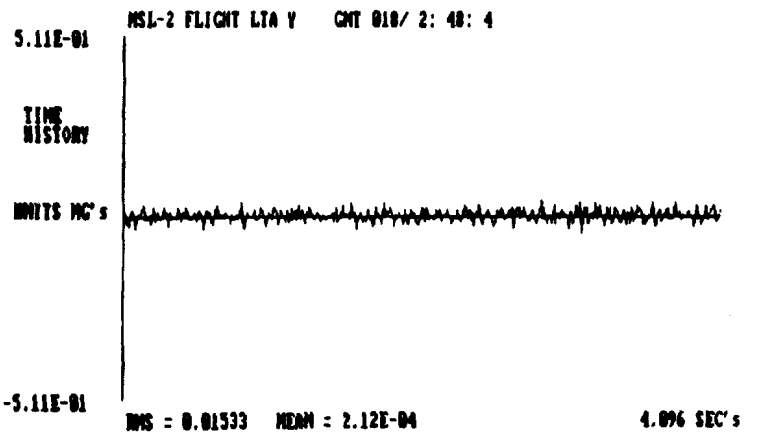

FIGURE 13. PUMP ON, 4-SEC TIME HISTORY

Again the filter-compensated PSD was taken to compare with the earlier sample (Figure 14). If peaks do not occur at the same frequency in each case, then the peak was most likely random or the situation measured changed from one 4-sec span to the next.

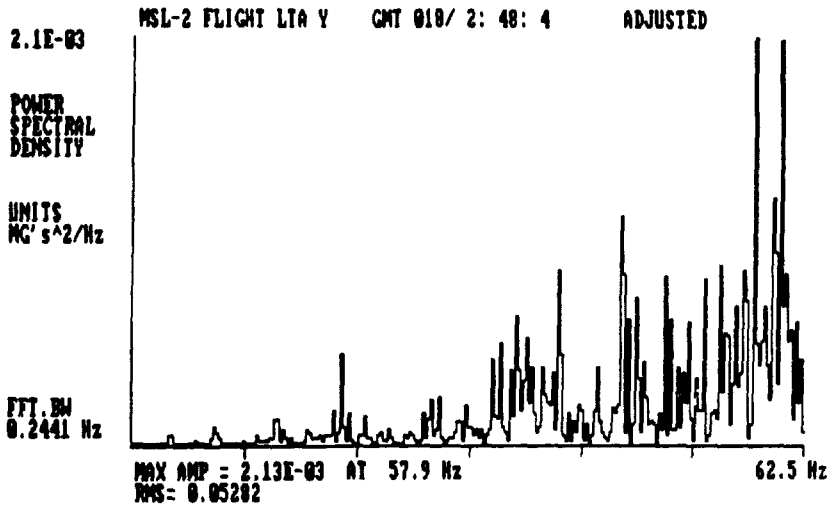

FIGURE 14. PUMP ON, ADDITIONAL 4-SEC PSD, ADJUSTED

If the sample is considered representative after comparison, then the composite time history with filter adjustment is obtained from the inverse FFT (Figure 15). This effectively reproduces the LTA signal as it was before the 20-Hz lowpass filter. It is possible to accurately report amplitudes greater than the 0.5-mg normal peak input of the LTA.

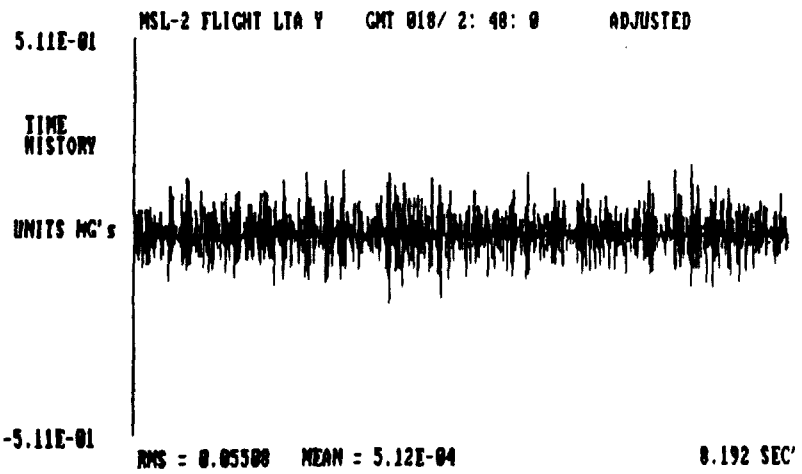

FIGURE 15. PUMP ON, COMPOSITE 8-SEC TIME HISTORY, ADJUSTED

The composite PSD obtained with filter compensation shows a probable spectral spike at 57.9 Hz (Figure 16). Since there is a possibility of some error being introduced by the filter-compensation amplification, both the adjusted and unadjusted 8-sec versions will appear in the flight report. All filter-compensated PSDs and time-history plots are denoted as "adjusted."

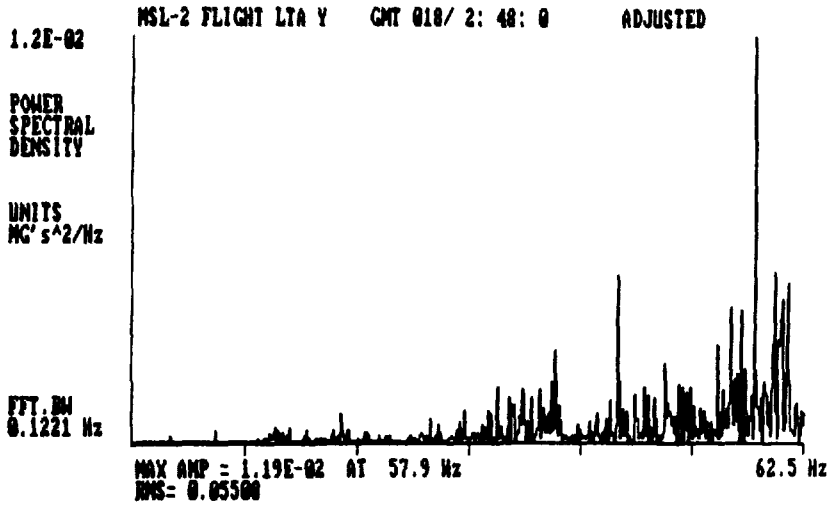

FIGURE 16. PUMP ON, COMPOSITE 8-SEC PSD, ADJUSTED

The low-frequency portion of the PSD is amplified (Figure 17) to show frequencies potentially more damaging to many experiments than the high-frequency spectra. If there is evidence of energy in the lower frequencies, the special processing technique is used to discern frequencies as low as 0.01 Hz by the application of a much longer time span of data.

The identical process, to the one performed for the pump-on case was repeated for the pump-off case shown in Figure 18. The adjusted time history appears much the same as that for the pump-on case.

The adjusted PSD of the pump off case (Figure 19) showed only slight variation from the pump-on case shown earlier. In fact, the rms value is slightly reduced.

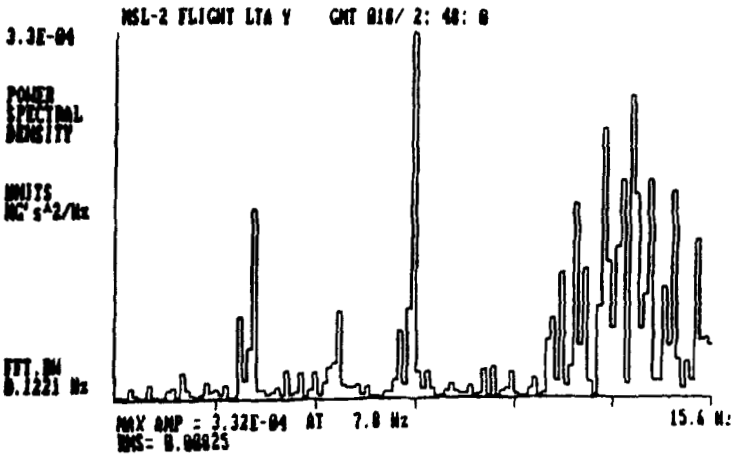

FIGURE 17. PUMP ON, LOW-FREQUENCY PSD

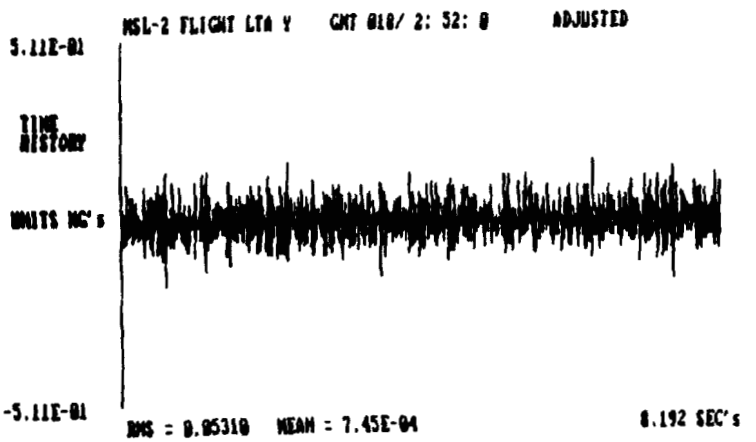

FIGURE 18. PUMP OFF, ADJUSTED TIME HISTORY

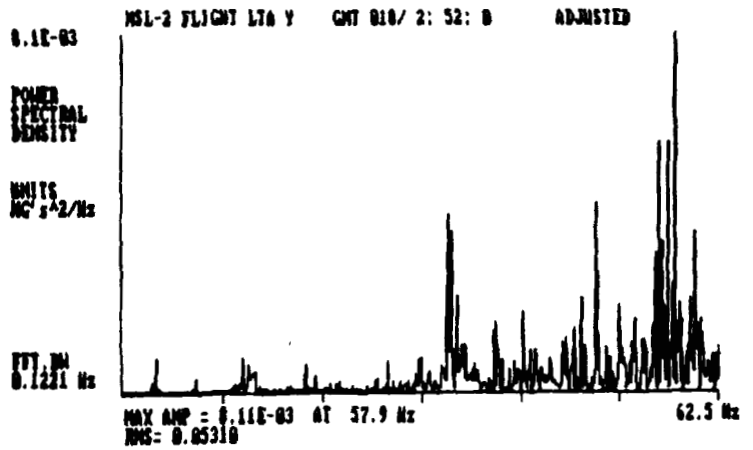

FIGURE 19. PUMP OFF, ADJUSTED PSD

As for the broad-frequency PSD, the low-frequency PSD shows little change with the pump off (Figure 20). From a comparison of data from all three LTA axes, it was concluded that operation of the Freon pump added little to the vibrations already present on the Shuttle.

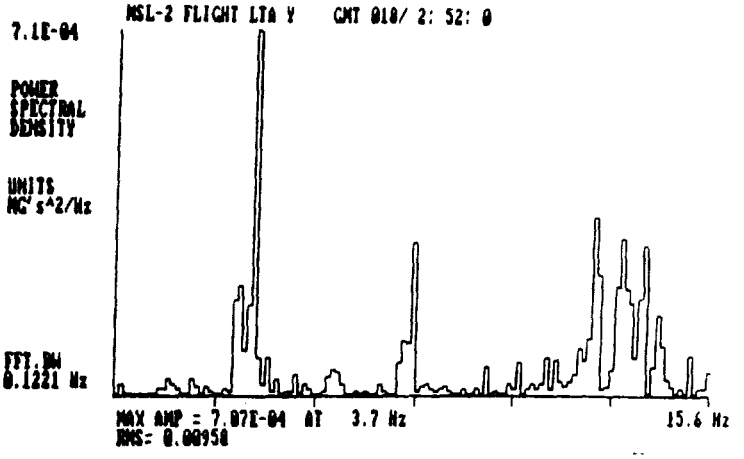

FIGURE 20. PUMP OFF, LOW-FREQUENCY PSD

As an added precaution, a PSD was taken from flight data with the LTA off to examine the possible presence of EMI or data system effects (Figure 21). This PSD was taken from flight data after the MSL System Control Unit, Freon pump, Experiment Tape Recorder, and Power Control Box had been activated but before the LTA was on. Had EMI been present on the data lines between the LTA and the MSL data acquisition system, it would be observable at this time. This PSD agrees with ground data that show RMS noise less than 0.1% for MSL measurements.

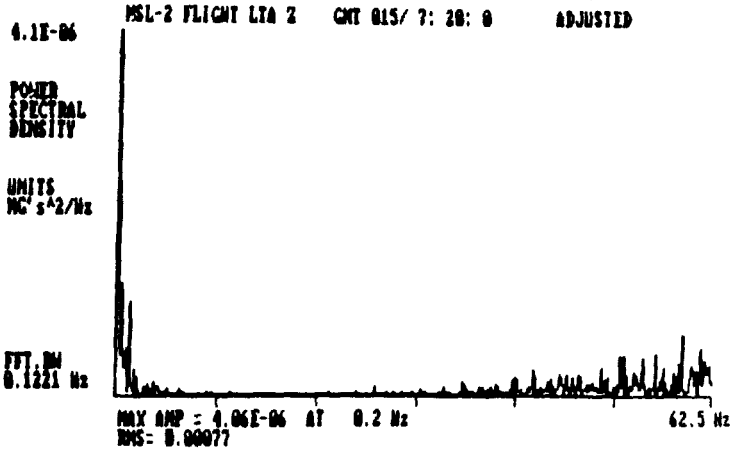

FIGURE 21. LTA OFF CASE

By contrast, data acquired during a crew exercise period using the treadmill show severe acceleration (Figure 22). It is difficult to estimate the true amplitude of the peaks because of saturation beyond ± 0.5 mg.

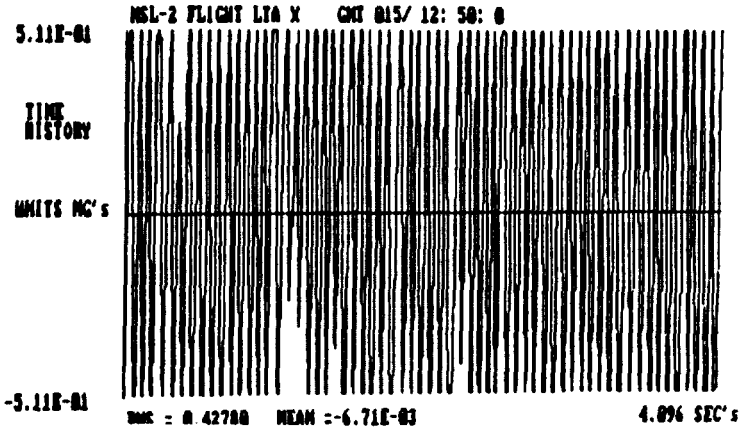

FIGURE 22. TREADMILL EXERCISE CASE, TIME HISTORY

As evident by the sinusoidal character of the time history, the PSD shows a predominant frequency (Figure 23). The greatest spectral amplitude is at 15.4 Hz. This and the energy in the frequencies within 3 Hz account for most of the 0.675-mg rms amplitude reported.

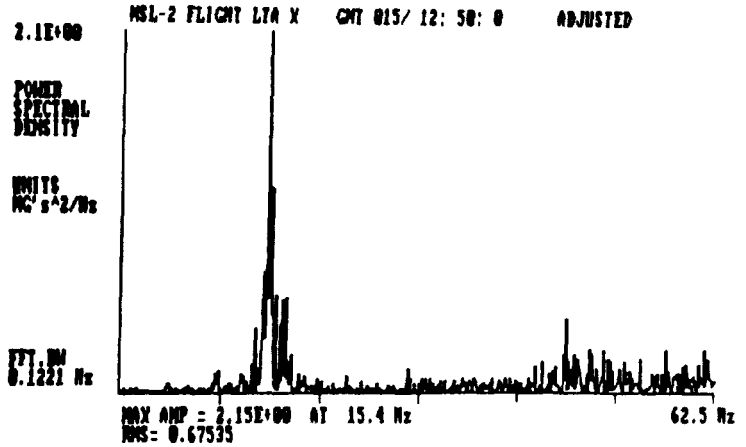

FIGURE 23. TREADMILL EXERCISE CASE, PSD

The 8-sec filter-compensated time history is difficult to interpret since it shows peaks at over twice the saturation level (Figure 24). Although possibly valid, the effects of saturated data may contribute to these apparent amplitudes. All that can be said with certainty is that the peak amplitude is greater than 0.5 mg.

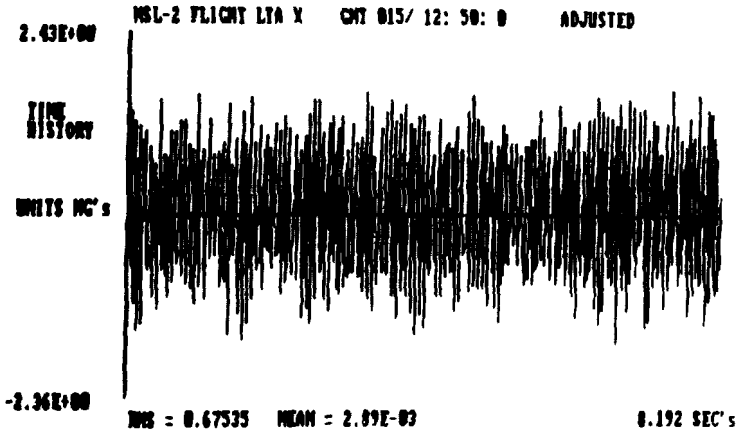

FIGURE 24. TREADMILL EXERCISE CASE, ADJUSTED

The low-frequency contribution appears small below 15.6 Hz (Figure 25). The absence of energy in the lowest portion of the spectrum appears to not justify extended low-frequency processing.

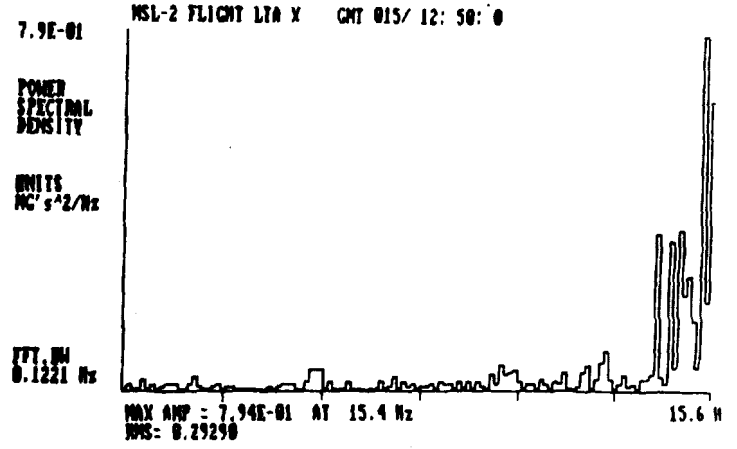

FIGURE 25. TREADMILL EXERCISE CASE, LOW-FREQUENCY PSD

Firings of the Reaction Control System (RCS) thrusters, like treadmill exercises, are intentional and occur only during crew periods of activity. X-axis accelerations are superimposed on higher frequency ringing of the structure. As with the treadmill case, a great degree of saturation occurs.

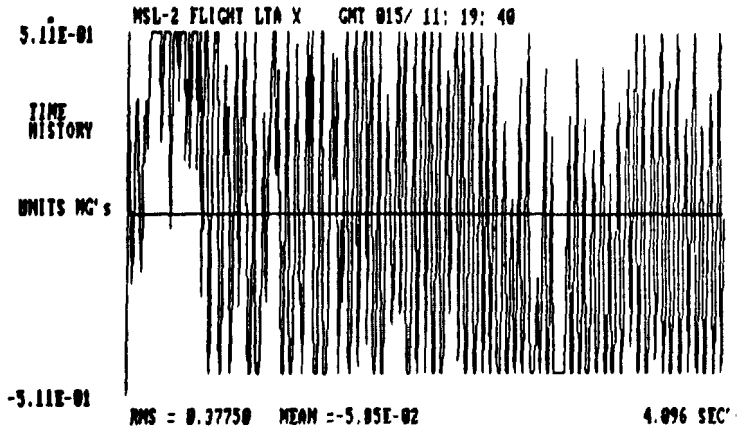

FIGURE 26. REACTION CONTROL SYSTEM, HOT FIRING, TIME HISTORY

As with the treadmill case, the apparent higher-than-saturation-level amplitudes of 2 mg (Figure 27) are possible manifestations of clipping and have not been proven valid. The actual peak amplitudes may be orders of magnitude greater.

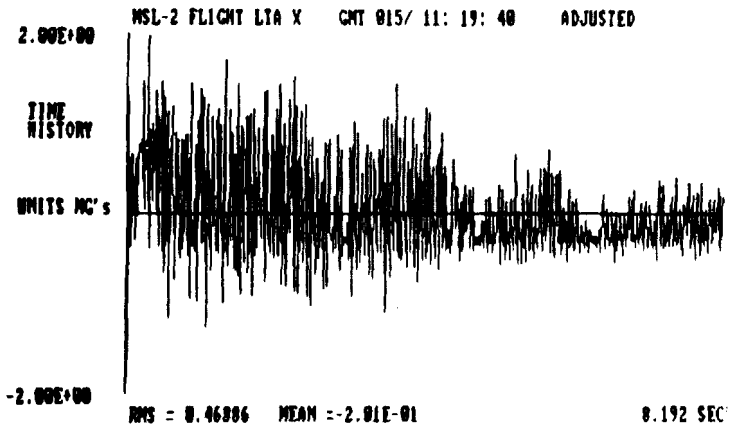

FIGURE 27. REACTION CONTROL SYSTEM, HOT FIRING, ADJUSTED TIME HISTORY

The PSD in Figure 28 shows a dominant frequency at 17.7 Hz, with a smaller contribution at low frequencies.

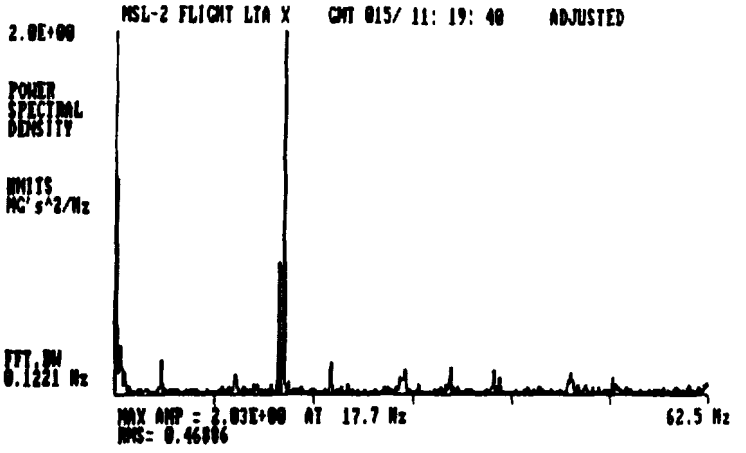

FIGURE 28. REACTION CONTROL SYSTEM, HOT FIRING, PSD

The low-frequency peak at 0.2 Hz appears significant in this case (Figure 29), with an rms amplitude of 0.13 mg. This is most likely the result of firing application rate.

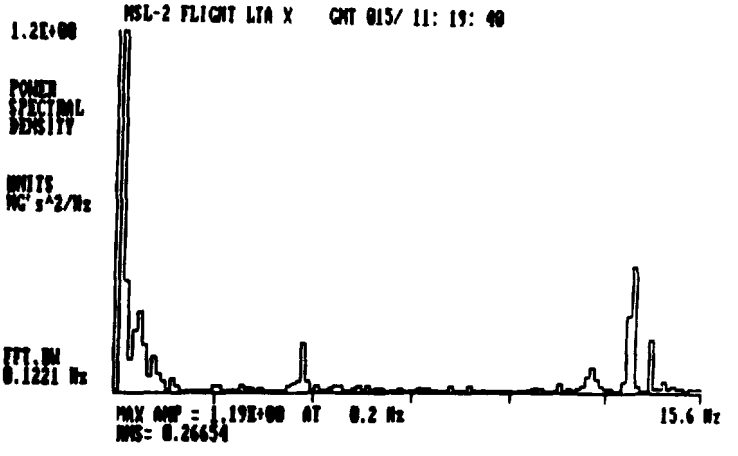

FIGURE 29. REACTION CONTROL SYSTEM, HOT FIRING, LOW-FREQUENCY PSD

The absence of crew activity does not guarantee moderate acceleration. Figure 30, taken well into the sleep period on January 15, shows a saturating acceleration during this 4-sec time history.

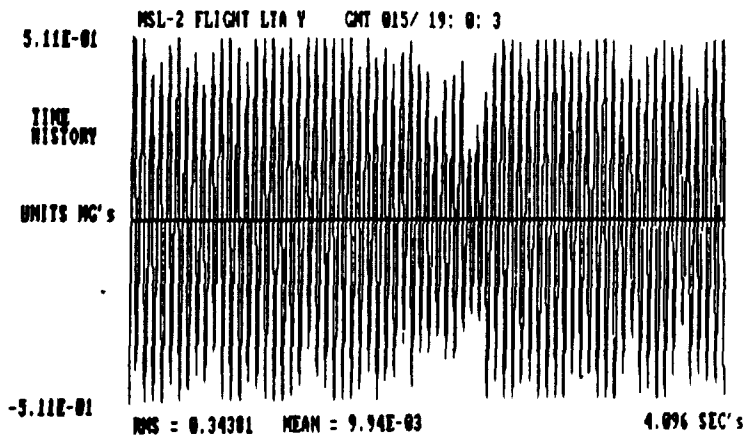

FIGURE 30. SLEEP PERIOD ON JANUARY 15, TIME HISTORY

The PSD in Figure 31 shows a highly dominant frequency of 17.1 Hz. Its cause has not yet been determined.

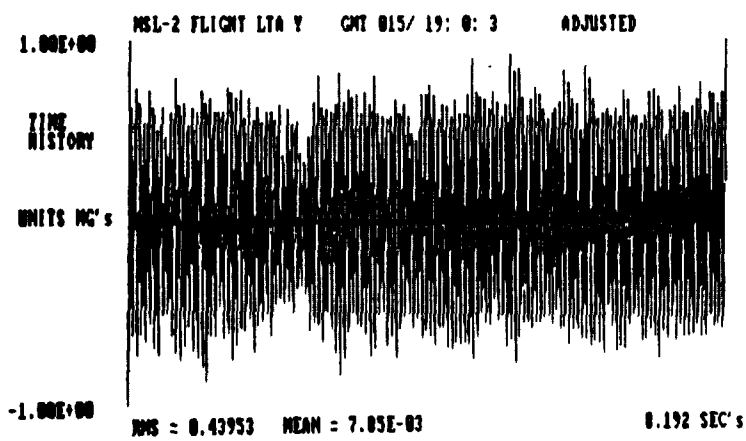

FIGURE 31. SLEEP PERIOD ON JANUARY 15, ADJUSTED TIME HISTORY

The adjusted time history (Figure 32) spans twice the period of the unadjusted time history shown before. The frequency is actually no different from that shown in Figure 30. Adjusted peaks appear to approach 1 mg.

The adjusted time history taken during a sleep period on January 17 (Figure 33) differs significantly from the January 15 case. Here, peak amplitudes do not exceed 0.2 mg over the 8-sec time span, and the total rms amplitude is 0.05 mg.

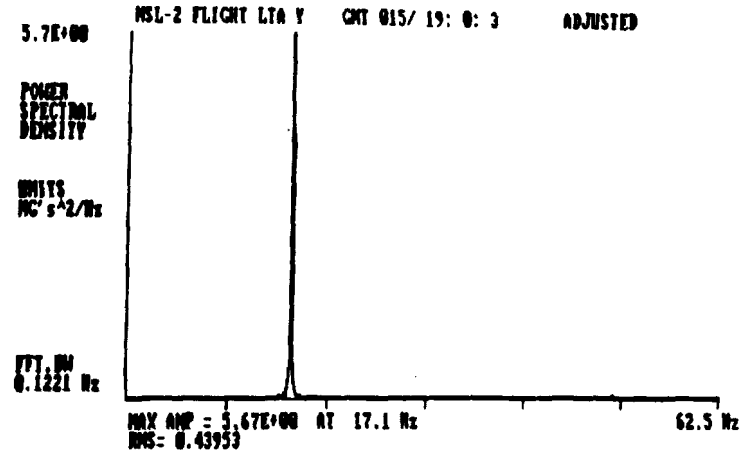

FIGURE 32. SLEEP PERIOD ON JANUARY 15, ADJUSTED PSD

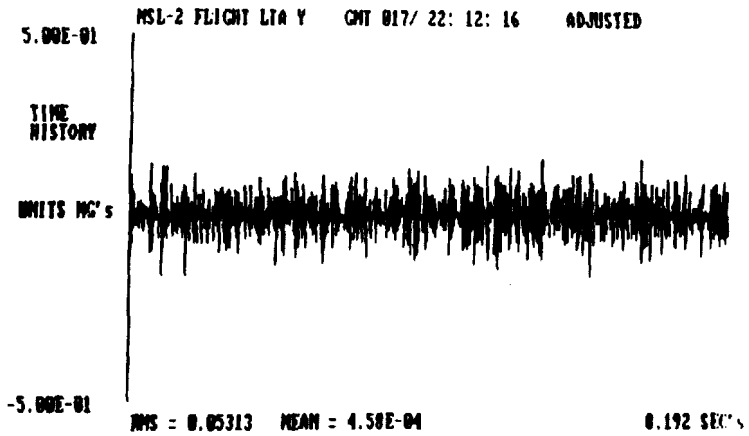

FIGURE 33. SLEEP PERIOD ON JANUARY 17, ADJUSTED TIME HISTORY

Also noticeable is the absence of a peak near 17 Hz in the PSD of the January 17 sleep case (Figure 34). The most prominent frequency of 57.4 Hz has an rms amplitude of less than 0.02 mg.

The LTA Y-axis was selected for this comparison since it exhibited greater acceleration on January 15. Both X and Z were greater than Y accelerations on January 17, with the X sensor reporting 0.1 mg RMS and the Z sensor reporting 0.011 RMS. Nevertheless, these amplitudes are significantly less in each case than those seen on January 15, and the 17-Hz component is absent in all three axes.

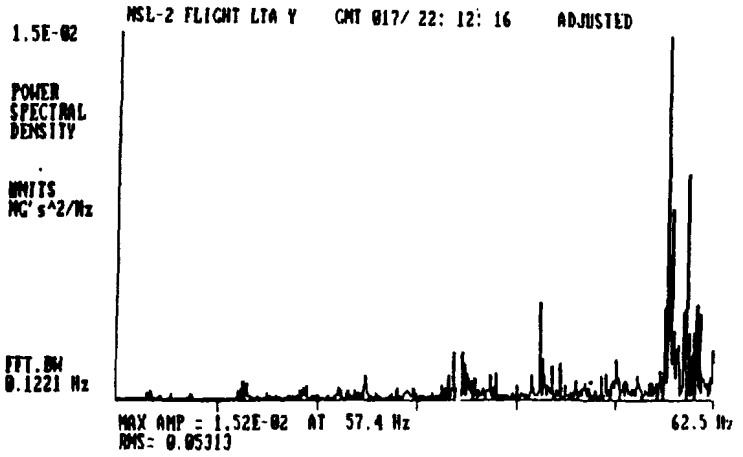

FIGURE 34. SLEEP PERIOD ON JANUARY 17, ADJUSTED PSD

The firings of vernier thrusters occur throughout the mission under control of the guidance and computer system. The IMU angle plot in Figure 35 was derived from a flight plot of yaw angular rate, and it shows the Orbiter attitude swinging between angular limits. The abrupt changes in direction are the result of firing of vernier engines located fore and aft of the Orbiter. Unless inhibited as a special operation for short periods, this activity continues throughout the mission. The case selected to show the effects of vernier firings corresponds to the first change in direction shown in this figure, during the sleep period on January 17.

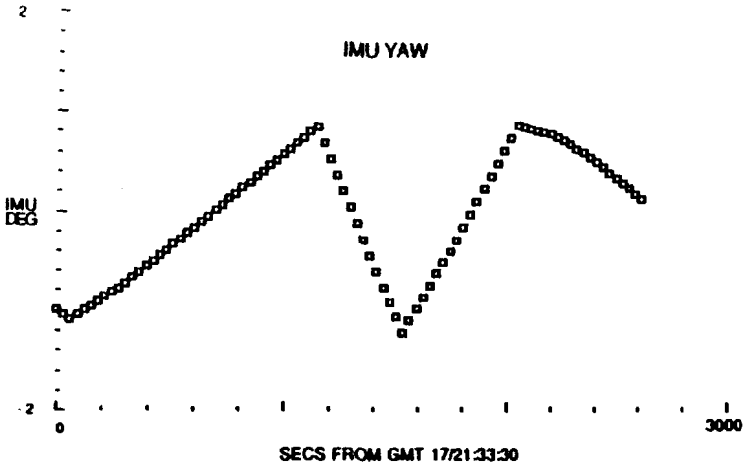

FIGURE 35. INERTIAL MEASURING UNIT (IMU) YAW, TIME HISTORY

Before looking at the LTA data, it is useful to examine the calculated steady-state response levels shown in Figure 36. These values, in milli-g's, have been corrected for the location of the LTA during the STS 61-C mission. Using the actual LTA location is necessary since rotational effects associated with the firings will affect the translational effects measured by the LTA. Although the combination of thrusters used for this correction may sometimes include more than the set required for pure yaw, an examination of angular position on all axes indicates no correction of rate error in pitch or roll at the same time; consequently, the plus yaw acceleration level of 0.157 mg shown here is applicable. The duration of the thruster firing required to correct the yaw rate would have been 0.3 sec.

	$\ddot{X}$	$\ddot{Y}$	$\ddot{Z}$
+ PITCH	-0.026	0.0	-0.415
- PITCH	0.014	0.0	-0.055
+ YAW	0.026	0.157	-0.191
- YAW	-0.051	-0.157	-0.225
+ ROLL	0.015	0.210	-0.275
- ROLL	-0.028	-0.210	-0.195

NOTES:

1. UNITS ARE IN mG'S.
2. DERIVED FROM ACTUAL MSL-2 LTA LOCATION AND NOMINAL ORBITER CG.
3. THRUSTER COMBINATIONS ARE TYPICAL. OTHER COMBINATIONS ARE POSSIBLE.
4. DURATION OF FIRINGS ARE MULTIPLES OF 80 msecs.

FIGURE 36. LTA SENSITIVITY TO VERNIER FIRINGS

The vernier firing effect was seen predominantly by the Y-axis accelerometer as vibration (Figure 37). Structural ringing at a moderate frequency is masking the short-duration input.

The principal frequency of 17.7 Hz predominates the PSD (Figure 38). This frequency was absent before the vernier firing. It would appear that the verniers excite the same mode that was excited during the sleep period on January 15, and as commonly seen during other times of severe vibration input.

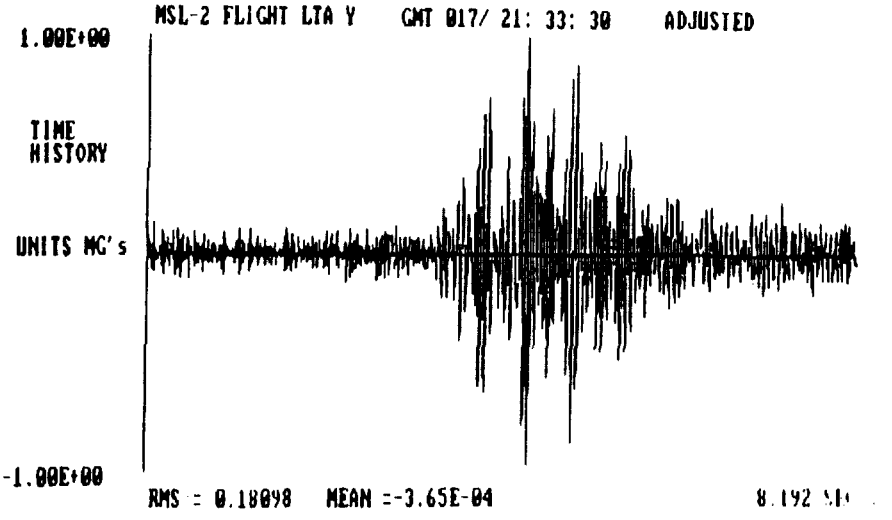

FIGURE 37. VERNIER FIRING, LTAY TIME HISTORY

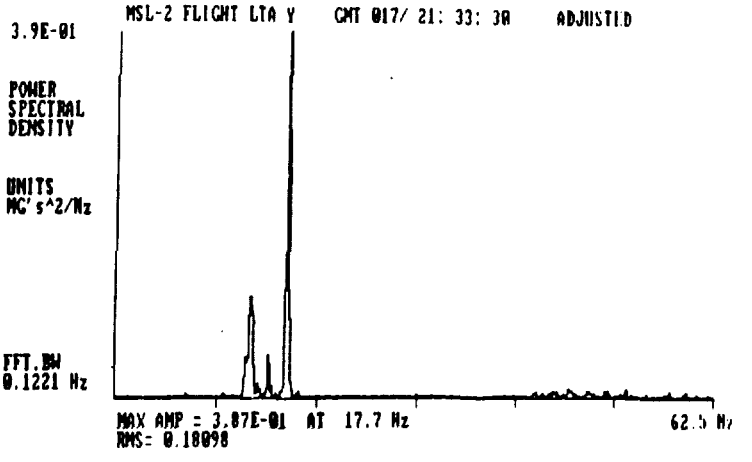

FIGURE 38. VERNIER FIRING, POWER SPECTRAL DENSITY

Other noise spikes, such as these shown in Figure 39, have no known origin. This plot shows two spikes of the same nature separated by 2 sec during the sleep period on January 12. A common occurrence, they may also occur singly or in pairs with opposing direction. There is frequently no apparent correlating activity on other axes.

Although not as spectacular as the treadmill and RCS hot fire cases shown earlier, these are possibly of more concern to acceleration-sensitive experiments since they represent an acceleration that is sustained for several tenths of a second above the 0.2-mg level.

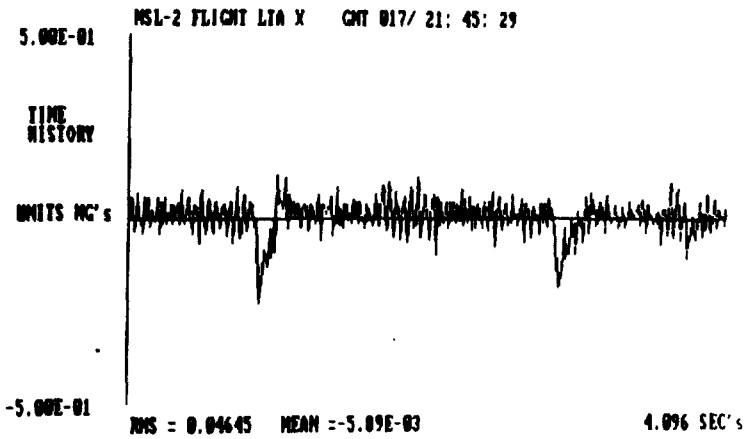

FIGURE 39. UNEXPLAINED SPIKES, TIME HISTORY

The PSD for the spike in Figure 40 shows a predominant frequency around 45 Hz. The 17-Hz source appears to not be excited.

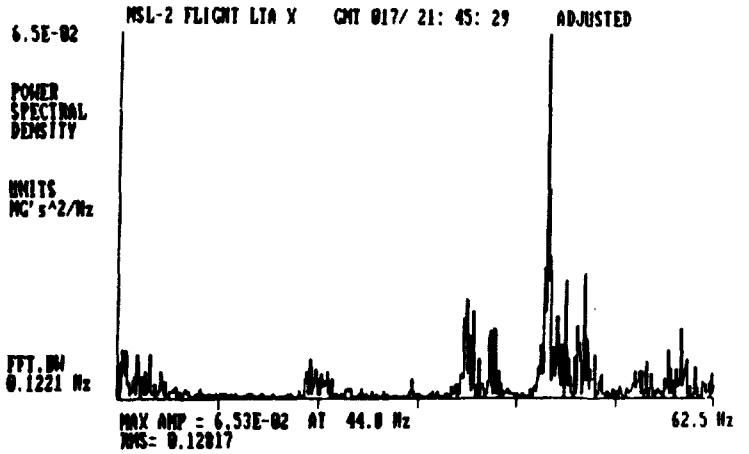

FIGURE 40. UNEXPLAINED SPIKES, PSD

Also seen during the sleep period on January 17 was this high-amplitude, short-duration burst on all three axes (Figure 41).

Figure 42 examines this burst to see its structure. It appears to begin at a higher frequency and rapidly ceases. The total duration of the burst is around 0.1 sec.

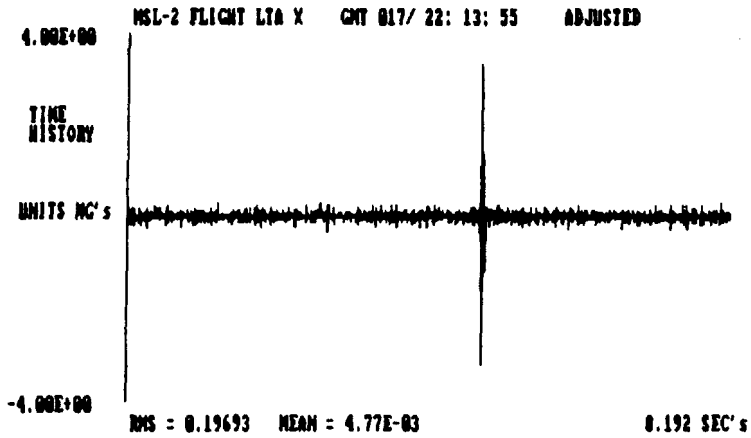

FIGURE 41. UNEXPLAINED BURSTS, TIME HISTORY

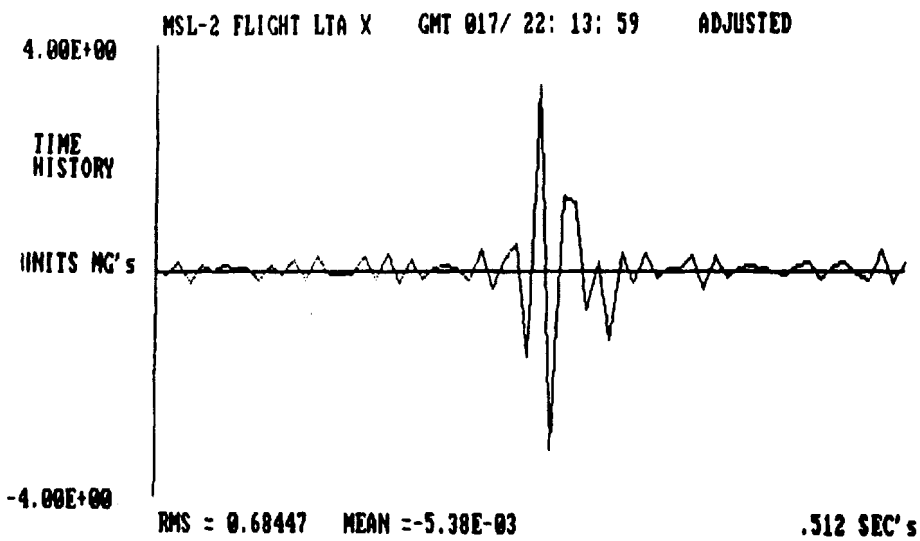

FIGURE 42. DAY 17 UNEXPLAINED BURST-EXPANDED TIME HISTORY

The PSD also indicates that no single frequency was predominant, but that the frequency range was primarily above 30 Hz (Figure 43). Possibly, the rapid stopping of rotating machinery could explain this occurrence.

To help explain the frequency of occurrence of these spikes and bursts, we examined all LTA data throughout the mission on 2-hour plots to identify periods of quiet and noise. Figure 44 is a sample of the results, which show the maximum periods of time, in minutes, between

saturations of each accelerometer axis. The first line shows that the maximum clear interval on January 17 between 17:00 and 17:30 was 2.5 min in X, 3.0 min in Y, and 3.0 min in Z. The maximum clear span of 7.5 min shown on the bottom line was duplicated several times on January 17 and 18 but was never exceeded.

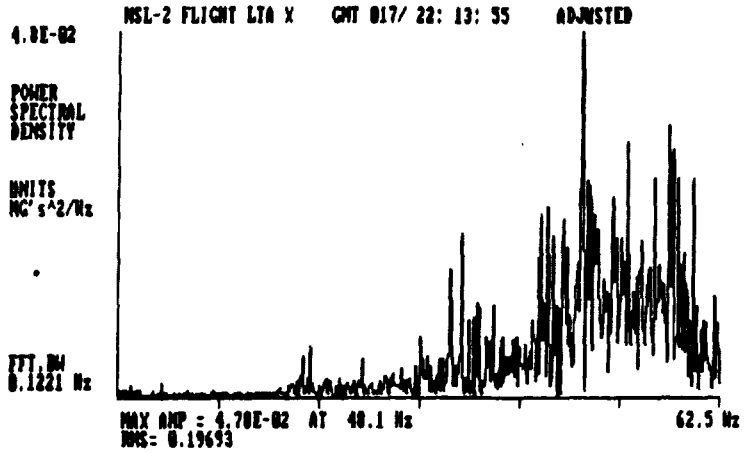

FIGURE 43. UNEXPLAINED BURSTS, PSD

	x	y	z
17/17:00	2.5	3.0	3.0
:30	7.5	8.0	2.0
17/18:00	2.5	4.0	2.0
:30	2.5	3.0	2.0
17/19:00	8.0	4.0	4.0
:30	2.5	7.0	1.0
17/20:00	4.0	2.5	1.5
:30	11.0	12.5	7.5
17/21:00	8.0	5.0	7.0
:30	6.0	15.0	10.0
17/22:00	5.0	2.5	7.5
:30	7.0	7.5	7.5
17/23:00	7.0	6.0	6.0
:30	8.0	8.0	7.5

FIGURE 44. MAXIMUM TIME BETWEEN SATURATIONS, GMT DAY 17

As a result of our study, we have drawn the following conclusions:

- The MSL carrier acceleration contribution is small with respect to other accelerations present on the Shuttle. We see no effect of MSL system operation in the LTA data.

- Although acceleration levels are greatly reduced in apparent severety by absence of crew activity, crew sleep periods do not ensure a quiet acceleration environment. Acceleration levels in excess of 0.5 mg occur throughout sleep periods.

- The use of gravity-gradient stabilization, which is difficult to achieve as a practical matter, will not guarantee low acceleration levels. Many 0.5-mg accelerations appear not to be connected with vernier thruster operation.

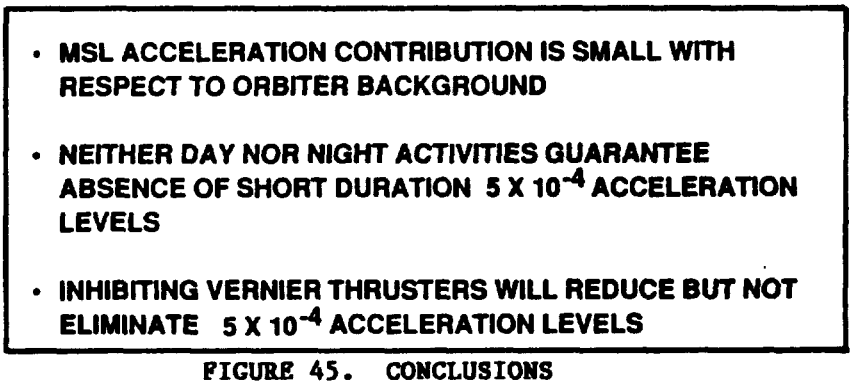

FIGURE 45. CONCLUSIONS

Question: I have a question about this power spectral density. The low-frequency interface part seems to be very low and flat, whereas in a real instrument you should have showing a certain frequency. So I was just wondering whether you don't have a high-pass filter just to see the disturbances, but you just filtered off the low-frequency end.

Henderson: There is a filter in the low-frequency end, is that the question? Is there anything filtering out the low-frequency part of it? Yes, there is, but it's way beyond the range that you see there. The low-frequency cutoff is 0.01 Hz, which is well beyond the range of that PSD.

Question: So low frequency is really that quiet, then, below 10 Hz.

Henderson: What we intend to do is to really blow up one long period of time during sleep and see what does crop up because we could be missing some frequencies of 0.05, 0.07 Hz unless we go to that amount of trouble, but there is nothing observable in what we have now.

Question: You had one chart, I believe, where you said you had the sensor cut off and we were looking at electronic noise.

Henderson: Yes, the LTA was off but the Command and Data Management System (CMDS) system was on.

Question: It seems that I recall seeing 1/F noise on that chart.

Henderson: Yes. Any random noise that was present there would be amplified by our inverse filter.

Question: I realize it was there and not when the sensor was on?

Henderson: I attribute that to the fact that there was random noise present getting through the system and so it would be amplified more because of that filter. The inverse filter is amplifying by a factor of 8 to 16, so any noise that is present there would be greatly accentuated.

Ulf Merbold, ESA/ESTEC: The 17-Hz resonant frequency, is there any information why it shows up so distinctly?

Henderson: We haven't found any; someone has pointed out that it might be a submultiple of 1,000 Hz, but it doesn't seem likely to me.

Question: That is close (17 Hz) to the structural frequency of the Orbiter, a major mode of the Orbiter.

Henderson: There is a major mode at much lower frequencies. I am not aware of a resonance at 17 Hz.

N91-12412

13. MECHANICAL ISOLATION FOR GRAVITY GRADIOMETERS

David Sonnabend, Jet Propulsion Lab

ABSTRACT

In principle, gravity gradiometers are immune to the effects of acceleration and vibrations. In real instruments, scale factor errors and structural compliance lead to undesired instrument outputs. This paper will describe the instruments and the fundamental sources of the problems, calculate the magnitude of the effects, demonstrate the need for isolation in the Shuttle (indeed, almost any spacecraft), and briefly describe the JPL eddy current isolation technique and its current development status.

The work I am going to report on today is generally in connection with the NASA program on gravity gradiometry and, referring to Figure 1, I'll give a few principles. The arrow symbol indicates an accelerometer and points along the sensitive axis. When you take two accelerometers and separate them on the ends of a rigid bar, you have a gradiometer. There are two ways in which you can build an accelerometer. The first arrangement shown in Figure 1 is a diagonal component gradiometer. Its output axes are in the same direction as the displacement, and so gives one of the diagonal components of the tensor gradient. You can also generate a cross-component device by changing the output axis as in the lower arrangement, and, in fact, instruments of both types exist today, or are under development. That is about all I am going to say about accelerometers. If you want to know more about gradiometers, consult H. J. Paik's paper in this workshop.

ACCELEROMETERS, GRAVIMETERS, and GRADIOMETERS

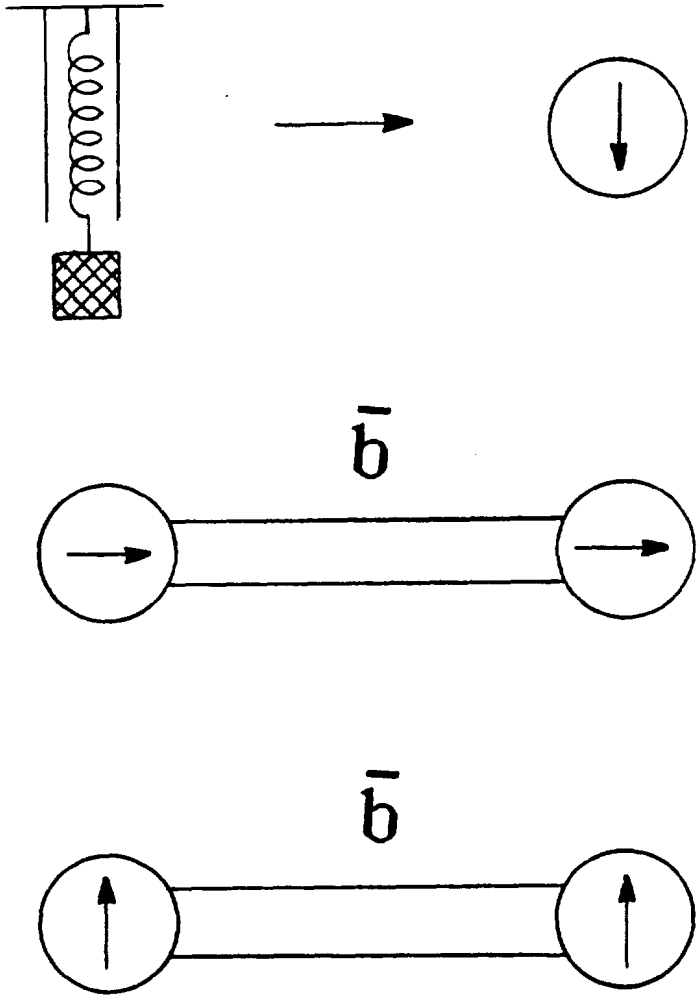

FIGURE 1.

I will discuss some of the reasons we are interested in acceleration and vibration. I will start with one of the most serious problems, acceleration. Suppose I built a general gradiometer of the type shown in Figure 2. It does not matter which type I have, and we will suppose there is an external acceleration on the instrument A along this direction and that there is some additional acceleration δ at the upper position. Moreover, we have a difference in the scale factors of the two accelerometers, given by ϵ. The output volts per input acceleration is off by ϵ in the second case. The output of an instrument like this is the difference between the two accelerometers. Multiplying this out, and throwing out the second order term, you get the expression in the middle of Figure 2, which is a gradient, H, multiplied by the baseline that separates them. So you have a contaminating error ϵA which is due to the acceleration field that doesn't really belong in there. This is what is called a scale factor error in the inertial instrument game.

Suppose you had a certain tolerance, H_{max}, for this kind of error. Then it is easy to compare these terms and decide in order to keep the overall error less than H_{max}, you would have to keep this ϵ below the ϵ_{max} in Figure 2. I have computed some numbers that are based on what you could resonably do. If you are in the laboratory, 10 m/sec^2 is the applied A, and I'm going to put the H in units we talk in this business which are Eötvös units and 1 E is 10^{-9} m/sec^2 the natural MKS unit of gradient. The reason I have put 1 E at the head of the table is because today's instruments actually deliver numbers of that order, or almost that, in the laboratory. So I put the tolerance and the field into this expression, and find out that I have to match to two parts in 10^{11}, which is really dramatic. The people who manage to bring off numbers of this order are really to be admired. I wouldn't care to believe that I could do it. But if we go to space, we find out that the acceleration is less. The numbers we have been talking about today are typically on the order of 10^{-4} m/sec^2. We need to lower this tolerance, because the reason for going to space in the first place is to get rid of this error, so I'll drop H_{max} 3 orders of magnitude, A five orders of

JPL

ACCELERATION

$$\Delta A = (1 + \epsilon)(A + \delta) - A = \delta + \epsilon A = bH$$

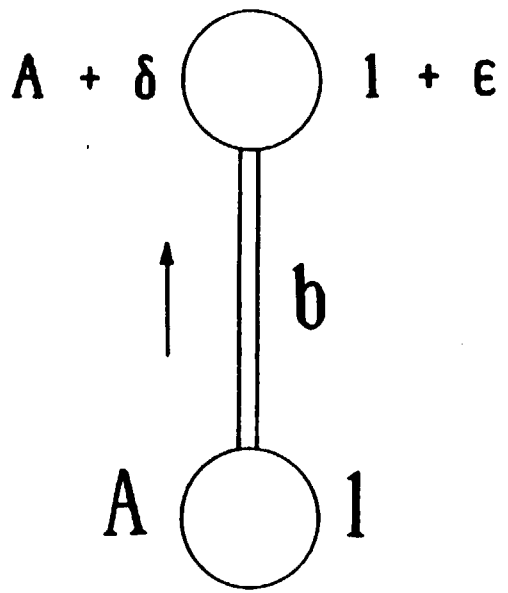

FIGURE 2.

$$\epsilon_{max} < \left| \frac{bH_{max}}{A} \right|$$

Case	H_{max} E	A m/s^2	ϵ_{max}
Lab (1g)	1	10	$2x10^{-11}$
STS	10^{-3}	10^{-4}	$2x10^{-9}$
Float	10^{-4}	10^{-10}	$2x10^{-4}$

magnitude, and we only need to match to parts in 10^9. This is matching over the entire range of the input acceleration. Even so, matching to parts in 10^9 is not an easy matter.

The last thing that we do to this instrument is to completely float it. In other words, if we remove all mechanical constraint so that there is no way of applying an acceleration or vibration, then we are getting numbers on the order of 10^{-10} m/sec^2 due to remnant effects like stray electrical charge on the instrument. We could then tighten our tolerance a little further, and we still only have to match parts in 10^4. That I can promise to do. I may be rash, but that is far easier. So this is the reason for going to space, the reason why we have to go to an actual floatation system.

The second problem we have to deal with is vibration, which is a real nuisance. Suppose I take an inline diagonal instrument, such as shown in Figure 3, and attach it to my rigid rod and shake it by grabbing it in the middle, as I must support it somehow. I grab it in the middle, and shake it up and down. The problem with that is the rigid bar that I supported the accelerometers with does not exist. We are forced to use real materials, and so it bends somewhat because these accelerometers have some mass. You can go through an elementary beam analysis on this and determine what happens. It is really quite peculiar. If you shake it up and down, the sensitive axes are bending in opposite directions and you measure a component of the shake. When you subtract these two you have something left over. Moreover, when the shake reverses, so do the scopes, so you get a result which is off in the same direction, whether up or down. This is a rectification process, a common instrument problem. Note that we get an output, even if the vibration frequency is outside the accelerometer bandwidth.

When elementary beam theory is used, the bias is as shown in Figure 3. Here, J is the amplitude of the applied vibration at the applied frequency ω, ω_y is the resonant frequency of the beam for this type of excitation. If you have a certain tolerance for this kind of

TRANSVERSE VIBRATION

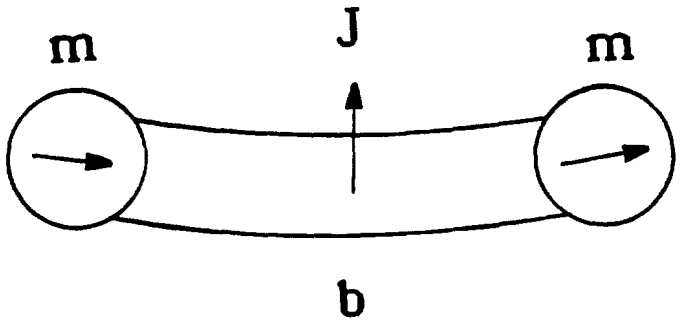

$$\Delta H_{xxbias} = -3\left(\frac{J\omega^2}{b\omega_y}\right)^2$$

$$J\omega^2 < b\omega_y\sqrt{H_{max}/3}$$

For: b = 0.2 m; m = 1 kg; $H_{max} = 10^{-4}$
0.1 m Diameter Tube; $m_{beam} = 0.4$ kg

	ω_y rad/s	$(J\omega^2)_{max}$ m/s^2
Aluminum	9500	3.5×10^{-4}
Beryllium	24000	8.8×10^{-4}

FIGURE 3.

error, H_{max}, you can solve the equation for $J\omega^2$ which is the vibration acceleration. Again, I put 20 centimeters in as the distance between the accelerometers, a kilogram for each one of the basic accelerometers, and the H_{max} at 10^{-4} E.

For standard accelerometers, which are hardly any bigger than your fist, many smaller, we can't make the diameter of the beam much larger than about 10 centimeters so I used that. The larger we make that the stiffer its going to be. Then, for the mass of the beam, I allowed 20 percent of the total accelerometer mass on the grounds that, if I made it more than this, elementry beam theory would no longer apply. That is not horrendously optimistic because then the beam mass itself would tend to lower the frequency so we would gain only a little. For 10 times that mass, we might get a factor of 2 increase in the resonant frequency.

If we use aluminum for the tube material, we get a resonant frequency of 9500 radians per second; and you have to admit that is a pretty stiff beam. Still, the allowable acceleration that turns out to be 3.5×10^{-4} m/sec^2 or 3.5×10^{-5} g's that everyone uses here. That number is much lower than the numbers quoted today for the Shuttle, or what is likely to be achieved on the Space Station. When I tried new materials it turned out that steel and titanium give almost identical results to the aluminum. Beryllium is really the only stuff that is significantly better and it leads to the answers shown in Figure 3, which are about a factor of 2.5 improvement. That's nice, but still nowhere near the actual vibration levels; so there is nothing for it, we can't permit the process to occur.

Our approach to both scale factor problems and vibration is total isolation. You turn the instrument fully loose and let it float. When your vehicle is about to collide with it, we apply a force using magnetic eddy currents. We have a set of coils that form a cage around the gradiometer and we force the thing back when it gets too close, but most of the time the forcing current is off, so it is drag free for the

periods between forces. The curve, Figure 4, has been presented today in different forms. You let something float freely long enough, and sooner or later it runs into whatever boundaries we establish. If you allow a gap between the experiment and the coils, eventually they get in the way. Reasonable numbers are toward the center of the chart, showing the spacecraft acceleration due to applied drag from all sources. You are then allowed the indicated number of seconds of free time between impulses. I would guess 10 to 20 seconds in the shuttle, maybe a little longer in the space station because it is still larger. Quite practical.

We have done a feasibility study on whether that would work with eddy currents. I won't bore you with the details, but there is a published paper on the subject.[1] I will say that at JPL we put together a small test facility to try this out in one axis in the laboratory, and this is shown in Figure 5. It is a torsion pendulum supported by a wire that comes from the top down through the center of gravity of the floated assembly. The assembly consists of a cross beam connecting an empty aluminum box and a counterweight. Not much lateral motion is allowed. When the box gets too close, we turn on the coils and push it away. Typical frequencies run around 50 kHz in order to make sure of totally expelling the field from the box. The thinner you make the box walls, the higher the frequency needed in order to do that. There are also position sensors shown that tie the sensor back to the amplifiers that drive the coils. We are beginning to work on that now.

We have what we believe is a pretty good position for the theory for this kind of eddy current work. Anybody who has tried to calculate eddy currents knows it is a horrendous mess so I put it out on contract with Arizona State University which has turned in terrific stuff; and I expect to have a solid report in a matter of months. There are papers on most of the subjects I've covered here in front of you. Any questions?

---

[1] C. H. Seaman and D. Sonnabend, "Semi Drag Free Gradiometry," J. Astron, SCI, Vol. 33, No. 4, p. 353, 1985

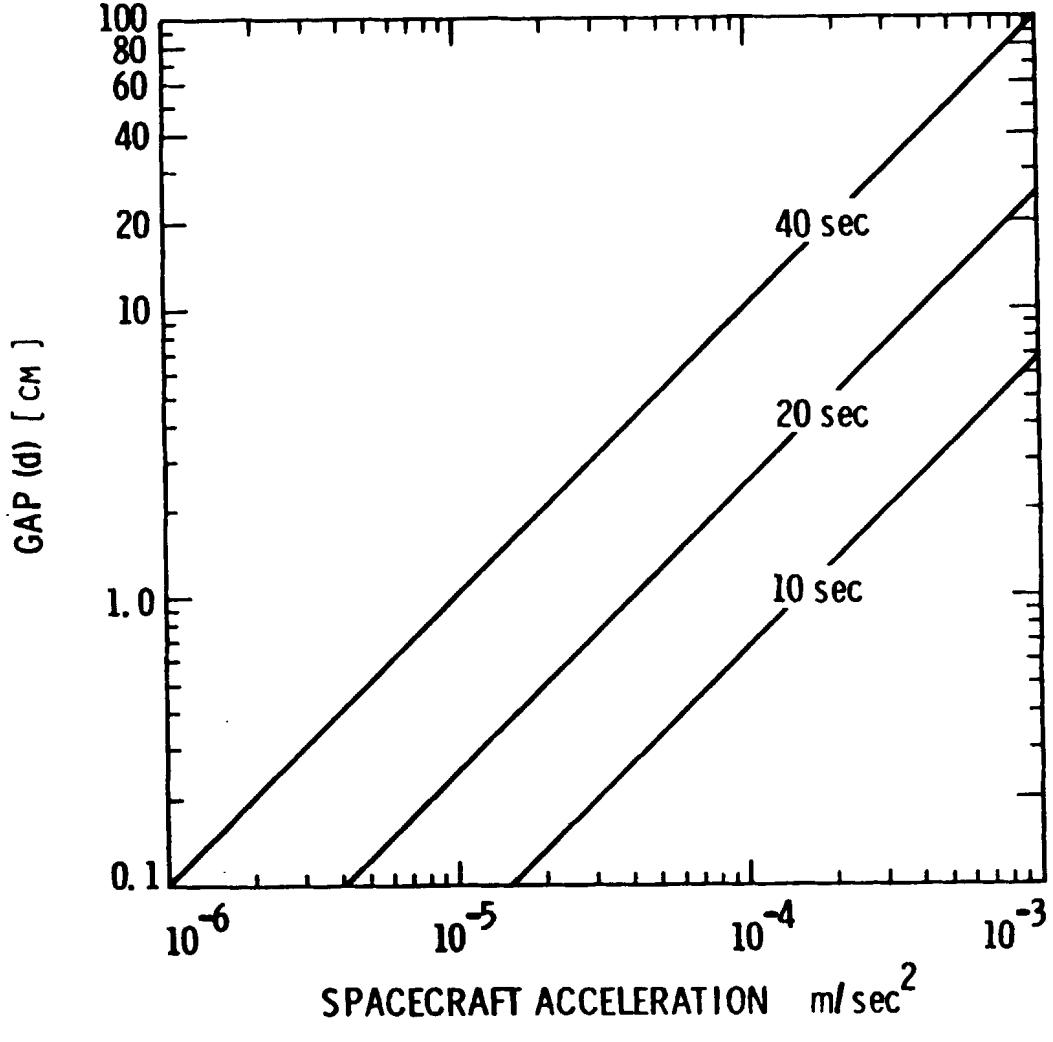

FIGURE 4. GAP VERSUS SPACECRAFT ACCELERATION

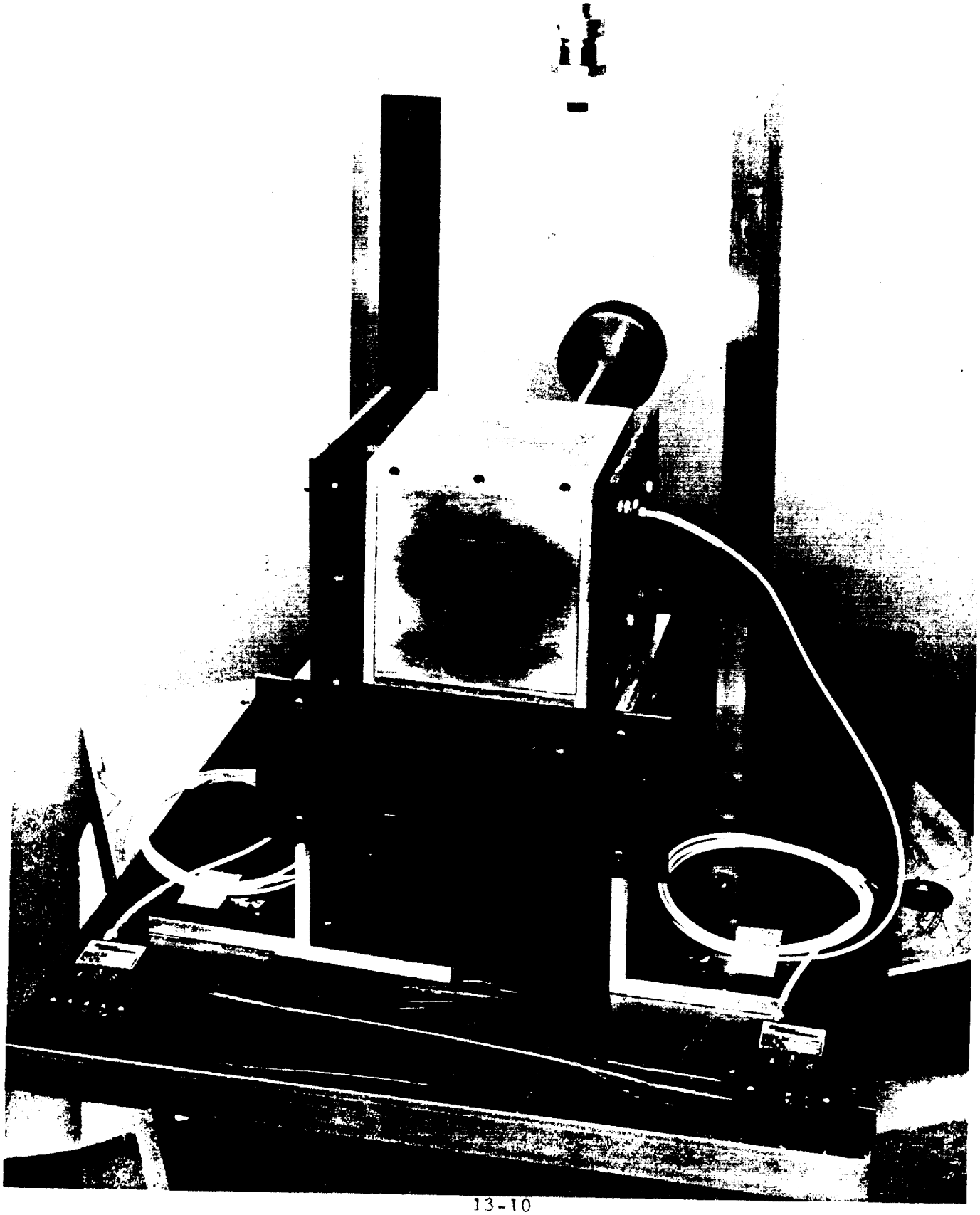

Bob Naumann, Marshall Space Flight Center: When you supply the restoring force using the eddy current link, wouldn't you excite vibrations in the gradiometer and would you not have to wait for them to die out to make measurements, because if you have something that stiff doesn't it take a long time for them to die out?

Sonnabend: We might have to put a little damping in for that; but we have not tried that yet, Bob. I would like to get as close to doing that as possible. We should be able to see it in this test facility. This is a pretty stiff box, I don't think its going to be easy to excite it.

ANSWER: Yes, the larger the package the worse that problem will get.

Ed Bergmann, C.S. Draper Laboratory: When those jets fired, that is a very abruptly applied acceleration and its not clear to me that your magnetic suspension is going to be stiff enough to accomodate that sudden an impulse.

Sonnabend: In this mode, as shown, the magnetic suspension is off and all that happens is that the vehicle approaches the floating package by some amount and you have to leave enough clearance for the largest excursion due to these impulses.

Bergmann: That means you must leave a significant amount of the clearance that you have trying to keep the wall far enough away to deal with that.

Sonnabend: If your package is a meter in diameter as we expect it to be, several 10's of centimeters is available to you. So I don't think you will have any problem with that. I haven't seen any amplitudes like that today. At the absolute worst, if you turn on really ferocious thrusters, there is nothing to stop you from caging this thing. We have to have some mechanism for doing that anyway. If you had to do that once a month I don't think anybody would complain.

Fred Henderson, Teledyne Brown Engineering: When it comes to accelerations other than the thrusters, we have a model using this MSL data, that shows all you would need is a thousandth of an inch.

Sonnabend: Yes, probably worse than thrusters is crew motion and we calculated crew motion. If I remember it right, it ran a millimeter or two for the shuttle and probably less with the space station. But that is just an arbitrary calculation I think we can easily allow for all of this.

N91-12413

14. THE MESA ACCELEROMETER FOR SPACE APPLICATION

William G. Lange and Robert W. Dietrich
Bell Aerospace Textron

ABSTRACT

An electrostatically suspended proof mass is used to measure acceleration in the submicro-g range.

Since no fixed mechanical suspension (such as springs or strings) is used, the constrainment scaling can be changed electrically after being placed in orbit.

A single proof mass can sense accelerations in three axes simultaneously.

It can survive high-g pyrotechnic-generated shocks and launch environments while unpowered.

1.0 INTRODUCTION

The word MESA is an acronym for Miniature Electrostatic Accelerometer (Figure 1). This accelerometer is designed specifically for low-g applications. Full scale is typically $\pm$1 milli-g up to $\pm$25 milli-g's. Often two more sensitive ranges are also provided.

What is significantly different about this accelerometer is that it has no mechanical spring. In other accelerometers used for low-g measurements, the mechanical spring is a large contributor to the bias instability and the time-dependent drift and temperature coefficient of the bias. The MESA does not have a mechanical spring; the MESA's proof mass is electrostatically suspended in all three axes. When it is in operation, there is absolutely no physical contact betwen the proof mass and any other part of the accelerometer.

FEATURES:

- ELECTROSTATIC SUSPENSION AND CONSTRAINMENT IN THREE AXES
- DESIGNED SPECIFICALLY FOR VERY LOW-G APPLICATIONS
- AUTOMATIC OR MANUALLY COMMANDED RANGE SWITCHING
- SURVIVE HIGH-G LAUNCH ENVIRONMENT

HISTORY:

- OVER 40 SINGLE-AXIS VERSIONS
- NINE THREE-AXIS VERSIONS
- THREE SINGLE-AXIS UNITS OPERATED FLAWLESSLY FOR FIVE YEARS IN SPACE

FIGURE 1. MINIATURE ELECTROSTATIC ACCELEROMETER (MESA)

Even though it is intended to measure very low g's, it is capable of surviving extreme launch environments. The MESA is unpowered during launch. In this nonoperating mode, it has been qualified to 15 g's linear acceleration, 20 g's rms random vibration, and 6000 g's pyro shock. After the high g's associated with launch have passed, the MESA can be powered up, and will be outputting valid low-g data within one minute.

Our first MESA accelerometers were single-axis instruments; although the proof mass is always electrostatically suspended in all three axes, we only instrumented one of the axes. Approximately 40 of these single-axis MESAs were built and flown. We were later asked if we perhaps could change the MESA to a three-axis version using a single-proof mass. We successfully instrumented the other two axes, yielding a three-axes MESA. Nine of these instruments have been built and flown.

2.0 HARDWARE

The MESA hardware is shown in Figure 2. The proof mass is a thin-walled, flanged cylinder. The inside diameter is approximately a half-inch and the length about one inch; the flange in the middle is about 1½ inches in diameter. The proof mass fits over the carrier, which is a ceramic rod with eight electrodes plated onto it. The outside diameter of the carrier is slightly smaller than the inside diameter of the proof mass, resulting in a very small radial gap between them when the proof mass is "suspended". The eight electrodes on the carrier are used in four constrainment loops to provide constrainment against linear and angular acceleration in two orthogonal axes.

On either side of the proof mass flange there are forcer assemblies. On each forcer there are three annular rings facing the proof mass flange. The middle ring on each forcer is used in a differential capacitive bridge for proof mass position sensing. The inner and outer rings on each forcer are used to generate the electrostatic rebalance forces required for constrainment. Between the forcers there is a

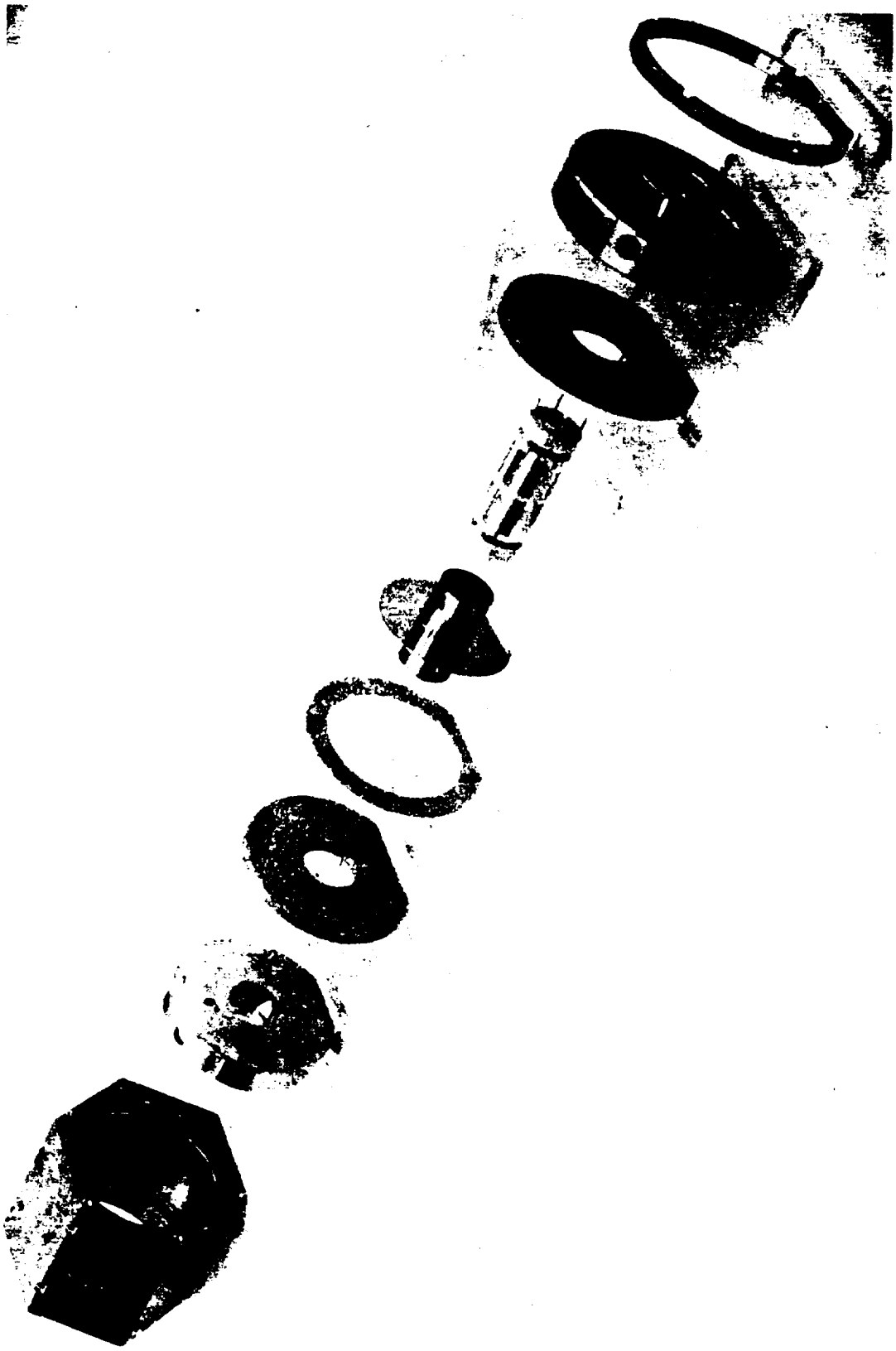

FIGURE 2. MECHANICAL ASSEMBLY

ceramic annular ring spacer which is slightly thicker than the proof mass flange; this difference establishes the pickoff and forcing gap. On the back side of each forcer there is a metallic retainer that supports an end of the carrier.

All the previously mentioned items are positioned in the housing and are held against a ledge in the hexagonal housing by a ring nut. The hermetically sealed housing is filled with a mixture of 90% dry nitrogen and 10% helium to provide gas damping of the proof mass for stable constrainment loop operation, and to protect the proof mass during the unpowered high-g launch environment.

Hermetically sealed terminals in the housing flats are used to connect the carrier and forcer electrodes to pickoff preamplifiers and forcer networks on p-c boards attached to the six housing flats.

The accelerometer has three mounting pads which are used to attach it to the vehicle structure at which the input acceleration is to be measured.

3.0 CONSTRAINMENT LOOPS

Figures 3 and 4 show the force rebalance loops in the Z axis and in the cross axes (X and Y), respectively.

A typical constrainment loop is shown in more detail in Figure 5. A cube-shaped proof mass is shown here (more will be mentioned about that later), but the principle of operation is independent of the proof mass shape.

The pickoff excitation generator provides push-pull sine wave excitation to a capacitive differential pickoff bridge consisting of two equal fixed capacitors, C_1 and C_2, and the capacitances between the two electrodes and the proof mass. The output of the bridge is summed by equal fixed capacitors C_3 and C_4, and is applied to the preamplifier.

If there is no input acceleration, the proof mass is centered between the two electrodes, causing the bridge to be balanced. The preamplifier input is thus zero, and no constrainment force is developed.

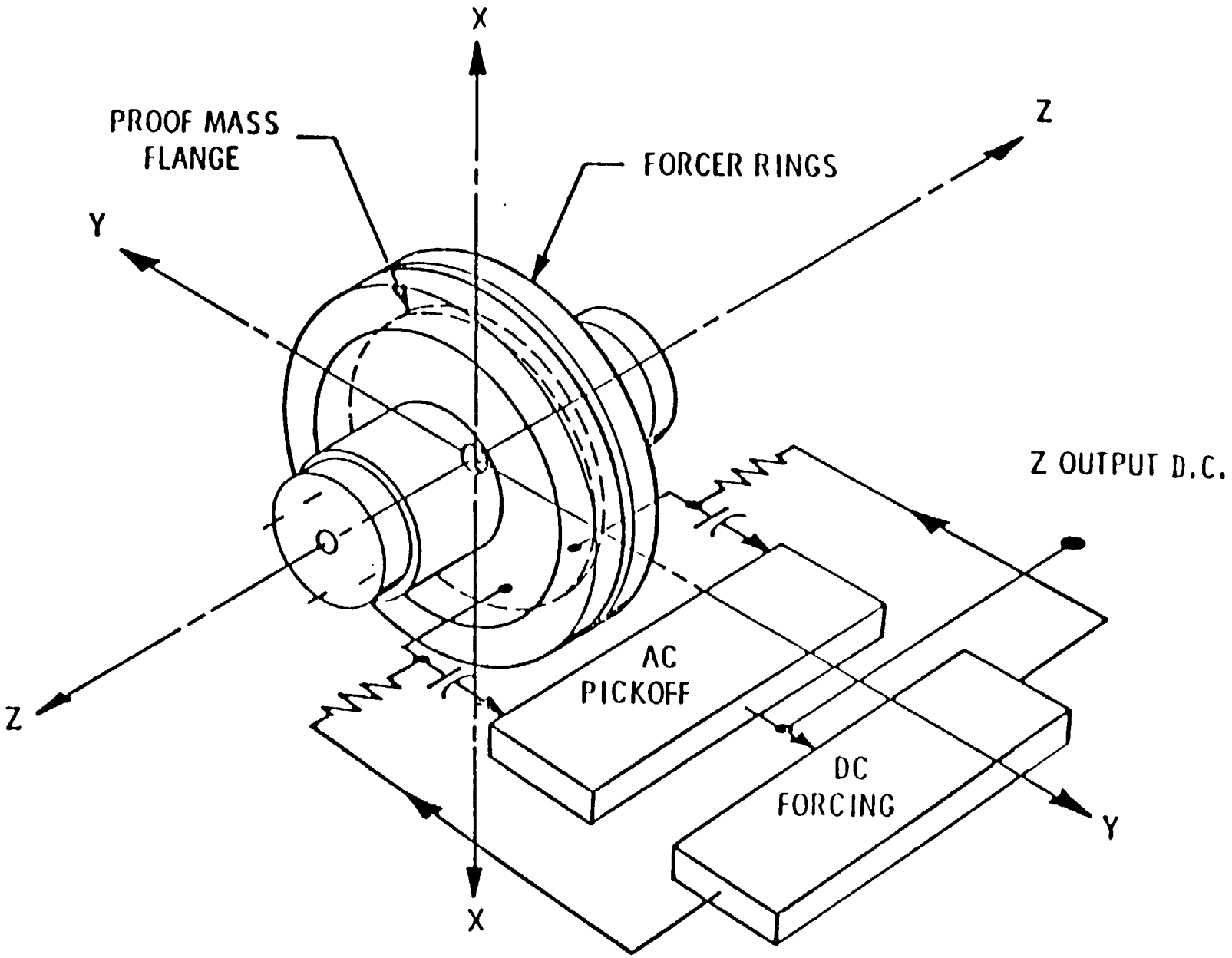

FIGURE 3. FORCE REBALANCE LOOP, Z AXIS

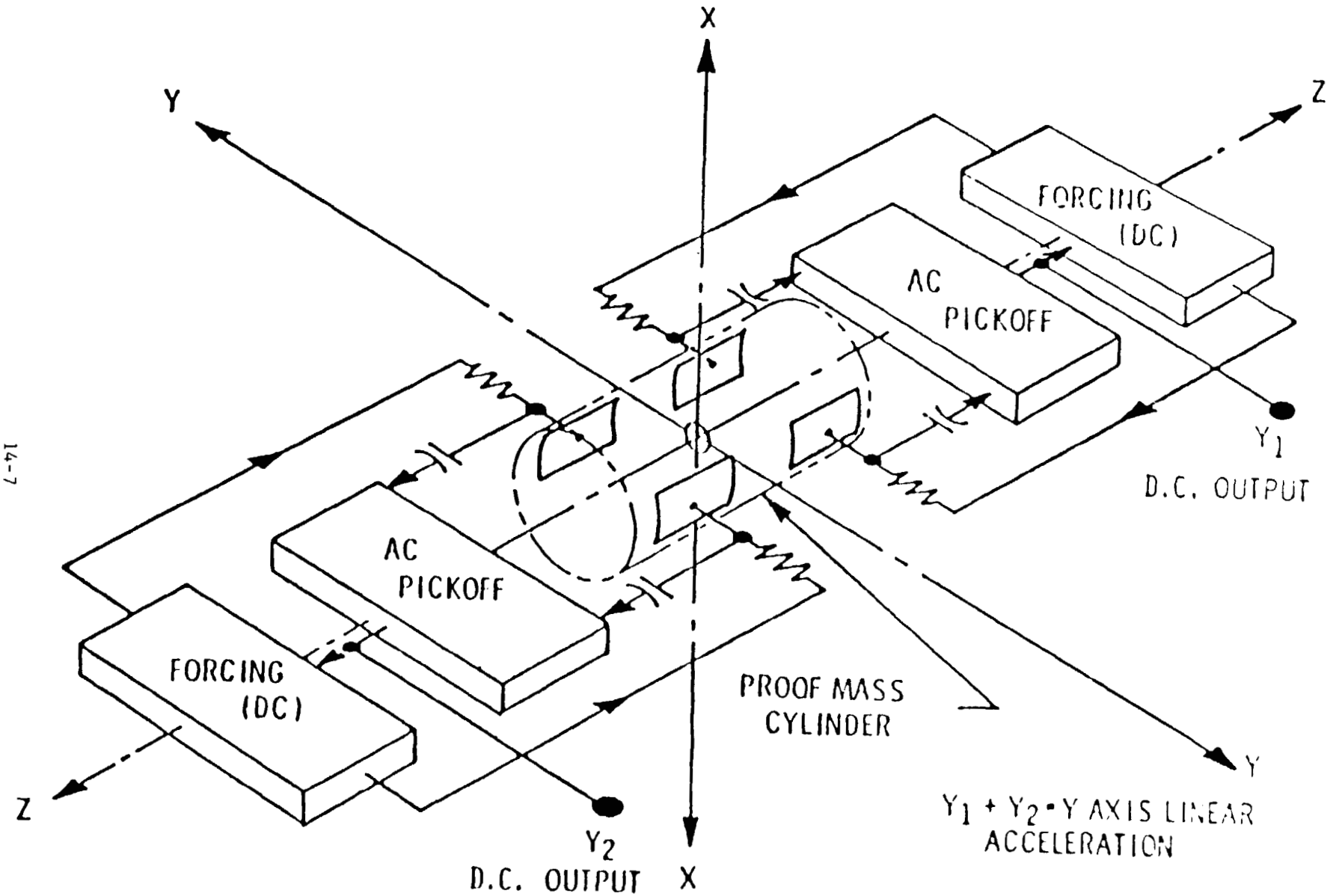

FIGURE 4. FORCE REBALANCE LOOP, X AND Y AXES (Y ONLY SHOWN)

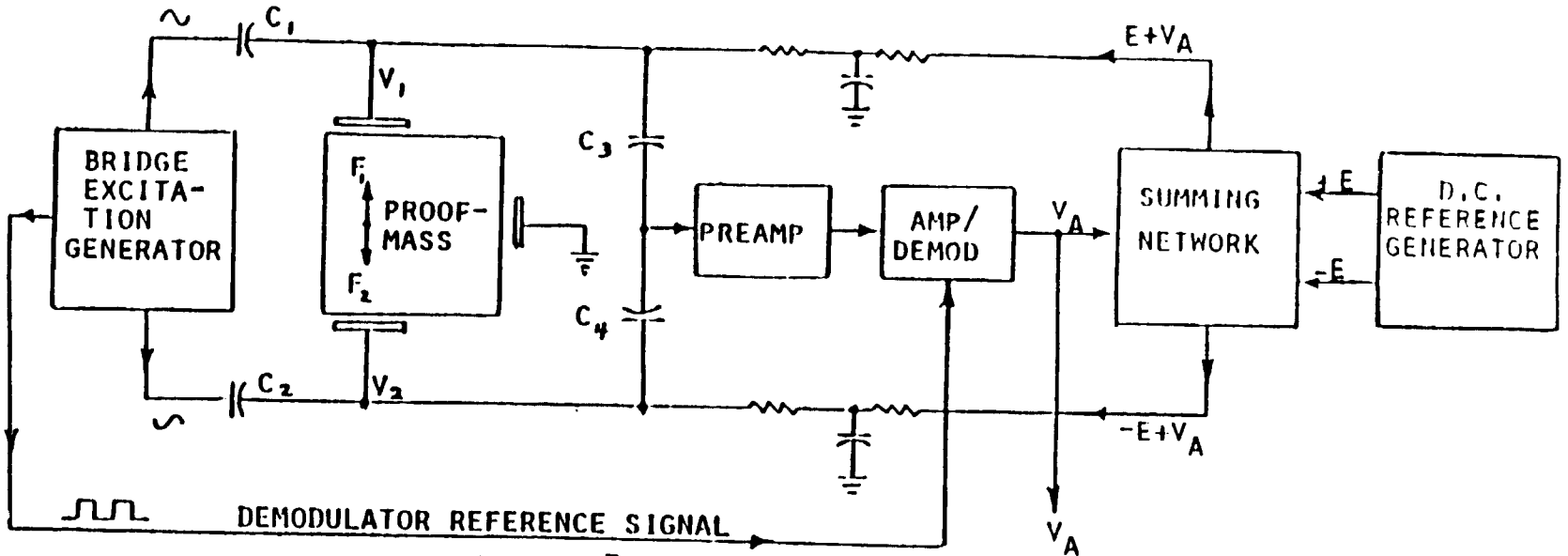

GENERAL EQUATION: $F = \frac{4.4 \times 10^{-7} K_A V^2}{s^2} = KV^2$

DEFINE $V_1 \equiv (E + V_A)$ AND $V_2 \equiv (-E + V_A)$

THEN $F_1 = KV_1^2 = K(E + V_A)^2$

AND $F_2 = KV_2^2 = K(-E + V_A)^2$

$(F_1 - F_2) = K(E + V_A)^2 - K(-E + V_A)^2 = 4KEV_A$

FIGURE 5. TYPICAL CONSTRAINMENT LOOP

If there is an input acceleration, the proof mass moves very slightly from its centered position. This causes the bridge to become unbalanced. The resultant bridge unbalance voltage is amplified by the preamplifier and amplifier, and then is phase-sensitive demodulated to provide d-c voltage, V_a.

The summing network combines error signal V_a with d-c reference voltages +E and -E to generate the two required d-c constrainment voltages, V_1 and V_2.

As shown in Figure 5, V_1 and V_2 cause forces F_1 and F_2, each one attracting the proof mass toward its forcer. The differential force (F_1 - F_2) is equal to $4KEV_a$; this constrainment force acts as a positive electrical spring to constrain the proof mass. Since the constrainment loop output voltage V_a is directly proportional to the constrainment force (F_1 - F_2), V_a is directly proportional to input acceleration.

4.0 FLIGHT DATA

Figure 6 shows some data taken in 1968 from a signle axis MESA used on the *SERT II (Space Electric Rocket Test)* vehicle in earth orbit. The MESA was used to measure acceleration due to thrust from an ion engine. The upper plot shows the expected 0.7 micro-g acceleration due to the gravity gradient; the ion engine was not thrusting at this time. The middle plot shows the acceleration with 30% and 80% engine thrust. The lower plot shows the acceleration with 100% engine thrust. There is an interesting phenomenom shown in this last plot; as far as we can determine, the perturbation in the acceleration was caused by the South Atlantic magnetic anomaly.

Figures 7 through 12 show some flight data from the 3-axes MESA used on spacecraft in an elliptical earth orbit.

Figures 7 through 9 are for normal flight operation. The MESA Z axis measured the along-track component of the vehicle acceleration. The MESA Z axis bias was approximately +3 micro-g's (the indicated

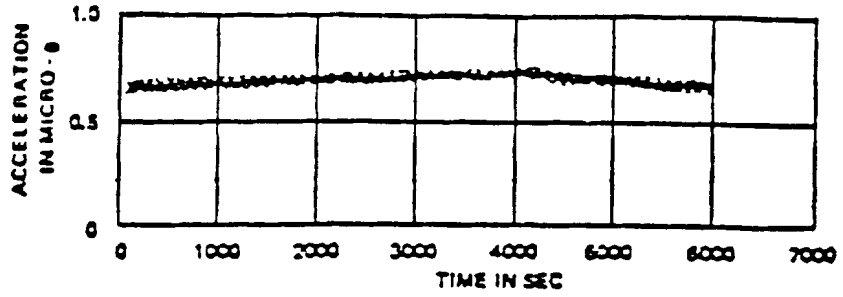

MESA Output for Gravity Gradient Input

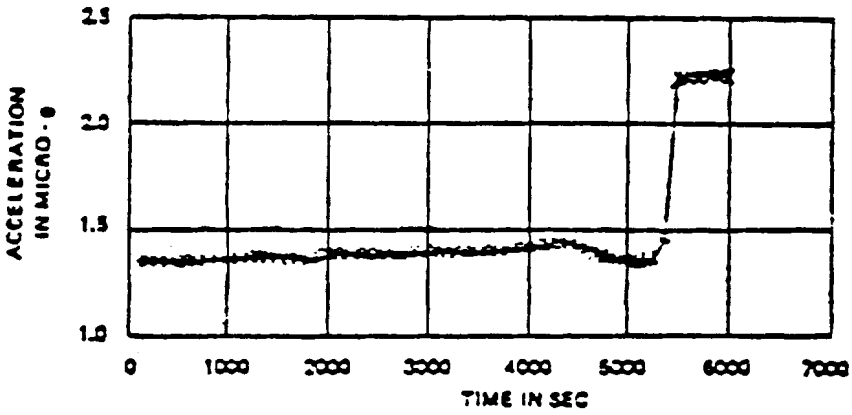

MESA output with 30% and 80% Engine Thrust

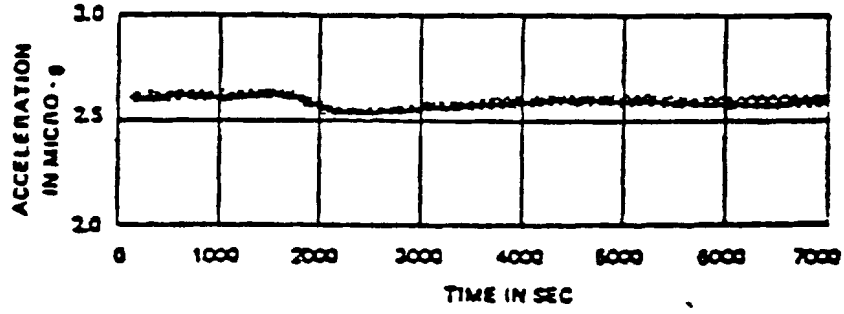

MESA output with 100% Engine Thrust

FIGURE 6. SERT II FLIGHT DATA

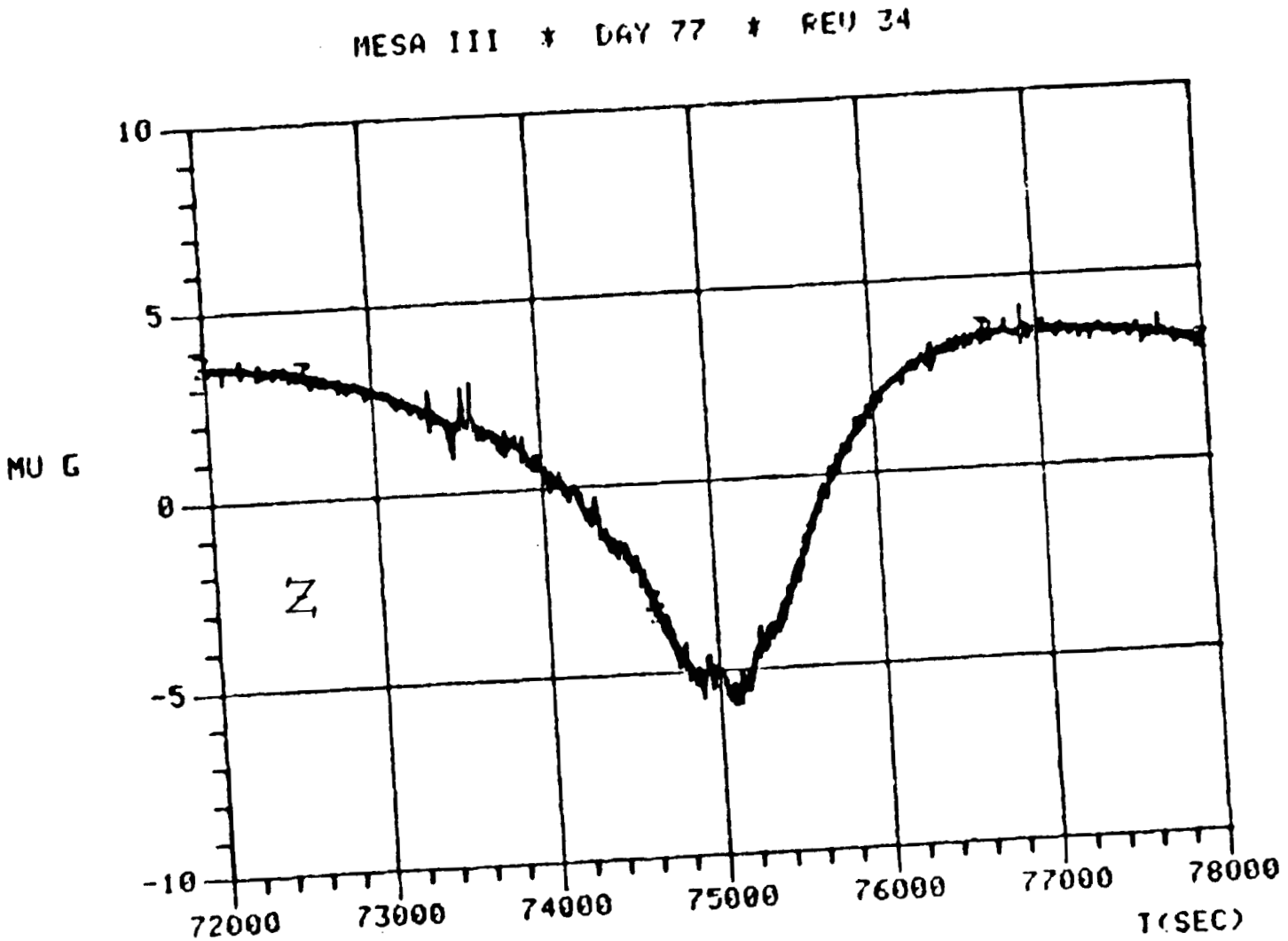

FIGURE 7. ALONG-TRACK COMPONENT

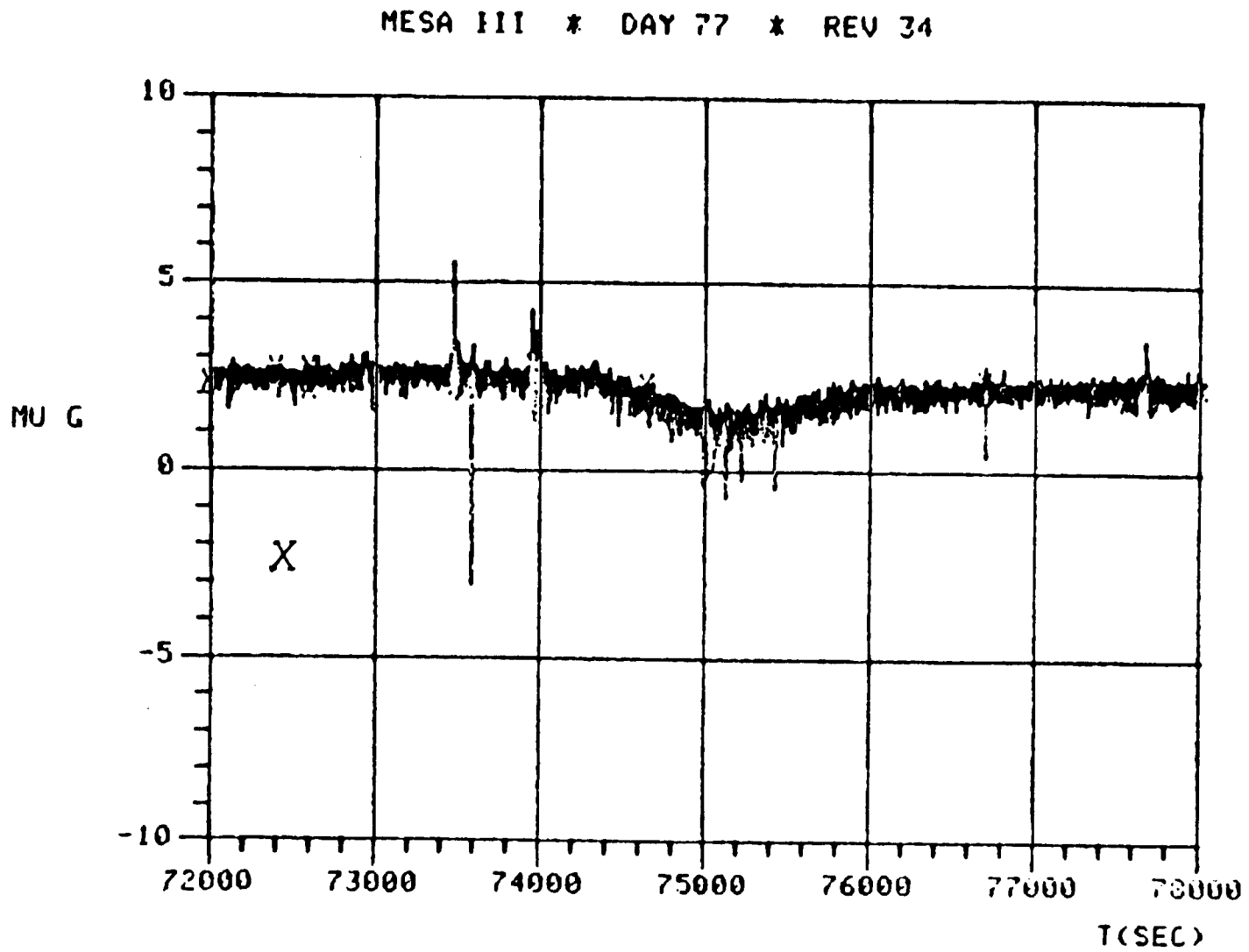

FIGURE 8. CROSS-TRACK COMPONENT

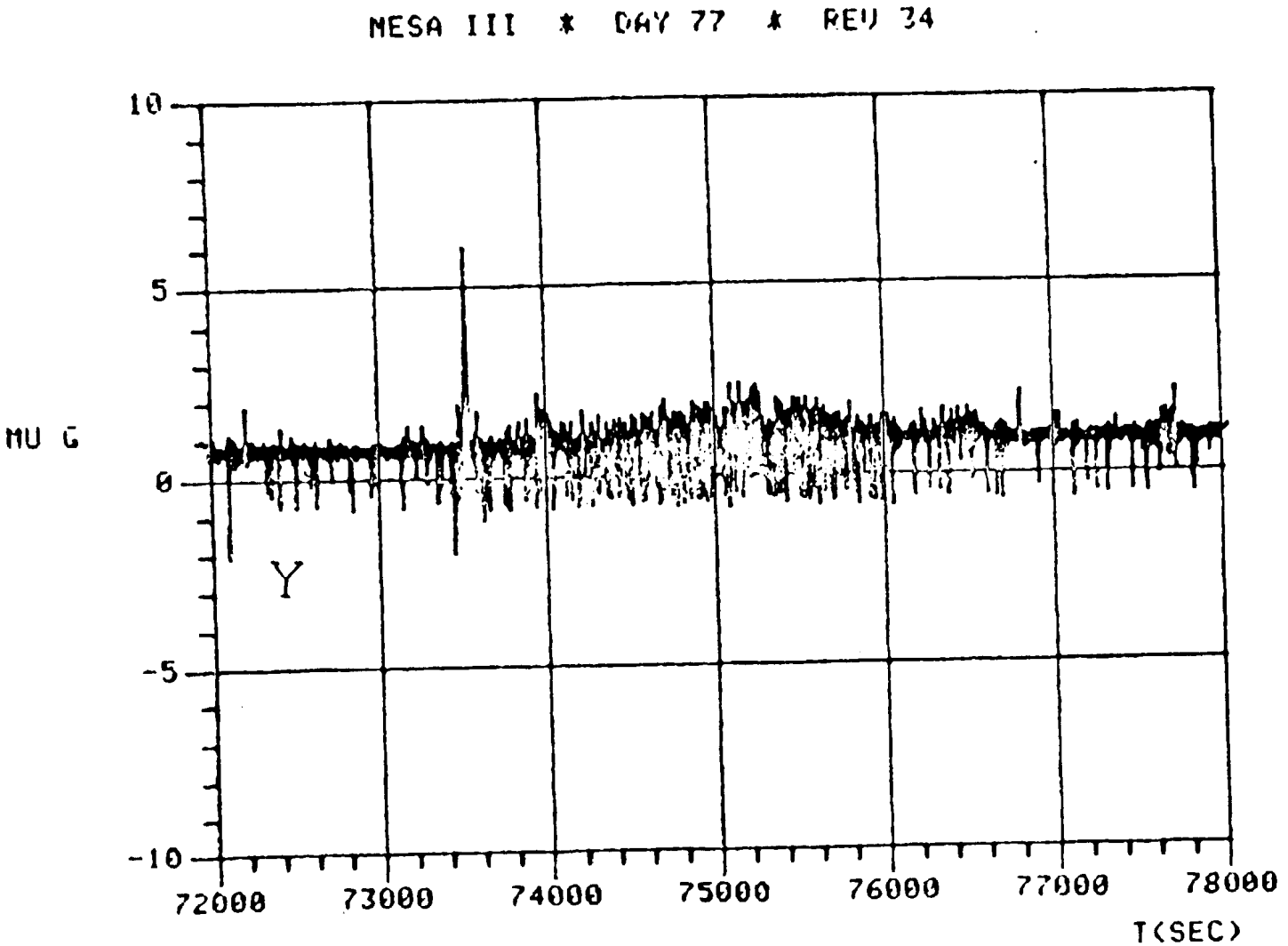

FIGURE 9. RADIAL

acceleration at apogee). As the vehicle approached perigee, the drag acceleration increased by approximately 9 micro-g's, resulting in an indicated acceleration of -6 micro-g's.

Figures 8 and 9 show MESA flight data in the X (cross-track component) and Y (radial component) axes. The spikes in the data are primarily from accelerations due to firing of the vehicle's attitude thrusters. Readily evident is the increased frequency of attitude thruster firings near perigee.

Figures 10 through 12 show data during an orbit-adjust thruster firing. The along-track component acceleration is approximately 10,000 micro-g's. The plots of the cross-track and radial components show some vehicle oscillations during the orbit-adjust thruster firing.

The MESA for which flight data are shown in Figures 7 through 12 is an autoranging instrument. Each axis has three ranges. During normal flight operation (Figures 7 through 9), all three axes were in their most sensitive ranges. When the acceleration suddenly increased due to firing of the orbit-adjust thrusters, the autorange circuitry caused upranging of the ranges as required to provide valid data. After the orbit-adjust thruster firing was completed, the autoranging circuitry caused downranging to the most sensitive ranges.

5.0 DEVELOPMENT AND FLIGHT HISTORY

As shown in Figure 13, development of the Bell electrostatic accelerometer started in 1958 with the ESA (Electrostatic Accelerometer); this was a larger version of the present MESA. Single-axis MESA's were flown on spacecraft, starting approximately 1963. Of particular interest is the MESA used on the Atmosphere Explorer Satellite AE-C. On this spacecraft there were three single-axis MESA's in a triad. This unit operated for five years in orbit until the satellite itself fell out of orbit and burned up.

In 1978, deliveries and flights of the three-axis version of the MESA began. Most have been used for navigation and for air density measurements. An exception is the MESA supplied for the Spacelab 3

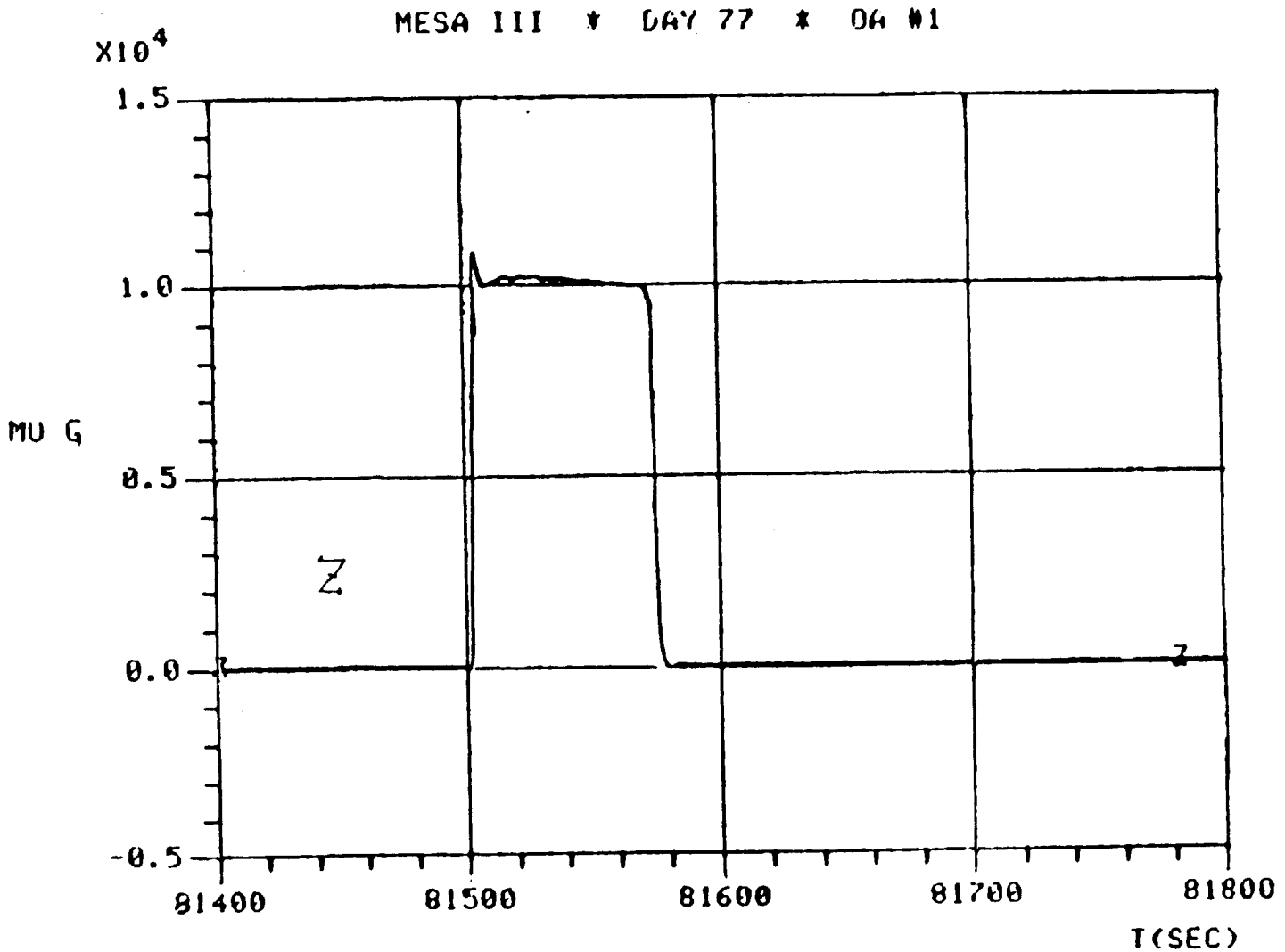

FIGURE 10. ALONG-TRACK COMPONENT

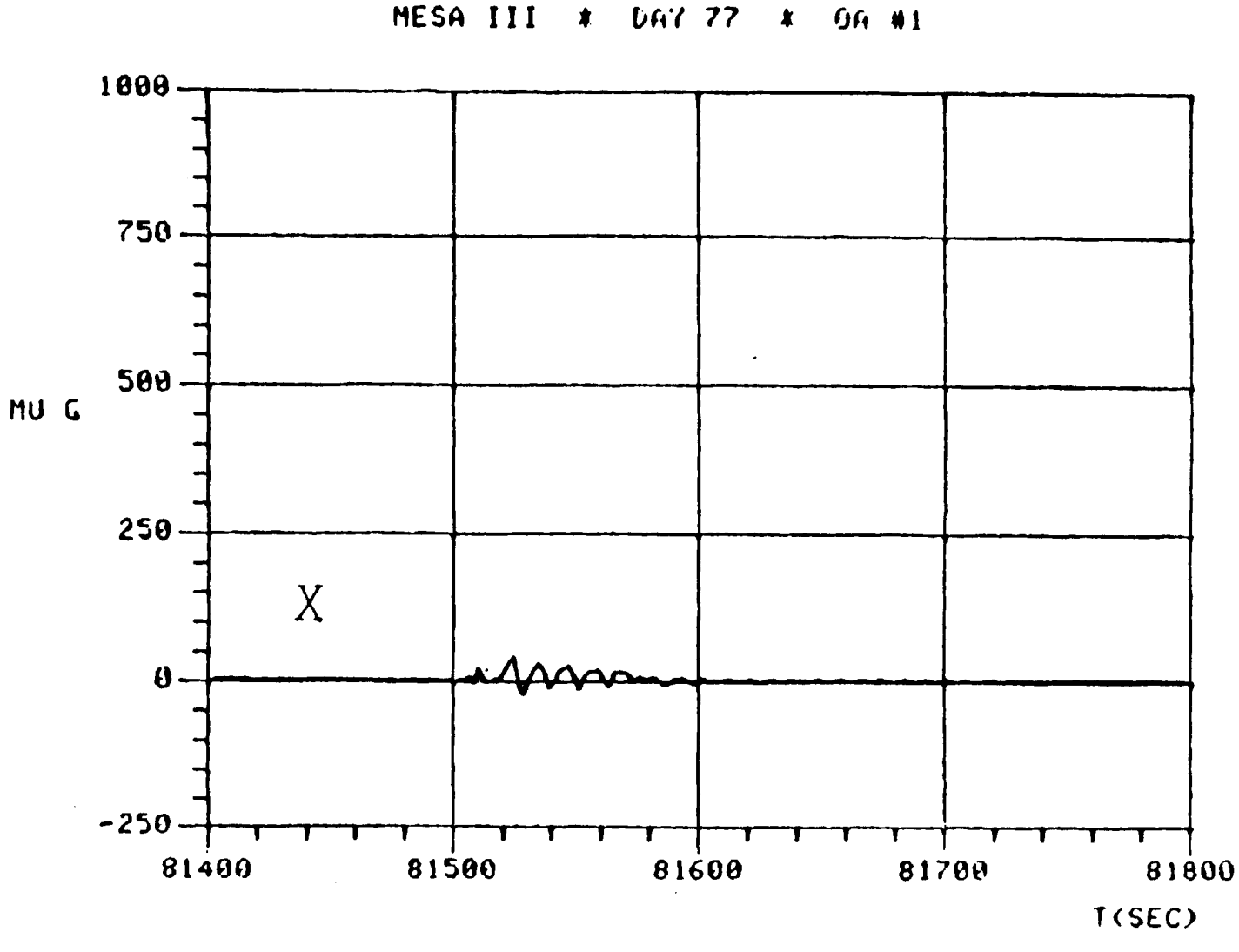

FIGURE 11. CROSS-TRACK COMPONENT

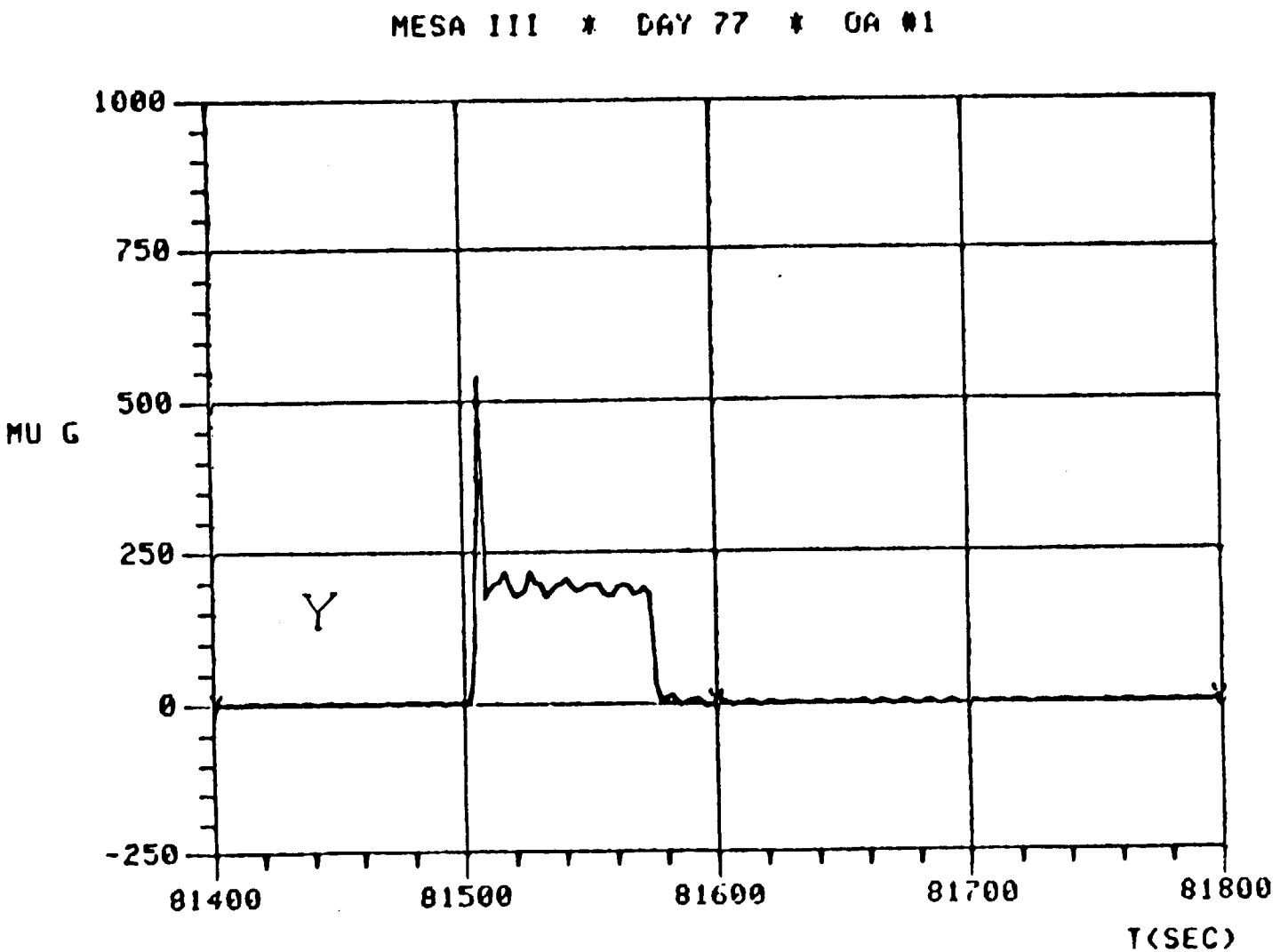

FIGURE 12. RADIAL

[SINGLE AXIS]	1958 - 1963	ESA, BASIC DEVELOPMENT (5)
	1963 - 1965	NASA LEWIS, FIRST FLIGHT SATURN 1B, JUNE 1966 (2)
	1964 - 1966	AIR FORCE, GENERAL DYNAMICS, CLASSIFIED (3)
	1966 - 1967	LOGACS (LMSC), FLOWN ON AGENA, APRIL 1967 (3)
	1966 - 1970	CANNONBALL/SPADES AFGL (12)
	1969 - 1970	MSFC, MASS ATTRACTION (1)
	1967 - 1968	SERT II, NASA LEWIS (2), ION ENGINE THRUST
	1968 - 1969	AF, MOL, GE, (9)
	1968 - 1969	PROJECT 110, LMSC, (7), ORBITAL DRAG MEASUREMENT.
	1970 - 1974	ATMOSPHERE EXPLORER SATELLITE AFGL/NASA, (9), AE-C 5 YEARS IN ORBIT.
	1975 - 1976	S73-5 AIR FORCE/BOEING SATELLITE, AFGL, AIR DENSITY (1).
	1978	ROCA, AFGL, (1), 90° ROTATING TABLE - SINGLE AXIS.
[THREE AXIS]	1978 - 1981	NAVPAC DMA/AFGL NAVIGATION AND AIR DENSITY (6)
	1979 - 1981	SL-3 MATERIAL PROCESSING (2) - FIRST SHUTTLE FLIGHT (2).
	1982 - 1984	S85-1 AIR FORCE - AIR DENSITY (1).
	1984 - 1986	OARE - NASA LANGLEY (1) WITH IN-ORBIT CALIBRATOR.
	1985 - 1986	CUBE - DEVELOPMENT - COMPANY SPONSORED.

FIGURE 13. ELECTROSTATIC ACCELEROMETER HISTORY

Material Processing in Space experiment; a wideband (50 hertz) instrument with an autoranging sampled data system was specified for this application. We are now working on a three-axis MESA for the OARE (Orbital Acceleration Research Experiment) for NASA/Langley; this MESA will be mounted in a centrifuge for veification of the calibration in orbit. As will be discussed in the next section, we are also developing a three-axes MESA with a cube proof mass.

6.0 *NEW DEVELOPMENTS*

An improved version of the MESA is now under development (see Figure 14). This new instrument uses a cube proof mass in place of the flanged cylinder, thus providing constrainment against six degrees of freedom instead of five. Elimination of the curved electrode and proof mass surfaces also results in equal performance in all three axes. A development model has been fabricated and testing will start in the near future.

The proof mass and electrode configuration is shown in Figure 15. The proof mass is a cube made of beryllium. Its outside dimensions are a nominal 0.5 inch, and the mass is one gram. Facing each of the six cube faces is a pair of electrodes. An electrode together with the corresponding electrode on the opposite face are used for the pickoff position and forcing functions in one of the six constrainment loops. Use of six pairs of electrodes in six constrainment loops provides constrainment against linear acceleration in three axes and against angular acceleration around three axes.

Figure 16 shows the force rebalance loop for the Y axis. The loops for the X and Z axes are identical. The Y output shown is the sum of the signals from the two constrainment loops; this output is proportional to Y axis linear acceleration. If the two constrainment loop outputs are differenced instead of summed, the resulting output will be proportional to the angular acceleration around the Z axis.

FEATURES:

- ELECTROSTATIC SUSPENSION IN 3 AXES
- PROOF MASS SYMMETRICAL IN ALL THREE AXES
- CONSTRAINED AGAINST 6 DEGREES OF FREEDOM (3 TRANSLATION, 3 ROTATION)
- MAY BE CALIBRATED IN 1G GROUND ENVIRONMENT
- SENSITIVITY GOAL IS 10^{-11}G
- PROOF MASS EXTREMELY RUGGED
- ORTHOGONAL ELECTRODES FOR MINIMUM CROSS COUPLING

FIGURE 14. 3 AXES CUBE PROOF MASS DEVELOPMENT

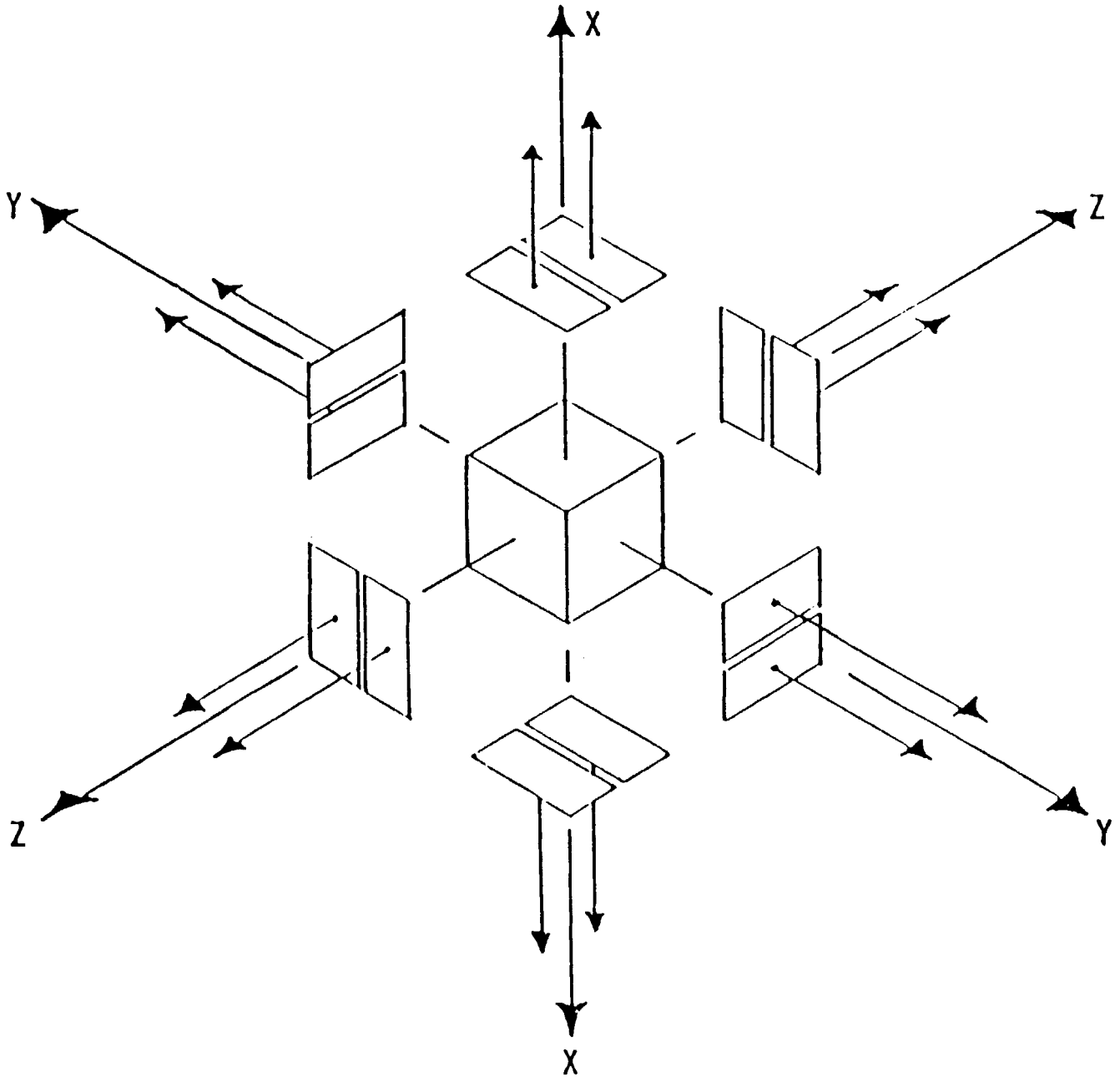

FIGURE 15. PROOF MASS AND ELECTRODE CONFIGURATION

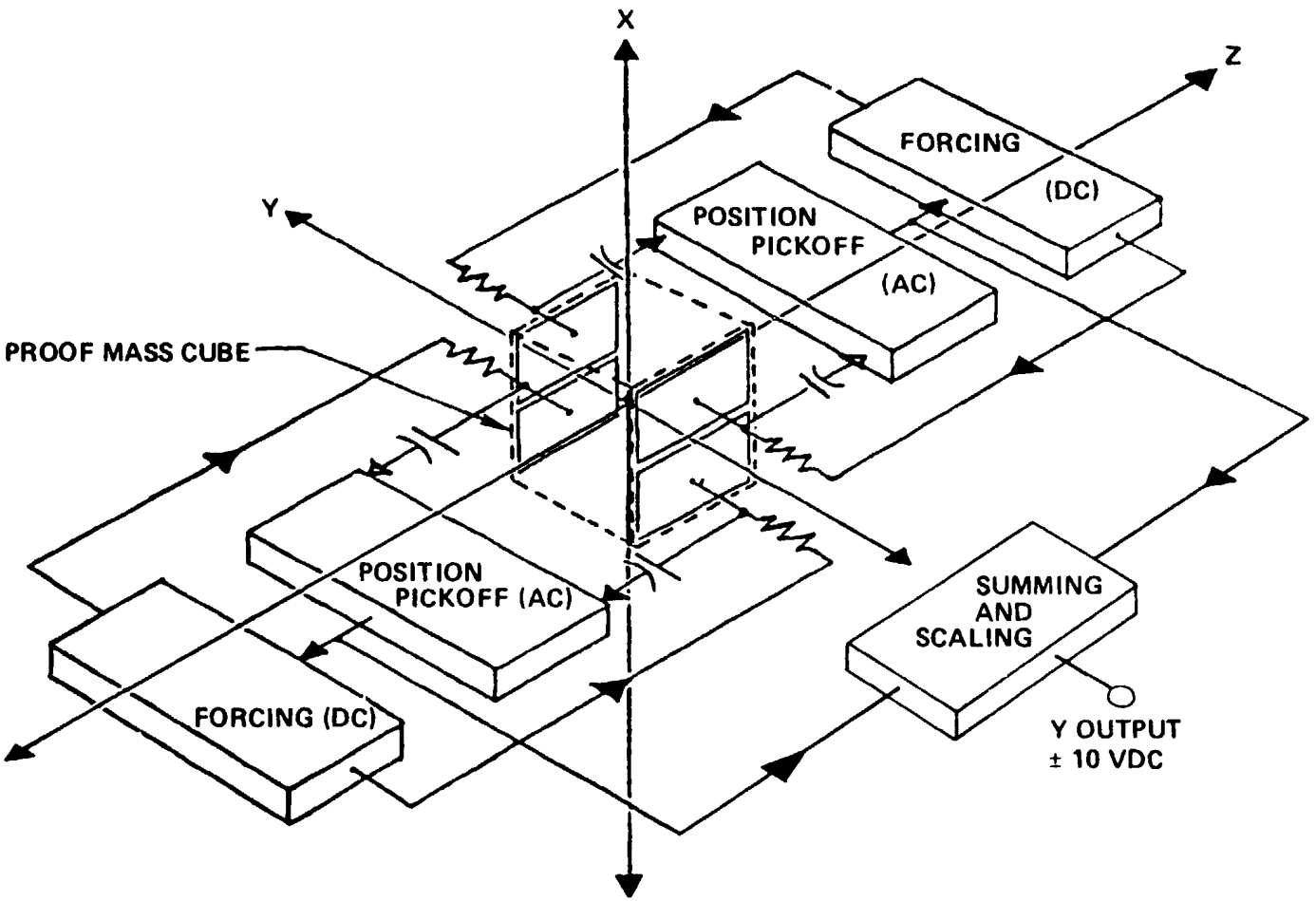

FIGURE 16. FORCE REBALANCE LOOPS (Y ONLY SHOWN)

The MESA cube proof mass mechanical assembly is shown in Figure 17. Each of the six identical electrode assemblies contains two electrodes which are insulated from each other and from the metal base by a ceramic insulator.

The gap between the electrodes and the proof mass is a nominal 0.002 inch and is maintained by the cylindrical-shaped cage into which all six electrode assemblies and the proof mass are assembled. The cage assembly fits inside the hermetically sealed hexagon-shaped housing, with the 12 electrode terminals exiting radially at both ends.

The six constrainment loop preamplifiers on individual p-c boards are attached to the external housing flats to provide short direct connections to the internal electrodes. The output of each preamplifier is at a low impedance and high signal level for connection to the rest of the constrainment loop electronics.

The instrument case has three mounting pads that are used to attach it to the vehicle structure at which the input acceleration is to be measured.

The case is hermetically sealed and filled with a mixture of 90% dry nitrogen and 10% helium to provide gas damping of the proof mass for stable constrainment loop operation, and to protect the proof mass during the unpowered high-g launch environment. The gas pressure is a nominal 1 atmosphere (15 psia).

Preliminary specifications for the Cube Proof mass MESA are given below.

Preliminary MESA - Cube Specifications

Type	Three Axis - Cube Proof Mass
Size	3.5 in. x 5 in. x 9 in.
Weight	5 lb
Power	9 Watts

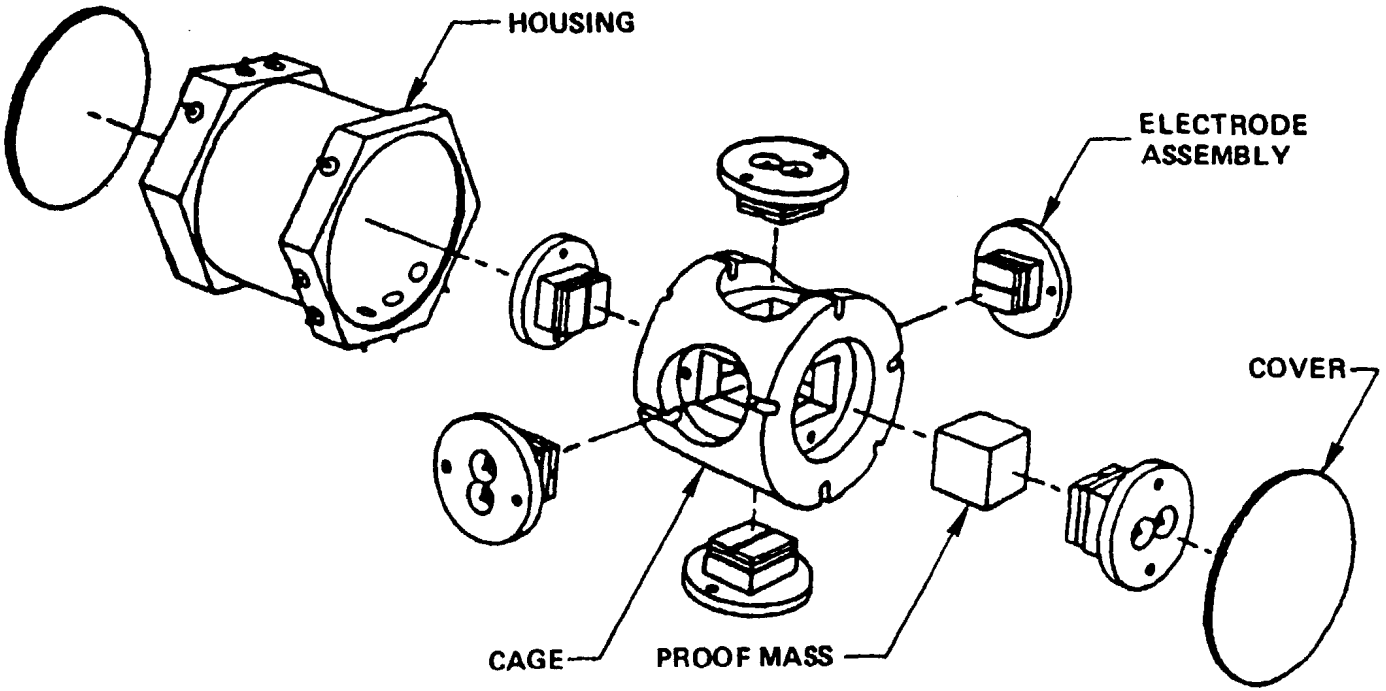

FIGURE 17. MESA CUBE PROOF MASS MECHANICAL ASSEMBLY

Sensitivity	10^{-9} g
+ Full Scale (Lowest Range)	10^{-5} g
+ Full Scale (Highest Range)	10^{-2} g
Scale Factor Accuracy	
Gnd Test Cal.	0.5%
On Orbit Cal.	0.05%
Output	$\pm$10 Vdc = $\pm$ Full Scale, all ranges
Ranges Available	3 from 10^{-2} to 10^{-5}
Environment:	
(Nonoperating)	
Temperature:	-25°F to +185°F
Shock:	50g, 8 msec, 3 axes
Vibration:	Sine: 20 to 2000 Hz 10 g's Random: 20 to 2000 Hz 20 g's rms Pyro: 6000 g's
Acceleration:	15g, 3 axes
Altitude:	Space
(Operating)	
Temperature:	-10°F to +160°F
Altitude:	Space

7.0 APPLICATION ENGINEERING

Potential users of low-g accelerometers always face the obvious problem of matching requirements against available instruments. This task is usually complicated by two factors:

1. Lack of precise knowledge of all the environmental and acceleration inputs which the instrument is expected to experience throughout its life, and

2. Lack of precise definition by the accelerometer manufacturer of all its characteristics and performance in terms that match each user requirement.

The questions that the user should ask himself in attempting to select an accelerometer generally fall into the following categories:

1. Maximum available power, weight, and size?
2. Single-axis or 3-axis sensing?
3. Range of input acceleration expected?
4. Maximum frequency of input acceleration to be measured?
5. Accuracy required?
6. Command and data interface requirements?
7. Environmental conditions such as temperature range, launch acceleration, pyro shock, electromagnetic interference levels, etc.
8. Delivery schedule and rate?
9. Dollar budget?

The accelerometer manufacturer, on the other hand, must characterize the instrument in these terms plus present possible options to each requirement that may be considered to accomplish the measurement in the most efficient manner.

Some available options are described in general terms. Precise electrical interface circuits involving data rates, voltage levels, impedances, etc. must be customized for each application.

Typical applications in which these instruments have been used or could be used are:

- Ion engine thrust measurement
- Air Density
- Solar Pressure
- Navigation and Guidance
- Fuel Venting Accelerations
- Mass Attraction
- Gravity Gradient
- Attitude Control
- Vehicle Acceleration Monitoring
- Vehicle Angular Acceleration.

A single package containing the mechanical instrument assembly and its associated electrostatic force rebalance constrainment loops represents the minimum hardware that can be purchased.

Various accessories are available which may be added to this basic hardware to perform a variety of functions. These generally fall into the six major categories listed below.

1. Power input conditioning
2. Signal output conditioning
3. Multiple ranges
4. Temperature control
5. In-flight calibration
6. Special packaging.

Power Input Conditioning

This converts any available input voltage to the voltages required to operate the constrainment loops. Total conditioning would normally include an EMI filter on the input line, a regulator, and a transformer coupled dc to dc converter followed by the normal power supply filter for each of the five dc voltages required.

Signal Output Conditioning

This converts the normal $\pm$10 Vdc voltages which represent $\pm$ full scale to the desired output voltage and impedance level. It can also convert the dc output to a serial digital data stream and filter and average the output either in analog or digital form.

Multiple Ranges

The constrainment loops may be switched to set full scale input limits at three different levels or ranges. Range selection may be by external command or by an internal autorange circuit. The latter will automatically adjust each axis to the appropriate scale required to accommodate the input acceleration level experienced at that particular time.

Temperature Control

This maintains the accelerometer case within $\pm 1^{\circ}F$ of a pre-set temperature. It is normally used if the environmental temperature range is large and scale factor temperature coefficients established during calibration cannot be used to correct the output data.

In-Orbit Calibration

This should be considered where the full scales selected may be lower than permitted by ground calibration. An alternative is to use higher scales to permit ground calibration and utilize a longer averaging time per data point to obtain the required resolution and sensitivity.

Special Packaging

The accelerometer may be packaged in various form factors. The instrument and its attached preamplifiers, if packaged separately, would occupy a box-shaped volume with dimensions of 3.5 in. x 4 in. x 4 in.

The instrument loop electronics, if packaged separately, is 3.5 in. x 5 in. x 6 in.

If combined in a single package, the total volume is slightly less, as shown on the specification sheets.

If packaged separately, the constrainment loop electronics should not be more than 10 inches from the instrument package. The accessory circuits described in the above six paragraphs may be located up to 48 inches from the constrainment loop electronics.

A single package configuration is always the most efficient from the standpoint of cost, volume, and performance.

N91-12414

15. A NEW ACCELEROMETER RECORDING SYSTEM FOR SHUTTLE USE

Dr. Byron Lichtenberg, Payload Systems, Inc.

ABSTRACT

Microgravity investigators are interested in enhancing the capabilities and improving the information return from accelerometers used in microgravity research. In addition to improving the accelerometer sensors, efforts should be directed towards using recent advances in microprocessor technology and system design techniques to improve:

a) Sensor calibration and temperature compensation;
b) Online data display and analysis;
c) Data reduction and information storage.

Results from the above areas of investigation should be combined in an integrated design for a spaceflight microgravity accelerometer package.

Good morning, thank you, it's nice to be here. I appreciate the opportunity to come and talk to all of you. As Dan said, we are not quite developing a new accelerometer, we are really developing an accelerometer data processing and recording system, which you are going to see in just a minute. It stemmed from some of our experiences on Spacelab 1 and some of the experiences that a lot of you have had out there in trying to get timely processed accelerometer data from the space shuttle, and from your experiments as well, and trying to figure out how to correlate these to particular operations that went on during experiment. We are going to talk about a system called Python. For all you NASA people, don't try to figure out what that stands for because it's not an acronym, it's just a name. Python is a microgravity accelerometer system made up of a variety of parts. Figure 1 shows a list of some of the design goals that we set for ourselves when we tried to put it together.

- Designed for use on the space shuttle.
- High performance accelerometers with temperature compensation to measure 1 micro-g in three orthogonal axes.
- Detachable sensor head allows micro-g acceleration measurements at the experiment location.
- Spaceflight-qualified version available which fits inside a middeck locker.
- Stand-alone system significantly reduces shuttle interface documentation and verification, and permits software refinements until shortly before launch.
- Removable high capacity data storage cassettes retain data during mission and allow early postflight data retrieval.
- Downlink data transmission capability.
- User-friendly system minimizes training time.
- Modular structure allows customization for a wide range of experiment requirements.
- Fully supported through mission integration and flight by PSI space experiment engineering personnel

FIGURE 1. PYTHON MICROGRAVITY ACCELEROMETER SYSTEM

First, it is designed for use on space shuttle, although that does not preclude use on the space station or free-flyers; it was designed initially for crew attended use on the shuttle. There will be a space flight qualified version because all the pieces we have used here have been flown or are going to fly and are space flight qualified. Because I'm a user, we wanted to make sure it's user friendly --that helps you understand how it works; it is easier for training people that use it, and for making changes and modifications. It has a detachable sensor head because we initially targeted this for the middeck, or spacelab module experiments (indoor sports where people are doing a lot of different experiments). It is a stand-alone system which significantly reduces interaction with the shuttle general purpose computers or the spacelab computer. This means you can do late software development and make late changes in your equipment just prior to flight, carry a small micro floppy disc and run your software without having to worry about going through all the extensive shuttle and spacelab verification procedures. We incorporated a data storage system, which is a magnetic tape cartridge system so that you can bring your data back immediately after flight. We will have downlink data transmission capability through the shuttle or spacelab, and Figure 2 shows what led us to doing this. The problem that we saw early on is that there is no available system now that can be used to control experiments, and that can be used on a variety of experiments with generic equipment. Also, there is no flight-certified data acquisition and display system that stands alone. A lot of systems do data acquisition, data storage, or downklink but there isn't one unified system that allows the crew to take a look at processed data during the flight. As I said before, we want to stay away from the Shuttle GPC and spacelab computers because of their limited availability, limited resources and capabilities as well as the difficult problem of interfacing with them.

When we take that process and apply it to our problem today, which is materials science and accelerometer and acceleration measurements, a little background is in order. There have been a lot of different systems developed to measure acceleration in the micro-g or

THERE IS NO AVAILABLE SYSTEM TO CONTROL SPACE EXPERIMENTS THAT CAN BE USED BY A VARIETY OF DISCIPLINES THROUGH CUSTOMIZATION OF A GENERIC GROUP OF EQUIPMENT.

THERE IS NO FLIGHT-CERTIFIED DATA ACQUISITION AND HANDLING SYSTEM THAT ENABLES REAL OR NEAR REAL-TIME PROCESSING AND DISPLAY THAT IS INDEPENDENT OF THE SHUTTLE OR SPACELAB COMPUTERS - BOTH OF WHICH ARE EITHER LIMITED IN THEIR PERFORMANCE OR ACCESSIBILITY AND REQUIRE EXTENSIVE INTERFACE VERIFICATION.

FIGURE 2. PROBLEM STATEMENT

milli-g ranges, but all of them have their own internal accelerometers that are not available to the users. The user has to rely on someone else's data. Remember we heard yesterday that some of the ASIP and HIRAP measurements were taken near the center of the mass of the vehicle and do not necessarily correspond to what a particular experiment might see if it is located, for example, in the middeck. So, a lot of these users develop their own systems and that leads to a lot of expense, or unnecessary duplication.

Somtimes they have an inappropriate bandwidth. As Dr. Hamacher mentioned yesterday, his scheme was to sample the peak acceleration during any one second, but he can't really reconstruct any time history from that. All he can do is put an envelope around the maximum acceleration values.

Another problem is that it takes a long time to get data back. Some of the materials science experimenters on Spacelab 1 and 2 waited over a year to get their reduced data.

Python is a modular, generic system that relies on commercially available equipment. It is built around a bus system with a user interface computer (we are using a GRiD case III, which I have here and will talk about later). We are using an STD bus so we have a distributed system that allows user interactive and iterative design. We can support a variety of sensors; we are not locked to any one accelerometer or thermocouple or other type of sensor. We are designing it for science and engineering applications, not for safety of flight or reliability issues, so we think we can push NASA a little bit in their flight qualification. Everything that we are using now has been flight-certified or flight-qualified or there is a version that's flown, so we are not looking at the tremendous problem of flight qualification. We want to stress the fact that this is not a safety-of-flight type of equipment and, therefore, we should be able to use more state-of-the-art equipment.

As I said, we use the STD bus modules and the STD system, which are widely commercially available. We do have customized software modules available to do a variety of things and we are concentrating on

distributed processors. As shown in Figure 3, our design philosphy is reverse from some of the other programs. We feel that now most hardware is really cheap, it's the custom-developed software that is much more expensive, so our philosophy is to separate these functions. Our data acquisition, data processing, and data handling systems design should be able to accommodate most hardware. We are not locked into any particular chip or particular system. We are trying to move beyond portable software, which in the past has been transferable from one machine to another. We did some software development that runs on a Compaq or IBM AT and they run without modification on the briefcase GRiD machine. This system is able to support different levels of hardware without being locked into any one system, as shown by the three goals on the bottom of Figure 3. We are going to do verification and validation on individual system elements such as plug-in modules, which makes it easier to customize to individual user needs.

Figure 4 shows some of the system elements that we are proposing for our Python system. The heart of the system is the STD data acquisition and control system that includes generic accelerometers, generic data storage devices, a generic user interface computer, and downlink interface.

For accelerometers, Sundstrand QA-2000's are the initial choice; because we feel that they have the best performance/cost ratio, as well as good power, weight, volume, frequency characteristics, and g-sensitivity. I'm not here to sell Sundstrands; if somebody wants to donate some MESAs, we can accommodate them. But if we are going to do our own development, then the Sundstrands look pretty good. Figure 5 shows some of the accelerometer characteristics on which we based our decision. The resolution accuracy that is claimed for the Sundstrand is 1 micro-g, and that is probably good enough for what we are doing on the shuttle or on the space station for quite awhile. It has good long-term stability, and they judiciously pick their accelerometers and test them so that they are well characterized in terms of the thermal characteristics. Sundstrand has a 4th order model that gives some idea of the histories of the temperature dependence of dc offset and thermal bias coeffici-

1. Hardware is cheap: separate functions.

2. Today's system design should be able to accommodate tomorrow's hardware.

3. Beyond portable software.

Easy to change system elements to achieve better performance

Easy to verify/validate individual system elements

Easy to customize system to each user's needs

FIGURE 3. PYTHON DESIGN PHILOSOPHY

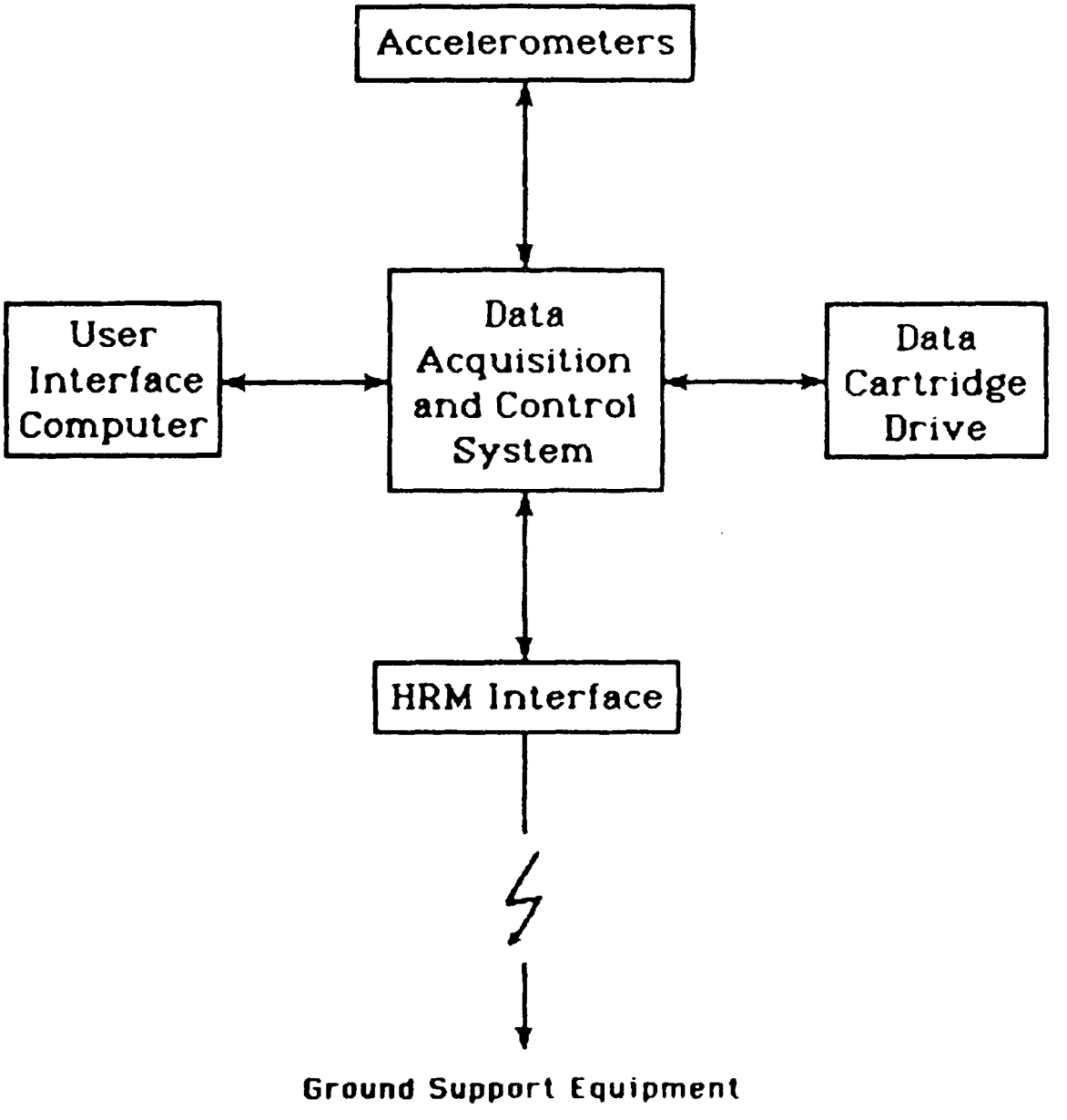

FIGURE 4. DATA ACQUISITION UNIT SYSTEM BLOCK DIAGRAM

INDEPENDENT OF PYTHON BUT CURRENT SPECIFICATIONS BASED ON SUNDSTRAND QA-2000

LOW POWER

LIGHTWEIGHT

HIGH PERFORMANCE TO COST RATIO

HIGH PERFORMANCE SERVO DESIGN

- RESOLUTION AND ACCURACY BETTER THAN 1 MICRO-G
- LONG TERM STABILITY OF DC BIAS, SCALE FACTORS, AND TEMPERATURE DEPENDENCE
- THERMAL CHARACTERISTICS WELL MODELLED AND DOCUMENTED
- SPACE FLIGHT CERTIFIED

FIGURE 5. ACCELERATION SENSORS

ents. So we can put those models into our system on the bus and do a real-time version of that data. Also, the QA-2000 sensors are already space-qualified.

The data acquisition and control systems and STD bus system were chosen from the large amount of commercially available equipment that works. There are CPU boards, memory boards, A/D boards, thermocouple boards, D/A boards, and open architecture boards available. Also, the small size means a low form factor so it's much smaller than some of the other busses that you might be familiar with. It is flexible enough to accommodate new processor chips and a new 19- or 20-bit A/D that's going to be available. There are also a lot of chips available in CMOS for low-power consumption and radiation protection. As I said before, our user interface computer is based on a GRiD case that was chosen because it is IBM compatible, and previous GRiD hardware has flown on the Shuttle. The GRiD case is now being certified for flight on the IML mission. We feel good about that but, as another example, if Hewlett-Packard or any other manufacturer gave us a certified lap top, we would not be against using their machine either.

For mass storage we are looking at a 3M data cartridge drive system, a version of which has already flown and has the ability to store 67 megabytes of data. It is a small cassette type of cartridge that you could put in your shirt pocket and bring home.

Figure 6 gives you an idea of how much recording time there is on one cassette. This is based on a 12-bit A/D word, three-channels of sample acceleration data, and 67-Mbyte capacity on the tape. We can change the sampling rates depending on what frequency ranges one is interested in. For example, a kilohertz sample rate in each channel gives 3¼ hours of continuous recording, before it is necessary to change the tape. At 200 Hz, you can get 16 hours of recording time, and if you only use 20 Hz bandwidth to get the 17-Hz signal of interest, you can go 163 hours (or nearly 7 days). If you want to run at the higher sampling rates, just bring several cassettes on board and have a crew member change them once every eight hours or so.

BASED ON A 12 BIT WORD, 3 CHANNELS OF SAMPLED DATA, 67 MBYTE CAPACITY

SAMPLING RATE	CONTINUOUS RECORDING
1 kHZ	3.25 hours
200 Hz	16.3 hours
20 Hz	6.8 days
1 Hz	136 days

FIGURE 6. CONTINUOUS RECORDING TIMES

Our Python system can simultaneously sample all the channels of data. Right now we are assuming three channels of acceleration (X, Y, Z) but more can be added. Each A/D board has eight differential inputs so one board can handle many more channels than the current baseline configuration.

We are using an interesting overlap scheme to get both dynamic range and resolution. By using two analog-to-digital converters per channel, we can get not only the dynamic range we want (which is a micro-g up to 1 g) but also the resolution in the vernier range, which is a micro g. It depends on how you scale the analog signal for the wide-scale range. If we have 1 micro-g resolution with a 12-bit A/D converter, we cover the range from 0 to $\pm$ 2 milli-g's. If we have a ½ milli-g/bit resolution on the high-range scale, we have an overlap. The wide range scale goes from ½ milli-g up to $\pm$1 g, at ½ milli-g resolution. You could change this to ¼ milli-g resolution to cover the range ¼ milli-g to $\pm$½ g.

We can simultaneously do digital filtering from 0 to 400 Hz because that looks like the frequency range of interest but that is also flexible. We can do on-line temperature compensation with stored models of the hysteresis curves. We can do dc offset corrections by letting the instrument float freely in the module for several seconds and as we have heard, the free-floating time before wall contact should last several seconds. In a confined space in the module or middeck of the orbiter, we can get less than 1 micro-g, and then use that as our dc offset with stored models of the hysteresis curves. We can also take measurements before and after the experiment to get a good idea of what happens to the sensor drift during a several day experiment.

Python can do Fourier transforms from the instrument coordinates to any experiment coordinates. People talk about power spectral densities and using fast Fourier transform algorithms. We can actually set up several different ranges so we can cover the low frequency range by taking long sampling periods of data and averaging points together. We can simultaneously do higher frequency FFT transforms as well.

We feel it is important, as Bob Naumann thought yesterday, to detect acceleration events. These are events that have an acceleration value above a user-set threshold. The goal is to measure the onset time of some excursion above the threshold, the peak acceleration, the time that the acceleration fell below the threshold, and the integrated value (the area under the curve). This gives a measure of the energy in the signal. This processing can be done simultaneously with FFTs and long-term running averages of acceleration.

We can also transfer data to the ground through the shuttle or the spacelab. We can display data to the crew members. Dr. Hamacher said yesterday that crew training can help in reducing the noise acceleration levels on board. Well, we feel this might be true, but if the crew has some feedback of acceleration, which they haven't had so far in real time, they can watch the values while they do a maneuver, or slam a door shut and see the effects of it right there. You can have a voice log so that it's all very nicely time-coordinated in one package. This can be with the full range of capabilities to command and control a variety of experiments in the indoor spaces.

The displays, commands, and controls can be used to alert crew members to off-nominal situations, give them access to the equipment, and let them take a look at the recorded data so that they can make real-time decisions about whether or not to be concerned. I certainly endorse the philosophy that if there are more scientists up there, they can truly assess the quality of data, not do data analysis on board, but take a look at it and see whether or not they want to change something.

Figure 7 shows a blow-up of the GRiD display. We decided to use a Lotus 1-2-3 type of menu across the top of the screen. We have a variety of commands to set A/D rates, stop A/D conversion, or exit back to a main menu. For example, if we were setting up an A/D rate we would set it in hertz, and the input shown in Figure 7 is 1,000 Hz. The tape and the time are self-explanatory, the data are time-tagged on the headers. We also have some digital data on the display that show the X,Y,Z axes of time-averaged RMS values. You can pick a time, say 10

Screen Display

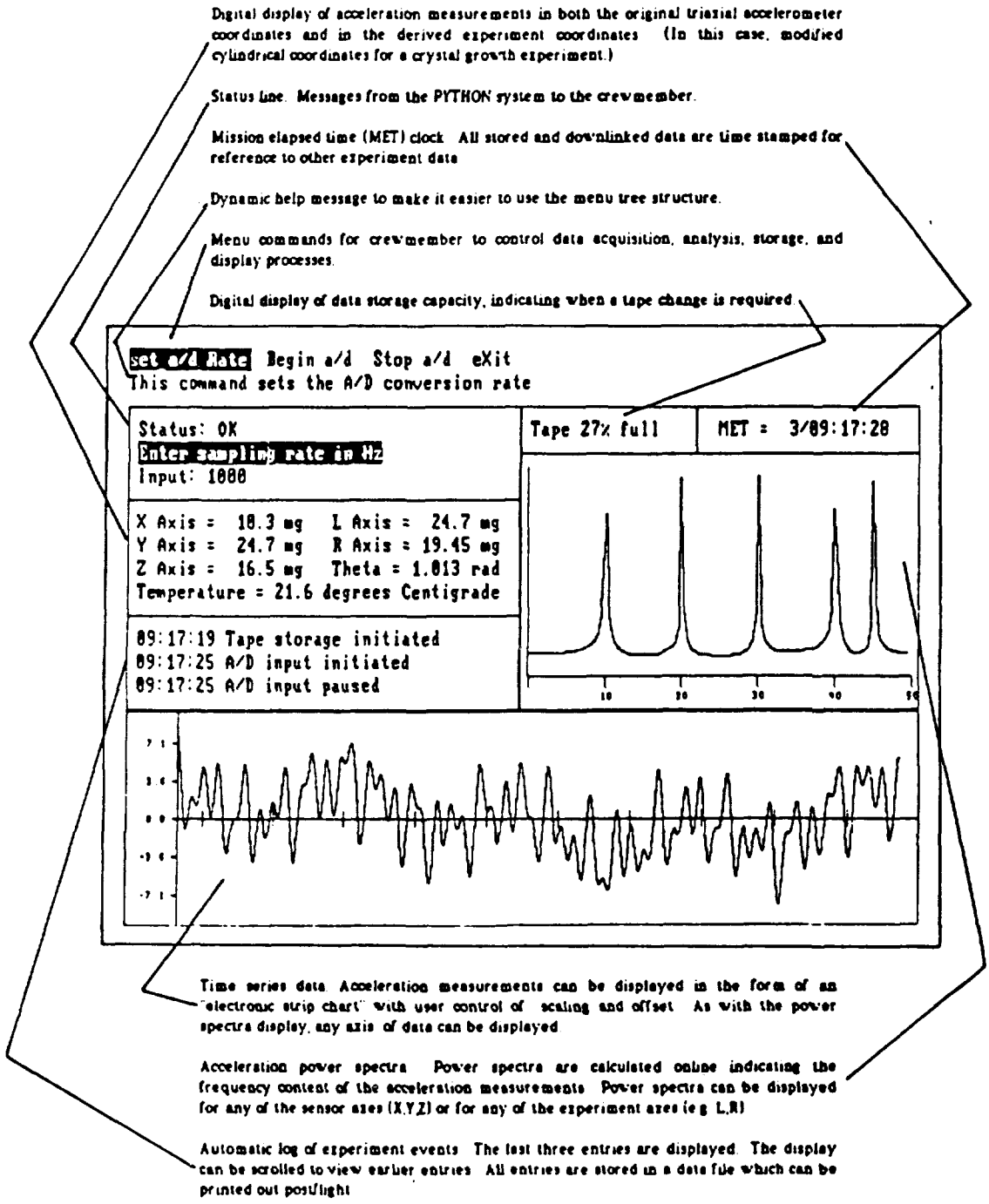

FIGURE 7. SCREEN DISPLAY

sec, and do an RMS so that once every 10 sec these quasi-steady dc values are updated. The temperature of the accelerometer package is used for temperature compensation. Those are examples of changes you can make. We have a log that gives you the time tag and what the commands were. It allows you to record the acceleration events as well and correlate them with the log.

Python can display other axes of data also, because it's not always true that your accelerometer axes (X,Y,Z) are appropriate to the experiment. Figure 7 shows cylindrical coordinates that could be appropriate if you're growing a crystal with a Bridgman technique, where you want longitudinal and radial acceleration.

Figure 7 also shows a quasi-random generated noise, some sine signal, and time axis data, but basically raw accelerometer data, with appropriate scaling. We also have the ability to have coprocessor chips on the bus system to do Fourier transforms. Figure 7 shows power spectral densities as well.

We are trying to put together a system that is flexible, customizable, useful, and gives you data the way you need it, when you need it, which is at the time the experiment is being conducted. We think our Python system has met the goals that we set for it, as shown in Figure 3. Again, just to recap, it was developed for manual use on the shuttle and space station. We have a space-qualified version that will be available. It is user-friendly with menu systems and custom software. Basing it on modular structure, we can swap components. We have disk drives so you can bring up your software at the last minute if you want one of the crew members to carry the disk in a shirt pocket. Python features a detachable sensor head, with the accelerometer of your choice or, if you trust us, our choice. And it is a stand-alone system so that we can reduce the verification and software integration requirements with the orbiter or space station. We have high-capacity data storage as well as data downlink transmission capability to all of you. The downlink transmission can be either the raw data, or the processed data. You can have a very low bit rate stream going down, which will give you just power spectral densities and maybe a 10-sec quasi-dc acceleration level.

Question: How do you get your data to downlink? I didn't know there were any wires from the shuttle middeck lockers.

Lichtenberg: The question was, how do you get your data down from the middeck? There are several ways. What we would prefer to do is use the payload data interleaver system, which will take data streams up to something like 44 kbits/sec, and downlink that. You can go through flex MDMs if you want also.

Question: Do you have hard wiring in the middeck lockers to do that?

Lichtenberg: Yes, there are some signal panels up in the payload specialist's compartment in the aft flight deck area, and I believe there have been wires for the continuous flow electrophoresis system that have been put in there that we could use. We end up going through the payload specialist station up in the middeck.

Ulf Merbold, ESA/ESTEC: One of the, I think, most important advantages of spacelab is the capability to do all the experiments interactively with the ground. How would you then hook that system into the data acquisition system on the Shuttle?

Lichtenberg: Okay, for the Spacelab, you're absolutely right. The question was, that the major advantage of doing crew-attended manned operations in Spacelab or the Shuttle is the ability to do things interactively with the ground so that you certainly want to be able to have these data down on the ground. Going in Spacelab it's very easy to get a dedicated port to the high-rate multiplexer with this, and, depending on what data streams you want to see, you can either set it up as a fairly low rate signal, in the range of tens of kilobits per second, or if you want to get all the data down you can go a little bit higher and have the raw data come down through a dedicated HRM port. So there's several different ways of doing it. It's our intention to allow that capability to get data down either from the module or from the middeck-type experiments.

Question: How can you synchronize your system with the shuttle or other accelerometers?

Lichtenberg: We have a question about how we can synchronize our system with the shuttle system or other accelerometers. We can do the time set function, and our feeling is we can get probably to within a tenth of a second. If you need it more than that, there are ways of pulling off the UTC, universal time, coming from the Orbiter, so that you can get a time code input. Our feeling was that somewhere less than a second of having a crew member input the GMT, or MET, into the computer when we start out will be good enough, at least it's going to get you in the ball park within one-half to one second.

Bob Naumann, NASA/MSFC: What does the system sell for now?

Lichtenberg: What does the system sell for? That's a good question. We have several systems. We have a ground-based version, and that would probably not consist of the GRiD because you can use an IBM, Compaq, or an AT or whatever, AT&T 6300, any IBM-compatible can be used, so we would put the ground-based system together and it's hard to come up with a price because we're not sure what you want.

Naumann: How about for the flight-qualified version?

Lichtenberg: Again, a little bit depends on what you want, but I can tell you that it certainly is going to be much less than the 1½, 2 million dollars that CDC is going to charge for their new little CMOS space flight computer, and we have data storage and also data displays. Much, much less than that.

Naumann: If your sample rate is high enough to reproduce the actual acceleration of the sample accelerometers, then you could conceivably average that and display a time-average up there if the user selects the right constants, is that correct?

Lichtenberg: The question was, it seems that our sampling rates are high enough that we can get an accurate reconstruction of the raw data and then do processing on it to do time averages and things, and that's exactly correct, Bob. We can set the A-to-D sampling rates. We figure that, probably something like a 200-Hz sampling rate is reasonable, that'll give you a reconstruction of at least 100 Hz or

below, so you're below the Nyquist frequency, but again it is settable, so if you have a very high vibration signal that you want to analyze, you can set the A-to-D rates at say 1,000 Hz and use a whole range of accelerometers. The Sundstrands are good to something like 600 Hz.

Question: Have you actually done that and shown that one can take all this grass, this noise, and actually time-average it and get zero?

Lichtenberg: Okay. Good question. No, we haven't done that yet. We're still in the process of developing the software.

Naumann: This is our big problem. The accelerometers are certainly sensitive enough, but when you try to time-average to get an average dc level, which is what most experimenters want, you get nonsense out. So it's kind of like trying to track a microvolt signal when you have millivolt noise.

Lichtenberg: The question is about the ability to take the data and to analyze as we're talking about, which is to have a fairly rapidly timed signal and to obtain a good average of it. RMS values seem like a pretty good way of doing it.

Ravindra Lal, Alabama A&M: Can the instrument take more than one sensor by a switch? Can the system take more than one sensor?

Lichtenberg: Oh, yes, can the system take more than one sensor? Yes. The STD bus cage that we're using has the ability to handle something like 8 to 10 cards. An individual A-to-D card, analog to digital card, can handle eight different signals. So you can stack up something like 80 different sensors without much of a problem at all. And what we would plan to do is to have distributed processing out there so we'd have some CPUs out in the bus that can do these dedicated tasks and then just bring the data in to display it on the user interface computer.

N91-12415

16. NEW ACCELEROMETERS UNDER DEVELOPMENT

Dr. Jerry Wald and Dr. M. Tehrani
Honeywell Systems and Research Center

ABSTRACT

The commercial viability of the Space Station requires that it provide a micro-g, or submicro-g environment to users. This represents significant improvement over existing systems.

Attainment of the lowest micro-g levels requires isolation systems. Passive and active systems have been evaluated. Best performance is achieved using active approaches where accelerometer sensors close feedback loops. Available accelerometers are reviewed elsewhere in this workshop. Two emerging accelerometer technologies are presented that have promise for meeting performance goals while achieving reductions of package size, weight, and power. The technologies addressed are Honeywell's design concept for an optical cavity locking accelerometer and the recent development of an integrated silicon accelerometer for government applications.

I. INTRODUCTION

NASA has asked its Space Station Work Package 2 contractor to evaluate the Space Station accommodation of acceleration environments needed for (1) scientific research, including materials processing in space (MPS) and life sciences; (2) engineering research and development of MPS, commercial preproduction scale-up of MPS and; (3) commercial production of material products. Mission data developed at the second Hampton Workshop showed science and commercial requirements for 10^{-5}g. Subsequent analyses showed, first, a need for 10^{-6}g or better, and second, that previous spacecraft (including Skylab, Shuttle, Spacelab, Soyuz) provided better performance than initial Space Station configurations because experiments are or were conducted close to the vehicles'

centers of gravity. These findings resulted in new analyses to assess the impact of payloads requiring $\leq 10^{-6}$g for extended periods on Space Station design.

II. ANALYSES AND RESULTS

NASA required that three options be addressed. The options are summarized in Table 1.

MPS requirements (including microgravity and cycle time requirements), MPS tolerance to accelerations and effects of disturbance sources have been investigated to determine if the NASA options can be met. Representative microgravity requirements related to processes are shown in Figure 1.

Acceleration responses for disturbance sources were analyzed and characterized, including crew motion, coarse pointing system and docking. Crew disturbance transfer functions were investigated. In addition, events, such as MRMS operation, reboost, and steady-state orbital effects, were considered. Typical disturbance envelopes appear in Figure 2. Based on the analyses performed, achievement of 10^{-5}g is limited by reboost and berthing operations and by crew motion; 10^{-6}g by venting, plume impingement, module placement and CG excursions; 10^{-7} by aerodynamics, air flow and sensor/servo errors. It has been concluded, however, that the micro-g environment looks achievable for extended time periods between major Space Station operation (e.g., docking, reboost, MRMS) if a mission equipment isolation system is used. One-tenth of a micro-g may be possible, but this will require tight center-of-gravity control, restrict scheduling to quiet sun periods or require continuous low thrust, restricts crew exercise for short periods, and requires a low-frequency isolation system.

The design of the isolator is influenced by power transfer methods and their associated restraint gradients. Analysis of isolation options show that the NASA requirements may be met using active and passive isolators to varying degrees. An ideal active isolator can

TABLE 1. SSP MICROGRAVITY MISSION REQUIREMENTS OPTIONS

DESIGN OPTIMIZATION: MICROGRAVITY MISSION ACCOMMODATION				
OPTIONS:	CORE SS VECTORIAL RESULTANT* MAXIMUM ACCELERATION LEVELS AT APPLICABLE EXPERIMENTS, MISSION PAYLOADS AND MTL			PERIOD OF DURATION AND NUMBER OF PERIODS
1.	10^{-5} G_o AS CURRENTLY STATED IN PDRD			30 DAYS MINIMUM
2.	10^{-6} G_o	0	$H_z < F < 0.032$ H_z	TARGET OF 9 PERIODS PER YR
	$\frac{10^{-5} G_o F}{0.32 \text{ Hz}}$	0.032	$H_z < F < 3.2$ H_z	
	$\frac{10^{-4} G_o F^2}{(3.2 H_z)^2}$	3.2	$H_z < F$	
3.	10^{-7} G_o	0	$H_z < F < 0.032$ H_z	90 MINUTES MINIMUM
	$\frac{10^{-6} G_o F}{0.32 H_z}$	0.032	$H_z < F < 3.2$ H_z	TARGET OF 18 PERIODS PER YR
	$\frac{10^{-5} G_o F^2}{(3.2 H_z)^2}$	3.2	$H_z < F$	

* THE VECTORIAL RESULTANT INCLUDES DRAG, GRAVITY GRADIENTS, ORBITAL LVLH FLIGHT, STATION MANEUVERS, PERIODIC/NON-PERIODIC DISTURBANCES, AND RESONANCES.

F = FREQUENCY

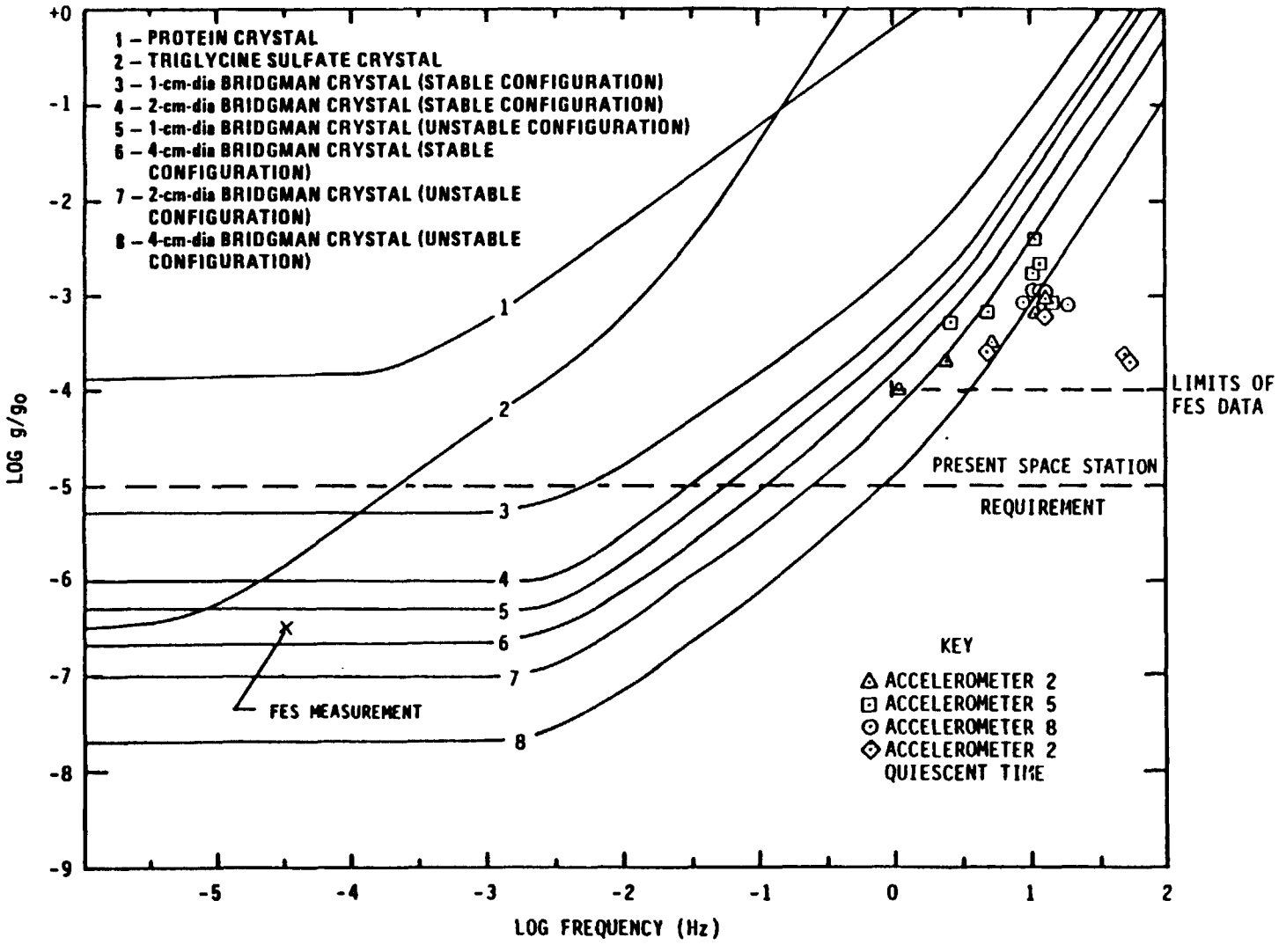

FIGURE 1. EXAMPLE MICROGRAVITY REQUIREMENTS RELATED TO PROCESS

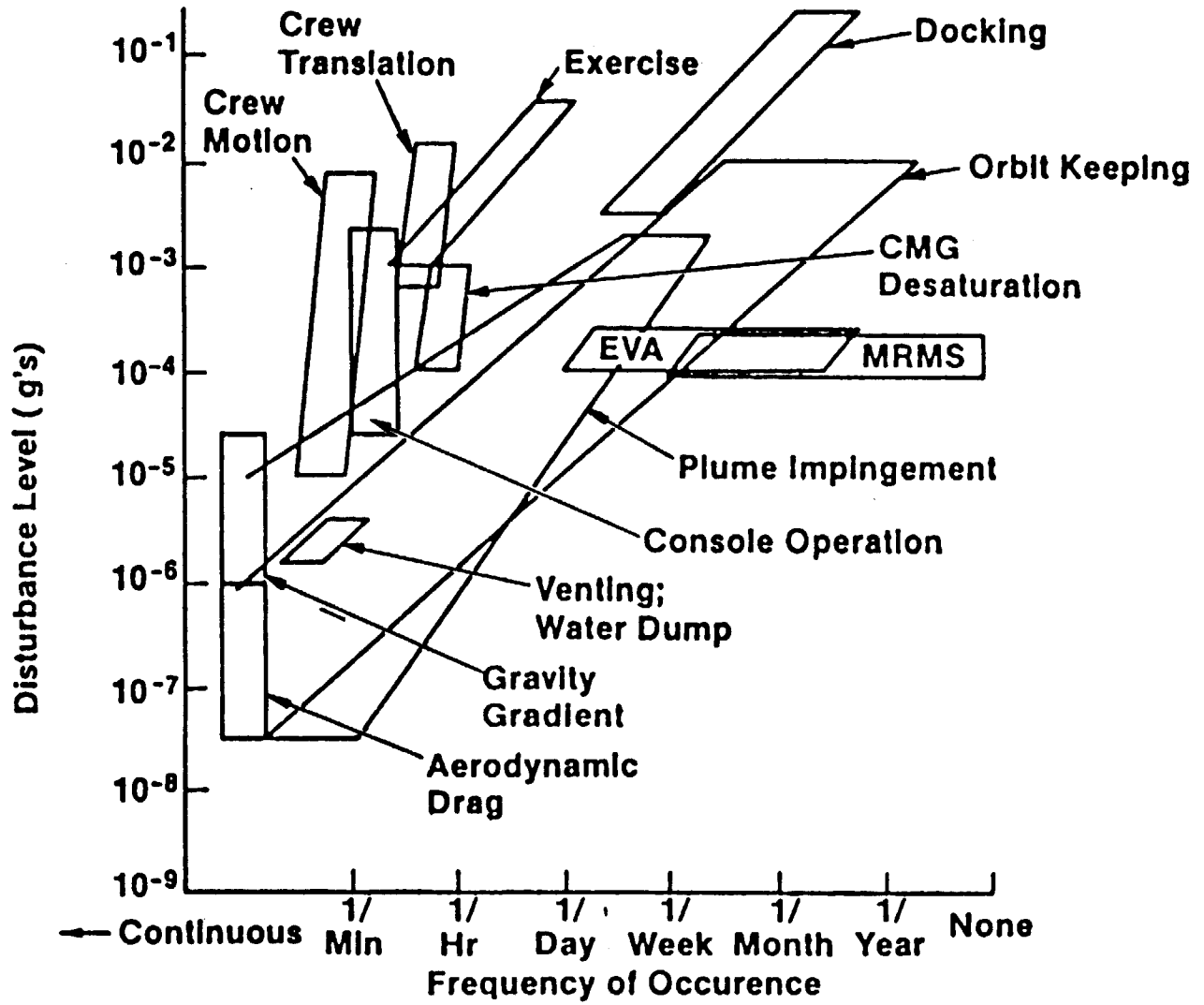

FIGURE 2. TYPICAL DISTURBANCE ENVELOPES

satisfy the isolation rquirements for all three options for low and high crew disturbance levels depending on the value of ξ. Analysis results are shown in Table 2.

Three isolation candidates are identified: passive mechanical, active servo; lead network and active servo; accelerometer. The passive mechanical system is possibly the lightest and cheapest system, but is sensitive to high-frequency input, is less versatile and sensitive to restraint (i.e., flex lines) gradient forces. The active network, lead network option is not as sensitive to high frequency outputs and is more versatile, but remains heavy, expensive, and sensitive to restraint gradient forces. The active servo accelerometer option is less sensitive to high-frequency inputs and restraint gradient forces and is versatile. But it too is heavy and expensive. Available accelerometers are the topic of another workshop paper. Two technical approaches offering the promise of reduced package size and weight are presented in the remainder of this paper. They are the design concept for an optical cavity-locking accelerometer and the technology for an integrated silicon accelerometer. Each approach is discussed in a section which follows.

III. THE CAVITY-LOCKING ACCELEROMETER (CLA)

Most accelerometer concepts considered to date use electrical pick-off schemes to detect the pendulum deflection under acceleration. Thus the accelerometer sensitivity is limited by the electronic pick off sensitivity. This limitation also dictates a sizable deflection of the pendulum structure for the accelerometer to respond to a given acceleration. The required deflection causes stress in the pendulum which enhances and propagates micro-creeps leading to bias problems under changing temperatures or as a result of aging.

One solution to this problem is to employ a pick-off technique with much higher sensitivities thereby reducing the pendulum deflection requirements for a given acceleration. Such a pick-off technique allows the use of a much thicker flexure or diaphragm structure which reduces the amount of stress developed in the structure. The Cavity-Locking

TABLE 2. MICRO-G ISOLATION ANALYSIS ISS RESULTS

CREW MOTION (STOCHASTIC)	IDEAL ISOLATOR CHARACTERISTICS	μGRMS @ EXP	SATISFIES SPEC. OPTION
QUIESCENT MOTION LOW-LEVEL (CASE B) • Console Ops • Resp, Cough, Sneeze • Arm Motion • Leg Motion • Swaying Motion RMS = 24.8μG @ HAB	PASSIVE ISOLATOR $\omega = .0062, \xi = .5$ PASSIVE ISOLATOR $\omega = .0062, \xi = .2$ ACTIVE ISOLATOR $\omega = .0062, \xi = .7$	1.30 0.26 0.02	1, 2 1, 2 1, 2, 3
UNINHIBITED MOTION HIGH-LEVEL (CASE A) • Torso Bowing • Crouch & Push-Off • Arm Flapping RMS = 105.0μG @ HAB	PASSIVE ISOLATOR $\omega = .0062, \xi = .5$ PASSIVE ISOLATOR $\omega = .0062, \xi = .2$ ACTIVE ISOLATOR $\omega = .0062, \xi = .7$	2.90 0.58 0.03	1 1, 2 1, 2, 3

Accelerometer (CLA) holds such a promise by virtue of its optical pick off technique which provides for several orders of magnitude increase in sensitivity. It will be shown here that the CLA can lead to accelerometers with nano-g (10^{-9} g) sensitivities while using rather thick diaphragms which should improve the bias stability.

The operational principle of CLA is based on tracking the resonance frequency of an optical (Fabry-Perot type) cavity. As shown in Figures 3 and 4, a probe beam provided by a coherent source (such as a laser diode) is injected into the cavity and the transmitted output of the cavity is measured by a photodetector. The strategy in the CLA is to assure that the frequency of the probe beam matches a resonance frequency of the interferometer cavity at all times. This can be accomplished either by adjusting the cavity length (as in Figure 3) so that the cavity resonance frequency matches the probe beam frequency or by adjusting the probe frequency (as in Figure 4), to match the cavity resonance frequency.

The cavity consists of two parallel mirrors with one mirror being attached to, or part of, a flexible diaphragm. A beam of light injected into the cavity undergoes multiple reflections and an output port is formed which is a function of the separation between the two mirrors as well as their reflectivities. Figure 5 shows such an output as a function of mirror separation for a number of different mirror reflectivities. It is seen that the intensity output exhibits successive peaks as the mirror separation changes by one-half of the probe beam wavelength. Furthermore, the peaks become sharper and sharper as reflectivity of the mirrors is increased. The peaks correspond to the resonance condition of the input (probe) beam frequency and the cavity length.

Acceleration along the cavity axis induces an inertial force in the diaphragm mirror, causing diaphragm deflection. This is followed by a change in cavity length which disturbs the resonance condition. An error signal is generated by the photodetector and the control loop restores the resonance condition. As stated earlier, the error signal can be applied to a PZT attached to the diaphragm thus driving the

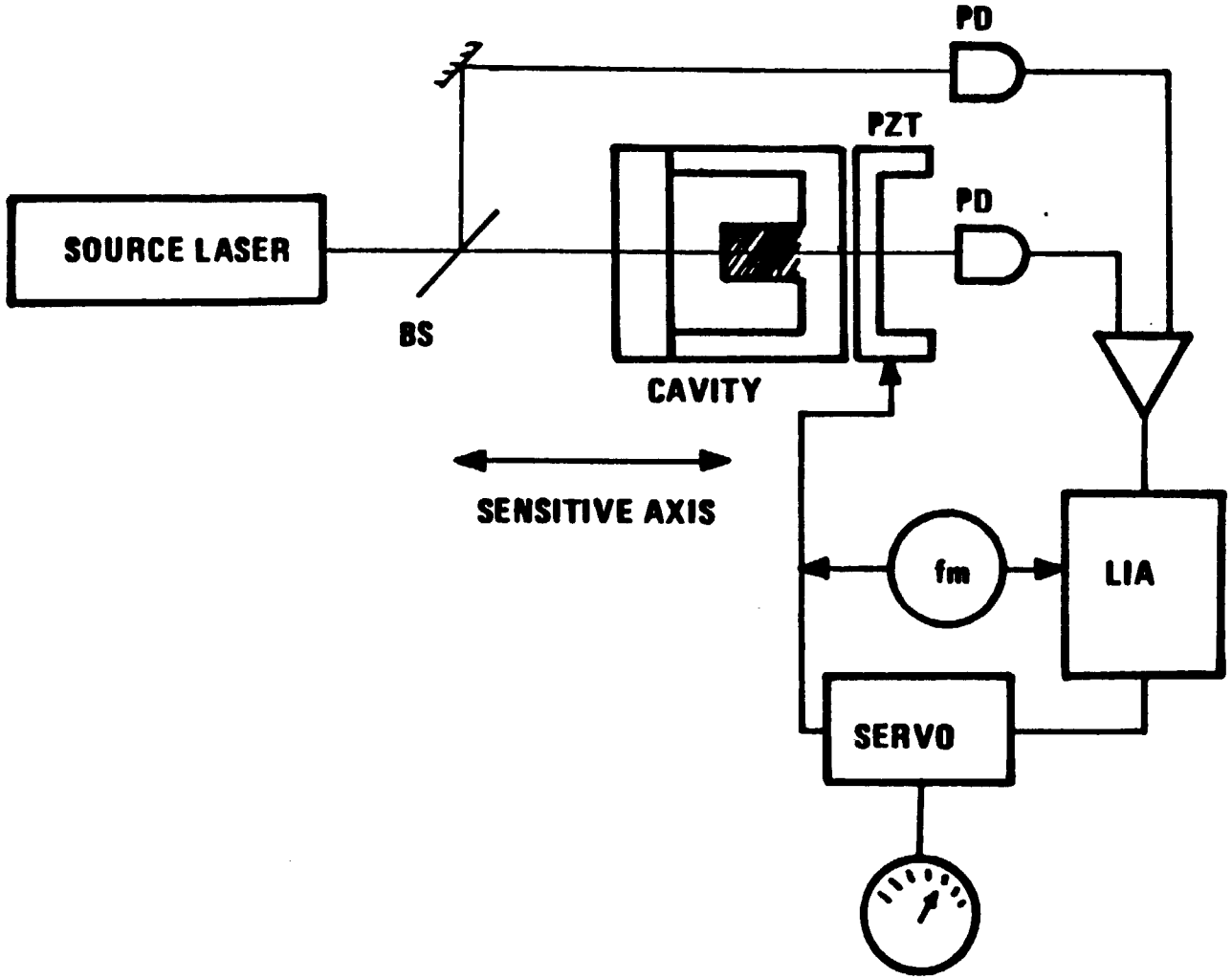

FIGURE 3. SCHEMATICS OF THE CLA WITH THE CAVITY LENGTH CONTROL TECHNIQUE

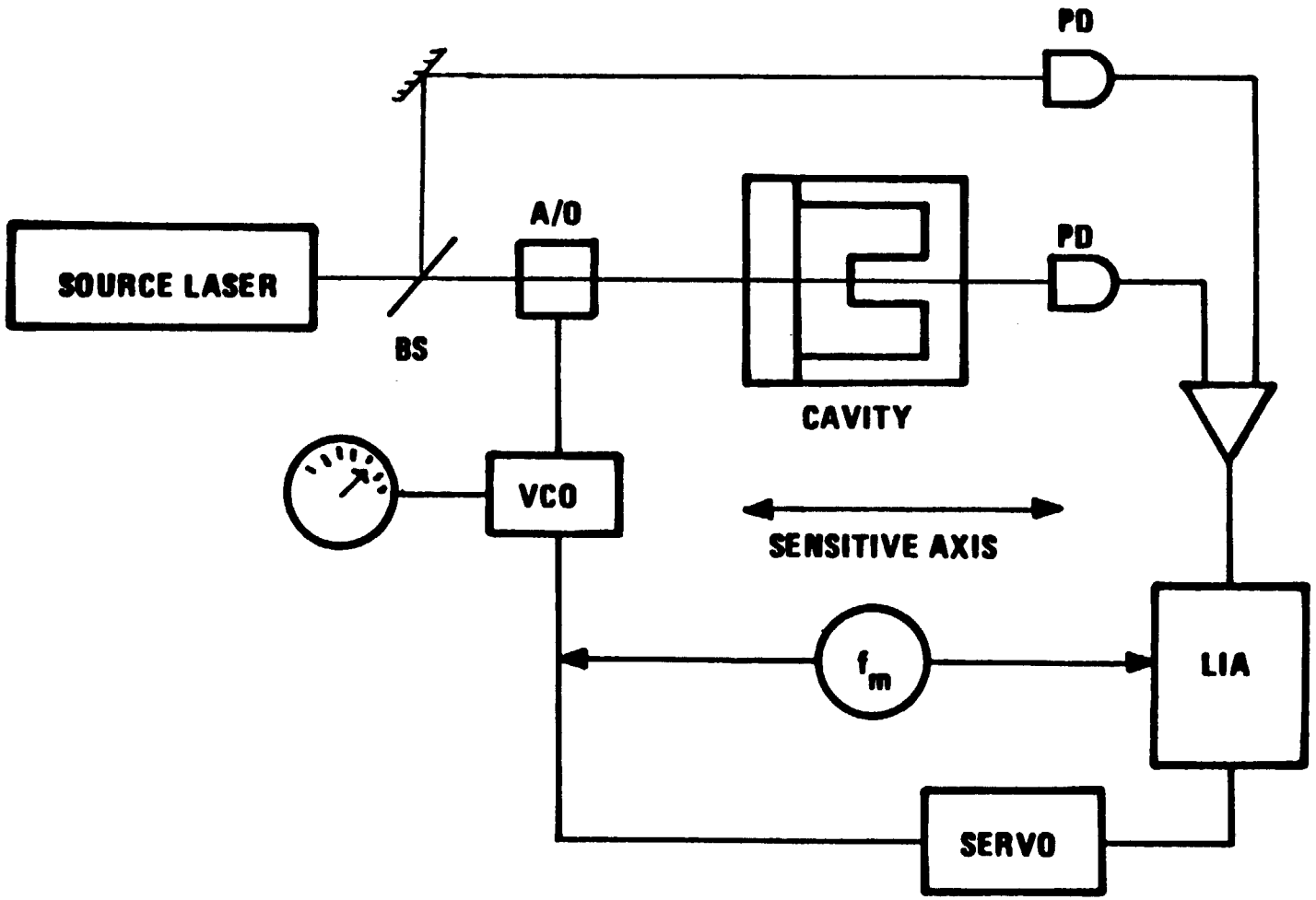

FIGURE 4. SCHEMATICS OF THE CLA WITH THE PROBE BEAM CONTROL FREQUENCY

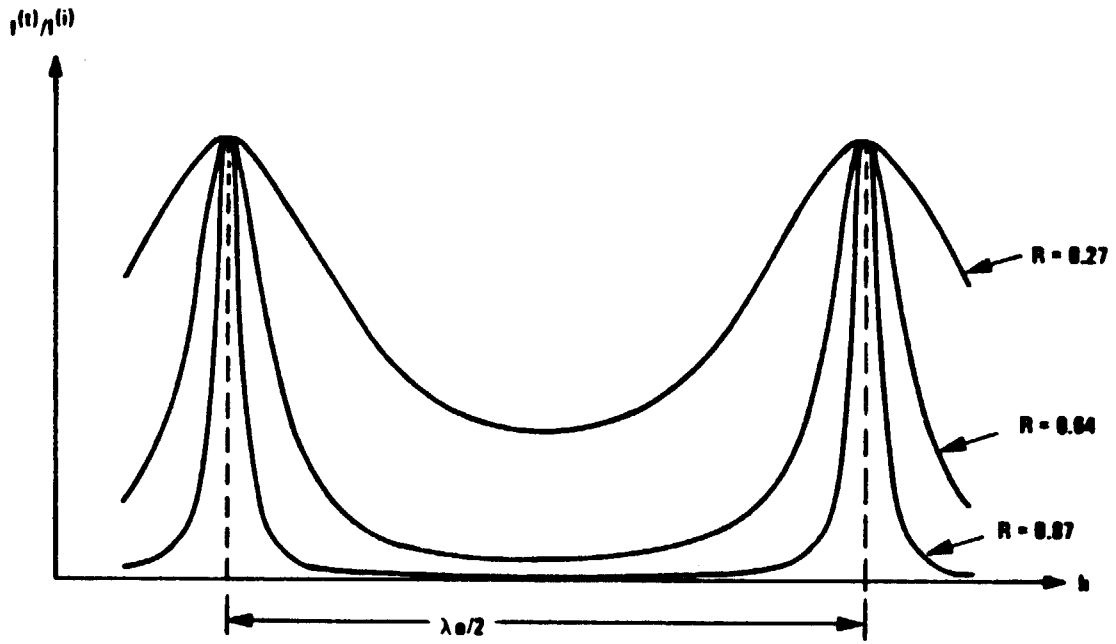

FIGURE 5. OUTPUT OF THE INTERFEROMETER AS A FUNCTION OF MIRROR SPACING

cavity length to the resonance condition or to an acousto-optic frequency shifter adjusting the probe beam frequency. A phase sensitive detection technique is used to achieve the resonance tracking. This technique which has been successfully employed in passive cavity gyros[1]-[3], is the main ingredient in achieving the high sensitivities in the CLA. Thus, referring to Figure 3, a modulating signal at a frequency f_m is applied to the PZT that scans the cavity length around its resonance and with an amplitude corresponding to the cavity linewidth (the resonance width in Figure 5). The detector output is demodulated at the same frequency by the phase sensitive detector (shown as LIA In Figure 3). Any departure of the cavity length from its resonance condition generates an error signal at $2f_m$ which is converted to a dc signal after demodulation. The dc signal is then applied to the PZT that restores the resonance. In Figure 4, the modulation and the error signals are applied to a frequency shifter that restores the resonance condition by adjusting the probe beam frequency. In either case, a second detector is used to monitor the probe beam intensity, and its output is subtracted from that of the first before demodulation. This provides for the common-mode rejection of changes in probe beam intensity.

Sensitivity Analysis. Sensitivity of the CLA is determined by the diaphragm configuration and the photodetection sensitivity. It has been demonstrated in passive cavity gyros that the detector shot noise is the main mechanism for limiting the photodetection sensitivity. We use the detector shot noise as the limiting mechanism of the CLA sensitivity.

Using the deflection equation of a circular diaphragm[4] and the detector shot noise equation, it can be shown that the acceleration sensitivity of the CLA is given by

$$S = \frac{8Et^3\ (1 - R)}{3\pi\ (1 - \nu^2)a^2\ M}\ \frac{\lambda}{\sqrt{N\eta\tau}}$$

where

S = acceleration sensitivity

t = diaphragm thickness

a = diaphragm radius

E = Young's modulus of diaphragm

ν = Poisson's ratio of diaphragm

M = mass of diaphragm mirror

λ = wavelength of light source

N = number of photons per second incident on the detector

η = detector quantum efficiency

τ = detector integration time

R = reflection coefficient of interferometer mirrors.

As an example, if a CerVit diaphragm is used for which $E = 13.37 \times 10^6$ psi and $\nu = 0.252$, and if $t = 0.1$ in., $M = 10$ gr., $\lambda = 0.8$ μm, $R = 0.995$, $\eta = 0.8$, $\tau = 1$ sec, and also $N = 4 \times 10^{15}$ sec^{-1} (corresponding to an incident power on detector of 1 mw), we obtain from Equation (1):

$$S = 1.54 \times 10^{-9}\ g \qquad (2)$$

Notice that such a sensitivity is achieved with a diaphragm whose thickness is 0.1 in., which is much thicker than the ones used in conventional accelerometers. Since the magnitude of stress in a loaded diaphragm is proportional to the inverse square of the diaphragm thickness[4], we expect the stress levels in the CLA be much reduced compared to conventional accelerometers which should alleviate the bias problems associated with the stress.

Dynamic Range. The maximum acceleration that the CLA can measure depends on the particular scheme of its resonance frequency tracking. In the configuration of Figure 3, where the control loop signal is applied to the PZT to rebalance the diaphragm and maintain the cavity length on resonance, the maximum applied acceleration depends on the operational range of the control loop. This is essentially an

electronic design issue which can be determined in a trade-off study of the control loop parameters. On the other hand in the configuration of Figure 4, where the error signal is used to adjust the probe beam frequency and the diaphragm is allowed to deflect, it is the tuning bandwidth that determines the maximum acceleration. It can be shown that the maximum allowable acceleration, γ max, for a given bandwidth is given by

$$\gamma \text{ max} = \frac{16\pi E t^3 h}{3(1 - \nu^2) a^2 M} \left(\frac{\delta\lambda}{\lambda}\right) \tag{3}$$

where

h = nominal distance between the cavity mirrors,

$\delta\lambda$ = tuning bandwidth of the probe beam.

All other parameters are the same as defined in Equation (1). The important parameter, from a component availability standpoint, is $\delta\lambda$. Tunable laser diodes are now available with a tuning bandwidth of 100 Angstroms. The frequency tuning in these diodes is achieved by varying the excitation current to the laser diode. The probe beam frequency can also be adjusted via the acousto-optic device, as shown in Figure 4. The frequency bandwidth of the available acousto-optic devices is limited to few gigahertz which corresponds to a $\delta\lambda$ of few hundredth of an Angstrom.

As an example, a frequency shifter with 3 GHz bandwidth yields a $\delta\lambda$ = 0.064 Angstroms. Using the same parameter values as in the sensitivity analysis and with h = 1 cm we obtain from Equation (3)

$$\gamma_{max} = 34 \text{ g} \tag{4}$$

Much higher accelerations can be measured if tunable laser diodes are used.

Although a good deal of experimentation and further analyses are needed to fully assess the potentials of the CLA, the concept does promise a significant improvement in sensitivity and bias stability based on the analysis presented here. These improvements are direct results of the optical pick-off technique employed in the CLA. As was

shown here, acceleration measurement sensitivities of the order of nano-g are possible using very thick diaphragms which develop much less stress during the accelerometer operation. Furthermore, such thick diaphragms are much less prone to micro-creeps and other damages during fabrication. If, as is often stated, such micro-creeps are the primary cause of the bias shifts then the thick diaphragms used in the CLA should provide it with much improved bias stability.

Finally, the CLA offers an interesting possibility for an all optical inertial navigation systems. If ring laser gyros (RLGs) are used in such systems, the probe beam of the CLA is already provided by one of the single beam output of an RLG. This would eliminate the need (and the corresponding cost) for highly stable coherent light source needed for the operation of the CLA.

IV. THE INTEGRATED SILICON ACCELEROMETER (ISA)

The ISA is an inertial grade accelerometer under development at Honeywell for application in strapdown RLG navigation systems. It is to be operated without temperature control, and contains no liquids, so as to be operational immediately after being turned on.

General Description of the Accelerometer. This is a pendulous accelerometer with torque rebalance. As shown in Figure 6, the pendulum is formed of single-crystal silicon, into which flexures are etched to provide suspension with a low stiffness. Mounted on the pendulum are rebalance coils, these coils and their bobbins forming most of the seismic mass. Pick-off of the pendulum deflection, to generate an error signal for rebalance, is by piezo resistive strain elements implanted into the flexures. Electronics for rebalance is processed directly on the silicon pendulum using existing IC technology (see Figure 7). The pendulum is sandwiched between two end caps which are bonded to it to form a capsule. The separation between the pendulum assembly and the end caps is small so that narrow gaps are formed, providing gas damping of the pendulum. This permits safe handling of the accelerometer when it is not operating.

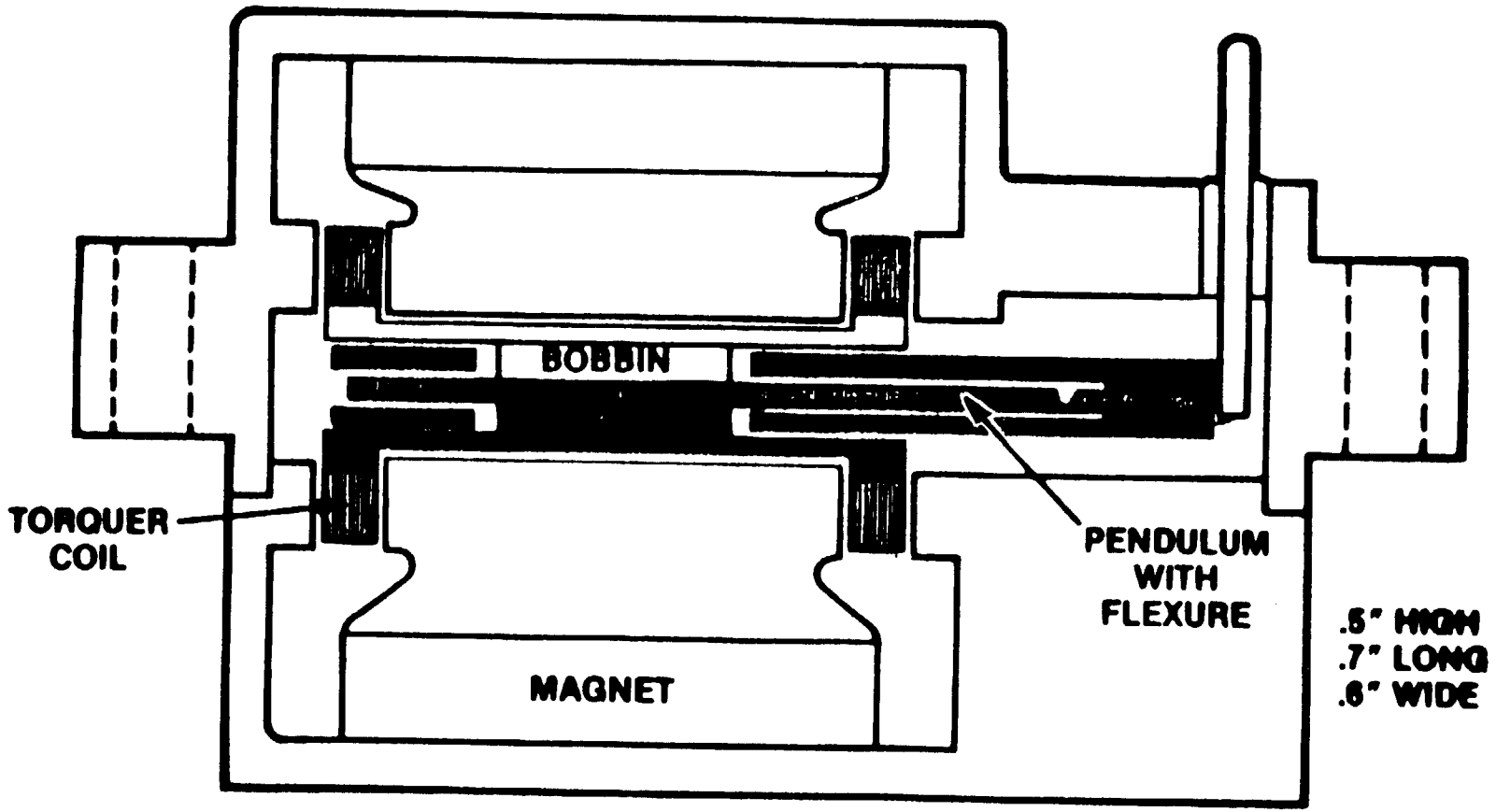

FIGURE 6. CROSS SECTION OF THE ISA

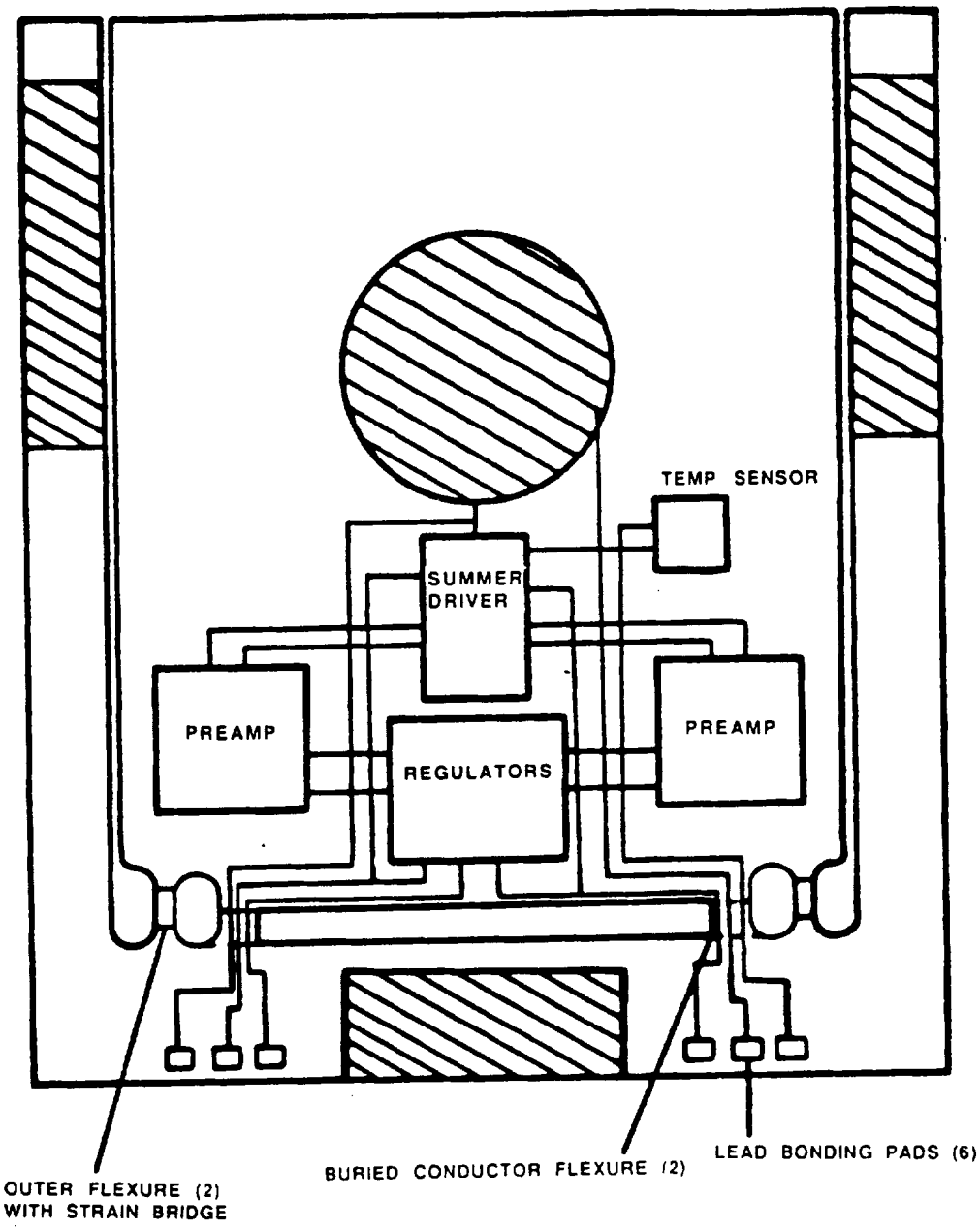

Figure 7. Schematics of the ISA Pendulum with On-board Electronics

The capsule is assembled into two Samarium Cobalt magnet assemblies which act also as the accelerometer case. Figure 8 shows the cutaway schematics of the assembly. Rebalance currents in the torque coils, in the fields of the magnets, produce the rebalance torque. The current through the torquer is an analog measure of the input acceleration. With analog-to-frequency conversion, the output is in a form suitable for the digital operations of a navigation system computer.

Development Goals. Goals for the development are roughly one order of magnitude beyond the state of the art in strapdown, fast reaction accelerometers without temperature control. Bias stability goals are 10 micro g's, (one sigma) short term and 20 micro g's, long term. The short term scale factor stability goal is 10 parts per million. Temperature sensitivity goal is 0.5 ppm per degree C, with software compensation. Input axis alignment stability goals are 5 micro radians short term, and 20 micro radians, long term.

The larger of two feasibility models now being evaluated measures 0.6 x 0.7 x 0.5 in.; this may be reduced in future development. It weighs 38.5 grams. The smaller unit weighs 20 grams.

The current breadboard results with the electronics off of the pendulum show an acceleration sensitivity of 1 micro-g. The limitation on sensitivity is mostly due to electronics noise. Detailed short- and long-term bias stability measurements are in progress.

V. CONCLUSION

Space Station micro-g performance goals are achievable through the management of operation, the design of isolation systems, and the use of accelerometers in active servo loops. New accelerometer designs are available to meet system micro-g requirements with reduced impact on system size, weight, and power.

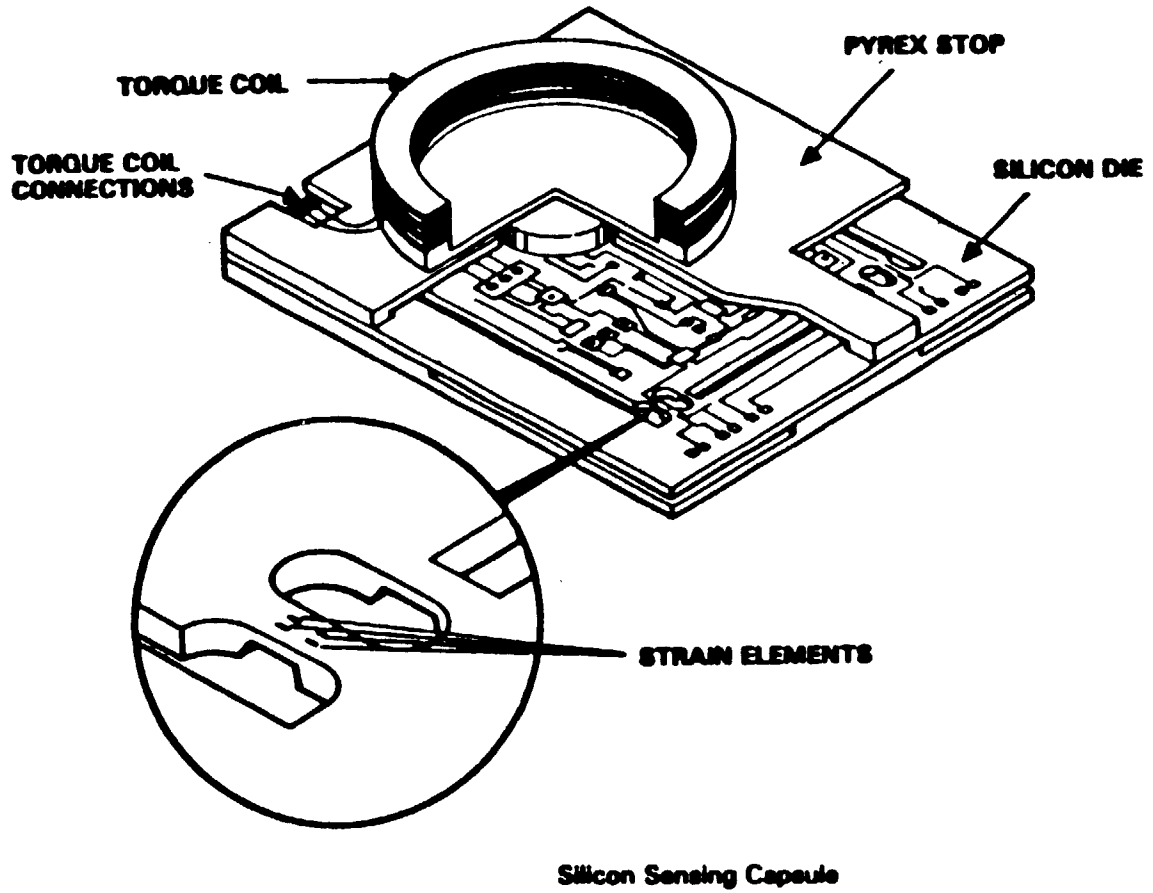

FIGURE 8. CUT-AWAY SCHEMATICS OF THE ISA ASSEMBLY

REFERENCES

1. S. Ezekiel and S. R. Balsamo, Appl. Phys. Lett. 30, 478 (1978)

2. G. A. Sanders, M. G. Prentiss, and S. Ezekiel, Opt. Lett. 11, 569 (1981)

3. M. M. Tehrani and J. A. Hoschette, Proc. SPIE, Vol. 412, P. 234 (1983)

4. R. J. Roark and W. C. Young, Formulas for Stress and Strain, Fifth Edition, McGraw-Hill Inc. (1975)

N91-12416

17. SUPERCONDUCTING SIX-AXIS ACCELEROMETER

Prof. H. J. Paik, University of Maryland

ABSTRACT

Highly sensitive superconducting accelerometers have been developed for application in gravitational wave detection and gravity gradiometry. A new superconducting accelerometer, capable of measuring both linear and angular accelerations, is under development at the University of Maryland. A single superconducting proof mass is magnetically levitated against gravity or any other drag force. Its relative positions and orientations with respect to the platform are monitored by six superconducting inductance bridges sharing a single amplifier, called SQUID (Superconducting Quantum Interference Device). Thus, the six degrees of freedom, the three linear acceleration components and the three angular acceleration components, of the platform are measured simultaneously. In order to improve the linearity and the dynamic range of the instrument, the demodulated outputs of the SQUID are fed back to appropriate levitation coils so that the proof mass remains at the null position for all six inductance bridges.

The expected intrinsic noise of the instrument is 4×10^{-12}m s^{-2} $Hz^{-\frac{1}{2}}$ for linear acceleration and 3×10^{-11} rad s^{-2} $Hz^{-\frac{1}{2}}$ for angular acceleration in 1-g environment. In 0-g, the linear acceleration sensitivity of the superconducting accelerometer could be improved by two orders of magnitude. We discuss the design and the operating principle of a laboratory prototype of the new instrument. Although such an advanced instrument is being developed primarily to satisfy the vibration and attitude measurement requirements for a space-borne superconducting gravity gradiometer, the superconducting six-axis accelerometer will have important applications in other terrestrial and space technologies.

INTRODUCTION

Applications in gravity survey and inertial navigation call for major improvements in the sensitivity of existing gravity gradiometers and accelerometers. A three-axis superconducting gravity gradiometer, which measures all three orthogonal in-line gravity gradient components, is being developed at the University of Maryland. Meanwhile, a prototype single-axis portion of a superconducting gravity gradiometer is being tested for its performance in a noisy terrestrial environment. Errors caused by common accelerations can seriously degrade the performance of the gradiometer because the ground has common accelerations which are several orders of magnitude larger than the extremely weak gravity gradient signals to be measured. An important error source of this kind comes from rotational motions which produce erroneous signals that are indistinguishable from gravity gradients. Although the errors along one of the three axes of a gradiometer caused by both torsional and tilting motions are minimized when that in-line axis is aligned with the vertical, such an orientation of the sensitive axis is not applicable to all the three orthogonal axes simultaneously. Availability of very sensitive accelerometers will provide knowledge of the exact motions of the gradiometer platform. Such precise information is useful to either develop a servo-controlled inertial platform or compensate for the errors caused by the motions of the platform. We are developing a "six-axis" superconducting accelerometer to measure all three linear and three angular accelerations of the platform. In this paper, we report the development status of the gradiometer including test results with the prototype gradiometer and also describe the principle and design of the accelerometer.

FEATURES OF THE GRADIOMETER

The design of the three-axis gravity gradiometer was given at another conference.[1] Here we describe the features of the instrument. The gradiometer consists of three pairs of coupled superconducting acceleration transducers mounted on the six faces of a precision cube.

Each acceleration transducer is a spring-mass type superconducting accelerometer[2] in which an applied acceleration signal produces a displacement of a proof mass suspended by a spring. The proof mass displacements for a pair of spring-masses in the common and differential modes of motion are detected by a coupled superonducting inductance-modulation circuit (Figure 1) and SQUID amplifiers. A passive coupling provided by the superconducting circuit with adjustable but persistent stored currents provide a quiet and stable means to accurately balance out the common linear accelerations for the measurement of the differential acceleration.

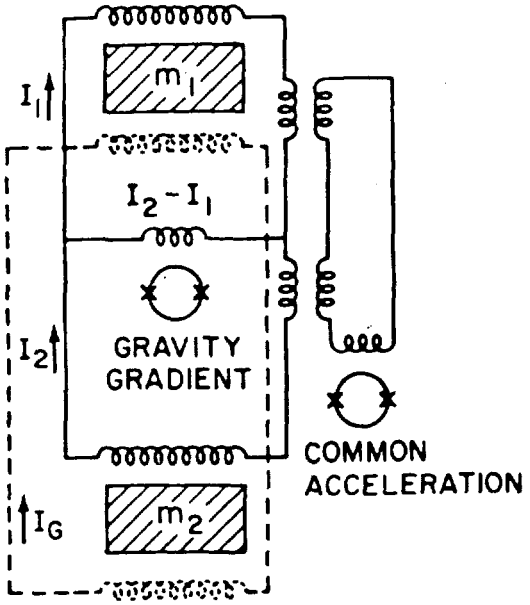

FIGURE 1. SCHEMATIC OF SUPERCONDUCTING CIRCUIT FOR EACH SINGLE-AXIS GRAVITY GRADIOMETER

The following considerations are important for each pair of coupled acceleration transducers:

1. In order to minimize the contamination of the signal by the SQUID amplifier noise, a very low proof mass resonance frequency in the differential mode is desirable in order to produce, for a given acceleration amplitude, a larger proof mass displacement before it is detected by the superconducting circuit.

2. The spring used in the suspension should have low loss in order to have lower thermal (Nyquist) noise from the spring.

3. A precise alignment of the sensitive axes together with a high degree of common mode rejection are needed in order to reject the relatively large common accelerations of the gradiometer platform.

As a compromise between alignment precision and sensitivity, a mechanical cantilever-spring suspension is used to confine the motion of the proof mass along a straight line. The mechanical suspension provides the convenience of employing mechanical precision to align the sensitive axes of a pair of in-line acceleration transducers along a common colinear direction and to align this common axis along a reference axis of the precision cube. The cantilever springs, which are relatively soft in the bending mode but stiff against stretching, provide the confinement for the motion of the proof mass to a one-dimensional motion. However, the mechanical suspension also raises the resonance frequency of the proof mass and hence sets an unnecessary limit on the sensitivity of the gradiometer to the order of 10^{-12} s^{-2} $Hz^{-1/2}$ for our present design. A passive superconducting negative spring, which lowers the resonance frequency without adding amplifier noise, is being developed[3] to extend the intrinsic sensitivity of the gradiometer.

Superconducting magnetic levitation of the proof mass against Earth's gravity also has an electromagnetic spring contribution. Yet, a pair of acceleration transducers can be combined in a "push-pull" configuration. By combining in series the levitation coils for a pair of proof masses, the electromagnetic spring constant of the coupled levitation coils becomes zero for the differential mode of motion but remains high for the common mode. The inductance modulations of the levitation coils in the differential mode add to zero for the series inductance so that no restoring force and hence no spring constant results.

The instrinsic instrument noise Γ_n of the gradiometer has a spectral density S_Γ given by[4]

$$S_\Gamma^2(f) = \frac{8\omega_0}{m\ell^2}\left[\frac{k_B T}{Q} + \frac{\omega_0}{2\beta\eta}\, E_n(f)\right], \text{ for } f < \omega_0/2\pi$$

where m, $\omega_0/2\pi$, Q, ℓ, E_n and $\beta\eta$ are the mass, differential-mode resonance frequency, quality factor, baseline, SQUID amplifier noise and energy coupling factor, respectively. The design values in our present gradiometer are m = 1.33 kg, $Q > 10^5$, ℓ = 0.19 m, $E_n = 3\times10^{-30}$ J Hz^{-1} (SHE dc SQUID at f > 0.1 Hz) and $\beta\eta$ = 0.5. Without using a superconducting negative spring, $\omega_0/2\pi$ is about 7 Hz and $\Gamma_n(f) = 2\times10^{-12}$ s^{-2} $Hz^{-1/2}$. With the negative spring and a lower loss ($Q>10^6$), the instrument noise can be improved by another order of magnitude. Such a high sensitivity imposes stringent requirements on the acceleration noise of the platform. With an angular velocity noise of $\omega\theta_n$ at a signal frequency $\omega/2\pi$ and a linear acceleration noise of a_n, the gravity gradient errors induced by these common accelerations are, respectively, $(\omega\theta_n)^2$ and $a_n\varepsilon/\ell$, where ε is a geometrical alignment error. With our present design values of the gradiometer, the estimated requirements on the uncertainty of the common accelerations are $a_n < 10^{-9}$ m s^{-2} $Hz^{-1/2}$ and $\omega^2\theta_n < \omega\times10^{-6}$ rad s^{-1} $Hz^{-1/4}$. These requirements are easily met by using superconducting accelerometers. Both linear and angular acceleration readouts are available as secondary outputs in a tensor gravity gradiometer[5] which has both in-line and cross-line gradiometers. With the present three-axis in-line gradiometer, only the linear common acceleration outputs are available. A desired ancillary instrument is a dedicated superconducting accelerometer that measures all the acceleration components.

DESIGN OF THE ACCELEROMETER

The six degrees of freedom of a platform are three linear and three angular motions. The "six-axis" accelerometer under development utilizes the same principles of the gradiometer with two major differences:

1. Because the accelerometer has no common mode balance requirement, only magnetic levitation (no mechanical spring) is used in the proof mass suspension. The proof mass resonance frequency can therefore be made low even in a simple design.

2. A single common proof mass has all the six degrees of freedom and can be conveniently shared by all the six component accelerometer circuits.

The design of the accelerometer is shown in Figure 2. The proof mass, which is shown in Figure 2a with a Cartesian coordinate system coinciding with the sensitive axes of the accelerometer, has 24 superconducting planes. Motion of the proof mass at these planes produces inductance modulations of 24 corresponding sensing coils which are mounted on 8 identical coil forms. Figure 2b shows one of these coil forms. A cross-sectional view of the proof mass together with the sensing and levitation coils is shown in Figure 2c on a zx plane (y = 1/4 times the proof-mass side length) through the four quadrants yzx, yz$\bar{x}$, y$\bar{z}\bar{x}$ and y$\bar{z}$x. The notation on each coil specifies the location of the particular coil by giving a three letter label of the quadrant in which the coil lies and by indicating the sensitive axis of the coil in capital letter.

Both orthogonality and parallelism are required of the proof mass. An umbrella orientation (one trigonal axis being vertical) gives symmetry for the proof mass towards levitation. The accelerometer can be integrated into the center cube of the gradiometer. The coils are then aligned with reference to the cube.

The linear and angular components of motion of the proof mass can be sensed by taking various combinations of the sensing coils to form six bridge circuits, each containing four coils. The choice of the combination should also minimize the coupling of each circuit to all but one component of motion. A scheme of achieving this decoupling, provided a cubic symmetry is maintained and the displacements of the proof mass relative to the coils are kept small, is shown in Figure 3 for the bridge circuits of one component linear acceleration a_x and one com-

ponent angular acceleration α_x, which are in the x direction. Figure 3 also shows the levitation coils with stored dc currents. Feedback is applied to the bridge circuit of these levitation coils in order to maintain the proof mass in the balanced positions of the bridges.

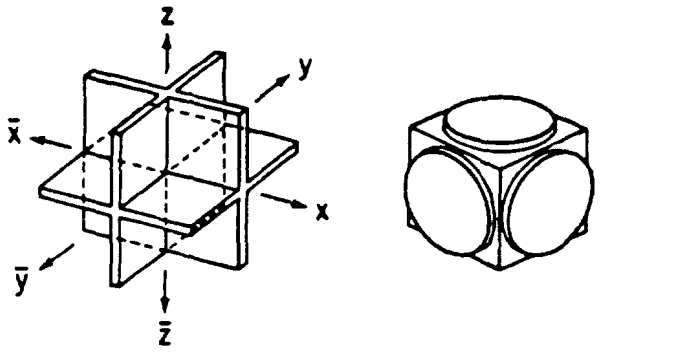

Proof mass (Niobium) Coil form (Macor ceramic)

(a) (b)

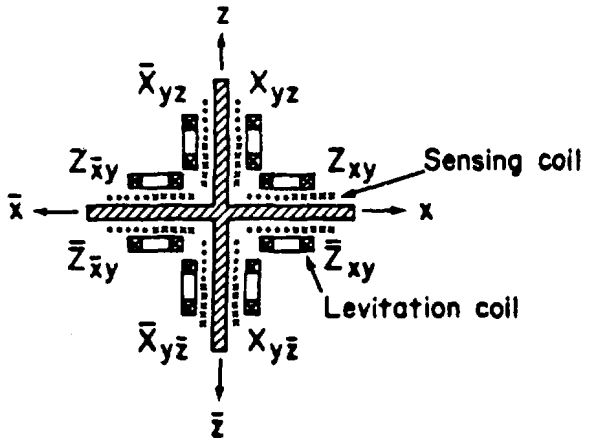

Coils (24 sensing coils + 24 levitation coils)

(c)

FIGURE 2. DESIGN OF A SIX-AXIS SUPERCONDUCTING ACCELEROMETER

Therefore, the feedback maintains the geometric symmetry of the system even in the presence of applied acceleration and minimizes the noise contribution from the driving oscillator of the bridge. Use of the ac bridge is intended to eliminate 1/f noise term due to the noise spectrum of the SQUID amplifier. A potentially economic and compact feature of

sharing one SQUID amplifier among more than one bridge circuit is possible by connecting the bridge circuits, which use different ac modulation frequencies, to the same SQUID.

The intrinsic instrument noise of the accelerometer has terms similar to that of the gradiometer and can be shown to be[6]

$$S_{ai}(f) = \frac{4\omega_{a0}}{M}\left[\frac{k_B T}{Q} + \frac{\omega_0}{2\beta} E_n\ (\omega_{ai}/2\pi)\right]$$

for each linear acceleration component a_i, and

$$S_{\alpha i}(f) = \frac{4\omega_{\alpha 0}}{I}\left[\frac{k_B T}{Q} + \frac{\omega_0}{2\beta} E_n\ (\omega_{\alpha i}/2\pi)\right]$$

for each angular acceleration component α_i. Here, I is the moment of inertia of the proof mass whereas $\omega_{ai}/2\pi$ and $\omega_{\alpha i}/2\pi$ are the respective driving frequencies of the ac bridges. The design values, using a proof mass of 5 cm in each side, are M = 0.1 kg, $I = 3\times10^{-5}$ kg m^2, $\omega_a 0 = 2\pi$ x 10 s^{-1}, $\omega_{\alpha 0} = 2\pi$ s^{-1}, T = 4.2 K, $Q = 10^5$, $\beta = 1/4$ and $E_n = 5 \times 10^{-29}$ J Hz^{-1} (SHE rf SQUID). The corresponding intrinsic noise levels are $\left|S_a(f)\right|^{1/2} = 4 \times 10^{-12}$ s^{-2} $Hz^{-1/2}$ and $\left|S_\alpha(f)\right|^{1/2} = 3 \times 10^{-11}$ rad s^{-2} $Hz^{-1/2}$. Sensitivity results are graphically shown in Figures 4 and 5.

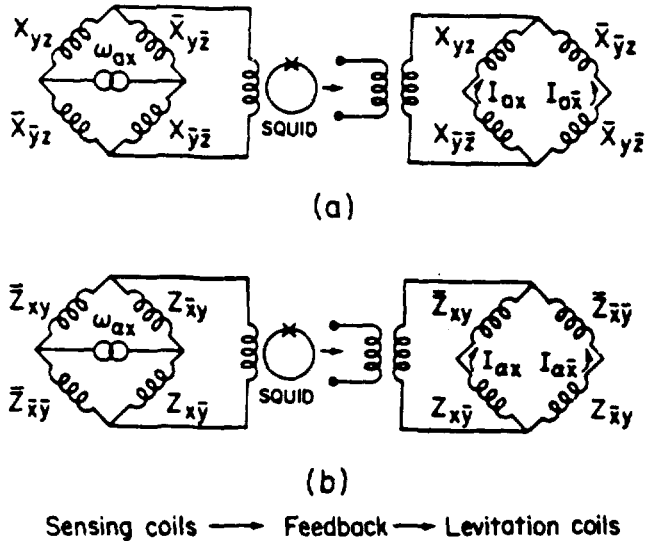

FIGURE 3. SCHEMATIC OF SENSING, LEVITATION AND FEEDBACK CIRCUIT FOR (a) A LINEAR ACCELERATION COMPONENT a_n, AND (b) AN ANGULAR ACCELERATION COMPONENT α_n

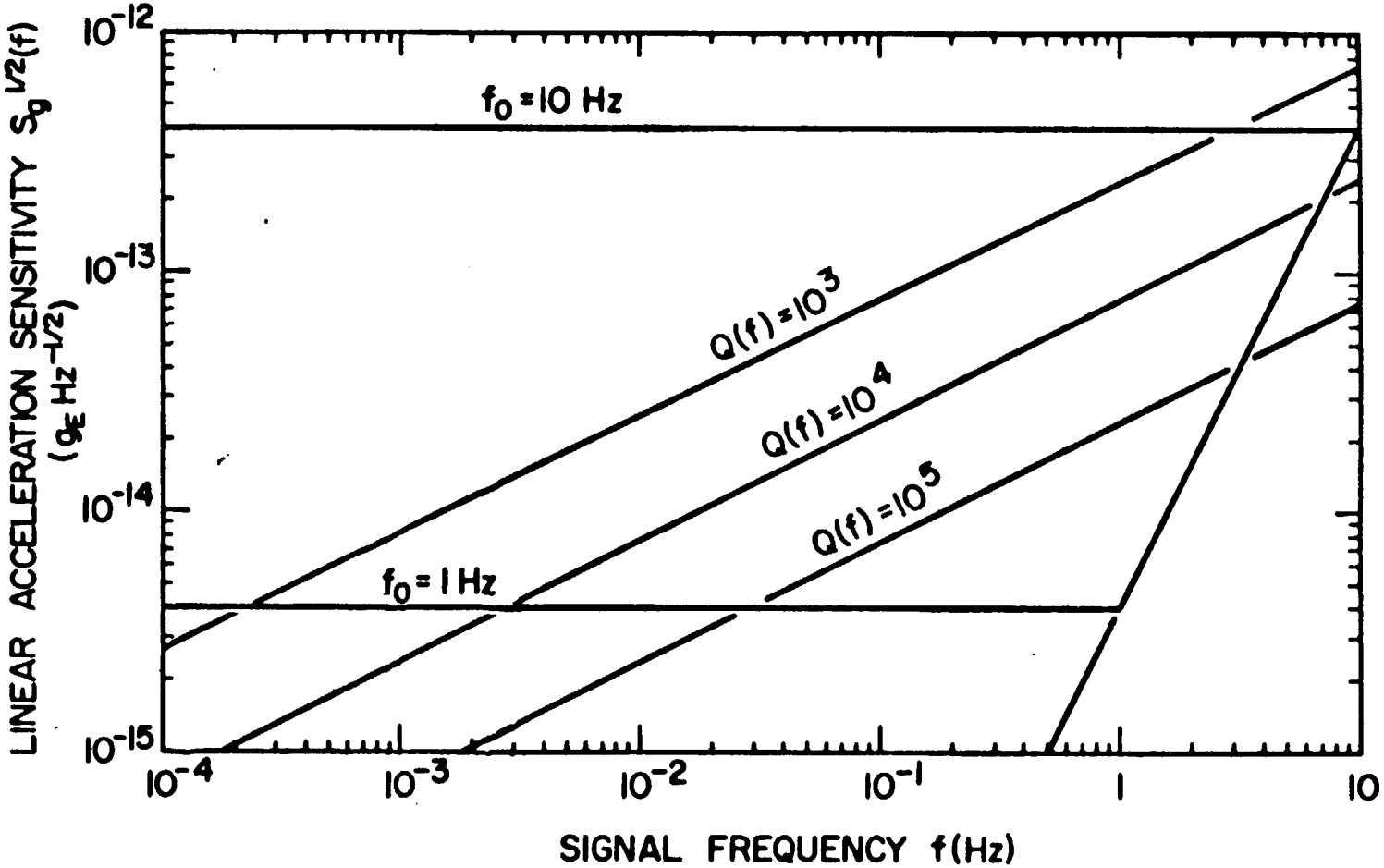

FIGURE 4. SIGNAL FREQUENCY f(Hz)

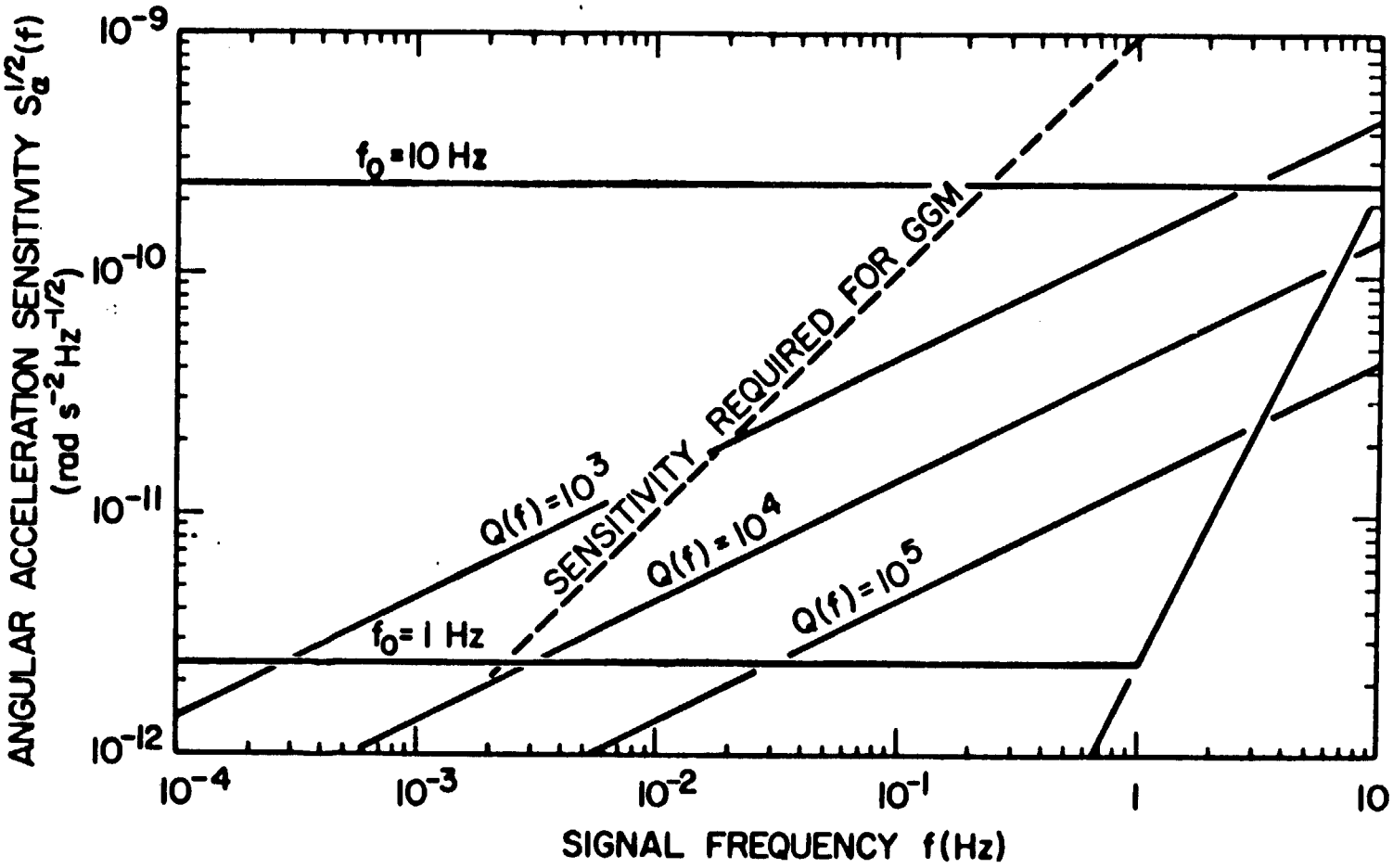

FIGURE 5. SIGNAL FREQUENCY f(Hz)

TEST RESULTS OF PROTOTYPE GRADIOMETER

A single axis prototype gradiometer, which is smaller in size and has a similar superconducting circuit to the one shown in Figure 1, is being tested in a noisy environment. The values of the parameters are $m = 0.4$ kg, $\ell = 15$ cm, $\omega_0 = 25$ Hz, $E_n = 5.9 \times 10^{-29}$ J $Hz^{-1/2}$ and $\beta_n = 0.1$. The measured Q of the gradiometer is over 30,000 making the thermal noise term of the gradiometer negligible compared with the SQUID amplifier noise term which is 7×10^{-11} s^{-2} $Hz^{-1/2}$. The linear acceleration noise of the gradiometer platform is measured by the gradiometer itself to be approximately 1.5×10^{-7} m s^{-2} $Hz^{-1/2}$ at below 1 Hz but the angular acceleration noise of the gradiometer platform at such low frequencies requires too high a sensitivity for room temperature instrumentation.

The gradiometer is mounted along one axis of a cube which has one trigonal axis vertical. The gradiometer platform is suspended from outside the dewar by a long vibration isolation filter which has a vertical resonance frequency of about 1.1 Hz and a pendulum frequency of 0.3 Hz.[4] High frequency vertical vibrations of the ground are attenuated by the passive filter. Horizontal vibrations at all frequencies are isolated by the pendulum but has a residual coupling to several degrees of motion of the platform due to the imperfect nature of the pendulum, which has to compromise between heat leak and rigidity, to several modes of motion. The heat leak through this filter and through radiation is small, but another source of temperature fluctuations at the gradiometer platform is a residual heat exchange with the Helium bath by conduction through the lead wires and through the residual gas of the vacuum. The thermal isolation of the gradiometer platform, together with a large heat capacity of the gradiometer system, behaves like a low-pass filter. A shaker is used to produce a vertical acceleration during the common mode balance procedure, and both this shaker and the dewar are shielded by μ-metal against electromagnetic interference.

The observed noise spectrum is shown in Figure 6. The upper trace of the figure shows the backgound common acceleration measured by the gradiometer when the gradiometer is charged with supercurrents in an accelerometer mode.[4] The instrument noise of the gradiometer, which has been determined indirectly from measurements of Q and amplifier noise, is indicated by a dotted line which is at a level of almost 10^5 below that of the acceleration noise. This instrument noise is what we expect

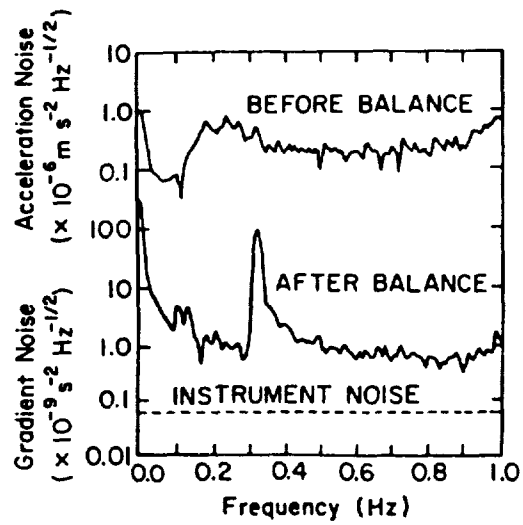

FIGURE 6. Noise measured by the gravity gradiometer before and after common mode balance when tested in terrestial environment. The vertical scale is the same continuous measure of common/ differential acceleration output of the gradiometer, although the lower region of the scale is expressed in terms of gravity gradient.

from the output of the gradiometer if it were tested in a quiet environment or if we can suppress the environment-induced noise. During the balance, (by adjusting the stored supercurrents) the measured (differential) acceleration output of the gradiometer lowers by an amount proportional to the degree of common mode balance achieved. This proportionality is well maintained until the level shown in the lower solid curve is reached. At this point, the gradiometer noise level no longer

decreases with the improvement of common mode balance. The noise floor is then 10 times higher than the indirectly measured intrinsic noise but is an improvement of about 10 dB over what we reported previously.[7] Besides noise peaks due to the modes of the vibration isolation used, excess noise is also evident near dc and a drift of about 10^{-8} s^{-2} per hour has been measured on a chart recorder. The cause of the excess $1/f^n$ noise is that temperature changes modulate the penetration depth and hence the inductances of the superconducting circuit.[8] The drift was about 10 times higher[7] when the He exchange gas pressure was higher and was thus giving a shorter thermal time constant.

CONCLUSIONS

Superconducting techniques can provide orders of magnitude of improvement for the instrinsic instrument noise of both gravity gradiometer and accelerometer. In the terrestial environment, however, the demonstration of the intrinsic noise of these gravity instruments also necessitates a careful suppression or compensation of environment-induced noise. Our prototype gravity gradiometer presently has its sensitivity limited by environment-induced noise to a noise floor of 7×10^{-10} s^{-2} $Hz^{-1/2}$. Availability of very sensitive accelerometers to monitor the motion of the gradiometer platform is an important error-reduction step towards demonstrating the intrinsic noise of a very sensitive gradiometer when used as a gravity survey system. A similar contribution is obtained from the gradiometer with respect to the accelerometer as an inertial navigation system. We are making parallel efforts in developing both of these superconducting gravity instruments.

REFERENCES

1. H. A. Chan, M. V. Moody, H. J. Paik and J. W. Parke, "Development of Three-Axis Superconducting Gravity Gradiometer," Proc. of 17th Int. Conf. on Low Temp. Phys., edited by U. Eckern et al, Elsevier Science Publishers B. V., 1984, pp. 927-928.

2. H. J. Paik, "Superconducting Turnable-diaphragm Transducer for Sensitive Acceleration Measurements," J. Appl. Phys., Vol. 47, pp. 1168-1178, 1976.

3. J. W. Parke, H. J. Paik, H. A. Chan and M. V. Moody, "Sensitivity Enhancement of Inertial Instruments by Means of a Superconducting Negative Spring," Proc. of 10th Int. Cryogenic Engineering Conf., Otaniemi, Finland, 1984.

4. H. A. Chan, "Null Test of Gravitational Inverse Square Law with a Superconducting Gravity Gradiometer," PhD thesis, University of Maryland, College Park, Maryland 1982.

5. H. J. Paik, "Superconducting Tensor Gravity Gradiometer for Satellite Geodesy and Inertial Navigation," J. Astronaut. Sci., Vol. 29, pp. 1-18, 1981.

6. H. J. Paik, private communication.

7. M. V. Moody, H. A. Chan and H. J. Paik, "Preliminary Tests of a Newly Developed Superconducting Gravity Gradiometer," IEEE Trans. Mag., Vol. MAG-19, pp. 461-463, 1983.

8. M. V. Moody, H. A. Chan, H. J. Paik and C. Stephens, "A Superconducting Penetration Depth Thermometer," Proc. of 17th Int. Conf. on Low Temp. Phys., edited by U. Eckern et al, Elsevier Science Publishers B. V., 1984, pp. 407-408.

N91-12417

18. PRESENTATION ON A SPACE ACCELERATION MEASUREMENT SYSTEM (SAMS)

Theodore L. Chase, NASA/LeRC

CONTENTS

		PAGE
1.0	INTRODUCTION	18-2
2.0	PROJECT SUMMARY	18-2
3.0	TECHNICAL PLAN	18-3
	3.1 General Technical Approach	18-3
	3.2 Description of System	18-3
	3.3 System Specifications	18-13
	3.4 First Flight System Configuration	18-16
	3.5 Baseline System Configuration	18-17
4.0	MANAGEMENT PLAN	18-17
5.0	PROCUREMENT APPROACH	18-18
6.0	PROJECT SCHEDULE	18-18

1.0 INTRODUCTION

A variety of Shuttle Orbiter experiments are currently under development as part of OSSA's Microgravity Sciences and Applications (MS&A) Program. These experiments generally require measuring and recording low gravity accelerations. Such measurements made to date have proven to be inadquate for certain microgravity experiments. As a result, Richard E. Halpern, Director of the MS&A Division at NASA Headquarters, requested that the Space Experiments Office of the NASA Lewis Research Center (LeRC) survey existing systems, establish general requirements, and formulate a plan for either procuring or developing a suitable acceleration measurement system. The survey was subsequently conducted, and it was found that no existing system met these requirements. It was therefore determined that LeRC should take the lead in developing such a system.

A preliminary set of technical specifications was then developed. Several references were consulted such as the Low Acceleration Characterization of Space Station Environment by Teledyne-Brown Engineering and the Feasibility Study for the Orbital Acceleration Research Experiment by KMS Fusion, Incorporated. In addition, a questionnaire was circulated in the microgravity science community to determine measurement requirements of potential users. In some cases, information was obtained from previous Shuttle experiments. The above inputs were used to develop a set of specifications. A plan to develop and qualify a Space Acceleration Measurement System (SAMS) meeting these specifications is presented herein.

2.0 PROJECT SUMMARY

The primary objective of the SAMS project is to provide an acceleration measurement system capable of serving a wide variety of space experiments. The design of the system being developed under this project takes into consideration requirements for MS&A experiments located in the middeck, in the orbiter bay, and in Spacelab. In addition to measuring, conditioning, and recording accelerations, the system will be capable of performing complex calculations and interactive control. The main components consist of a remote triaxial sensor head, a microprocessor-driven data acquisition system and an optical storage device. In operation, the triaxial sensor head produces output signals in response to acceleration inputs. These signals are preamplified, filtered and converted into digital data which is then transferred to optical memory. The system design is modular, facilitating both software and hardware upgrading as technology advances. The microprocessor chosen is code-compatible with the IBM PC-XT allowing maximum compatibility with the majority of experiments. The electronics package, utilizing CMOS technology, is on the STD-BUS modular interconnection system.

The project is managed and implemented "in-house" at Lewis with fabrication, drafting, engineering analysis and software development performed under contract, where appropriate. Support contractors will be used for the safety and integration documentation.

Two complete acceleration measurement flight systems will be built and tested under this project. The initial system is to be flown to acquire preliminary data in support of the JPL-managed Lambda Point Experiment. The initial system will be housed in a GAS can in the Shuttle bay with the sensor head located on an MPESS carrier. The second system will be built in a general purpose or baseline configuration and will be capable of supporting a wide variety of experiments. After the initial system has been flown, it will be retrofitted to the baseline configuration. Both these systems will then be made available to the space experiments community. In addition to the two flight units mentioned above, a complete set of spare parts, an engineering development system, and a breadboard system will also be provided.

The duration of this activity from initiation to completion is estimated to be 27 months with the first flight system scheduled for shipment in 20 months.

3.0 TECHNICAL PLAN

3.1 General Technical Approach

The Space Acceleration Measurement System (SAMS) will be comprised of a triaxial acceleration sensor head connected by an umbilical cable to an electronics package. The electronics package will be microprocessor-driven and will be designed to accommodate a wide variety of functions through the use of plug-in boards. The electronics package will be both modular and software-driven to facilitate future additions or modifications. The electronics package will be equipped to communicate with other electronics systems, e.g., other experiments, the Shuttle communications and control system. The data gathered from the sensors as well as ancillary data will be stored in an optical memory system. The SAMS will be equipped with its own power conditioning circuitry allowing operation from 28 VDC Shuttle power or self-contained batteries. The SAMS is designed to fit into a small volume, draw minimal power and operate over a wide temperature range so that it may be used in a wide variety of configurations. Figures 1 and 2 show the SAMS configured to fly in a middeck locker and a GAS can, respectively. Figure 3 shows alternate SAMS configurations.

3.2 Description of System

3.2.1 Hardware Description

The accelerometer sensor is a pendulous inertial type, employing a quartz flexure suspended proofmass, producing an acceleration output current independent of output load. The

National Aeronautics and Space Administration

Lewis Research Center

SPACE EXPERIMENTS OFFICE

NASA

SPACE ACCELERATION MEASUREMENT SYSTEM

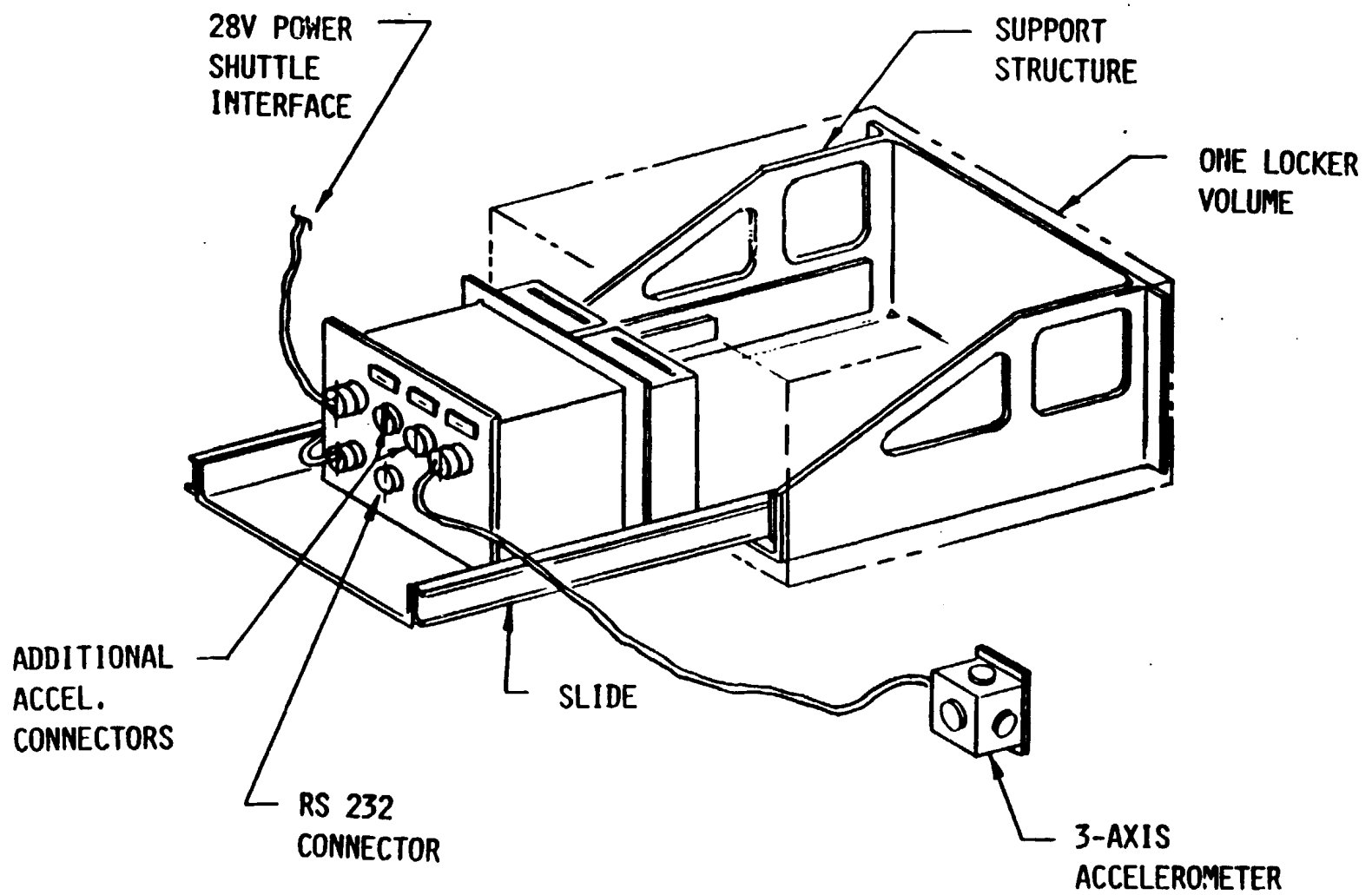

FIGURE 1

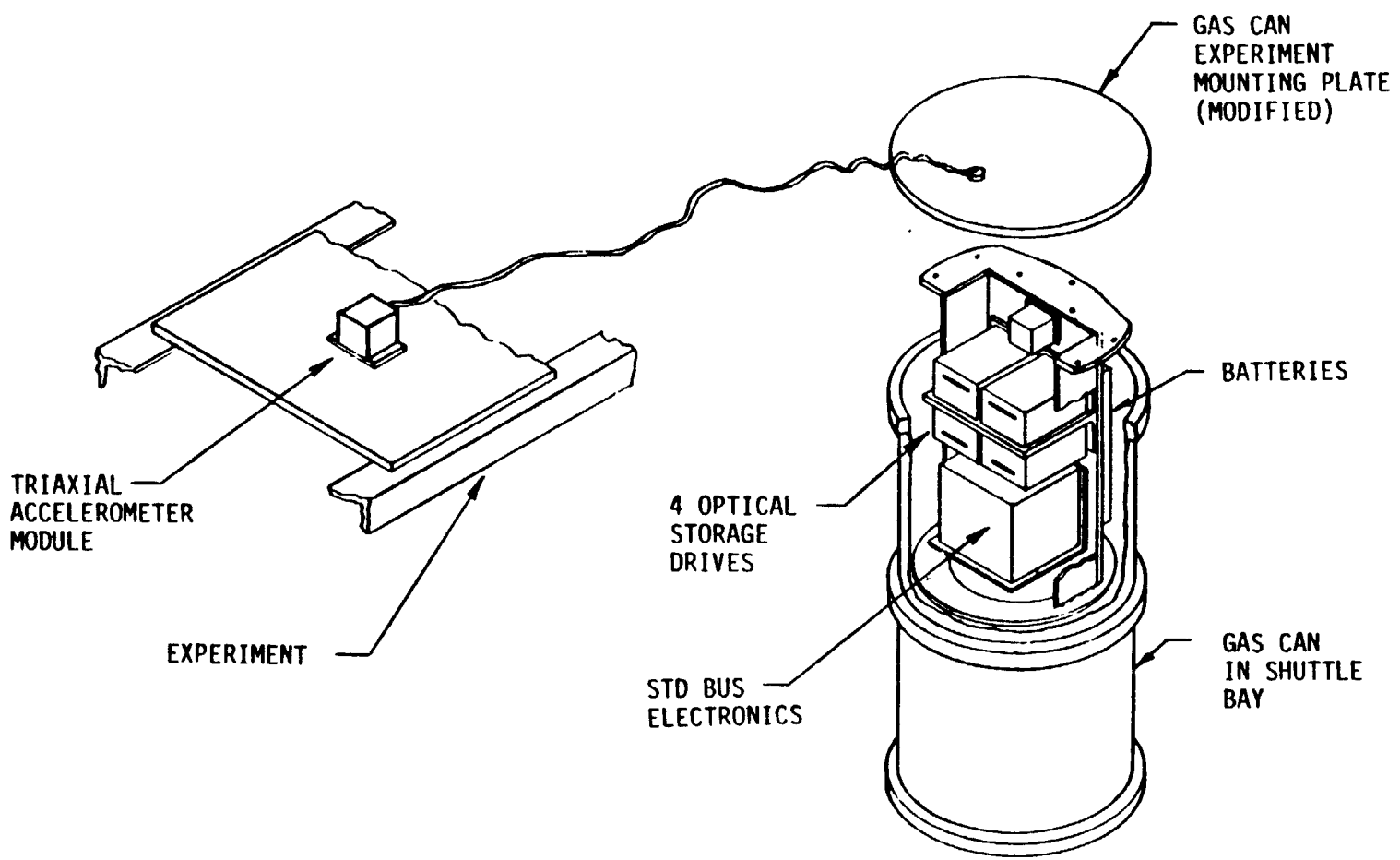

FIGURE 2 - SAMS-GAS CAN CONCEPT

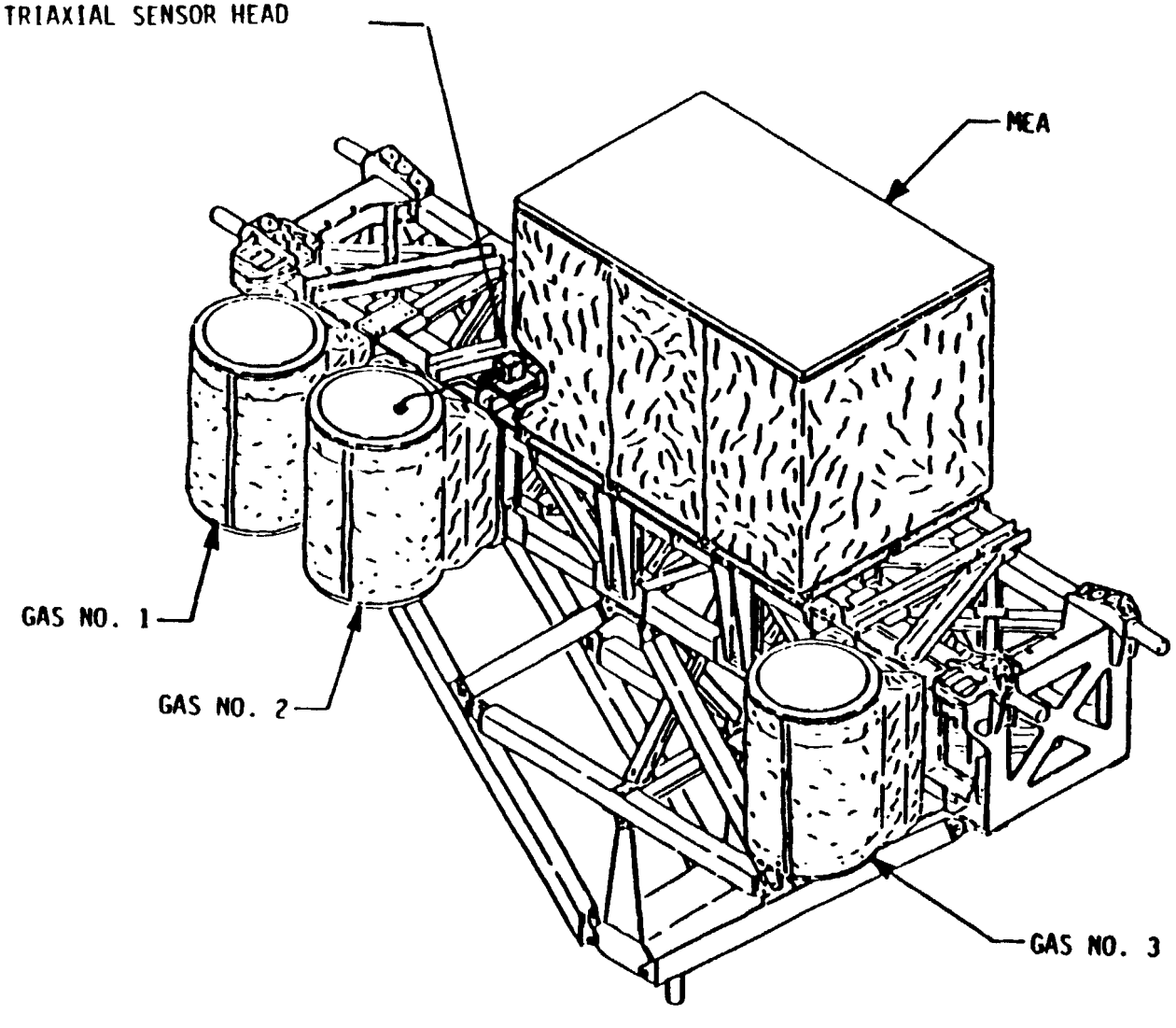

MEA-1 PAYLOAD CONFIGURATION

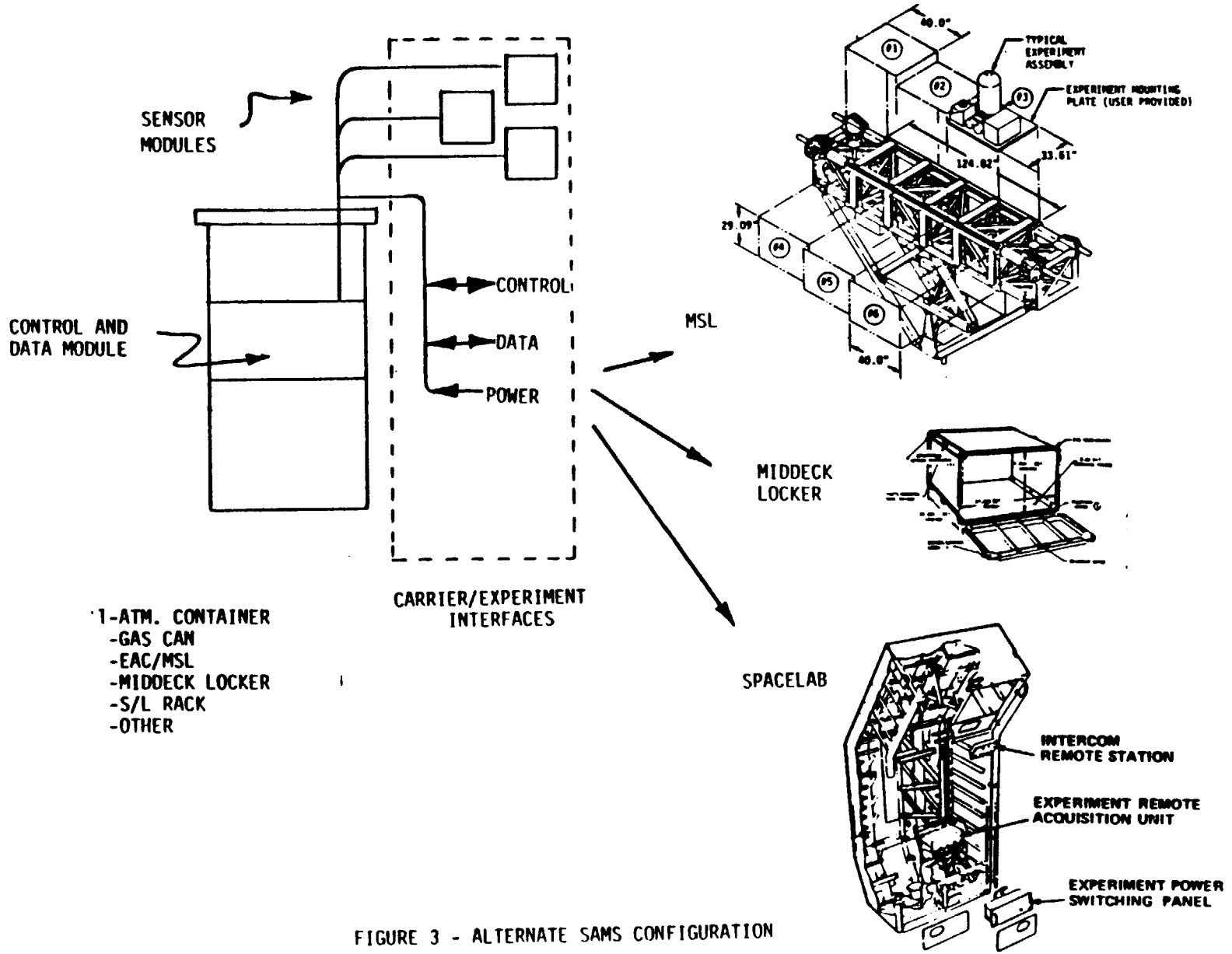

FIGURE 3 - ALTERNATE SAMS CONFIGURATION

Sundstrand Model QA-2000 high performance single axis-type sensor is to be used. Three such sensors will be mounted in a triaxial sensor head. The triaxial sensor head will also contain conditioning electronics. The sensor head will be separated from the electronics package by an umbilical cable. A range of cable lengths will be accommodated depending on experiment requirements. Each accelerometer will be equipped with a solid-state temperature sensor to enable correction of triaxial sensor output based on temperature.

The electronics package functional schematic is shown in figure 4. The design is based on the STD-BUS system. This industry standard interconnection system allows the utilization of modular electronic circuit boards incorporating a wide variety of functions. At present, at least 40 manufacturers provide products for the STD-BUS. Where possible, CMOS technology will be utilized to minimize power consumption and thermal dissipation.

A 16-bit Analog/Digital (A/D) converter card will be used to convert the accelerometer inputs as well as the temperature from each sensor.

An Input/Output (I/O) card will be used to provide bidirectional communications with the experiment.

The bytewide memory card will be used to temporarily hold data for transfer to the optical drives. This card can also be utilized to store firmware routines in ROM.

The central processor card will be equipped with the IBM PC-XT compatible 8088 Central Processing Unit (CPU). In addition, this card will be equipped with a math coprocessor, a real time clock, on-board monitor software, Read Only Memory (ROM) and capacity for 64K bytes of plug-in memory. The card will also have one RS-232 port. The RS-232 interface combined with the monitor will provide on-board checkout and verification capability through a dumb terminal.

The Small Computer Systems Interface (SCSI) card will be used to interface the optical drives to the STD-BUS.

The optical drive is the Model 5984 from OPTO-TECH, Incorporated. It uses Write Once Read Mostly (WORM) technology and occupies the same physical space as a standard 5.25" full-height floppy disk drive. It is possible to store 400 megabytes of formatted 8-bit data on two sides of the media. For unattended operation, only 200 megabytes are accessible. The system will accommodate up to four drives.

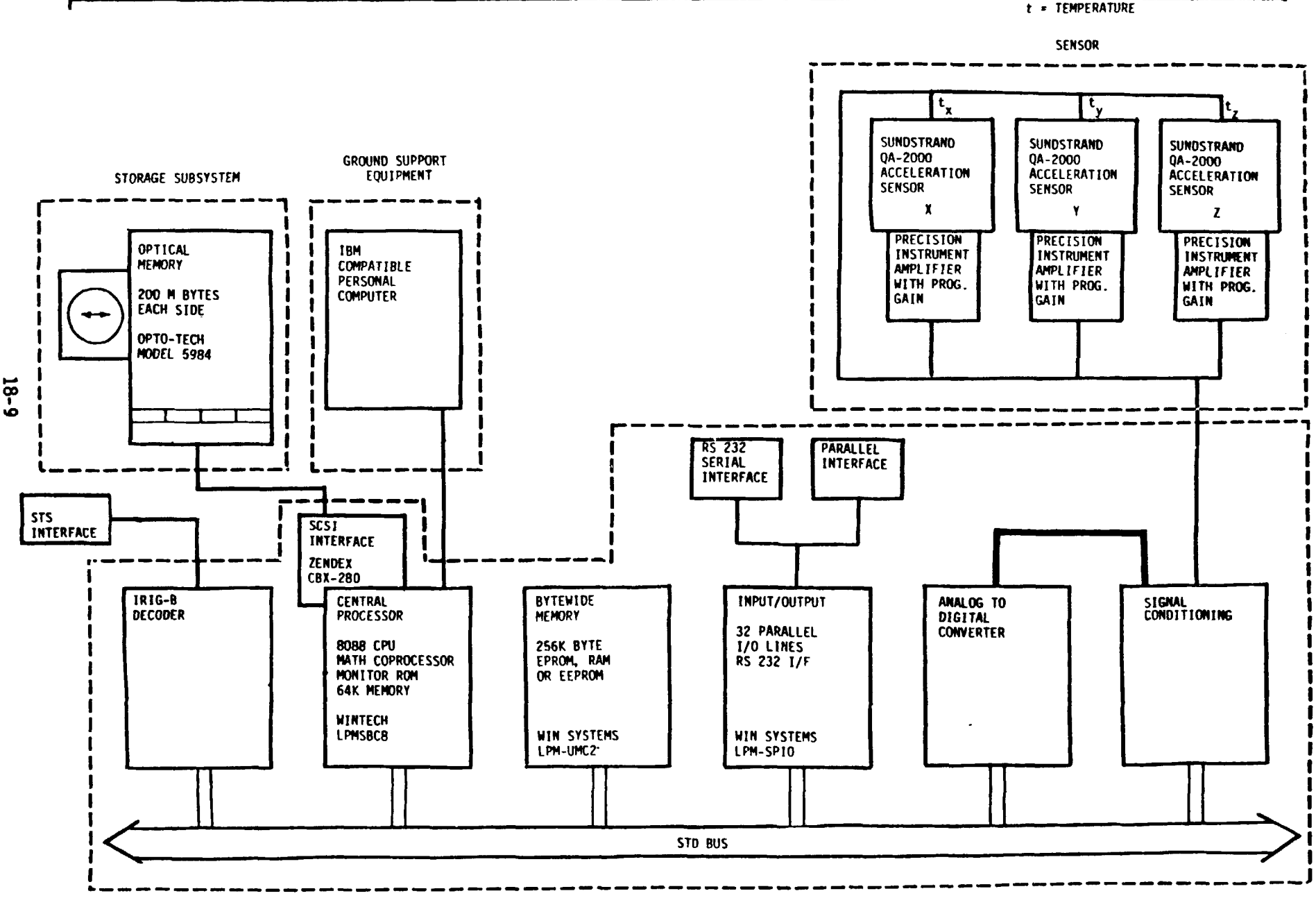

FIGURE 4 - FUNCTIONAL SCHEMATIC OF SPACE ACCELERATION MEASURMENT SYSTEM

The data transfer rate of the optical drive is 2.2 megabits/sec while the access time is 305 milliseconds (max). The mean time to failure of the drive is 20,000 hours. A ruggedized version of this drive is being developed by the Goddard Space Flight Center (GSFC). That activity will be followed closely to provide maximum benefit to the SAMS program.

Cards may be switched or added to this system to accommodate new requirements as they evolve.

Sufficient power conditioning electronics will be supplied with the package to allow the system to run from batteries or the Shuttle 28 Volt power bus.

3.2.2 Software

The software concept is shown in figure 5 and is based on the STD-DOS operating system. This DOS is IBM-capatible allowing the utilization of a wide variety of software written for the IBM-PC. This includes such things as utilities, interface drivers and high-level math routines. The three categories of application software which must be included as part of this measurement system are described below:

3.2.2.1 Input/Output

The input/output routines allow each component part of the system to communicate. All routines run on a microprocessor which is part of the STD-BUS CPU card. The memory card is used to store constants, temporary data, or systems software.

The accelerometers communicate with the STD-BUS through the analog to digital converter card. The software drivers in this case take temperature and acceleration data from each accelerometer sensor and transfer it to the optical memory.

The input/output card allows communication between the STD-BUS and devices external to the acceleration measurement system. The software drivers provide communications to experiments via parallel digital or serial (RS-232) ports. Typically, these interfaces would support the following functions: turn data gathering off and on; read data to or from experiment; flag an abnormal acceleration value; and time correlation.

The SCSI card couples the optical memory to the STD-BUS. The software drivers associated with this card provide read-write capability as well as formatting and error checking to the optical drive.

3.2.2.2 Utilities

Included among the software utilities are those that allow checkout, monitoring, and execution of developed software.

The SAMS is also equipped with a unique set of routines specifically oriented toward acceleration measurements. This includes tests of hardware such as accelerometers, A/D converters, optical drives and the serial/parallel interface.

3.2.2.3 System Software

The system software routines are defined as those which provide certain repetitive operations necessary to gather acceleration information and are as follows:

- Send and receive data over serial/parallel interface to external packages.
- Monitor peak value of acceleration and set a flag.
- Provide auto gain change for acceleration inputs based on acceleration levels or external commands.
- Read or write blocks of data from/to the optical drive.
- Provide moving window data acquisition based on either acceleration levels or external commands.

3.2.2.4 Calculations

This software provides the math routines which will utilize the math coprocessor. The math routines (1) convert accelerometer input from raw data to temperature compensated data via a polynomial calculation, and (2) digitally filter data based on certain input parameters.

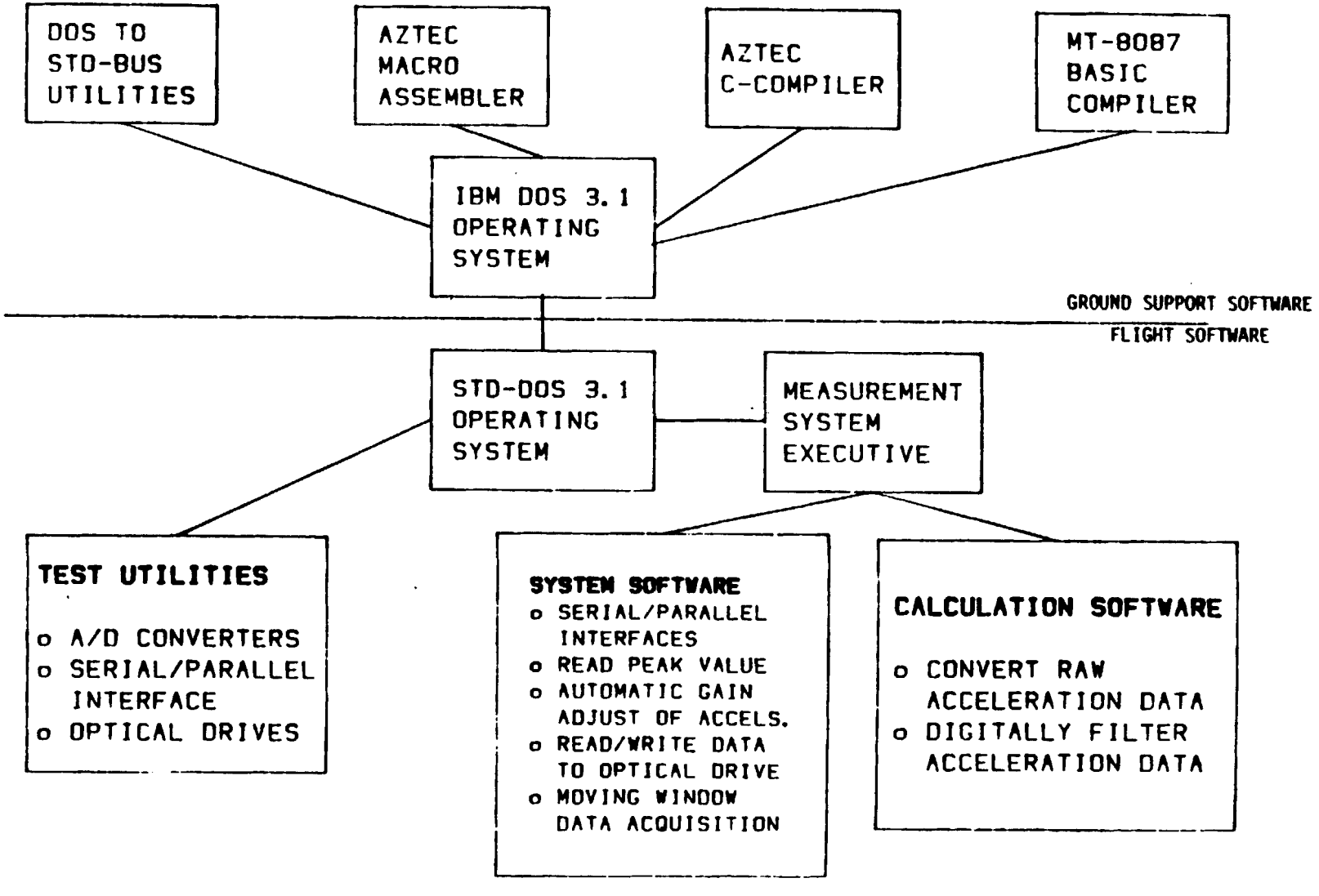

FIGURE 5 - SAMS SOFTWARE CONCEPT

3.3 System Specifications

The system specifications are defined below based on the flow of data from the sensor through to the optical recorder.

3.3.1 Acceleration Sensor

Pendulous inertial sensor employing a quartz flexure suspended proofmass, producing an acceleration output current independent of output load.

Internal temperature sensor mounted in each accelerometer to correct accelerometer output for bias, scale factor and alignment.

Sensor frequency response: 0-100 Hz +/- .2 %.

Sensor resolution and threshold: 1 micro-g.

Sensor absolute value: 10 micro-g +/- 1 micro-g

3.3.2 Sensor Package

Sensors integrated in a triaxial sensor head which includes dynamic over range prefiltering and amplification.

Sensor axes mutually orthogonal to within .0005" True Indicator Runout (TIR).

Amplifier computer-controlled with gains of 1,10,100,1000.

Sensor output standardized to +/- 1 G equal to +/- 10 volts output.

Range switching with the following ranges (16-bit word).

+/- 1 G to +/- 3×10^{-5} G's

+/- .1 G to +/- 3×10^{-6} G's

+/- .01 G to +/- 3×10^{-7} G's

+/- .001 G to +/- 3×10^{-8} G's

Triaxial sensor head operating temperature range: -55 to 95 deg. C

Triaxial sensor head separated from electronics package by a cable up to 20' in length.

3.3.3 STD-BUS Electronics Package

The electronics package is based on the STD-BUS system. The overall package will allow proper operation over a temperature range from -55 to 95 deg. C.

3.3.3.1 Signal Conditioning Board

Low pass filters configured for DC to 100 Hz.

Seventh order low pass anti-aliasing filter (-42 DB/octave).

Sensors placed into a test mode via computer control for calibration purposes.

Output controls sensor amplifier gain.

3.3.3.2 Analog to Digital Converter Card

Full 16-bit A/D conversion.

Sampling rates up to 500 samples per second, per channel.

X, Y, and Z axis inputs taken simultaneously.

3.3.3.3 Central Processor Board

IBM-XT compatible 8088 CPU chip.

8087 math coprocessor chip.

On board real time hardware clock.

Monitor ROM allowing communication via dumb terminal.

Socket space for 64K bytes of additional memory.

One RS-232 or RS-422 interface.

Programmable interrupt controller with 8 interrupts.

Direct addressing to 1 megabyte.

Precision power-on/brown out detect circuit.

iSBX module expansion connector.

iSBX to SCSI piggyback card (attaches to CPU card).

- Provides interface to the optical storage system.

3.3.3.4 Bytewide Memory Board

Stores up to 256K bytes of information.

Used for temporary storage of data.

Can be used for ROM or EPROM storage.

3.3.3.5 Input/Output Board

Allows communication with peripheral equipment.

32 lines of digital input/output (TTL or CMOS).

One RS-232 serial port.

3.3.4 Optical Recorder

Interfaced to STD-BUS system through SCSI interface.

SCSI interface supports up to four drives.

Recording capacity: 200 megabytes per drive without operator intervention.

Drive access time: 305 ms maximum.

Corrected bit error rate: 10^{-12}.

Mean time before failure: 20,000 hours.

Mechanically conforms to standard 5-1/4" full height floppy.

3.3.5 Recording Times

Assume one triaxial sensor head, three temperature inputs, time coding and assorted ancillary signals.

16 bits x 3 heads + 8 bits (all others) = 56 bits/sample

Sampling Rates	Freq. Resp.	Time to Fill 200 Megabytes (8 bits/byte)
500/sec	100 Hz	15.9 hrs
250/sec	50 Hz	31.7 hrs
50/sec	10 Hz	158.7 hrs (6 days, 14 hrs)
25/sec	5 Hz	317.4 hrs (13 days, 5 hrs)
5/sec	1 Hz	1587 hrs (66 days)

3.3.6 Power System

Sufficient power conditioning will be included in the package to allow the system to run from batteries or the Shuttle 28 volt DC power bus. DC to DC converters will be utilized to convert 28 volt power to +/- 15 volts, 12 volts, and 5 volts.

3.3.7 System Power Requirements

Triaxial accelerometer system	2 W
STD-BUS electronics package	10 W
Optical memory	15 W
	27 W

(Assumes DC to DC converter efficiency of 80%)

TOTAL POWER REQUIRED	35 W*

* Does not include heating or cooling energy that may be required; thermal analysis to be performed to define requirements.

3.4 First Flight System Configuration

The first SAMS built is planned to be flown in the Shuttle bay in a GAS can (see figure 2). The system will be used to determine the response to low-level acceleration of the MSL-3/MPESS carrier containing the MEA and three GAS cans. The data gathered will be used to determine the isolation requirements for the Lambda Point Experiment managed by JPL. The data gathered should also be of interest to the space experiment community at large. In this configuration, the SAMS will be equipped with a battery pack to supply power to the electronics. Any additional power required to thermally stabilize the package will be supplied by the Shuttle 28 VDC power bus. External control of the SAMS will be accomplished through the use of the Autonomous Payload Control System (APCS). This will allow the astronauts to remotely control three latching relays located at the base of the GAS can. This system will provide the ability to power up, reset and time syncronize SAMS.

In this configuration, the triaxial sensor head will be mounted on top of the MPESS structure adjacent to the MEA as shown in figure 6. This location appears to be an optimum one for characterizing the MPESS structure. The sensor head will be insulated, heated and thermally isolated from the MPESS structure. This will insure that the sensors remain within a tolerable temperature range.

The general specifications outlined above in Section 3.3 apply to this configuration with the following exceptions:

Data will be recorded over a DC-100 Hz frequency range only.

All data will be stored as raw information.

No preprocessing or digital filtering of data will be employed.

Ten hours worth of data will be recorded.

Data will be taken in bursts ranging froom 10 to 20 minutes long.

Automatic range switching will be employed.

3 5 Baseline System Configuration

The baseline system configuration will conform to the general specifications given in Section 3.3 above. Two completely operational general purpose systems will be developed under this project. The initial system will be configured to meet the first flight requirements as specified in Section 3.4. After the initial system has been completed and in process, the second system will be assembled using the baseline configuration. Once the initial system has been returned from flight, it will be retrofitted such that both systems will be identical. The balance of the funding through 1991 will be used to adapt the SAMS to specific space experiments as requirements arise.

4 0 MANAGEMENT PLAN

The Space Acceleration Measurement System (SAMS) project will be managed by the Space Experiments Office (SEO) of the Aerospace Technology Directorate (ATD) of the Lewis Research Center. The organization charts for LeRC, the ATD, the SEO and the SAMS project are presented in figures 7 through 10, respectively. Other divisions at Lewis that will support the project include the R&QA Office, the Test Installations Division for testing and assembly, the Fabrication Support Division, and the Procurement Division.

Because the system being developed is a general purpose one designed to accommodate a wide-range of experiments, there will be no assigned principal investigator. However, since the initial system is to be used to take preliminary data for the Lambda Point Experiment, special consideration will be given to that project in developing the acceleration measurement system. The JPL-managed Lambda Point Experiment requires acceleration data as soon as possible to finalize experiment requirements.

The Marshall Space Flight Center will be responsible for payload integration with the MSL. LeRC will support the safety meetings and project integration documentation required by Marshall. MSFC will also supply the GAS can which attaches to the MSL and contains the SAMS hardware. Lewis will coordinate directly, but informally, with appropriate offices to insure that the system is readily adaptable to a variety of Shuttle Orbiter environments, viz., GAS cans, middeck, and Spacelab.

Progress will be reported in the MICS report submitted by LeRC SEO and Headquarters MSAD. Status will also be provided to Headquarters personnel during biweekly telecons.

5.0 PROCUREMENT APPROACH

The SAMS will be designed, fabricated, and assembled within LeRC. Engineering support will be supplied by an on-site support service contractor. Components, materials, and fabrication will be purchased through the normal Lewis purchase request system. Parts will be bought by the Procurement Division, and fabrication will be performed or contracted by the Fabrication Support Division of Lewis. Two systems will be developed for flight and one set of spares will be provided.

Accelerometer sensors and optical disk drives represent long lead-time items for this project.

6.0 PROJECT SCHEDULE

The project schedule is shown in figure 11. The project was initiated in March of 1986. The first unit is scheduled for delivery in 20 months (October of 1987), the time required to develop a general purpose system of sufficient capability to gather data for the Lambda Point Experiment. The second unit will be available in in June of 1988, 27 months after project start.

A PERT chart will be generated to assist the project manager with respect to hardware development, purchasing and fabrication. This chart will be updated periodically.

Dick Gates, Boeing: Can your system handle more than one sensor head as well as the Python?

Chase: It can support three sensor heads as it's configured. It is limited by the standard bus system to how many boards you can plug in. We have nine slots. The only other limitation will be the number of connectors you can get on the box that you're putting it into. We configured it so that there will be three connectors there allowing us to go to a total of three.

Bob Naumann, NASA/Marshall Space Flight Center: You said you completed a survey and found those other instruments inadequate. Yet I don't see anything terribly unique about this equipment. Can you tell me what this equipment does that others don't do.

Chase: We found that the instrumentation was either limited in the g-range, limited in frequency, and a little bit of this and a little bit of that, but nothing that would operate over the whole spectrum. Also, things like low power consumption, the ability to be able to go into one locker, mid-deck locker space, power, there are a number of considerations.

Naumann: What really worries me is that one of the biggest inadequacies is that we have not had a system that will integrate to get the background dc acceleration we know we're supposed to see. And you're saying that you had a hard time, I think you said it was a resolution of 1 Micro-g, with a 10-micro-g absolute accuracy. So if you're only working with 10 micro-g that's 10^{-5}, but that's the top end of the dc level we want to see. So that won't even sense the environment we hope to have on the Space Station.

Chase: That's true. That is dependent upon where you're going with the sensor technology. There's nothing magic about the Sundstrand. Those are the limitations attached to the Sundstrand. If you want to go to a Bell Model 11 that's a different story. If you want to pay the price penalty. That's something that the experimenter will have to determine. Again, there's nothing magic about the sensor, ...

it's the same as Byron's system. If you want to change the sensor, that's up to you.

Naumann: So the big problem there is in the noise at the low frequencies to the Sundstrand head, which you previously talked about, is that basically it?

Chase: Yes.

N91-12418

19. ACQUISITION AND ANALYSIS OF ACCELEROMETER DATA

Keith R. Verges, Teledyne Geotech

ABSTRACT

Acceleration data reduction must be undertaken with a complete understanding of the physical process, the means by which the data are acquired, and finally, the calculations necessary to put the data into a meaningful format.

This paper will discuss the acceleration sensor requirements dictated by the measurements desired. Sensor noise, dynamic range, and linearity will be determined from the physical parameters of the experiment.

The digitizer requirements will be discussed next. Here the system from sensor to digital storage medium will be integrated, and "rules of thumb" for experiment duration, filter response, and number of bits will be explained.

Data reduction techniques after storage are next. Time domain operations including decimating, digital filtering, and averaging will be covered. Frequency domain methods, including windowing and the difference between power and amplitude spectra, will be discussed. Simple noise determination via coherence analysis shall be included.

Finally, an example experiment using the Teledyne Geotech Model 44000 Seismometer to measure accelerations from 10^{-4}g to 10^{-10}g over a bandwidth from 1 Hz to 10^{-6} Hz will be discussed. The sensor, data acquisition system, and example spectra will be presented.

INTRODUCTION

In order to acquire and analyze data in such a way as to characterize the acceleration environment, one must consider three primary areas:

1. The sensor(s) themselves. The accelerometers must be selected carefully in order to be certain that they are suited to measuring the anticipated signals.

2. The Data Acquisition System. For later analysis, the data must be converted to a digital form and stored. This process involves signal conditioning, analog to digital conversion, and storage. These steps must dovetail with the sensor such that they do not adversely affect the experimental goals.

3. The Analysis Techniques. The digital representation of the data must be operated upon in some way to provide meaningful, standard data. The methods used have inherent limitations and assumptions. One must have a good working knowledge of these factors in order to make quantitative judgments.

This paper will briefly discuss each of these three areas to explain techniques and terminology. Finally, an example experiment involving vertical accelerometer data will be presented. The data set is from a Teledyne Geotech Model 44000 Seismometer and was collected continuously over an interval of 72 hours. Signals due to teleseismic earthquakes, tidal fluctuations, and system noise were recorded. Acceleration levels as low as 10^{-12} g were discernible from system noise. The data was Fourier Transformed to yield spectral components with frequencies as low as 3×10^{-6} Hz.

SENSOR REQUIREMENTS

Dynamic Range

The dynamic range refers to the ratio between the largest and smallest signals measured. Obviously, the sensor selected must meet or exceed that dynamic range.

In the case of the Spacelab experiments, the anticipated signal is not well defined. Accelerations as low as 10^{-8} g may be expected, particularly at low frequencies. At higher frequencies, 10^{-3} g is likely during a typical experiment. The sensor chosen must therefore have an intrinsic dynamic range of at least 10^5 or 100 dB. A single figure can be misleading, however. Generally, we know what the peak acceleration permissible without distortion is. The minimum measurement will be limited by the system noise, which will in general have some variation with frequency. Bandwidth, too, is important in determining dynamic range requirements.

Consider a simple case where an instrument has 10^{-18} g^2/Hz noise, flat from dc to 100 Hz. If we were to integrate this power over a bandwidth from dc to 1 Hz, then the rms power would be 10^{-9} g. However, if we were interested in low frequencies and limited our bandwidth to 10^{-4} Hz, the rms power would be only 10^{-11} g. The important point here is that the average signal amplitude in time can translate to vastly different power spectral densities, dependent upon the bandwidth of interest.

Dynamic range is then actually a function of frequency. The sensor noise and full scale range are intertwined with the dynamic range.

Noise

After determining the dynamic range, this scale must be referred to an absolute value. The sensor should not have noise any higher than the smallest anticipated signal. In fact, a good rule of thumb is that the sensor noise at any given frequency should be at least 10 dB below the anticipated signal. Specific processing methods may require an even lower noise margin. This must be remembered as part of the sensor selection.

For the space station case already mentioned, we might want an accelerometer with internal noise no greater than 10^{-18} g^2/Hz, particularly at low frequencies. This also implies that the dynamic range requirements have been increased to 10^6 or 120 dB.

Linearity

Imagine that a full scale pure sine wave signal at a given frequency is applied to our sensor. If the response of our sensor is not purely linear, then the output signal will have components at all integer multiples of that frequency. If a pair of sine waves are applied, then both the difference and sum frequencies will appear at the sensor output. Hence, large signals at high frequencies can produce apparent signals at much lower frequencies due to response nonlinearity.

Since nonlinear behavior is not a one-to-one function, processing cannot extract the original input signal. We must rely on the instrument itself to provide output with high fidelity.

The expected signal range must not be such that harmonics or sum/difference signals will be created in other parts of the spectrum. If we define nonlinearity to be the size of the first harmonic of a full scale signal, then the nonlinearity must be less than 10^{-5} if the full dynamic range is to be utilized at the harmonic frequency.

All the above is really only an introductory discussion of noise and dynamic range requirements. A hypothetical case is shown in Figure 1. Here, the three performance specifications, dynamic range, noise, and linearity are drawn as a function of frequency from 1 to 10^{-6} Hz. Now consider a signal spectrum as shown in Figures 2a and 2b. The sensor has gain that is 20 dB at all frequencies. The input and output spectra are shown superimposed on our hypothetical sensor performance curves. Figure 2a will be represented properly at the sensor output, as it does not exceed the performance of the sensor. Figure 2b shows the effects of nonlinearity and excessive noise. The noise is apparent in the output spectrum, as is the harmonic of the input peak that exceeded the sensor linearity.

DATA ACQUISITION SYSTEM

With an appropriate sensor selected, the signal must be interfaced with some system in order to provide digital data for later pro-

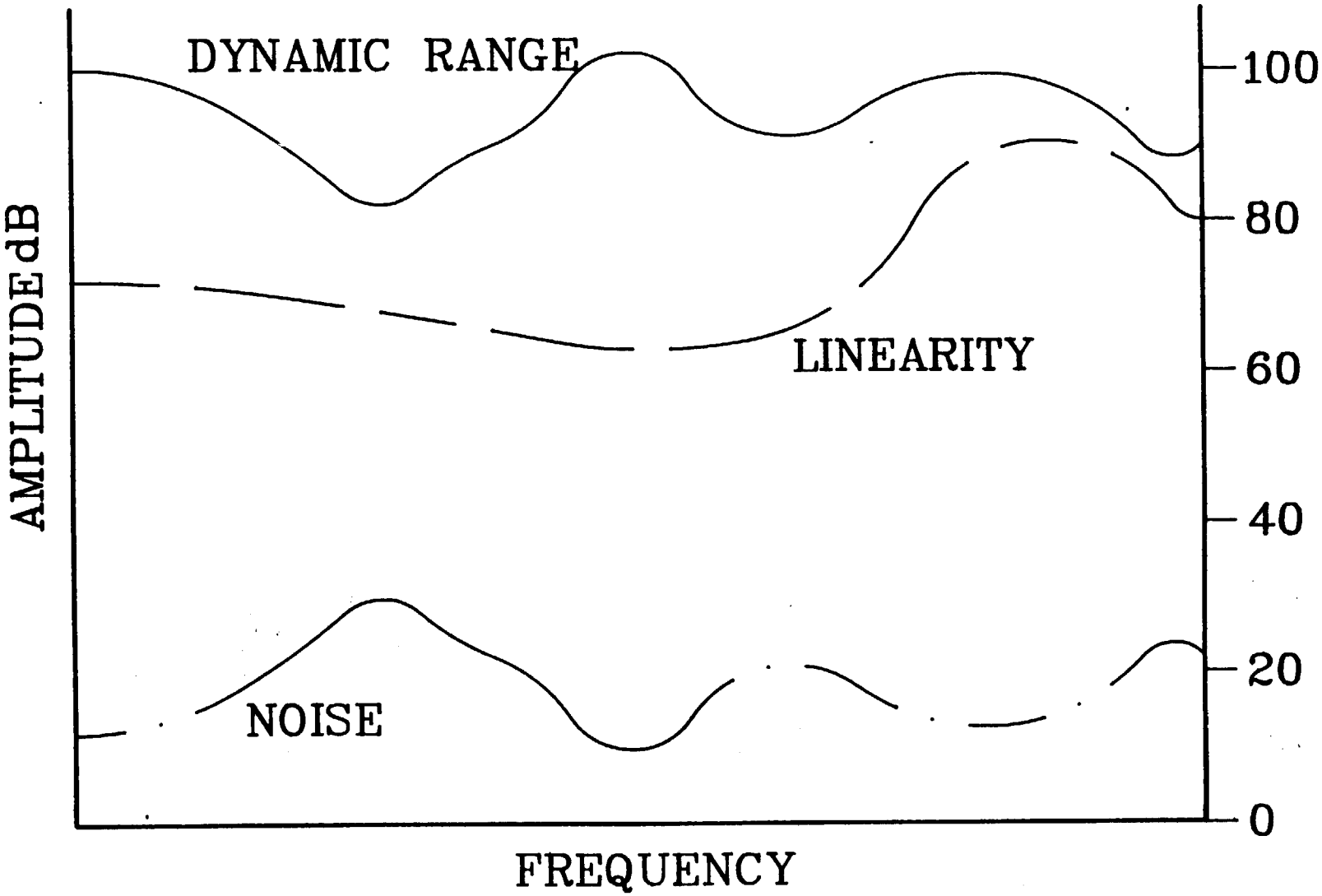

FIGURE 1. SENSOR CHARACTERISTICS

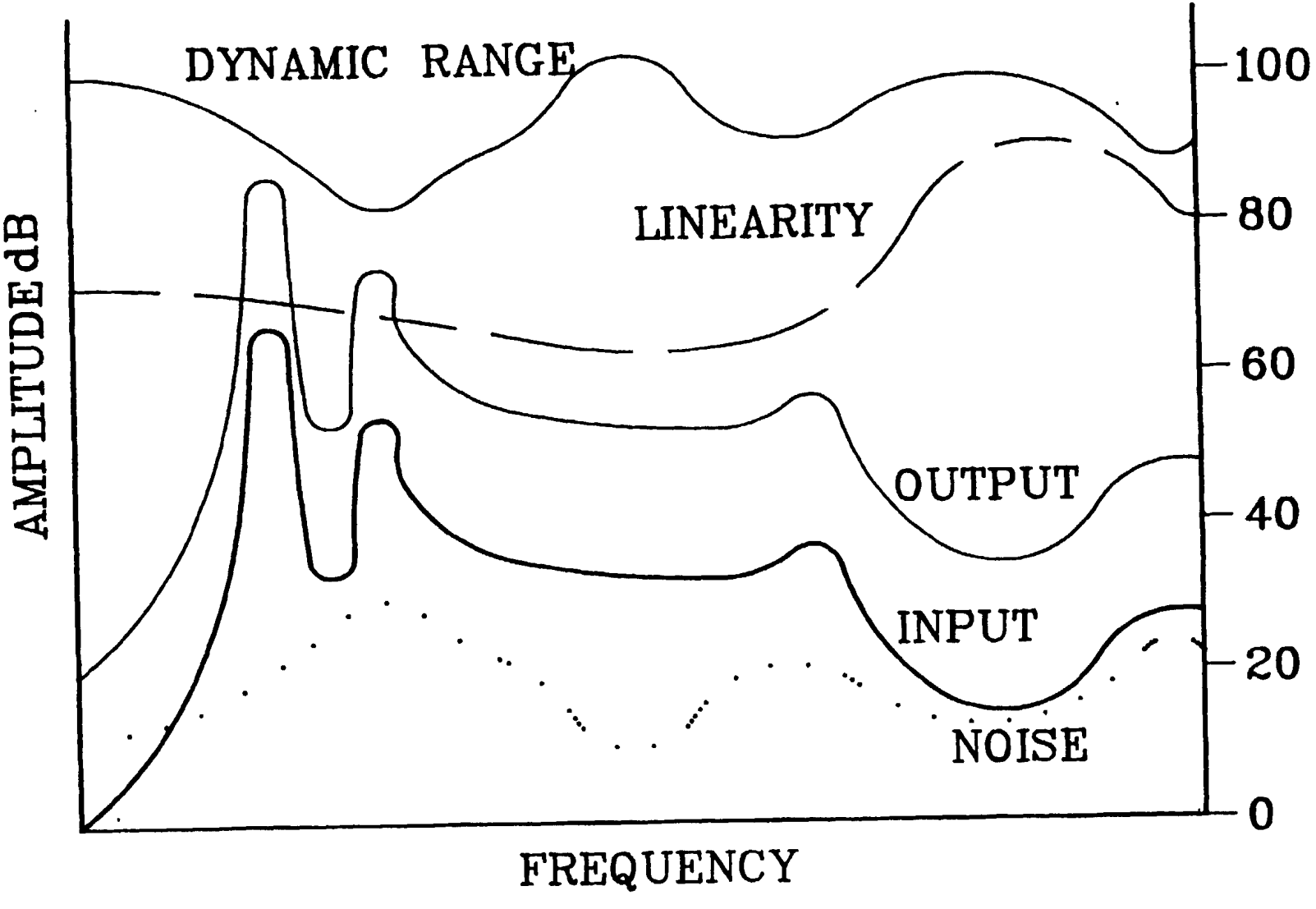

FIGURE 2a. SIGNAL THROUGHPUT (ADEQUATE SENSOR SELECTION)

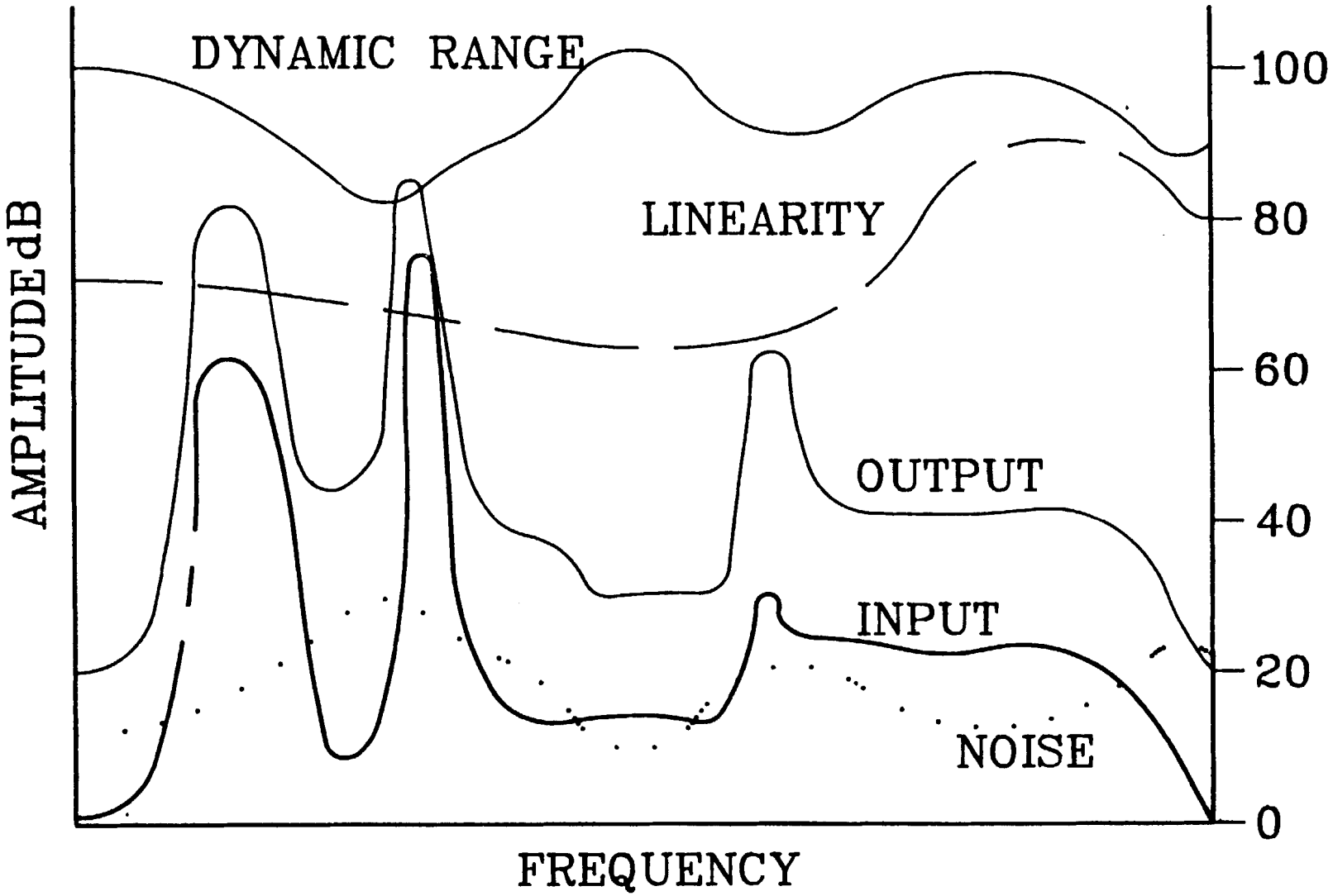

FIGURE 2b. SIGNAL THROUGHPUT (POOR SENSOR SELECTION)

cessing. The data must be stored on some medium suitable for the processing computer to read and work with. Discussion of some of the most important specifications follow.

Signal Conditioning

In the case where the sensor signal is an analog voltage, there will most likely be a requirement to condition that data prior to digitization. The most important areas include gain and filtering.

The gain serves to match the noise and dynamic range of the sensor to that of the digitizer.

Filtering prevents aliasing. Figure 3 shows the effect of sampling on a spectrum. The signal spectrum is folded about the axis at w=0 and repeated at every interval of the sampling rate. If at frequencies greater than the sampling rate divided by two (Nyquist Frequency) the input signal has non-zero frequency components, then they will be "folded" back into the spectrum. This can be avoided by filtering the input spectrum such that the signal at the Nyquist frequency is below the resolution of the digitizer. The sample rate and digitizer resolution then dictate the required filter response. Figure 4 shows the filter requirements as a function of sample rate, digitizer dynamic range, and desired signal bandwidth.

Sample Rate

The sample rate requirements have been briefly mentioned already. The sample rate is driven by two factors:

1. Signal Bandwidth. The desired signal bandwidth along with the anti-alias filter response help specify the minimum Nyquist frequency.

2. Oversampling requirements. If the quantization noise spectrum is too large for a given digitizer, the noise spectrum can be reduced by an increase in sample rate followed by digital filtering (as opposed to building/buying a higher resolution digitizer).

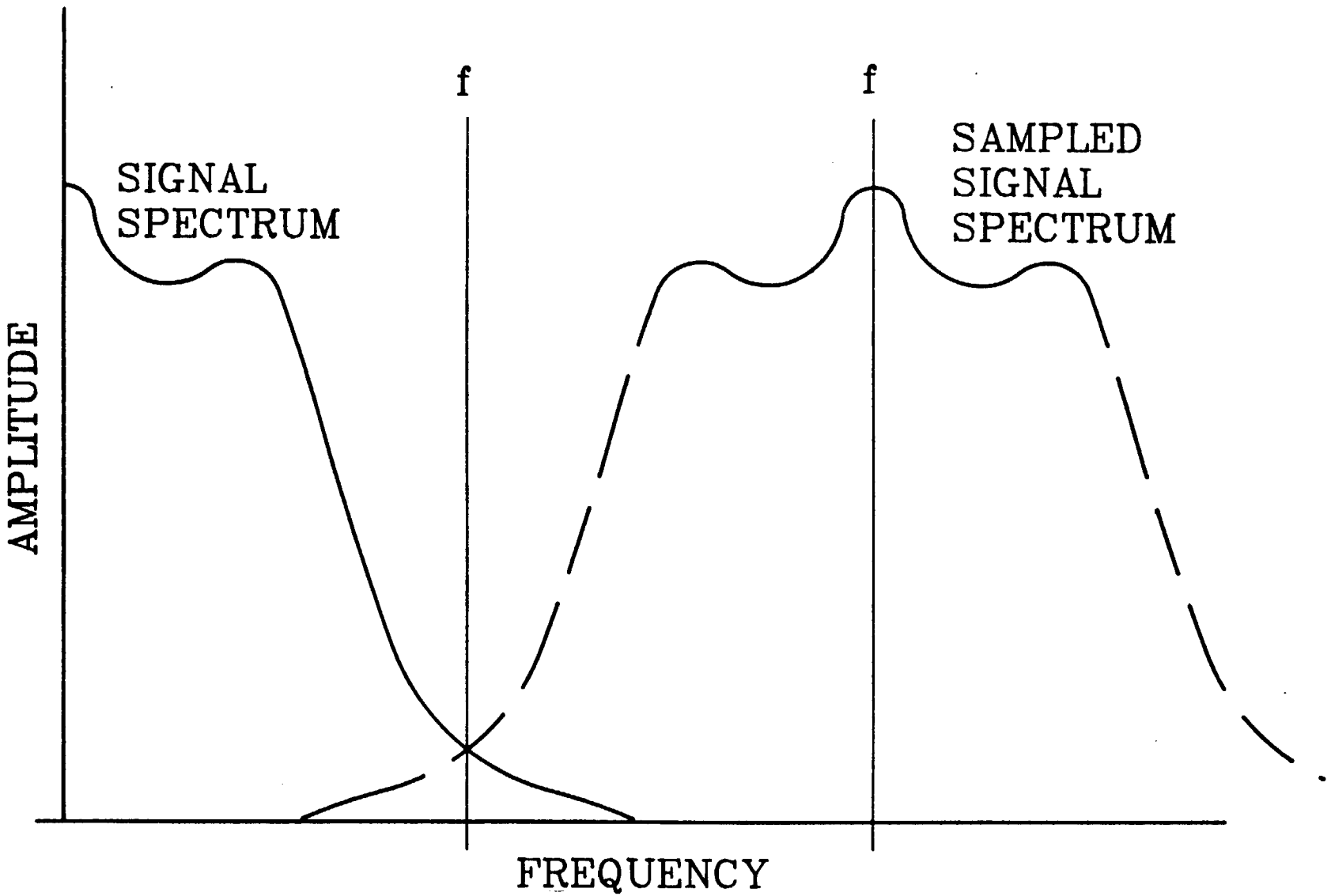

FIGURE 3. ALIASED SIGNAL

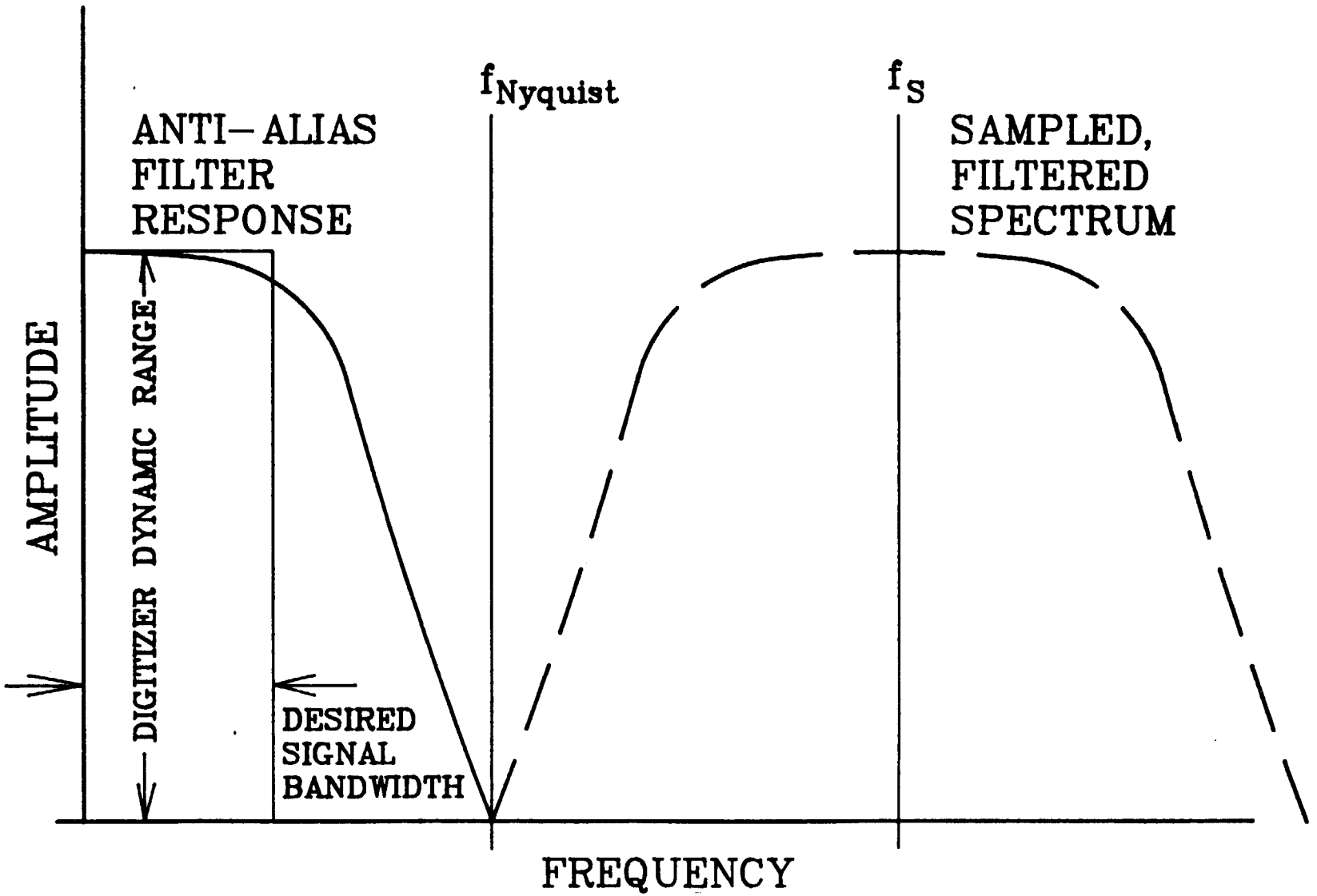

FIGURE 4. ANTI-ALIAS FILTER

Signal bandwidth refers here to the frequency interval over which we want to see the data. If the filter has a 3 dB corner at the edge of this band, it will roll off to a point below the digitizer resolution at some higher frequency f_{co}. The Nyquist frequency must be at least this great, hence the sample rate $f_s > 2f_{co}$. Refer to Figure 4, where $f_{co} = fN_y$. Of course the f_{co} can be decreased by a steeper roll-off in the filter response. The tradeoffs here are between the filter response and sample rate. A more complex filter is required to have the signal bandwidth a larger fraction of the Nyquist Frequency.

Oversampling is mentioned here as a means of decreasing the in band quantization noise. The enhancement as a function of sample rate will be discussed further in the following section.

Resolution or Number of Bits

A digitizer with sufficient dynamic range to complement the sensor must be selected. It would be foolish to use an 8-bit ADC for the purpose of digitizing a voltage with 100 dB dynamic range. Here the digitizer must be specified in much the same way as the sensor so that they will complement one another in terms of dynamic range and noise.

Scaling: The input amplifier must be set up to match the full scale range of the sensor to that of the digitizer. Figure 5 shows a simplified block diagram of a digital acceleration measurement system. If we have a maximum voltage for the ADC defined as V_{MAX}, then we do not want to exceed this value through the sensor and filter/amplifier. If the transfer functions for the sensor and filter/amplifier are F_s ($V/m/s^2$) and F_A (V/V) respectively, then we can express the desired V_{MAX} to a_{MAX} (both values are 0 to peak measurements) relationship:

$$V_{MAX} = F_s F_A \, a_{MAX}.$$

We simply adjust F_A to make the maximum anticipated acceleration a_{MAX} yield the V_{MAX} for the ADC. The anticipated acceleration should be estimated conservatively, as exceeding this limit will result in a hard clip of the data acquisition system.

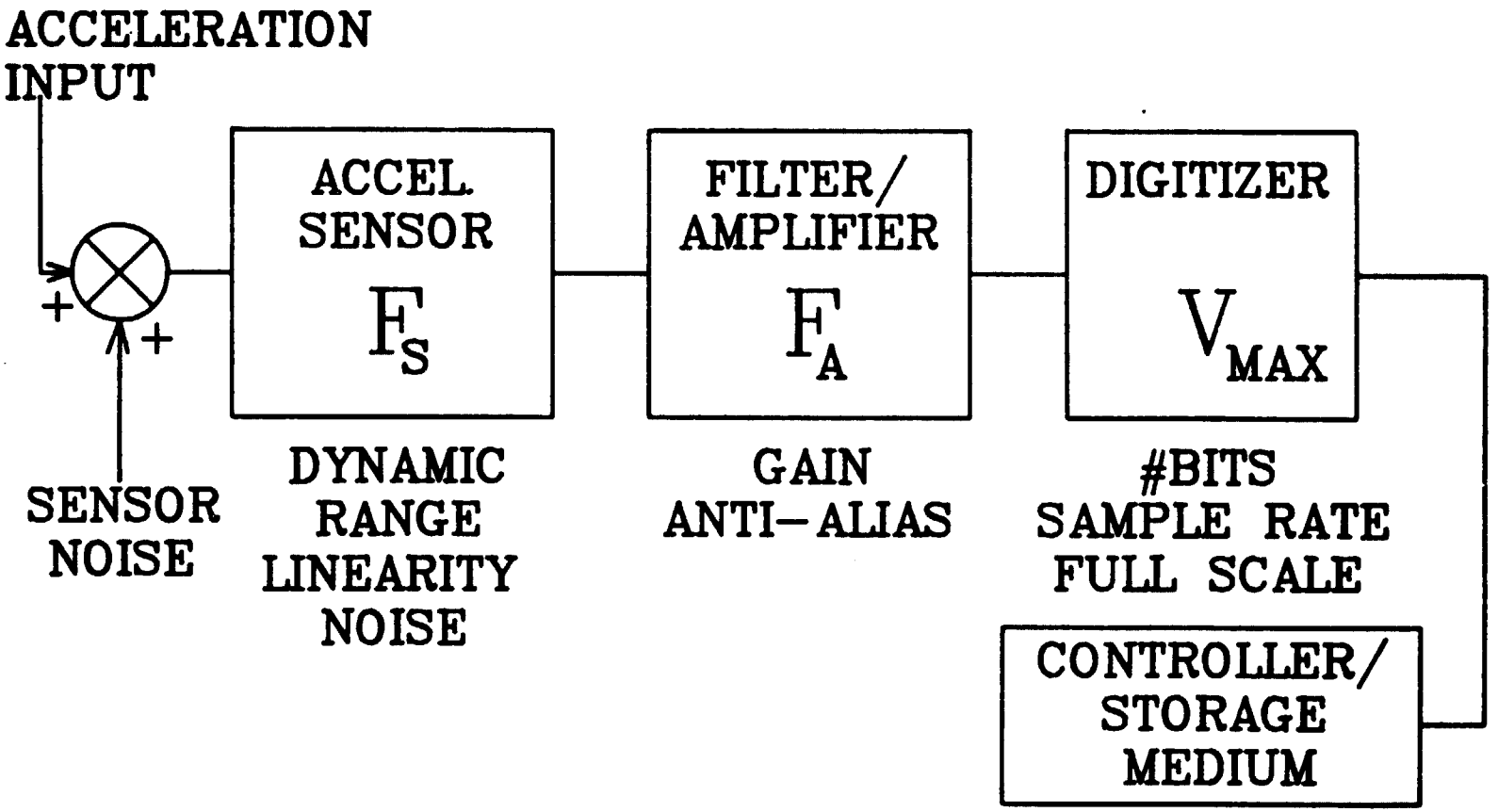

FIGURE 5. SYSTEM BLOCK DIAGRAM (SIMPLIFIED, SINGLE CHANNEL)

Dynamic Range: The required dynamic range for the ADC can be specified in number of bits N. This is a function of the sample rate and least significant bit Q. The root mean square noise for a digitizer is:

$$\bar{V}_{ND}^2 = Q^2/12$$

If the signal is much larger than Q, then this noise is white and its spectrum is distributed over the band from $-fN_y$ to fN_y. fN_y is the Nyquist frequency and is one half of the sampling frequency f_s. Figure 6 shows the spectra of two different sampling processes. The lower plot has twice the sample rate of the upper plot. The rms amplitude in each case is the same, but the energy is spread out over a greater bandwidth in the lower case. The spectrum of the quantization noise has amplitude:

$$\bar{V}_{ND}^2 = Q^2/12fs$$

Relating this to acceleration:

$$\bar{V}_{ND}^2 = F_s^2 F_A^2 a_{MAX}^2/3fs2^{2n}$$

Here we have used the fact that for a digitizer of resolution N, Q is related to V_{MAX}:

$$Q = V_{MAX}/2^{N-1}$$

If we look at the quantization noise spectrum referred to acceleration, we can get an estimate of the dynamic range requirements:

$$\bar{A}_N^2 = a_{MAX}^2/3f_s2^{2N}$$

For example, imagine an experiment where the maximum acceleration was to be 10^{-3} g. If we used a 16-bit ADC and 100 Hz sample rate, then the power spectral density of the quantization noise can be calculated:

$$\bar{A}_N^2 = 7.8 \times 10^{-19}\ g^2/Hz$$

or

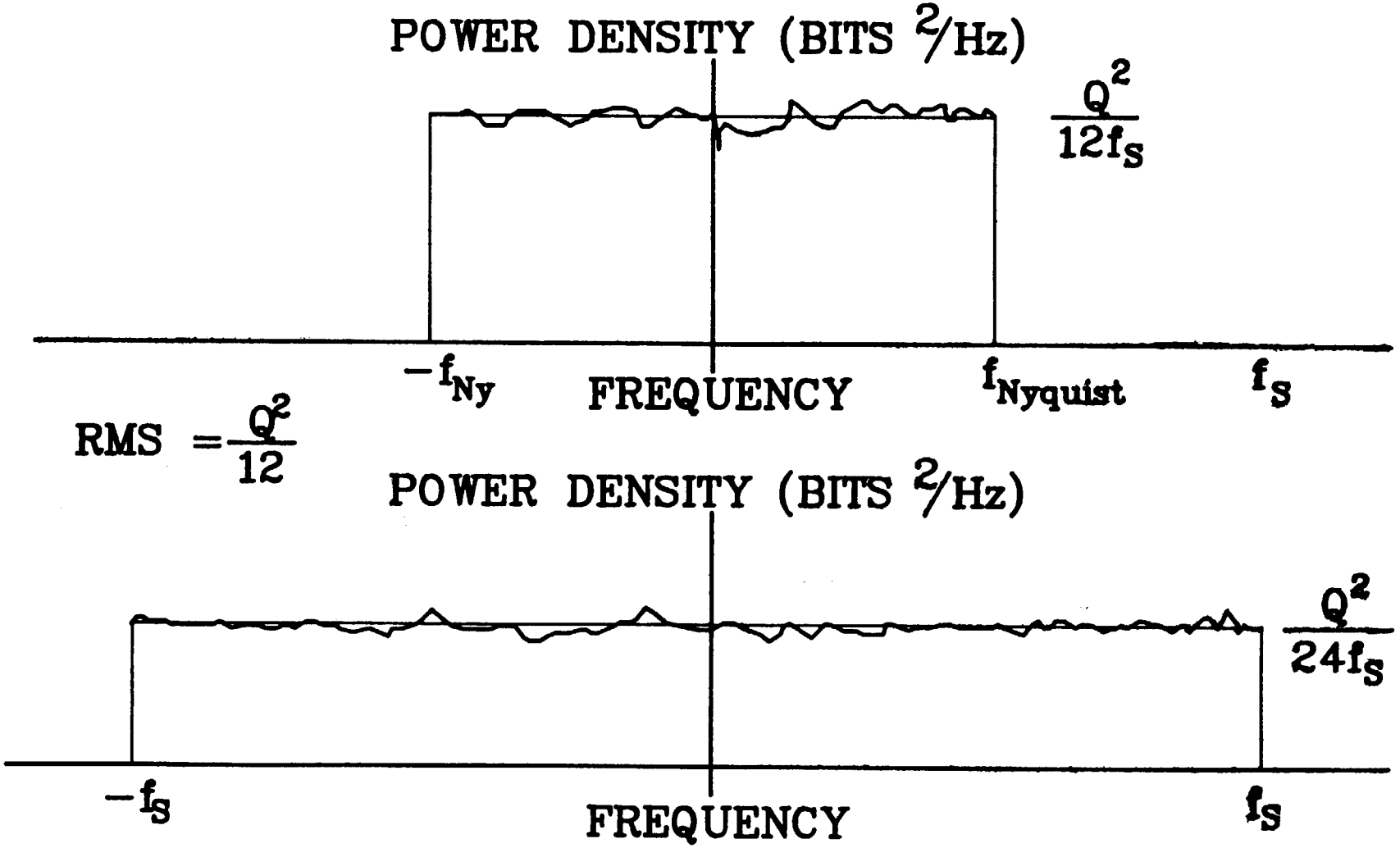

FIGURE 6. QUANTIZATION NOISE (FOR DIFFERENT SAMPLE RATES)

$$\bar{A}_N = 8.8 \times 10^{-10} \text{ g}/\sqrt{\text{Hz}}$$

We see that we can reduce the quantization noise density simply by increasing the sample rate. If storage capacities permit, the sample rate can be increased as much as desired to capitalize on this phenomenon. The tradeoff here is with the maximum sample rate achievable, along with storage and computation limitations.

Importantly, no single figure for the dynamic range has been specified here. This is because the scaling was done using an estimate of the time signal. The spectral nature of this signal will change experimental signal-to-noise ratio. If, for example, the signal were a pure sine wave, then the spectral power would be confined to a small part of the spectrum and would be very large. If, on the other hand, the signal was Gaussian and distributed evenly over all frequencies, then the spectral power at each frequency would be far smaller. Clearly, the dynamic range calculations would be very different for these two cases.

ANALYSIS AND COMPUTING

After the experiment is over, we will have some data set consisting of time samples in a digital format. This data will be of interest in both the time and frequency domain.

Time Analysis

For a start, we may at least want to see the signal as a function of time, "strip chart" style. However, if we have data that was sampled every 10 milliseconds, the strip chart over a period of a day could be pretty long. Furthermore, the computation time to operate on such a large array can be prohibitive.

Size Reduction

The physical process of filtering and sampling the acceleration data during the experiment limits the bandwidth and resolution obtainable in the analysis. A typical broad-band experiment can produce many

Mbytes of data for any given channel. This data set cannot be operated on in any but the most rudimentary way as a whole. We will want to break the entire set down or compile it in such a way as to make these subsets more manageable.

If we simply take a subset of the data, this makes things more manageable, but places limitations. A Fourier transform of a set of data with duration T_{EXP} and sample spacing T_s will have spectral resolution and bandwidth:

Minimum frequency	$= 1/T_{EXP}$
Frequency resolution	$= W/T_{EXP}$
Maximum frequency (or bandwidth)	$= 1/2T_s$

Where W is the window factor, always greater than unity. Windowing is discussed further below.

The simple subset has as high a bandwidth as could be possible under the constraints of the experiment, but the frequency resolution and minimum frequency suffer from the truncation process.

Decimation

We would decimate the data set to a more manageable size. By picking every N^{th} sample the array size will be decreased by an equal factor. This process can induce aliasing, so the decimation process must be preceded by digital filtering.

Digital Filtering

The raw digital data set can have a bandwidth too great to permit practical calculation of Fourier transforms of low-frequency components with high resolution. We can simply filter the data digitally down to a smaller bandwidth and decimate in order to "zoom in" on the lower frequency components.

Two basic techniques for digital filtering are in common use. The filters are often designated as recursive or nonrecursive.

Recursive filters: These filters calculate a single time element from a linear combination of previous input and output time elements. "Recursive" refers to the fact that previously output samples are "fed back" to the calculation process. They require little computational time, since typically only a few previous elements are used in each calculation. However, a precise desired response can be hard to form from this technique.

A typical recursive filter design is based on analogy with analog filters. Desired poles and zeros are used to determine the Laplace transform of an analog filter. The Laplace transform can then be converted to a Z-transform. Finally, the Z-transform coefficients yield the time series domain function required for the filter. This process is generally approached from a pole-zero starting point. An arbitrary frequency response cannot in general be obtained from a recursive filter.

Other disadvantages of recursive filters arise from their close analogy with analog filters. The existence of poles in their response can cause calculations to "explode" during the filtering process. Furthermore, the phase response of a recursive filter is nonlinear function of frequency. Hence different frequency components of the time series will have different time delays through the filter. This can distort the time series of some discernible "event" significantly.

Nonrecursive or Finite Impulse Response (FIR) Filters: Another class of digital filter is the FIR filter. This filter is simply a linear array of coefficients that are convolved with an equal number of elements of the time series to yield a single filtered time series element. Figure 7 shows the operation of calculating a single filtered element from a time series. The filter coefficients (top) operate on the time series (below):

$$Y_m = \sum_{n=o}^{N} a_n X_{m-n}$$

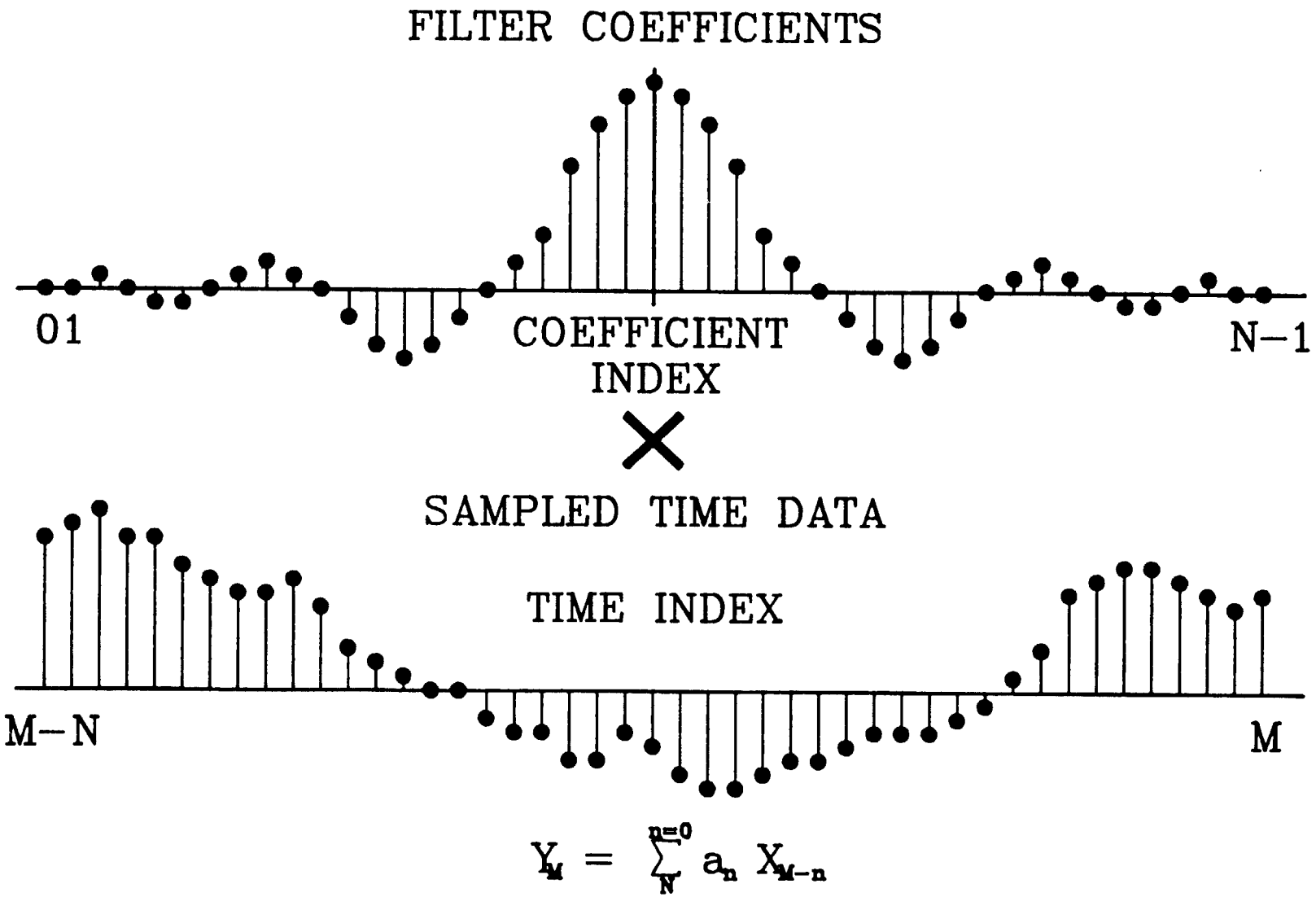

FIGURE 7. FIR FILTER OPERATION

Where N is the length of the filter, whose coefficients are the a_n. Y_m is the output and X_m is the input of the filter.

As you might expect, this can require a significant amount of computation for long filters. The beauty of this technique is the fact that the Fourier transform of the FIR filter coefficients is the response. Likewise, any desired frequency response can be simply inverted to yield a filter. The limitation here is that there must be a sufficient number of coefficients calculated in order to provide adequate accuracy in the frequency response.

This filter suffers from none of the weaknesses of the recursive filter. Phase response is linear with frequency. Furthermore the finiteness of the number of elements used in the calculation precludes the possibility of a numerical overflow.

Typically, unless the application is real time, FIR filters are the best choice for data reduction. They can be shortened at the expense of response accuracy and suffer from none of the other ailments of recursive filters.

Decimation versus Different Sample Rates

The process of digitally filtering a huge data set in order to band limit it sufficiently for decimation can be an excessively long effort. Furthermore, if we were to sample at 100 Hz continuously over a period of 10 days, we would generate 173 Mbytes of data! (assuming 2 bytes per sample). This can present something of a storage problem in addition to requiring large processing times. An alternative method exists, namely to filter several channels from each sensor and record them each at different sample rates. These separate data sets would be almost the same as postprocessed data already discussed.

The largest weakness to this scheme is the loss of bit enhancement for the low frequencies. Since they would be sampled differently, their quantization noise spectral densities would differ accordingly.

Obviously, additional hardware in the form of filters, multiplexers and/or digitizers would be required. This option is not considered in detail here, but the same techniques used can be applied to each of the channels at their different sample rates.

Frequency Domain Processing

The time data, even after filtering, is not terribly useful for quantitative evaluation. We can determine peak and rms amplitudes of given time series. Usually, only if a known process is occurring, is the time series useful for calculation. For example, an individual walking very near the accelerometer might leave a discernible "fingerprint" in the data. For environmental calculation, we will likely need an estimate of the frequency dependence of the measured acceleration.

Fourier Transforms

A function in time will have a Fourier transform defined by:

$$F(w) = \int_{-\infty}^{+X} f(t)e^{-iwt}dt$$

Likewise, the inverse transform is as follows:

$$f(t) = \frac{1}{2\pi} \int_{-\infty}^{+X} F(w)e^{-iwt}dw$$

A function that is sampled in time is in essence multiplied by the sampling function. Figure 8 shows the effect of sampling on a waveform. The sampling function is simply a series of infinitely narrow pulses of unity amplitude.

If this sampling function in time is assumed to be evenly spaced at time intervals T_s, with unit amplitude, it can be shown that the Fourier transform of the sampling function is a series of Dirac delta functions at all positive and negative integer multiples of $1/T_s$.

A sine wave can be shown to have a Fourier transform that consists of a pair of delta functions at +/-(1/T), where T is the period of the sine wave.

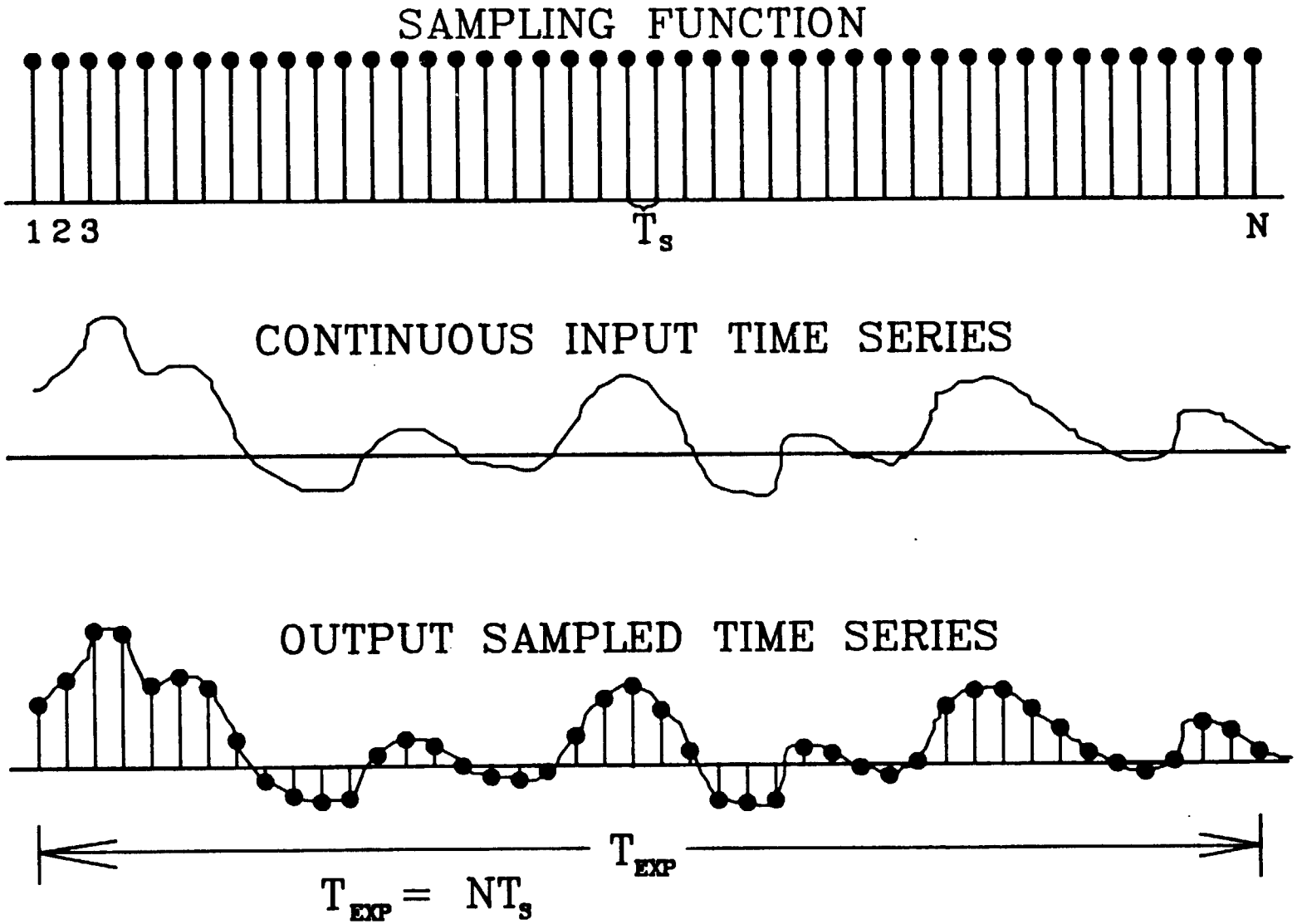

FIGURE 8. SAMPLED CONTINUOUS DATA

Of course, we cannot measure the signal for infinite time, so we must window the signal somehow. Figure 9 shows the Fourier transforms of a sine wave, the sampling function, and a rectangular window, each alone.

So now we are ready to calculate the Fourier transform of a finite set of data. We simply multiply (signal) X (sampling function) X (window) and transform. The convolution theorem states that the result is simply the convolution in the frequency domain of the three individual Fourier transforms.

For simplicity let the signal be the pure sine wave. Then the result is easy, since delta functions convolve quite nicely with anything else. Figure 10 shows the result of this process. We see immediately why we were so careful about aliasing, since the spectrum repeats itself every $1/T_s$. Also very important is the fact that the window effectively spreads the energy of the sine wave into other frequencies.

Windowing

The fact that we cannot look at a signal for infinite time necessitates the use of a window. As shown in Figure 10, the presence of a window will distort the spectrum in comparison with that in the case of a perfect transform. In the case of a rectangular window, the sidelobes are down in amplitude only 13 dB. The main lobe is only $1/T_w$ wide, however. Figure 11 shows the Fourier transforms of three popular windows, the rectangular, Hann, and Flat Top. The Flat Top window has the minimum amplitude sidelobes, but the main lobe is now five times as wide. If we want to distinguish two different frequencies, the minimum spacing between the two is now $5/T_w$.

This provides the criteria for selection of time span for the experiment and the subsets of the data. For example, if we want to distinguish frequencies as small as 10^{-6} Hz, then the window must be at least 5×10^6 sec long if we use the Flat Top window. This translates to an experiment duration of almost 58 days. If we used the

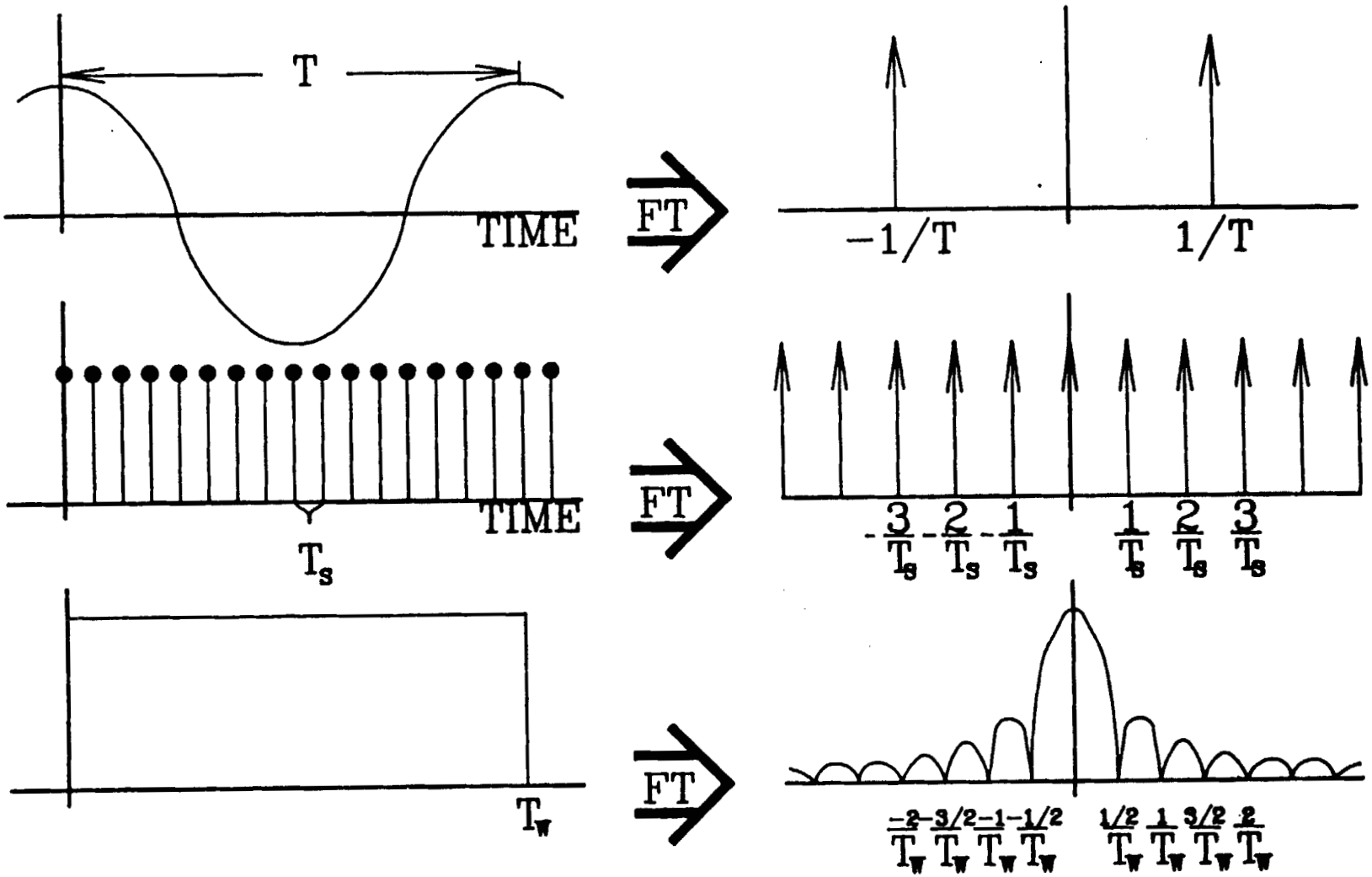

FIGURE 9. FOURIER PAIRS

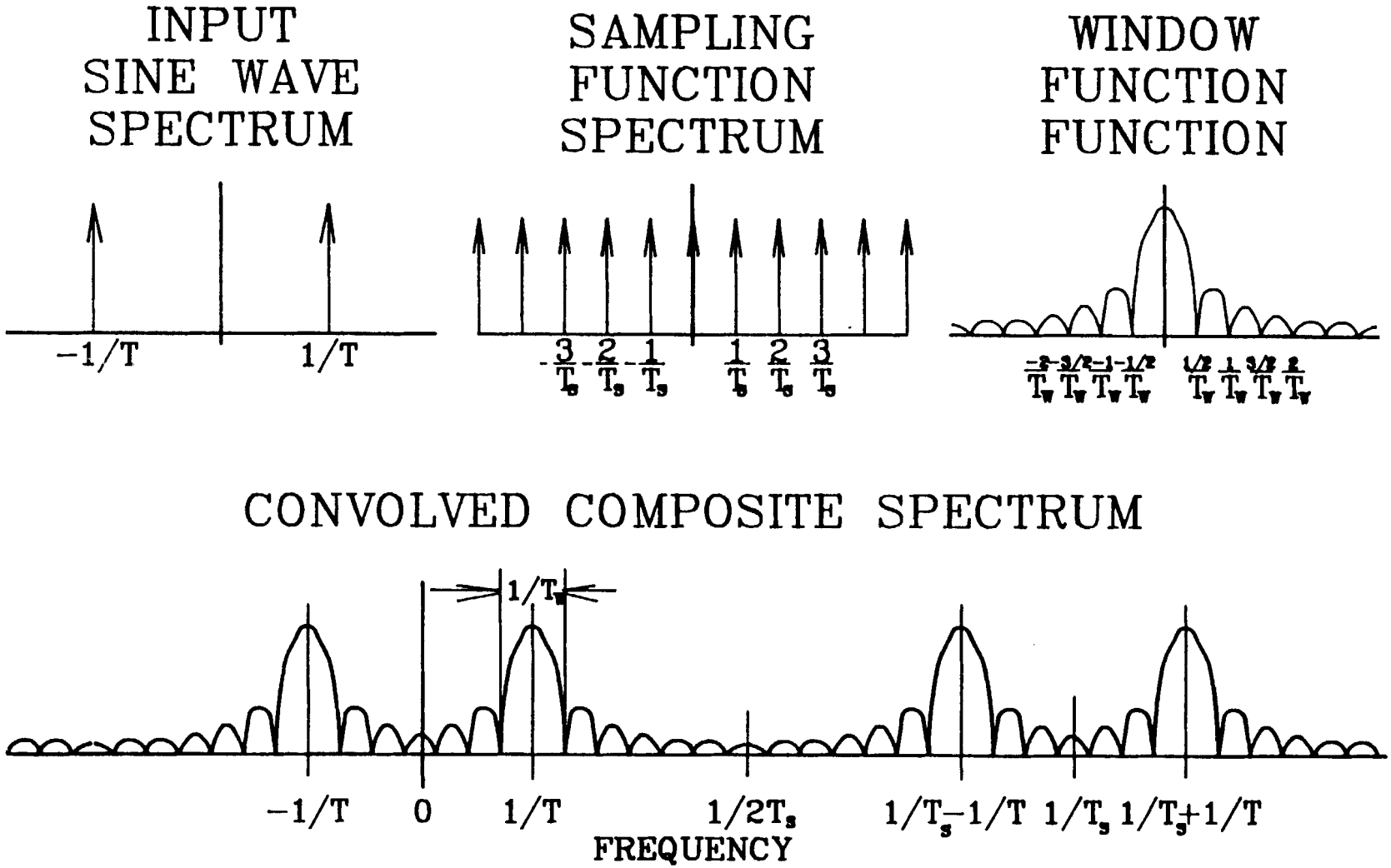

FIGURE 10. SINE WAVE SPECTRUM

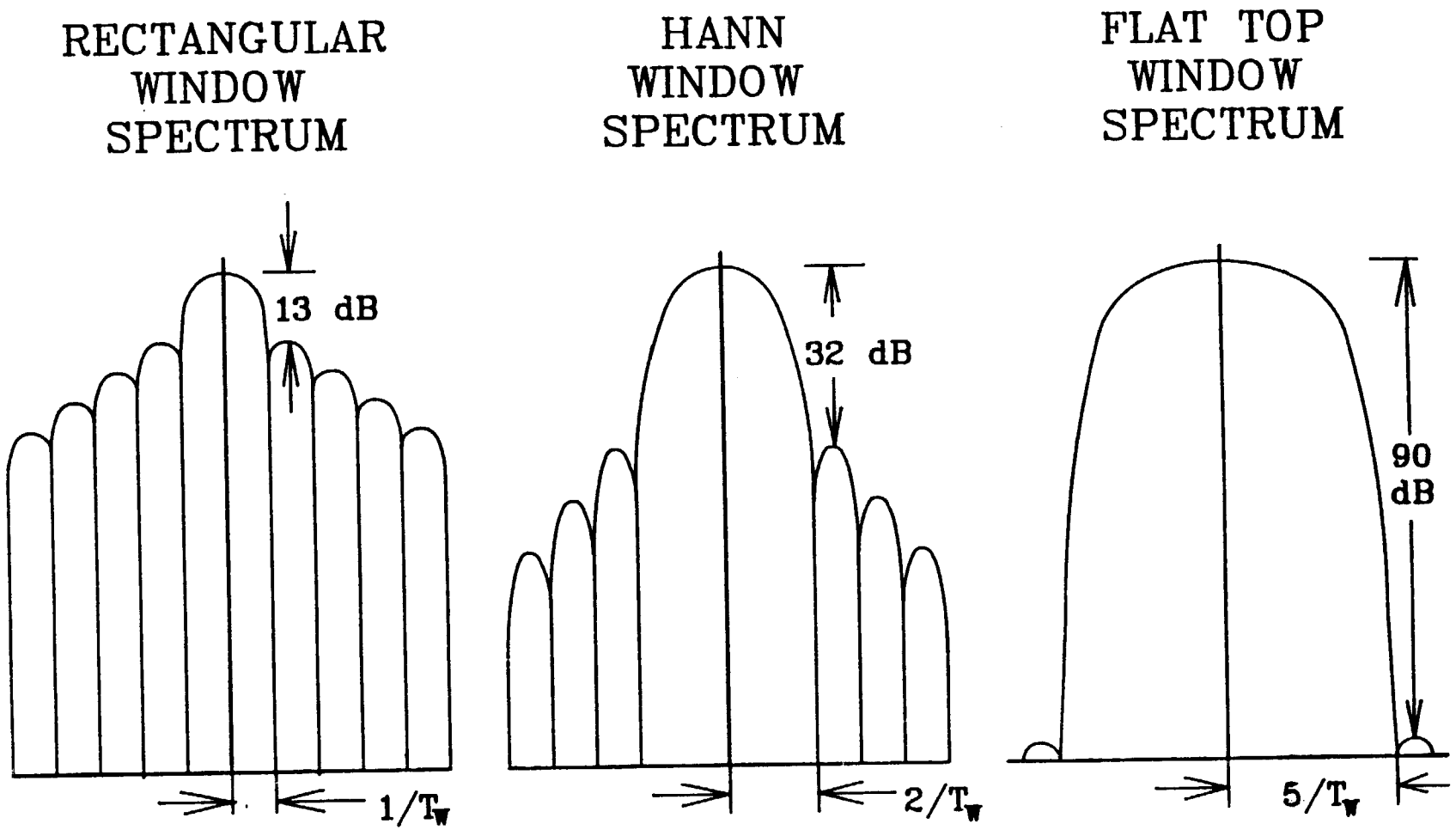

FIGURE 11. WINDOW FUNCTIONS

rectangular window, we would still need over 11 days. Also, if the spectral intensity of two adjacent (about $1/T_{EXP}$ apart) peaks differs by more than 13 dB, then the rectangular window will not be suitable for picking them out.

Averaging

If we have a data set that is sufficiently long that the required window length for our frequency resolution measurements is some fraction of the entire length, we have averaging options. The purpose of averaging is to improve the measurement of random processes.

Power Spectrum Averaging: If we average successive power spectra, the main improvement is in the standard deviation of the random signal measurements. For a Gaussian process whose amplitude is constant across the window bandwidth, the normalized standard deviation of the amplitude measurement, σ is as follows:

$$\sigma = 1/\sqrt{(B_w K T_{RECORD})}$$

Where B_w is the window bandwidth, K is the number of records averaged, and T_{RECORD} is the record time length.

This process will not enhance the signal-to-noise ratio. Any signal that is "buried" in the noise will not be enhanced, since the noise amplitude will not be altered. Only our confidence in the accuracy of the random process measurements will be improved.

Time Averaging: Subsets of the time data can be averaged before taking the spectra and the signal-to-noise ratio for some periodic signal in a noisy environment enhanced. We must have some reference for this process in order that the phase for the periodic process be the same in the successive time records. If not, destructive interference between averaged data sets can eliminate the signal-to-noise improvement.

Numerically, the signal will be increased by a factor K by adding K spectra. Random processes will only increase by a factor of $\sqrt{K}$.

Hence, time averaging K spectra will yield a signal to noise ratio improvement of $\sqrt{K}$.

This might be useful if we wanted to see the effect of some process like the repeated firing of a correction rocket, whose times could be accurately determined from some other source. These times could then be used to properly synchronize the time averaged data sets.

In general, the process most often used to estimate acceleration background on the earth is to average spectra. Here we assume that the processes are random in nature. A qualitative look at the time data will show whether there are any discernible nonrandom processes. These signals require special attention to identify the source. Otherwise, spectral averaging will provide the most accurate estimates of amplitude.

EXAMPLE EXPERIMENT

During July 1986, a Teledyne Geotech Model 44000 Borehole Seismometer was used to record acceleration data over a period of several days. The data set discussed here spanned 72 hours, from approximately 12 PM 15JUL86 to 12 PM 18JUL 86. The primary purpose of the experiment was to observe earth background from 1 Hz to the primary tidal frequencies, 12 and 24 hours.

Sensor Selection

The Model 44000 Seismometer is a very high resolution accelerometer. The package is tubular, approximately 6 feet in length and 3.75 inches in diameter. Three orthogonal axes of accelerometer reside within. The sensors use a capacitive position sensor and active feedback for response stabilization.

Anticipated tidal accelerations were approximately 100 nano-g peak. The instrument noise floor is lower than 10^{-20} g^2/Hz, with a bandwidth of 4 Hz in its present configuration. Optional bandwidths at higher frequencies are possible by changing the feedback parameters.

Small signal linearity is greater than 10^6, and dynamic range is greater than 120 dB. The response was set for 2 X 10^4 V/m/s^2 from dc to 4 Hz. The maximum anticipated signal output was 10^{-6} g. We anticipated no significant dynamic range or noise problems, as the predicted spectral intensity of the tidal fluctuations was expected to be greater than 10^{-13} g^2/Hz.

Amplifier and Filter

A special filter with dc to 0.1 Hz bandwidth was employed with a gain of 50 in the passband. The filter has response that is down by over 100 dB at 2.5 Hz, the Nyquist frequency for this experiment.

Digitizer

A 16-bit digitizer running at a 5-Hz sample rate was used to collect the filtered data. The quantization noise, referred to as acceleration, was 1.6 X 10^{-23} g^2/Hz. The digitizer LSB was 3 X 10^{-11} g. With 96 dB of dynamic range, the anticipated spectral intensity was within the limits of the digitizer. The data were recorded on standard 1/2 inch, 9-track, 1600 BPI magnetic tape.

Analysis

The raw data were decimated by 10, since the spectral content was not sufficient to induce aliasing in this process. Next, a linear trend was removed. The final time domain process was to digitally filter and decimate by another factor of 10 in order to yield a data set of 12,960 samples over a period of 259,200 sec with a sample rate of 0.05 samples/sec. Figure 12 shows the time record in comparison to pure calculated tidal data. The bar shows an amplitude of 50 μgal, which is equal to 50 nano-g. The glitches are teleseismic earthquakes. Quite good agreement with the theoretical data is shown.

The data set was transformed using a standard Fast Fourier Transform (FFT). The result is shown in Figure 13. The minimum

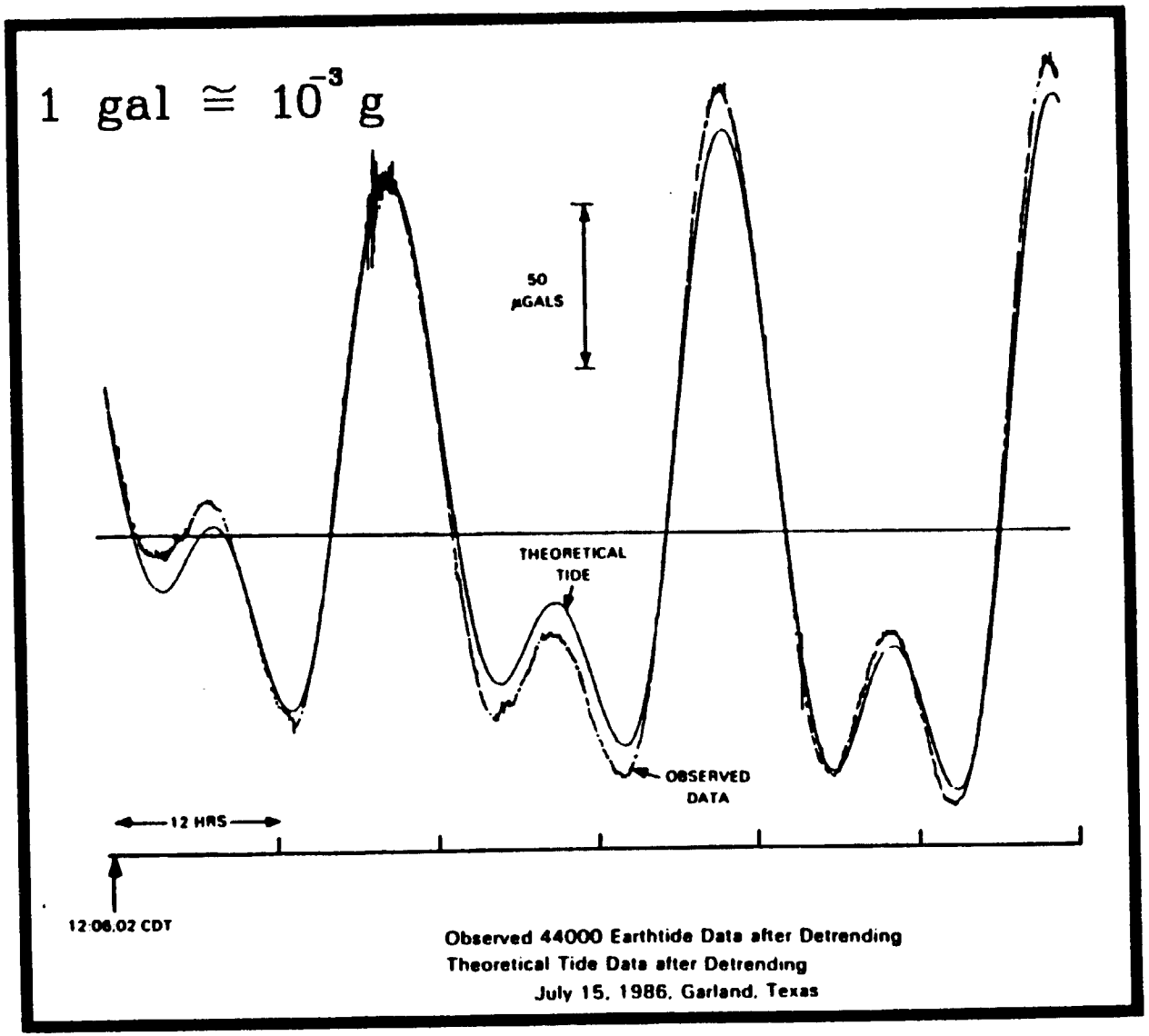

FIGURE 12. TIME SERIES DATA

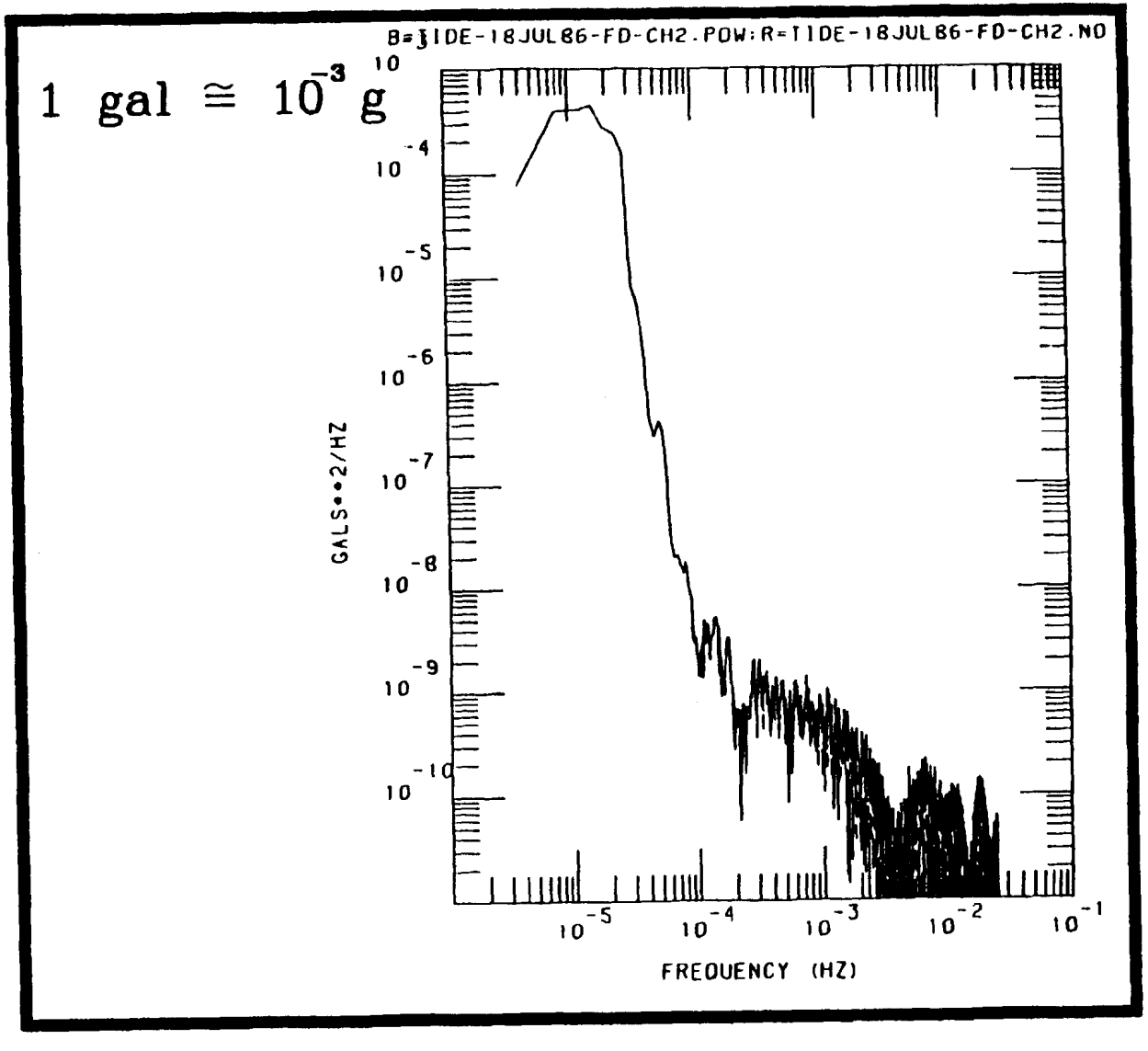

FIGURE 13. POWER SPECTRUM

frequency was 3.86 X 10^{-6} Hz, which is simply the reciprocal of the record length. Peaks at 1.2 X 10^{-5} Hz and 2.3 X 10^{-5} Hz overlap one another. In this case, the experiment was not long enough to discern both peaks spectrally. The time series clearly shows the presence of both, however.

This experiment is intended to show the potential resolution at long periods, and the problems associated with long period data analysis. We were able to obtain good data for frequencies as low as 10^{-5} Hz, even though our minimum frequency was lower. The experiment duration was 3 days. To resolve frequencies as low as 10^{-6} Hz, a continuous experiment of one month would be necessary!

CONCLUSION

The discussion above has been intended essentially as a primer on the topics of acquisition and analysis of acceleration data. Both areas require careful consideration if an experiment is to be successful and meaningful.

It is the author's belief that careful design of the experiment is the first step in data analysis. For long periods, the experiment duration must be adequate. Issues such as power stability, data storage capacity, and reliability become very important for ultra low frequency measurements.

The sensor must also be selected carefully, since stability and low noise at ultra long periods are essential to the acquisition of high quality data.

Finally, even simple analysis has caveats and assumptions that must be kept in mind throughout any experiment. The very nature of sampling and the finiteness of the experiment alter the Fourier transform of the measured signal. An understanding of the basics is important to proper interpretation of end results.

REFERENCES

1. Bennet, W. R., Spectra of Quantized Signals, Bell System Technical Journal, 27, pp. 446-472, 1948.

2. Oppenheim, Alan V. and Schafer, Ronald W., Digital Signal Processing, Prentice-Hall, 1972.

3. Classen, Theo A.C.M., Mecklenbrauker, W.F.G, Peak, J.B.H. and Hurck, N.V., Signal Processing Method for Improving the Dynamic Range of A/D and D/A Converters, IEEE Trans. on ASSP, ASSP-28(5), 1980.

4. Terrell, Trevor J., Introduction to Digital Filters, Macmillan Press, 1980.

5. Jayant, N.S. and Rabiner, L.R., The Application of Dither to the Quantization of Speech Signals, Bell System Technical Journal, pp. 1293-1304, 1972.

6. Gordon, Bernard M., Digital Sampling and Recover of Analog Signals, EEE, 1970.

7. Blackman, R.B. and Tukey, J.W., The Measurement of Power Spectra, from the point of view of communications engineering, Dover Publications, 1958.

8. Priestly, M.B., Spectral Analysis and Time Series, Academic Press, 1981.

N91-12419

20. CHARACTERIZING PERFORMANCE OF ULTRA-SENSITIVE ACCELEROMETERS

Dr. Henry Sebesta, Applied Technology Associates, Inc.

ABSTRACT

This presentation gives an overview of methodology and test results pertaining to the characterization of ultra sensitive accelerometers. Two issues are of primary concern. The terminology ultra sensitive accelerometer is used to imply instruments whose noise floors and resolution are at the state of the art. Hence, the typical approach of verifying an instrument's performance by measuring it with a yet higher quality instrument (or standard) is not practical. Secondly, it is difficult to find or create an environment with sufficiently low background acceleration. The typical laboratory acceleration levels will be at several orders of magnitude above the noise floor of the most sensitive accelerometers. Furthermore, this background must be treated as unknown since the best instrument available is the one to be tested.

A test methodology has been developed in which two or more like instruments are subjected to the same but unknown background acceleration. Appropriately selected spectral analysis techniques were used to separate the sensors' output spectra into coherent components and incoherent components. The coherent part corresponds to the background acceleration being measured by the sensors being tested. The incoherent part is attributed to sensor noise and data acquisition and processing noise. The method works well for estimating noise floors that are 40-50 dB below the motion applied to the test accelerometers.

The accelerometers being tested are intended for use as feedback sensors in a system to actively stabilize an inertial guidance component test platform. The frequency band of interest for tests on the platform extends from a 90-day

period to 100 Hz. The residual motion on the platform is required to be below 10 nano-g's for translation and 10 nano-radians for rotation. Accelerometers used in controlling this platform are required to exhibit noise floors at or below a nano-g. The parallel test methodology has been used successfully to demonstrate availability of accelerometers which are capable of resolving nano-g level motion in the band 0.001 Hz to 100 Hz. No one instrument was found acceptable over the entire frequency bandwidth. Instruments were found which cover the mid-frequency band (0.001 to 1 Hz) and the high-frequency band (1 to 100 Hz).

Tests were conducted at the Advanced Inertial Test Laboratory, which is part of the Central Inertial Guidance Test Facility operated by Air Force's 6585 Test Group. Other tests were conducted in a mountain cave constructed for seismic instrument tests by the Albuquerque Seismological Laboratory. These facilities provide sufficiently quiet backgrounds so that the parallel method is able to extract accelerometer noise floors at or near the nano-g level.

In our discussions of accelerometers and the development of new accelerometer technology, we've heard about the problems of trying to characterize instruments. In order to characterize something, you normally think about having an instrument that's better than the one you're testing and evaluating, and if you're at the state of the art, that's a chicken and egg type situation. It turns out that there are some tools that come from the spectral analysis world that Keith Verges and a number of other speakers talked about, that allow you to extract noise floors considerably below the signal level. When you're trying to characterize an accelerometer that's capable of measuring nano-g and micro-g acceleration levels, the problem we face is finding a location that's quiet enough so that you can see the capability of the accelerometer.

I intend to talk about where our work comes from, and that agency in particular has much interest in accelerometers, not so much for space flight, but for guidance and control. This particular agency is the Central Inertial Guidance Test Facility at Holloman Air Force Base, which is a DoD-wide support agent for calibrating and certifying navigation and flight control systems. I plan to talk about the challenges associated with characterizing precision accelerometers and the methodology that can be brought to bear on the problem. Then, I will discuss some examples of results, and then a wrap-up.

Several years ago, we at Applied Technology Associates got involved with this particular work. The objective was to develop a laboratory facility, and the technology to support the evaluation of components for guidance and navigation systems, accelerometers and gyros in particular. (Figure 1) What we would like to be able to do is create an environment on the Earth, in the laboratory, where we can isolate and stabilize a test item down to nano-g and nanoradian levels. These are the levels that flow from certain performance requirements. The frequency band of interest is 90 days to 100 Hz. The general feeling was that as accelerometers improved for these new applications, and we got advances in the state of the art, that the capabilities and the facilities to support testing and calibration of these instruments needed to also move upward in their state of the art.

One of the things that we've been involved with also was supporting a Central Inertial Guidance Test Facility in identifying what are the trends associated with accelerometers. So about 6 to 8 months ago, we conducted a study program which had the purpose of identifying operational needs for advanced guidance test capability. We did this in response to the requirements of the agency by looking at performance capabilities associated with components in current DoD programs. We then looked at the vendor community and what they projected capabilities of new instruments to be, and then estimated what the current and projected test capability is (Figure 2).

INTRODUCTION

- ACTIVE CONTROL SYSTEM FOR CIGTF SEISMICALLY STABLE PLATFORM

  GOAL: DESIGN, FABRICATE & DEMONSTRATE TECHNOLOGY

  -ISOLATION/STABILIZATION TO 10 NANO-G AND 10 NANO-RADIAN RMS LEVELS

  -FREQUENCY BAND OF 1E-7 TO 100 Hz

- STATE OF ART ACCELEROMETERS REQUIRE IMPROVED TEST CAPABILITY

- TRENDS ARE TOWARD EVEN BETTER ACCELEROMETERS

FIGURE 1

- **PURPOSE:** DETERMINE EXTENT/CRITICALITY OF OPERATIONAL NEED FOR AN ADVANCED GUIDANCE TEST CAPABILITY

- **DATA**
  - — PERFORMANCE CAPABILITIES OF CURRENT DOD PROGRAMS
  - — PROJECTED INSTRUMENT PERFORMANCE UP TO 2010
  - — CURRENT/PROJECTED TEST CAPABILITY

- **SPONSOR:** 6585TH TEST GROUP/CIGTF
  HOLLOMAN AFB, NEW MEXICO

FIGURE 2

Primarily, this was done by contacting the various agencies, first by telephone, then through a mail-out survey, and then some of the key vendors and key using agencies by actual site visits and interviews with people involved (shown in Figure 3).

We were very pleased to get participation by a large number of organizations, and Figure 4 summarizes the organization numbers that were involved. We certainly got a lot of very useful data and a feeling for where the guidance component industry and technology was going.

Figure 5 shows the noise floor, (scale is in G^2/Hz, for the PSD level) which also implies that there's a bandwidth, which we generally didn't try to deduce. The little dots represent actual respondees' current capabilities and then also capabilities that they expect to reach over the next couple of decades. This graph also shows the current capability for testing accelerometers, using the best available equipment and test methodologies. We identified that there is a problem in that as instruments get better our capability needs to improve also.

Figure 6 shows the threshold characteristics.

Figure 7 shows the methodology for testing an instrument where the environmental noise is considerably above the basic capability of the instrument. In other words, you're trying to deduce noise floors of an accelerometer and its performance at maybe 2 or 3 orders of magnitude below the background level of the facility in which you are operating. So the basic problem is: we don't have another sensor to determine what X is. X, in this case, is the unknown acceleration that you're subjecting the instrument to. The concept here is to utilize like instruments operating side by side at the same location and sensing the same unknown acceleration. Then theoretically, if the instruments had no noise, you would see the same output signals. The procedure is to record and process the data from these two instruments, and to look at that data using full knowledge of spectral analysis theory. We have a sensor, and we model that sensor as a device that gives an output signal proportional to the input acceleration plus some noise that's unknown. The same situation is true for the second sensor. The noise in sensor 1 and

- **SURVEY OF DOD, NASA, AND VENDORS**
  - — TELEPHONE
  - — MAIL
  - — SITE VISITS
- **LITERATURE SEARCH**
- **CIGTF CAPABILITIES REVIEW**
- **COMPILE RESULTS/DATATRIEVE**
- **ANALYSIS OF RESULTS**
- **DOCUMENT RESULTS (AFR57-1)**

FIGURE 3

	DOD	OTHER	TOTAL
TELEPHONE CONTACTS	46	71	117
QUESTIONNAIRES SENT	25	32	57
QUESTIONNAIRES RECEIVED	10	17	27
ORGANIZATIONS VISITED	7	12	19

FIGURE 4

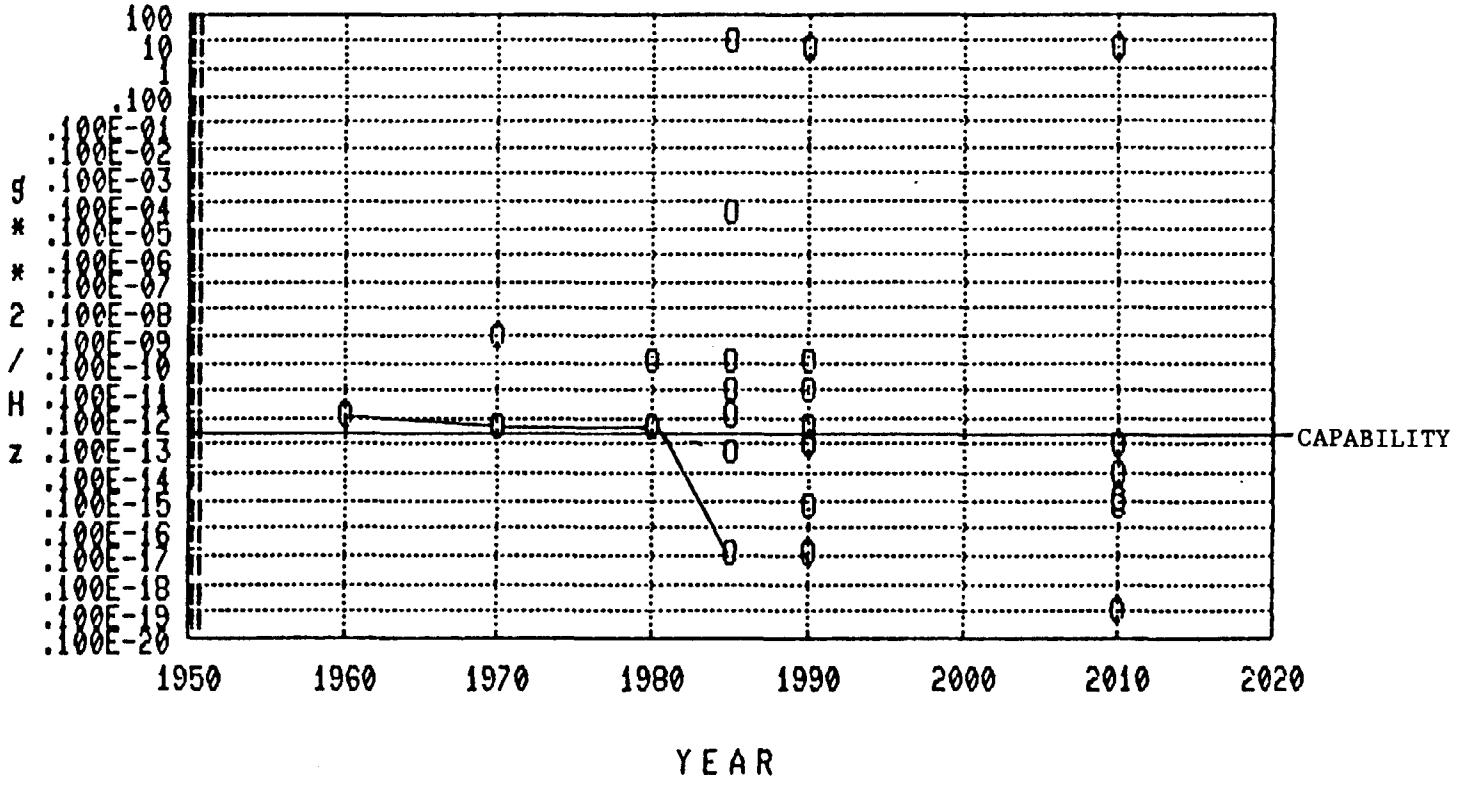
100
10
1
.100
.100E-01
.100E-02
.100E-03
.100E-04
.100E-05
.100E-06
.100E-07
.100E-08
.100E-09
.100E-10
.100E-11
.100E-12
.100E-13
.100E-14
.100E-15
.100E-16
.100E-17
.100E-18
.100E-19
.100E-20
g * * 2 / H z
1950
1960
1970
1980
1990
2000
2010
2020
YEAR
CAPABILITY

FIGURE 5

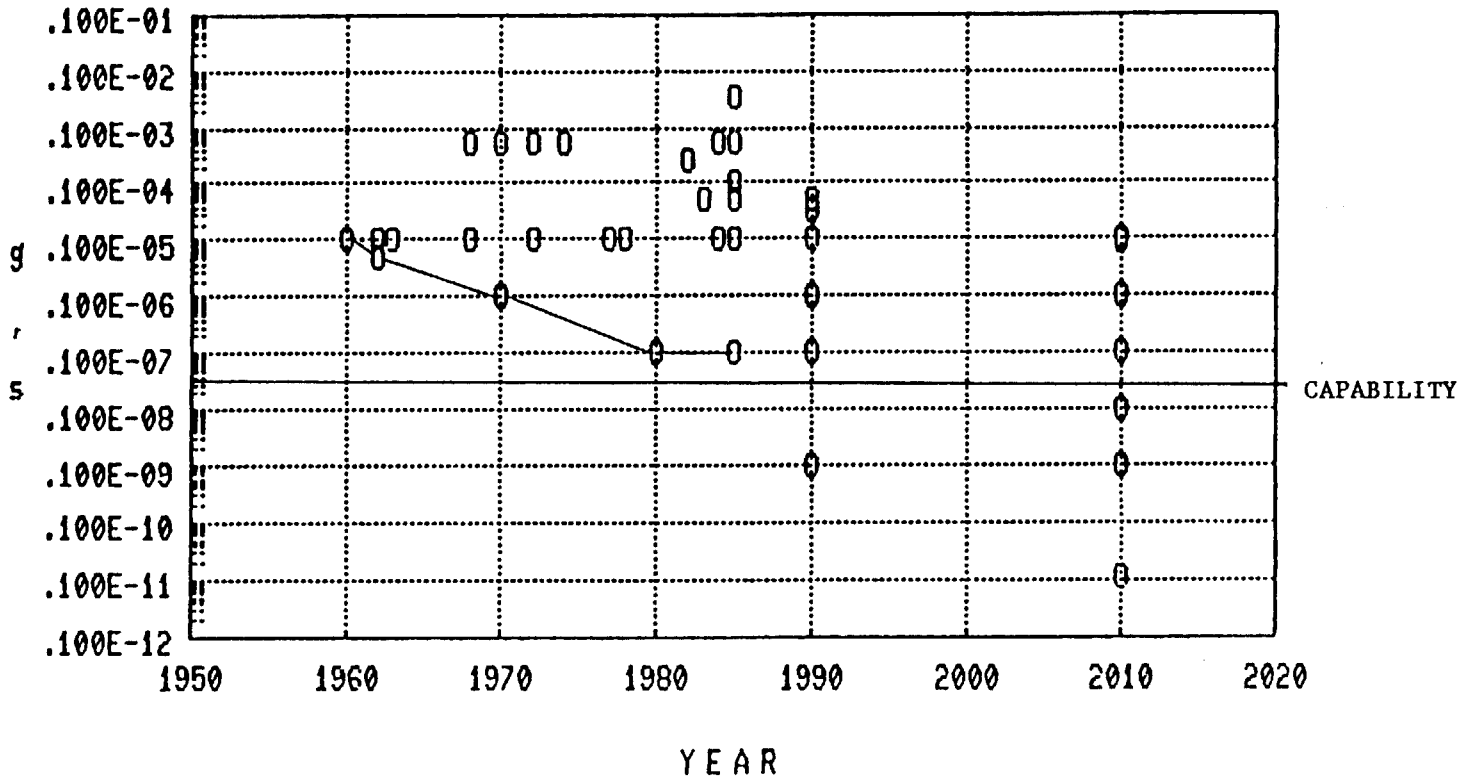
.100E-01
.100E-02
.100E-03
.100E-04
.100E-05
.100E-06
.100E-07
.100E-08
.100E-09
.100E-10
.100E-11
.100E-12
g
s
1950
1960
1970
1980
1990
2000
2010
2020
YEAR
CAPABILITY

FIGURE 6

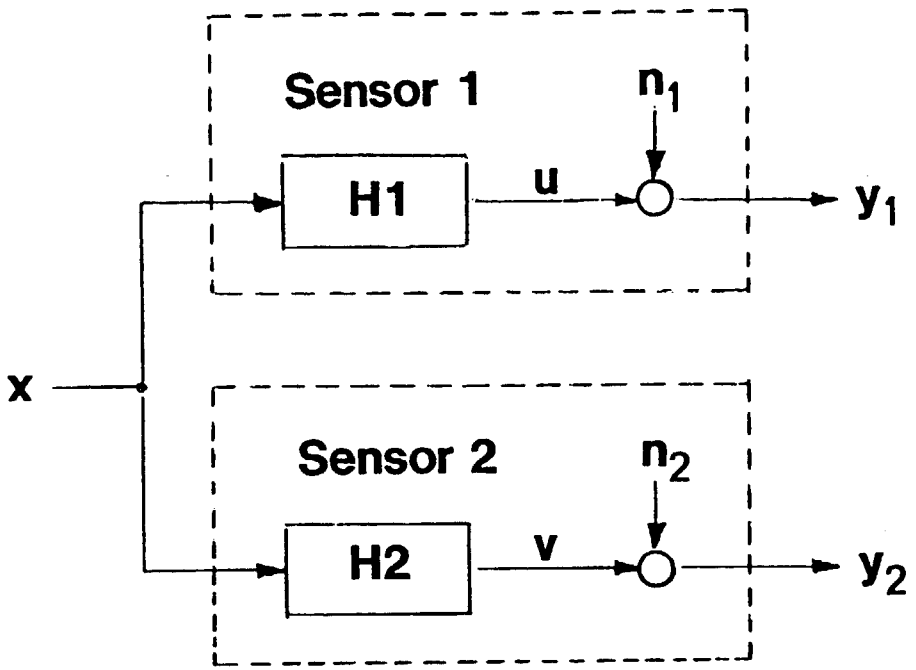

$$G_{11} = H1^{*} H1\ G_{xx} + G_{n1\,n1}$$

$$G_{22} = H2^{*} H2\ G_{xx} + G_{n2\,n2}$$

$$G_{12} = G_{uv} = H1^{*} H2\ G_{xx}$$

$$\gamma^2_{12} = \frac{|G_{12}|^2}{G_{11} G_{22}}$$

FIGURE 7

the noise in sensor 2 are typically uncorrelated. In other words, they're each independent of one another. Now the signals per se, the U and the V, we expect to be correlated. Both sensors are measuring the same thing, and should be responding in the same way. The processing involves calculating the auto spectrum for Y_1, which is the sensor output plus the noise, and the auto spectrum for Y_2, which is the other sensor's output, and these are defined in terms of a mathematical relationship. The important thing here is a frequency-dependent function called the coherence function that you can also calculate. That coherence function is the magnitude of the cross spectral density, which is the relationship between these two signals, divided by the auto spectrum signal of sensor 1 and the auto spectrum signal of sensor 2. This coherence function is a measure of how well these two signals, Y_1 and Y_2, are correlated with one another.

Figure 8 shows one of the math relationships that describes that estimate. In other words we can make an estimate of the sensor noise or the unexplained part of the output. It can be thought of as the auto spectrum of sensor 1 minus the coherence function times the auto spectrum, or 1 minus the coherence times the auto spectrum. The basic premise of this particular relationship is that all of the noise is due to sensor 1, there's no noise on sensor 2. This is what you might call a worst-case assumption. Figure 9 shows other assumptions that can be used.

If you assume that the model for the sensor system at each input of the sensor has equal noise, you can calculate an estimate of the noise floor spectrum of the sensor as the auto spectrum minus the square root of the coherence function times the auto spectrum. This gives a better estimate of what the sensor noise might be: typically, for two sensors that are alike, you would expect the noise to be somewhat similar in character.

A little bit more complicated relationship is given in Figure 10, where you make the assumption that both of the output noises are the same. All these things can be easily calculated with digital signal processing tools. The typical digital signal analyzer that you might

$$\hat{G}_{n1\,n1} = G_{11} - \gamma^2_{12} G_{11}$$

- **ASSUMPTION : Other sensor noise zero**

- **EASY CALCULATION (2 keystrokes on HP5420)**

FIGURE 8

$$\hat{G}_{n1n1} = G_{11} - \gamma_{12} G_{11}$$

- **ASSUMPTION : Input noises equal**

- **REQUIRES $\sqrt{\ }$ FUNCTION**

FIGURE 9

$$\hat{G}_{nn} = \frac{(G_{11}+G_{22})-\sqrt{(G_{11}-G_{22})^2+4|G_{12}|^2}}{2}$$

- **ASSUMPTION : Output noises equal**

- **DIFFICULT CALCULATION**

FIGURE 10

buy from HP or Nicolet will have buttons that you can push and generate these noise floor estimates. This enables you to generate the auto spectrum, the cross spectrum, coherence function, and calculate the noise spectral plot. And so you have an estimate of what the noise floor looks like as a function of frequency for the particular sensors that you're evaluating.

Figure 11 depicts power spectral density plots that represent results from sensors that we've tested. Our first job in developing an actively isolated platform was to find sensors that would do the job from 90 days to 100 Hz. It turns out that we were able to find sensors from about 0.001 Hz to 100 Hz, two different sensors, not the same sensor over the whole bandwidth. We were also able to find sensors that had PSD noise floors on the order of a nano-g squared per hertz. And that's the goal we set for outselves, because we were trying to get an actively controlled system with a noise floor of 10 nano-g in translation. We set our sensor requirement for a feedback system 1 order of magnitude below that. Obviously if you try to control something with a noise on the feedback sensor, then the system response can't be better than your feedback sensor, so you have to have a feedback sensor that's better than the isolation goal of the system. We did a fairly comprehensive survey of the people that made sensors, both in the aerospace and the seismic community. We ended up with sensors from the seismic community that are capable of sensing nano-g accelerations. These sensors are manufactured by a little company called Streckeisen in Switzerland. What we're looking at in Figure 11 is the PSD of the motion that we measure on the floor of the Advanced Inertial Test Lab at Holloman. That particular lab is a facility that's designed to provide as quiet an environment as we know how to do. It includes special air-handling features, seismic pads, and then the active isolation system goes on top of that. The peak on the curve at about 0.1 Hz, or about a 10-sec period, is actually the ocean waves pounding on the continental shelves, so-called microseismic peaks. You can see this same character at any continental location, basically, as far as the PSD of the low-frequency end of the spectrum is concerned.

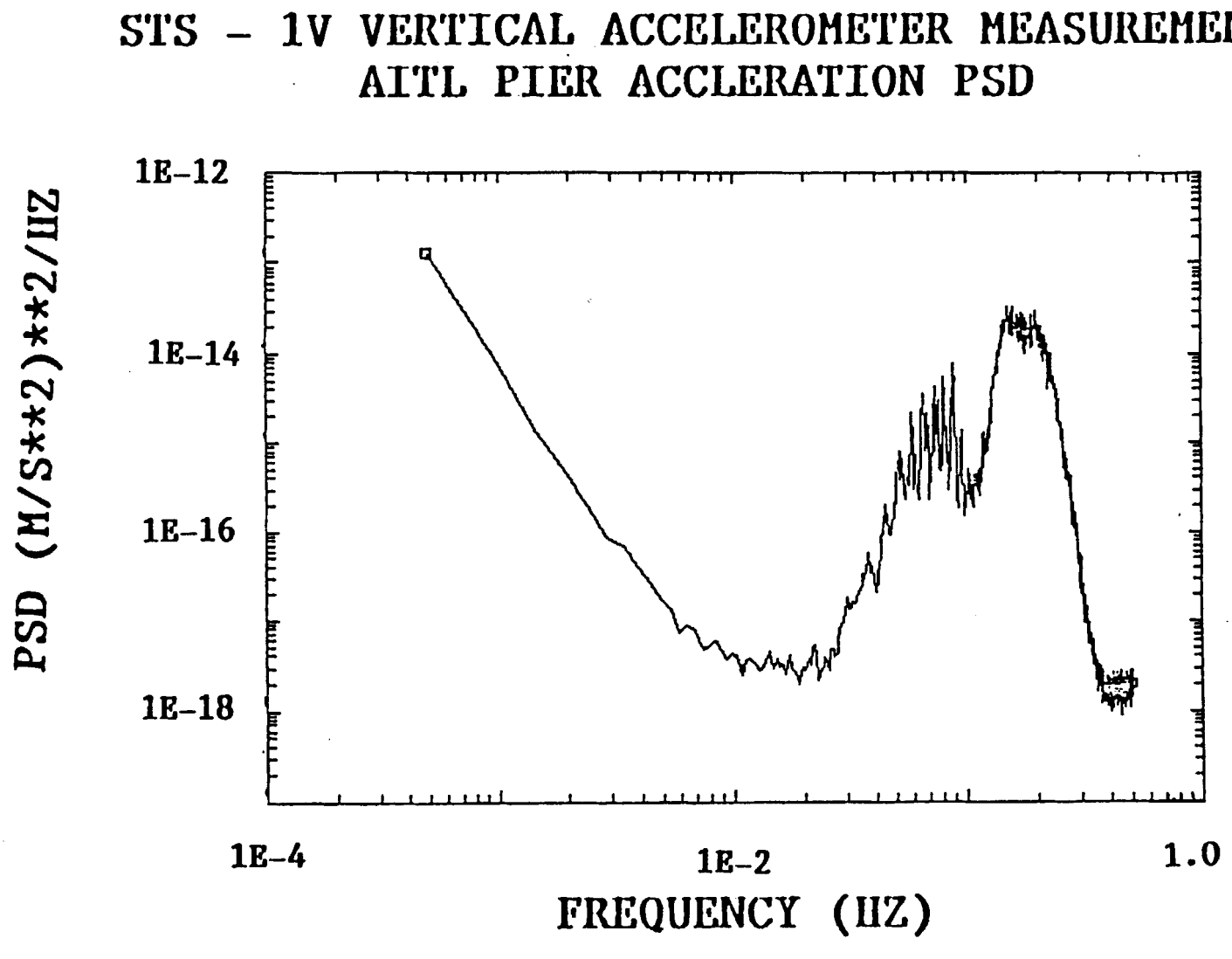
STS – 1V VERTICAL ACCELEROMETER MEASUREMENTS
AITL PIER ACCLERATION PSD
PSD (M/S**2)**2/HZ
1E-12
1E-14
1E-16
1E-18
1E-4
1E-2
1.0
FREQUENCY (HZ)

FIGURE 11

Figure 12 shows the noise PSD, or the incoherent power taken from two STSs measuring the same input, at the same location. This corresponds to a nano-g squared per hertz level of noise floor, and what we're able to see from this plot is that these sensors, their inherent noise floor, from something on the order of 0.002 Hz up to about 1 Hz, which is the bandwidth of the sensor, is below a nano-g squared per hertz, as a noise floor.

Figure 13 shows some of the Streckeisen-predicted noise or theoretical noise floors, and we found that they were very close to what we were able to measure.

Figures 14 and 15 are from instruments that are intended to work from about 0.1 Hz to 100 Hz. These happen to be Teledyne Geotech S-750s. This particular set of data was not obtained by us but by Sandia National Labs in some work that they were doing, to evaluate this particular seismometer. The PSD of sensor 1 and PSD of sensor 2 are the auto spectra, and we have the coherence function in Figure 16. The point to be made here is that the coherence is near to 1, which says that basically the outputs from each of these sensors are essentially correlated. The idea being that both are seeing the same input, so they should be showing the same output; and if there's not noise in the problem, then it will be the same. The coherence is a measure of how small that noise is. Noise can come from any of several sources. One source is the acquisition and processing algorithms themselves. There's a neat little trick that you use to verify that your acquisition electronics and amplifiers and all your algorithms are not dominating the noise. The procedure is accomplished by taking one sensor output and putting it into two parallel paths, and then looking at the incoherent power from that one sensor output through the two separate independent processing paths. That would be the equivalent of replacing the output signal of one of the instruments onto both of the processing channels. You can look at the coherence function for this setup and it should correspond to very low noise. Indeed, you expect that noise to be below the sensor noise. This is a technique that came from Teledyne Geotech. It's one of their standard processing tools to validate their acquisition and

STS – 1V VERTICAL ACCELEROMETER MEASUREMENTS
INCOHERENT COMPONENT PSD

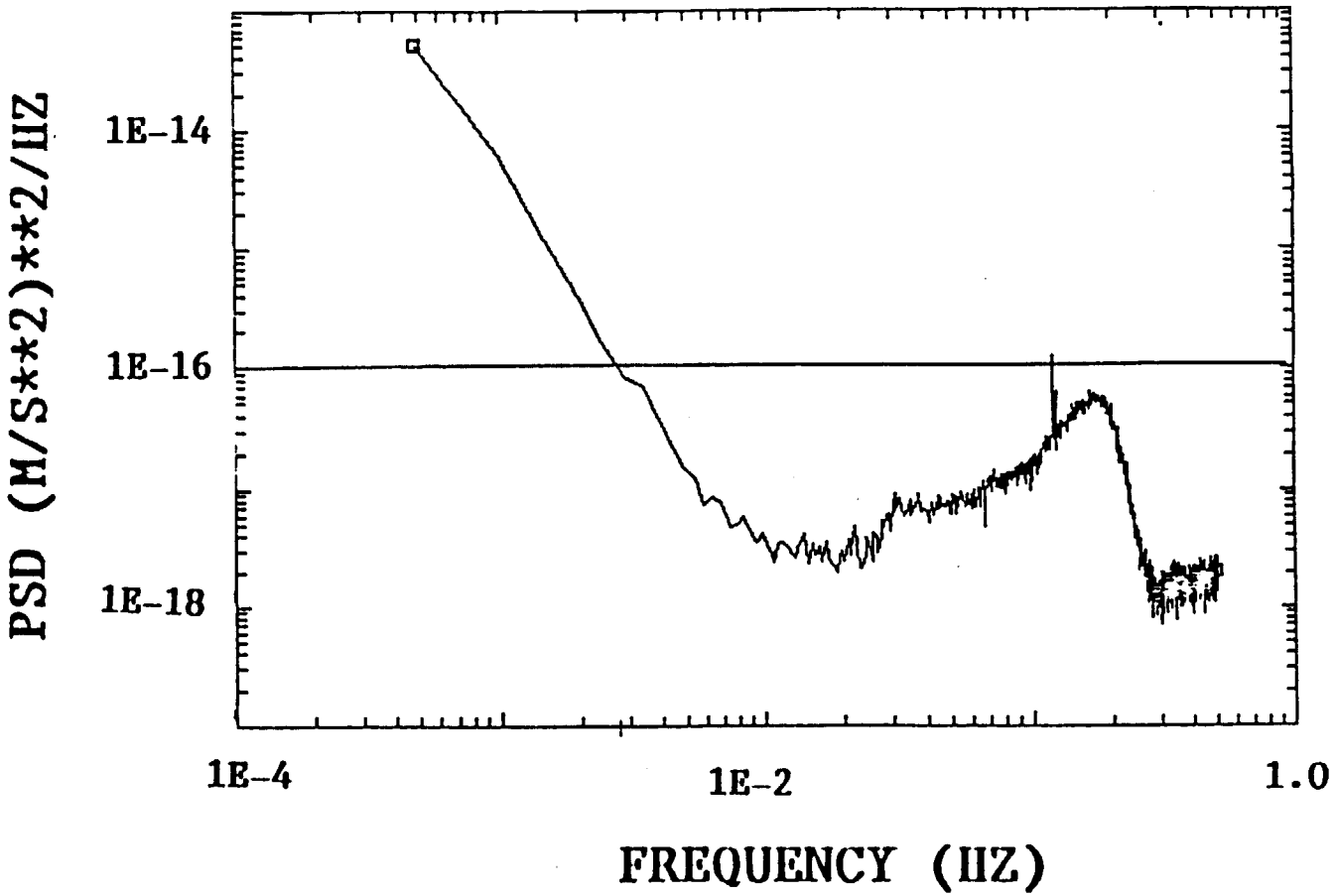

FIGURE 12

STRECKEISEN STS - PREDICTED ACCELEROMETER NOISE PSDS

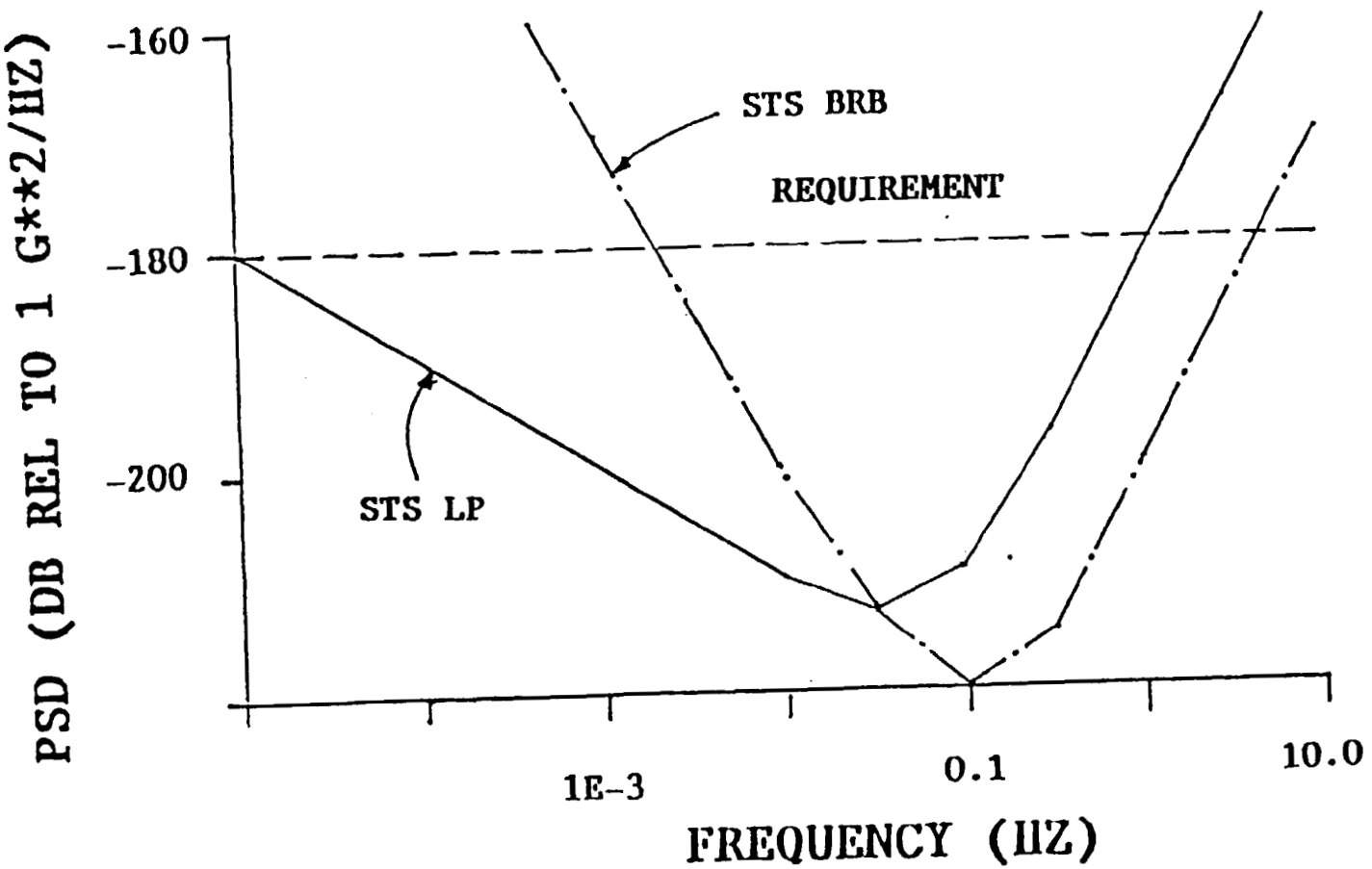

FIGURE 13

instrumentation system. The plot in Figure 17 is the incoherent part. Our requirement was to try to get to nano-g squared per hertz levels. We didn't quite get there with this particular instrument, but we were close enough that it would meet our requirements as far as the closed-loop stabilization system was concerned.

Figure 18 illustrates the active isolation system that is part of the Advanced Inertial Test Laboratory facility at Holloman. The whole thing is in a very quiet environment. The base is 20 ft below ground level, in a test cell that is also below ground level, sitting on a big concrete seismic mass. The apparatus that's sitting on top of it is equivalent to two optical benches. They're mounted on pneumatic airbag isolators, one mass on top of the other. So theoretically you're getting the equivalent of two inertial mass passive type of isolation system. At high frequency it works in a passive mode. At low frequency, we have actuators and the accelerometers, which we described earlier, as feedback sensors to actively suppress motions and forces that are acting on these masses.

A very busy overlay from a number of different sources is shown in Figure 19. In the low frequency range from 1 Hz down, we expect a seismic background that is pretty much similar in any location on the continent. You can get slight variations, if you live near the coastlines or a storm happens to be in the ocean or there is earthquake activity or something like that. But predominantly the low frequency characteristics will be the same. One of the things we noticed, is that some of these asymptotes are not quite the same. Our hypothesis is that the graphs include sensor noise that hasn't been eliminated from those measurements. As you get to lower and lower frequencies, you have other variables involved in the sensor output, such as barometric pressure and temperature variations, that may not be eliminated from the sensor output. If you can't control those variables, they influence the output and, as far as the measurement is concerned, it doesn't know the difference. Theoretically, we can look at analysis processes where we do a multiple coherence calculation that takes several variables, like temperature, pressure, and the combined parallel sensor outputs, and

S750 ACCELEROMETER MEASUREMENTS (QUIET ENVIORNMENT)

SENSOR 1 PSD

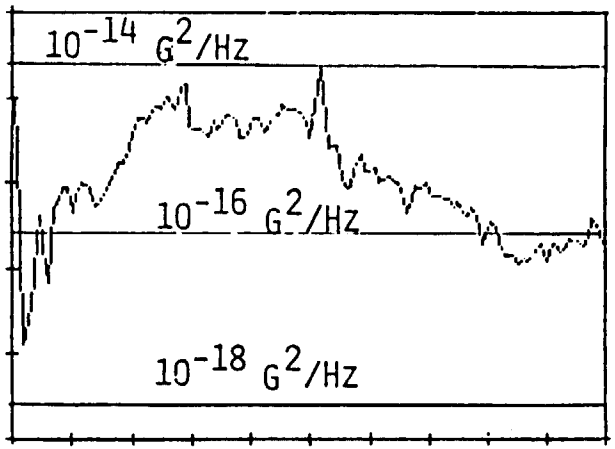

COHERENCE FUNCTION

FIGURE 14

SENSOR 2 PSD

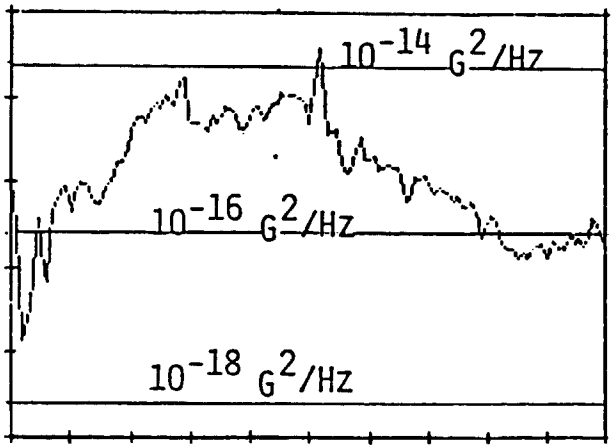

INCOHERENT COMPONENT (NOISE)

FIGURE 15

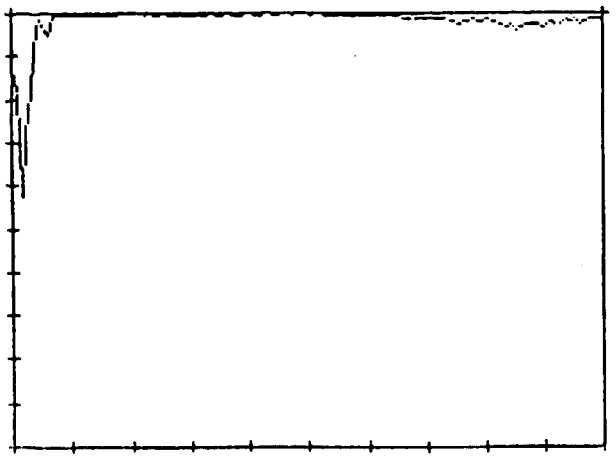

FREQUENCY (HZ) 100 HZ

FIGURE 16.

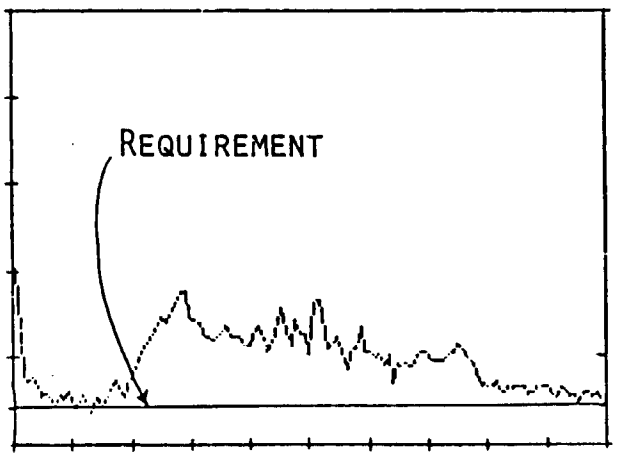

FREQUENCY (HZ) 100 HZ

FIGURE 17.

ILLUSTRATION OF THE SEISMICALLY STABLE PLATFORM

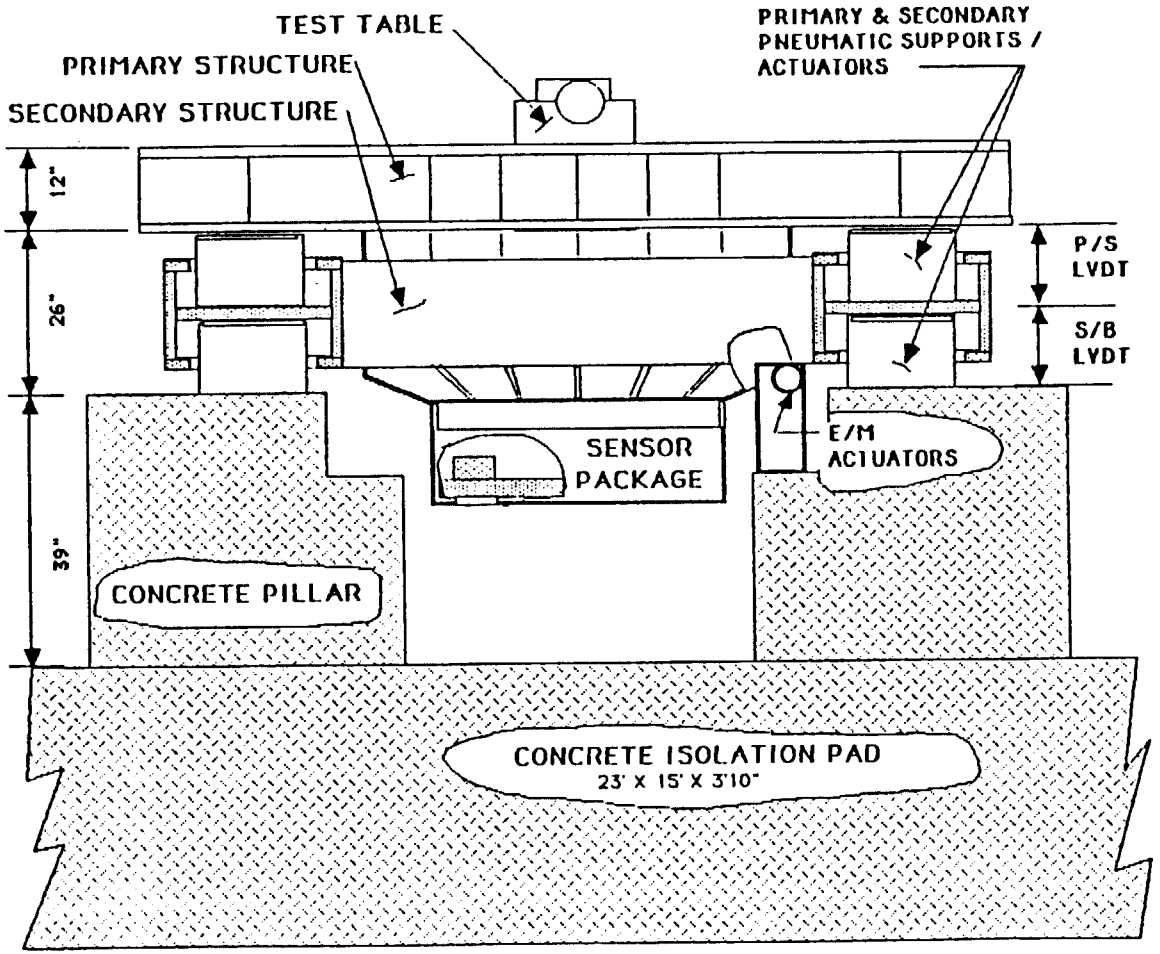

FIGURE 18.

DISTURBANCE FOR THE VERTICAL TRANSLATION AXIS

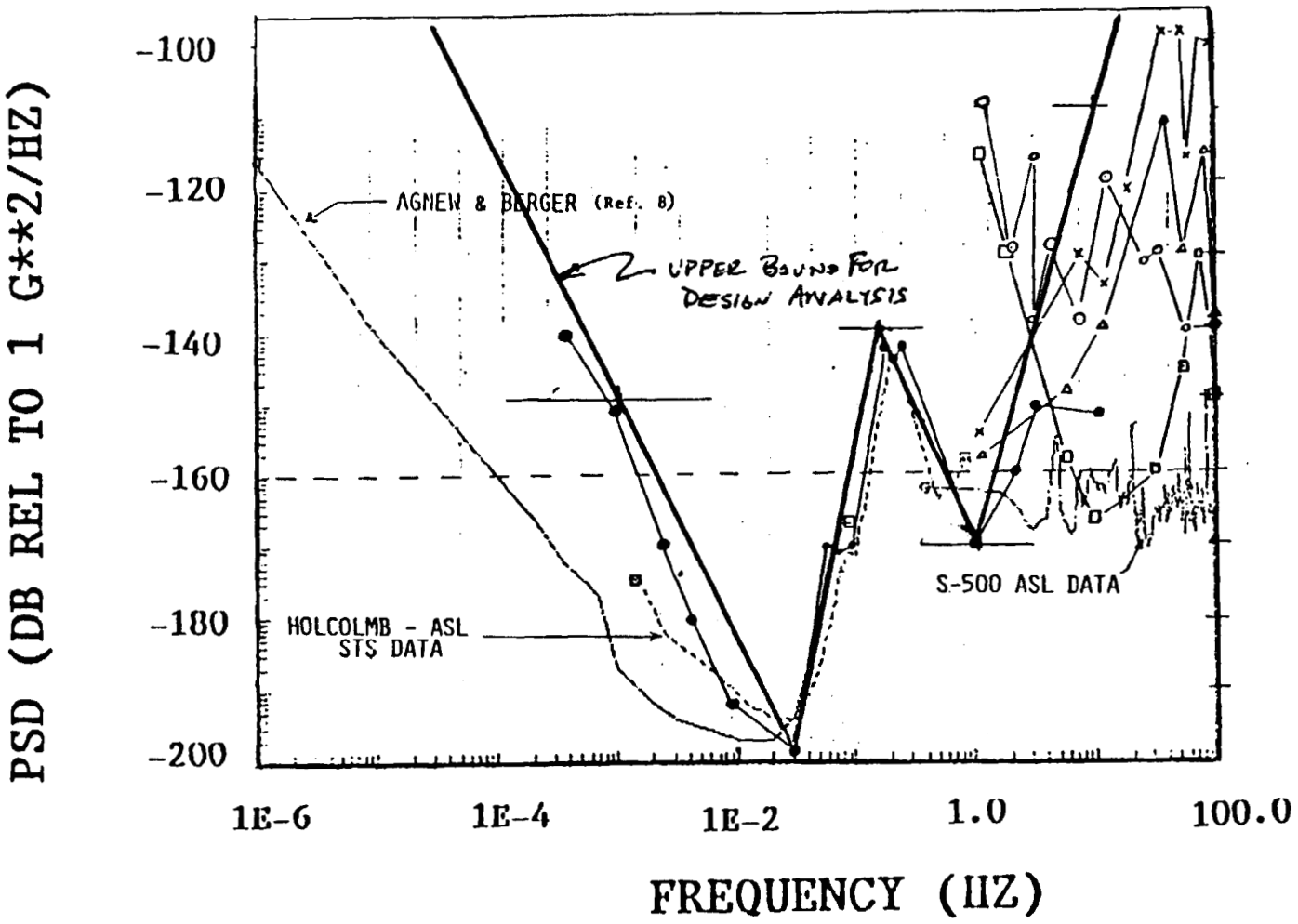

FIGURE 19.

explain their connection to the output. We can actually do a much better job than we have been doing as far as the low frequency end is concerned. In the upper end, what you really see is a wide variety of contributions that depend on your location. You have local machinery, local highways, rivers, and so on that contribute to the general spectra shape and levels from 1 Hz up. Figure 19 includes a curve that's down around 160 dB, which represents data that we took in a cave in the Monzano Mountains near Albuquerque. It's a part of a USGS facility where they do calibrations of seismic network instruments. It's a very quiet location. You can go to the back of the cave, about 60 meters into the mountain, and set up your instruments in parallel and establish the noise floors of an instrument fairly well.

The other data represent various conditions on top of the test platform with air conditioners on, air conditioners off, etc. But we basically took the solid dark line as an envelope that we're considering to be our disturbance input and designed our system to work against that.

The system that is being implemented currently involves basically two major loops: disturbance cancellation loops that actively control the pressure in the pressure bags, and an acceleration loop which actively controls some electromagnetic actuators to give us a high bandwidth control. The predicted performance is illustrated in Figure 20 by the lowest curve. The curve represents the residual acceleration, on top of the platform, with all the control loops working. What we're shooting for is the 10-nano-g residual environment.

I would like to summarize by saying that, if you want to characterize ultraprecise accelerometers, you have to find a quiet environment. Even with parallel testing, the best we were able to do is to see acceleration signals that might be 40, 50, or 60 dB below the inherent background. The inherent background in most places may range from micro-g's to tens of milli-g's. So if you're trying to characterize a sensor down to sub-micro-g level, you have to create a quiet environment. The parallel test methodology with this spectral analysis gives you the ability to do that with the current technology and current types

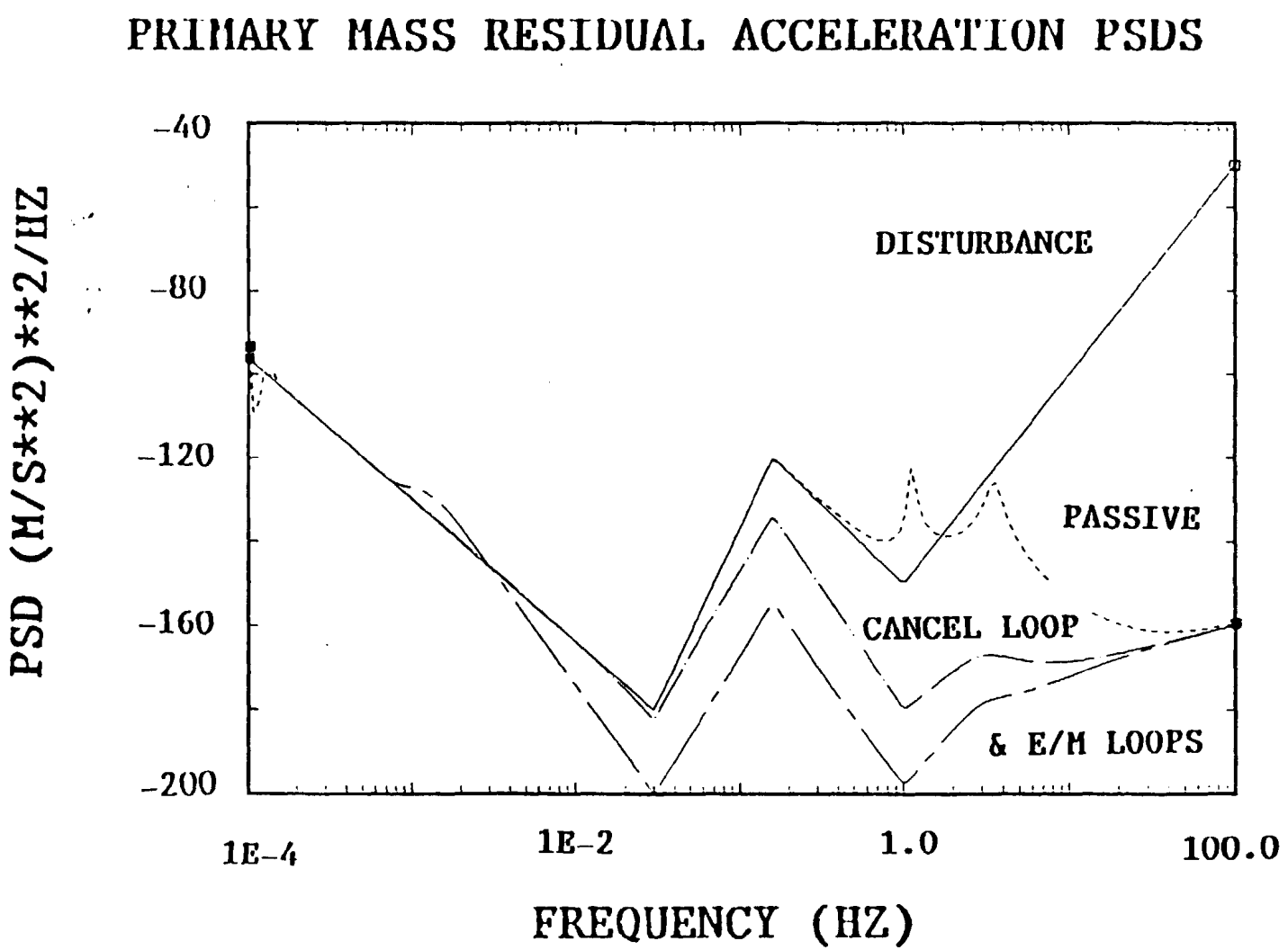
PRIMARY MASS RESIDUAL ACCELERATION PSDS
PSD (M/S**2)**2/HZ
-40
-80
-120
-160
-200
DISTURBANCE
PASSIVE
CANCEL LOOP
& E/M LOOPS
1E-4
1E-2
1.0
100.0
FREQUENCY (HZ)

FIGURE 20.

of facilities. There are accelerometers available that can be used as calibration instruments that are capable of noise floors at 1 nano-g over a fairly broad bandwidth, at least from 0.001 Hz to 100 Hz.

Question: Are those seismic accelerometers flight-qualified?

Sebesta: The answer to that is no. As far as I know, none of the ones that we've been involved with have been designed for flight environments. Most of them are fragile instruments. But the technology is there, and they could probably be brought to that environment, but they haven't been. Keith Verges from Teledyne can talk about their particular applications.

21. FREE-FLOATING EXPERIMENTS IN ORBITER AND SPACE STATION

Owen K. Garriott, EFFORT, Inc.

ABSTRACT

Manned spacecraft will never be free of acceleration perturbations due to necessary motions of crewmembers. However, in most cases, the perturbations can be minimized or even isolated from sensitive experiments when required. The principal disturbances will be mentioned below and methods of isolation described.

As the crew moves about the spacecraft, no external forces are applied and the average acceleration remains near zero. External force will be exerted when jets are fired for spacecraft attitude control or translation, and these must be transferred to the microgravity experiments.

Transitory acceleration and vibration are produced by crew and equipment. The most significant on Orbiter have been "wall push-offs" used for body translation within the spacecraft, the exercise conducted on a treadmill within the middeck area, closing doors of stowage compartments and the vibration of some machinery, such as a sample centrifuge. For short periods of perhaps a few minutes, crew and equipment motion can be largely inhibited, but not for much longer intervals.

It may be necessary to mount especially sensitive experiments on an "isolation table", which can greatly reduce the acceleration transferred to the experiment. Either weak mechanical springs or, even better, a computer-controlled electromagnetic suspension can be used to effectively insulate the table from vibration at frequencies above about 0.01 Hz.

Another option is to "free-float" an experiment table within the spacecraft. All of the above-mentioned perturbations can be eliminated for some minutes if the entire experiment package is allowed to "free-float" within teh spacecraft until a wall contact is made. Package

accelertion levels should be maintainable below 10^{-8} g_o in this way. To achieve maximum float periods, it is necessary to release the experiment package with a precisely controlled initial velocity relative to the spacecraft. The initial velocity must be near zero, but a substantial increase in float time is possible with careful control of the initial velocity components. Typical initial values are a few mm/sec (Friedlander, private communication) and accuracy to about 10% is required. Examples of the free-floating trajectories will eb shown.

Even longer periods of free floating can be achieved and small spacecraft accelerations can be made to offset atmospheric drag. At Space Station altitudes, the drag will probably be less than 10^{-7} $g_o \approx 10^{-6}$ m/sec^2, requiring very low levels of offsetting thrust. For a Staton mass of 100 tonnes, a force of about 0.1 newton or less is all that is required to offset atmospheric drag. A small "resistojet" minithruster, expelling very hot wasted gases, is being considered for station drag make-up and would also allow free-floating experiments of many tens of minutes, depending upon the precision of the release velocity.

For experiments compatible with any of these modes of operation, the advantages of crew participation can be retained.

22. MICROGRAVITY ACCELERATION MODELING FOR ORBITAL SYSTEMS

Dr. Walter Knabe, MBB-ERNO, Bremen

In the absence of a manuscript of Dr. Knabe's paper, the editors of the Proceedings Volume wrote the following short synopsis.

In view of the decisive importance of a disturbance-free environment on the Space Station, and on other orbital systems, for materials processing experiments, the author undertook a theoretical and semi-experimental analysis of the acceleration environment to be expected on large orbiting spacecraft.

A unified model of such spacecraft cannot be established; therefore, a number of sub-models representing major components of typical large spacecraft must be investigated. Assumptions must be made, in parametric form, about elastic responses, dynamic behavior, damping coefficients, rigidity, materials used for structural components, and general design features. Natural frequencies and resonance effects can be estimated on the basis of these assumptions. Gravity gradient and atmospheric drag produce low-level, low-frequency accelerative forces; superimposed over their spectrum are forces caused by running machinery, mass movements, docking maneuvers, activities and movements by the astronauts, and other sources.

In order to obtain experimental data of these latter forces, a typical spacecraft - an engineering model of ERNO's Spacelab - was suspended on long ropes in a high-bay hanger, and equipped with a number of accelerometers. Active components on the Spacelab (fans, pumps, air conditioners, valves, levers) were operated, and "astronauts" moved boxes, drawers, sleds, and their own bodies. Generally speaking, the response of the Spacelab structure was very similar to the environment measured on Spacelabs SL-1, SL-2, and D-1. At frequencies in the broad range between 1 and about 100 Hz, acceleration peaks reached values of 10^{-3} and 10^{-2} g_o, and even higher.

Dr. Knabe will extend his theoretical and experimental studies; they will include Spacelab, the Space Station, Columbus, Eureca, and Free Flyers of various designs.

N91-12422

23. LOW-G PAYLOAD PLACEMENT CONSTRAINTS FOR SPACE STATION

Anita S. Carpenter and Stanley N. Carroll
NASA/Marshall Space Flight Center

ABSTRACT

Payloads onboard the Space Station will be subjected to a steady state acceleration level dominated by gravity gradient and aerodynamic drag forces. The g-level due to gravity gradient forces depends on the payload location relative to the center of mass, whereas the g-level due to aerodynamic drag may be assumed nearly constant throughout the Space Station. The vector of acceleration due to aerodynamic drag can always be broken down into three orthogonal components, in the direction opposite to the velocity vector, along the local vertical, and perpendicular to the orbit plane. It will be shown that the gravity gradient term has two components, which are orthogonal to one another. One component is along the local vertical and the other is perpendicular to the orbit plane. Thus, the combination of all components form an orthogonal triad of vectors. This paper will address the payload location constraints to satisfy the requirements of 1 micro-g. The permissible locations are within an open-ended tube having an elliptical cross section, which is aligned with the velocity vector and centered on the system center of mass.

INTRODUCTION

Payloads onboard the Space Station are subjected to a steady state g-level dominated by gravity gradient and aerodynamic drag forces (Figure 1). The g-level due to gravity gradient depends on the payload location relative to the center of mass, whereas the g-level due to aerodynamic drag is constant throughout the Space Station. This briefing addresses the payload location constraints to satisfy a requirement of 1 micro-g maximum acceleration.

OVERVIEW

- ACCELEROMETER EQUATION/ASSUMPTIONS.
- GRAVITY GRADIENT BOUNDARY CONSTRAINT FOR MICROGRAVITY PAYLOADS.
- EFFECT OF ALTITUDE ON BOUNDARY CONSTRAINT.
- AERODYNAMIC DRAG EFFECT.
- ACCELERATION DUE TO RCS FIRINGS DURING REBOOST.
- ADDITIONAL DISTURBANCES TO BE CONSIDERED.

FIGURE 1.

Additional disturbances to the microgravity environment, such as the accelerations expected during reboost will also be presented.

ACCELEROMETER EQUATION/ASSUMPTIONS

An accelerometer senses the vector sum of all gravitational, inertial, and external accelerations. Or stated in terms of forces, the accelerometer senses the vector sum of all gravitational, inertial, and external forces.

The acceleration equation (Figure 2) with the station in a circular orbit and in a local vertical orientation contains both an in-the-orbit plane term and an out-of-the-orbit plane term.

The g-level for a payload at a specified distance from the center of mass has one gravity gradient component along the local vertical and another perpendicular to the orbit plane.

The permissible microgravity payload locations are within an open-ended tube having an elliptical cross section. This elliptical boundary constraint is aligned with the velocity vector and centered on the trajectory of the system center of mass.

ONE MICRO-G BOUNDARY CONSTRAINT WITHOUT AERODYNAMIC DRAG EFFECT

The payload location constraint for a maximum acceleration level of one micro-g and a 220 nm circular orbit is shown in Figure 3. The velocity vector is into the paper. Since the boundary is determined only by distance from the center of mass it is independent of the station configuration.

To obtain boundaries for g-levels other than one micro-g, it is only necessary to scale both axes by the same amount. The curve will always be an ellipse with a three to one ratio between major and minor axes, with the tighter constraint being in the axis aligned with the local vertical.

Ex: For a 10 μg requirement,

Major axis = 10 (major axis for 1 μg) = 10 (50.4 ft) = 504 ft

Minor axis = 10 (minor axis for 1 μg) = 10 (16.8 ft) = 168 ft

ACCELEROMETER EQUATION/ASSUMPTIONS

ACCELERATION SENSED BY ONBOARD ACCELEROMETER:

$$\underline{A} = \dot{\underline{\omega}} \times \underline{r} + \underline{\omega} \times (\underline{\omega} \times \underline{r}) + \Omega_o^2 \underline{r} - 3\Omega_o^2 \underline{u} \cdot \underline{r}\, \underline{u} \qquad (1)$$

WHERE,

$\underline{\omega}$ IS THE INERTIAL ANGULAR VELOCITY.

$\dot{\underline{\omega}}$ IS THE INERTIAL ANGULAR ACCELERATION.

$\underline{r}$ IS THE VECTOR FROM THE CENTER OF MASS TO THE ACCELEROMETER (I.E., PAYLOAD LOCATION).

Ω_o IS THE ORBITAL RATE OF THE CIRCULAR ORBIT.

$\underline{u}$ IS A UNIT VECTOR ALONG THE LOCAL VERTICAL.

FOR CONVENIENCE, VECTORS WILL BE REPRESENTED IN TERMS OF IN-THE ORBIT PLANE (SUBSCRIPT p) AND OUT-OF-THE ORBIT PLANE (SUBSCRIPT o) TERMS,

$$\underline{r} = \underline{r}_p + \underline{r}_o = r_p \underline{u}_p + r_o \underline{u}_o$$

FOR SPACE STATION IN LOCAL VERTICAL ORIENTATION,

$$\dot{\underline{\omega}} = 0$$

$$\underline{\omega} = \Omega_o \underline{u}_o$$

EQUATION (1) NOW REDUCES TO,

$$\underline{A} = \Omega_o^2 \underline{r}_o - 3\Omega_o^2 \underline{u} \cdot \underline{r}_p \underline{u}$$

FIGURE 2.

ACCELEROMETER EQUATION/ASSUMPTIONS (CONTINUED)

IN TERMS OF STATION BODY AXES ($\underline{u} = \underline{u}_z$, $\underline{u}_o = \underline{u}_y$) EQUATION (2) BECOMES,

$$\underline{A} = \Omega_o^2 \, y \, \underline{u}_y - 3\Omega_o^2 \, z \, \underline{u}_z$$

EXPRESSING THE ACCELERATION LEVEL IN UNITS OF G'S,

$$\underline{g} = \frac{\Omega_o^2}{g_o} \, y \, \underline{u}_y - 3 \, \frac{\Omega_o^2}{g_o} \, z \, \underline{u}_z$$

THE ABOVE COEFFICIENT IS CALCULATED AS,

$$\frac{\Omega_o^2}{g_o} = \frac{1/R_o}{(1+h/R_o)^3}$$

WHERE, R_o IS THE EARTH'S RADIUS

h IS THE ORBIT ALTITUDE

THE STRUCTURE OF THE ACCELERATION EQUATION IS,

$$\underline{g} = \frac{y}{\alpha} \, \underline{u}_y - \frac{z}{\beta} \, \underline{u}_z$$

WHERE, $\alpha = \left(\frac{\Omega_o^2}{g_o} \right)^{-1}$ AND $\beta = \frac{\alpha}{3}$

EXPRESSING THE MAGNITUDE ONLY,

$$g^2 = \frac{y^2}{\alpha^2} + \frac{z^2}{\beta^2}$$

THIS EQUATION FOR AN ELLIPSE IN THE Y-Z PLANE DEFINES THE ACCELERATION BOUNDARY CONSTRAINT IMPOSED BY GRAVITY GRADIENT FORCES.

THE DESIRED MAXIMUM G-LEVEL IS USED FOR THE VARIABLE g.

FIGURE 2. (Concluded)

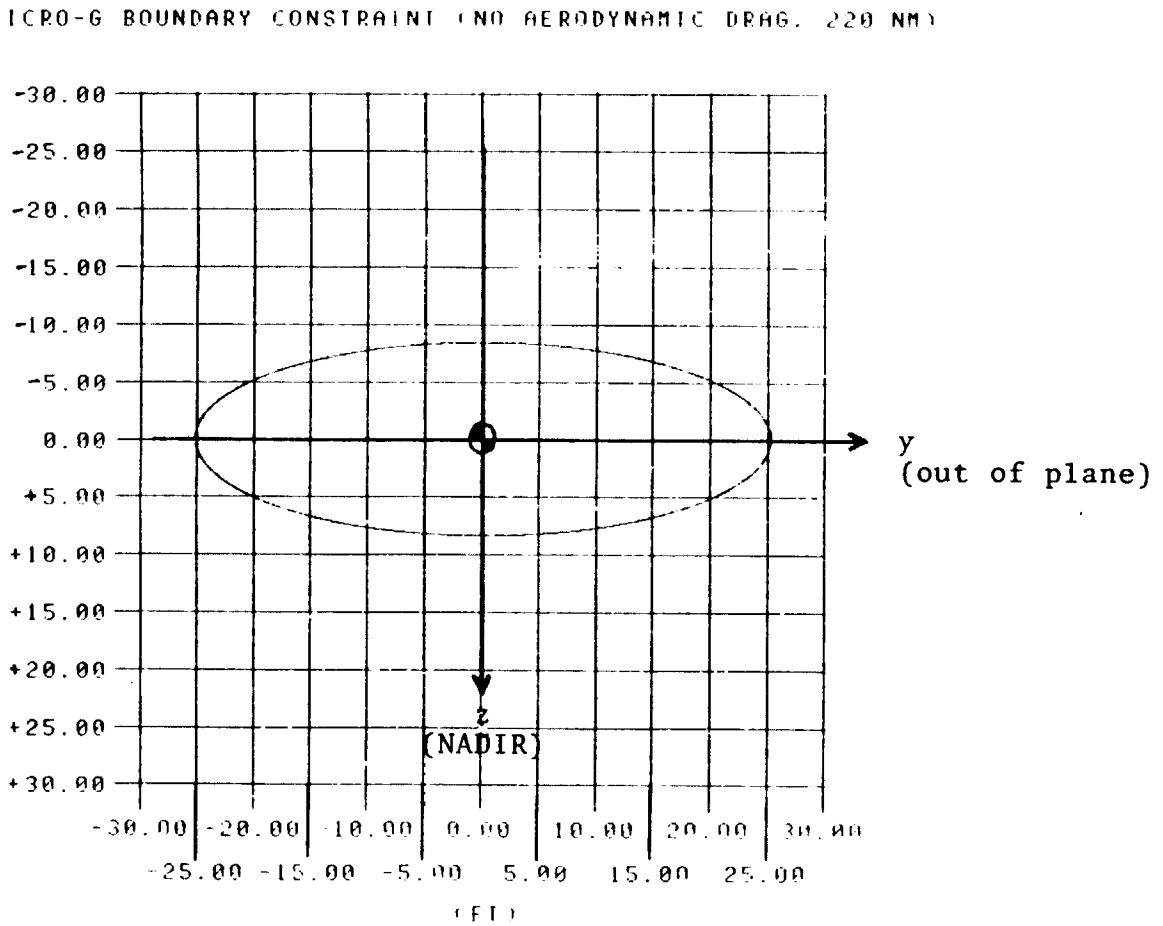
1 MICRO-G BOUNDARY CONSTRAINT (NO AERODYNAMIC DRAG, 220 NM)
-30.00
-25.00
-20.00
-15.00
-10.00
-5.00
0.00
+5.00
+10.00
+15.00
+20.00
+25.00
+30.00
y
(out of plane)
z
(NADIR)
-30.00 -20.00 -10.00 0.00 10.00 20.00 30.00
-25.00 -15.00 -5.00 5.00 15.00 25.00
(FT)

FIGURE 3.

It is important to realize that knowledge of the center of mass location may be no better than a 1-ft-diameter sphere, even with good bookkeeping of fuel usage, payload repositioning, etc. Thus, it appears that locating payloads to receive less than 10^{-6} g acceleration may be unrealistic on the Space Station. Active control or movement of the center of mass will also be difficult after the operational configuration is established. A rough calculation shows that it would require approximately 33,000 lbm added to the far end of the station to move the center of mass one truss cube (16.4 ft).

VARIATION OF ALPHA AND BETA COEFFICIENTS WITH ALTITUDE

The α (semimajor axis) and β (semiminor axis) coefficients vary almost linearly, but very slightly, with altitude (Figure 4).

Previous plot was arbitrarily calculated for a 220 nm orbit since actual operational altitude is uncertain and could be a variable, constant density altitude profile.

AERODYNAMIC DRAG EFFECT

The vector of acceleration due to aerodynamic drag can always be resolved into three orthogonal components, in the direction opposite to the velocity vector, along the local vertical, and perpendicular to the orbit plane. It is assumed to be uniform over the station structure.

The effect of aerodynamic drag on the boundary constraints is to reduce the dimensions of the ellipse. In the limiting case, as the g-level due to aero approaches the maximum requirement level, the ellipse contracts down to a point. There is no further meaning to boundary constraints if the aerodynamic contribution exceeds the requirement level.

ONE MICRO-G BOUNDARY CONSTRAINTS FOR SEVERAL VALUES OF AERODYNAMIC DRAG

The open-ended elliptical constraints for a requirement of one micro-g total acceleration are shown for aerodynamic drag components of 0., 0.25, 0.5, and 0.75 micro-g's, assuming that the drag force acts

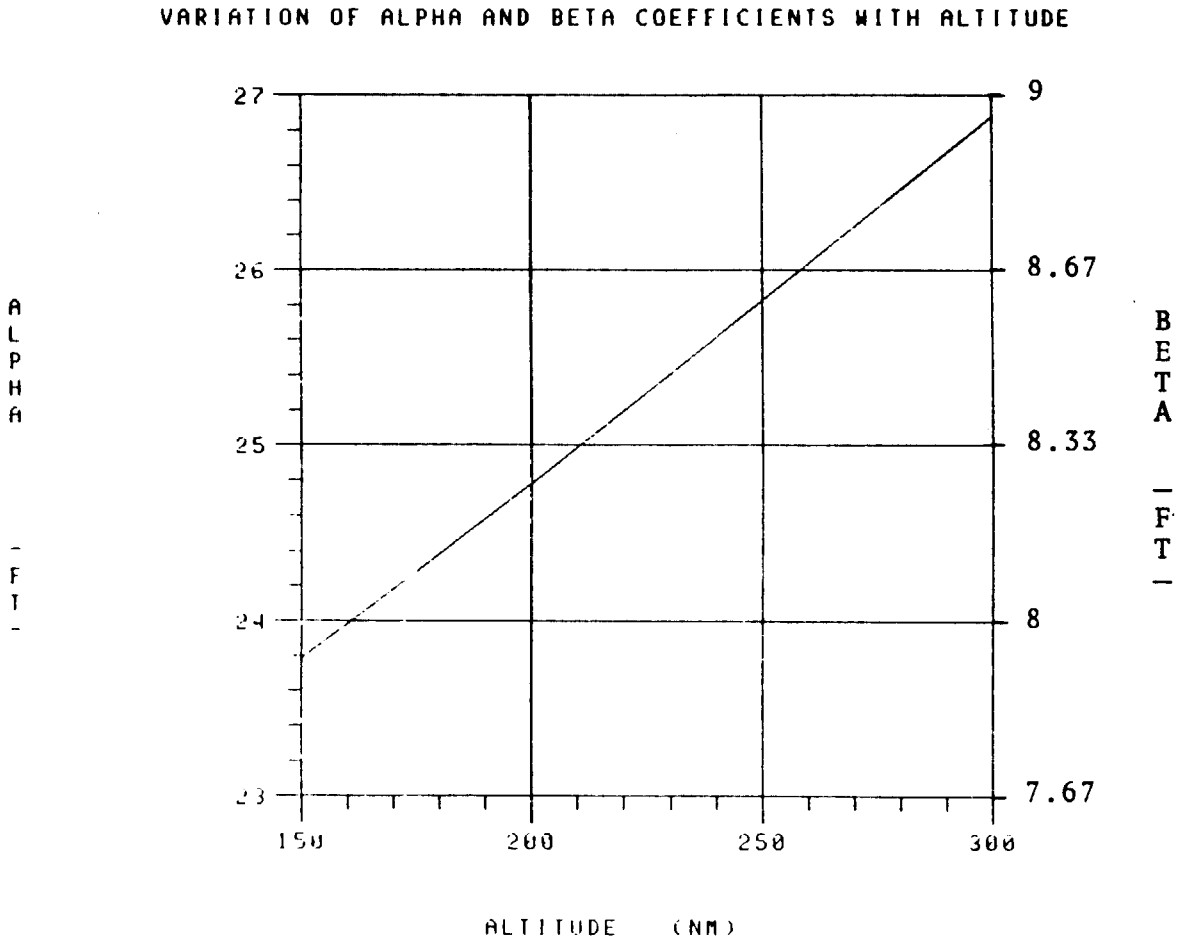
VARIATION OF ALPHA AND BETA COEFFICIENTS WITH ALTITUDE
27
26
25
24
23
9
8.67
8.33
8
7.67
150
200
250
300
ALTITUDE (NM)
ALPHA - FT -
BETA - FT -

FIGURE 4.

only in the direction of the velocity vector. It can be seen that the size of the ellipse decreases rapidly with increasing aerodynamic drag (Figure 5).

Actually, the vector of the drag force will always have components in all three orthogonal directions; their magnitudes change periodically during each orbit because of the periodic attitude change of the solar panels. The "ellipses" of constraint, therefore, will become non-symmetrical contour lines under the influence of aerodynamic drag.

ACCELERATION DUE TO RCS FIRINGS DURING REBOOST

The Space Station will need to be reboosted approximately every 90 days during normal operation. For the 9-ft truss dual keel configuration, six (+X) 25-lb engines are on nominally with the appropriate engines off-modulated for attitude control.

Figure 6 shows the X acceleration profile as sensed near the module cluster during a representative portion of the reboost burn. A rigid station is assumed. The accelerations in the Y and Z directions are approximately one order of magnitude smaller than those in the X (flight path) direction.

ADDITIONAL "STEADY STATE" DISTURBANCES

Although the gravity gradient and aerodynamic drag are the dominant "steady state" disturbances, several other unavoidable disturbances will be affecting the acceleration environment (Figure 7). These include crew motion, rotating machinery, fluid loops, and momentum management maneuvers.

Larger, infrequent disturbances such as reboost, shuttle and OMV docking, RMS operation, and others will dictate an interruption of sensitive microgravity payloads.

Question:

Ken Demel, NASA/Johnson Space Center: On these assumptions of constant drag, we have done some computations with rotating the panels through

1 MICRO-G BOUNDARY CONSTRAINTS FOR SEVERAL VALUES OF AERODYNAMIC DRAG

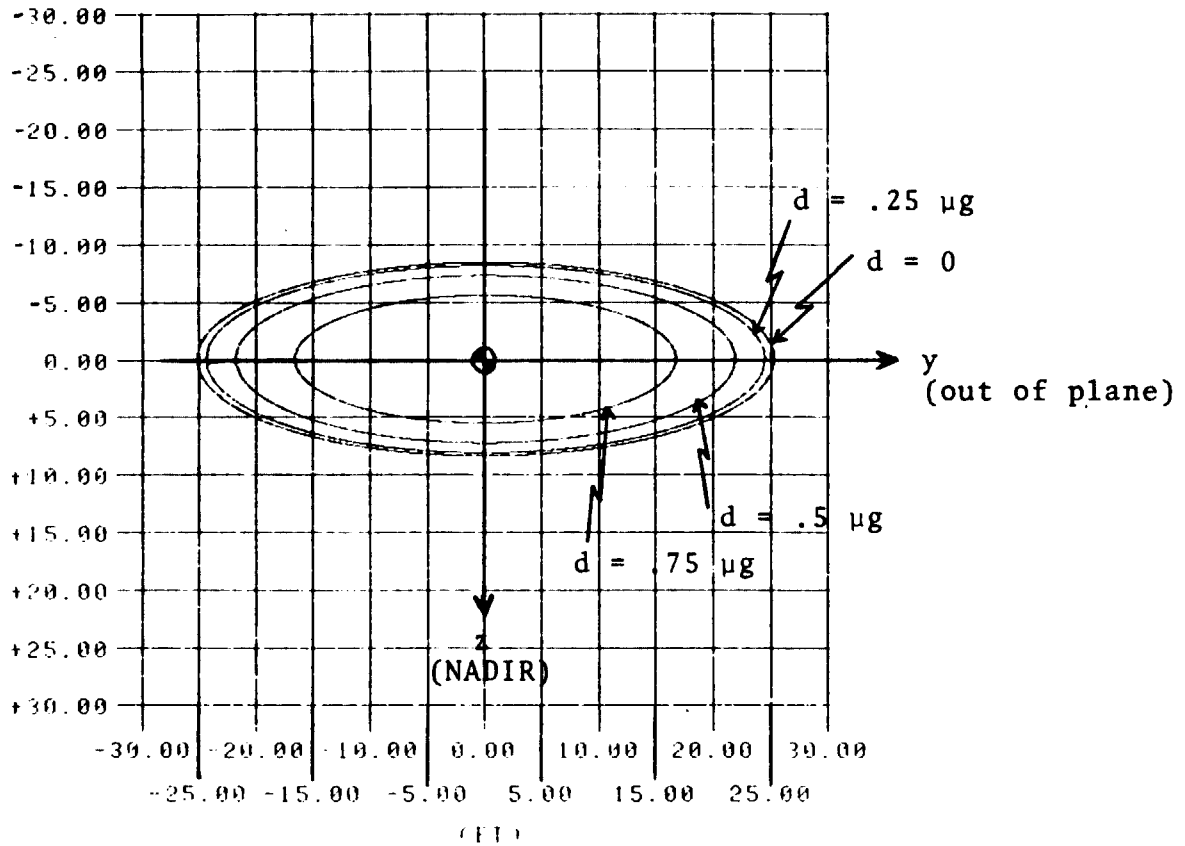

FIGURE 5.

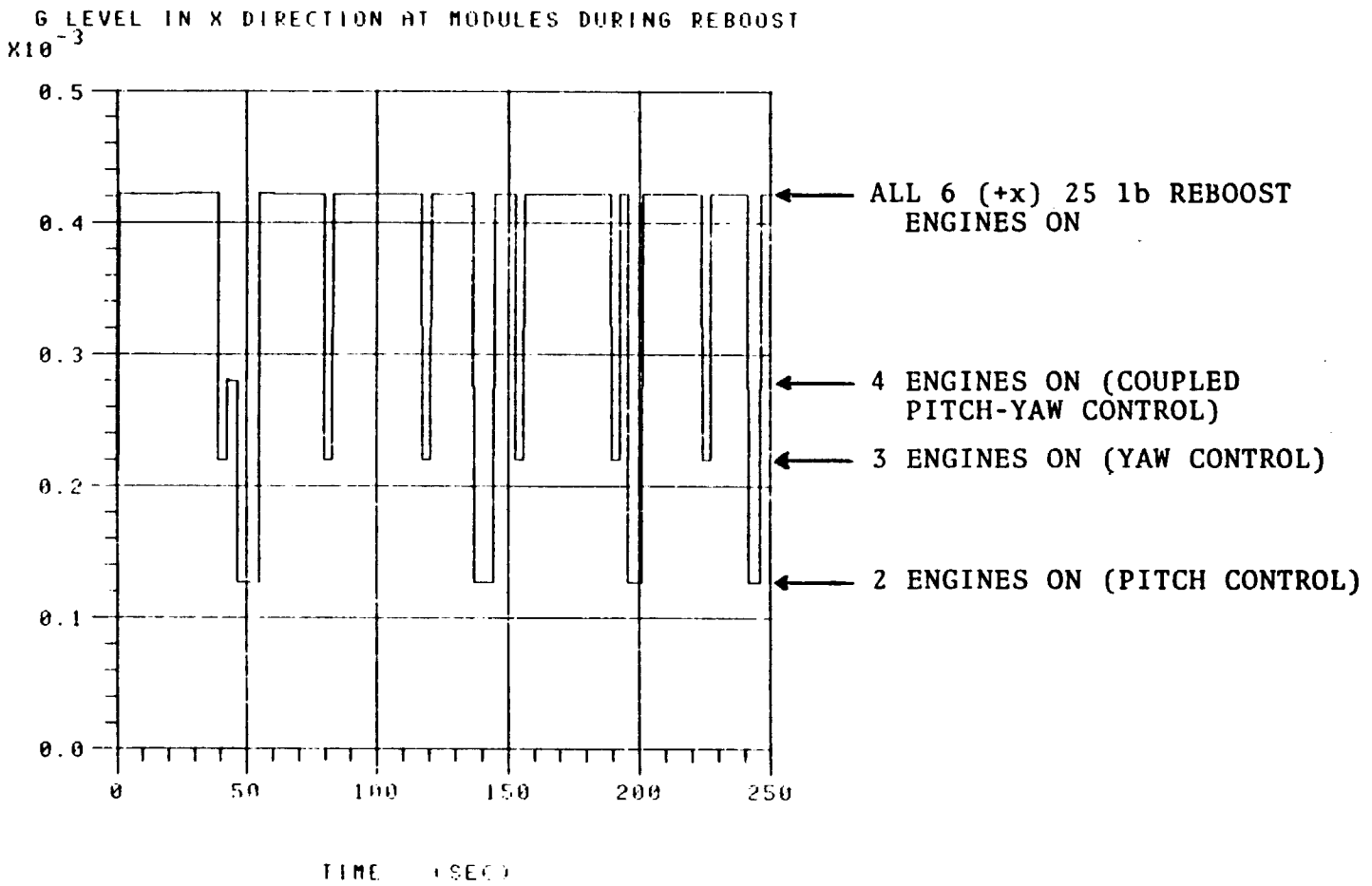
G LEVEL IN X DIRECTION AT MODULES DURING REBOOST
X10⁻³
0.5
0.4
0.3
0.2
0.1
0.0
G LEVEL
0
50
100
150
200
250
TIME (SEC)
ALL 6 (+x) 25 lb REBOOST ENGINES ON
4 ENGINES ON (COUPLED PITCH-YAW CONTROL)
3 ENGINES ON (YAW CONTROL)
2 ENGINES ON (PITCH CONTROL)

FIGURE 6.

ADDITIONAL "STEADY STATE" DISTURBANCES

- CREW MOTION - RANDOM, 10 LB FORCE AT C.G. WOULD RESULT IN 14-20 μg ACCELERATION.
- ROTATING MACHINERY - CMG'S.
- ROTATING APPENDAGES - SOLAR ARRAYS, RADIATORS, ANTENNAS.
- FLUID LOOPS FOR ECLS AND THERMAL CONTROL.
- SOLAR DYNAMIC POWER SYSTEM.
- MOMENTUM MANAGEMENT MANEUVERS - ADDED ANGULAR COMPONENT OF $0\text{-}10^{-10}$ g.
- STRUCTURAL OSCILLATIONS.

FIGURE 7.

the diurnal bulge as you fly through an orbit. The minimum drag in the orbit is about a twentieth of a micro-g and the maximum in the orbit is about a half of a micro-g. So, when you vectorially add that to the gravity gradient form you wind up with a fan of vectors that is rotating. The vectorial resultant of the two is rotating through about 20 to 25 degrees. I don't know whether people have really looked at it in that detail, but up will not always be in the same direction as you go though the orbit. Some of these assumptions of constant drag tell you what is going to happen to your altitude but they don't tell you anything about what is happening over about a 10- to 15-minute period and if a particular crystal growth is sensitive to the symmetry condition, that rotation is really going to degrade it over several hours. So, I'd like to see the actual drag profiles through an orbit taken into account.

Carpenter: Of course I guess you are going to have to design your experiment to withstand the worst case aerodynamic drag.

Demel: But we might want to look at those effects as they really occur and not assume constant effects, and maybe that drives us to requiring drag makeup as we go.

Ed Bergmann, C.S. Draper Laboratory: You assumed that the space station was in a local vertical attitude and you threw out some terms because it was maintaining that attitude. The shuttle when it holds attitude limit cycles because of the finite reslution of the jets and there may be a similar effect on the space station so you may have small angular rates superposed on the local vertical rate.

Carpenter: Yes, the local vertical is going to be at the torque equilibrium attitude.

Stan Carroll, NASA/Marshall Space Flight Center: That is basically why that tube in the X direction is going to close up on you too is because the angular rate in pitch. So you won't have an empty tube sitting on the dead band. It depends on the dead band and the control rate.

Ray Yoel, Boeing: In the acceleration effects, you didn't have the satellite servicing in there, and you mentioned that you could narrow it down to within an inch, the center of gravity. The satellite servicing guys, I heard, are planning to bring a 700-pound satellite through the airlock, put it on a slide, and slide it down to the work station and work on it there. To keep track of the center of gravity, as you have a 700-pound satellite sliding through the habitat module might be a little difficult.

Carpenter: No, it's just a very preliminary thing here.

Question: You quoted some numbers though that said how sensitive you were in terms of a very large mass, 33,000 pounds, 200 feet away. Could you clarify that?

Carpenter: I said it would take 33,000 pounds added at 200 feet away to move the center of mass one truss cube. So that is a lot of weight that is going to have to be added to move the CG around if we are going to try to actively control the position of the CG. The station needs to be built up right in the first place, that is the main point.

N91-12423

24. SPACE STATION DYNAMICS

Reg Berka
NASA/Johnson Space Center

ABSTRACT

Structural dynamic characteristics and responses of the Space Station due to the natural and induced environment are discussed. Problems that are peculiar to the Space Station are also discussed. These factors lead to an overall acceleration environment that users may expect. This acceleration environment can be considered as a loading, as well as a disturbance environment.

I've tried to re-orient this briefing to emphasize some of the micro-g aspects that everybody's been talking about. We've been hearing a lot about the requirements for the Space Station and how to measure that environment. What I'd like to talk about is what we at the Johnson Space Center think we can expect on Station. The reason is because it really has a very significant effect on the configuration. The requirements that I've heard over the last few days seem to have a very wide range, and will have a dramatic impact on the Space Station configuration. Yet we're very uncertain as to whether 10^{-3} or 10^{-8} g's are needed. 10^{-5} is our current requirement, and remember those exponents are orders magnitude and as such have a large effect on Space Station design. I want to encourage both the user side and the Station performance side that we need to really work together to make sure that we understand exactly what we need. These requirements don't come cheap and we have an $8 billion budget to bring this thing in under.

The configuration can't solve this entire problem. It seems like every speaker at this workshop has put a note in my notebook about another problem with micro-g materials processing, and frankly it seems that the work of the user community in this area is really just begin-

ning. There seems to be a lot of different problems and I think the best we can do as far as Space Station is concerned is to try to present an environment that will be benign to your conditions, because you're going to find out that you never really understand it until you do get on orbit. So from a configuration standpoint, we'll just try not to do anything stupid that will really aggravate a situation that is already a very difficult engineering problem. To that effect we've changed from the power tower (which had featured modules at the bottom of a long beam) to the dual keel, primarily because of this micro-g requirement.

There seems to be a whole host of other problems, including dynamic effects and things like that. Another thing to consider is Owen Garriott's speech about a free-floating type of experiment that may release us completely from the configuration issue, in the sense that the free flyer becomes its own spacecraft and we don't have to worry about it quite as much. Again, I want to emphasize that we really need to work together to resolve this issue because it's an important thing to the Space Station configuration. We need to nail these things down and work toward resolving what those real requirements are.

Work Package 2 represents work that is going on at the Johnson Spacecraft Center (in our own dynamics area), Rockwell in Downey, and McDonnell Douglas in Huntington Beach.

Space Station dynamics separate into rigid and flex, and I'm going to talk about what the characterization and the different disturbances are in each of these areas and what we've been trying to address.

Now one of the major configuration issues is the flight mode, and some of this has been opened up recently again to try to study the solar inertial and Local Vertical, Local Horizontal (LVLH) modes (Figures 1 through 3). The solar inertial flight mode essentially points at the Sun. The reason for doing this is because Space Stations are solar powered, and you can look at it like it's a giant payload on the Station that has to be pointed at the Sun. The issue is whether or not you point the rest of the Station at the Sun, or whether you point the rest

SPACE STATION FLIES WITH PRINCIPAL AXES IN ORBIT PLANE

- All Points On Structure Have Drag Acceleration Opposite To V-Bar (250 NM <0.7 μG's)
- Points On Structure Above Or Below SS CM WRT Earth Have A Component Of Acceleration Force Towards CM Parallel To The Earth Radius Vector
- Points To Side Of Orbit Plane Have A Component Of Accelerations Force Away From Orbit Plane
- Points In Front Or Behind CM Along V-Bar Have A Component Of Acceleration Force Away From CM And Parallel To V-Bar, Which Adds To The Drag Acceleration

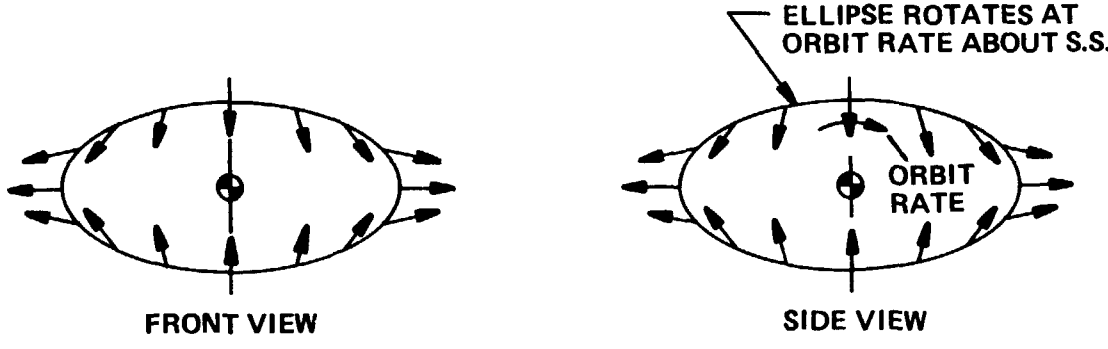

FIGURE 1. SOLAR INERTIAL FLIGHT MODE

LVLH FLIGHT MODEL

- Space Station (SS) Assumed To Rotate About Perpendicular To Orbit Plane
  - All points on structure have a drag acceleration opposite to V-Bar (@ 250 NM <0.7 μGs)
  - Points on structure above or below SS CM have a component of acceleration force towards CM parallel to the earth radius vector
  - Points to side of orbit plane have a component of accelerator force away from orbit plane

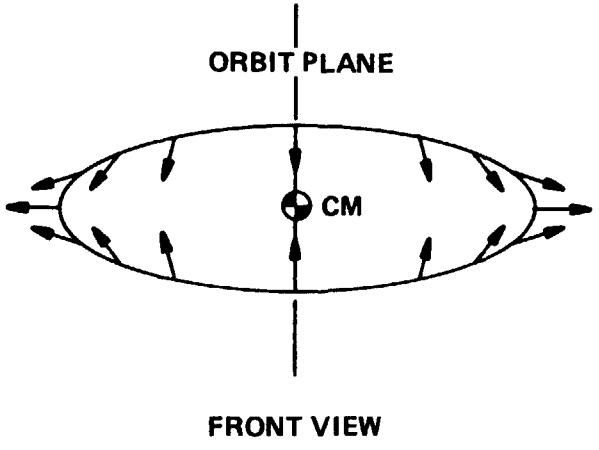

FIGURE 2. LVLH FLIGHT MODE/MICRO-GRAVITY ENVIRONMENT

of the Station at the Earth. The solar inertial flight mode is a very cost-effective way to go. You can eliminate many of the articulating systems and thereby simplify the dynamics issues and analysis. But if we have to go to the LVLH mode from a micro-g standpoint, or from an Earth-viewing standpoint, then we have to do it, but we want to know what the cost is and identify those things and know what the benefits are.

- **CONCLUSIONS:**
  - BOTH SI AND LVLH FLIGHT MODES HAVE THE SAME μG ACCELERATION COMPONENT PERPENDICULAR TO THE ORBIT PLANE
  - THE COMPONENT OF ACCELERATION PARALLEL TO THE RADIUS VECTOR FOR THE LVLH FLIGHT MODE IS APPROXIMATELY 50 PERCENT GREATER THAN FOR THE SI FLIGHT MODE
  - THE μG COMPONENTS OF ACCELERATION IN THE ORBIT PLANE FOR THE SI FLIGHT MODE AVERAGES OVER THE ORBIT TO <1.0 μG

FIGURE 3. CONCLUSIONS

Figure 4 shows a reference configuration that is being studied at the Johnson Space Center. This Station configuration has been studied both from the solar-oriented standpoint and from a local vertical, local horizontal configuration. One of the features that is different from the reference dual keel is the lack of the keels. A major benefit of this is that it allows the Space Station to be very compact, and that yields very advantageous dynamics effects.

I was asked to show some of the isogravs, a word that I think we made up at JSC. Figure 5 shows the isogravs on a solar inertial station. You get constant gravity just like you do on the LVLH station as you come out of the orbit plane. The five micro-g circle is the outer one, two and a half the inner. In-plane isogravs are a set of ellipses (Figure 6) and they will rotate with respect to the body, or vice versa.

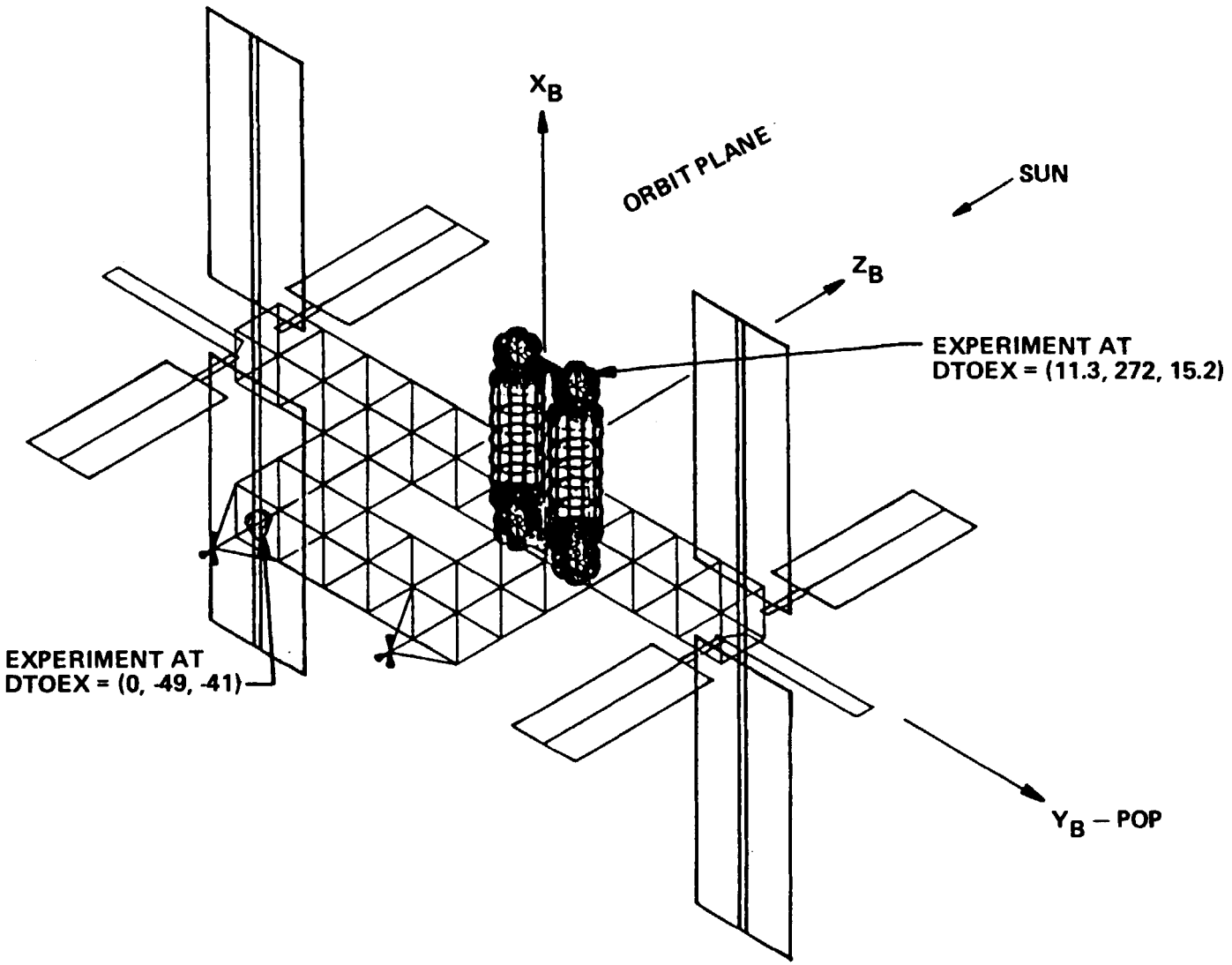

FIGURE 4. SOLAR ORIENTED SPACE STATION

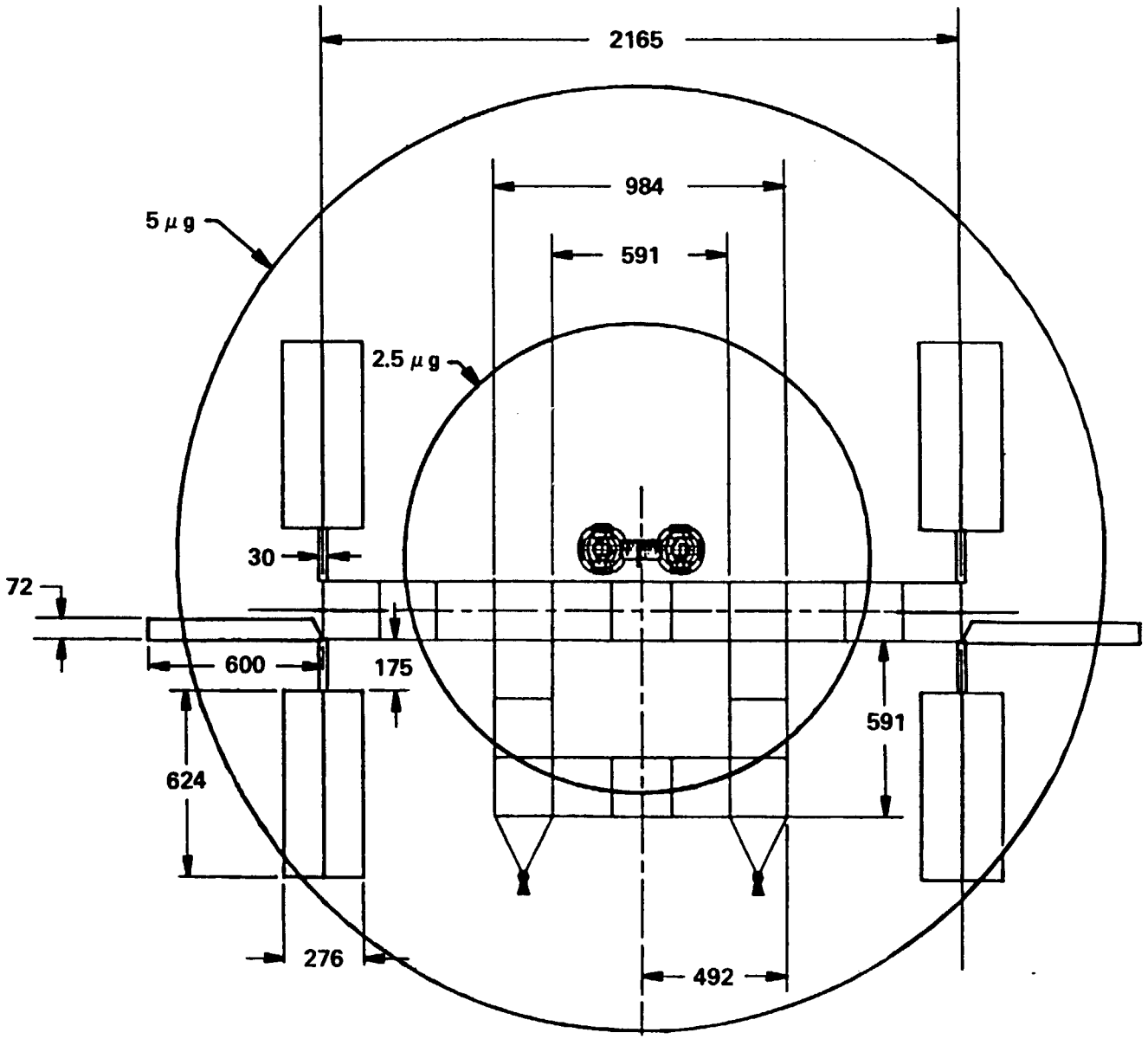

FIGURE 5. SOLAR INERTIAL FLIGHT MODE, TOP VIEW

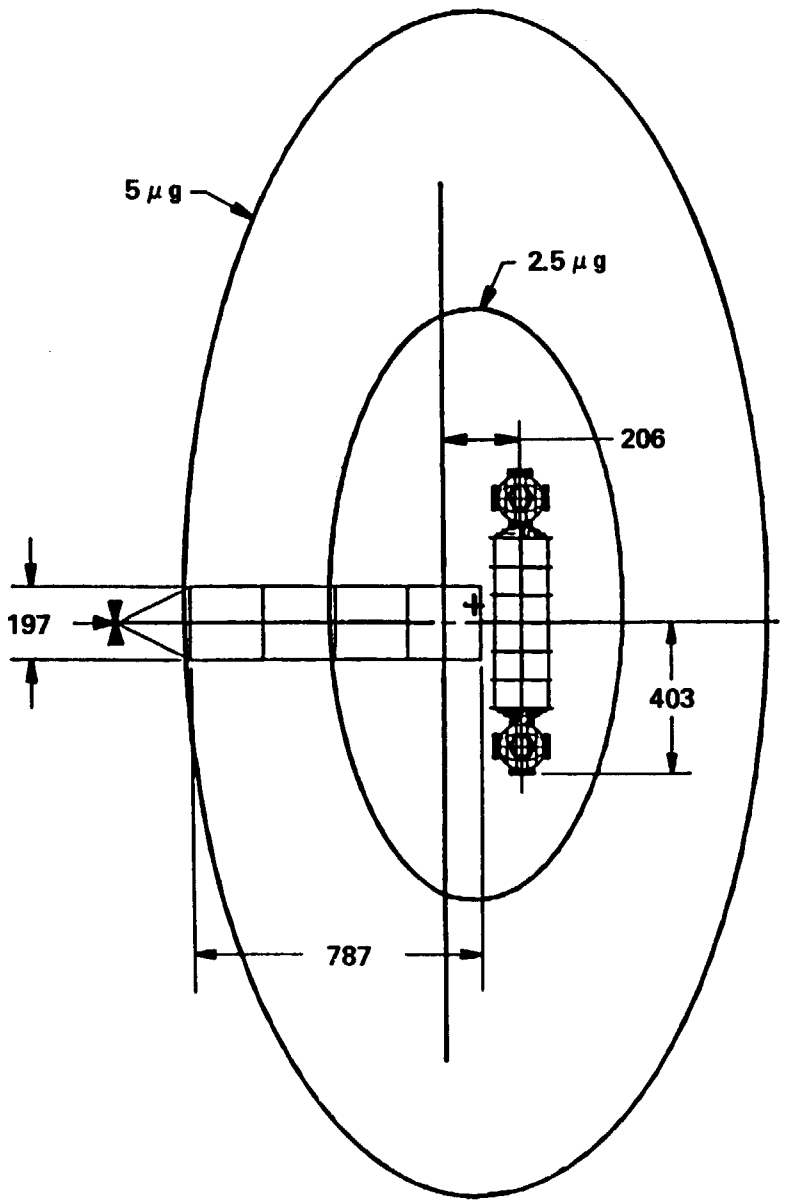

NOTE: MICROGRAVITY (μg) CONTOURS CLOCK AROUND STATION AT ORBITAL RATE, FOR POP S.I. FLIGHT MODE

FIGURE 6. SOLAR INERTIAL FLIGHT MODE, SIDE VIEW

This characteristic has caused some people in this materials processing community some concern. We're just trying to explore that, and as dynamicists we try to identify the environment and then try and get user's reaction to it.

Figure 7 shows isogravs in the LVLH mode.

Figure 8 shows rigid body accelerations of the two flight modes. This figure tries to address what the actual magnitude of that acceleration is. The number 4 curve includes the aero effects, but I'd like to point out that the model really varies a great deal over whatever assumptions you make in terms of solar cycle so you have to be really careful. It's a difficult thing to quantify. This example is a rather extreme atmosphere, but I think it's the case that's been consistently analyzed. The number 5 line shows a magnitude that results from a solar inertial flight mode on this particular station. It is consistent with respect to atmospheric drag. You would see the same thing if this were on the dual keel or a power tower or anything else. You're going to get a reduction in magnitude from the solar inertial standpoint, but also some fluctuation. On the LVLH mode, you get a constant type of acceleration and it's going to be a little larger. The cycle period is going to be somewhere around half of an orbit, and whether or not a materials processing experiment can respond in 45 minutes to this cycle is questionable. An experiment will get a reduced amount of acceleration in the SI mode, but it's going to be changing a little bit.

Bob Naumann mentioned yesterday the possibility of rotating experiments. Those things have to be investigated because, from the configuration standpoint, we can only present an environment that is amenable to the solution of the problem, we're not going to be able to solve the whole problem. There's still going to have to be something done at the point of the experiment, but from the other problems that I've heard about over the last few days, I think you're going to have to do that anyway. The kind of environment that we can expect from the solar inertial flight mode is reduced, but not constant.

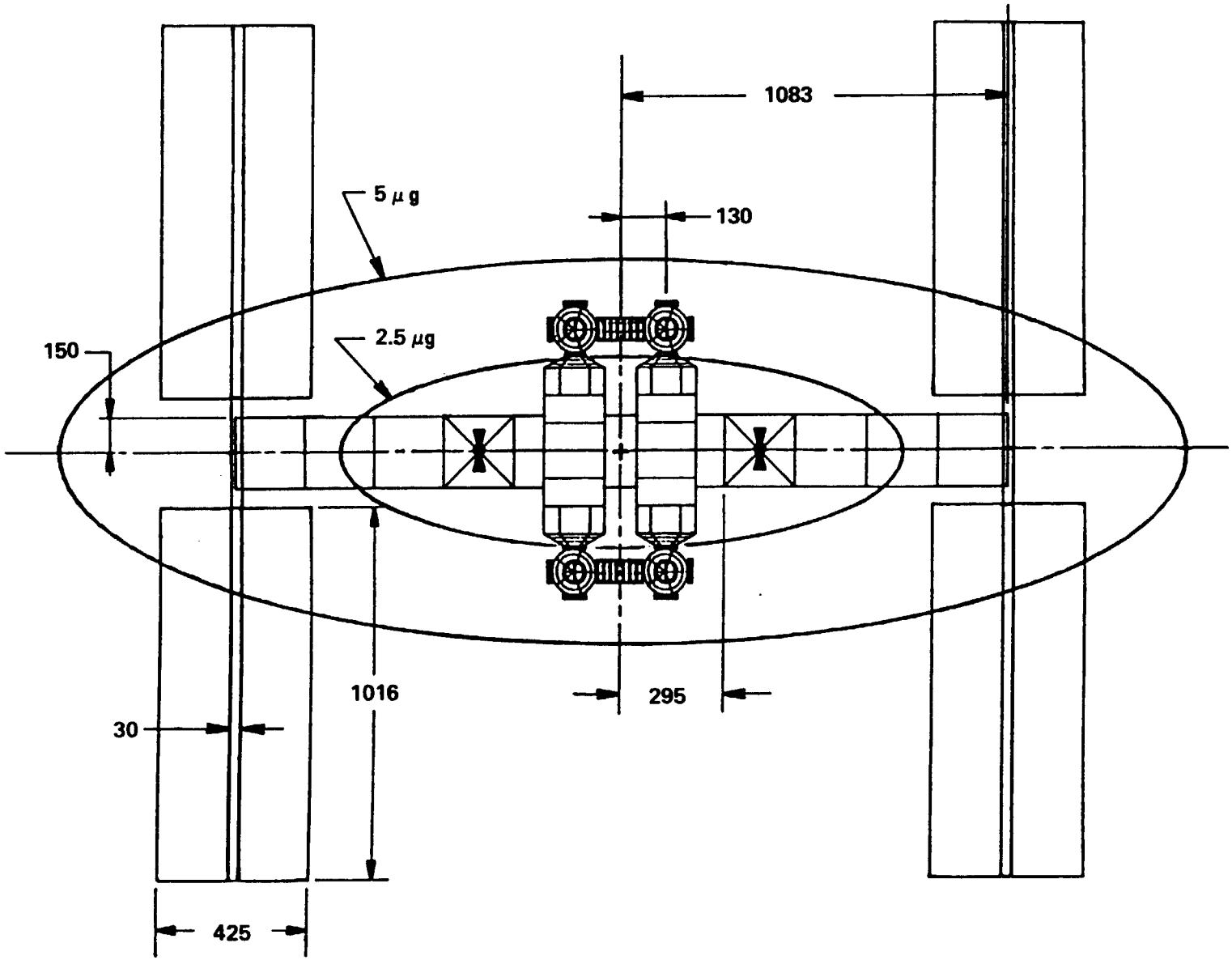

FIGURE 7. LVLH FLIGHT MODE, SIDE VIEW

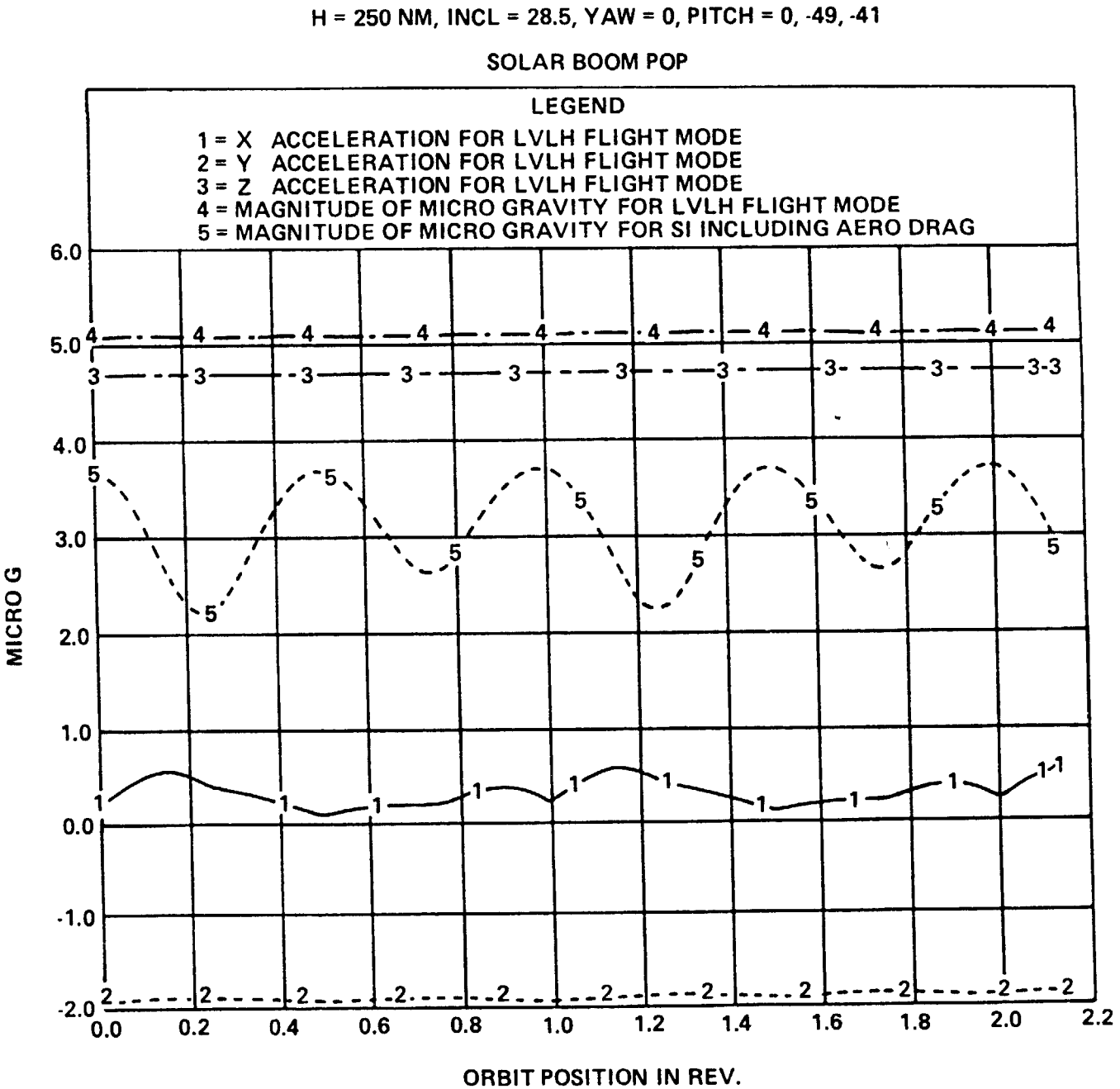

FIGURE 8. RIGID BODY ACCELERATIONS

Figures 9 through 10 show a breakdown of the magnitude value into its components. You do get a sinusoidal activity that has a 45-minute period. There is phasing difference as a function of the position. Line 4 shows the aero disturbance. The thing that I'm trying to learn, with reference to what I heard yesterday about the worst kind of thing, is a steady state acceleration, but I don't know whether this may be too low a frequency. We need to explore that a little more, but certainly as you integrate this as an average (reference again to Dr. Naumann's presentation yesterday) you're going to get a very low net acceleration.

The flight mode is really a very basic and fundamental issue to the configuration. It's probably the first fork in the road. When we start solving micro-g problems from the first fork in the road, we cascade that into an impact on a lot of other systems. So as we try to do the systems engineering on the Space Station, what happens at the very top level can have a very dramatic effect on what happens later on. And that's the concern about the impact of micro-g on flight mode: its significance to the configuration.

Now the conclusions that we're drawing from the analysis is that both the solar inertial and LVLH flight modes have the same micro-g acceleration components out of the orbit plane. It's only in the orbit plane that it shows a difference. If somebody wants a steady-state value, you can locate an experiment at the center of mass and out of the orbit plane leading to a higher static or steady-state value. I'm getting the impression that's probably not a good way to go because the component of acceleration parallel to the radius vector for the LVLH flight mode is approximately 50 percent greater than the solar inertial flight mode. That was what the first chart was trying to demonstrate. Micro-g components of acceleration in the orbit plane for the solar inertial flight mode average over the orbit to less than a micro-g because of the sinusoidal components. We want to hear what impact that has on the materials processing. That is, how you really feel about this difference in flight modes.

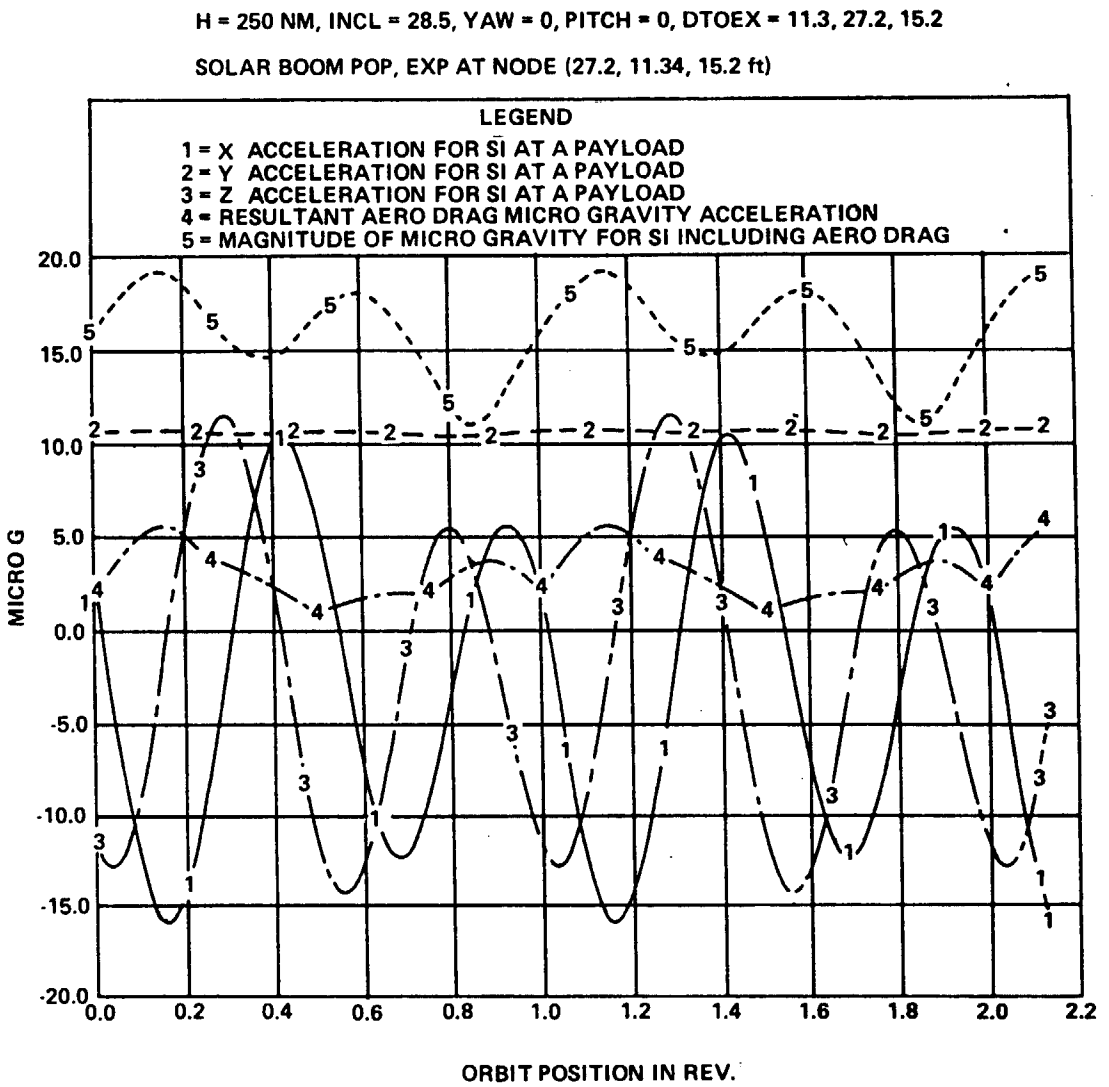

FIGURE 9. COMPONENTS OF ACCELERATION AT A PAYLOAD

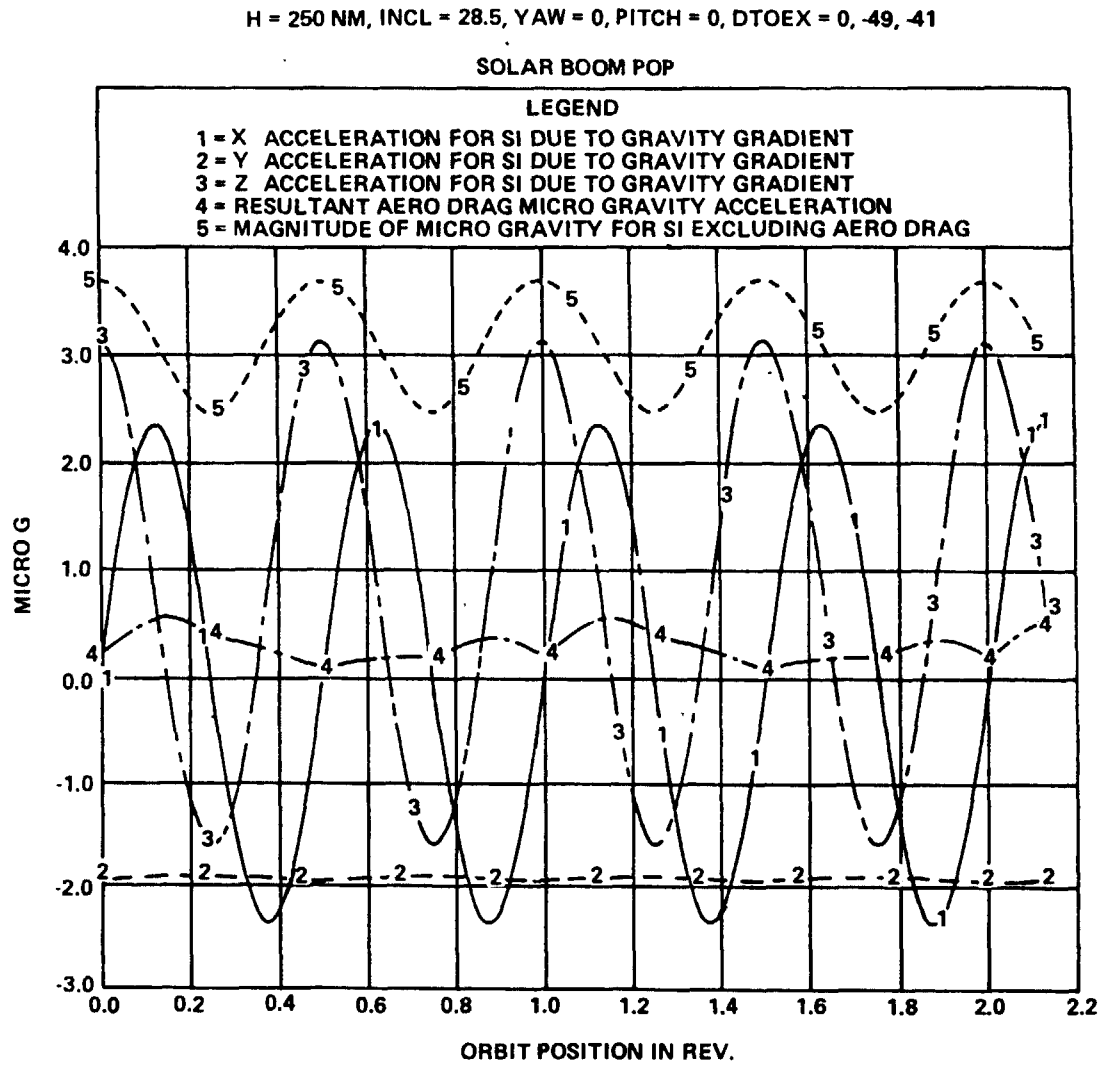

FIGURE 10. GRAVITY GRADIENT COMPONENTS

The operational impacts of orbital rate have become very dramatic from a rigid body standpoint, because there's a lot happening on the Station besides micro-g materials processing experiments. This is what cascades from a very early systems decision, there will be effects that may have been otherwise unexpected. As an example, on the dual keel we ran into several problems conserving angular momentum, moving masses from the upper boom down toward the modules. If you take something out of the orbiter (docked in the middle) and move it out to the upper and lower booms, you've got to conserve a great deal of momentum because in the LVLH flight mode, we have an orbital rate to contend with. The whole system has a certain angular momentum that has to be conserved. Now this has resulted in an impact to the mobile service center, the old MRMS. It now has about 2 feet per minute maximum speed given the design condition of a 30,000-lb payload. Torque equilibrium must be conserved, a gravity gradient torque on the vehicle must counter that angular momentum change. The speed that the mobile servicing center moves is roughly 20 times slower than the mobile launch platform at KSC. This leads to operational impacts. If you go to a solar inertial mode, you don't have angular momentum that has to be conserved, and mass can be moved about the station in a much more expeditious fashion. This, therefore, is one of the impacts that we're concerned about. The mass management for an SI mode can be served by more compact geometry (Figure 11). Inertia changes can be minimized because it's an MX^2 function. We are trying to drive the configuration to be more mass compact. The LVLH modules and the solar inertial power system complicate the rigid body dynamic analysis. There are many problems with coupling the alpha joint control system to the attitude control system. We can provide the LVLH attitude, but it's going to cost and on an $8 billion station budget we need to make sure that we're getting what we pay for. We recently talked with Bob Naumann at MSFC as one of the respondents to a poll. We were trying to get more of a feel for what the user community was looking for in terms of flight mode. The poll came out and interviewed about 18 or so people in the materials science area to get

their flight mode preference. It's not a fair question, granted, but in that poll, just over half of the respondents said they had no preference. Of the people that did, the majority of those preferred LVLH flight mode, as you might expect. However, there was some solar inertial preference as well. When I got that information, I asked all my dynamics friends, and they overwhelmingly supported the solar inertial mode as you might understand. So we are on both sides of the fence of this flight mode issue and I just want to try to start a dialogue such that we can work out these problems.

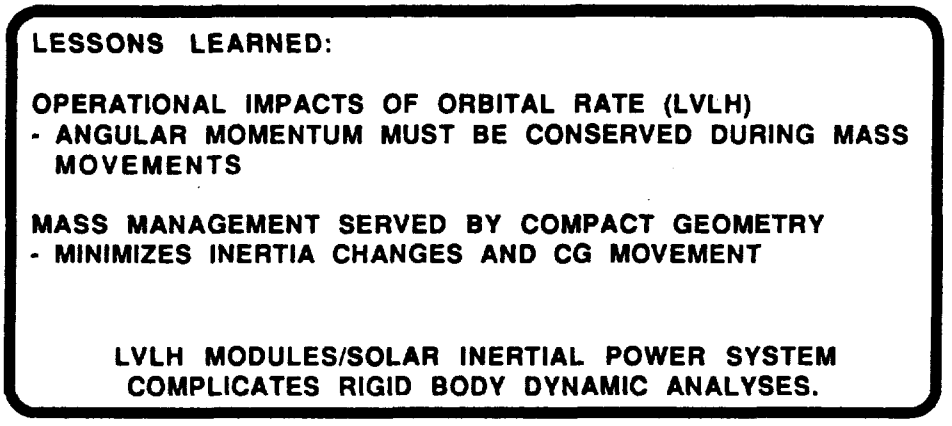

FIGURE 11. RIGID BODY DYNAMICS

The flex body dynamics of the station are very interesting. The Station is a very peculiar thing to analyze because about every day somebody walks in with something different they want to do on station and adds to our disturbance environment. Figure 12 shows a very short list here, but it gets longer by the day. I'm very concerned, not about the growth in loading conditions, but the spontaneous way that different loading conditions can pop up. Here the disturbances are crew motion, machinery, payload slewing, and mobile servicing center (MSC) operations. The Space Station peculiarities include changing mass properties as things move about the station. The mass properties are changing, and thereby change the modes and frequencies. That's something we're just

going have to live with on the Space Station. We can make some configuration changes by keeping the geometry compact, but we're going to have to live with these problems on an operational station. A solar array rotation, on the other hand, is something that really complicates the modal analysis. We can solve all these problems, that's not the question, it's just whether or not we should. To get in under an $8 billion budget, we need to be eliminating those problems not solving them. The coupled control system is another issue that must be solved from a dynamics standpoint, that is, dynamic interaction between adjacent payload pointing systems. Alpha joint and attitude control is another interaction that we have to consider on an LVLH station.

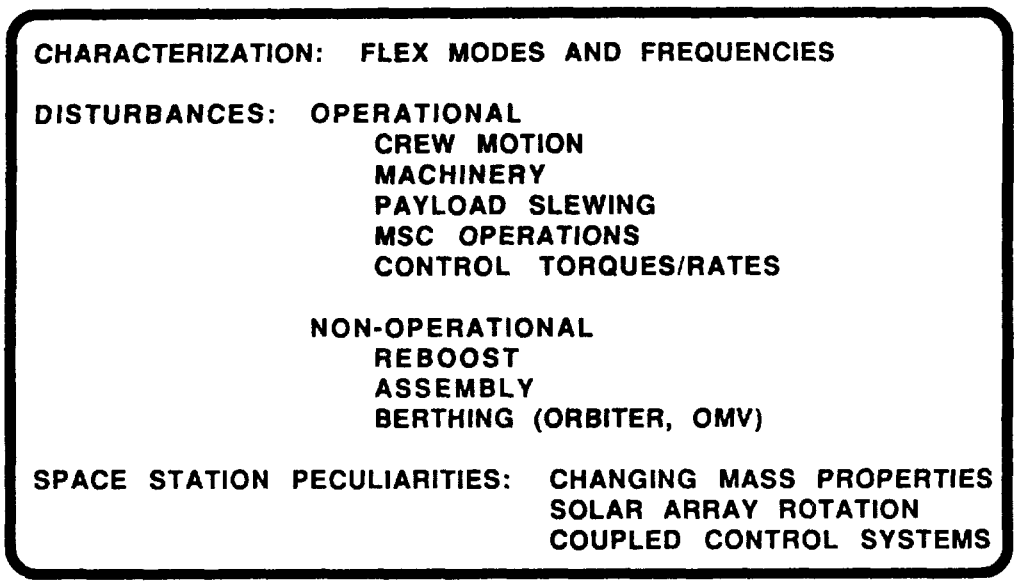

FIGURE 12. FLEX BODY DYNAMICS

Figure 13 shows the dual keel power tower with hybrid power. This station is built up of truss work which contributes to the stiffness rather substantially. There are a lot of pieces on this station, and you can see that the center part is the LVLH part and the outboard parts are the solar inertial aspects of the station. With a large num-

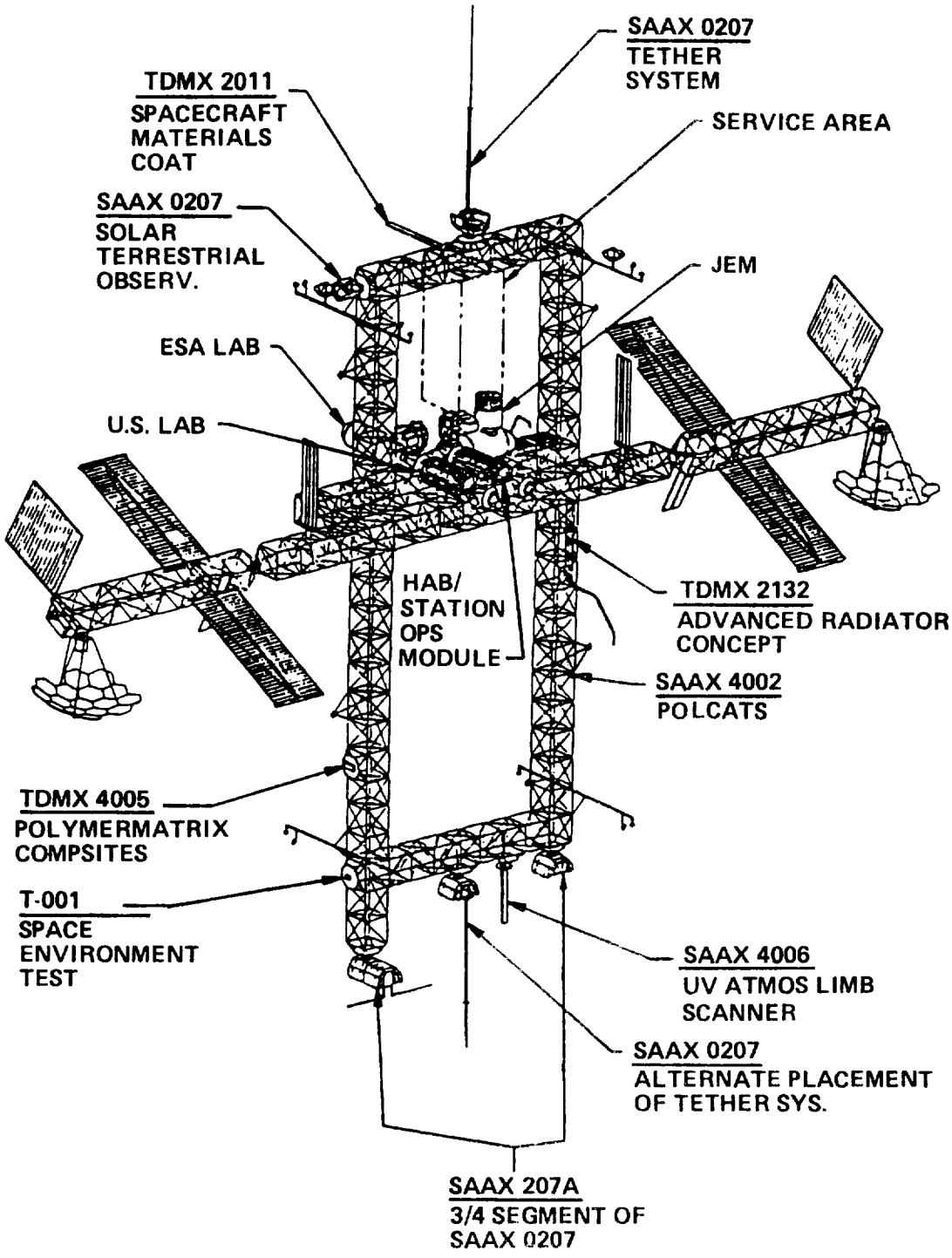

FIGURE 13. INTERNATIONAL SPACE STATION CONFIGURATION

ber of cantilevers like that, there are always a lot of opportunities for little cantilever modes. The mode set is very clustered and quite complicated with this configuration, and the more you put things on it and introduce other flexibilities, the more modes you get.

Assembly is another key loading environment for the Space Station. I guess we're not going to have the micro-g conditions during assembly (Figure 14). The Orbiter's primary reaction control system can overload a large beam very easily. We are baselining use of the vernier reaction control system during assembly; however, we would like to have some kind of back-up capability. The primary system is such an adverse loading environment that we can very easily break some of the truss members. Figure 15 is a growth model, and if you stare at it long enough I'll guarantee it will start moving. Look closely and you can see the first bending mode of the solar transverse booms. These growth versions are a real challenge from the dynamics standpoint.

Next I'd like to talk about the acceleration responses to the loading. I want to point out that we try to separate the environments between an operational and a non-operational environment. We're trying to work the micro-g problem in the context of the operational environment, crew motion and that sort of thing, and not worry about it too much during a reboost condition or Orbiter docking.

We've already hit this Station and looked at the responses (which violate 10^{-5}) and, therefore, we may need isolation on the system (Figure 16). I'm not real sure we do, because if it's peaked one way and peaked the other the average over time may be acceptable. Impulse forces acting on the Station can get significant attenuation and reduce that g-level. It's simply an experiment that's been modeled and located in the lab module and the response to the crew motion. But again we're leaning toward isolation, which means that we're spending money on isolation systems. And we need to know if we need isolation. It looks as though we do, because we're violating 10^{-5}, but we're spending money as we talk, and we'd certainly hate to walk downstream developing isolation systems that we can't use because we didn't define the requirements properly early on.

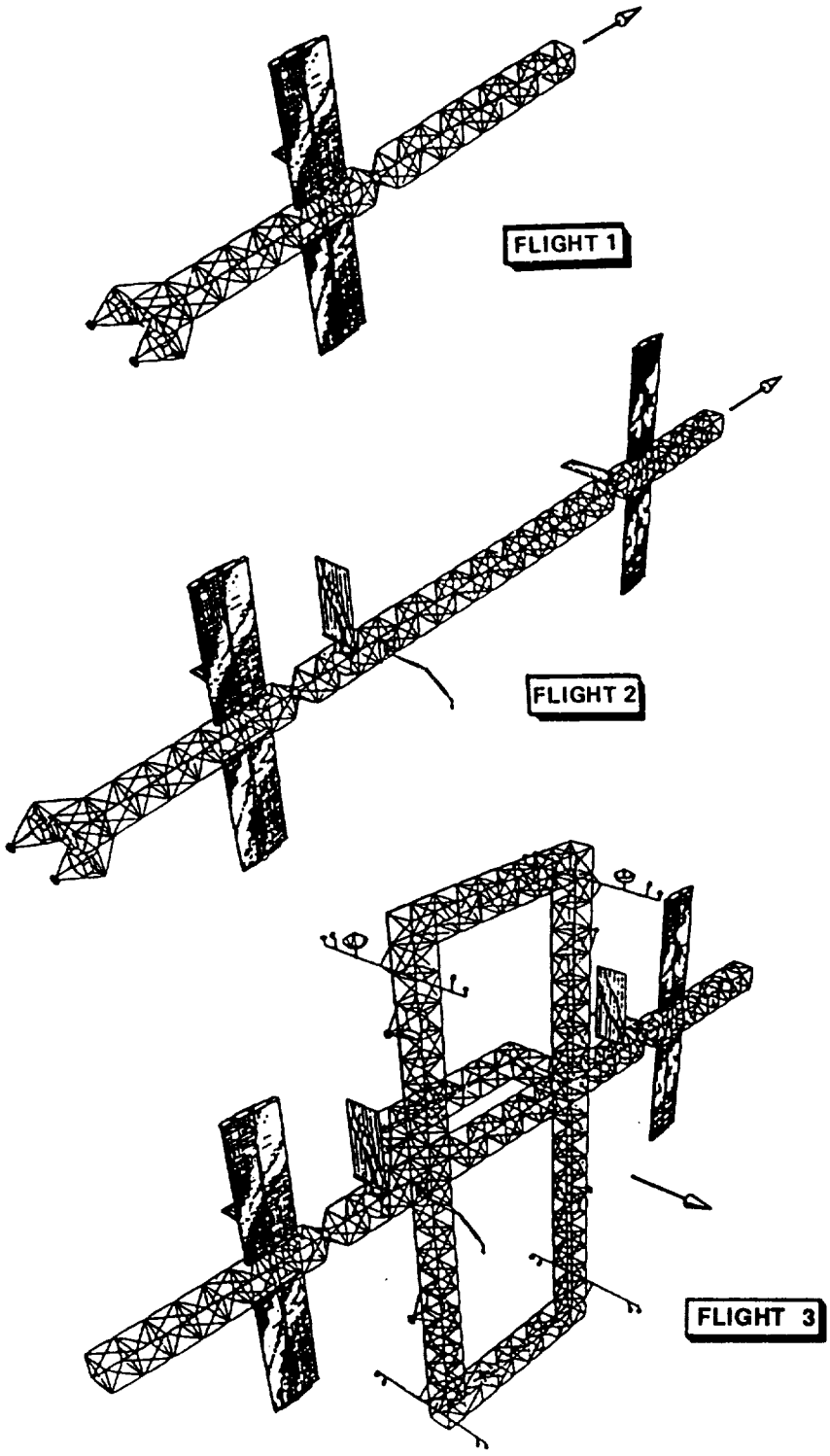

FIGURE 14. FLIGHT ASSEMBLY CONFIGURATIONS

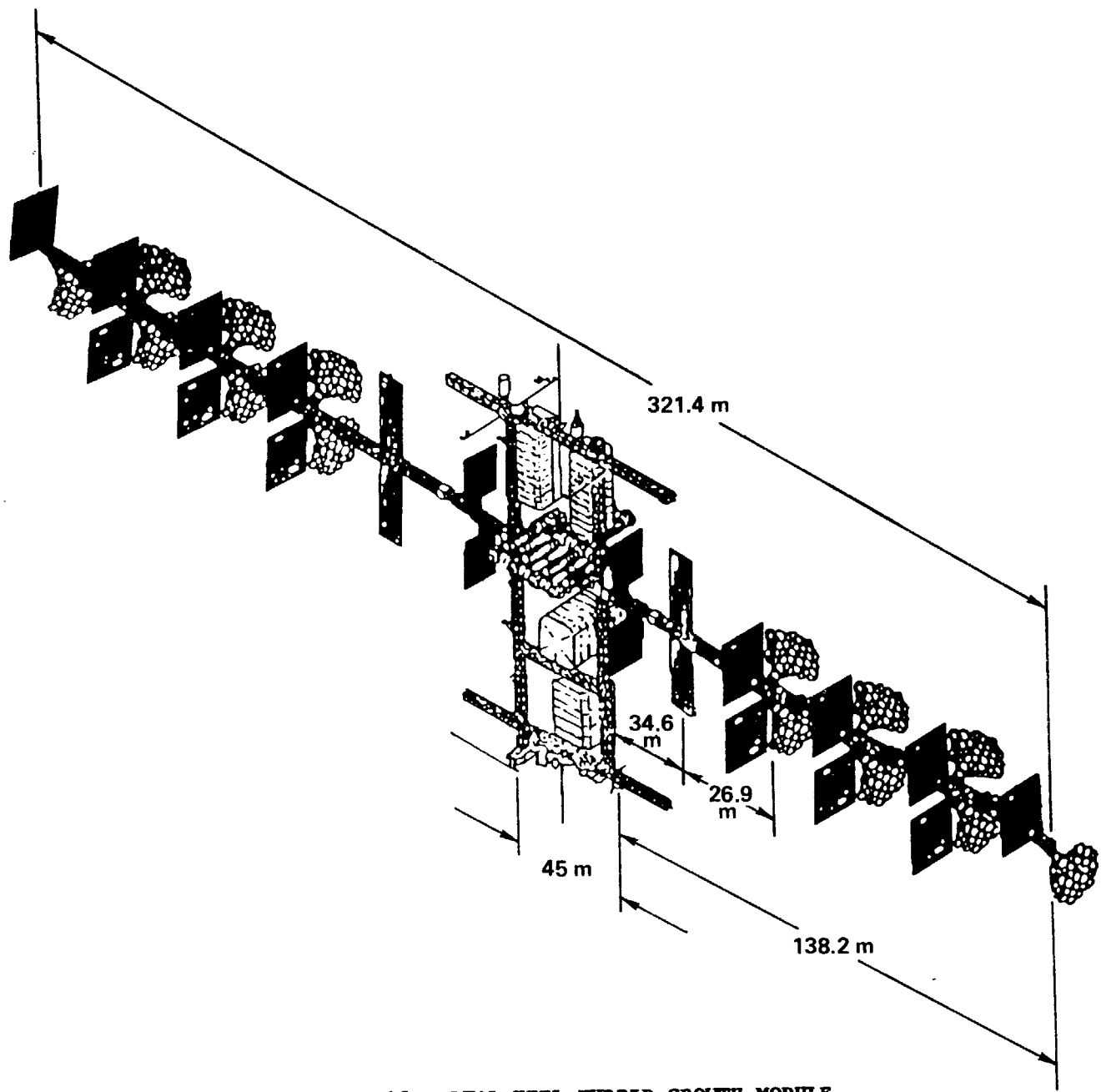

FIGURE 15. DUAL KEEL HYBRID GROWTH MODULE

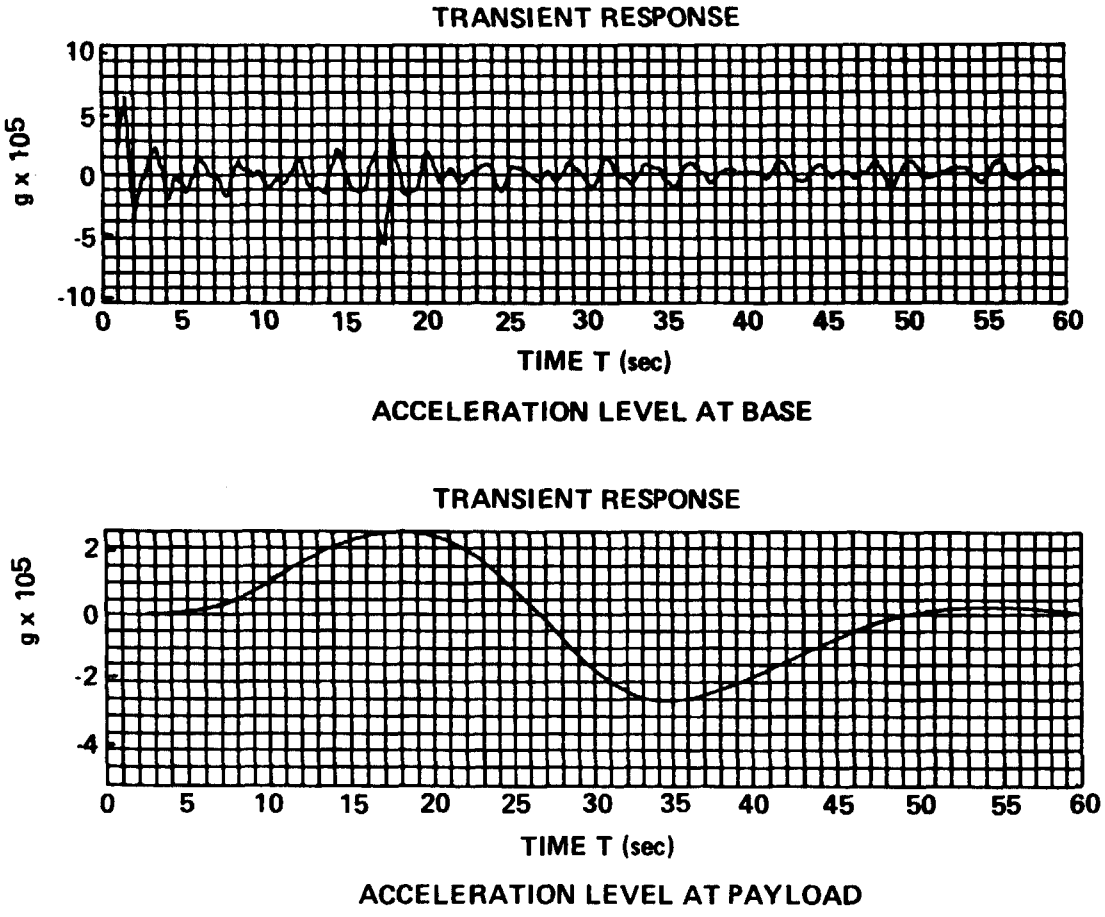

FIGURE 16. ISOLATOR REDUCES CREW DISTURBANCE G-LEVEL

The low-frequency content of the reboost forcing function makes attenuation difficult. I don't think anybody can count on maintaining a micro-g environment during reboost (Figure 17).

Another issue is that dynamicists, if given enough rope, will try to design the most perfect linear system possible. The concern that many of us have is that we might go off and design a completely predictable and linear space station -- tight joints and tight interfaces and all the rest -- and then somebody pushes off a wall and the thing rings like a tuning fork for a day and a half. We don't want to back ourselves into a corner that way and so we're trying to consider different ways of passive damping. We've had concepts for putting in different shock absorbers, where they can go, and what kind of passive damping systems might be employed. Oddly enough, a study of the closed-loop system using a completely tight linear structure showed that all the distributed control systems that weren't put on for damping, but to point payloads and to control the alpha joint, contribute to the damping fairly well. When the controllers have 70% damping, even at some of these frequencies, there is an effect of these distributed control systems as they start to damp out some of the vibration.

The other concern that we had was that in this low frequency system, these big beams with masses at the ends the thing starts to shake as our projector screen did a moment ago. We were very concerned that there was going to be a sea-sickness condition for the crew on board. So we did a study to try to determine what level of acceleration and frequency could be tolerated by the crew so that we didn't give somebody a sailing boat lesson in orbit. Figure 18 shows a result of that. When you see the acceleration requirement 640×10^{-5} that's with respect to the crew-allowable; it's not a micro-g condition. But you can see here how fast things are starting to damp out because of the distributed controllers. I must admit that you have to be a little careful about that as to whether or not you can rely on it. I don't think this solves the problem because any distributed system that's put on there for other reasons certainly can't be counted on in different configurations.

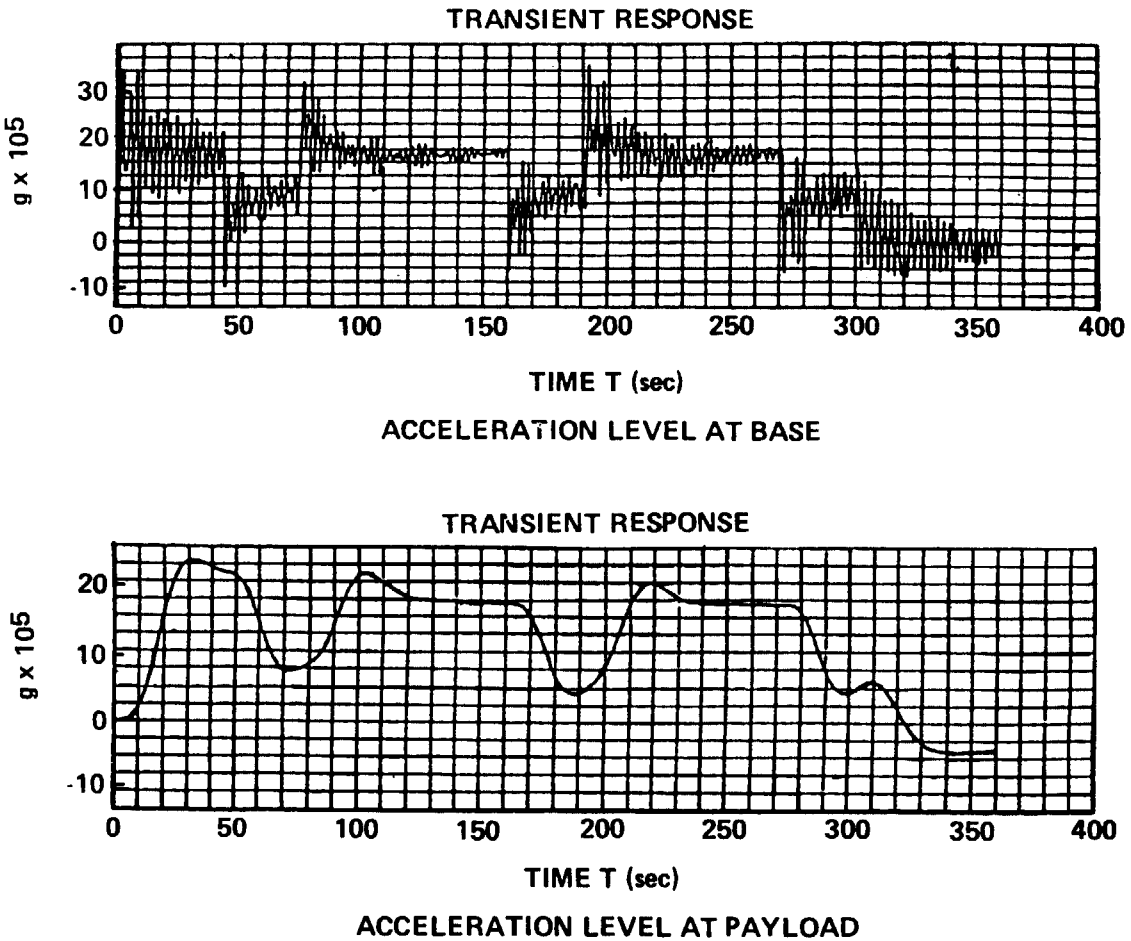

FIGURE 17. MICRO-G ENVIRONMENT CANNOT BE MAINTAINED DURING REBOOST

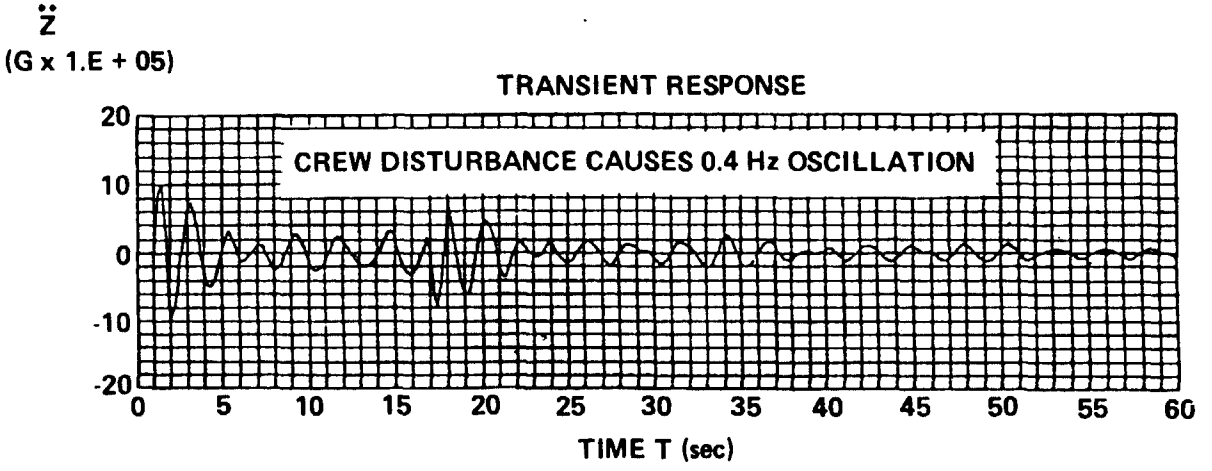

- MODAL DAMPING CAUSED BY STRUCTURAL DAMPING AND CONTROL DAMPING EQUALS 7%
- ACCELERATION REQUIREMENT IS 640 x 10^{-5} gs
- PEAK ACCELERATION IS 10 x 10^{-5} gs
- ACCELERATIONS DO NOT EXCEED HABITABILITY REQUIREMENT
- TRANSIENT DAMPS TO HALF AMPLITUDE IN 3 sec

FIGURE 18. CREW DISTURBANCE ACCELERATION LEVEL IS ACCEPTABLE AND TRANSIENT DAMPS TO HALF AMPLITUDE IN 3 SECONDS

The same thing can be said about the reboost transient (Figure 19). Four percent damping to a structures analyst is a lot of damping. So we've come a long way in the damping, and from looking at this, we've learned that we are getting some contribution to the damping effects from the distributed controllers. But I still want to hold the door open on whether we need some passive damping at this point. I think we can provide some damping by designing viscoelastic joints.

I'd like to summarize the micro-g aspects from the flex body standpoint. The micro-g is a design driver since it limits the applied loads. When we try to decide how fast the mobile servicing center can move, we need to accelerate it. When we try to accelerate, it means a force. The force level that we can have comes under our operational category of loads. So when it's under that operational category, we try to maintain the micro-g, and therefore we backed into what the amount of loads can be. As people were saying yesterday, the most benign loadings can violate a 10^{-5} g limit. There are these limits to the amount of loads that can be put into the MSC or how we can slew a payload that determines the different design conditions. The accelerations for most disturbances exceed the 10^{-5} value which is a very small level of acceleration. If that becomes a problem we need to consider isolation very carefully.

Now do periodic or transient disturbances offer relief (Figure 20)? The requirements need to specify this because we're not going to be able to respond with anything in the dynamics area, whether it's flight mode or Space Station configuration, unless it's in terms of the requirements. So we need to narrow the requirements down from between 10^{-3} and 10^{-8} and really be sure of ourselves. Isolation appears necessary, but we are certainly willing to rethink that. That should be done right away, and in earnest (Figure 21).

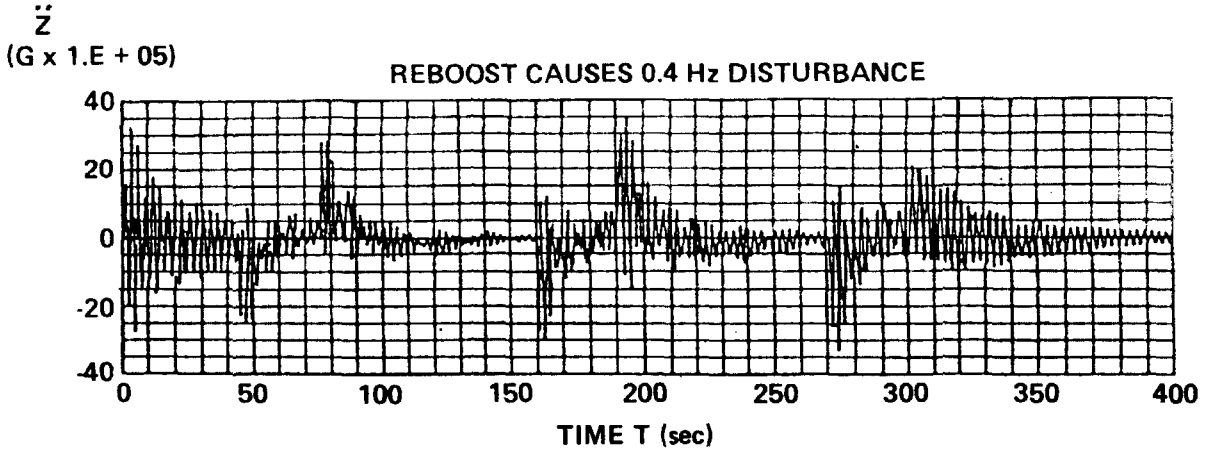

- MODAL DAMPING CAUSED BY CONTROLS EQUALS 4%
- ACCELERATION REQUIREMENT IS 640 x 10^{-5} gs
- PEAK ACCELERATION IS 33 x 10^{5} gs
- ACCELERATIONS DO NOT EXCEED HABITABILITY REQUIREMENT
- TRANSIENT DAMPS TO HALF AMPLITUDE IN 8 sec

FIGURE 19. REBOOST TRANSIENT ACCELERATION LEVEL IS ACCEPTABLE AND TRANSIENT DAMPS TO HALF AMPLITUDE IN 8 SECONDS

- MICRO-G IS A DESIGN DRIVER SINCE IT LIMITS APPLIED LOADS.
- ACCELERATIONS FROM MOST DISTURBANCES EXCEED 10 MG.
- DOES PERIODIC OR TRANSIENT DISTURBANCES OFFER RELIEF?
  - SPACE STATION SPELLS RELIEF.

"REQUIREMENTS"

- ISOLATION APPEARS NECESSARY
- PROBABILISTIC APPROACH BEING INVESTIGATED.
  - ACCELERATION THRESHOLD CROSSING PROBABILITY.

FIGURE 20. MICRO-G ASSESSMENT SUMMARY

LESSONS LEARNED:

DYNAMIC ISOLATION REQUIRED.

MICRO-G LIMITS OPERATIONAL ACTIVITY.

APPENDAGES LEAD TO CLUSTERED MODES.

DISTRIBUTED CONTROL SYSTEMS CONTRIBUTE TO SYSTEM DAMPING.

LVLH MODULES/SOLAR INERTIAL POWER SYSTEM COMPLICATES FLEX BODY DYNAMIC ANALYSES.

FIGURE 21. FLEX BODY DYNAMICS

Another thing that came up yesterday was the probabilistic nature of the crew disturbance. I'd like to address that. The way that we're looking at solving this problem is from a probabilistic standpoint, which is a method of determining the probability of exceeding certain limits by doing a threshold analysis. For fatigue analysis, the

amount of time that stress in a part exceeds a certain stress level generates a stress cycle curve. That same approach can be used to analyze the acceleration environment. A constant acceleration, like 10^{-5}, can be used as the threshold. Then, what is the probability of crossing that threshold? Without isolation, let's say that value is 50%, that means that 50% of the time it might be above this value, then we may need to go to isolation systems. Maybe, with isolators, we can raise that level of probability from 50% to say 95%. The way the analysis is done and the requirements are set is, as Ken Demel said yesterday, doesn't fit to a PSD in terms of units. We can work some more in that area, but we're trying to do this from a probabilistic standpoint. Issues can be raised about stationarity and ergodicity with this approach and it needs more attention. That's our approach to the problem. We are treating it from a probabilistic and not a deterministic standpoint.

The dynamic isolation system now looks necessary. The micro-g acceleration requirement is the limitation to our activity in the design of many systems. The appendages are going to lead to clustered modes. The distributed control systems are contributing to the system damping. I'd like to hear some more interchange. Give me a call sometime. We're really interested in understanding more about this.

Owen Garriott, EFFORT, Inc.: You said you're spending money on isolation systems. What are you isolating from what? Where are you spending your money?

Berka: What we're trying to do is work this problem from understanding what the size of the payloads are, and, given a base acceleration that we predict through our flex body models, what is the attenuation you can get force transmissibility across that interface? Now we're looking at it from a passive standpoint, we've got studies at Yale University on a passive system of just springs and masses and dampers...

Garriott: Excuse me. Are you isolating whole modules from the rest of the structure?

Berka: Oh no. We're isolating a mass, it's of suitcase size. You can vary the mass parametrically. We're not isolating modules, we're isolating some device.

Garriott: An experiment in a module from the rest of the module?

Berka: Exactly.

Garriott: Electromagnetic, mechanical, or what?

Berka: We've got studies going on in electromechanical, in strictly passive systems, and recently we've been working on an air jet system that actually flies, there's two ways of doing this, but one of them is similar to an MMU, only with an air jet, floated in a module. It seems very similar to the thing you're talking about. Fly that thing in formation with respect to the module. Those are the kinds of things that we're doing in the isolation area.

Ken Demel, Johnson Space Center: One comment on the flying things inside the module. There's limited aisle volume in a module, and we're trying to maximize the amount of payload capability for the user and his apparatus. Right now it looks like we're getting to the 60 to 65 percent of 44 double racks for user equipment. Now when we start floating things in the aisle, we probably preclude access to a large number of those user racks and operating them like you'd like to. I suspect that free-floating things in the aisleway are going to be very special cases. You may be shutting down the operations of 25 other guys while you do this.

Berka: Yeah, and I'm not trying to advocate that, but I want to say that I think we'd be remiss without looking at that. But it just points again to the critical volume problems that we're running into in the modules, because everybody's trying to get in there.

Demel: I want to make a point that custom integration people have been looking at those kinds of questions and tried to balance, make sure we have a balanced program. The other thing on the solar inertial rotating vectors, turns a lot of material processing things from a stable configuration thermally to a de-stable configuration thermally. When you do that, go to the unstabilizing situation, the g requirements go down by an order of magnitude. That is going to really affect how we scale up

research activity to get the development data for commercial production, and if we don't look at commercial activities as the goal I think this support for research is going to have a real problem.

Berka: Yes. And I appreciate that kind of feedback. I'd like to know more about that stability thing and its effect, but, as I said, the idea of LVLH and solar inertial has such an impact on the other aspects, if there's any flexibility there on the user side, we want to hear about it.

Alex Lechoczky, Marshall Space Flight Center: I'm going to speak up here. I come from the user side here. Basically, your argument of averaging out acceleration over a period of several hours to zero, and defining the microgravity requirement in that terms, you should not do that. Let's just look at acceleration, what the definition is. You take the second derivative of position as x equals 0, and these arguments about averaging out acceleration, if you chose your frame of reference correctly, I can sit right here on the ground and I can define for you a frame of reference where if I average it over time, I am in my zero-g. So I am really bothered about the loop you're going around and trying to come up with an explanation how you get rid of requirement by using arguments of averaging accelerations over days or whatever it is. So it turns out if you do a solidification experiment, you don't average out. Because while you are in one half of the cycle, you have grown a segment of material. Then you come back, where the g's in the opposite direction, well you're not going to remelt that material. So whatever you froze in there is in there. So most solidification experiments don't have averaging effects. So any argument you use vis a vis averaging just doesn't work in most of the crystal growth experiments.

Berka: Bob, would you like to comment on that?

Bob Naumann, Marshall Space Flight Center: I follow up on what Alex is talking about. The times that we are safe to average over are response times of the fluid itself. That's on the order of seconds, not thousands of seconds, which is what Alex is talking about. And I guess the thing that worries me is basically same thing Alex is saying here. The

only place that you can locate an experiment, where one would have a reasonably well-defined g vector, and I guess I said yesterday, that the steady-state acceleration is what really gets you. The only thing worse than the steady-state acceleration would be a slowly varying periodic acceleration which varies over an orbital period or some fraction thereof. And so the problem is that when I went through the calculations yesterday, I showed a Δt as a typical thing of say 10 degrees. Well that would be the radial gradient that you would have in crystal growth. But the horizontal gradients are more like a hundred or several hundred degrees. So the 10^{-6} g's we were talking about assumes that you were lined up with the growth axis. But if you go perpendicular with that, then the requirements drop by at least an order of magnitude or two orders of magnitude. And then what's worse is, it will go unstable and the whole thing turns over on you. So you've really got a mess. You really cannot grow crystals in an environment where the g-vector is walking around. So the only place that you can grow a crystal in solar inertial would be on that line perpendicular to the orbital plane through the center of mass. Now you've got a problem with the fact that well yes, the gravity gradient is constant, but now the velocity vector walks around. So I'm now having to continually horizontal control, which is going to drive convection also. So I guess, for the crystal growth community, I think what Alex and I are both saying is that we really don't like the solar inertial at all.

Berka: Well, Bob, the thing that comes to mind is that, regardless of the gravity conditions, what you're really going to end up with is not a static single thing pushing in one direction anyway. That's going to be one component of many things. We've already talked about the aero resultants and things like that. You're going to get something that's going to vary anyway. And so I feel like you're going to have to start dealing with that problem regardless of the flight mode. The other thing is, when we talk about the frequency and the time thing, and then for crew motion I understand your point. But, I've got to deal with things that are changing in acceleration and direction anyway because of

aero and other disturbances that are going to exist. The gravity gradient condition is a very very low frequency and it's of less value by 50% or more, depending on where you are in the thing. So the value is less. If a thing thinks that that's just a quasi static, it's almost like a quasi static response to whatever experiment location you have. It's like a quasi static response. It's lower. I know we can't solve that here, but I just want to get that out to you that this is the kind of thing that we're having to think about. Get back to me about it. If it creates a problem we want to know.

Byron Lichtenberg, Payload Systems, Inc: I'd like to add some comments from the user community. It seems like you're going to push the solar inertial mode when you said you get half of your materials science respondents saying that in fact they either preferred LVLH first. Nobody said that for solar inertial. If the engineers do prefer that, that's understandable, but the engineers aren't the user community. Besides micro-gravity sides you have Earth observations people who look like they're always looking at the ground. You have astronomy, solar physics, a variety of solar astronomy people that want to look out. And there are a whole bunch of different communities here, and I urge you to go very carefully in trying to push some sort of a solar inertial mode, because a whole spectrum of people that don't want that.

Berka: First of all, the poll that we've taken, I'm sorry I don't have that data with me. Over half of the respondents said they had no preference between the two.

Lichtenberg: I don't think they understand what it means.

Berka: I admit, it's probably not a fair question, but there were some solar inertial preferential respondents to that. The other thing is about the Earth pointing community, we've certainly had to deal with those people, too. A configuration meeting just week before last that answered that they had a very limited Earth viewing requirement at 28½ degrees. With most user viewers preferring the polar platform.

About all you can see from there (28° orbit), is water and tropical rain. These are the kinds of things that if we were going to go LVLH it's fine I'm not trying to push that from the standpoint of that's

the way we should go, but I want to make sure that people understand from our side that it does complicate the station in terms of what we need to do to analyze, what it's going to cost us to put that system in orbit. We want to make sure we're getting something back from that.

Lichtenberg: Make sure the station is, as you said in the beginning, going up there to support users.

Berka: There are a lot of users that are not, like servicing and things like that, that we didn't talk about at all. We can talk about this later. Bob?

Naumann: I just wanted to say one other thing. One of the ways of driving the cost up the wall is those acres of solar cells we have to have up there. Our good friends over at SDI area have an SP-100 reactor, which can put out somewhere between 100 kW and a megawatt.

Berka: You've found the solution to both of our problems. We can go nuclear and forget all this.

N91-12424

25. SPACE STATION STRUCTURAL PERFORMANCE EXPERIMENT

Dick Gates, Boeing Aerospace Co.

Reg Berka (Paper #24) mentioned some of the Space Station disturbances that need to be dealt with. The Space Station can be used as a testbed for the determination of structural dynamics resulting from these disturbances. It will be one of the first very large space structures to be put into orbit that can't be tested totally on the ground. We need a means to hone our analytical methods by comparing actual results on orbit with those predictions that we've made analytically. The NASA/Langley Research Center has contracted us to define a flight experiment that could be used to measure Space Station dynamics during and after its assembly. By integrating sensors into the structure to measure its ambient dynamic responses, it will provide some information as to how it behaves during its evolution. The objectives of the experiment are to define a series of experiments to measure the dynamic responses due to disturbances to establish the experiment scenarios, and to identify the locations of the instrumentation that can be integrated into the structure. We have also defined the Space Station resources that are required so that they can be included in the Mission Requirements Data Base (MRDB). We used the 16-flight-assembly scenario that was recommended by Rockwell as the baseline. Figure 1 shows a cartoon of the structure that goes up on the first flight. It consists of one-half of the transverse boom including a pair of solar arrays and power radiator. Located on this drawing are the accelerometers, strain gauges, acoustic emission sensors, thermocouples, and a laser optical measurement system that can be used to measure the structural characteristics of that piece of structure. Accelerometers are placed at several locations along the beam so that its dynamic response can be measured and used to verify the preflight predictions. I will talk mostly about the accelerometers since that is the subject of the workshop. Low g accelerometers are envisioned for this structure. Because we don't plan

Work Package A - Technology Mission/ Experiment Definition

FLIGHT 1

- PORT TRANSVERSE BOOM
- PORT SOLAR ARRAYS
- ACA MODULE
- ENERGY STORAGE MOD
- 4 BATTERIES
- ALPHA JOINT
- BETA JOINT
- BERTHING RING
- EPS RADIATOR

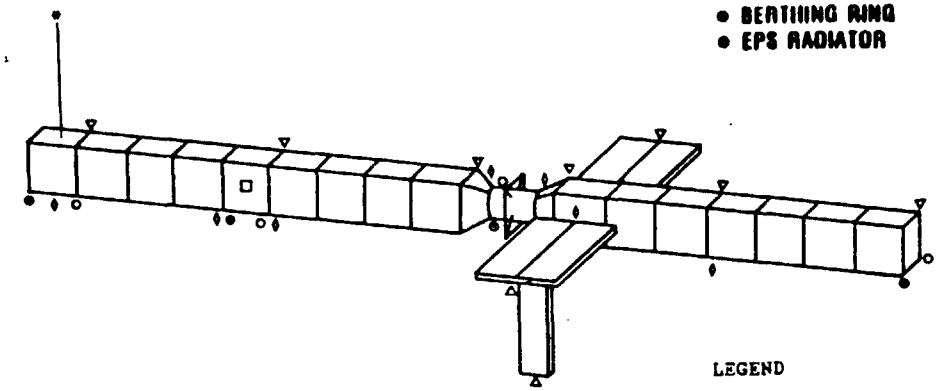

LEGEND

- △ Accelerometers
- ↕ Strain gauges
- ● Acoustic emission sensors
- ○ Thermocouples
- ✱ Laser optical system
- □ Remote data processors
- ■ Central data processor

FIGURE 1

to put up an excitation system on the structure to excite the structural dynamics, we will rely on the ambient excitation caused by control system forces and other disturbances. Accelerometers are located at the tip, between the tip and the alpha joints, and on each side of the alpha joint. There are other accelerometers located where the vertical keel will fasten into the structure, and close to the center of the transverse boom of the final configuration. At these locations we specified six linear accelerometers so that angular accelerations as well as linear accelerations can be measured. For instance, a triaxial accelerometer, a biaxial accelerometer, and a single-axis accelerometer can be used to measure the rotational accelerations along with the linear accelerations.

Figure 2 shows a mirror image of the transverse boom that would be attached on the other side. It is instrumented in a very similar fashion to the first half. I won't go through all of the 16 flights to show where the accelerometers are, but I will show enough so that you will see where the accelerometers are located for at least the major portion of the structure.

The upper keel boom is constructed on the third flight (Figure 3). The accelerometers are located at the junction with the transverse boom, half way up, at the corners, and in the middle of the upper keel.

On each of the major pieces of structure, we postulate the use of a remote data processor that would handle the data measured by the instrumentation on that portion of the structure. The remote data processors will have the capability of storing data, and of transferring them to a central data processor, which will be located in one of the modules.

During Flight 4 (Figure 4), the radiator and the instrumentation that is needed to measure its dynamics are added.

On Figure 5, the lower keel has been added. It is instrumented in a fashion similar to the upper keel. The module support structure is also added in this flight. It is also instrumented with accelerometers to measure its response before and after modules are attached.

Work Package A - Technology Mission/ Experiment Definition

FLIGHT 2

- STB TRANSVERSE BOOM
- STB SOLAR ARRAYS
- ENERGY STORAGE MOD
- 4 BATTERIES
- ALPHA JOINTS
- BETA JOINT
- 2 RCS MODULES
- EPS RADIATOR

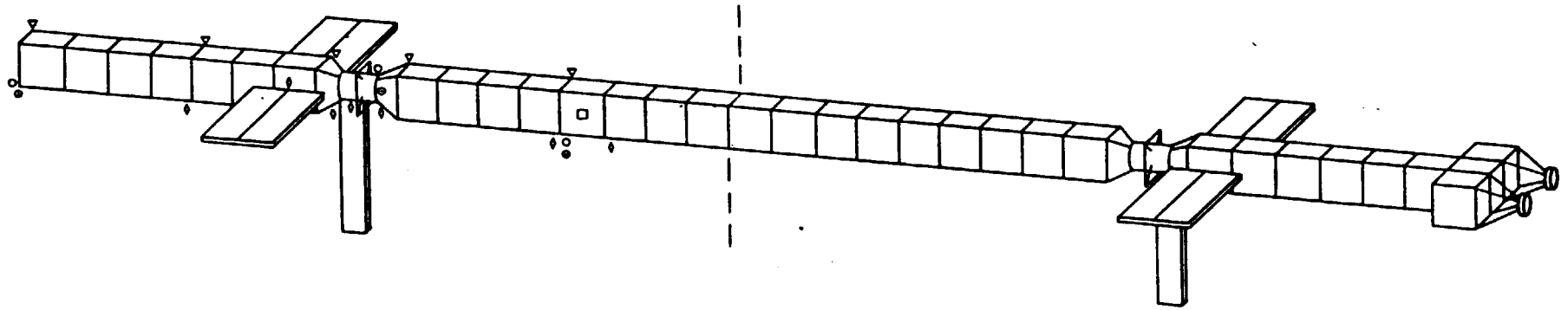

LEGEND

- △ Accelerometers
- ◊ Strain gauges
- ⊕ Acoustic emission sensors
- ○ Thermocouples
- ✱ Laser optical system
- □ Remote data processors
- ■ Central data processor

FIGURE 2

Work Package A - Technology Mission/ Experiment Definition

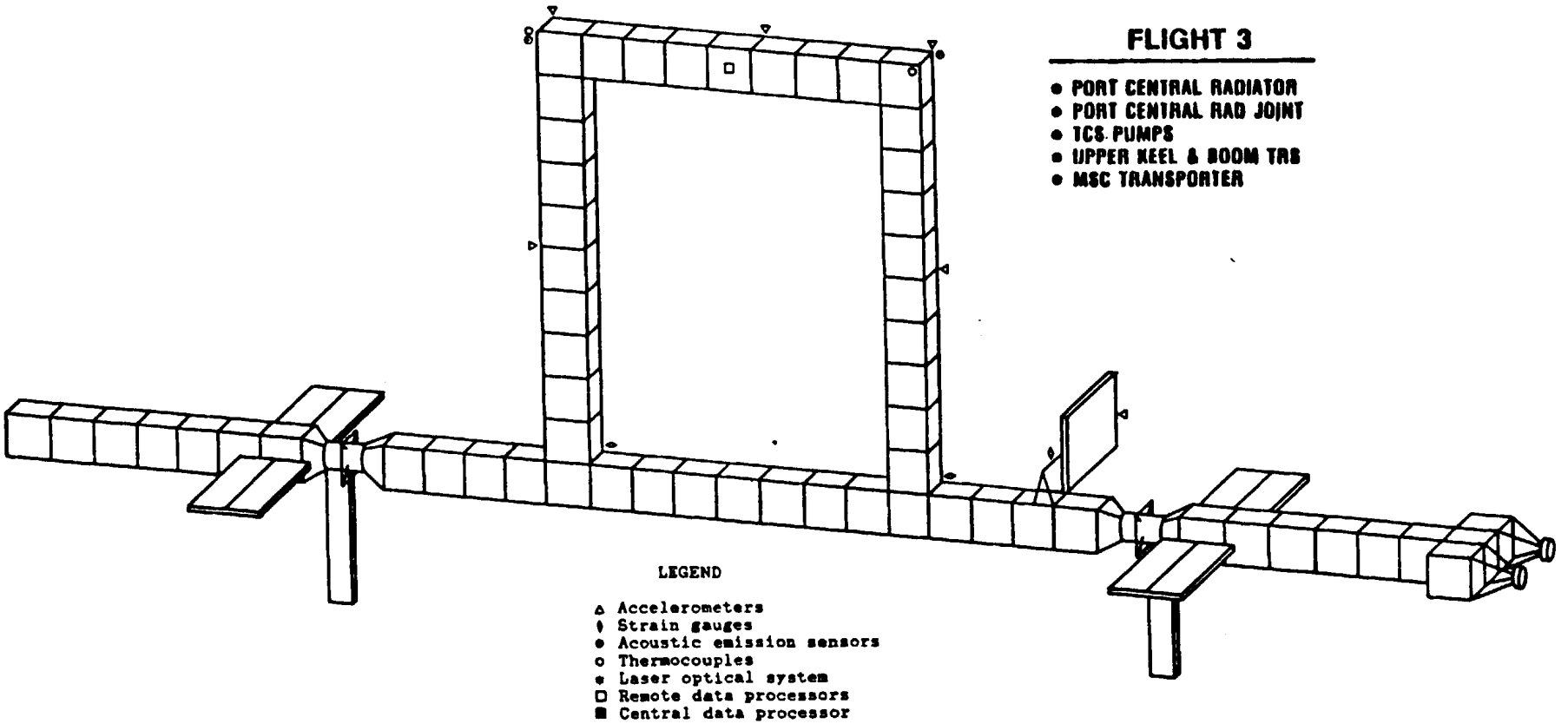

FIGURE 3

Work Package A - Technology Mission/ Experiment Definition

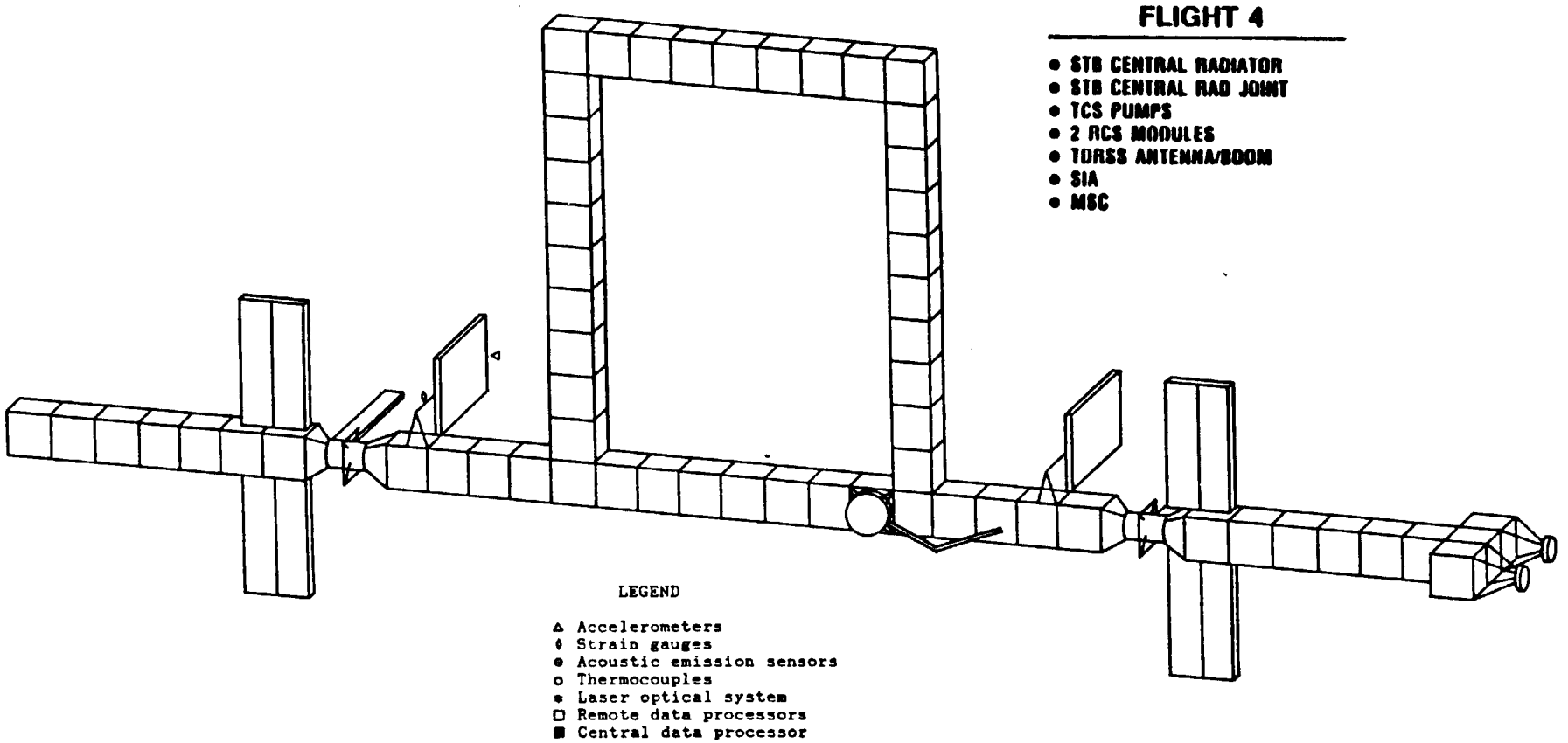

FIGURE 4

Work Package A - Technology Mission/ Experiment Definition

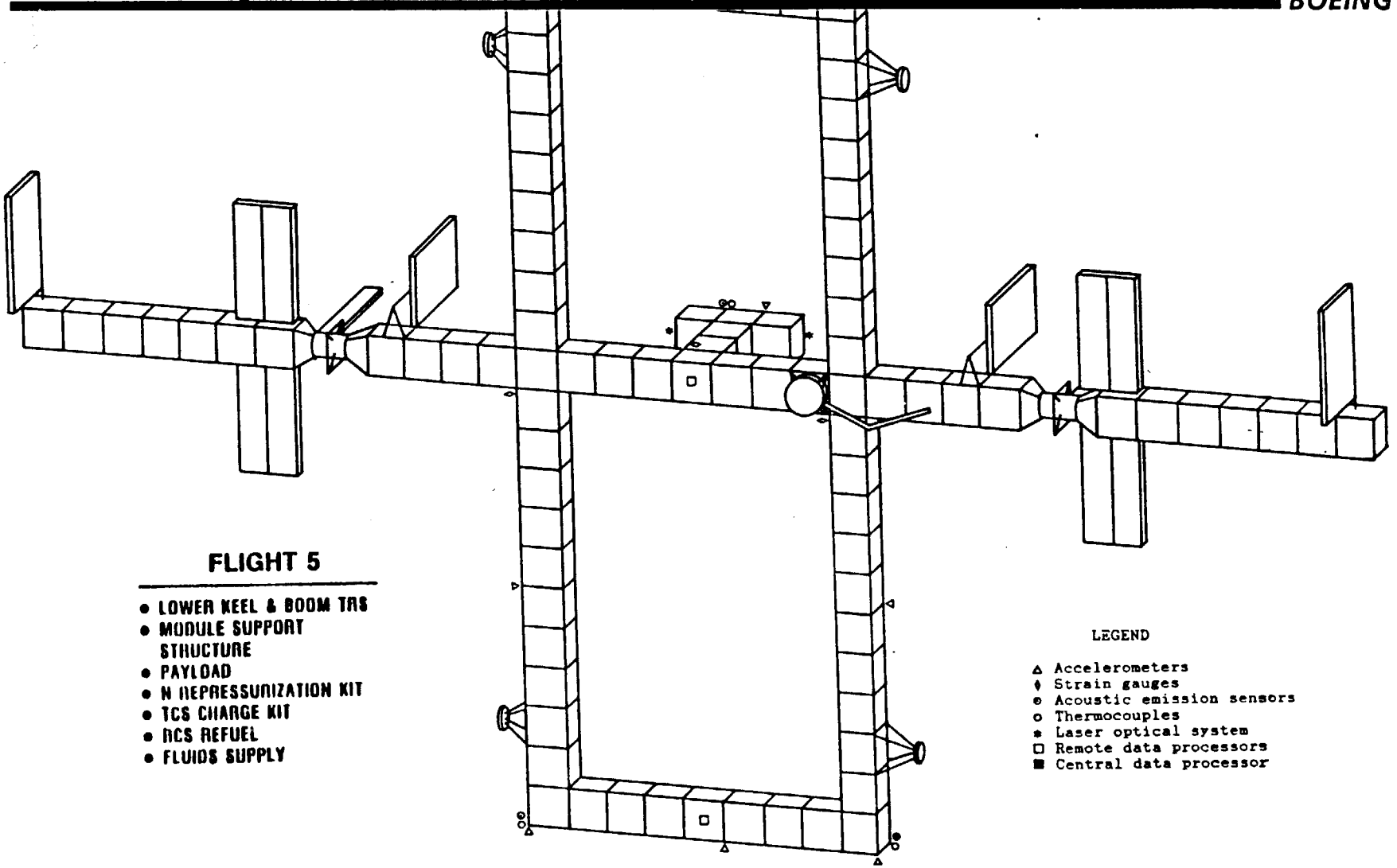

FLIGHT 5

- LOWER KEEL & BOOM TRS
- MODULE SUPPORT STRUCTURE
- PAYLOAD
- N REPRESSURIZATION KIT
- TCS CHARGE KIT
- RCS REFUEL
- FLUIDS SUPPLY

LEGEND

- △ Accelerometers
- ♦ Strain gauges
- ⊕ Acoustic emission sensors
- o Thermocouples
- ✱ Laser optical system
- □ Remote data processors
- ■ Central data processor

FIGURE 5

The first module is attached during Flight 6 (Figure 6). Accelerometers in the module or attached to the module measure its rigid body response. The module structures are very rigid compared to deployable components and the truss. Therefore it is expected that they will behave as rigid bodies.

The other part of the task was to identify resource requirements for these flights (Figure 7). We looked at the power requirements of the instrumentation, the volume requirements, mass requirements, and data storage requirements. It is obvious that most of the instrumentation is delivered on the first few flights. On later flights, less and less instrumentation is needed.

This structural performance experiment will become a valuable tool in verifying the analytical predictions of the dynamics of the Space Station, and to determine the dynamic behavior the Space Station during its mission. Any questions?

Bob Walker, NASA/MSFC: Have you established any performance requirements on the accelerometer?

Gates: We've postulated the use of some of those accelerometers which you've seen mentioned before, such as the Sundstrand QA 2000. You want to measure accelerations on the order of 10^{-5} g's, because since we aren't exciting the structure on purpose, the ambient excitations are going to be fairly small, and we will have to measure some very small accelerations.

Question: I think that's probably not quite good enough for what I have in mind; do you have the possibility of ascertaining where the center of gravity of the array is located by looking at the outputs of the accelerometers?

Gates: No, but Ken Demel mentioned that that sort of thing is being postulated, comparing the torque inputs to the response of the Space Station.

Work Package A - Technology Mission/ Experiment Definition

SPACE STATION

BOEING

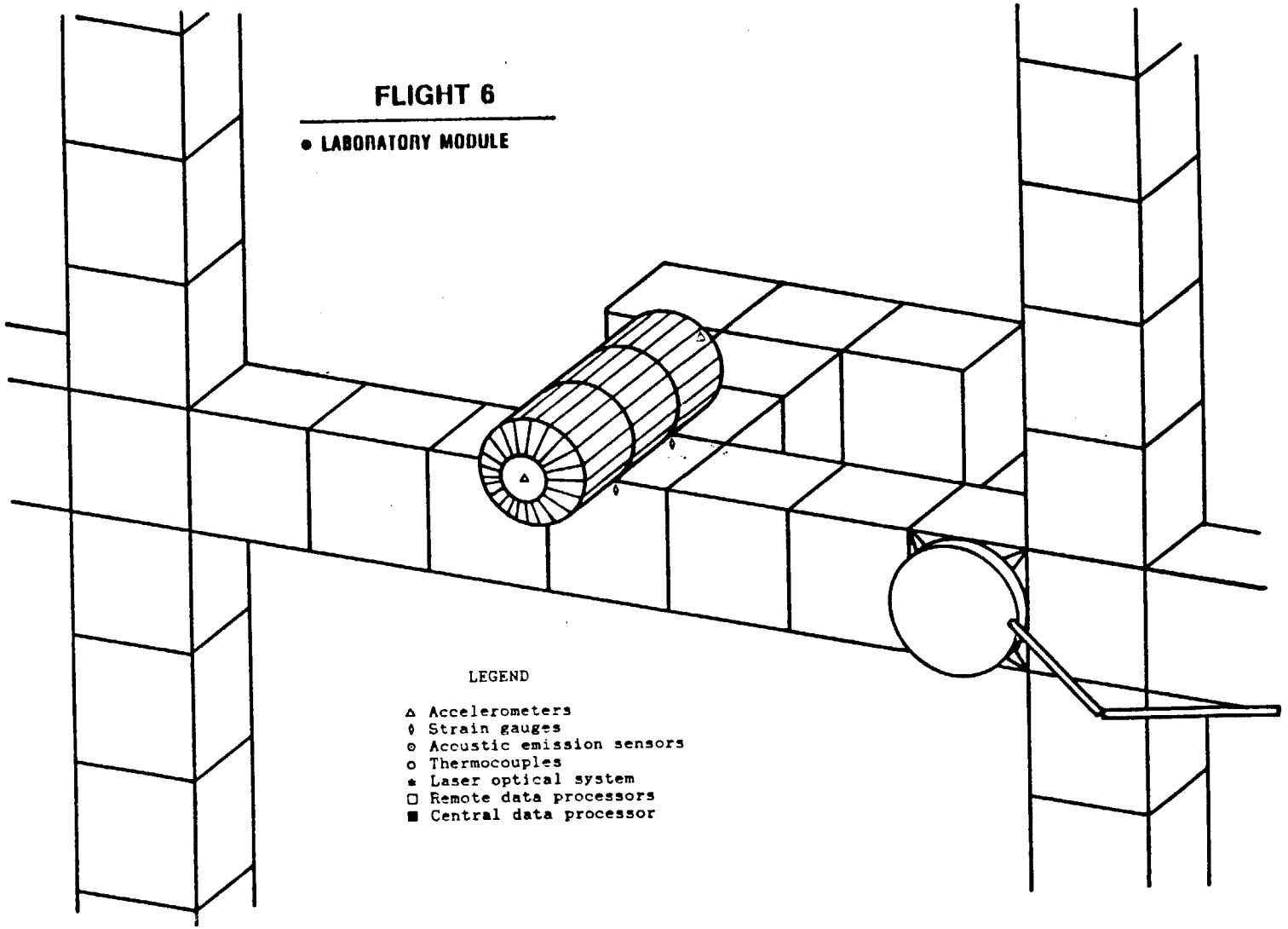

FIGURE 6

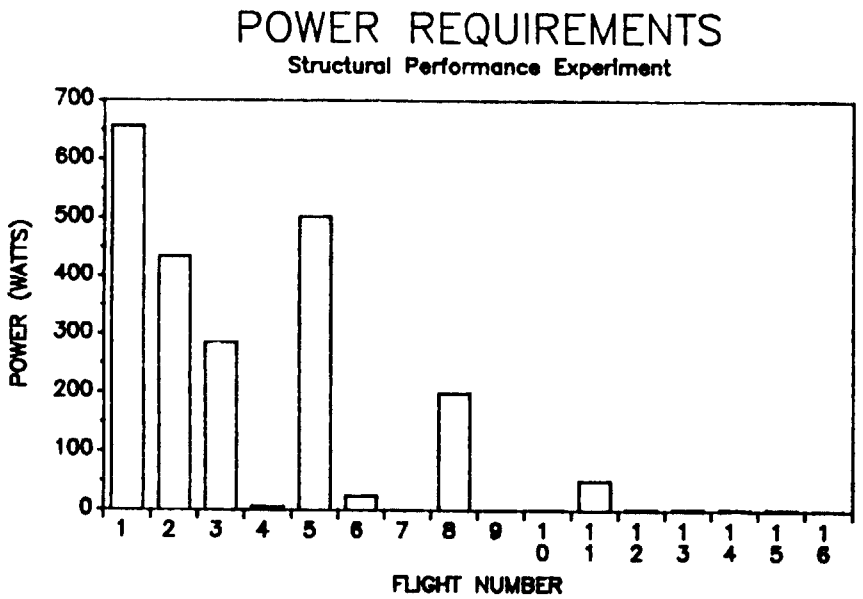
POWER REQUIREMENTS
Structural Performance Experiment
POWER (WATTS)
700
600
500
400
300
200
100
0
1 2 3 4 5 6 7 8 9 10 11 12 13 14 15 16
FLIGHT NUMBER

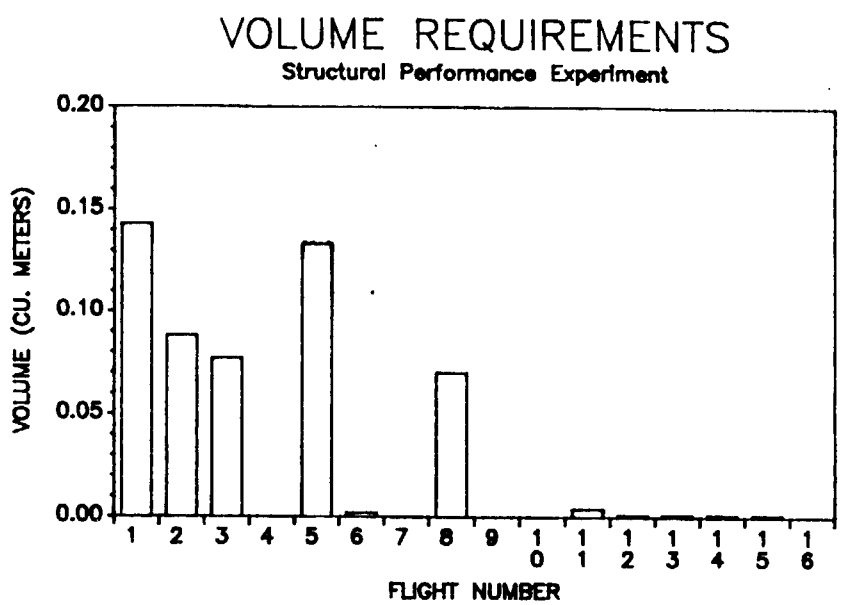
VOLUME REQUIREMENTS
Structural Performance Experiment
VOLUME (CU. METERS)
0.20
0.15
0.10
0.05
0.00
1 2 3 4 5 6 7 8 9 10 11 12 13 14 15 16
FLIGHT NUMBER

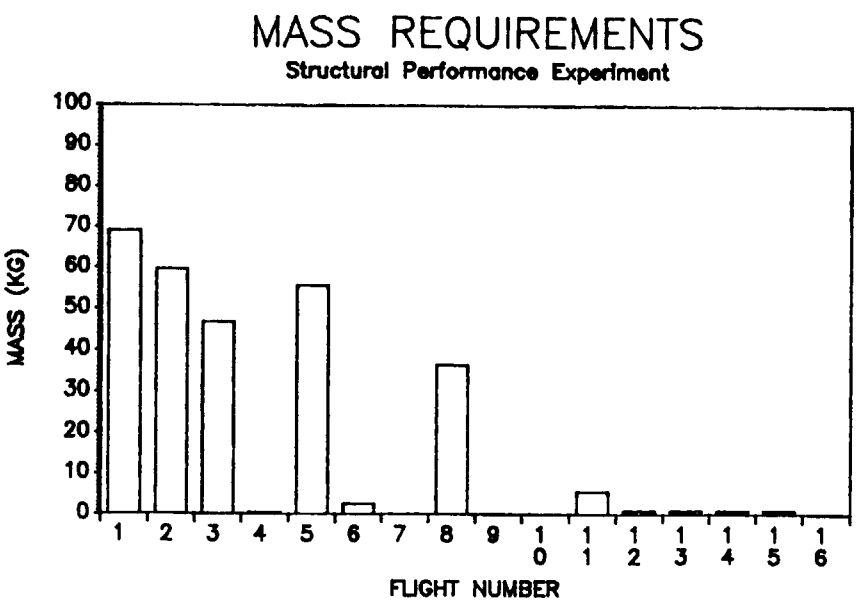
MASS REQUIREMENTS
Structural Performance Experiment
MASS (KG)
100
90
80
70
60
50
40
30
20
10
0
1 2 3 4 5 6 7 8 9 10 11 12 13 14 15 16
FLIGHT NUMBER

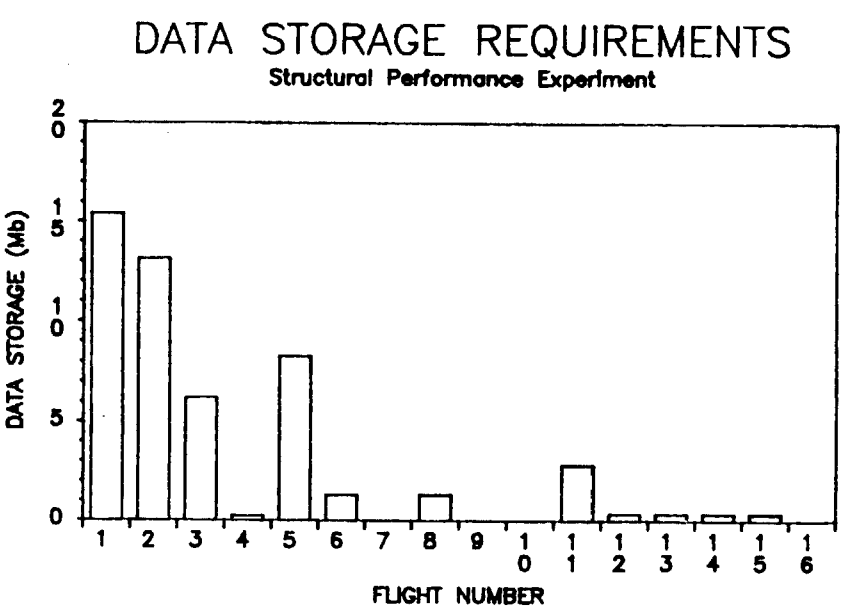
DATA STORAGE REQUIREMENTS
Structural Performance Experiment
DATA STORAGE (Mb)
20
15
10
5
0
1 2 3 4 5 6 7 8 9 10 11 12 13 14 15 16
FLIGHT NUMBER

FIGURE 7

Question: You had some laser sensors. Are they measuring range to targets at specific points on the structure?

Gates: Yes. The purpose of those sensors was to measure the as-built accuracy of the structure and also to measure the thermal deformations as it goes in and out of the shadow.

Question: What kind of data reduction scheme will you use to analyze the data?

Gates: We don't have any. We haven't calculated any typical responses of the structure; our job is to identify the experiment, and we haven't postulated the data reduction schemes.

N91-12425

26. EFFECT OF SCIENCE LABORATORY CENTRIFUGE ON SPACE STATION ENVIRONMENT

Nancy Searby, Lockheed

I represent a completely different user community, the life sciences. It has been a good opportunity to be here and listen to what life sciences often considers the other side of the fence, materials sciences. Hopefully, I can share a little of the life sciences rationale with regard to the centrifuge. One of the projects we are working on at Lockheed, as an independent development project, is a specimen research centrifuge. Consequently, this is proprietary data for Lockheed.

The National Commission on Space report, released recently, states the rationale for a specimen research centrifuge. It says that we really don't understand the life sciences aspects of the effects of gravity. Materials scientists are interested in the effects of residual gravity levels on the order of 10^{-4} to 10^{-7} g. The life sciences community is interested in slightly different levels, between 10^{-3} and 1 g, which are only obtainable in the Space Station or in a spacecraft environment using a centrifuge.

Several potential medical problems arise for spacecraft crew in space. The heart becomes deconditioned, the skeleton demineralized, and the muscles lose mass. The body stops reacting to the 1-g force that is always felt on the ground. The Russians found that after 237 days in space, their cosmonauts had many problems adapting to Earth's gravity again. In fact, it took them 45 days back in Earth's gravity before they could even play catch, because they had lost their coordination. Consequently, these microgravity effects pose a very serious problem. And, although it brings a variety of horrifying pictures to many people's minds to have this large rotating device up there, the centrifuge is essential if we're going to go further in manned space exploration.

In this presentation I will discuss the rationale for the research centrifuge, to give some background information about our need for it. I will also discuss the configurations that are currently being considered, and the dynamics of the centrifuge. I will then describe a system that we have developed, with the help of Sperry Corporation, that should ease the worries about the centrifuge.

The primary reason for the centrifuge is to identify gravity's role in biological, physical, and chemical processes. We must also evaluate the requirements for artificial gravity on long-duration manned missions. Some of the Russian cosmonauts have said that they don't know if the human body could withstand a round trip to Mars. We could go there, without a problem, but upon return to the Earth environment, it is not certain our bodies could re-adapt to 1-g. We also don't understand the effects of fractional g. The Moon has 1/6 Earth's gravity and Mars 1/3. It has always been a dream to colonize Mars, but we are not sure if we can tolerate that level.

We must provide a controlled acceleration environment for comparison with microgravity studies. One of the criticisms of biological experiments that have been conducted to date in the Shuttle, is that we can not be sure the effects we are seeing are from microgravity unless we have a control group. It is normal practice to have a control group, where we vary only that one parameter, microgravity. So if we have a centrifuge and a microgravity holding facility that use the same habitat configuration, we are able to vary that one parameter of gravity.

We also can use the centrifuge to provide a 1-g environment to supply specimens free of launch effects for long-term studies. After going through launch and into orbit, the specimens may already have adapted quite a bit to zero-g. If we had them on the centrifuge we could simulate a 1-g environment (as though they were on Earth), and we could immediately transfer them to microgravity. We could then detect any rapid changes as they occur.

Finally, one of the objectives proposed by the National Commission in Space is to have a large-diameter, experiment-carrying capsule or module at the end of a tether or some very large rotational system where we could actually investigate the effects of varying artificial gravity on humans. The Space Station centrifuge allows you to test the necessary rotational systems.

Figure 1 shows the scientific bounds on centrifuge size. The most constraining bound on the size of the centrifuge, assuming we want it to be inside the Station, is the inner radius of the module. The upper limit of the angular velocity is set by the coriolis acceleration. It is bounded on the lower side by the need to create 1 1/4 g at the perimeter, which should make about 1 g at the specimen's heart. Figure 1 illustrates the relationship. The vertical lines indicate the radius an animal can handle with a $\pm$10% gravity gradient across its body. If you were on a centrifuge, you wouldn't want the gravity at your feet to be completely different from the gravity at your head; that would not simulate Earth. Scientists think specimens can probably handle a plus or minus 10% or a 20% gradient across their bodies, thus determining the centrifuge size limits for a rat, a squirrel monkey, a rhesus monkey, and a human. To have a rat on a centrifuge and to simulate Earth gravity, we need a centrifuge diameter of at least a couple of feet. We can't fly squirrel monkeys on the centrifuge unless its radius is almost 6 ft, and we'll notice that for radially oriented humans to be on the centrifuge, we need a 38-ft-radius centrifuge, which would require a variable gravity research facility separate from any modules of the Station.

Another capability that scientists would like to have is various radii simultaneously available to provide different g-levels. They would like the centrifuge to have positions at 1 g, 0.8 g, and 0.6 g so that they can study the effects on the specimens of fractional gravity in the same experimental time frame.

SCIENTIFIC BOUNDS TO CENTRIFUGE SIZE

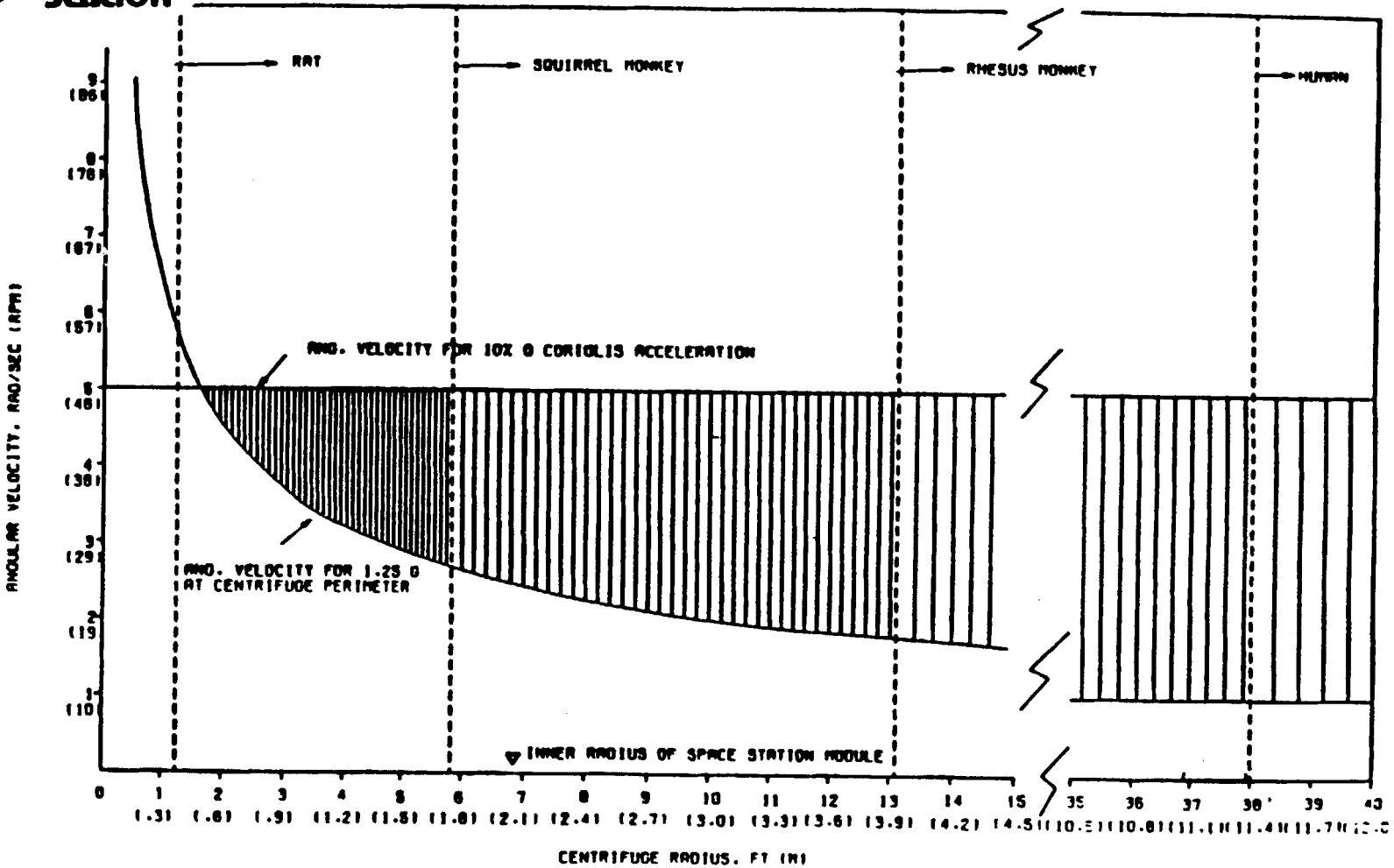

ASSUMES: ± 10% GRAVITY GRADIENT
0.3 KG RAT, 2.5" BACK TO BELLY
1.2 KG SQUIRREL MONKEY, 11" HEAD TO BUTTOCKS
14 KG RHESUS MONKEY, 28" HEAD TO BUTTOCKS
92 KG 95TH % MALE, 73" HEAD TO FOOT
SPECIMEN MOTION OF .1 M/SEC

FIGURE 1

A controversial issue at this time is whether we need a servicing rotor. If we must create and maintain a continuous 1-g, Earth-like environment on the Station, we wouldn't want to stop the centrifuge and expose all the 1-g specimens to micro-g every time we need to take a sample or clean a cage. There are some scientists who believe we need to have a separate rotor that spins up, matches the spin rate of the centrifuge, engages with the centrifuge, removes two specimen packages, and spins back down again, so that we expose only that two specimen packages to microgravity (see Figure 2).

We also want to support samples ranging in size from cells all the way up to humans. Acceleration levels shown range from 0.001 to 2 g, and acceleration rates from 0.01 to 0.25 g/sec. The centrifuge should not create vibration for the Station. Also, the variation of the g-level on the centrifuge should not exceed 10^{-3} g.

Figure 3 shows a concept that would fit in the Station. The 6-ft-diameter centrifuge takes the space of two double racks on a Space Station module. On this centrifuge we can put rodents and small plants, but we can't do squirrel monkey research.

A full-module-diameter centrifuge which provides the scientists with the large radius that they want, but has a very large hub with a hole through the center, is shown in Figure 4. In fact, the hub has the same diameter as the diagonal dimension of the hatch. And it's stationary, so as far as the crew is concerned, it's just a tunnel that they go through. Another solution is an attached module containing both the centrifuge and the stationary specimen holding facilities. The centrifuge would have a small hub and therefore support more specimens. The specimens would be isolated from the material sciences and the other parts of the station.

The mass for the 6-ft-diameter centrifuge is about 270 kg, while for the 12-ft diameter it is approximately 1,000 kg. The moments of inertia are correspondingly larger on the large centrifuge. To create 1 g at the perimeter, the spin rate of the 6-ft centrifuge is 31.5 rpm,

SPACE STATION

12 FOOT CENTRIFUGE WITH SERVICING ROTOR IN 14 FT MINIMODULE

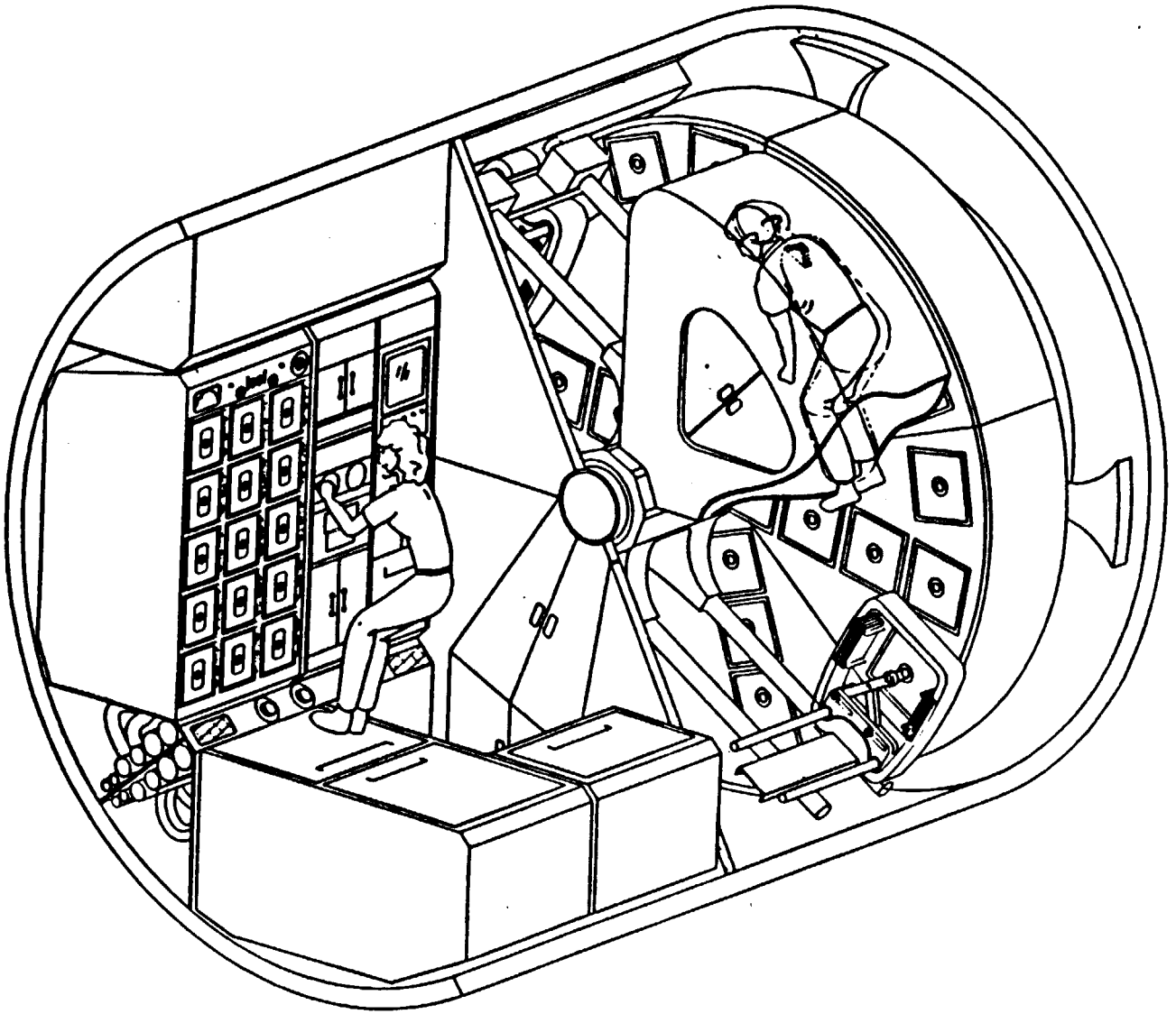

FIGURE 2

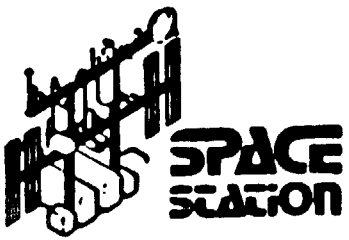

6 FOOT DIA RACK MOUNTED CENTRIFUGE WITH AUTOMATED SERVICING

Lockheed

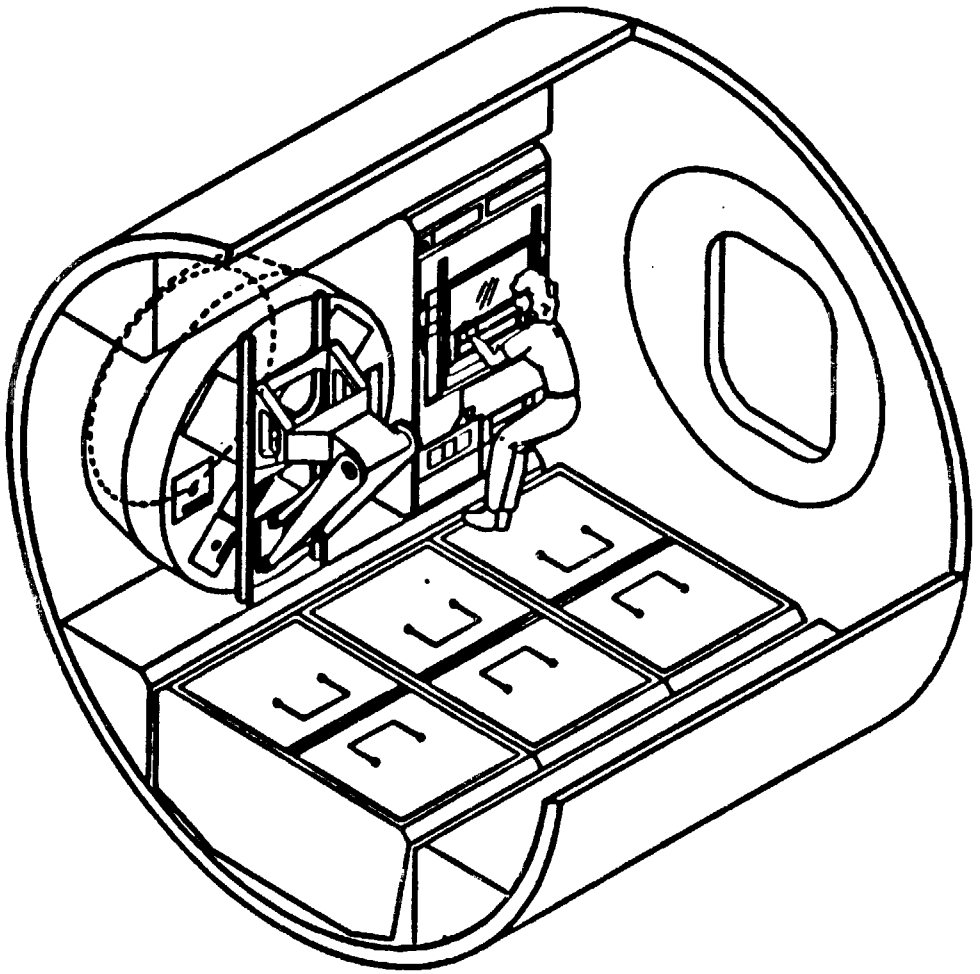

FIGURE 3

12 FOOT CENTRIFUGE WITH SERVICING ROTOR IN MODULE END OR 14 FT MINIMODULE

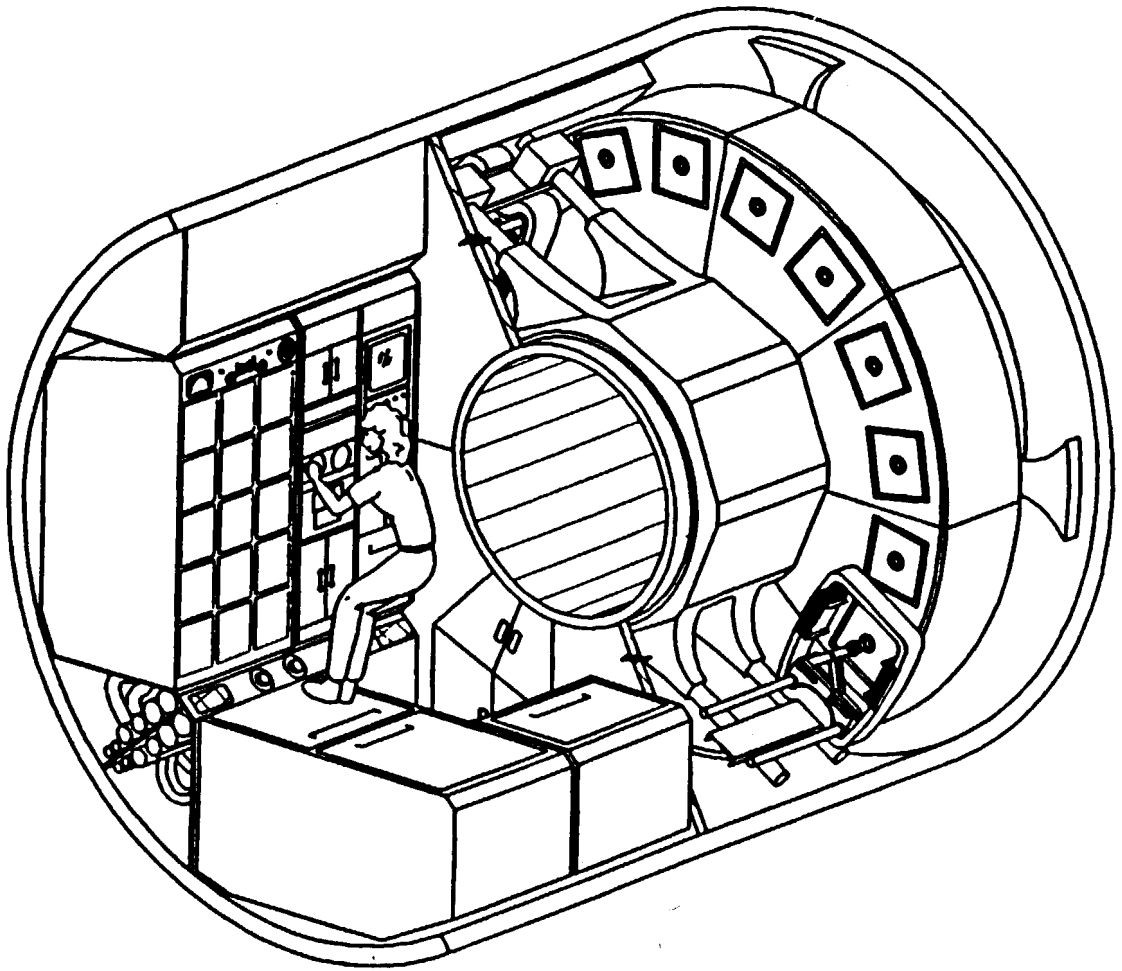

FIGURE 4

while it is almost 22 rpm on the large-diameter centrifuge. The spin-up time for nominal 1-g operations is about 2 min for the principal rotor. That doesn't require a lot of torque. The angular momentum for this case is 363 N m sec for the 6-ft, and about 4,800 N m sec for the 12-ft centrifuge. Our assumption has been that uncompensated momentum and torque should not exceed 1 to 3%, and that the Station control system can handle that much residual.

Figure 5 was put together to eliminate some misconceptions about the centrifuge and illustrate how we have eliminated or solved many potential problems. The first misconception is that the centrifuge will create an unacceptable disturbance of the microgravity environment. The system that we have designed is a magnetically suspended and dynamically balanced centrifuge. That eliminates the majority of the problems of vibration disturbance. Another concern was that the centrifuge would cause a torque on the Space Station and cause it to precess. We've designed the centrifuge with a counter-rotating inertia wheel, which absorbs both the gyroscopic effects and the starting and stopping torques of the centrifuge. Another concern is that such a large centrifuge will be dangerous, but the centrifuge really rotates slowly, only at about 22 rpm. Also, we plan on enclosing it in a structural honeycomb absorption barrier system so there won't be any problems if something should come loose. We also have touchdown bearings to contain the centrifuge in case of power loss. Other concerns were that the magnetic suspension system would generate electromagnetic interference and that the magnetic suspension system presents a big development risk. In response, the system is designed so that magnetic flux cannot escape. This suspension technology has been used before on momentum control gyros and on vibration-isolated pointing systems.

Another major design driver is that the centrifuge must be assembled on orbit. The hatches are 50 in. square with a 12-in.-radius corner which gives a 60-in. diagonal. Even the 6-ft centrifuge would not fit through the hatches. Consequently, we have designed both centrifuges to break into separate components which can be passed through the hatches. The drive motor is an ironless armature, dc-drive, brushless, noncontacting system.

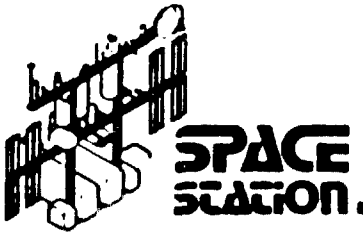

CENTRIFUGE FACT SHEET

Lockheed

MYTH	FACT
THE CENTRIFUGE WILL CAUSE UNACCEPTABLE DISTURBANCE OF THE MICROGRAVITY ENVIRONMENT	THE CENTRIFUGE DOES NOT MAKE PHYSICAL CONTACT WITH THE SPACE STATION. IT IS MAGNETICALLY SUSPENDED AND AUTOMATICALLY BALANCED
THE CENTRIFUGE WILL EXERT A TORQUE ON THE SPACE STATION, CAUSING THE STATION TO PRECESS	A COUNTER-ROTATING INERTIA WHEEL ABSORBS GYROSCOPIC, STARTING, AND STOPPING TORQUES
SUCH A LARGE ROTATING SYSTEM IS DANGEROUS TO THE CREW AND STATION	THE CENTRIFUGE ROTATES SLOWLY (~22 RPM). AN INTERLOCKED PHYSICAL BARRIER IS PROVIDED BETWEEN THE CREW AND THE ROTATING CENTRIFUGE. AN ENERGY-ABSORBING HONEYCOMB SHIELD ENCLOSES THE CENTRIFUGE. DESIGN IS FAIL-SAFE AND INCLUDES TOUCH-DOWN BEARINGS TO PROVIDE CONTAINMENT IF POWER FAILS
THERE WILL BE ELECTROMAGNETIC INTERFERENCE FROM THE MAGNETIC SUSPENSION AND MOTOR	SIMILAR MAGNETIC BEARINGS ARE USED ON THE MAGNETIC ISOLATOR DEVELOPED TO FLY IN A SHUTTLE MID-DECK LOCKER, DESIGNED TO SHUTTLE EMI REQUIREMENTS
THERE WILL BE MAGNETIC FIELD INTERFERENCE BETWEEN THE MOTOR, SUSPENSION, AND ROTARY DATA AND POWER TRANSFER DEVICES	DESIGN IS BASED ON MAGNETIC ATTRACTION. FLUX IS CONFINED TO THE AIR GAP AND DIES OUT TO BELOW EARTH'S MAGNETIC FIELD WITHIN ONE FOOT
MAGNETIC SUSPENSION AND PROPULSION REPRESENTS A SIGNIFICANT HARDWARE DEVELOPMENT RISK	TECHNOLOGY IS SIMILAR TO THAT USED IN SATELLITE CONTROL MOMENT GYROS, TALON GOLD VIBRATION ISOLATION POINTING SYSTEM, AND HIGH RATE GAMMA SCANNER FOR SANDIA

FIGURE 5

To determine how the centrifuge will perform on the Station -- because we not only have to isolate the Station from the centrifuge, but also the centrifuge from the Station -- we modeled the Space Station for manned push-off, treadmill, and control moment gyro forces. We obtained an environment for the Space Station as shown in Figure 6. Then we did a similar analysis for the centrifuge, also shown in Figure 6. It is obvious that the centrifuge is really not the major driver for microgravity concerns; there are more problems with the crew push-offs, treadmill, man movements, pumps, fans, and other forces.

In Figure 7, the centrifuge characteristics were superimposed on a chart showing representative disturbances. The centrifuge comes in below many of the transient responses, but above the steady-state accelerations.

You will recognize the chart taken from a Teledyne Brown Engineering study, shown in Figure 8; it has been discussed repeatedly in the past few days. The centrifuge data are plotted with the requirements that are postulated by the material sciences. The centrifuge data are located far enough to the right in frequency so that the centrifuge would not disrupt even the lower than 10^{-5} g requirements of the materials sciences in the lower frequency regime.

This is our first cut at the large centrifuge. We continue our analyses, and as the Station configuration is defined more closely, we will be able to do more work on the design to ensure we don't adversely impact experiments. One of the challenges that faces the centrifuge program is to determine if we need the service rotor. We are already facing a complex dynamic problem by having two wheels rotating, the counter-rotating inertia wheel and the centrifuge. An independent service rotor will add complexity because the counter-rotating inertia wheel has to compensate for that additional rotation. If we don't have a service rotor the centrifuge must be stopped for servicing, and all the specimens must be serviced at once.

CENTRIFUGE DISTURBANCE COMPARED TO SPACE STATION ENVIRONMENT

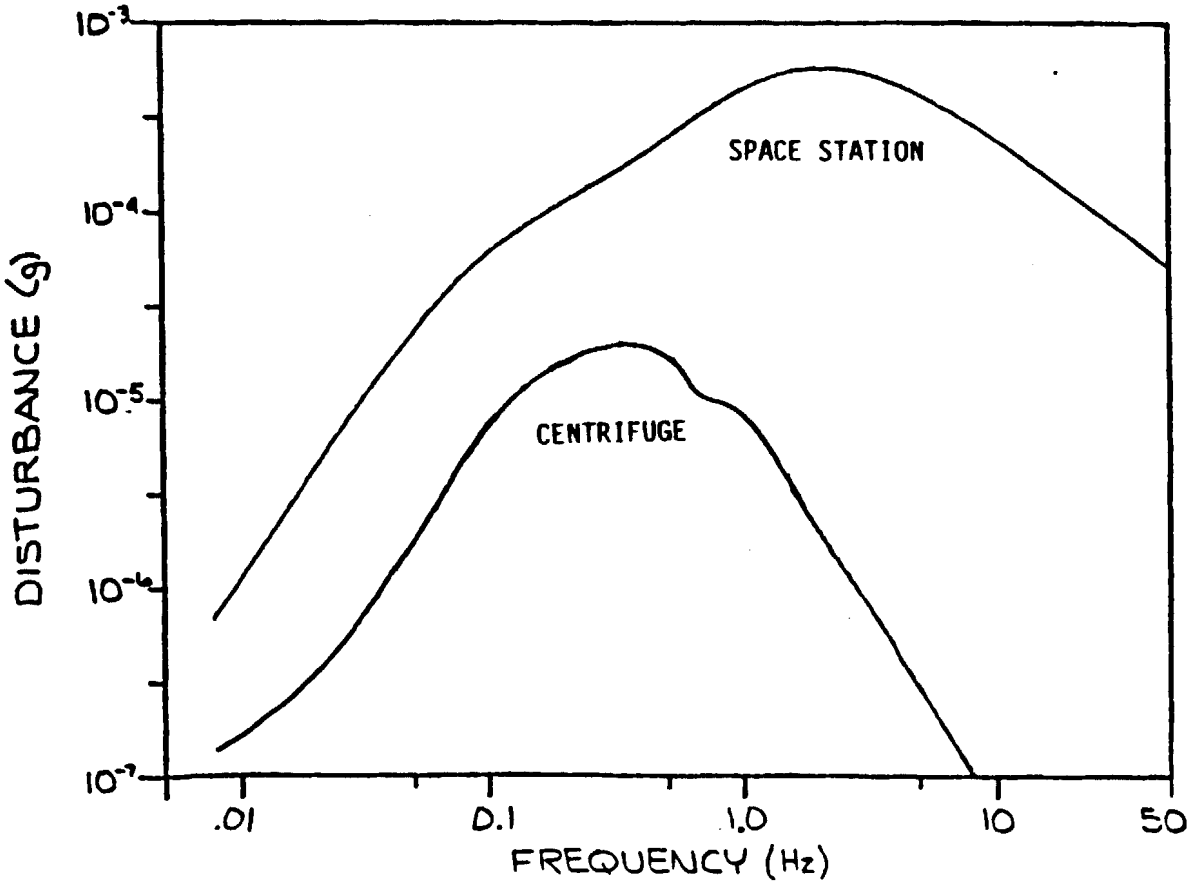

FIGURE 6

SPACE STATION ACCELERATION ENVIRONMENT

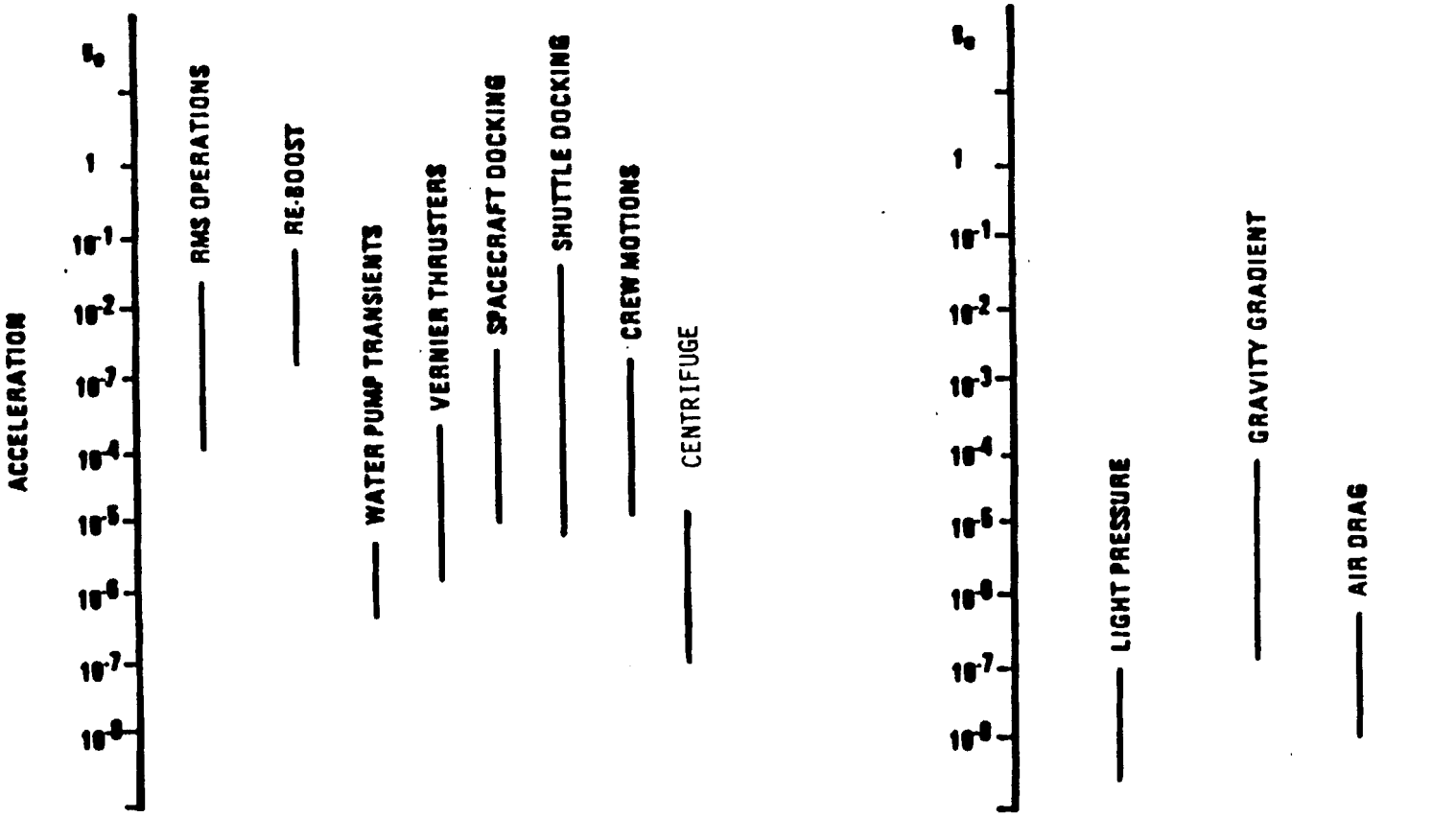

TRANSIENTS
COVERING A FREQUENCY SPECTRUM
FROM ABOUT 10^{-3} TO 10 Hz

STEADY STATE ACCELERATIONS
(0 TO 10^{-3} Hz)

FIGURE 7

ACCELERATION SENSITIVITIY OF MATERIALS PROCESSING

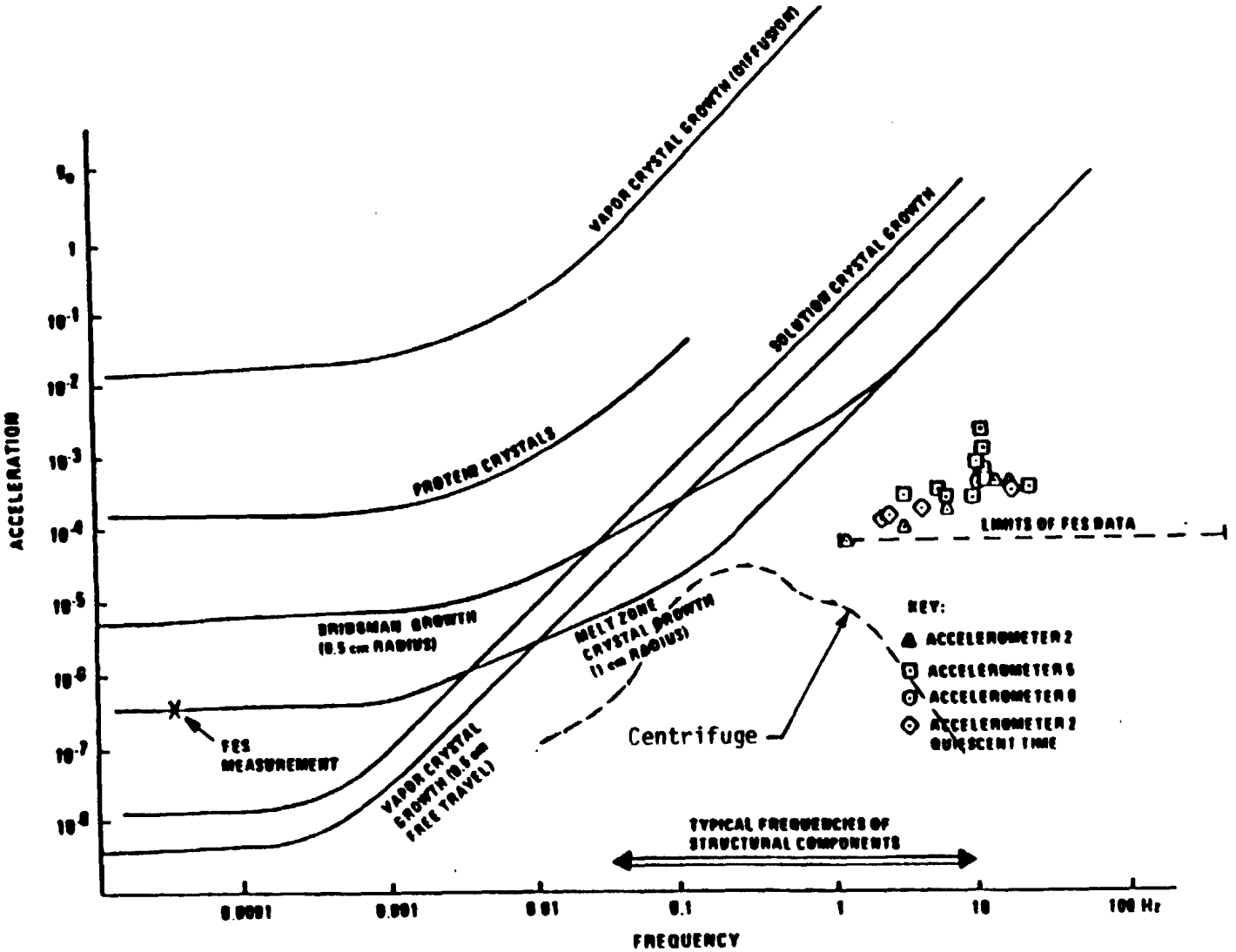

FIGURE 8

Another study that needs to be undertaken is the analysis of the dynamic interactions between the Station and the centrifuge to make sure the centrifuge doesn't excite any structural resonances. A further, important step will be the integration of all the dynamic disturbances, and the verification that they do not exceed the allowable limits.

In summary, as shown on Figure 9, the life sciences community and the Space Station program need the centrifuge. Lockheed has been working on centrifuge designs that satisfy the science objectives as much as possible, while also keeping in mind that the centrifuge must be designed to have the smallest possible dynamic impact on the Space Station.

Question: For all the dynamicists present, I will tell you that you will save yourself a ton of grief if you will bring that compensating rotor a lot closer to your main rotor.

Question: Is there a mechanism for taking into account animal movement back and forth in there, and how that might drive resonances in the Station?

Douglas Havenhill, Sperry Corporation: The balancing system was designed only to take out static imbalance. However, the magnetic isolation, or the magnetic suspension system, also provides a certain amount of isolation. Although we have not looked at it in any detail, we certainly think that animal motions are going to be much less than any kind of crew motion.

Searby: The philosophy was that you isolate against the dynamic imbalances, and you compensate for the static.

Question: The issue still is, will you drive the resonant frequencies of the Station?

Havenhill: There is a certain amount of isolation that's built into the suspension system. Whether there will still be an excitation of resonances, we don't know.

- WE NEED A CENTRIFUGE

- WE HAVE CENTRIFUGE DESIGNS WHICH SATISFY SCIENCE OBJECTIVES

- THE CENTRIFUGE IS BEING DESIGNED TO HAVE THE SMALLEST POSSIBLE DYNAMIC IMPACT ON THE SPACE STATION

FIGURE 9

Searby: I pointed out how important that integration aspect is. Hopefully, it will be an iterative process where we'll have a first cut, analyze it, and then go back and forth until we reach a situation where we don't excite those structural resonances.

Question: I'm having a little trouble with your first step, which seems to be Newton's law of reaction. If an animal moves in the centrifuge, giving an unbalanced situation, how does the fact that you have magnetic rather than mechanical suspension prevent you from coupling the reaction of that unbalance into the Space Station?

Havenhill: It does not prevent the forces from being transmitted across the magnetic gap. But, if there is a spike of the force, for instance an animal jumping, the magnetic suspension will tend to smooth out that spike because it represents an isolation system.

Question: So if an animal moves a matter of a meter or so, you get maybe a kg-m unbalance in the system....

Answer: An animal cage is really small. These cages are only on the order of 20 cm square, so the animals are not going very far. If they jump, they jump only a little, and come down very quickly.

N91-12426

27. NOISE POWER SPECTRAL DENSITY OF THE SUNDSTRAND QA-2000 ACCELEROMETER

Information Supplied By: Rex Peters and David Grindeland

Sundstrand Data Control, Inc. Redmond, WA

ABSTRACT

There was no paper presented at the acceleration workshop. However, as several acceleration measurement systems use the Sundstrand sensor, the editors have included some noise PSD information of typical hardware. Figures 1 through 6 reflect measured data.

Comments by Rex Peters:

There are no good data on low frequency (<0.1 Hz) PSD for the Q-Flex accelerometer. We have, however, made some preliminary stability measurements over periods of 12-24 hours and demonstrated stability <0.5 micro-g over >12 hours. The test data appear to contain significant contributions from temperature variations at that level, so the true sensor contribution may be less than that. If what we saw could be construed as a true random process, it would correspond to about 0.1 micro-g rms over a bandwidth from 10^{-5} Hz to about 1 Hz. Other studies of low frequency PSD in flexure accelerometers have indicated that material aging effects tend to approximate a first order Markhov process. If we combine such a model with the spectrum obtained at higher frequencies, it suggests the spectrum shown in Table 1 and in Figure 7 as a conservative estimate of Q-Flex noise performance.

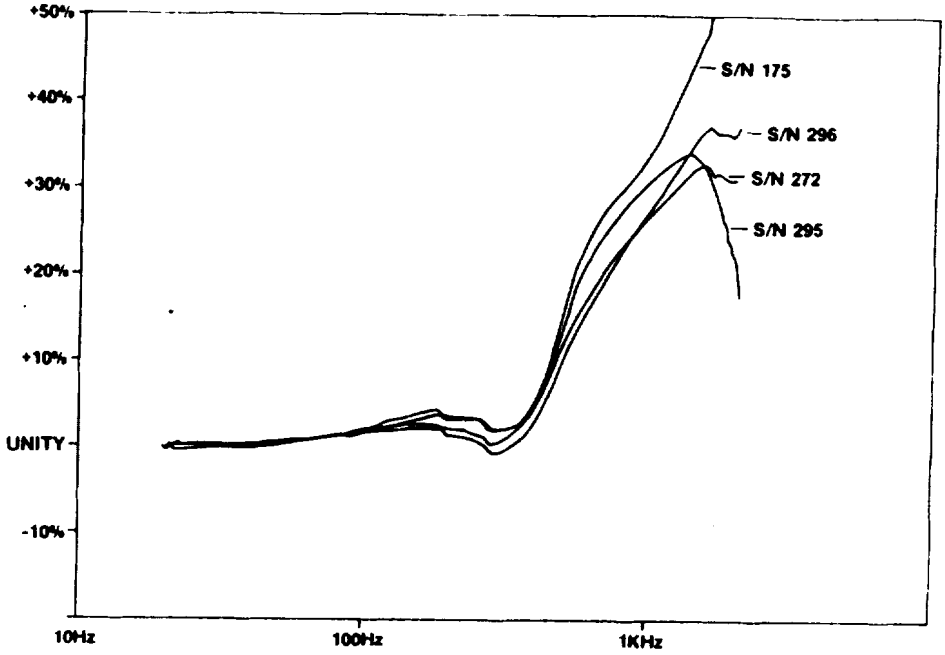

FIGURE 1. QA-2000 AMPLITUDE RESPONSE

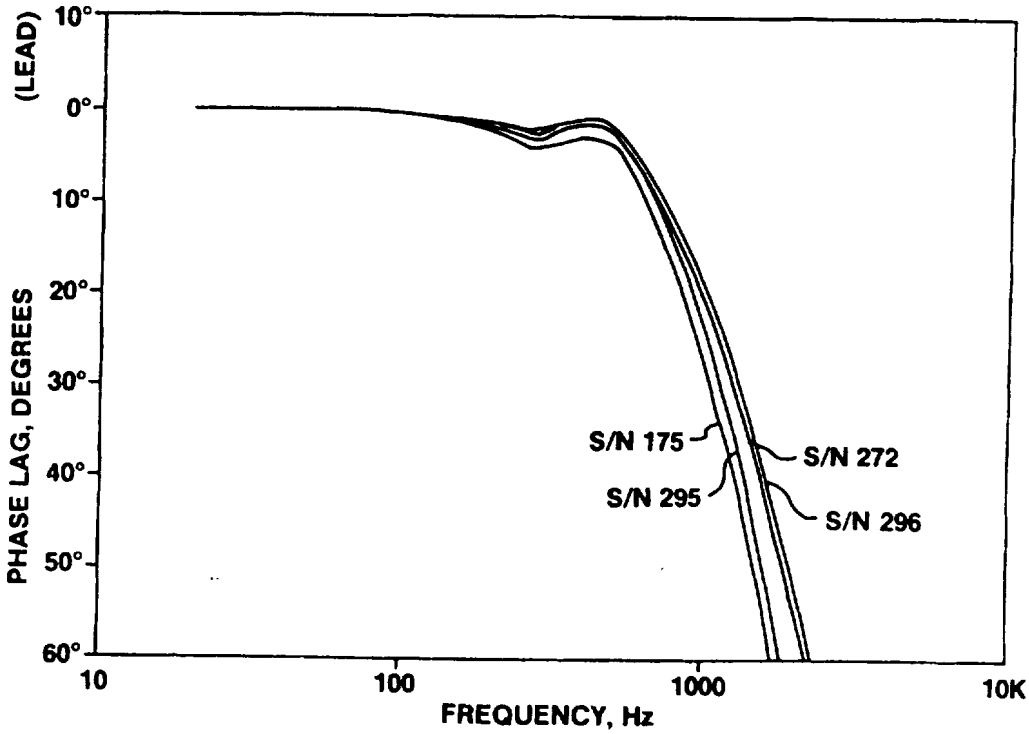

FIGURE 2. QA-2000 PHASE RESPONSE

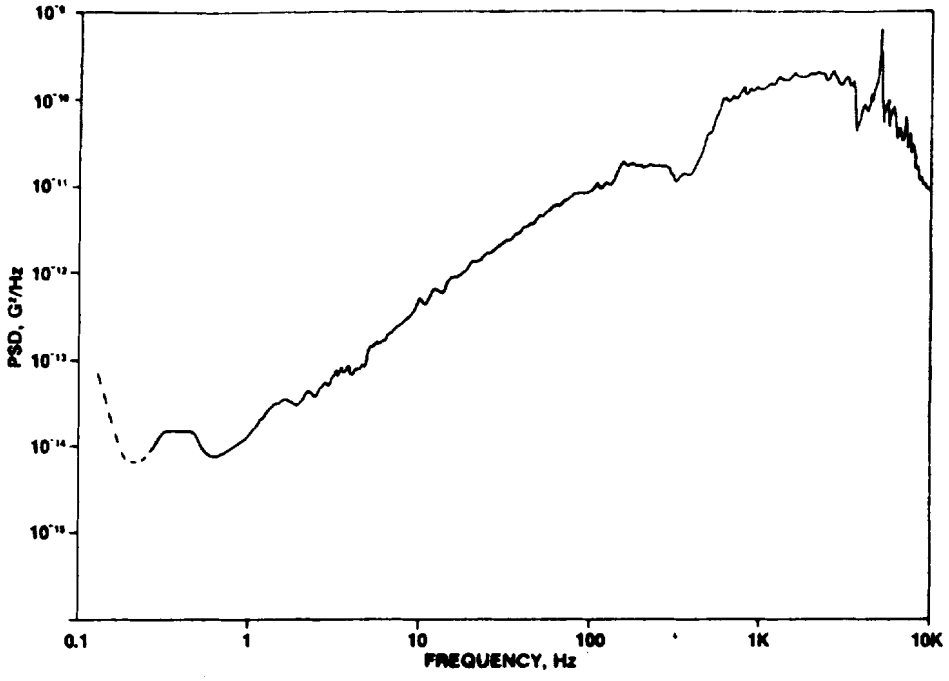

FIGURE 3. NOISE POWER SPECTRAL DENSITY QA-2000-002 SERIAL NO. 175

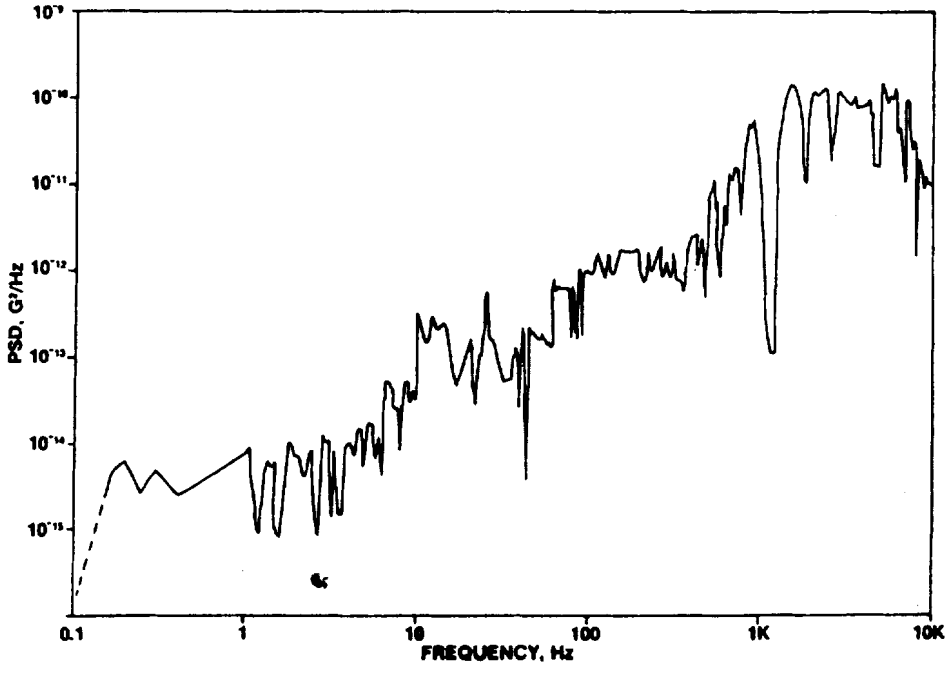

FIGURE 4. NOISE POWER SPECTRAL DENSITY QA-2000-001 SERIAL NO. 272

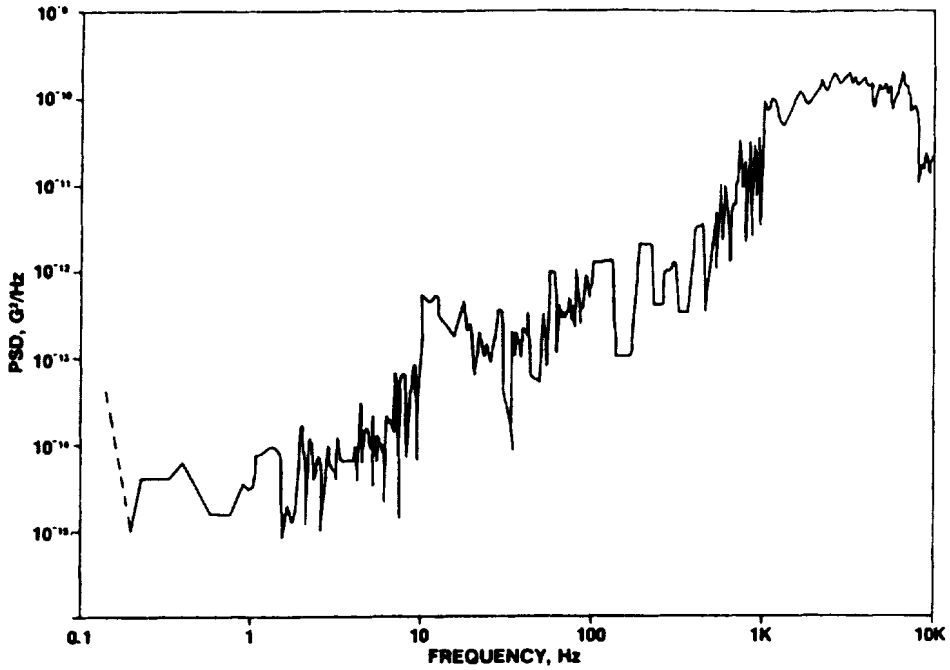

FIGURE 5. NOISE POWER SPECTRAL DENSITY QA-2000-001 SERIAL NO. 295

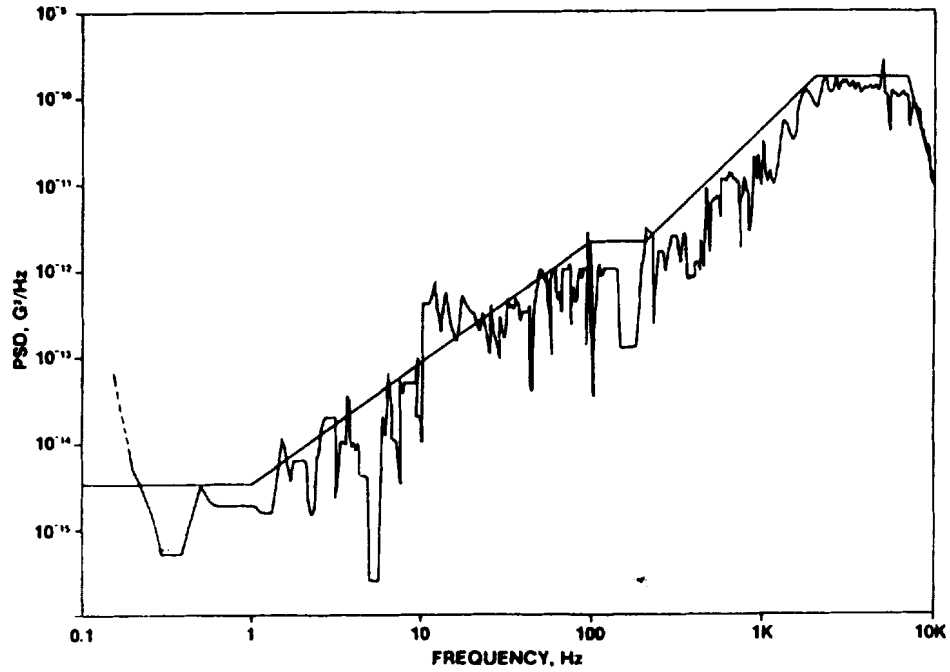

FIGURE 6. NOISE POWER SPECTRAL DENSITY QA-2000-001 SERIAL NO. 296

TABLE 1. ESTIMATED Q-FLEX NOISE PERFORMANCE

BANDWIDTH	g (rms)
10^{-5} Hz to 5 x 10^{-3} Hz	8.7 x 10^{-8}
10^{-5} Hz to 1 Hz	10.2 x 10^{-8}
10^{-5} Hz to 50 Hz	11 x 10^{-6}
10^{-4} Hz to 5 x 10^{-3} Hz	2.7 x 10^{-8}
10^{-4} Hz to 1 Hz	6.1 x 10^{-8}
10^{-4} Hz to 50 Hz	11 x 10^{-6}
10^{-3} Hz to 1 Hz	5.5 x 10^{-8}

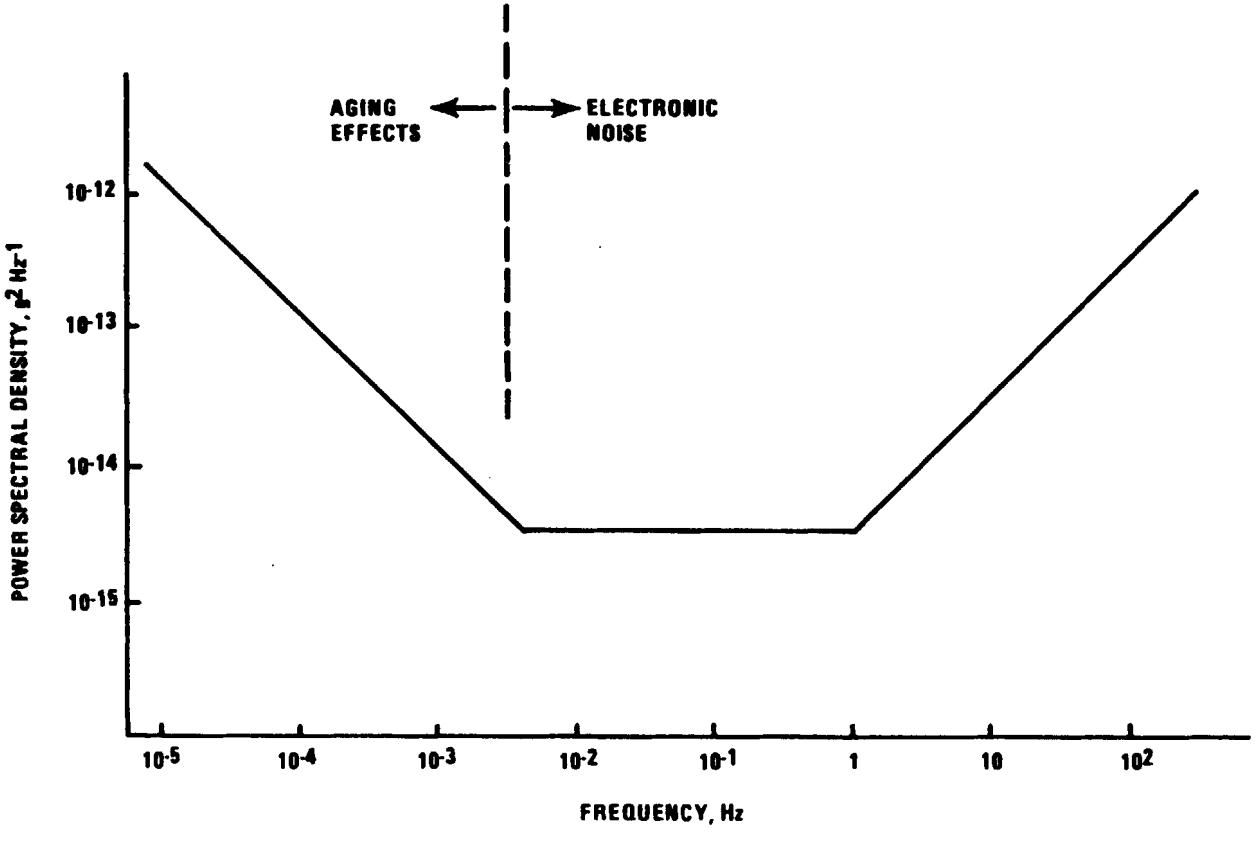

FIGURE 7. NOISE POWER SPECTRUM OF Q-FLEX ACCELEROMETER

SUMMARY OF WORKSHOP

28. THE PERFECTLY IDEAL ACCELEROMETER

Dr. Ernst Stuhlinger, Teledyne Brown Engineering

ABSTRACT

This summary paper gives a condensed version of the results and conclusions that developed during the Workshop. Upper limits of residual accelerations that can be tolerated during materials processes, presented as "acceptable" and as "desirable" limits, are shown. Designs and capabilities of various accelerometers, and their inherent problems, are compared. Results of acceleration measurements on Spacelab flights are summarized, and expected acceleration levels on the Space Station under various conditions are estimated.

Our workshop consisted of four main sessions, a panel discussion, a summary session, and a joint dinner with speech. The titles of the main sessions reflect the problem areas that were to be addressed at the workshop: 1) desired acceleration and frequency limitations of disturbances; 2) residual acceleration levels measured on spacecraft; 3) accelerometer systems; and 4) the Space Station acceleration environment.

We heard two and one half days of presentations, discussions, and debates about a subject that is not new, but has moved into the limelight for spaceplanners during the past one or two years. It is the question of determining to what degree of weightlessness our materials processing experiments in space should be, and will be, exposed during orbital flight.

Fifteen years ago, when we began considering materials processing experiments in space, we talked glibly about zero-g. We prepared experiments for Skylab, but we did not even think of measuring the degree of weightlessness our spacecraft would offer. As the years went by, studies were made about the level of residual accelerations our experiments could tolerate, and also about the acceleration environment to which these experiments would be exposed. Our vernacular changed from zero-g to micro-g. Then, acceleration measurements were made on rockets and on Spacelabs, and our vernacular changed promptly from micro-g to milli-g. We then felt the urge to organize a workshop that would help us shed some light on a problem area that proved to be more important and more complex than most of us had previously thought.

How low should the low-acceleration environment for space processing of materials be, and how can we measure and characterize the residual levels of acceleration that prevail during our materials experiments in space?

The first session was originally planned to address effects that residual accelerations will have on materials processes under near weightlessness. Although much study work has been done during past years to clarify this subject, we still have only a poor understanding of the exact mechanism by which residual accelerative forces produce lattice defects or otherwise imperfect crystals. Robert J. Naumann, NASA/MSFC, reviewed the various sources of low-level accelerations on spacecraft. Steady accelerations, as produced by gravity gradients and by atmospheric drag, are of greater influence than accelerative forces of higher frequencies as they are generated by running machinery or by transient motions of masses onboard the spacecraft. Based on theoretical studies in which movements of particles or volume elements due to convection or diffusion were compared with movements caused by accelerative forces, diagrams were drawn that showed for various crystal growth processes those critical accelerations as functions of frequency above which homogeneous crystals would not be expected to grow without developing lattice defects.

Figure 1 shows this function in a "desirable" and an "acceptable" version for the most sensitive processes presently envisioned for space experiments.

It is obvious that these diagrams cannot claim to be more than very broad, qualitative guidelines for the planners of space experiments. They badly need confirmation, or improvement, by further studies, and by systematic experiments in the laboratory and in space. It is even not quite clear how these experiments should be interpreted. If, for example, a vibration existed that is caused by two sinusoidal excitation functions with closely spaced frequencies, $f(1) \approx f(2)$, each with a peak acceleration of a(o), should the resulting vibration be entered into the diagram of Figure 1 as two points at $f(1)$; a(o) and $f(2)$; a(0) , or as one point at $f(1) + f(2)/2$; 2a(o) ? In the first case, the two points may fall below the critical curve, and would be judged acceptable; in the second case, the one point may fall above the line, and the vibration would be judged inacceptable.

Ken Demel, JSC, expressed his concern even more drastically: "If you had a bad acceleration event of a few seconds duration, you could dissolve it into a million monochromatic sinusoidal oscillations, each with a little different frequency, but with a real tiny acceleration. Each would have its own point in the diagram, and each point would lie way below the critical curve. Would that be a true representation of what we want to know?"

Lively discussions developed around this question of how to define critical acceleration levels, how to measure them, and how to formulate specifications for spacecraft designers.

Proposals were made to measure and plot the power spectrum density, rather than acceleration of the acceleration environment. However, a power spectrum density diagram would not show those features either that are considered decisive in the growth of homogeneous crystals. It is quite obvious that a simple acceleration versus frequency plot, as shown in Figure 1, can certainly not provide more than qual-

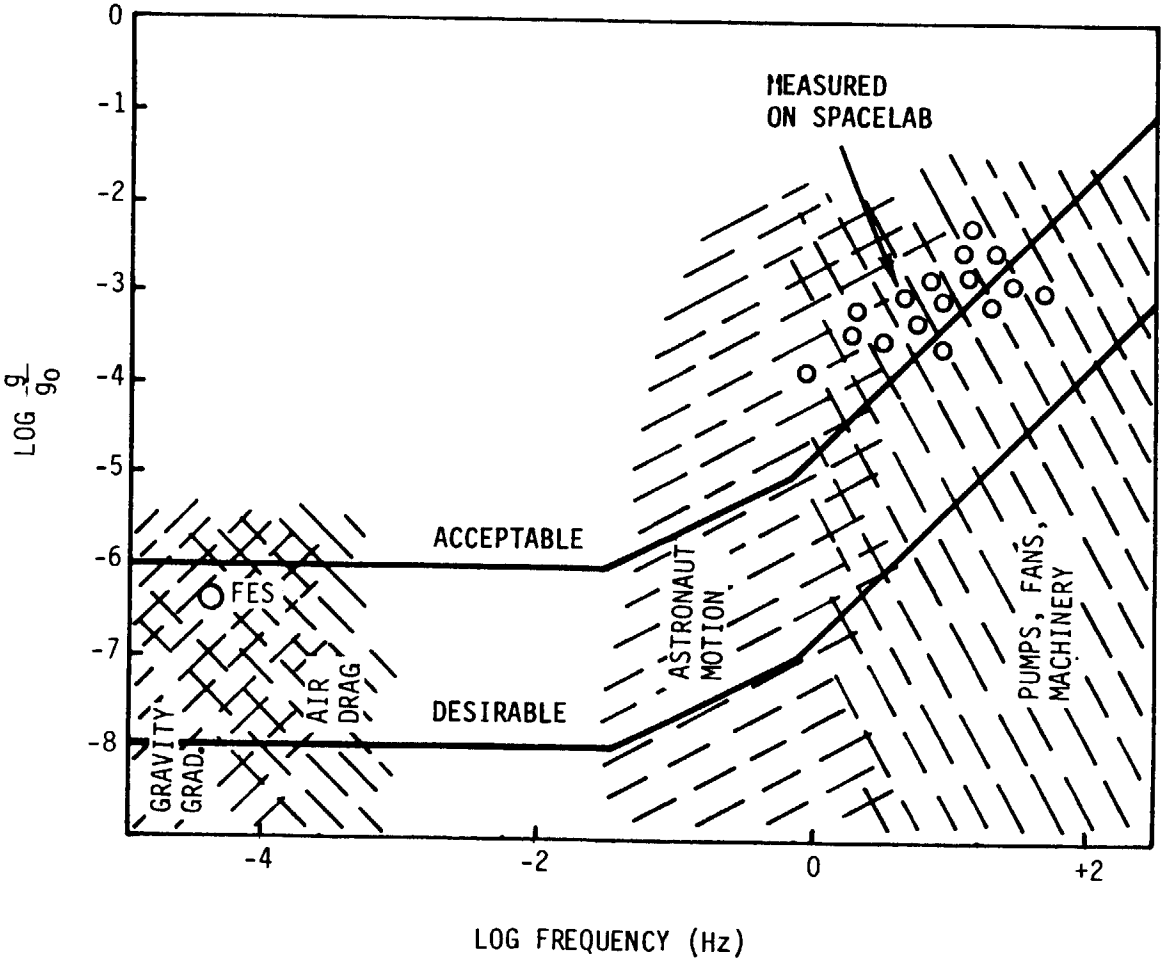

FIGURE 1. PROPOSED ACCELERATION LIMITS

itative guidelines for designers; but in view of the broad uncertainties that still prevail in the question of acceptable levels of residual accelerations, this way of presentation may at present be the most helpful one for Space Station designers. In Dr. Naumann's words, "we set requirements as best as we could." The degree of uncertainty may be illustrated by this remark from the audience: "What does gravity have to do with space processing? We don't really know!" -- a remark that would not have been subscribed by all the attendees, though.

Naumann suggested that the most relevant quantity that would characterize the quality of the acceleration environment would probably be the "moving window average" of the acceleration, as described in Paper No. 19 in these Proceedings.

The most dangerous accelerations affecting materials processes are produced by steady and slowly varying forces, such as gravity gradients, and atmospheric drag. Expected accelerations caused by these forces are shown in Figures 2a, 2b, and 3.

Gravity gradient accelerations can be minimized by placing the sensitive experiments close to the line of the center of gravity on the Space Station, not more than about 0.3 m apart for 10E-7 g.

Deceleration of the Space Station by atmospheric drag forces can be compensated by a continuously working thruster system whose thrust level is controlled according to the drag. With electrothermal thrusters using waste products (water) as propellant, a yearly mass consumption on the order of 10 to 20 tons, and an average electric power of about 5 kWe, would be sufficient to compensate aerodynamic drag forces on a continuous basis. This scheme would also make re-boost maneuvers unnecessary.

Another group of accelerating forces is caused by running machinery, such as fans, pumps, compressors, and alternators, and by functions that include the rapid motion of mechanical parts, such as valves and switches. The frequency spectrum of these disturbances covers a range approximately from 1 to 100 Hz, with acceleration peaks

DISTANCE FROM CG (m)	ACCELERATION (10^{-6} g_o)	
	VERTICAL	LATERAL
R	A_V	A_L
1	0.375	0.125
2	0.75	0.25
4	1.50	0.50
8	3.00	1.00
16	6.00	2.00
32	12.00	4.00
64	24.00	8.00
ORBIT ALTITUDE: 270 n.mi, 500 km		

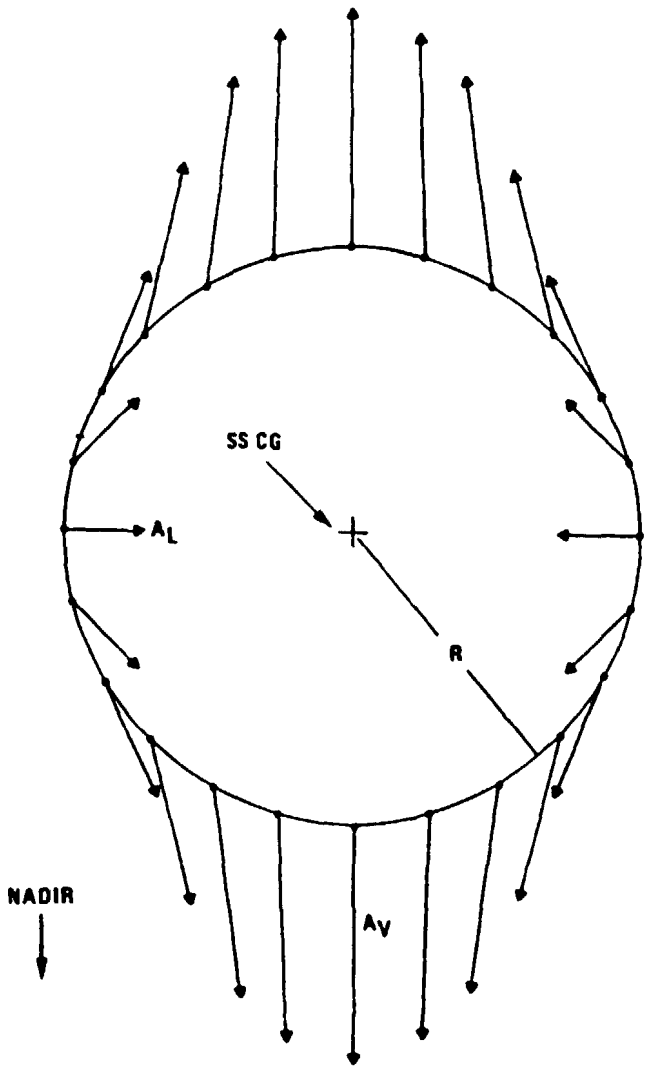

FIGURE 2a. GRAVITY-GRADIENT VECTORS ON A CIRCLE AROUND CENTER OF GRAVITY ON AN ORBITING SPACECRAFT IN A PLANE PERPENDICULAR TO FLIGHT DIRECTION

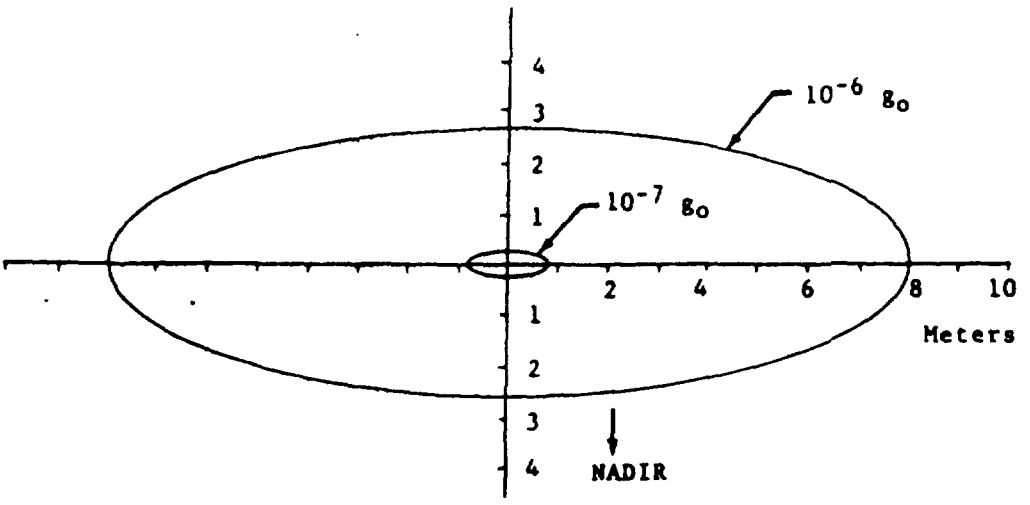

CONTOURS OF CONSTANT GRAVITY GRAIDENT ACCELERATION IN A PLANE PERPENDICULAR TO THE PATH OF THE SPACECRAFT'S CENTER OF GRAVITY (450 km ORBIT)

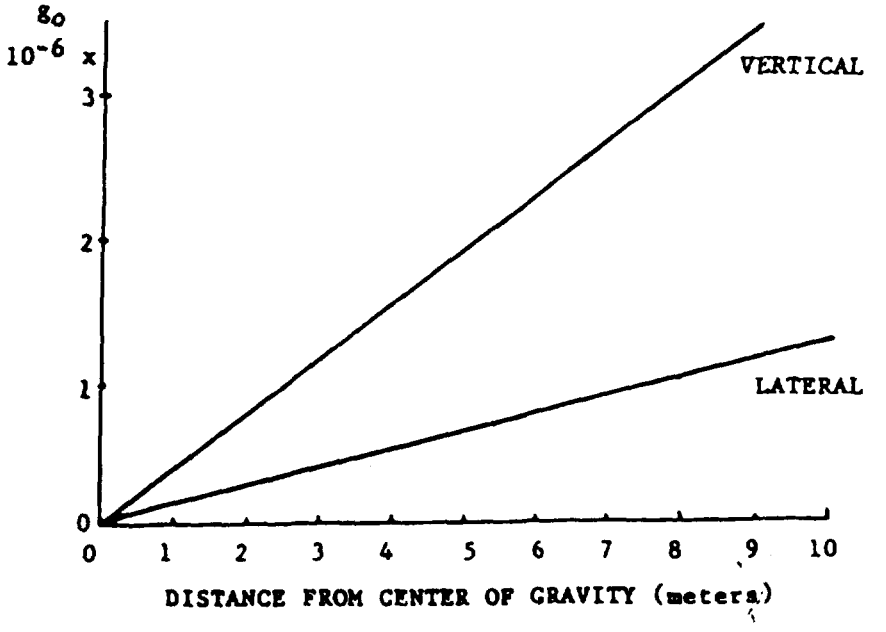

FIGURE 2b. GRAVITY GRADIENT ACCELERATION IN RADIAL AND LATERAL DIRECTION AS A FUNCTION OF DISTANCE FROM THE CG (450 km ORBIT)

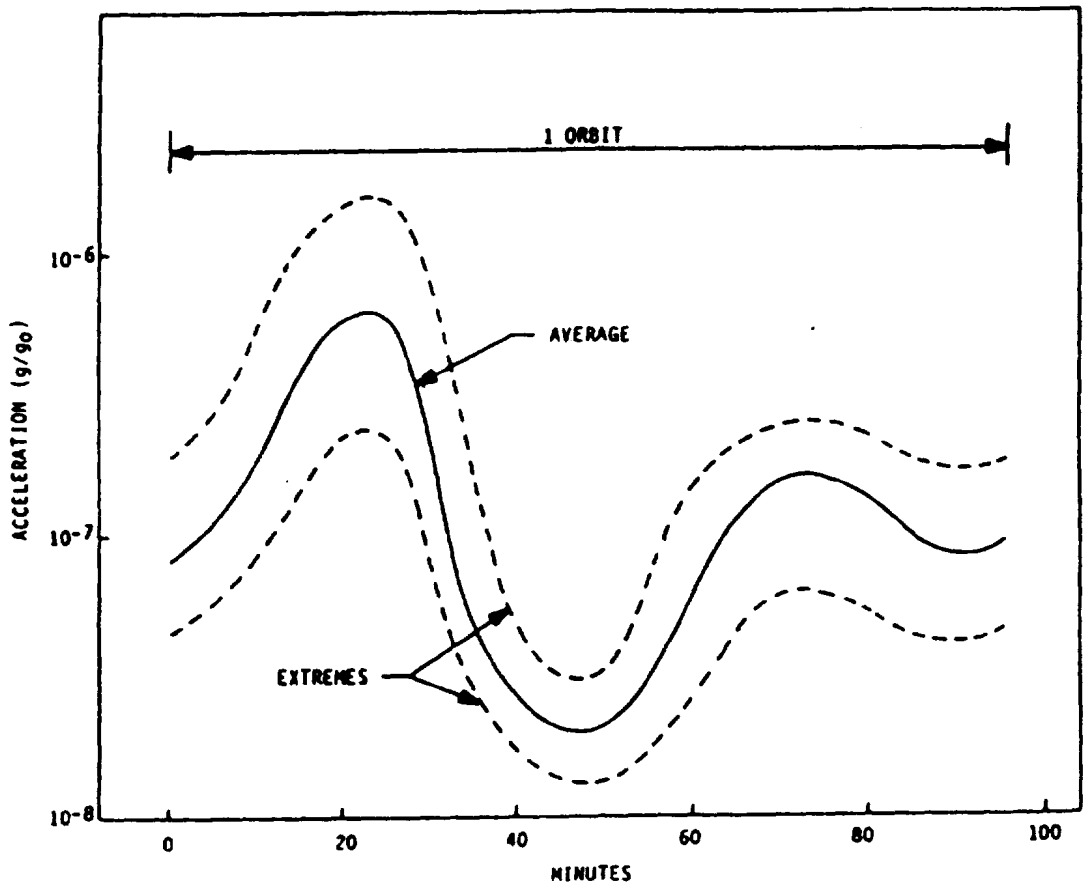

FIGURE 3. DECELERATION OF SPACE STATION CAUSED BY ATMOSPHERIC DRAG

Variations of deceleration result from changes of aspect angle, day-night cycles, and varying solar activity.

up to about 5 x 10E-3 g. It is likely that materials processing experiments can be protected against most of these disturbances by proper shockmounts and other vibration-isolating systems.

A further potentially dangerous group of disturbances falls between these two regions. Caused by the movement of masses onboard the Station (motion of astronauts; docking and undocking of spacecraft; transfer of propellants, waste materials, and freight; change of experimental set-ups), accelerative forces in this group may reach 2 x 10E-2 g with frequency spectra covering a wide range from about 10E-3 to 10 Hz. It may be necessary to avoid such mass movements entirely by proper timelining of activities while high-sensitivity materials processing experiments are underway.

Several acceleration measurements were made on Shuttle flights, particularly by West German investigators, and also on ballistic flights (SPAR Project). They typically show a frequency spectrum reaching from about 1 Hz to 100 Hz, with peak accelerations up to about 2x10E-3 g (Figures 4 and 5)*. Some of the more prominent frequencies could be attributed to specific sources (fans, pumps); shock-like accelerations were obviously caused by astronaut activities (operation of sled; opening and closing of rack drawers). Below a frequency of about 0.5 Hz, the recorded data were not good enough to allow a meaningful analysis.

These measurements were taken on the ground, with the Spacelab suspended on ropes. It is believed that the results are representative of the acceleration environment in flight, except for the effects of air drag and gravity gradient.

Trying to determine a steady-state or slowly varying acceleration component on the order of 10E-5 to 10E-6 within this very lively acceleration environment by analyzing a recorded accelerometer readout as shown in Figures 4 and 5 would seem almost hopeless.

Naumann and co-workers (Papers 4 and 6) tried to determine the quasi-steady state acceleration during a Spacelab flight by analyzing the movie picture record of a crystal floating within a solution. The

*D. Eilers and W. Knabe, Technical Report PRV-TB-I2/80
ERNO Raumfahrttechnik, Bremen, BRD, 12/15-80.

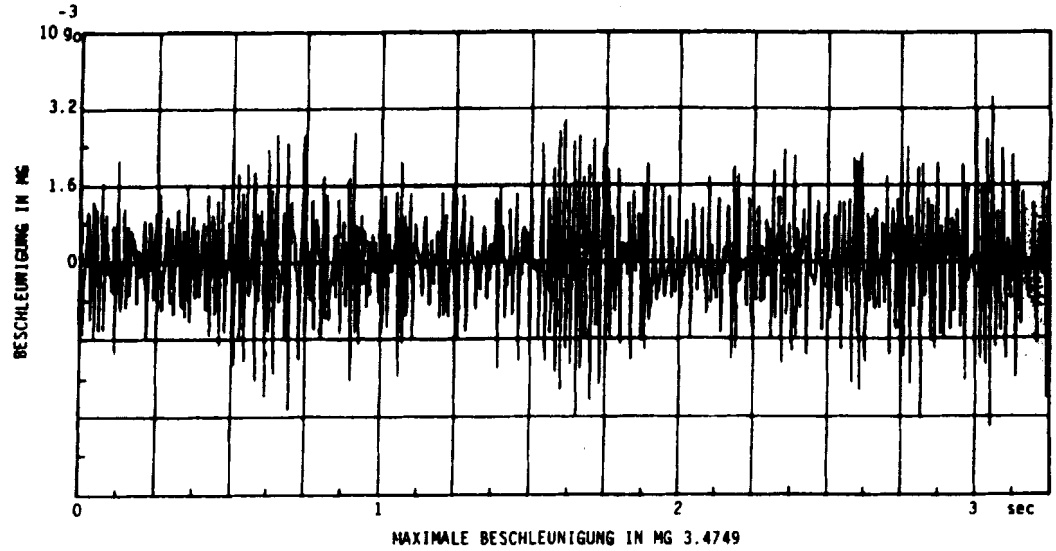

Abb. 3-1-15: Step A4 MP 1y
Spacelab aktiv, Storpegel am Control Center Rack

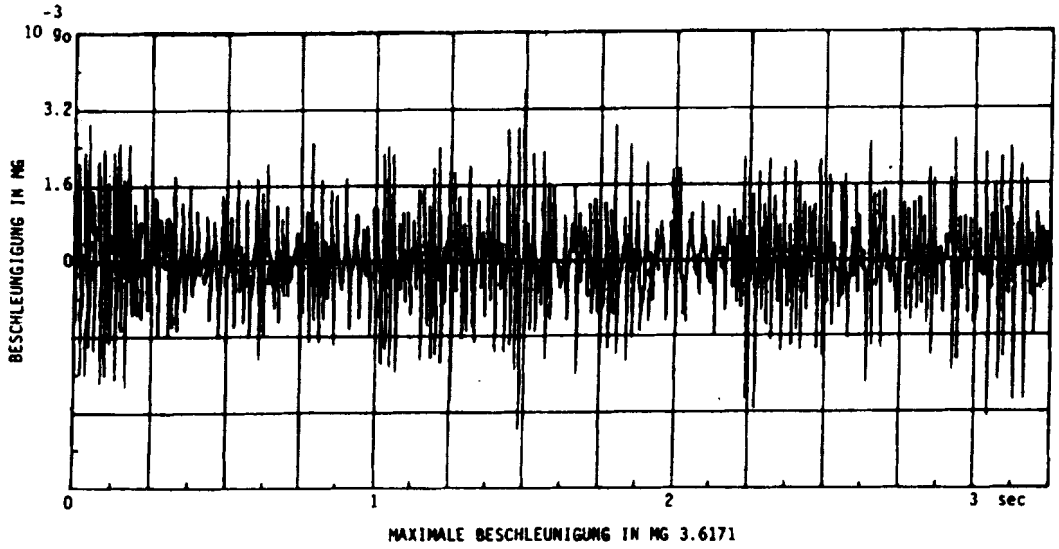

Abb. 3-1-16: Step A4 MP 1Sy
Spacelab aktiv, Storpegel am Control Center Rack

FIGURE 4

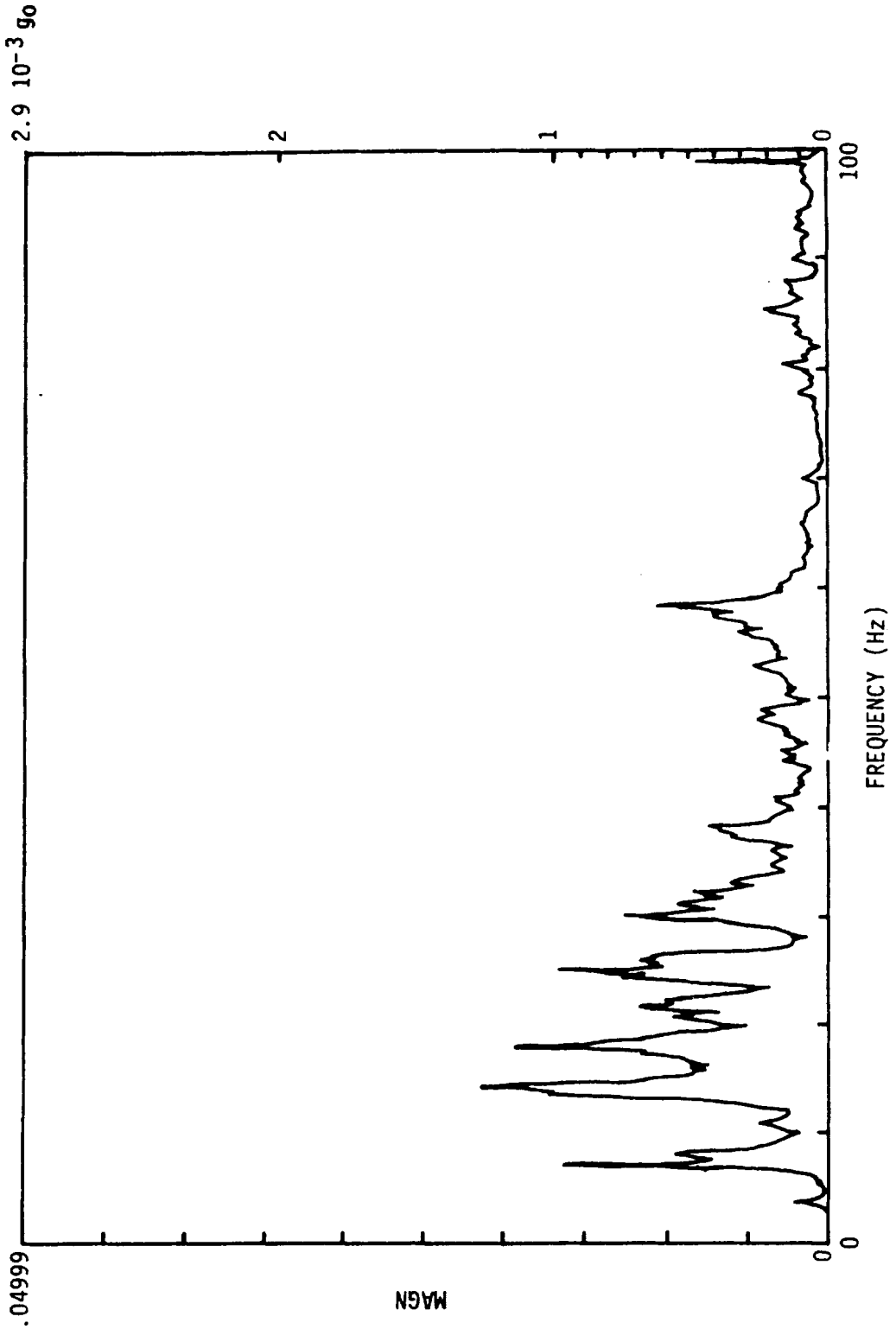

Abb. 3.2-2: Synthetisches Spektrum aus Step A4 MP 1Sy/Step B14 MP 1Su Spacelab aktiv, plus Simulation von Handhabungsstoßen

FIGURE 5

C 7

result, shown in Figure 1 as FES, agrees with expected values. However, since a number of those factors that influenced this measurement are not well known, only limited importance can be attributed to this observation. On the other hand, experiments like this may still offer the best method to determine low-level, quasi-steady state accelerations onboard a spacecraft in the presence of accelerations of higher levels and higher frequencies.

A number of presentations (Papers #14 to 20) describe existing or planned accelerometers; most of them have impressive capabilities regarding sensitivity, frequency response, and accuracy. Among the accelerometers presented or at least brought up during discussions were accelerometer systems developed by Bell Aerospace Textron, Payload Systems, Inc., Honeywell, Inc., University of Maryland, Teledyne Geotech, Applied Technology Associates, Inc., Sundstrand Data Control, Inc., Systron Donner, and NASA/Lewis Research Center.

It became obvious that several types of accelerometers either are, or soon will be available that will be able to measure the acceleration environment that is of interest in materials processing experiments. However, several remaining problems were pointed out during the Workshop; they should be given careful attention.

First, it will be difficult to obtain an accurate record of very low steady or near-steady accelerations against the background of a very restless environment as illustrated in Figure 4. Second, in view of the great sensitivity of some materials processes even to disturbances as short as a fraction of a second, it is hard to imagine how the huge amount of acceleration data accruing over the length of an experiment (hours, and even days or weeks) can be recorded, transmitted to the ground, stored, analyzed, and correlated with materials processing samples, within a reasonable volume of effort. Third, a proper way to correlate specific acceleration events with particular crystal lattice defects or other inhomogeneities has not yet been established. Fourth, in order to obtain a complete picture of the acceleration environment,

one should determine the accelerations in three translational and three rotational coordinates at the location of each of the sensitive experiments. This requirement alone will considerably increase the amount of data to be handled. Fifth, the cost of some of the commercially available accelerometers is high, on the order of $300,000 -- each.

The "ideal accelerometer" as conjectured by space planners -- which, naturally, will never exist in reality -- would measure accelerations over an acceleration range from about 10E-9 to 1 g, and over a frequency range from zero to about 100 Hz. It would be strictly linear over both these ranges, and it would measure continuously three translational and three rotational components of the acceleration (Figures 6 and 7). It would provide continuous records on tape of all these accelerations as functions of time.

It would also provide, through an appropriate filter system, continuous readouts of these accelerations in a number of different frequency regimes, such as 0 to 10E-3 Hz; 10E-3 Hz to 0.1 Hz; 0.1 to 1 Hz; 1 to 10 Hz; and 10 to 100 Hz, all as functions of time.

The system would also provide, through a proper network and on a continuous basis, for each coordinate the average acceleration during a specified time interval delta t ("moving window average"). Several displays of this average acceleration, each for a different delta t, would be available.

All these data would be stored on tape for later transfer to earth. They would also be put on telemetry links for immediate transmission to ground stations. Visual displays on a real-time basis would be available, at least on an as-wanted basis, for the scientist astronauts onboard the Station.

Each "ideal" accelerometer would produce data for six coordinates, and each of the sensitive experiments would be equipped with at least one accelerometer. The immense volume of data coming from this system, plus the uncertainties regarding interpretation and correlation of acceleration data with respect to crystal growth experiments, repeat-

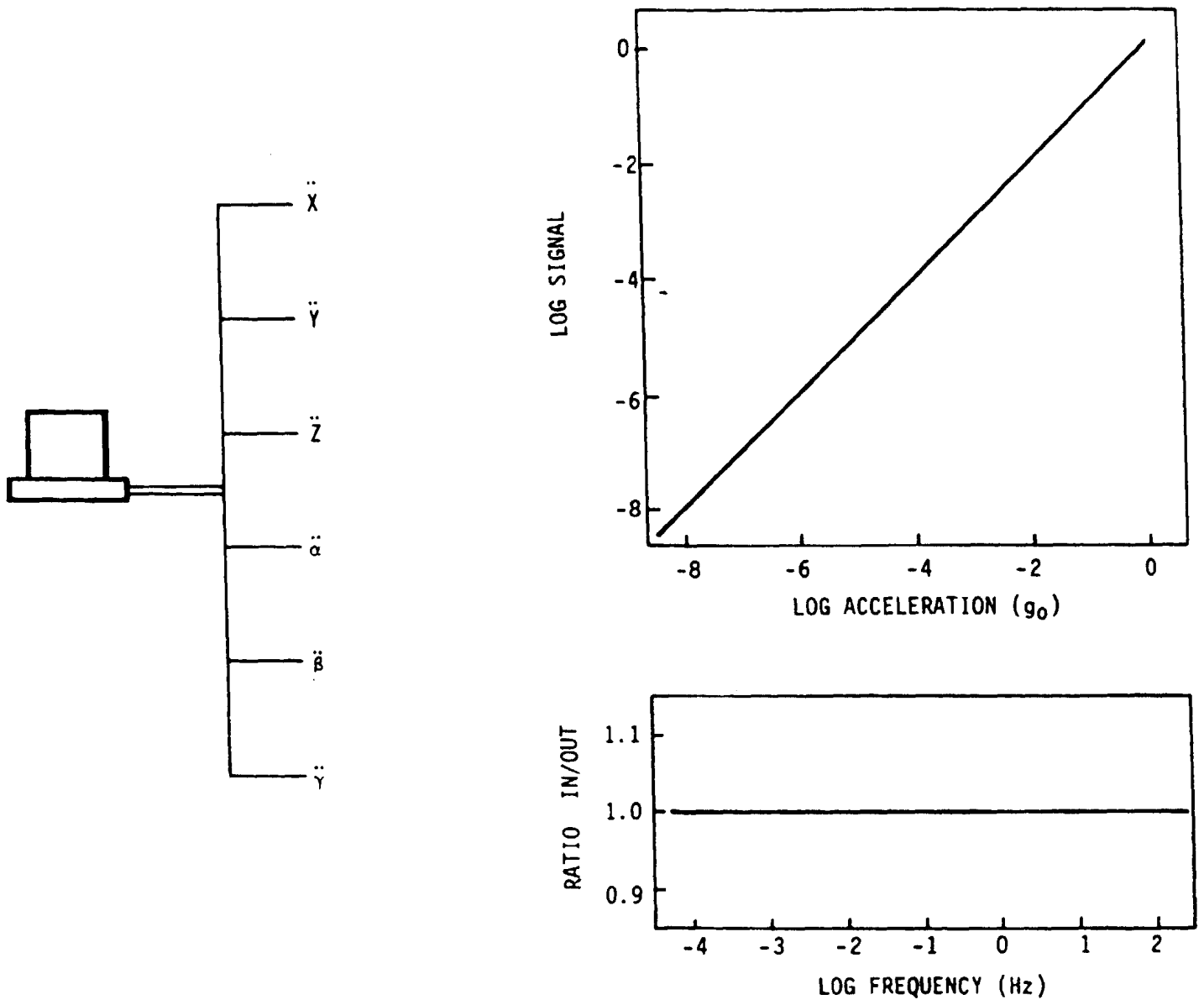

FIGURE 6. THE IDEAL ACCELEROMETER

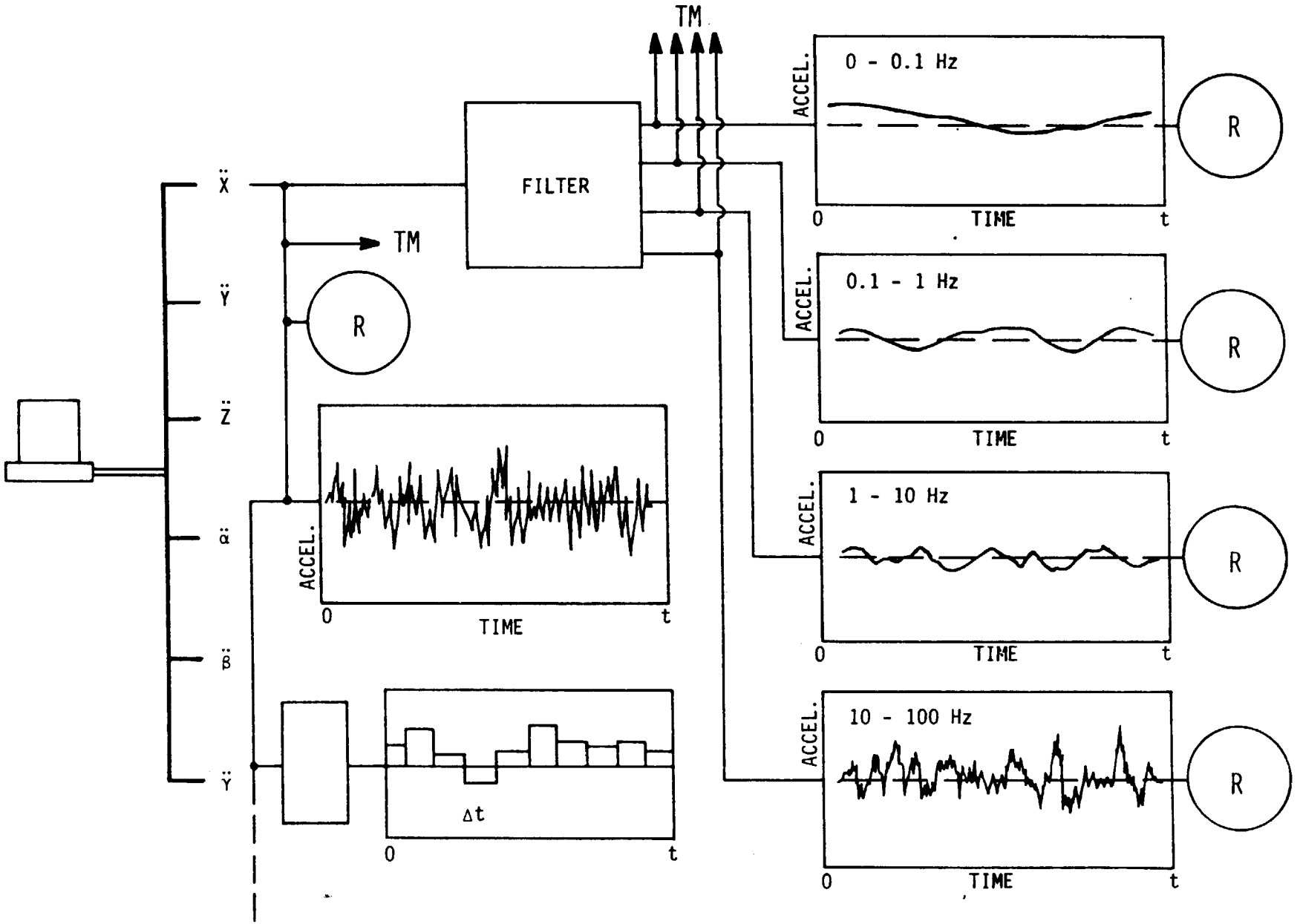

FIGURE 7. IDEAL ACCELEROMETER MEASUREMENTS

edly prompted remarks at the Workshop to the effect that this entire problem area could be avoided by putting the more sensitive materials experiments on free-flying platforms that would operate in conjunction with, but physically separated from the Space Station or the Shuttle. Acceleration levels on a Free Flyer can be expected to remain below 10E-7 g during the total duration of the detached flight. A sketch of a Free Flyer with eight materials processing chambers is shown in Figures 8 and 9.

Throughout the Workshop, the interchange of thoughts between astronauts, scientists, instrument manufacturers, spacecraft engineers, and project planners generated interesting suggestions of great mutual benefit. Among them were the following:

Astronauts' Advice:

Do in space only what cannot be done on the ground. Conduct sample preparations and elaborate evaluations in earth-bound laboratories. Store flight data on tape and transport these to earth.

Do not overburden payload scientists in orbit. Give them enough time to operate, adjust, and repair your instruments. Operational timelines must allow contingencies for unforeseen events.

Familiarize astronaut scientists thoroughly with your instruments and with your research objectives before flight. Once they are in orbit, do not try to guide them on a minute-by-minute basis. They should be prepared to use their own judgement and initiative.

Remember: As soon as a person is in orbit, he -- or she -- is a totally different human being!

Scientists' Concerns:

All the raw data should be stored onboard, and later transferred to earth. Filters, networks, and selection systems compromise the original data, often to the detriment of the value of the experiment.

FIGURE 8. FREE FLYER FOR MATERIALS PROCESSING

FIGURE 9. SERVICING OF MATERIALS PROCESSING FREE-FLYER ARRAY OF MODULES EXCHANGED SIMULTANEOUSLY

Information on steady, and near-steady accelerations, even in the presence of higher-frequency vibrations, is badly needed.

Scientists need far more time for theoretical and experimental ground work, and for a series of systematic flight expriments, before they can define systems for the manufacturing of materials in space.

Designers' Pleas:

The Space Station is for users. They should define what they need.

Specifications for the residual acceleration levels that can be tolerated by the experimenters are badly needed. Requirements as to the upper limits of acceptable acceleration and frequency levels should be established.

Advice to Designers:

Atmospheric drag compensation by continuously operating thrusters may be necessary. Design studies for such systems should be made.

Structural damping systems, and shock mounts for materials processing chambers, may be needed to provide some protection against accelerative forces.

The Space Station should be designed for acceleration-sensitive experiments. Moving systems, such as fans, pumps, compressors, bearings, hinges, latches, valves, switches, drawers, and doors, shold produce as little of a disturbance as possible.

The Space Station should always be oriented in such a way that the long axis of the Lab Module is parallel to the line along which the center of gravity moves. That line should coincide as closely as possible with the line along which the sensitive materials processing experiments are located within the Lab Module.

Remember: The Space Station must be designed for users!

Several more guidelines for Space Station designers and users, and for space program managers, resulted from discussions during the Workshop. They included the following:

Far more flight experiments are badly needed, perhaps including systematic investigations under different levels of acceleration. Such experiments could be carried out with centrifuges, or with tethers, onboard a Shuttle or the Space Station, or on a free-flying platform with a controllable thruster system.

More analysis and modeling of Space Station dynamics is needed.

Free Flyers, operating in conjunction with, but detached from the Shuttle or Space Station, would provide a long-term acceleration environment of less than 10E-7 g. The use of such spacecraft for automated or remotely controlled materials processing experiments would eliminate all problems caused by residual accelerations above that level.

☆U.S. GOVERNMENT PRINTING OFFICE: 1990-727-064/26001

NASA

Report Documentation Page

1. Report No.	2. Government Accession No.	3. Recipient's Catalog No.
NASA CP-3088		

4. Title and Subtitle	5. Report Date
Measurement and Characterization of the Acceleration Environment on Board the Space Station	August 1990
	6. Performing Organization Code
7. Author(s)	8. Performing Organization Report No.
Charles R. Baugher, Editor	
	10. Work Unit No. M-639
9. Performing Organization Name and Address	11. Contract or Grant No.
George C. Marshall Space Flight Center Marshall Space Flight Center, Alabama 35812	NAS8-36122
	13. Type of Report and Period Covered
12. Sponsoring Agency Name and Address	Conference Publication
National Aeronautics and Space Administration Washington, DC 20546	14. Sponsoring Agency Code

15. Supplementary Notes

These proceedings are the results of papers presented at a three-day workshop held at Lake Guntersville State Lodge in Guntersville, Alabama on August 11-14, 1986. The workshop was implemented by Teledyne Brown Engineering under Contract NAS8-36122 with the Marshall Space Flight Center.

16. Abstract

Although experimentation in materials processing in the space micro-gravity environment has been in progress for over a decade, there is still uncertainty in the influences of low level carrier induced perturbations on the physics of the processes. Additionally, the magnitude, duration, source, and frequency distribution of the disturbances themselves has not been cataloged in an organized fashion, even though a number of measurements have been made during various manned flight missions. Finally, it is apparent the instrumentation utilized in past flights has not been specifically suited to the task of measuring the disturbance environment actually encountered.

This workshop provides a comprehensive overview of the work and status of each of these areas to provide a basis for establishing a systematic approach to the challenge of avoiding these difficulties during the Space Station era of materials experimentation. The discussions were arranged in the order of: the scientific understanding of the requirements for a micro-gravity environment, a history of acceleration measurements on spacecraft, the state of accelerometer technology, and the current understanding of the predicted Space Station environment.

17. Key Words (Suggested by Author(s))	18. Distribution Statement
Accelerometers, Micro-gravity Materials Processing in Space Spacecraft Vibration Environment	Unclassified - Unlimited Subject category: 88

19. Security Classif. (of this report)	20. Security Classif. (of this page)	21. No. of pages	22. Price
Unclassified	Unclassified	588	A25

NASA FORM 1626 OCT 86

For sale by the National Technical Information Service, Springfield, VA 22161-2171